Development of Antimicrobial Peptidomimetics

DIANA KOLOS

Development of Antimicrobial Peptidomimetics

A Thesis Presented for the Degree of Doctor of Philosophy

The Department of Chemistry

Durham University, Ustinov College

Diana Maria Kolos

Supervised by Prof. Steven Cobb

2024

Author's Declaration

I declare that this thesis is a presentation of original work, and it is the work of the author unless otherwise stated. This work was conducted in the Department of Chemistry and Biosciences at Durham University and collaborative work was mentioned where applicable. The work has not been submitted for a degree in this or other university.

Abstract

Peptoids (oligomers of *N*-substituted glycines, NSGs) represent a class of peptidomimetics that offers notable advantages over peptides, including proteolytic stability and enhanced biological function, all while maintaining the capability to target the intricate landscape of protein-protein interactions. This thesis aimed to establish links between peptoid structure, physical properties, and antimicrobial efficacy while minimising toxicity to mammalian cells. Novel peptoid frameworks were developed to expand the chemical diversity with therapeutic promise, including long peptoid chains and macrocycles.

Chapter 1 introduces peptoids and focuses on their secondary structures, pharmacokinetics, and their biological properties. It also summarises peptoid limitations such as unfavourable hydrophobicities and amide bond heterogeneity.

In **Chapter 2**, a library of dodecamer peptoids incorporating fluorinated alkyl, **31** and **32**, and cationic quaternary ammonium peptoid (**49** – **51**) building blocks. The biological evaluation of this library unveiled that the incorporation of these monomers led to peptoids showcasing the highest SI values reported thus far for clinically relevant pathogens, including *E. coli* and *S. aureus.* Notably, **Pep. 27** and **Pep. 31** exhibited SI values of 16 and 32, respectively, for these two species. It was further observed that the inclusion of tertiary cationic ammonium monomers decreased peptoid cytotoxicity.

Chapter 3 focused on the design and synthesis of polar tyrosine-type peptoid monomers, outlining the synthetic strategies employed in their development. Detailed discussions include the determination of amide bond geometry through NMR and X-ray crystallography. The incorporation of hydrogen bond donors in the ortho position of the hydroxy(aryl) moiety of **104** (*No*Tyr) resulted in hydrogen bonding between the hydroxyl and the backbone O_{i-1}, yielding a $K_{cis/trans}$ value of 8.70 in CD_3CN and thereby inducing α-helical peptoid structures. Surprisingly, the *o*-amino(aryl)-containing acetamide **170** exhibited a full *cisoid* amide bond population, attributed to hydrogen bonding between the *ortho* amino substituent and the O_{i-1}.

The tyrosine-type and amino(aryl) monomers were employed in peptoid synthesis in **Chapter 4**, wherein eight nonamer peptoids were synthesised and their biological activities against Gram-positive and gram-negative bacteria were assessed. In addition, the partition coefficients between octanol and water were evaluated for these peptoids and revealed that increasing the number of hydroxyl groups decreased peptoid partitioning into octanol. **Pep. 54**

containing the *cis* inducing **104** monomer showed the highest SI values for *E. coli* (SI of 16), *S. aureus* (SI of 64) and *B. subilitis* (SI of 64) whilst being non-toxic.

Finally, development of a novel TFP-based peptoid cyclisation method is discussed in **Chapter 5**. This method explores the employment of *N*Tyr and *N*Lys residues in the formation of cyclic peptoid structures. Furthermore, the methodology was extended to the formation of cyclic peptides. **Pep. 93** displayed significant efficacies against Gram-positive bacteria with its MIC and ED_{50} values indicating potential therapeutic applications for TFP-stapled structures (*S. aureus* MIC of 12.5 μM; *B. subtilis* MIC of μM 3.13 μM; HepG2 ED_{50} of 100 μM).

Partitioning experiments were carried out for all the linear and cyclic peptoids studied in this thesis. Peptoids with log *D* values close to 0 exhibited the highest efficacy against pathogens, whilst reducing peptoid hydrophobicity correlates with decreased toxicity.

Acknowledgements

I want to express my deepest gratitude to my academic supervisor, Prof. Steven Cobb, for his optimistic approach, fantastic support, and guidance throughout this endeavour. His willingness to embrace my experimental detours added depth to my research.

Dr William Brittain deserves a special mention for his invaluable assistance in the laboratory, especially during the tough times of Covid-19 laboratory access restrictions, and Dr Gary Sharples for generously facilitating antimicrobial testing and providing bacterial cultures. Thanks to Prof. Paul Denny for providing HepG2 cultures and Dr Robert Pal for consenting to my work in the Clean Room. I further thank Prof. AnnMarie O'Donoghue's group for showing me how to use the UV-vis spectrometer.

I am profoundly grateful to Durham University's NMR, mass spectrometry, and X-ray crystallography services, particularly Dr Juan Aguilar, Dr David Parker, Mr. Peter Stokes, Dr Dmitri Yufit, and Dr Toby Blundel, whose work was essential for the completion of this thesis.

My sincere thanks go to the members, past and present, of the Cobb Group, including Dr Carissa Lloyd, Dr Yazmin Santos, Dr Hirunika Perera, Izzy Zawadzki, Katie Dowell, Eleanor Taylor-Newmann, Liam Beardmore, and Lewis Picken, who made this journey memorable and fulfilling.

I couldn't forget to mention that this would not have been possible without my network of friends who continued to be there for me every step of the way. This journey began years ago, and I would not have been able to come this far without the supervision of Sylvain Regeon, who, once a colleague, has become a dear friend.

My parents deserve my utmost gratitude for their endless belief in me, for their emotional support, for having my back even when the world was seemingly falling apart.

Abbreviations

Å	Angstrom
^{o}C	Degree(s) Celsius
μL	Microlitre
μM	Micromolar
AA	Amino acid(s)
a.m.u.	Atomic mass unit
Ac_2O	Acetic anhydride
AcCl	Acetyl chloride
ACN	Acetonitrile
ADME	Adsorption, distribution, metabolism, excretion
$AgClO_4$	Silver perchlorate
Ala	Alanine
Alloc	*N*-Allyloxycarbonyl
Ama.	Amastigotes
Arg	Arginine
AMPs	Antimicrobial peptides
Arg	Arginine
Asn	Asparagine
B. brevis	*Bacilus brevis*
B. subtilis	*Bacillus subtilis*
Bnz	Benzyl (protecting group)
Boc	*tert*-Butyloxycarbonyl (protecting group)
Boc_2O	Di-*tert*-butyl dicarbonate
BzBr	Benzyl bromide
Ca^{2+}	Calcium ion(s)
CAMPs	Cationic antimicrobial peptides
cat.	Catalyst
Cbz	Benzyl formate (protecting group)
CD	Circular dichroism
CD_3CN	Deuterated acetonitrile
CD_3OD	Deuterated methanol
$CDCl_3$	Deuterated chloroform
conc.	Concentrated
COSY	Homonuclear correlation spectroscopy
Cs_2CO_3	Cesium carbonate
CuAAC	Cu-catalysed cycloaddition via click-chemistry
Cys	Cysteine
d	Doublet
Da	Dalton(s)
DCM	Dichloromethane

dd	Doublet of doublets
Dde	2-Acetyl-5,5-dimethyl-1,3-cyclohexanedione
DIAD	Diisopropyl azodicarboxylate
DIC	*N,N'*-Diisopropylcarbodiimide
DIPEA	*N,N'*-Diisopropylethylamine
DMF	Dimethylformamide
DNA	Deoxyribose nucleic acid
DMSO	Dimethyl sulphoxide
DNA	Deoxyribonucleic acid
E. coli	*Escherichia coli*
ED_{50}	Median effective dose
EDC	1-Ethyl-3-(3-dimethylaminopropyl)carbodiimide
eq	Equivalents
ESI-MS	Electrospray ionisation mass spectrometry
EtI	Ethyl iodide
EWG	Electron withdrawing group
FC	Flash column
Fmoc	9-Fluorenylmethyl carbamate (protecting group)
Fmoc-Osu	9-Fluorenylmethyl-succinimidyl carbonate
g	Gram(s)
Gln	Glutamic acid
Glu	Glutamine
Gly	Glycine
h/hr	Hour
H_2	Hydrogen gas
H_2O	Water
H_2SO_4	Sulphuric acid
HBr	Hydrogen bromide
HCl	Hydrochloric acid
HG2	Hoveyda-Grubbs Catalyst 2nd Generation
His	Histidine
HOAt	1-Hydroxy-7-azabenzotriazole
HOBt	Hydroxybenzotriazole
HOMO	Highest occupied molecular orbital
HPLC	High-performance liquid chromatography
HMBC	Heteronuclear multiple quantum coherence spectroscopy
HRMS	High resolution mass spectrometry
HSQC	Heteronuclear single quantum coherence spectroscopy
HSV-1	Herpes simplex virus
Hz	Hertz (unit of frequency)
Ile	Isoleucine
IUPAC	The International Union of Pure Applied Chemistry
K	Kelvin

kcal	Kilocalorie(s)
K_2CO_3	Potassium carbonate
KF	Potassium fluoride
$KHCO_3$	Potassium bicarbonate
L. mexicana	*Leishmania Mexicana*
LC_{50}	Lethal concentration 50
LC-MS	Liquid chromatography mass spectrometry
LDH	Lactate dehydrogenase
$LiAlH_4$	Lithium aluminium hydride
$LiOH.H_2O$	Lithium hydroxide monohydrate
LL-37	Cathelicidin
Log *D/P*	Octanol/water partitioning constant – measure of hydrophobicity
LRMS	Low resolution mass spectrometry
LPG	Lipophosphoglycan
LRMS	Low resolution mass spectrometry
LUMO	Lowest unoccupied molecular orbital
Lys	Lysine
M	Molar
MBHA	4-Methylbenzhydrylamine hydrochloride
Mg^{2+}	Magnesium ion(s)
MHB	Mueller-Hinton broth
m/z	Mass to charge ratio
Me	Methyl group
mg	Milligrams
$MgSO_4$	Magnesium sulphate
MeOH	Methanol
MIC	Minimum inhibitory concentration
Min(s)	Minute(s)
m/z	Mass to charge ratio
mol	Mole
MHz	Megahertz (unit of frequency)
mL	Millilitre(s)
mm	Minimetre(s)
Mmt	Monomethoxytrityl
mM	Millimolar
MRSA	Methicillin-resistant *S. aureus*
MS	Mass spectrometry
MTT	3-(4,5-dimethylthiazol-2-yl)-2,5-diphenyltetrazolium bromide (a dye)
MW	Molecular weight
N_2	Nitrogen gas

Na_2CO_3	Sodium carbonate
NaH	Sodium hydride
$NaHCO_3$	Sodium bicarbonate
NAD(P)H	Reduced form of nicotinamide adenine dinucleotide (phosphate)
nm	Nanometre(s)
NMR	Nuclear magnetic resonance
NOESY	Nuclear overhauser effect spectroscopy
NSG	*N*-substituted glycine(s)
o/n	Overnight
OMe	Methoxy
P. aeruginosa	*Pseudomonas aeruginosa*
PBS	Phosphate buffered saline
Pd(0)/(II)	Palladium(0)/(II)
Pd/C	Palladium on charcoal (10%)
$Pd(PPh)_3$	Tetrakis triphenylphosphine palladium
pdt	Product
PFP	Pentafluoropyridine
Pg	Protecting group
pH	Potential of hydrogen
Ph	Phenyl group
Phe	Phenylalanine
PhSiH	Phenyl silane
PPh_3	Triphenylphosphine
PPI/PPII	Polyproline type I/type II
ppm	Parts per million
Pro	Proline
Prom.	Promastigotes
QToF	Quadrupole time of flight (mass spectrometry)
Quant.	Quantitative
R	Gas constant
RCN	Ring-closing metathesis
RNA	Ribonucleic acid
RP-HPLC	Reverse-phase high performance liquid chromatography
rpm	Revolutions per minute
RT	Room temperature
S. aureus	*Staphylococcus aureus*
S. epidermis	*Staphylococcus epidemis*
SAR	Structure activity relationship
Ser	Serine
S_N2	Nucleophilic substitution
S_NAr	Nucleophilic aromatic substitution
SO_2	Sulphur dioxide

SPPS	Solid phase peptide/peptoid synthesis
t	Triplet
T	Temperature
T_1	Spin-lattice relaxation time constant
Trt	Trityl
^{t}Bu	*Tert*-butyl (protecting group)
TEA	Triethylamine
TFA	Trifluoroacetic acid
TFP	Tetrafluoropyridine (protecting group)
THF	Tetrahydrofuran
TIPS	Triisopropylsilane
TLC	Thin-layer chromatography
Trp	Tryptophan
Trt	Trityl
Ts	Tosyl
Tyr	Tyrosine
TQD	Triple quadrupole (mass spectrometry)
t_R	Retention time
Tyr	Tyrosine
UV-Vis	Ultraviolet-Visible (spectroscopy)
v/v/v/v	Volume concentration
Val	Valine
w.r.t.	With respect to
Z-OSu	*N*-(Benzylcarbonyloxy)succinimide

Contents

Chapter 1: Introduction to Biologically Active Peptoids

1.1. Introduction to antibiotic resistance and antimicrobial peptides

The emergence of antimicrobial resistance (AMR) has resulted in a fatality rate exceeding 700,000 deaths per year globally while predictions indicate the annual death count of 10 million by 2050.[1] Therefore, the finding of new antibacterial resources has become an urgent need engaging attentions of research groups all over the world.

In the 1960s, following the discovery of brombinin and lactoferrin,[2-4] and the continuing rise of multi-resistance microbial pathogens, research into host defence peptides also known as antimicrobial peptides (AMPs) increased significantly. In 1981, a study carried out by Boman reported induction of a potent AMP after injection of bacteria into Cecropia silk moths.[4] In 1987, in a breakthrough study by Zasloff, the cationic AMPs (CAMPs) called magainins were isolated and characterised from the African clawed frog *Xenopus laevis*.[5] Magainins were found to possess potent antimicrobial and tumoricidal activities.[6,7] Successively, in 1990, Zanetti reported the discovery of the cathlecidin CAMPs in bovine neutrophils.[8] Following this discovery, four years later, Gallo discovered the presence of cathlecidins in mammalian skin cells.[9]

Cathelicidins (such as LL-37), together with defensins and histatins, are small CAMPs which are activated proteolytically and are found in neutrophils and leukocytes, secreted by skin and epithelial cells, and in the case of histatins are found in saliva. They play an important role in the mammalian host innate immune system. In addition to being effective against Gram-positive and Gram-negative bacteria, CAMPs have also been found to cause cell death in fungi[10], enveloped viruses[11] and protozoa.[12,13]

The cationic nature of AMPs allows for the formation of pores in bacterial membrane bilayers, via ‘barrel-stave’, ‘toroidal-pore’ and carpet-like (‘micelle’) mechanisms (**Section 1.1.2**).[14-18] The disruption of bacterial cell membranes leads to cell death, and some CAMPs have been found to cross bacterial cytoplasmic membranes and disrupt intracellular processes such as protein folding and degradation, and DNA/RNA synthesis.[19-20]

1.2. Antimicrobial peptides (AMPs)

1.2.1. AMP secondary structures

AMPs are highly conserved components of the innate immune system in all organisms. Typically, AMPs consist of between 10 to 50 residues, with >50% being hydrophobic and the inclusion of numerous charged residues (e.g. Lys and Arg) renders them overall cationic. It should be noted that while highly uncommon in nature a number of anionic AMPs do exist, including several lantibiotics produced by Gram-positive bacteria.[21-24]

The secondary structures of AMPs can roughly be divided into four distinct groups (a – d), as illustrated in **Figure 1.1.**

(a) α-helical structures, e.g. magainin. This type of peptide secondary structure is the most prevalent, self-stabilising motif in the family of structure conformations seen for AMPs. Naturally occurring α-helices are amphipathic, and right-handed with ca. 3.6 residues per turn, and are made of 4 – 40 amino acids.[5,24]

(b) α-hairpin and loop conformation, e.g. protegrin I. A β-hairpin consists of two antiparallel peptide strands, where the *N*-terminus of one is adjacent to the *C*-terminus of the other. They can exist in isolation or collectively comprise a β-sheet.[25]

(c) β-sheet-containing, such as α- and β-defensins. These molecules are heterogenous in length, belong to CAMPs and are non-glycosylated. Their characteristic secondary structure can be attributed to the six cysteine amino acids which form three disulphide bridges. This results in a triple beta sheet structure. A β-sheet conformation is less stable than α-helices due to 'dangling' hydrogen bonds.[26,27]

(d) Extended AMP conformation, such as indolicidin. Such peptides do not fold into any defined conformation, and this is often the result of predomination of a single amino acid such as proline, tryptophan or arginine.[26]

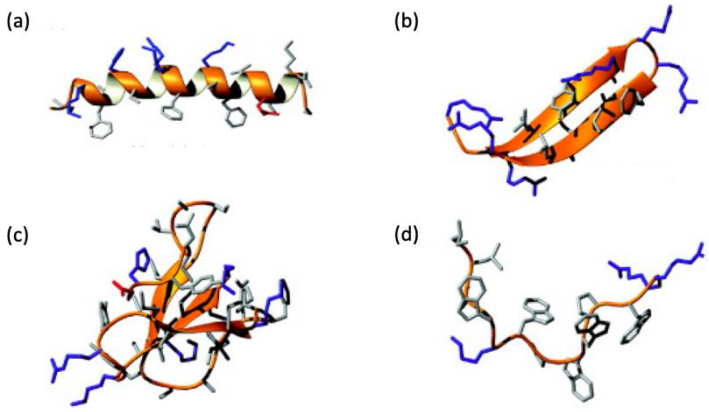

Figure 1.1. Examples of the four structural families of naturally occurring AMPs: (a) α-helix; (b) β-sheet; (c) β-hairpin; (c) extended structure. (Figure adapted from Nguyen *et al*., 2012)[24]

APMs are typically amphipathic, and they often adopt a helical shape, (**Figure 1.1.a**) where the hydrophobic and hydrophilic parts align on opposite sides. This arrangement allows AMPs to be soluble in water whilst also having properties that interact favourably with hydrophobic surfaces. Within an aqueous solution, AMPs often have highly disordered structures but upon entering a non-polar environment, such as the bacterial bilayer lipid membrane they can adopt highly ordered, amphipathic alpha helices (**Figure 1.2**).[24,27] This feature facilitates perturbation of peptides through bacterial cell membranes by electrostatic interactions. Hence, in contrast to the action of traditional antibiotics, CAMPs interact with bacterial membranes by neutralising the negative charge before penetrating through them, leading to the formation of channels.[28] Due to this specific type of membrane targeting, emergence of resistance to AMPs is not as prevalent as in the case of antibiotics.

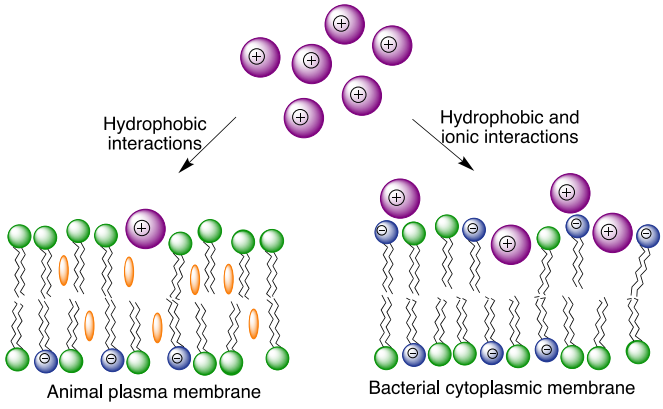

Figure 1.2. Interaction of CAMPs with animal and bacterial membranes. There is no charge outside of animal membranes while bacterial cells possess cationic phospholipids on the outer face of their membranes.

Moreover, as AMPs often display broad-spectrum antimicrobial activity[10-13,29] they could in theory be used to treat complex polymicrobial infections e.g. multispecies biofilms which can occur in diseases such as pneumonia.

1.2.2. Interactions of AMPs with bacterial membranes

There exist a large range of different AMPs which adopt various secondary structures, when acting upon the bacterial lipid membrane by translocation. Three key poration mechanisms by which AMPs target bacteria include: the barrel stave, toroidal and micelle mechanism (**Figure 1.3**).[14-18]

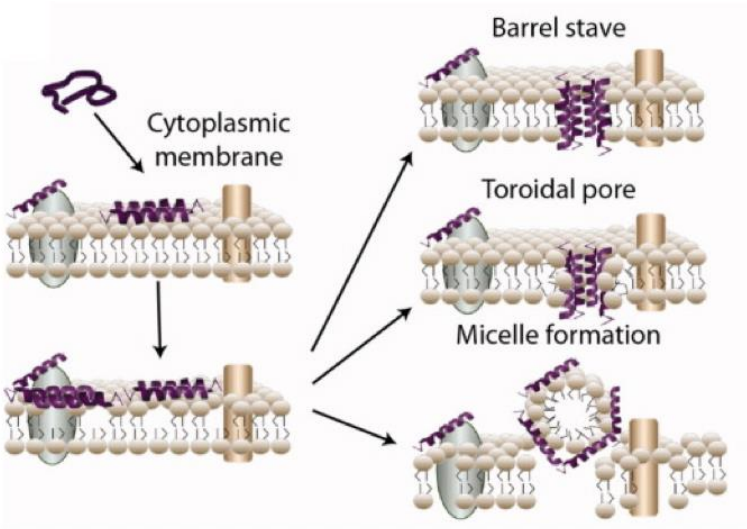

Figure 1.3. Schematic representation of barrel stave, toroidal pore, and micelle mechanisms by which AMP can disrupt the bacterial lipid membrane. (Figure adapted from Buer *et al.*, 2012)[30]

(1) The *barrel stave* mechanism suggests that peptide amphipathicy leads to peptides assembling and orienting on the bacterial membrane surface. In high concentrations this leads to peptide aggregation and insertion into bacterial membranes.

(2) The *toroidal pore* formation model sees self-association of peptide helices aligned to the plane of the membrane. This results in the formation of a protein-lined pore and, similarly to the carpet mechanism, it leads to curvature strains and membrane disruption. The AMP magainin acts via this mechanism; it penetrates the lipid membrane headgroup region, destroying the lipid-lipid interactions, resulting in positive curvature strains and thinning of the membrane.

(3) In the *micelle formation*, the AMPs interact with the bacterial lipid membrane and essentially cover the surface of the membrane which leads to curvature strains and

membrane breakage. This mechanism will lead to the formation of micelles, comprising of bacterial phospholipids 'carpeted' with AMP chains. The membrane disruption commences with association of the AMP with the membrane via electrostatic interactions, e.g. between the AMP arginine residue and the membrane phosphate functionalities.

There are known factors which affect the mechanisms by which AMPs insert into the membranes such as peptide size, charge, hydrophobicity, secondary structure, as well as membrane composition. The translocation mechanisms are most commonly passive, but some peptides such as cyclosporin (a cyclic AMP) can be taken up by cells via active transport.[24]

1.2.3. Limitations of AMPs with respect to therapeutic development

AMPs are an evolutionarily conserved part of the innate immune system and therefore the design of non-natural peptide libraries based on innate peptides would be a logical path to take in the quest to tackle antimicrobial resistance. However, multiple studies applying this strategy reported not only toxicity to microbial cells but also cytotoxicity to host cells as well as haematotoxicity when AMPs were applied in quantities necessary to destroy pathogens.[31,32] Therefore, it is common that a synthetic AMP, showing a potent activity against a microbial target *in vitro*, rarely reaches *in vivo* testing. Despite it being unclear what causes toxicity to eukaryotic cells, it has been observed that the use of hydrophobic amino acid residues, when designing AMPs, can contribute to it. The poor selectivity index (SI) for many synthetic AMPs is attributed to these hydrophobic peptides interacting not only with lipids within the bacterial membranes but also with the phosphatidylcholine lipid moieties located in eukaryotic cell membranes.[33] In addition, many AMPs show a high degree of conformational flexibility, which sometimes results in activation of more than one target (poor specific biodistribution). This can lead to side effects and there is a risk of immunogenic effects.

It is worth noting however, that the significance of cytotoxicity might be lower in living organisms compared to laboratory settings. In 2009, Pasupuleti and co-workers[34], reported that several Phe- and Trp-tagged AMPs showed reduced cytotoxicity to eukaryotic cells in the presence vs. absence of serum. The short AMPs used in this study were derived from kininogen, KNKGKKNGKH, and it was recognised that end-tagging of these short peptides with Phe and Trp residues leads to minimal haemolysis. This observation was rationalised by

a higher binding affinity of these peptides to bacterial cell membranes, leading to liposome rupture. The effect of the peptides on eukaryotic cells is shown in **Figure 1.4**.

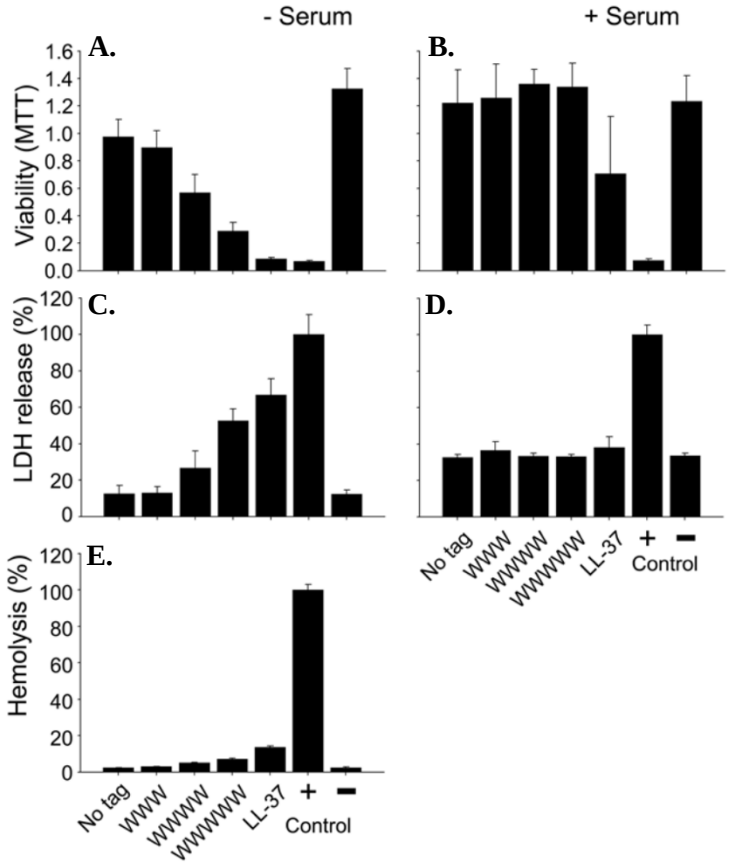

Figure 1.4. Effect of kininogen-derived peptides, with variable Trp (W) tagging on eukaryotic cells in the absence and presence of human serum. **A** & **B**: MTT viability assay which is NAD(P)H-dependent. **C** & **D**: LDH assay results indicate membrane integrity. **E**: Haemolytic effect on the cells. LL-37 is a benchmark antimicrobial peptide used in the study, (-) indicates negative control, (+) indicates positive control, where 2% Triton X-100 (cell lysis) was used. For MTT and LDH assays in serum, the differences in values between non-tagged and tagged peptides are not statistically significant. This is also the case for haemolysis values. Figure adapted from Paspuleti *et al*.[34]

In recent years numerous research groups have focussed on controlling the cytotoxicity and antimicrobial activities of AMPs by tuning both their overall and positional hydrophobicity. Attempts have been made to replace/remove as well as re-position the hydrophobic residues and hence rationally design *de novo* peptides.[31]

In addition, all peptides, not just AMPs, are hampered by an inherent poor oral bioavailability due to their susceptibility to proteolytic cleavage at the amide bond. Their propensity to be rapidly metabolised, is the primary reason that peptides are often viewed as

poor drug candidates.[35] Nevertheless, the growing number of small-molecule drugs being abandoned in clinical trials has led to peptides seeing a revival of interest as potential drugs.

1.3. Peptidomimetics

1.3.1. Peptidomimetic classes

Peptidomimetics are molecules which are designed to mimic the properties and structures of naturally occurring peptides. Given their unnatural structures, they have the potential to circumvent some of the major issues, such as proteolytic degradation, associated with naturally occurring peptides including AMPs. Four main classes of peptidomimetics are: 1) foldamers such as D-peptides, which are mirror images of naturally occurring α-peptides; 2) macrocycles, where peptides bearing adopt cyclic ring structures; 3) β/γ-peptides, which consist of β/γ-amino acids where the amino group is bonded to the $C^{\beta/\gamma}$; 4) peptoids, such as α-peptoids, where the side chain functionality is bonded to the nitrogen atom of the amide bond rather than C^{α}, but β- and γ-peptoids are also possible. For the representation of these different peptidomimetic structures see **Figure 1.5**.

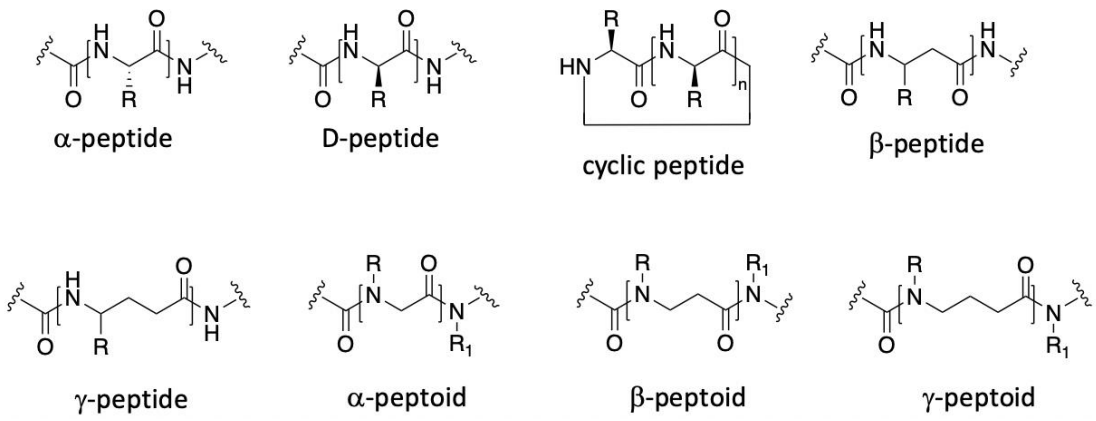

Figure 1.5. Comparison of different peptidomimetic structures.

1.3.2. Peptoids

Peptoids were firstly reported in the 1980s and are a class of non-natural polymers which can be accessed via synthetic methods.[36] In contrast to peptides, which have their side chains attached to C^{α}, peptoids can be described as foldamers consisting of *N*-substituted glycine oligomers. There are factors which have to be kept in mind when looking to design new peptoid libraries:

1) Within peptoids the lack of amide hydrogen bonding capacity affects the formation of rigid and stable secondary structures and controlling their formation can be more difficult to achieve than in the corresponding peptide systems.
2) Lack of chirality on the peptoid backbone leads to peptoids having no intrinsic handedness and together with the presence of tertiary amide bonds it leads to the chains being able to adopt either of the nearly isoenergetic *cis* or *trans* conformation (rotations about ω, see **Figure 1.6**).

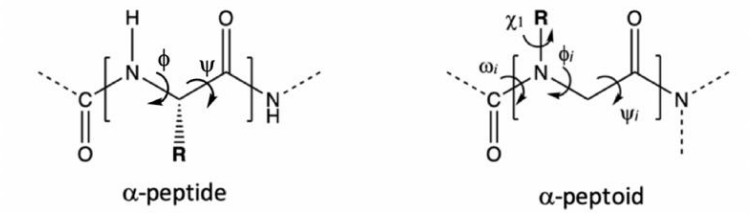

Figure 1.6. An illustration of the rotational architecture of peptides and peptoids.

Given the aforementioned challenges, *de novo* design of peptoids is much more problematic than the design of chiral peptides. A number of research groups have focused their research efforts on developing methods to achieve full structural control of peptoid chains by restricting backbone conformation.[37-42] The utilisation of different functionalities bonded to the amide side chains makes it possible to attain full structural control through electrostatic and steric interactions, work in this area is further discussed in **Chapters 2** and **3**.

1.4. Synthesis of α-peptoids

1.4.1. Monomer approach

The original monomer method to synthesise α-peptoids requires the synthesis of *N*-terminus and side chain protected building blocks which are then reacted together via amide coupling to form the desired peptoid chains.[43] The formation of the peptoid monomers can be performed by S_N2 reaction where a primary amine of choice selectively displaces an alkyl halide. Alternatively, reductive amination can also be used.[44] Following this, *N*-protection with an Fmoc group is performed (**Scheme 1.1**).

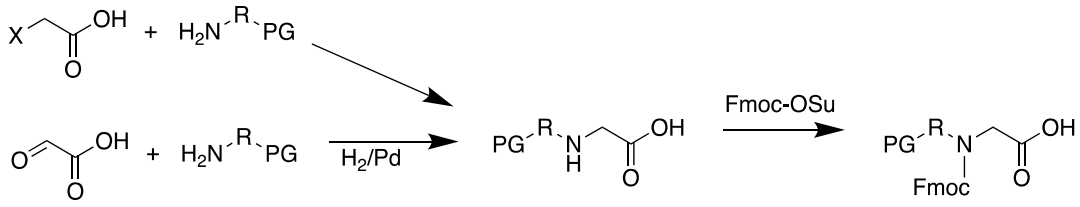

Scheme 1.1. A scheme showing the formation of an Fmoc-protected α-peptoid building block (PG = protecting group).

The monomer strategy, shown in **Scheme 1.2**, has been traditionally applied when synthesising long α-peptide chains as Fmoc-protected α-amino acid building blocks are commercially available. In the synthesis of peptoids, coupling step is followed by Fmoc-deprotection, performed with a solution of piperidine in DMF, is repeated until the desired sequence is achieved. The peptoid is then cleaved from the resin using a cleavage solution, typically consisting of trifluoroacetic acid (TFA) and a scavenging agent such as triisopropylsilane (TIPS).[43]

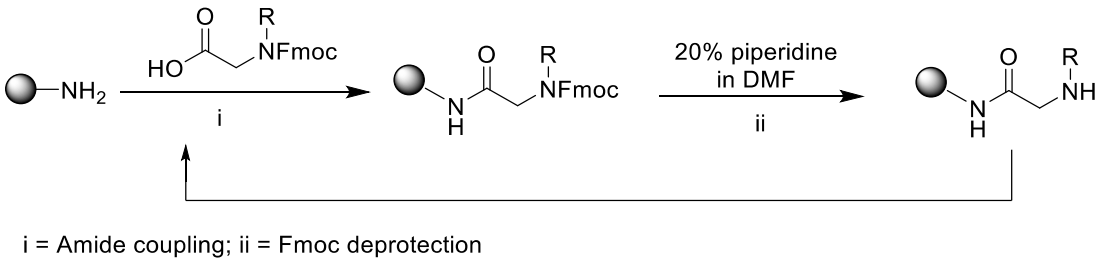

Scheme 1.2. A schematic representation of the monomer method used to synthesise α-peptoids.

Nevertheless, the utilisation of the monomer method does not come without its synthetic challenges. Firstly, the coupling of secondary amines, in peptoid synthesis, can result in much lower yields when compared to the formation of secondary amide bonds, as in standard Fmoc SPPS. Secondly, the solution phase synthesis of the required Fmoc-protected peptoid building blocks can be challenging. This latter issue can render monomer peptoid synthesis lengthy and laborious when numerous different monomers are required for the synthesis of a given peptoid or library of peptoids for biological testing.

1.4.2. Submonomer method

In 1992, in the group of Zuckerman, the submonomer method was developed.[45] This method typically employs Rink amide resin and utilises haloacetic acid (1.2 M; 20 eq), such as bromo- or chloroacetic[46] acid (iodoacetic acid[47] has also been used via *in-situ* Finkelstein reaction), activated by *N*,*N*-diisopropylcarebodiimide (DIC) (20 eq). The activation by DIC forms an isourea intermediate, which then reacts with the resin-bound amine through amide coupling. This acylation step typically takes about 15-20 minutes at room temperature.

The halide is displaced by the primary amine of choice (1.0 – 2.0 M; 20-40 eq) to form a peptoid building block. The advantage of this technique is that the side-chain of interest can be incorporated into the growing chain by a S_N2 reaction using a primary amine. Hence, it guarantees that the reaction of the peptoid chain will result in a much higher overall yield, compared to the monomer approach, which requires the coupling of secondary amines. This method also avoids the synthesis of Fmoc-protected peptoid building blocks, thereby rendering it much more efficient when synthesising long and varied α-peptoid oligomers.[36] The submonomer approach can be carried out under ambient conditions and, depending on the nature of the primary amine used, the reaction times can vary from ca. 30 mins to 120 mins. Subsequently, the amine solution can be recovered and reused.

Peptoids are cleaved from Rink amide resin using a solution of TFA/TIPS/H_2O (95:2.5:2.5 *v/v/v*), just like in standard solid phase peptide synthesis (SPPS). The submonomer method allows for a cost-effective and timely means to synthesise vastly diverse peptoids due to commercial availability of a large range of primary amines.[36] The technique can also be automated and tens of peptoids can be synthesised simultaneously. The submonomer method is illustrated in **Scheme 1.3**.

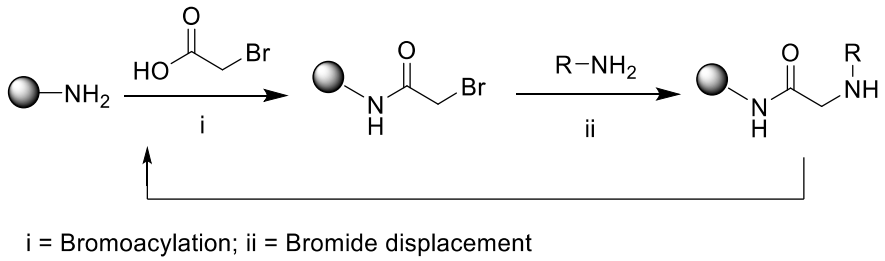

Scheme 1.3. A schematic representation of the sub-monomer method used to synthesise α-peptoids.

1.5. Secondary structure of peptoids

1.5.1. Control of peptoid secondary structure

In peptides the secondary structure is dictated by the sequence of amino acids and the internal hydrogen bonding which is facilitated by the presence of the amide hydrogens along the peptide backbone. The absence of backbone hydrogen bonding in α-peptoids leads to isomerisation between *cis* and *trans* amide bond conformations occurring much more readily than in the case of α-peptides.

The control of peptoid secondary structure has been extensively explored and researchers have been able to achieve stable helices, turn and loop structures. This has been possible via the installation of monomers with side chains that are able to restrict backbone conformation. These side chains can give rise to forces which control the secondary structure of peptoids:

1) Repulsive forces between bulky side chains[48], such as aromatic functionalities due to steric hindrance, or negatively charged moieties which would lead to charge-charge repulsions with backbone carbonyls;
2) π stacking interactions[39] between aryl side chains;
3) n → π* interactions[37] between two carbonyls or a backbone carbonyl and an aryl side chain; (**Figure 1.7**)
4) Electronic interactions between backbone carbonyls and highly electronegative side chain, such as fluorinated side chains[38]; (**Chapter 2**)
5) Hydrogen bonding has been explored in monomers which were used to lock the peptoid amide bond in the *cis* conformation.[49,50] (**Chapter 3**)

trans amide *cis* amide

Figure 1.7. A depiction of n → π* interactions between neighbouring backbone carbonyls (trans amide), giving rise to a β-turn and n → π_{Ar}* interactions between a carbonyl and an aryl side chain (cis amide), giving rise to an α-helix. (Figure adapted fron Gorske et al, 2007).[37]

1.5.2. α-helical structure

Peptoids with magainin-type structures are oligomers adopting a PPI helix when exposed to a hydrophobic environment.[5] The utilisation of different peptoid monomers allows for precise control of secondary structure. Some peptoid monomers which encourage the *cis* amide bond conformation within a peptoid are shown in **Figure 1.8**.

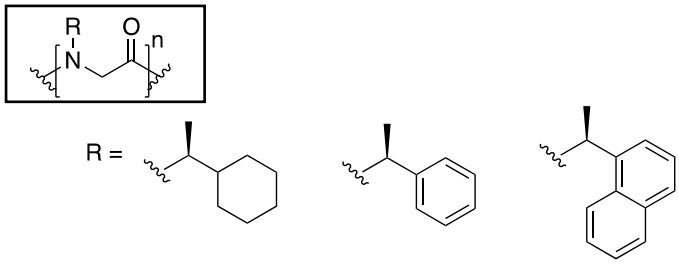

*N*sch **1** *N*spe **2** *N*s1npe **3**

Figure 1.8. Peptoid monomers which encourage α-helical structure formation.[5]

The α-helix (**Figure 1.9**) is the most explored peptoid secondary structure, and peptoids which fold to form α-helices exhibit excellent thermal and chemical stabilities. They provide a platform for making peptoids which mimic biopolymers. It has been evidenced that linear peptoids consisting of as few as five monomers adopt α-helical conformation. Furthermore, the process of stapling peptoids can lead to stable α-helices. Peptoid helicity is especially promoted in chains containing ≥50% α-chiral residues or in chains with α-chiral side chain groups positioned every third residue (*i, i+3*), and α-chiral residue at the *C*-terminus.[51,52]

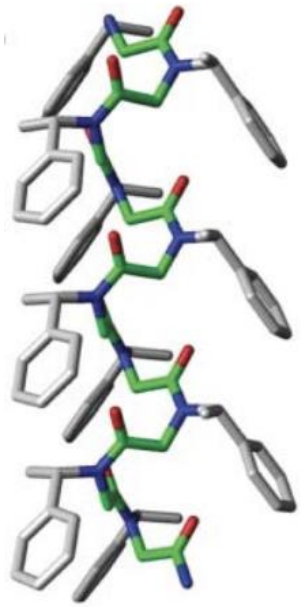

Figure 1.9. NMR structure of an α-helical (PPI helix) peptoid (*N*spe)$_{10}$, which was generated by 2D NMR analysis.[53] (Structure adapted from Fowler *et al*., 2009)

In a study carried out by Wu and co-workers, homooligomeric peptoids were studied using X-ray crystallography. The results revealed that these peptoids adopt an α-helical structure with a pitch of 6.0 Å.[51] In this context, the "pitch" refers to the vertical distance along the helix axis that one complete turn of the helix spans. This α-helical structure contains three residues per turn, meaning that every 6.0 Å along the helix, the structure completes a full rotation and three peptoid residues are positioned along this segment. Further analysis of the structure by 2D NMR showed very high backbone amide $K_{cis/trans}$ values. This is indicative of homogenous structures in solution. The aromatic ring of the α-branched benzylic-type monomer utilises the n → π^*_{Ar} electronic interaction between the backbone carbonyl oxygen (O_{i-1}) (HOMO) to the submonomer antibonding orbital (LUMO) (residue *i+1*) to stabilise the *cis* amide structure and therefore achieve the α-helical conformation.[37,51]

The utilisation of the electronic properties of side chains of a non-aromatic nature has also been studied. Such side chains which contain electronically deficient groups exploit the n→ π* interactions between the carbonyl and the side chain, in turn lowering the gap between the n (HOMO) and π* (LUMO) orbitals in the system. This modulation of orbital energies influences the overall folding and stability of the peptoid, thus providing a three-dimensional control of peptoid secondary structure. By precisely controlling these electronic interactions,

researchers can predict and manipulate the three-dimensional conformation of the peptoid, enhancing its structural stability and functional properties.

It is the balance between the n → π* interactions in **4** and **5** that determines the isomerisation of the amide bond. PPI (type I polyproline) helix consists of amide bonds in *cis* conformation, but there exists a less popular PPII (type II polyproline) helix which can be achieved by incorporating side chains adjacent to the amide nitrogen which encourage the *trans* amide bond conformation. Such groups include aryls which result in low $K_{cis/trans}$ values.[54] PPII-type structures are further discussed in **Section 3.1.1.**

1.5.3. Threaded loop peptoid structure

The threaded loop structure was first identified in a homononamer of *N*spe. Unique to nonamers with α-chiral side chains, it was first found by well-defined local interaction and it has been firstly described by the Barron group in 2000s.[55] The circular dichroism (CD) spectrum of such a structure appears highly distinct from an α-helix and it shows a single broad peak at 203 nm.[51] Due to its novel appearance, its structure was confirmed by high resolution 2D NMR. The hydrogen bonding between backbone carbonyls on three residues (*N*Spe submonomers 5, 7, and 9, **Figure 1.10.**) and *N*-terminal secondary ammonium play an important role in the stabilisation of this structure. Additionally, one intramolecular hydrogen bond between residue 2 (backbone carbonyl) and C-terminal primary amide (residue 9) has been assigned to further assist structure stabilisation.

The threaded loop conformation contains four *cis* and four *trans* amide bonds. Reportedly, this structure was found to form in acetonitrile, where the peptoid used was a homooligomer $(Nspe)_9$. Interestingly, the use of a solvent mixture such as MeOH/ACN (1:1) causes the structure to disassemble, converting it to an α-helix. This can be explained by MeOH being able to disrupt the formation of intramolecular hydrogen bonding, demonstrating its importance in the formation of the threaded loop conformation.

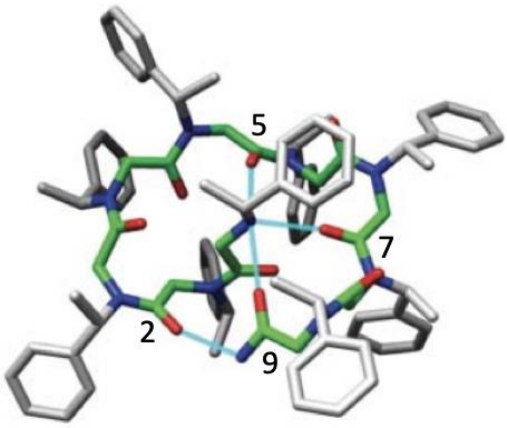

Figure 1.10. A depiction of a threaded-loop structure of (*N*spe)$_9$ peptoid. This structure was generated by 2D NMR analysis.[53] (Structure adapted from Fowler *et al*., 2009)

To date, attempts have been made to discourage the formation of the threaded loop structure and stabilise the formation of α-helices. For example, in the Blackwell group, efforts have been made to achieve this by incorporating electron withdrawing groups adjacent to the amide nitrogen. Nitro-aromatic (**4**) and fluorinated (**5**) moieties (**Figure 1.11**) were used to modulate the intramolecular hydrogen bonding and in turn affect the loop conformation.[51] Moreover, the Kirschenbaum group employed covalent bonding to stabilise the α-helix of **Pep. 1**, forming **Pep.2**, and to prevent it from converting into the threaded loop structure.[56] (**Figure 1.12**)

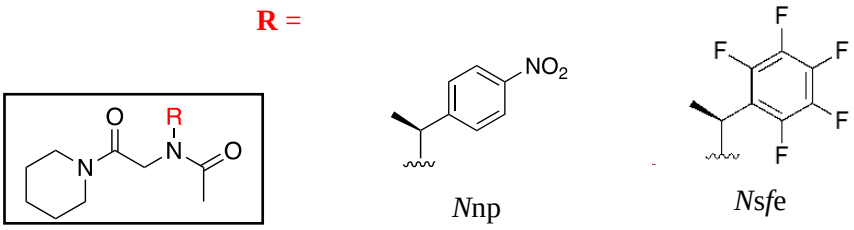

Figure 1.11. Fluorinated and nitro-aromatic monomers used by Blackwell[37] to control the conformation of the peptoid loop structure.

A.

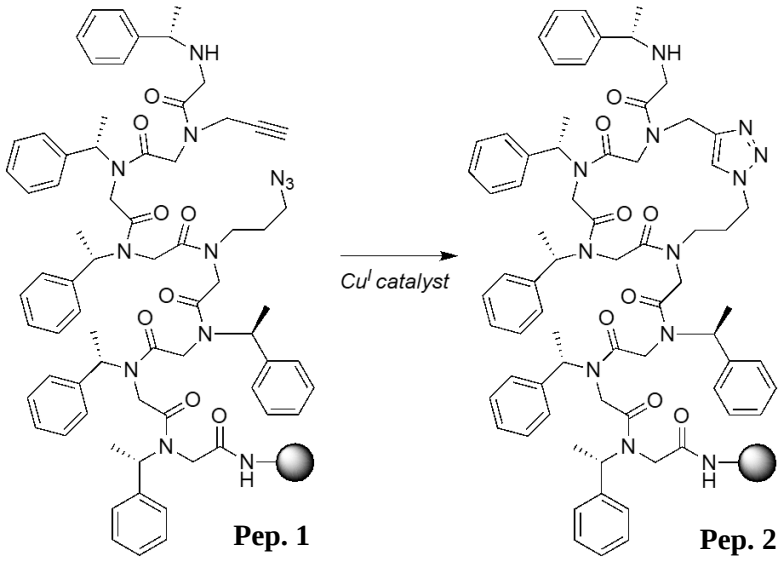

B.

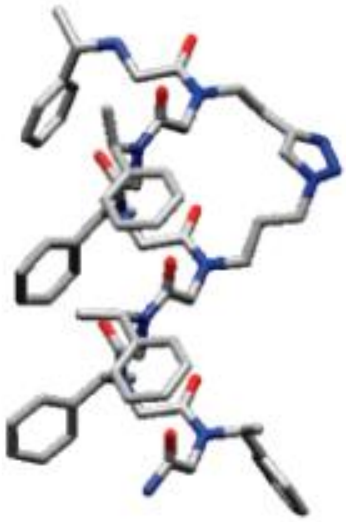

Figure 1.12. A. Illustration of covalent macrocyclic constraint in **Pep. 2** formed by pre-organising the reactive groups (at *i*, *i+3* positions) of **Pep. 1** across one turn of the helix, via a click reaction using a Cu(I) catalyst on resin, which can prevent it from transitioning into a threaded loop structure. **B.** Structure of the **Pep. 2**, generated by 2D NMR analysis.[56] (Structure adopted from Kirschenbaum *et al*., 2007)

1.5.4. Peptoid turn structure

Unlike α-helices, β-turn structures in peptoids have not been well established. The formation of such structures is heavily dependent on the incorporation of side chain moieties.[56] β-turns first explored by Appella,[57] who demonstrated that incorporation of a geometrically constrained triazole ring in a peptoid chain (**Pep. 3**) will lead to the stabilisation of a turn structure in linear peptoids which mimics the β-hairpin structure in peptides. (**Figure 1.13**)

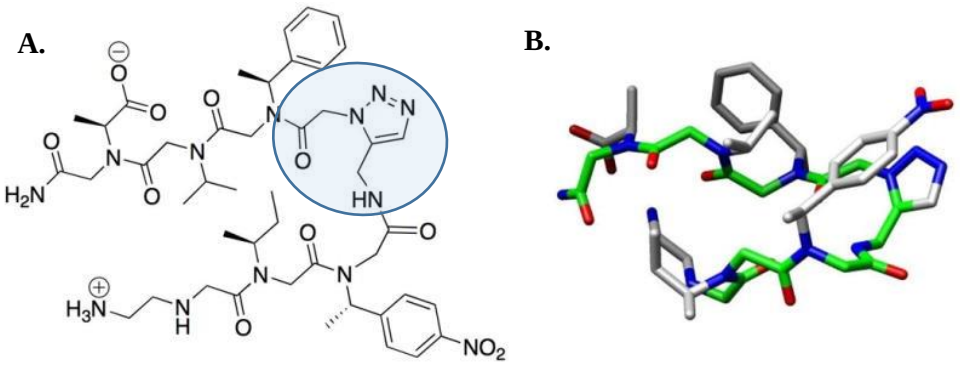

Figure 1.13. A. A molecular structure of a β-turn, reported by Appella[56]. This peptoid is a mimic of a β-hairpin and contains a triazole turn unit (upper right corner). **B**. Structure of **Pep. 3**, generated by 2D NMR analysis.[57] (Structure adapted from Pokorski *et al*., 2009)

1.5.5. Peptoid secondary structure determination

CD spectroscopy is the most commonly used analytical technique in peptoid secondary structure determination. The measurements for CD analysis can be carried out quickly and require samples of low concentrations (as low as 1 mg/mL). Importantly, it can be used to monitor peptoid secondary structure changes in a variety of environments, such as different pH, temperature, solvent nature or presence of denaturants. CD spectroscopy requires a molecule to possess one or more chiral light-absorbing groups (chromophores) and it utilises the difference in the absorption of left- and right-handed circularly polarised light. The absence of chiral species in a peptoid will result in the absence of a signal.[56,57]

The feature which makes it possible to investigate peptoid secondary structures by CD spectroscopy is the low-energy electronic n → π* and π_0 → π* transitions, which take place within the *N*-substituted amide bond. The intensity of the absorption observed on a CD spectrum is dependent upon the quantity of the electronic transitions. Therefore, higher absorptions are seen for longer peptoid chains. The most extensively studied are peptoids with α-helical structures and on a CD spectrum they show a well-defined double minimum at 202 and 218 nm, and a maximum at 190 nm (**Figure 1.14**). Furthermore, peptoids with exclusively α-chiral side chains, such as in the case of **Pep. 6** (**Section 1.7.2.**), show a shallow double minimum at 200 and 205 nm, and a maximum at 210 nm.[51,58,60,61]

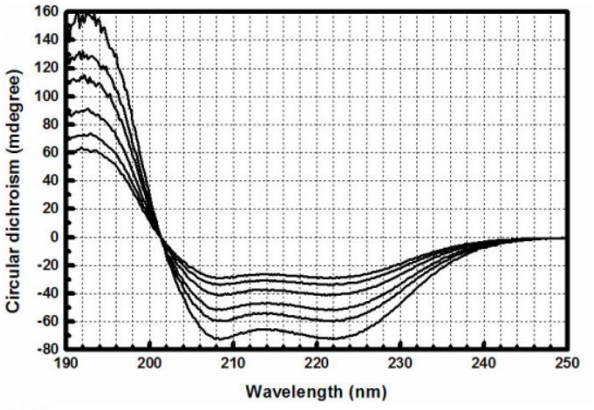

Figure 1.14. Far-UV CD spectrum of a helical species in various concentrations, whereby the most defined trace represents the most concentrated solution (highest degree of helicity).[58]Adapted from Corrêa *et al*., 2009.

Analysis of peptoid conformations by NMR spectroscopy is more time-demanding than CD spectroscopy and often employs 2D-NMR techniques such as NOESY and HSQC. While NOESY can confirm the n → π* interaction between the backbone carbonyl and an aryl side chain, the use of $^{1}H–^{13}C$ HSQC spectra is useful in the investigation of the *cis*/*trans* equilibrium within a peptoid chain, caused by a particular submonomer, and is used to determine the preferred isomer formation. The $K_{cis/trans}$ value, which can be calculated using the integration values of the NMR signals corresponding to the *cis* and *trans* helical isomers, gives an indication of the isomer formation preference. This value often varies slightly depending on the solvent in which the NMR analysis was carried out, and it can be used to find the free energy difference between the *cis*- and *trans*-isomers.[37,51,61,62]

The use of X-ray crystallography in secondary structure determination of peptoids is less common due to the flexibility of most linear peptoids. This is because due to their flexible nature, peptoids are not crystalline. Therefore, this technique is more commonly used to resolve structures of cyclic peptoids which are more conformationally restricted.[53] Cyclic peptoids are discussed in detail in **Chapter 5**, where a crystallographic representation of a peptoid cyclohexamer, obtained by Kirshembaum[63], is depicted.

1.6. Pharmacokinetics and pharmacodynamics of peptoids

Peptides often showcase exceptional *in vitro* antipathogenic properties. However, linear unmodified peptides show poor pharmacokinetics because of the presence of enzymatically cleavable peptide bonds, resulting in short plasma half-lives. Consequently, the permeability

of peptides across the intestinal epithelium is remarkably poor rendering them rarely orally bioavailable. Therefore, peptide therapeutics are typically administered intravenously, intramuscularly, or subcutaneously.

The past few decades have seen an increase in techniques including the development of automated methods allowing a diversity of chemical modifications to be introduced into oligomeric libraries. The incorporation of not only genetically encoded L-amino acid residues, but also D-amino acids as well as *N*-substituted glycines (NSGs) allowed for the efficient and cost-effective generation of unprecedented number of compounds. This allowed for screening of huge numbers of compounds over very short time periods.

The non-natural synthetic strategies which can be implemented have the potential to improve the limitations of peptides by refining their pharmacokinetic profiles. There are four pharmaceutical properties limiting peptides which researchers seek to improve often without success: i) adsorption, ii) distribution, iii) metabolism, iv) excretion (ADME). Oligomers mimicking α-peptides serve a more immediate promise to improve these deficiencies than peptides. This is especially the case when designing therapeutics which are sought to be administered orally.[64,65]

The enzymatic degradation of a series of hexameric oligomers was investigated by Miller and co-workers.[66] In the study, L-peptides, D-peptides, peptoids, and retro-peptoids were prepared and then screened against enzymes naturally present in the digestive tract. The results are shown in **Figure 1.15**. Indeed, the *in vivo* bio-stability of L-peptides is very low as these molecules bind well to the enzymatic active sites. As expected, the *N*-substituted peptides do not undergo enzymatic cleavage as the peptide bond is not readily available for nucleophilic attack. The side chains attached to the amide nitrogen cause misalignment of the carbonyl groups preventing hydrolysis.

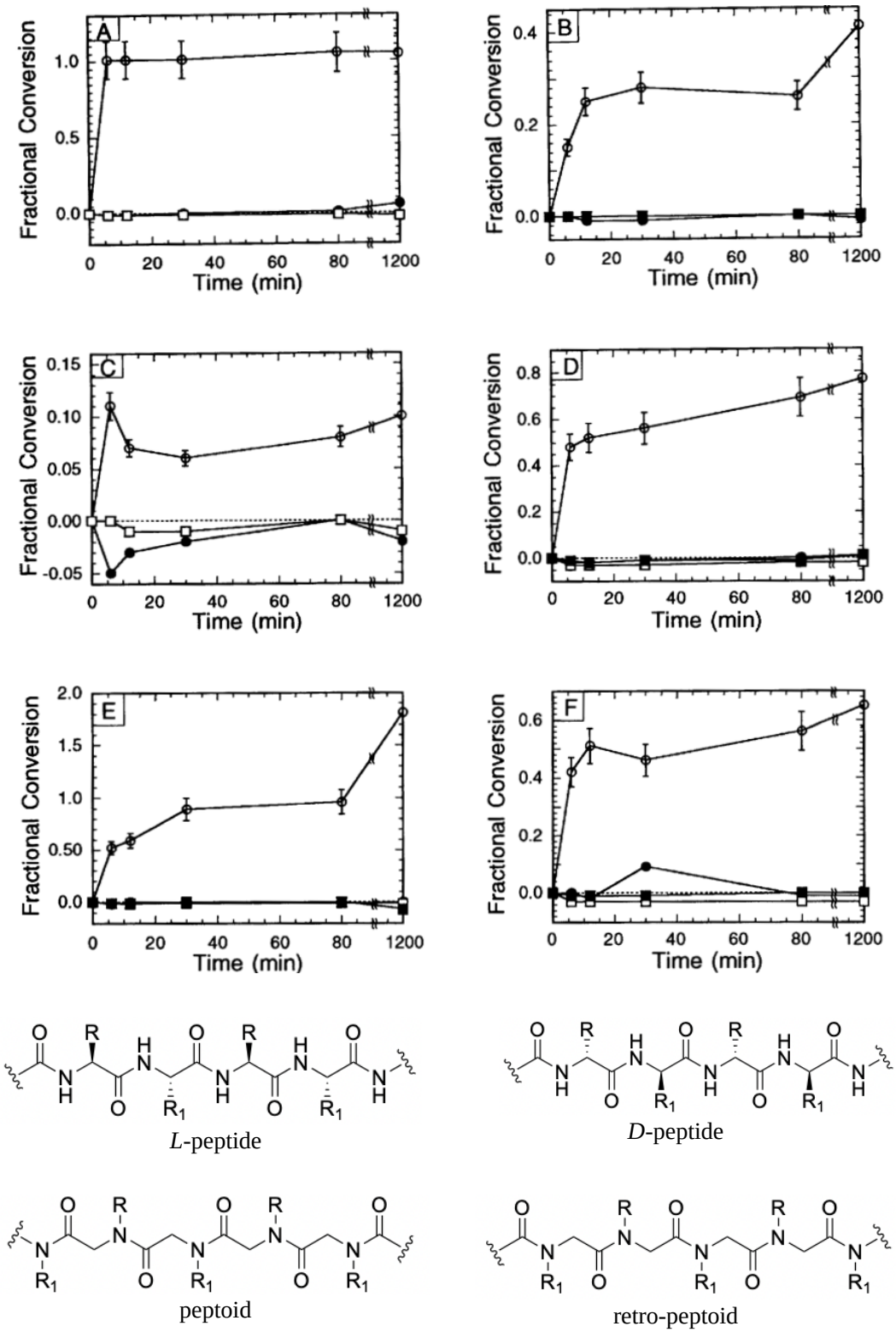

Figure 1.15. Fractional conversions (proportion of the original substrate enzymatically converted into products) of peptides and peptoids in simultaneous reactions together with oligomer structures. The enzymes chosen to carry out the study: (**A**) carboxypeptidase A, (**B**) papain, (**C**) pepsin, (**D**) trypsin, (**E**) elastase, (**F**) chemotrypsin, which are enzymes present naturally in digestive tract. The oligomers investigated: (○) L-peptide, (●) D-peptide, (□) peptoid, (■) retro-peptoid.[66] Figure adapted from Miller *et al.*, 1995.

In 1999, a group of researchers at Novartis illustrated the absorption and disposition of a trimeric peptoid (**6**) relative to its backbone counterpart peptide species (**7**) in rats. In this study, **6** and **7** of similar molecular size and structure were used, and the only difference between the species was the presence or absence of peptide bond.[67] The data collected for the two molecules are presented in **Table 1.1**.

Table 1.1. A tripeptoid **6** and its tetrapeptide **7** counterpart, together with their five physicochemical properties (Lipinski's Rule of 5. Hydrogen bond donors and acceptors are combined).[67]

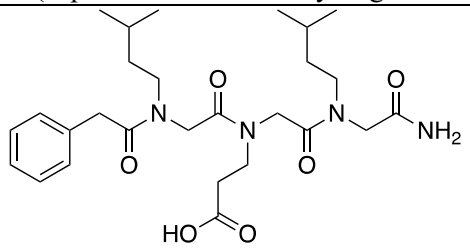

M.W. = 513.7 Da

6

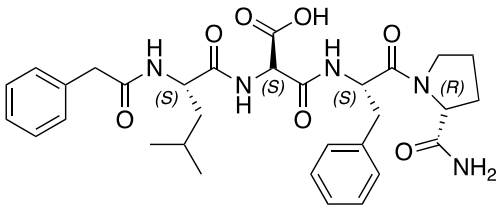

M.W. = 593.7 Da

7

	Tripeptoid 6	**Tetrapeptide 7**
H-bonding sites	13	9
Absorptive clearances (mL min^{-1} cm^{-1})	4.8 x 10^{-4}	6.7 x 10^{-4}
Octanol/water partition constant	0.39	0.30
Oral absorption (%)	3.0 – 8.0	>75

The physicochemical properties of these molecules, including their degree of H-bonding, molecular size, and comparable octanol/water partition coefficient (log *D*) determined their intestinal permeabilities which were found to be similar. However, the *in vivo* absorptions and dispositions differed between the two molecules. The absorption of the peptide was measured by the absorption of metabolised radioactive fragments. In the case of the tetramer **7**, the rapid metabolism is attributed to the presence of standard amide (peptide) bonds along the main backbone chain. Conversely, where the amide nitrogen is tertiary, as in the trimeric α-peptoid (**6**) an enhanced *in vivo* stability compared to its peptide counterpart was found. However, it is important to note that this improved proteolytic stability was accompanied by the drawback of rapid elimination from the body, caused by the increase in overall hydrophobicity.[67] In previous work by Schwochert,[68] it was found that there is a positive correlation between permeability and absorption. In this study however, it was shown that this is true for peptides but not for peptoids. In summary, while stability towards proteolysis can be

easily achieved there are still *in vivo* challenges that need to be overcome when developing optimal peptoid structures as drug candidates.[68]

1.7. Antipathogenic peptoids

1.7.1. Biological applications of peptoids

Biological interest in peptoids can in part be attributed to their ability to form a variety of different secondary structures that mimic peptides such as α-helices (PPI) and type I and type II β-turns. Single amphiphilic peptoids helices can be assembled into structures with hydrophobic cores.[5] Most interestingly, peptoids often exhibit much better cellular permeability compared to their peptide analogues. In a study carried out in the Barron group, a series of structurally different peptoids were reported to act as excellent cellular transporters.[69]

Goodson and co-workers screened over 800 peptoids, of which several trimeric peptoid isomers was identified to possess antimicrobial activity.[70] **Trimer 8** (**Figure 1.16**) was found to be the most potent of the series, and it displayed activity against resistant Gram-positive and Gram-negative bacteria. The MIC values of this peptoid trimer against the chosen multi-resistant pathogens (including *E. coli*, *S. aureus*, *S. epidermis* and *P. aeruginosa*) were in the range of 3.12-12.46 μM. The remaining five isomers of this type, which were screened, showed a reduced MIC against Gram-negative bacteria but similar MIC against Gram-positive strains.[70] The activity of the peptoids screened in this study is non-specific and therefore indicates that they target the bacterial cell membranes rather than intracellular components such as ribosomes.

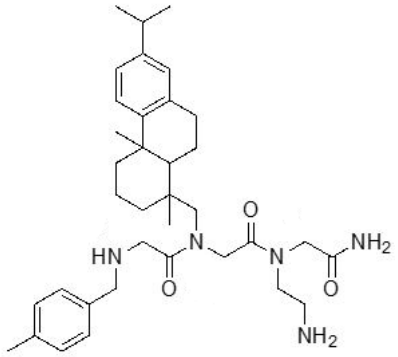

8

Figure 1.16. A trimeric peptoid (**8**) screened against resistant bacteria which showed the most potent activity.[70]

In a more recent study,[71] brominated peptoids, previously known for their antimicrobial activities and minimal cytotoxicities,[72] have demonstrated effectiveness as antiviral agents. Ten peptoids underwent screening against the herpes simplex virus (HSV-1), revealing that MXB-9 (**Pep. 4**) exhibited particularly potent antiviral activity, relative to the naturally occurring cathelicidin LL-37. Moreover, it was observed that HSV-1 susceptibility was strongly influenced by molecular structure, as the MXB-9 analogue MXB-10 (**Pep. 5**) showed no impact on viral propagation. The researchers attributed this lack of effect to an increased overall hydrophobicity. The effect of peptoid hydrophobicity was analogous to that exerted on bacteria. Indeed, the antimicrobial effects of peptoids are influenced by their hydrophobicity; once a certain threshold is surpassed, the activity diminishes.[71,72] Upon closer examination, it was discovered that **Pep. 4** exhibited a tendency to self-assemble into stable core-shell micelle, while **Pep. 5** formed long cylinders. This variation in structural configuration could explain the contrasting activities observed for these analogs.[71] (**Table 1.2)**

Table 1.2. Activity of peptoids and LL-37 against HSV-1. Structures of **Pep. 4** and **Pep. 5** are also included.[71]

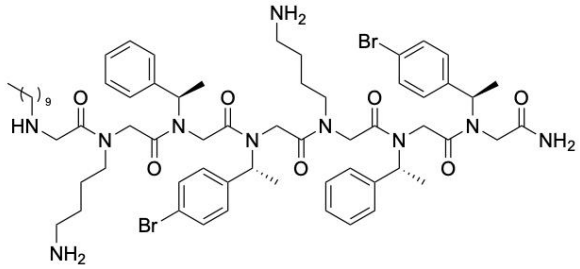

Pep. 4
H-*N*dec-(*N*Lys*N*spe*N*spe(*p*-Br))$_2$-NH_2

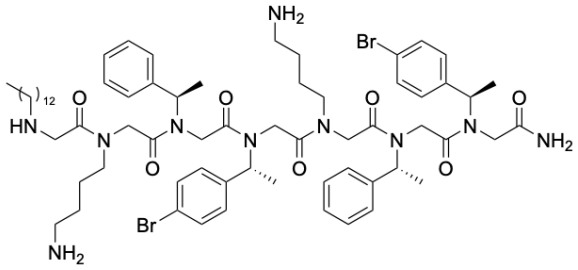

Pep. 5
H-*N*tridec-(*N*Lys*N*spe*N*spe(*p*-Br))$_2$-NH_2

No.	HSV-1 DNA levels relative to (LL-37)	ED_{50} (µM) EpiOral cells
LL-37 (control)	1.0	>100
Pep. 4	0.5	>100
Pep. 5	1.4	>100

1.7.2. Parameters controlling antimicrobial properties of peptoids

A number of research groups have focussed their efforts on structure-activity relationship (SAR) investigation of peptoids against their biological targets. The variation in chain length, hydrophobicity, overall charge, chirality, single monomer substitutions and lipidation of peptoid oligomers are the most studied structural modifications.

In a pioneering study by the Barron group,[73] a peptoid (**Pep. 6**) was designed to mimic LL-37, showing a PPI-like helix of α-peptoids. This peptoid consisted of four repeat units made of two α-chiral aromatic *N*spe (**2**) monomers and one cationic *N*Lys monomer (**Figure 1.17**). It contained a positive charge of +4 and was found to possess potent antimicrobial and tumoricidal activity. The incorporation of the *N*Lys at every third position creates a cationic face on the peptoid. Since this discovery, the majority of peptoids designed and screened against various antimicrobial targets have a similar structural composition to **Pep. 6**, consisting of >50% of aromatic residues and typically possess an overall charge of +4.[42,51,73-75]

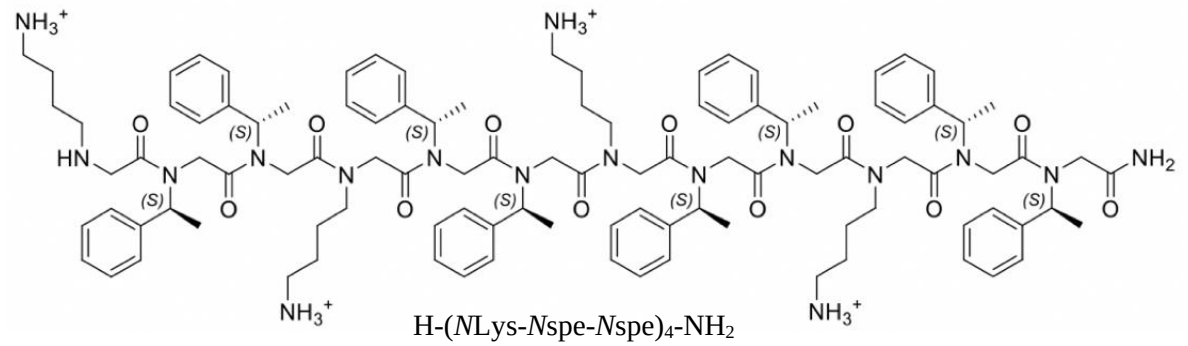

H-(*N*Lys-*N*spe-*N*spe)$_4$-NH$_2$

Pep. 6

Figure 1.17. **Pep. 6**, a 12-mer peptoid comprised of four repeating trimer motifs. The overall charge of the molecule is +4. The peptoid mimics a liner, cationic, facially amphipathic helical antibacterial peptide magainin.

An early study by Barron and co-workers, carried out in 2008 against *E. coli* and *B. subtilis* led to a number of key observations.[75] Interestingly, it was shown that α-peptoids act via the same mechanisms AMPs do and their design should be based on the knowledge obtained about AMPs. The effectiveness and integration of the peptoid enantiomer into the receptor sites are not reliant on specific interactions based on stereochemistry. Indeed, this has also been observed for AMPs, and the insertion of these oligomers into the cell membrane occurs via the interaction with the heads and tails of the liposome layer positioned in the cell membrane. In this study, all chains were based on **Pep. 6**.

The Cobb group found that increasing the overall peptoid chain length corresponded to an enhancement in its antibacterial potency. This can be attributed to the differences in hydrophobicity which increased proportionately with peptoid length. However, the drawback of the increased hydrophobicity is an increased haemolytic activity (**Pep. 6** MIC = 2 – 50 μM for the bacterial species tested: on the contrary, shorter **Pep. 8** showed no antibacterial activity). Similar effect was found for the (*N*Lys*N*Phe*N*Phe)$_n$ oligomers **Pep. 9** – **11**, whereby **Pep. 9** MIC values ranged between 2 – 50 μM, while **Pep. 11** showed no potency against the bacterial species screened against. (**Table 1.3.**) There exists an optimum hydrophobicity past which peptoids show enhanced haemolytic but not antimicrobial properties. 12-mer peptoids were found to be the optimum length oligomers and many research groups base their studies upon this length. For instance, **Pep. 9** (ED_{50} = 36 and >100 μM) offered a more optimal balance between cytotoxicity and antimicrobial activity compared to **Pep. 10** and **Pep. 11** (ED_{50} = >100 μM for both peptoids, for both HaCaT and HepG2).[75,76]

In addition to oligomer length, it was found that the peptoid chains showing the greatest antimicrobial properties had an overall cationic charge of +4.[75] Like in the case of AMPs, the overall peptoid α-helicity, detected by CD, can have a disadvantageous effect on the haemolytic activity. It follows that strongly α-helical structures confer haemolysis. These parameters are essential to be taken into consideration when designing peptoid libraries.

Table 1.3. Toxicity, antibacterial activity of peptoids of varying lengths.[76]

No.	Sequence	ED_{50} (μM)		MIC (μM)		
		HaCaT	**HepG2**	***E. coli***	***P. aeruginosa***	***S. aureus***
Pep. 6	(*N*Lys*N*spe*N*spe)$_4$	20	29	25	50	2
Pep. 7	(*N*Lys*N*spe*N*spe)$_3$	>100	>100	13	>100	2
Pep. 8	(*N*Lys*N*spe*N*spe)$_2$	>100	>100	>100	>100	>100
Pep. 9	(*N*Lys*N*Phe*N*Phe)$_4$	36	>100	13	50	3
Pep. 10	(*N*Lys*N*Phe*N*Phe)$_3$	>100	>100	50	>100	25
Pep. 11	(*N*Lys*N*Phe*N*Phe)$_2$	>100	>100	>100	>100	>100

1.7.3. Hydrophobicity of peptoids

Hydrophobicity of peptoids is generally influenced by the nature of the side chains as well as the length of the peptoids. To date, various research groups have determined

hydrophobicity of peptoids by HPLC (high pressure liquid chromatography) retention times (t_R).[71,73,77,78]

In 2017, the very first study of hydrophobicity of α-peptoids by log *D* measurements was carried out in the Cobb group.[79] Log *D* measurements represent the partitioning of a peptoid between aqueous and lipid phases.[780] The Cobb group reported that the hydrophobicity values determined by HPLC t_R differed vastly from values which were measured in this way. Two peptoids whose biological activities were compared based on their hydrophobicities are shown in **Table 1.4**.

Pep. 6 and **Pep. 12** showed similar HPLC t_R but their log *D* measurements were strikingly different. **Pep. 12** showed a significant movement to the hydrophobic phase (octanol) resulting in a negative log *D* value. Interestingly, it was found that the helical structures adopted by these peptoids were the same in both octanol and PBS (aqueous) phases. Therefore, the vastly different log *D* values could be caused by different folded hydrophobicities, and the shorter cationic moieties present in peptoid **Pep. 12** are shielded to a greater extent from the solvent.

Table 1.4.. A summary of **Pep. 6** and **Pep. 12,** their hydrophobicities as described by the HPLC t_R and log *D* values. The biological activities against Leishmaniasis parasites and bacterial targets are also shown.[76]

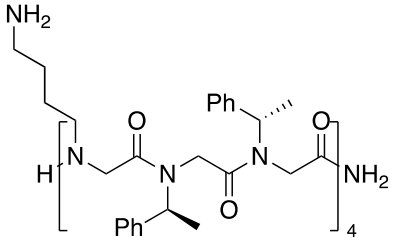

(*N*Lys*N*spe*N*spe)$_4$
Pep. 6

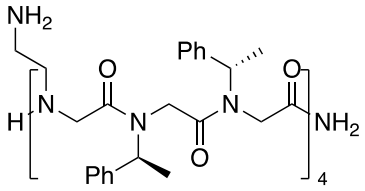

(*N*ae*N*spe*N*spe)$_4$
Pep. 12

No.	MW (g/mol)	**ED$_{50}$ (μM)**		**MIC (μM)**		**HPLC t_R (min)**	**log *D***
		L. mex prom.	*L. mex ama.*	*E. coli*	*S. aureus*		
Pep. 6	1819.32	8	>100	25	2	14.9	1.21
Pep. 12	1707.11	7	17	>100	2	16.7	-1.85

Given the HPLC t_R for **Pep. 6** and **Pep. 12**, and considering their very similar structures it would be appropriate to speculate that their biological activities would be very similar if not the same. However, **Pep. 6** exhibits significantly higher activity against *L. mexicana* amastigotes, with an effective median dose (ED_{50}) of 17 μM, compared to 100 μM for **Pep. 12**. Similarly, **Pep. 6** also shows high activity against *E. coli*, with an ED_{50} of 25 μM versus 100 μM for **Pep. 12**.[77] This difference can possibly be attributed to the differing log *D* values. It also suggests that the biological potential of a peptoid depends on its ability to fold in solution, and this is best portrayed by the biphasic environment in which log *D* is measured.

1.8. Project objectives

Peptoids are oligomers based on a poly-*N*-substituted glycine backbone. It has been well evidenced that this modification results in their chemical stability and makes peptoids highly resistant to proteolytic degradation, when compared to their peptide counterparts.[66] However, unlike peptides, peptoids lack the ability to form hydrogen bonds, leading to numerous research groups focussing on the development of methods to control the formation of peptoid secondary structures.

Moreover, many antimicrobial peptoids which have been developed, to date, contain over 50% of hydrophobic chiral building blocks, and are designed so that they mimic the α-helical magainin-2. It was aimed to utilise interactions induced by alkyl fluorinated peptoid monomers in order to explore their effect on antimicrobial efficacies of peptoids, but also aim to decrease peptoid cytotoxicity and increase selectivity against antimicrobial targets.[38,49]

A preliminary study within the Cobb group found that HPLC t_R is not a good measure of peptoid hydrophobicity in biological environments.[79] Log *D* measurements were found to offer a more useful tool allowing the analysis of peptoid activities. Designing new peptoid sequences that allow a wider range of log *D* values to be accessed offers an approach to achieve more rational design elements into development of future antimicrobial peptoid libraries. This is planned to be achieved by establishing connections between peptoid structure (determined by CD spectroscopy), physicochemical attributes, and antimicrobial efficacy.

Although the stability profile of peptoids is better than that of peptides their physicochemical properties still need to be improved in order to compete with small molecules as pharmaceuticals. One potential concern with peptoid design is their limited ability to be absorbed orally and their less-than-ideal elimination from the body, which is primarily attributed to their high hydrophobicity.[67] In order to tackle the hydrophobicity issues in peptoids, it was aimed to develop new polar submonomers, which are to be introduced into peptoid oligomers. The nonamer hydrophobicities will be determined by log *D* measurements and HPLC t_R values and will be comparted to their apolar counterpart. Moreover, the biological properties of these peptoids will also be evaluated.

Additionally, it was sought to explore novel macrocyclic structures, with a subsequent plan to subject them to antimicrobial screening and hydrophobicity analysis.

1.9. References for Chapter 1

[1] O'Neil, J., 2016, Tackling Drug-Resistance Infections Globally: Final Report and Recommendations. Available online: https//https://amr-review.org/sites/default/files/160518_Final%20paper_with%20cover.pdf (accessed on 30/01/2024)
[2] Groves, M. L., 1960, *J. Am. Chem. Soc*., 82, 3345-3350.
[3] Montreuil, J., Tonnelat, J., Mullet, S., 1960, *Biochim. Biophys. Acta*, **45**, 413-421.
[4] Steiner, H., Hultmark, D., Engström, Å., Bennich, H., Boman, H. G., 1981, *Nature*, **292**, 246-248.
[5] Zasloff, M., 1987, *Proc. Natl. Acad. Sci. USA*, **84**, 5449-5453.
[6] Anghel, R., Jitaru, D., Bădescu, L., Bădescu, M., Ciocoiu, M., 2013, *BioMed Res. Int.*, 2013.
[7] Lehmann, J., Retz, M., Sidhu, S. S., Suttmann, H., Sell, M., Paulsen, F., et al., 2006, *Eur. Urol.*, **50**, 141-147.
[8] Zanetti, M., Litteri, L., Gennaro, R., Horstmann, H., Romeo, D., 1990, *J. Cell Biol*., **111**, 1363-1371.
[9] Gallo, R. L., Ono, M., Povsic, T., Page, C., Eriksson, E., Klagsbrun, M., et al., 1994, *Proc. Natl. Acad. Sci. USA*, **91**, 11035-11039.
[10] López-García, B., Lee, P. H., Yamasaki, K., Gallo, R. L., 2005, *J. Invest. Dermatol.*, **125**, 108-115.
[11] Tripathi, S., Tecle, T., Verma, A., Crouch, E., White, M., Hartshorn, K. L., 2013, *J. Gen. Virol.*, **94**, 40.
[12] Giacometti, A., Cirioni, O., Del Prete, M. S., Skerlavaj, B., Circo, R., Zanetti, M., et al., 200, *J. Antimicrob. Chemother.*, **51**, 843-847.
[13] Haines, L. R., Thomas, J. M., Jackson, A. M., Eyford, B. A., Razavi, M., Watson, C. N., et al., 2009, *PLoS Negl Trop Dis*, **3**, e373.
[14] Oren, Z., Shai, Y., 1998, *Pept. Sci.*, **47**, 451-463.
[15] Shai, Y., 1999, Biochim. Biophys. *Acta - Biomembranes*, **1462**, 55-70.
[16] Ehrenstein, G., Lecar, H., 1977, Q. Rev. *Biophys*., **10**, 1-34.
[17] Pouny, Y., Rapaport, D., Mor, A., Nicolas, P., Shai, Y., 1992, *Biochemistry*, **31**, 12416-12423.
[18] Ludtke, S. J., He, K., Heller, W. T., Harroun, T. A., Yang, L., Huang, H. W., 1996, *Biochemistry*, **35**, 13723-13728.
[19] Ho, Y. H., Shah, P., Chen, Y. W., Chen, C. S., 2016, *Mol. Cell. Proteomics*, **15**, 1837-1847.
[20] Le, C. F., Fang, C. M., Sekaran, S. D., 2017, *Antimicrob. Agents Chemother*., **61**.
[21] Lei, J., Sun, L., Huang, S., Zhu, C., Li, P., He, J., et al., 2019, *Am. J. Transl. Res*., **11**, 3919.
[22] Harris, F., Dennison, S. R., Phoenix, D. A., 2009, *Curr. Protein Pept. Sci*., **10**, 585-606.
[23] Becucci, L., Valensin, D., Innocenti, M., Guidelli, R., 2014, *Soft Matter*, **10**, 616-626.
[24] Nguyen, L. T., Haney, E. F., Vogel, H. J., 2011, *Trends Biotechnol*., **29**, 464-472.
[25] Tang, M., Hong, M., 2009, Mol. *Biosyst.*, **5**, 317-322.
[26] Chan, D. I., Prenner, E. J., Vogel, H. J., 2006, *Biochim. Biophys. Acta - Biomembr*., **1758**, 1184-1202.
[27] Huang, W., Seo, J., Lin, J. S., Barron, A. E., 2012, *Mol. Biosyst*., **8**, 2626-2628.
[28] Hollmann, A., Martinez, M., Maturana, P., Semorile, L. C., Maffia, P. C., 2018, *Front. Chem*., **6**, 204.
[29] Park, C. B., Yi, K. S., Matsuzaki, K., Kim, M. S., Kim, S. C., 2000, *Proc. Natl. Acad. Sci. USA*, **97**, 8245-8250.
[30] Buer, B. C., Marsh, E. N. G., 2012, *Protein Sci*., **21**, 453-462.
[31] Eckert, R., 2011, *Future Microbiol*., **6**, 635-651.
[32] Tossi, A., Sandri, L., Giangaspero, A., 2000, *Pept. Sci*., **55**, 4-30.
[33] Matsuzaki, K., 2009, *Biochim. Biophys. Acta - Biomembr*., **1788**, 1687-1692.

[34] Pasupuleti, M., Schmidtchen, A., Chalupka, A., Ringstad, L., Malmsten, M., 2009, *PLoS One*, **4**, e5285.
[35] Vlieghe, P., Lisowski, V., Martinez, J., Khrestchatisky, M., 2010, *Drug Discov. Today*, **15**, 40-56.
[36] Zuckermann, R. N., 2011, *Pept. Sci*., **96**, 545-555.
[37] Gorske, B. C., Bastian, B. L., Geske, G. D., Blackwell, H. E., 2007, *J. Am. Chem. Soc*., **129**, 8928-8929.
[38] Gimenez, D., Zhou, G., Hurley, M. F., Aguilar, J. A., Voelz, V. A., Cobb, S. L., 2019, *J. Am. Chem. Soc*., **141**, 3430-3434.
[39] Gorske, B. C., Blackwell, H. E., 2006, *J. Am. Chem. Soc.*, **128**, 14378-14387.
[40] Caumes, C., Roy, O., Faure, S., Taillefumier, C., 2012, *J. Am. Chem. Soc*., **134**, 9553-9556.
[41] Roy, O., Caumes, C., Esvan, Y., Didierjean, C., Faure, S., Taillefumier, C., 2013, *Org. Lett.*, **15**, 2246-2249.
[42] Fowler, S. A., Luechapanichkul, R., Blackwell, H. E., 2009, *J. Org. Chem*., **74**, 1440-1449.
[43] Simon, R. J., Kania, R. S., Zuckermann, R. N., Huebner, V. D., Jewell, D. A., Banville, S., et al., 1992, *Proc. Natl. Acad. Sci. USA*, **89**, 9367-9371.
[44] Massolo, E., Pirola, M., Benaglia, M., 2020, *Eur. J. Org. Chem*., **2020**, 4641-4651.
[45] Zuckermann, R. N., Kerr, J. M., Kent, S. B., Moos, W. H., 1992, *J. Am. Chem. Soc*., **114**, 10646-10647.
[46] Meyer, J. P., Davis, P., Lee, K. B., Porreca, F., Yamamura, H. I., Hruby, V. J., 1995, *J. Med. Chem*., **38**, 3462-3468.
[47] Horn, T., Lee, B. C., Dill, K. A., Zuckermann, R. N., 2004, *Bioconjug. Chem*., **15**, 428-435.
[48] Stringer, J. R., Crapster, J. A., Guzei, I. A., Blackwell, H. E., 2011, *J. Am. Chem. Soc*., **133**, 15559-15567.
[49] Wijaya, A. W., Nguyen, A. I., Roe, L. T., Butterfoss, G. L., Spencer, R. K., Li, N. K., et al., 2019, *J. Am. Chem. Soc*., **141**, 19436-19447.
[50] Stringer, J. R., Crapster, J. A., Guzei, I. A., Blackwell, H. E., 2010, *J. Org. Chem*., **75**, 6068-6078.
[51] Wu, C. W., Sanborn, T. J., Zuckermann, R. N., Barron, A. E., 2001, *J. Am. Chem. Soc*., **123**, 2958-2963.
[52] Webster, A. M., Cobb, S. L., 2018, *Chem.–Eur. J*., **24**, 7560-7573.
[53] Fowler, S. A., Blackwell, H. E., 2009, *Org. Biomol. Chem*., **7**, 1508-1524.
[54] Sui, Q., Borchardt, D., Rabenstein, D. L., 2007, *J. Am. Chem. Soc*., **129**, 12042-12048.
[55] Huang, K., Wu, C. W., Sanborn, T. J., Patch, J. A., Kirshenbaum, K., Zuckermann, R. N., Barron, A. E., Radhakrishnan, I., 2006, *J. Am. Chem. Soc*., **128**, 1733-1738.
[56] Holub, J. M., Jang, H., Kirshenbaum, K., 2007, *Org. Lett*., **9**, 3275-3278.
[57] Pokorski, J. K., Miller Jenkins, L. M., Feng, H., Durell, S. R., Bai, Y., Appella, D. H., 2007, *Org. Lett.*, **9**, 2381-2383.
[58] Corrêa, D. H., Ramos, C. H., 2009, *Afr. J. Biochem. Res*., **5**, 164-173.
[59] Wu, C. W., Kirshenbaum, K., Sanborn, T. J., Patch, J. A., Huang, K., Dill, K. A., Barron, A. E., 2003, *J. Am. Chem. Soc*., **125**, 13525-13530.
[60] Patch, J. A., Kirshenbaum, K., Seurynck, S. L., Zuckermann, R. N., Barron, A. E., 2004, in Pseudo-Peptides in Drug Discovery, Nielsen, P. E., Ed., Wiley-VCH: Weinheim, pp. 1-31.
[61] Butterfoss, G. L., Yoo, B., Jaworski, J. N., Chorny, I., Dill, K. A., Zuckermann, R. N., Voelz, V. A., 2012, *Proc. Natl. Acad. Sci. USA*, **109**, 14320-14325.
[62] Sternberg, U., Birtalan, E., Jakovkin, I., Luy, B., Schepers, U., Bräse, S., Muhle-Goll, C., 2013, *Org. Biomol. Chem*., **4**, 640-647.

[63] Shin, S. B. Y., Yoo, B., Todaro, L. J., Kirshenbaum, K., 2007, *J. Am. Chem. Soc*., **129**(11), 3218-3225.
[64] Di, L., 2015, AAPS J., **17**, 134-143.
[65] Qvit, N., Rubin, S. J., Urban, T. J., Mochly-Rosen, D., Gross, E. R., 2017, *Drug Discov*. *Today*, **22**, 454-462.
[66] Miller, S. M., Simon, R. J., Ng, S., Zuckermann, R. N., Kerr, J. M., Moos, W. H., 1995, *Drug Dev. Res.*, **35**, 20-32.
[67] Wang, Y., Lin, H., Tullman, R., Jewell Jr, C. F., Weetall, M. L., Tse, F. L., 1999, *Biopharm*. Drug Dispos., **20**, 69-75.
[68] Schwochert, J., Turner, R., Thang, M., Berkeley, R. F., Ponkey, A. R., Rodriguez, K. M., Kalgutkar, A. S., 2015, *Org. Lett.*, **17**, 2928-2931.
[69] Huang, W., Seo, J., Lin, J. S., Barron, A. E., 2012, *Mol. BioSyst.*, **8**, 2626-2628.
[70] Goodson, B., Ehrhardt, A., Ng, S., Nuss, J., Johnson, K., Giedlin, M., Giacona, M. B., 1999, *Antimicrob. Agents Chemother*., **43**, 1429-1434.
[71] Diamond, G., Molchanova, N., Herlan, C., Fortkort, J. A., Lin, J. S., Figgins, E., Bopp, N., Ryan, L. K., Chung, D., Adcock, R. S., Sherman, M., 2021, *Pharmaceuticals*, **14**(4), 304.
[72] Molchanova, N., Nielsen, J., Sørensen, K., Prabhala, B., Hansen, P., Lund, R., Barron, A., Jenssen, H., 2020, *Sci. Rep.*, 10, 14805.
[73] Patch, J. A., Barron, A. E., 2003, *J. Am. Chem. Soc*., **125**, 12092-12093.
[74] Stringer, J. R., Crapster, J. A., Guzei, I. A., Blackwell, H. E., 2011, *J. Am. Chem. Soc*., **133**, 15559-15567.
[75] Chongsiriwatana, N. P., Patch, J. A., Czyzewski, A. M., Dohm, M. T., Ivankin, A., Gidalevitz, D., Barron, A. E., 2008, *Proc. Natl. Acad. Sci. USA*, **105**, 2794-2799.
[76] Bolt, H. L., Eggimann, G. A., Jahoda, C. A., Zuckermann, R. N., Sharples, G. J., Cobb, S. L., 2017, *MedChemComm*, **8**, 886-896.
[77] Mojsoska, B., Zuckermann, R. N., Jenssen, H., 2015, *Antimicrob. Agents Chemother*., **59**, 4112-4120.
[78] Lee, J., Kang, D., Choi, J., Huang, W., Wadman, M., Barron, A. E., Seo, J., 2018, *Bioorg. Med. Chem. Lett.*, **28**, 170-173.
[79] Bolt, H. L., Williams, C. E. J., Brooks, R. V., Zuckermann, R. N., Cobb, S. L., Bromley, E. H. C., 2017, *Peptide Sci*., **108**, e23014.
[80] Kah, M., Brown, C. D., 2008, *Chemosphere*, **72**(10), 1401-1408.

Chapter 2: Antimicrobial Peptoids

2.1. Fluorine in biological and medicinal chemistry

2.1.1. Use of fluorine in medicinal chemistry

Fried's pioneering work on 9-fluorohydrocortisone acetate[1] (**9**) (**Figure 2.1**) sparked an interest into the introduction of fluorine atoms into biologically active compounds by showing that this could be used to impart favorable effects on their properties.[2] Since this seminal work fluorine has been increasingly used to modulate the physicochemical properties of molecules to enhance their biological properties or make them more biostable and hence orally available.[1]

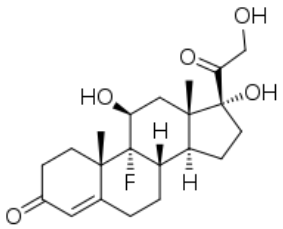

9

Figure 2.1. Structure of 9α-fluorohydrocortisone acetate (**9**), a corticosteroid.[1]

Fluorine has a number of properties which enable it to modulate the physicochemical properties of molecules:

- The relative size of a fluorine atom is comparable to that of hydrogen, although slightly larger (relative van der Walls radii of 1.47 Å vs 1.20 Å). Fluorine is a known hydrogen mimic[3] and it exerts minimum steric effects when substituting a hydrogen;
- Fluorine is a highly lipophilic element and therefore it enhances the binding affinity of a compound to its target active site;
- Fluorine is the most electronegative element with a value of 3.98 on the Pauling scale.[4] Due to the C-F bond being highly polar and of low polarisability, it is known to change the properties of functional groups within proximity to the fluorinated sites by affecting the pKa, dipole moment and the overall reactivity of the neighbouring groups (**Section 2.1.2**).[5,6]

- The strength of the single covalent C-F bond (485 kJ mol^{-1}) is the highest known and is more stable than the C-H bond (439 kJ mol^{-1}). The metabolic stability is therefore greatly enhanced when incorporating this element into a molecule.[7]

The effect of fluorine on synthetic systems is routinely explored in the context of drug discovery. For example, to enable the regiocontrolled synthesis of target compounds,[8,9] or to enhance the in *vivo* stability of a compound.[10] Fluorine's electron withdrawing property mean it can be used to control the regiochemistry of aromatic substitution (SEAr) reactions, favouring the *ortho/para* substitution which is stabilised by conjugation. (**Scheme 2.1**)

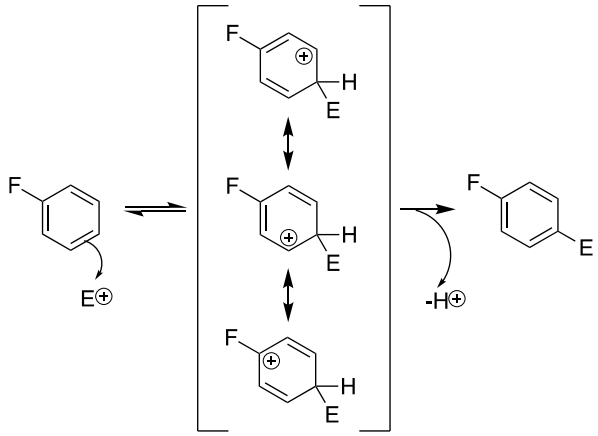

Scheme 2.1. A scheme showing the *ortho/para*-directing property of fluorine through strong resonance effects. Delocalised electron cloud in the aromatic ring attacks the highly electrophilic group, E^+. The formation of cyclohexadienyl cation follows; this species is also known as a Wheland intermediate, and the conjugation stabilises the position of attack. A proton, H^+, is the leaving group.

2.1.2. Fluorine's effect on hydrophobicity and lipophilicity

Lipophilicity (log *P*) denotes a compound's ability to partition between two immiscible solvents, most commonly *n*-octanol and water.[11] Log *P* is routinely utilised in drug discovery as a measure of the hydrophobic properties of a compound and is one component of the Lipinski's Rule of 5. Determining log *P* can also be used to predict a compounds bioavailability. Compounds which are hydrophobic (positive log *P*) tend to target cell membranes more readily, whilst hydrophilic molecules localise more readily in aqueous environments such as plasma.

Fluorination has a very profound effect on compound lipophilicity. Due to its relatively small size, substitution of hydrogen with fluorine atoms exerts relatively insignificant steric

impact on a molecule. Nevertheless, due to the C–F bond polarisation the introduction of fluorine into aromatic compounds increases log *P* values, indicating greater lipophilicity. In terms of fluorination patterns, mono-, di-, and trifluorination exert varying effects on lipophilicity. Among these, mono- and trifluorination have the most pronounced impact because these functionalities exhibit stronger dipole moments.

The studies carried out by Muller/Carreira and Linclau (**Table 2.1**) documented that the relative increase or decrease in lipophilicity is dependent not only on the degree of aliphatic fluorination but also on the position of the substitution.[12,13] Both groups reported that the inclusion of a trifluoromethyl (CF_3) in place of a methyl (CH_3) led to a moderately decreased log *P* value in both the 3'-substituted indole and alkanol. Furthermore, the decreased fluorination level on the terminal aliphatic methyl resulted in a decreased lipophilicity. The introduction of geminal difluorinated moieties in place of the terminal trifluoromethyls rendered the molecules less lipophilic (log *P* Δ -0.4 for **12**, **Table 2.1**, **Entry 3**; and Δ -0.85 for **21**, **Table 2.1**, **Entry 12**). Meanwhile, the monofluorinated congeners **13** (log *P* Δ -0.5, **Entry 4**) and **23** (log *P* Δ -1., **Entry 14**) marked the greatest attenuation in log *P* values compared to **10** (log *P* 3.3, **Table 2.1**, **Entry 1**) and **16** (log *P* 1.51, **Table 2.1**, **Entry 7**), respectively. The increasing lipophilicity with an increased degree of fluorination can be explained by the degree of polarisation of the C–F bond, as the increased dipole moment is counterbalanced by an increased hydrophobic surface of the molecule. Therefore, amplified molecular polarity in these instances will not result in reduced hydrophobicity. This is further evidenced by **15** (**Table 2.1**, **Entry 6**), whereby the inclusion of five C–F bonds increases the log *P* value (Δ +0.21) compared to the non-fluorinated parent molecule **16** (**Table 2.1**, **Entry 7**).

Notably, altering the position of the fluorine-rich moieties relative to the indole/alcohol groups leads to opposite effects for each molecule. In the case of the indoles studied by Muller,[13] it was noted that when $–CF_2–$ is in closer vicinity to the heteroaromatic ring (**13**, **Table 2.1**, **Entry 4**) it attenuates the log *P* value by 0.1 compared to **12** (**Table 2.1**, **Entry 3**). On the other hand, the inclusion of terminal geminal difluoromethyl leads to a greater reduction in lipophilicity compared to its alkanol counterparts where the fluorinated group is moved closer to the OH moiety (log *P* Δ -0.96, **Table 2.1**, **Entry 12** vs. log *P* Δ -0.80, **Table 2.1**, **Entry 10**). A shorted distance between the $–CF_2–$ group and the hydroxyl reduces the hydrophobicity of pentanol. Finally, the incorporation of an additional monofluorinated moiety has a profound effect on the lipophilicity of the pentanols. The inclusion of a terminal C–F to **20** (**Table 2.1**, **Entry 11**) attenuated log *P* by 0.11 (**21, Table 2.1**, **Entry 12**), and by

incorporating a vicinal C–F into **22** (**Table 2.1**, **Entry 13**) the log *P* value of **23** (**Table 2.1**, **Entry 14**) was reduced to +0.11 (vs +0.52 for **23**).

Table 2.1. A selection of aliphatic fluorination and lipophilicity values which involved various patterns, in relation to a non-fluorinated parent compound (**10**). Data extracted from Muller and Linclau. NOTE: Log *P* = log([octanol]/[water]).[11,12]

Entry	No.	Compound	Log *P*	Entry	No.	Compound	Log *P*
1	**10**	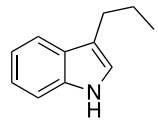	+3.3	**6**	**15**	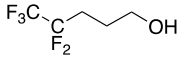	Δ +0.21
				7	**16**	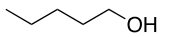	+1.51
2	**11**	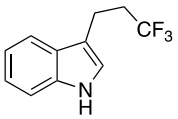	Δ -0.2	**8**	**17**	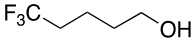	Δ -0.29
				9	**18**	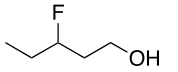	Δ -0.76
3	**12**	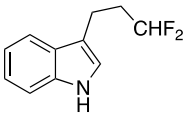	Δ -0.4	**10**	**19**	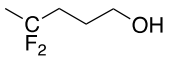	Δ -0.80
4	**13**	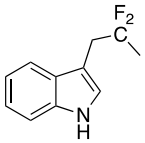	Δ -0.5	**11**	**20**	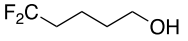	Δ -0.85
				12	**21**	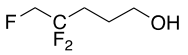	Δ -0.96
5	**14**	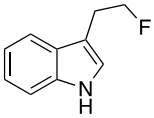	Δ -0.5	**13**	**22**	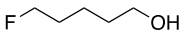	Δ -0.99
				14	**23**	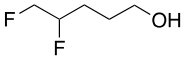	Δ -1.40

Log *P* values account for lipophilicity of neutral molecules, but since most molecules possess ionisable functionalities (such as $–NH_2$), it is necessary to consider their ionic states. This becomes particularly important when considering pH environments in the body. For instance, blood is maintained at the physiological pH 7.4, whilst the pH within the GI tract varies greatly (pH 1 – 8). Log *D* is a pH dependent coefficient of water-octanol distribution is therefore more applicable when it comes to determination of compound's drug-likeness. Optimising the log *D* value of a compound is essential for enhancing the bioavailability of a drug candidate.[11]

2.1.3. Fluorine *Gauche* effect

Due to its small size and highly electronegative properties fluorine containing molecules often exhibit a '*Gauche* effect' whereby the *gauche* conformation is the most stable (**Figure 2.2**). Electrostatic and steric interactions make this conformation counterintuitive as it would be expected that the molecule would adopt an *anti*-conformation due to repulsive interactions, as is the case with other halogens. The effect is driven by hyperconjugation between σ_{CH} (HOMO) and low-lying energy σ^*_{CF} (LUMO) orbitals. The electronegativity of fluorine makes the σ^*_{CF} orbital a better electron acceptor than σ^*_{CH} orbital, while the σ_{CH} orbital is a better electron donor than the σ_{CF} orbital. Therefore the $\sigma_{CH} \rightarrow \sigma^*_{CF}$ electron delocalisation is more stabilising than $\sigma_{CF} \rightarrow \sigma^*_{CH}$. This was demonstrated by O'Hagan's work on 3-fluoro-GABA **24** (**Figure 2.2**), which adopted a low-energy structure showing *gauche* interaction, where the C-F bonds form 60° angles relative to each other, rather than 180° as in the anti-conformation.[14,15]

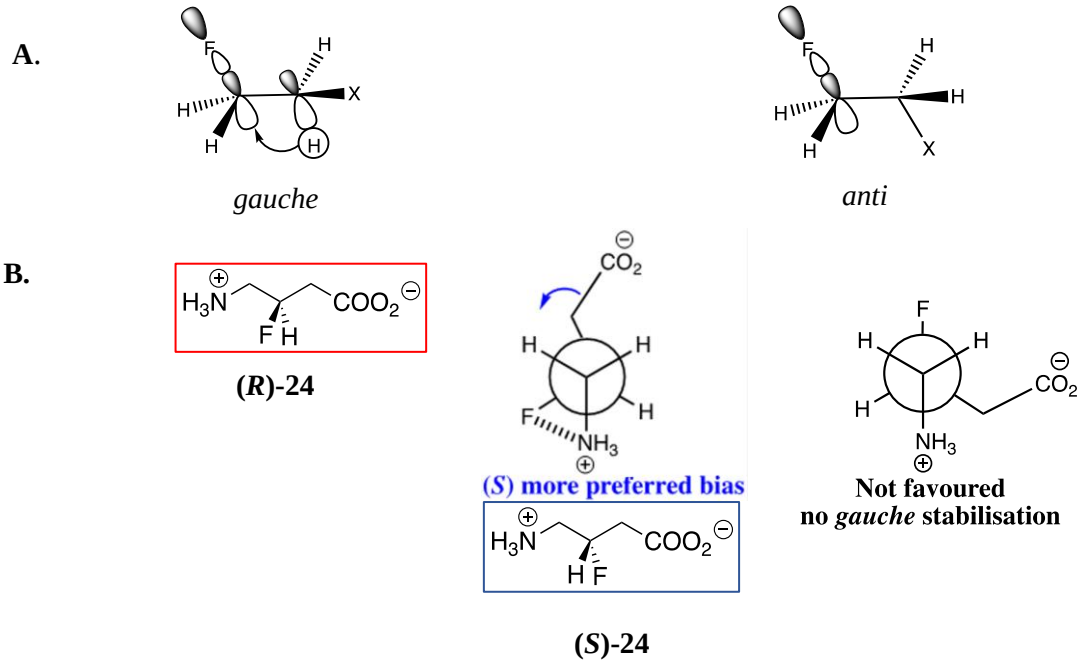

Figure 2.2. A. Hyperconjugation models explaining the *gauche* effect. **B.** Newmann projection showing the topological structures of staggered conformations around C3 and C4 in 3-fluoro-GABA, and the (*R*)- and (*S*)-enantiomers. The *gauche* conformations are low energy, whilst the *anti*-conformation is high energy.[14]

2.1.4. Fluorinated amino acids and peptide secondary structure

The incorporation of novel fluorinated amino acids into peptides and proteins is a unique way to modulate not only their physicochemical properties but also their secondary structure.

Fluorinated amino acids are more hydrophobic than their natural counterparts and given that peptide and protein folding is largely governed by hydrophobic interactions it is not surprising that the incorporation of such amino acids can lead to the stabilisation of protein structures. To date, most studies have focussed on the incorporation of fluorinated leucine (hFLeu **25** and tFLeu **26**), valine (tFVal, **27**), isoleucine (tFIle, **28**). However, there exists work which also includes amino acids such as phenylalanine (pFPhe **29**), as well as glycine (tFeG) (**30**).[2,15,16] (**Figure 2.3**)

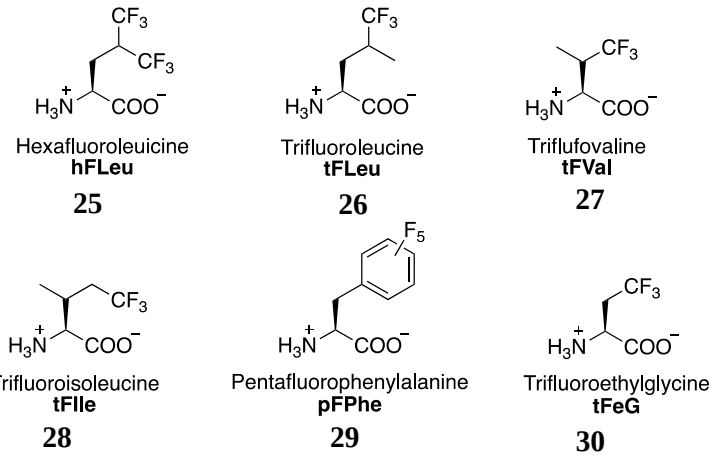

Figure 2.3. Some of the perfluorinated amino acids which have been incorporated into peptide chains. tFLeu (**25**) and tFVal (**27**) are chiral building blocks.

Bilgiçer and co-workers investigated the effects of substitution of amino acids for their fluorinated counterparts on the coil-coiled domain of a transcription factor GCN4. This study pioneered the use of fluorine's unique properties in design and synthesis of self-segregating proteins with a hydrophobic centre. The "synthetic" fluorinated GCN4 retained the function of the native protein but showed an increased stability.[17,18] The modelled crystal structure of the protein is shown in **Figure 2.4**.

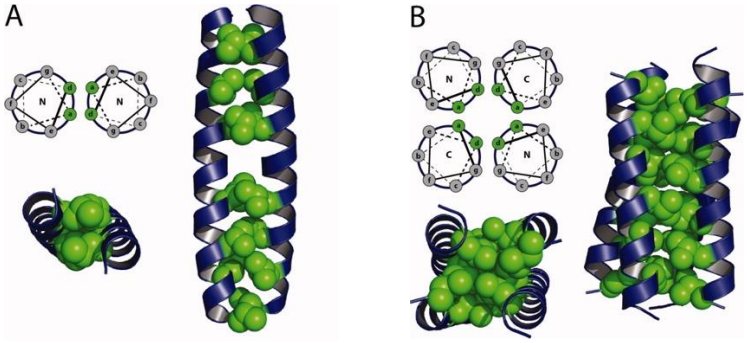

Figure 2.4. Coiled-coil domains used in the work performed by Bilgiçer *et al*. The wheel diagrams showing a heptad repeat **A** and **B**: positions a and d, shown in green, have been replaced with fluorinated counterparts. **A**. The demonstration of hydrophobic packing in the dimeric parallel coiled-coil GCN4 using a model crystal structure showing positions which have been modified with fluorous residues. **B.** The demonstration of hydrophobic packing in the tetrameric antiparallel coiled coil α4. A model crystal structure representing positions which have been modified with fluorous residues.[19] (Figure adapted from Buer *et al*., 2012)

Perfluorinated compounds are extremely hydrophobic and lipophilic which results in their unusual phase separating properties. This phenomenon has been dubbed the 'fluorous effect'. This property is utilised in the extraction of perfluorinated compounds from reaction mixtures using fluorinated solvents.[20,21]

The unusual properties of fluorine make perfluorinated compounds exhibit the fluorous effect and this gave rise to the concept of self-assembling fluorinated proteins. The effect may be responsible for specific protein-protein interactions between the fluorinated side chains which are orthogonal to the protein-protein interactions between native amino acid side chains. Kumar reported that in the presence of native chains the fluorinated peptides self-associated to form parallel coiled coils both in solution and membrane environments. [17,22,23] Mixing of the native peptide chains with *de novo* fluorinated peptides was not favoured (<3%).[19] Interestingly, it had been shown that the fluorine rich peptides formed tetramers rather than dimers like in the case of native coiled coils. The slightly bulkier fluorinated counterpart of Leu might not be compatible with this structure.[24]

In 2008, Gottler and co-workers performed a set of ^{19}F NMR titrations on Leu-rich and tFLeu-rich tetramers.[25,26] It was found that in the presence of α_4H the α_4F_6 ^{19}F NMR signals experienced a downfield shift. This was attributed to the increasing concentration of mixed tetramers (**Figure 2.5**). This provided evidence that there must have been another force which governed the tetrameric stability, and it was stronger than the fluorous effect. A more recent study, showed that this was indeed the case, and the steric hindrance exhibited by all-fluorine tetramers was optimised upon introduction of non-fluorinated chains.[27] Although fluorine does

aid protein stability and self-assembling properties of fluorine-rich proteins, the overall core packing and accommodation of side chains were also shown to be important.

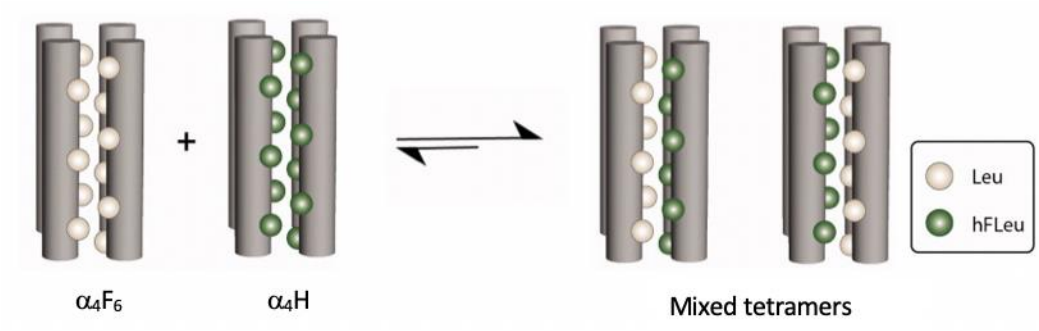

Figure 2.5. An illustration of the displaced equilibrium between α_4H and α_4F_6, and the resulting mixed tetramers.[15] (Figure adapted from Buer *et al*., 2012).

Cheng *et al.* reported that in the case of single α-helix strands the effect on the secondary structure stability is the opposite. While the general trend of increasing structure stability correlates with an increasing fluorine content within a small globular structure, incorporating fluorinated amino acids into single helices leads to a decreased helix propensity. In the study, tFeG (**30**), hFLeu (**26**) and pFPhe (**29**) residues were investigated and an eight-fold decrease in α-helical structure was found by circular dichroism (CD).[28]

2.1.5. Use of fluorine to modulate properties of AMPs

The most common mode of action of antimicrobial peptides (AMPs) involves the targeting and disruption of bacterial cell membranes often without exerting any intracellular activities, such as interruption of protein-protein interactions involved in protein chaperoning or specific interruption of DNA replication. Fluorine can be used in the modulation of physicochemical properties of AMPs by affecting their lipophilicity.[29]

AMPs are susceptible to *in vivo* proteolysis by endogenous and bacterial proteases and overcoming this issue by increasing the dosage of a peptide drug being administered is not an option as it can lead to haemolysis. This limitation is attributed to non-specific hydrophobic interactions between a peptide and the cell membrane. Such interactions can be overcome by utilising fluorinated amino acids without compromising biological activity.[1] The Marsh group was one of the first groups to investigate the effect of fluorinated amino acids on peptide stability to degradation.[25] The group worked on replacing Leu and Ile residues in melittin (MSI-

78), with tFLeu (**26**). They discovered that the *de novo* peptide, fluorogainin-1, showed an increased interaction with the bacterial cell membranes. It was also found that the fluorine-rich peptide had a greater partitioning into liposomes and an increased stability to proteolysis.

The slight perturbation of secondary structure of MSI-78 (**Figure 2.6**) also influenced the *in vitro* antimicrobial activity and showed lower MIC values compared to MSI-78 when screened against *S. aureus* and *K. pneumoniae*: both 16 μg mL^{-1}, which is four- and 16-fold lower, respectively. While MSI-78 disrupts the bacterial cell membrane through the toroidal pore mechanism, fluorogainin-1 acts through the barrel-stave mechanism.[25]

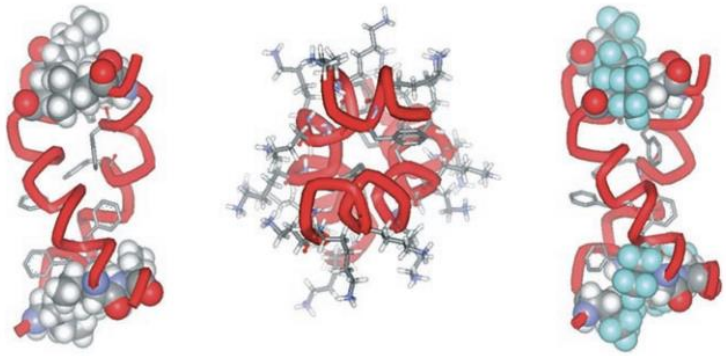

Figure 2.6. *Left*: Model crystal structure of the MSI-78 dimer protein bearing Leu and Ile amino acids. *Centre*: Top view of the MSI-78 protein which shows the arrangement of Leu and Ile residues. *Right*: Model crystal structure of fluorogainin-1 bearing tFLeu (**26**) residues.[25] (Figure adapted from Gottler et al., 2008)

2.1.6. Control of peptoid secondary structure using fluorine

It can be challenging to control peptoid secondary structures because of the tertiary amide bonds present within their backbones, negating the option of hydrogen bonding. Early work in this area conducted by the Barron group put an emphasis on the use of sterically bulky, preferentially aromatic monomers (e.g. *N*spe, **2**) to encourage the formation of a PPI-like helix which was found to mimic the antimicrobial peptide mangainin-2.[30,31] The conformational heterogenic nature of the amide bond sets a difficulty in the introduction of other peptoid building blocks to favour the *cis* amide bond conformation. It therefore is unsurprising that a plethora of studies (see **Chapter 3** for further discussion on this) investigating the *cis/trans* equilibrium control focused on the carbonyl-carbonyl and carbonyl-aromatic n → π* interactions between the peptoid backbone carbonyl and submonomer *N*-side chain.[22]

Fluorine possesses the ability to affect the reactivity and preorganisation of neighbouring functional groups. This is most prominent when it is in β-position from an electron withdrawing (EWG) group, giving rise to the *gauche* effect. The use of fluorinated building blocks in this area was first reported by Gorske who investigated the effect of different building blocks on the *cis/trans* equilibrium within a peptoid model (**Table 2.2**). Amongst several R-groups used in this investigation there was α-chiral pentrafluoroaromatic monomer *Nsfe* **5**. The report focused on n→π_{Ar}* interactions between backbone carbonyls and aromatic side chains, this electron-withdrawing system led to $K_{cis/trans}$ value of 3.84 for **5**, while the revised $K_{cis/trans}$ value for **4** was found to be three-fold lower.[32]

Table 2.2. Peptoid model system structures. Amide cis/trans ratios in $CDCl_3$ together with the free energy differences (calculated using $\Delta G_{cis/trans} = -RT \ln (K_{cis/trans})$.[32]

	Side chains – R	**$K_{cis/trans}$ value**	**$\Delta G_{cis/trans}$ (kcal/mol)**
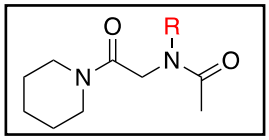	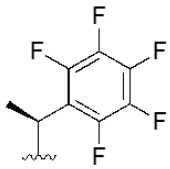 *Nsfe* **5**	3.84	-0.79
	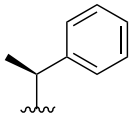 *Nspe* **2**	1.26	-0.15

In 2018, the Cobb group envisaged that the electron withdrawing property of fluorine could stabilise the *cis* amide conformation of the α-peptoid backbone via the inductive effect exerted by the C-F bond. The investigation was based on Banks's report of α-fluoroamides adopting the *trans*-periplanar arrangements (**Scheme 2.2**).[33-35]

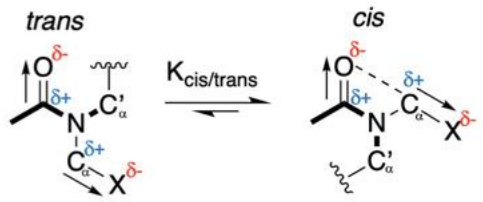

Scheme 2.2. The projected dipole interactions between electronegative groups and the neighbouring carbon atoms in α-fluoroamides, where X represents a flourous group. The cis conformation is stabilised by the inductive effects, and the NCIs between the C=O and the CX (fluorinated group) are shown as a dotted line.

In this work, novel fluorinated peptoid monomers were investigated with the aim of controlling the α-peptoid secondary structure conformation.[33,34] The work focused on utilising the strong electron withdrawing properties of fluorine. Five *de novo* fluorinated acetamides, shown in **Figure 2.7**, were designed, and synthesised in the quest to investigate how the inductive effect of fluorine would influence the *cis/trans* ratio of the amide bond. The monomers used were of three types: alkyl, aromatic and chiral. It was found that in the case of the fluorinated alkyl monomers (**Figure 2.7**, **32** – **34**), the reliance on the non-covalent n → π_{Ar}* interactions to induce α-helical peptoid conformation was eliminated.

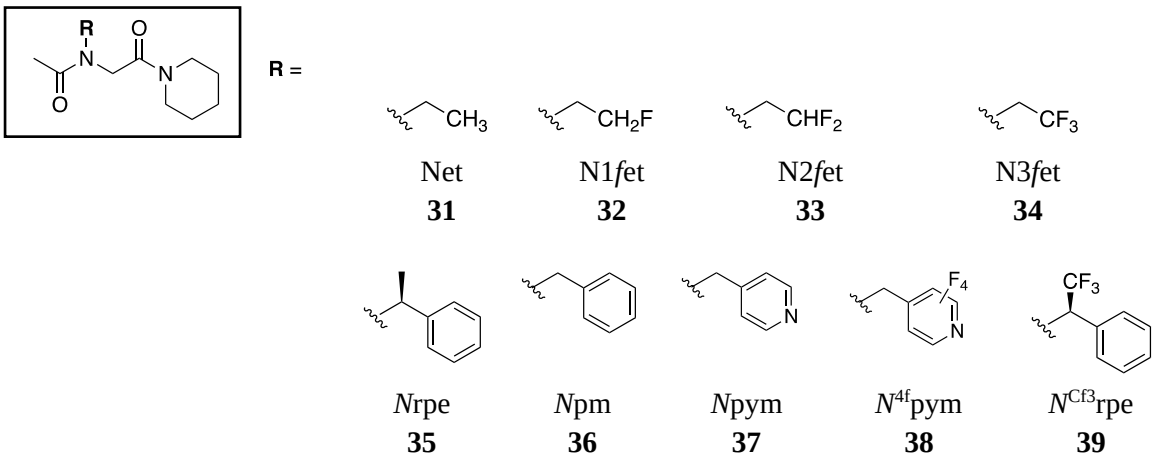

Figure 2.7. Novel fluorous alkyl, aryl and chiral amines used in Cobb's study.[33,34]

Among the fluorine containing alkyl monomers, the *cis* amide bond conformation was enhanced by increasing the degree of fluorination. **34** (*N*3*f*et) showed the highest $K_{cis/trans}$ value of 2.24±0.12 in CD_3CN, which exceeded that seen for **35** (*N*rpe) $K_{cis/trans}$ (2.08±0.12). In addition, **33** (*N*2*f*et) exhibited a $K_{cis/trans}$ value comparable to **35** (2.05±0.12). Overall, withdrawing effects of fluorine and $K_{cis/trans}$ values indicated a strong linear correlation. In the

presence of CD_3OD the general trend of increasing *cis* amide preference confirms the $K_{cis/trans}$ values in CD_3OD and this disclaims the involvement of hydrogen interactions. (**Table 2.3**).[33]

Again, the $\Delta G_{cis/trans}$ values show the same correlation as the $K_{cis/trans}$ values where **33** stabilises the *cis* amide conformation to a greater extent than *N*rpe (in CD_3CN). Interestingly, the free energy of the **34**-containing peptoid in $CDCl_3$ favours the *trans* amide conformation, which was suggested to be caused by apolar solvents disfavouring large dipoles within the peptoid. This preference can be further explained by the overall dipole moment being lower in the *trans*-isomer of the model peptoid.

Table 2.3. $K_{cis/trans}$ values for **31-39**, including alkyl, aryl and chiral model peptoids, together with the corresponding $\Delta G_{cis/trans}$ values. ($\Delta G_{cis/trans} = -RT\ln K_{cis/trans}$).[33,34]

No.	CD_3CN		$CDCl_3$		CD_3OD	
	$K_{cis/trans}$	$\Delta G_{cis/trans}$ (kcal mol^{-1})	$K_{cis/trans}$	$\Delta G_{cis/trans}$ (kcal mol^{-1})	$K_{cis/trans}$	$\Delta G_{cis/trans}$ (kcal mol^{-1})
31 (*N*et)	0.66±0.07	0.28±0.08	0.19±0.01	0.97±0.01	0.51±0.04	0.43±0.05
32 (*N*1*f*et)	1.15±0.09	-0.09±0.04	0.76±0.03	0.16±0.02	0.74±0.07	0.16±0.05
33 (*N*2*f*et)	2.05±0.12	-0.42±0.04	1.28±0.08	-0.16±0.03	1.17±0.04	-0.09±0.02
34 (*N*3*f*et)	2.24±012	-0.48±0.03	0.54±0.06	0.35±0.01	1.23±0.03	-0.13±0.01
35 (*N*rpe)	2.08±0.12	-0.43±0.04	0.94±0.05	0.05±0.04	1.35±0.04	-0.18±0.02
36 (*N*Phe)	1.20±0.06	-0.11±0.03	0.27±0.01	0.79±0.03	0.71±0.03	0.20±00.03
37 (Npym)	1.66±0.06	-0.30±0.02	0.46±0.01	0.45±0.02	1.15±0.02	-0.08±0.01
38 (N^{4f}pym)	3.22±0.12	-0.69±0.03	1.41±0.16	-0.20±0.08	2.22±0.04	-0.47±0.01
39 (N^{Cf3}pym)	5.82±0.23	-1.04±0.03	5.17±1.12	-0.95±0.19	6.41±0.13	-1.10±0.02

Following the investigation of fluorinated alkyl monomers on the amide bond conformation, the influence of the inductive effects was investigated upon aryl and chiral monomers. Introduction of a heteroaromatic group β to the amide group (**37** to **38**) led to a shift in the *cis/trans* equilibrium in all solvent systems. It was envisaged that upon fluorination of the heteroaromatic, electron withdrawing **38**, the *cis* amide bond conformation preference would be increased further. Indeed, comparing to its non-fluorinated counterpart, **38** showed an increased preference for the *cis*-isomer ($K_{cis/trans}$ in CD_3CN= 3.22±0.12 for **38** comparing to 1.66±0.06 for **37**). The $K_{cis/trans}$ values for the heteroaromatic monomers followed the same trend in MeOD and CD_3Cl. In the case of the chiral monomer containing peptoid model, the amide bond conformation showed an extremely strong preference for the *cis*-isomer ($K_{cis/trans}$ value 5.82±0.23) in CD_3CN. This result was also predominant in the other two solvents. While,

the non-fluorinated counterpart, **35**, showed no preference for either the *cis*- or *trans*-isomer in $CDCl_3$ ($K_{cis/trans}$ ~1), the presence of polar solvent strongly enhanced the *cis*- amide bond conformation.[31,33] Moreover, **39** showed highest $K_{cis/trans}$ values in all solvents, and its *cis*-inducing preference was highest in a protic solvent.[34]

Furthermore, the Cobb group designed and synthesised seven model peptoids **Pep. 13** – **19** to investigate the ability of the fluorinated alkyl monomers to form stable peptoid helices.[33] These peptoids consisted of fifteen peptoid monomers, where *N*spe (**2**) was incorporated into the peptoid *C*-terminus to serve as a chiral reporter for the CD spectroscopy.

These model peptoids were analysed and apart from the molar ellipticity and helical structure analysis carried out by CD spectroscopy. The effect of fluorine on α-peptoid secondary structure was established to be cumulative, where an increase the molar ellipticity correlated with increasing the number of fluorine atoms present in the peptoid. It has been identified that the CF_3 group in **34** and CH_3 group in **31** have volumes of 40.47 Å and 29.63 Å, respectively, explaining the decreased synergy between the neighbouring **39** which resulted in decreased overall α-helical character of the peptoid.[33] (**Figure 2.8**)

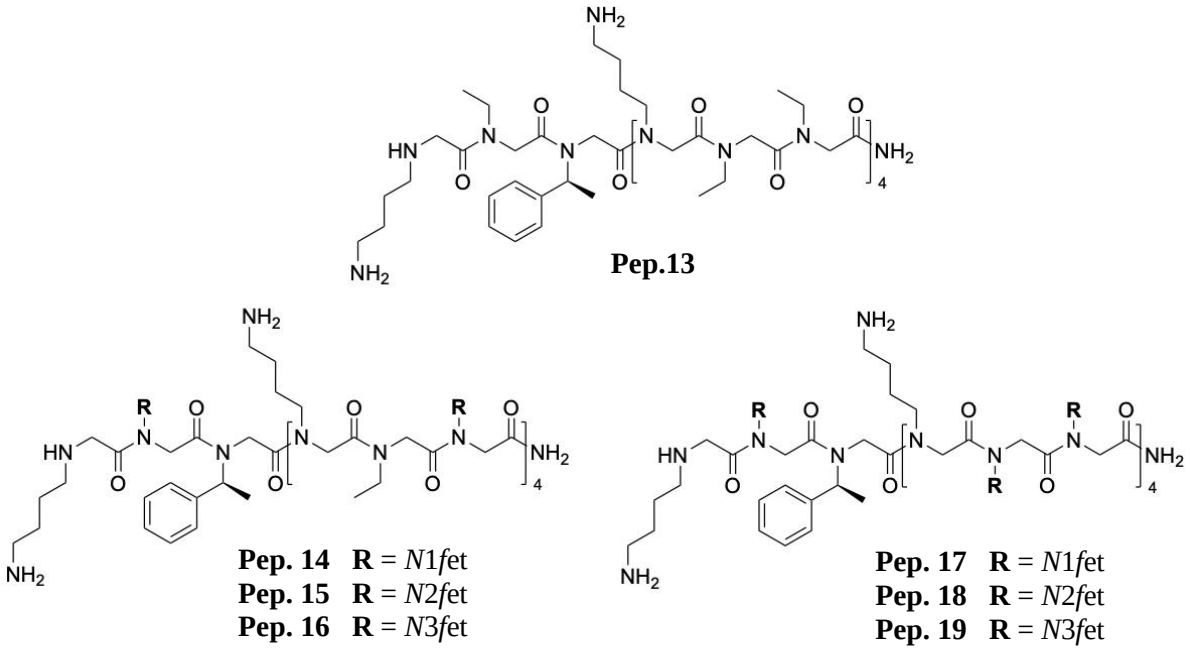

Figure 2.8. Chemical structures of peptoids **Pep. 13** – **19**.

2.1.7. Fluorinated monomers and peptoid efficacy against pathogens

Bolt *et al.*,[36] reported incorporating achiral *meta*- and *para*-substituted fluorobenzyl monomers **42** (*N*mfb) and **41** (*N*pfb) into α-peptoid chains to investigate their effect on peptoid antimicrobial properties. (**Figure 2.9**) Incorporation of the fluorinated monomers led to an increase in antibacterial properties against Gram-positive bacteria studied (for comparison, see biological data for **Pep. 6, 20 – 24**, **Table 2.4**). Additionally, combining fluorinated achiral monomers with *N*spe monomers further boosted antibacterial effectiveness, as seen in **Pep. 23**. Notably, **Pep. 24** exhibited reduced toxicity, relative to **Pep. 6** and **Pep. 20 – 23**. This observation underpins the study carried out by Chongsiriwatana[37], who reported the need for defined α-helical structures in antimicrobial peptoids to not be of a great importance. Instead, other effects such as hydrophobicity and the overall charge play a significant part in designing peptoids with highest antimicrobial activities.

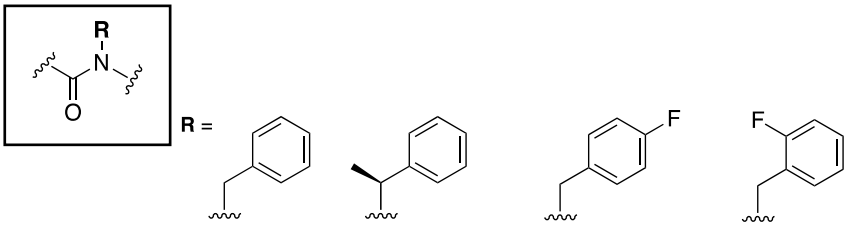

*N*Phe **40** | *N*spe **2** | *N*pfb **41** | *N*mfb **42**

Figure 2.9. Structures of aryl peptoid monomers used in the synthesis of peptoids in **Table 2.4**.

Table 2.4. Activities of peptoids screened against mammalian (HaCat) and bacterial cells.[36]

No.	Sequence	ED_{50} (μM) *HaCat*	MIC (μM) | Average selectivity			
			E. coli	***P. aeruginosa***	***S. aureus***	***S. epidermis***
Pep. 20	*(NLysNPheN*Phe)$_4$	36	13 | 6	50 | 2	3 | 23	2 | 34
Pep. 6	*(N*Lys*N*spe*N*spe)$_4$	20	25 | 1	50 | 1	2 | 13	1 | 25
Pep. 21	(*N*Lys*N*mfb*N*mfb)$_4$	25	25 | 1	25 | 1	6 | 4	3 | 7
Pep. 22	(*N*Lys*N*pfb*N*pfb)$_4$	46	13 | 3	25 | 2	2 | 19	1 | 38
Pep. 23	(*N*Lys*N*pfb*N*spe)$_4$	20	13 | 2	13 | 2	2 | 12	2 | 12
Pep. 24	*[(N*Lys*N*pfb*N*pfb) *(N*Lys*N*spe*N*spe)]$_2$	>100	6 | 13	50 | 2	2 | 39	1 | 78

2.2. Objectives for Chapter 2

Previously, stable 15-mer α-peptoids, **Pep. 13** – **19** (**Figure 2.8**), have been synthesised and subjected to structural analyses. The effects of fluorinated alkyl monomers on the biological properties of α-peptoids have not been investigated yet but such systems provide an attractive platform to study the effects of fluorine's unusual properties on bacterial membrane interactions. Thus, one objective of this work is to design and synthesis a library of peptoids containing a mixture of fluorinated and cationic quaternary ammonium peptoid monomers. This library would then have its biological properties assessed.

Through this work it was sought to improve peptoid antimicrobial to haemolytic activity ratios (i.e. selectivity indices, SI). To achieve this, a library of dodecamer peptoids was to be subjected to minimum inhibitory concentration (MIC) assays, and cytotoxicity assays which will be performed on the immortal cell line HepG2. It was further endeavoured to measure exact log *D* values of these peptoids to aid the rational peptoid design, as reverse-phase (RP) HPLC t_R values were found to not be an accurate prediction of hydrophobicity of peptoids, which is an important component of Lipinski's Rule of 5.

2.3. Chapter 2: Results and discussion

2.3.1. Synthesis and purification of fluorinated peptoids (Pep. 13 – 19)

Initial efforts focussed on the synthesis of the fluorinated peptoids **Pep. 13** – **19**, and it very quickly became apparent that the strongly electron withdrawing fluorine made the synthesis challenging. The bromine displacement step of the sub-monomer method proved to be time-consuming due to long reaction times which ranged from 90 to 270 minutes per step. This was particularly evident where **33** and **34** were used as monomers. In fact, the use of fluorinated submonomers further in the synthesis saw a need for increased reaction times of up to three hours. The formation of deletion sequences, and undesired side products made the separation of the desired product from impurities challenging, and several sequences needed to be re-synthesised. A detailed synthesis, and cleavage from the resin, of **Pep. 19** is shown in **Scheme 2.3**, as an example.

Purification of the peptoids was performed using RP HPLC at 220 nm and this also proved to be challenging. Initial attempts were made to purify the fluorinated peptoids at a concentration of 10 mg/mL (50:50 ACN/water), where 1 mL of the solution was injected. This, however, needed to be revised due to peptoids being flushed out of the column at the beginning of each run. This result was attributed to the poor interaction of the fluorinated peptoids and the RP HPLC column, as well as solubility issues with the selected HPLC solvent system. Eventually, after a number of runs and low recovery yields, it was determined that high dilution of peptoid solutions was necessary and 4 mg of crude product, in 1 mL of 95% H_2O + 5% ACN, was injected per run. This aided the purification process and allowed suitable amounts of the required products to be obtained, to allow biological screening and physical analysis to be carried out.

The general behaviour of the fluorinated peptoids and their poor interaction with the HPLC column alkyl chains led to a need to optimise each peptoid purification. In particular, the less UV-active peptoids, primarily **Pep. 13** and **Pep. 17**, required longer run times per injection, up to 80 mins leading to more gradual gradients, and a slower flow of 1 mL/min instead of 2 mL/min. An example HPLC run, where such method was employed is shown in **Figure 2.10**.

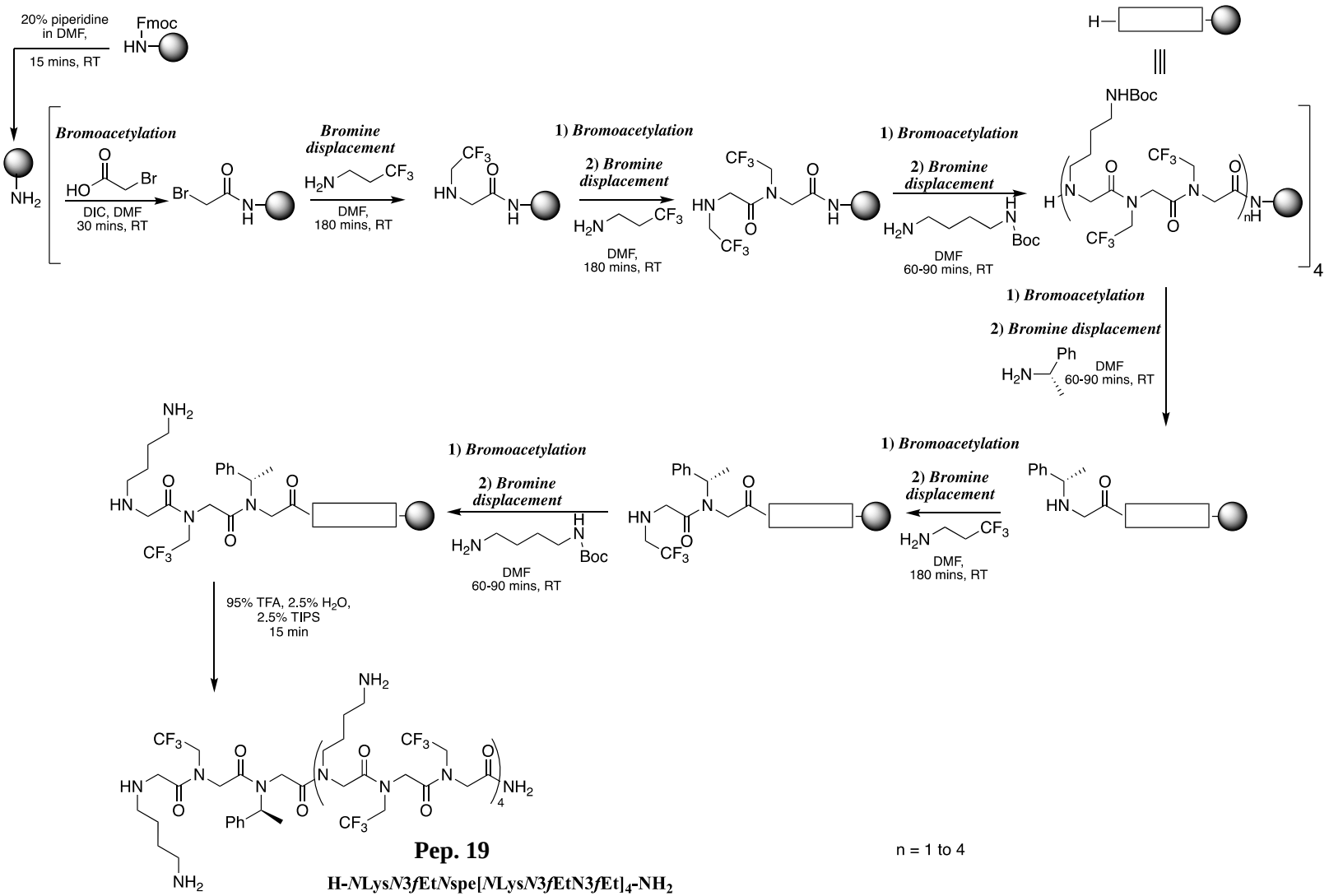

Pep. 19

n = 1 to 4

H-*N*Lys*N*3*f*Et*N*spe[*N*Lys*N*3*f*EtN3*f*Et]$_4$-NH$_2$

;p

Scheme 2.3. A detailed route for the synthesis of **Pep. 19**.

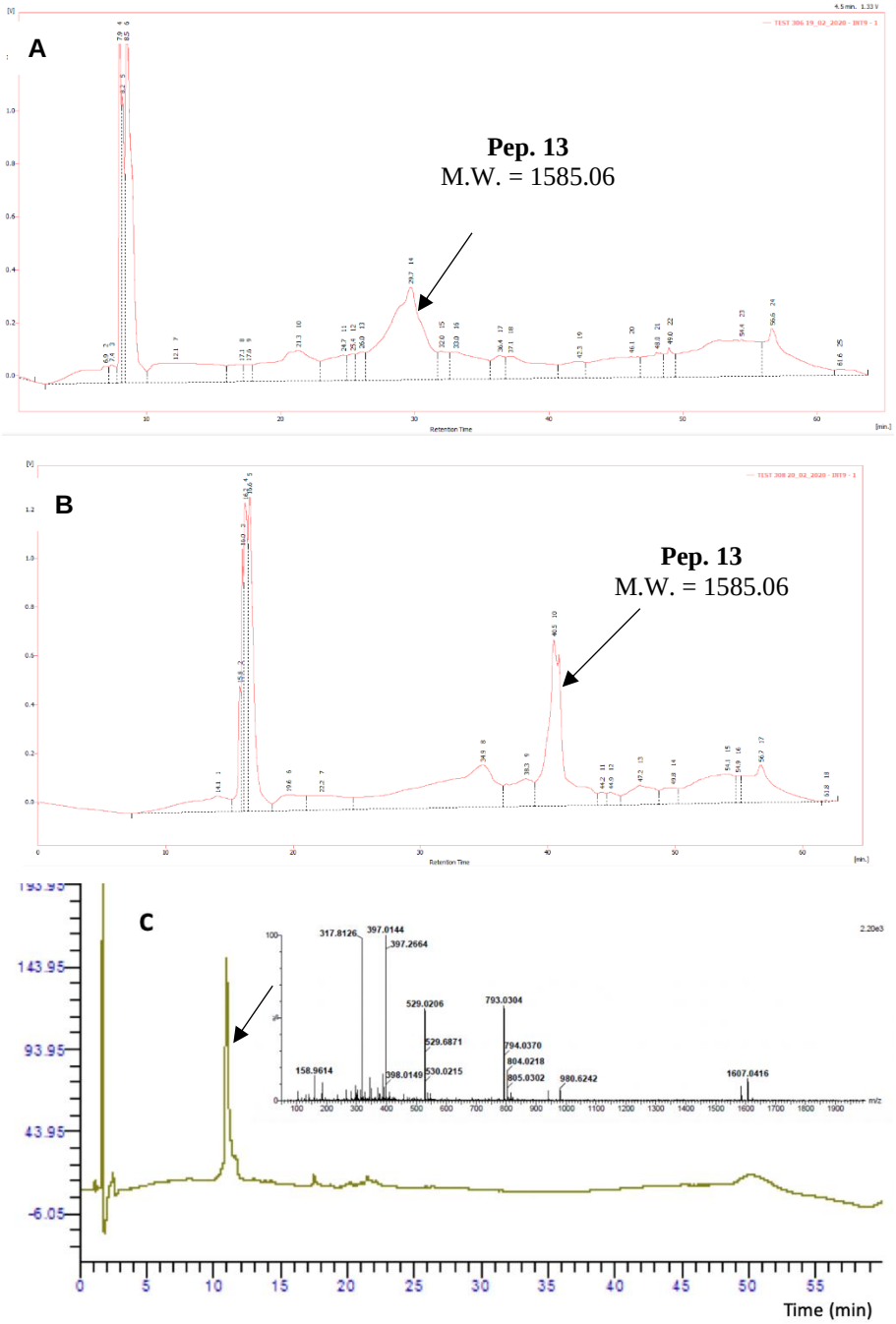

Figure 2.10. RP HPLC run of **Pep. 13** at 220 nm, 4 mg/mL. **A**. Purification conditions: 0-65% Solvent B, 60 min gradient, flow of 2 mL/min. **B**. 0-90% solvent B, 80 min gradient, flow of 1 mL/min. [V] = voltage. The arrows indicate the double peak corresponding to two regioisomers of **Pep. 13**. **C**. An analytical HPLC run together with the corresponding MS trace of pure **Pep. 13**. [2M+ACN]/2 = 1607.0416; [M+2] = 793.0304; [M+3] = 529.0206; [M+4] = 397.0144. Traces of impurities are present.

The presence of deletion sequences in the final crude product mixture (**Figure 2.11**) interfered with the purification of the peptoids. This was particularly troublesome in the case of peptoid **Pep. 19** where HPLC t_R of the deletion sequences were like that of the desired

peptoid. The bromine displacement step performed with trifluoroethylamine required extended reaction times of at least two hours.

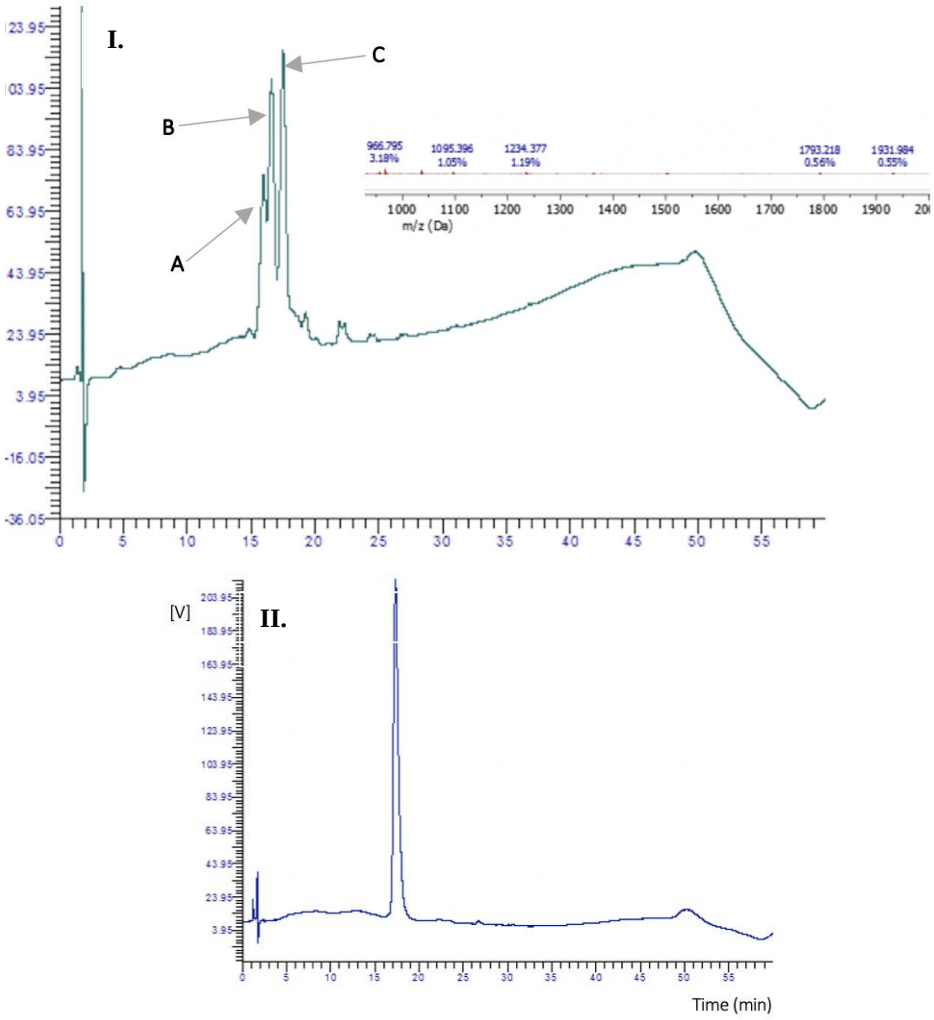

Figure 2.11. I. HPLC trace of crude **Pep. 19**. The three peaks correspond to the desired **Pep. 19** and two deletion sequences. **A**. *N*Lys*N*spe*N*3*f*et[NLys*N*3*f*et*N*3*f*et]$_3$*N*Lys–NH_2, t_R = 16.0 min, [M+1] = 1793.218; **B**. *N*Lys*N*spe*N*3*f*Et[*N*Lys*N*3*f*et*N*3*f*et]$_3$*N*Lys*N*3*f*Et –NH_2, t_R = 16.5 min, [M+1] = 1931.984; **C**. *N*Lys*N*spe*N*3fet[*N*Lys*N*3*f*et*N*3*f*et]$_4$–NH_2, t_R = 17.4 min, [M+2+NaCl] = 1095.306. **II**. HPLC trace of pure peptoid **Pep. 19**.

Despite the challenges encountered, the successful synthesis and purification of all of the target fluorinated peptoids was achieved (**Table 2.5**). As an example, the analytical HPLC traces of crude and pure peptoids **Pep. 16** and **Pep. 18** are shown in **Figure 2.12**.

Table 2.5. A tabulated summary of **Pep. 3 – 9**, showing their HPLC t_R, the amount of crude product obtained, the purification conditions, and the amounts of pure products obtained after HPLC runs.

No.	MW ($gmol^{-1}$)	HPLC t_R (min)	Crude pdt (mg)	Purification conditions	Pure pdt (mg)
Pep. 13	1585.06	12.5	88.3	0-90% B; 1.0 mL/min; 80 mins; 220 nm	5
Pep. 14	1675.02	10.5	88.0	0-100% B; 2.0 mL/min; 60 min; 220 nm	4.6
Pep. 15	1764.97	12.7	82.0	0-100% B; 2.0 mL/min; 60 min; 220 nm	18.9
Pep. 16	1854.92	16.7	118.9	0-100%; 2.0 mL/min; 60 mins; 220 nm	27.1
Pep. 17	1745.98	10.0	90.0	0-80%; 1.0 mL/min; 80 min; 220 nm	11.1
Pep. 18	1908.89	14.0	133.0	0-70% B; 2.0 mL/min; 60 mins; 220 nm	27.3
Pep. 19	2056.82	17.4	136.0	0-70% B; 2.0 mL/min; 60 mins; 220 nm	6.9

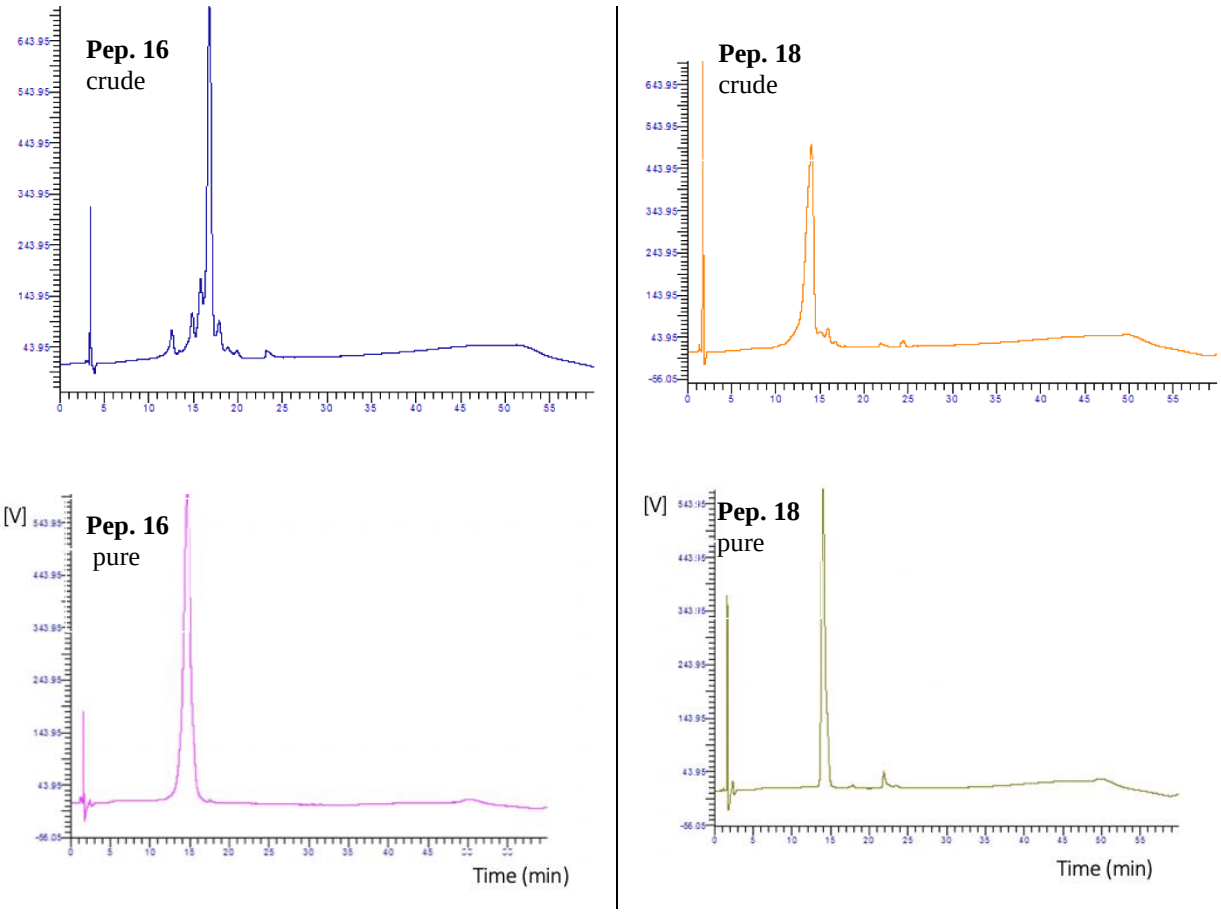

Figure 2.12. Analytical HPLC traces of crude and pure **Pep. 6** and **Pep. 8**.

2.3.2. Synthesis and purification of non-fluorinated peptoids (Pep. 6, 12 and 25)

In addition to the fluorinated peptoids, **Pep. 13** – **19**, a selection of previously screened non-fluorinated peptoids **Pep. 6**, **Pep. 12** and **Pep. 25** were identified for resynthesis (**Figure 2.13** and **Table 2.6**). These peptoids were specifically chosen due to their high biological activities against pathogenic targets (**Table 2.6**).[38] **Pep. 25** has an overall charge of +3, which is relatively uncommon as the overall charge has been reported to play a key role in antimicrobial properties of peptoids, and the optimum charge has been reported to be +4.[37]

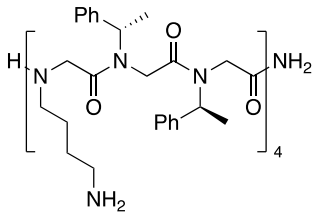

[*N*Lys*N*spe*N*spe]$_4$-NH$_2$
Pep. 6

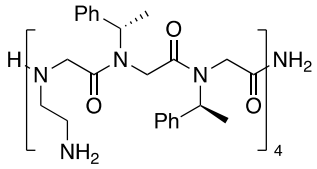

[*N*ae*N*spe*N*spe]$_4$-NH$_2$
Pep. 12

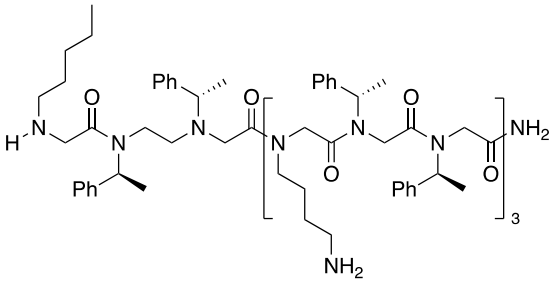

*N*amy*N*spe*N*spe[*N*Lys*N*spe*N*spe]$_3$-NH$_2$
Pep. 25

Figure 2.13. A selection of most active peptoids screened against biological targets.

Table 2.6. Biological activities of **Pep. 6**, **12** and **25** when screened against *L. mexicana*, the causative agent of leishmaniasis, and bacteria. Their haemolytic activities are also shown. [38]

No..	M.W. (g/mol)	HPLC t_R (min)	ED50 (μM)			MIC (μM)	
			HaCat	*L.mex prom.*	*L. mex ama.*	*E. coli*	*S. aureus*
Pep. 6	1594.93	14.9	20	8	>100	25	2
Pep. 12	1707.11	16.7	29	7	17	>100	2
Pep. 25	1876.15	19.3	12	8	21	50	2

In contrast to the fluorinated oligomers, the non-fluorinated peptoids required much shorter reaction times of only 1 hour (bromine displacement step), followed by comparatively

trouble-free purifications. In fact, the amount of peptoid purified per injection often exceeded 10 mg.

The cleavage of these peptoids from the resin repeatedly resulted in a *m/z* detection of sequences corresponding to 105 a.m.u. less than the *m/z* of the desired sequences. Indeed, this corresponded to an acid-catalysed elimination of a phenylethyl moiety **43** (**Scheme 2.4**), leading to the formation of side products. These side products did appear to have very similar HPLC t_R to the desired peptoids; however, their separation was relatively trouble-free, and the products obtained were of high purity (**Table 2.7, Figure 2.14**). In fact, this side reaction occurred during cleavage of the fluorinated peptoids from the resin, but this was minimal. However, decreasing the reaction times did not assist in overcoming this issue.

Side reactions where electron-rich benzylamines showed instability in acidic conditions have previously been documented in literature.[39] It has been reported that reducing the amount of TFA used during this step can help to minimise the occurrence of this side reaction. A cleavage cocktail of TFA/DCM/H_2O/TIPS (47.5/47.5/2.5/2.5 *v/v/v/v*) is suggested as an alternative.

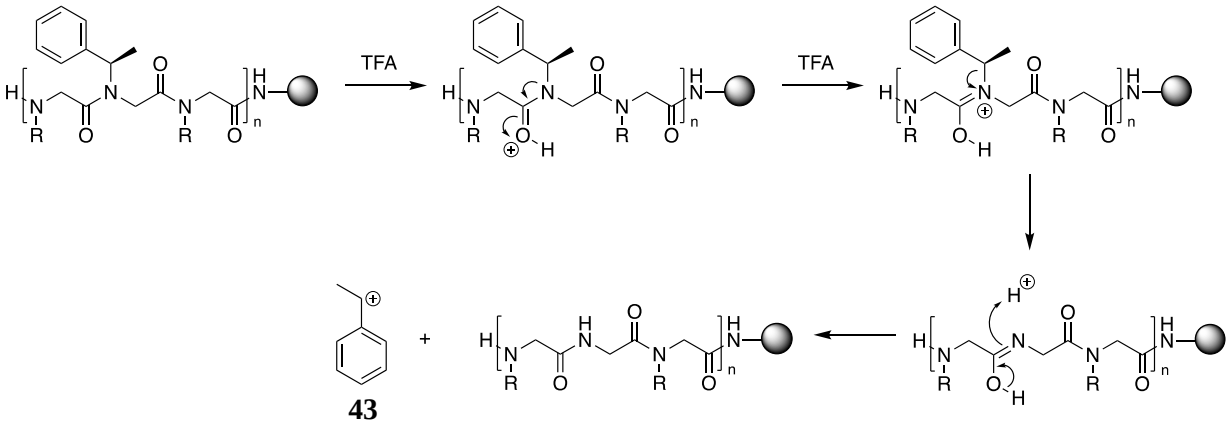

Scheme 2.4. A proposed reaction scheme, which illustrates the TFA-catalysed phenylethyl cleavage.

Table 2.7. A tabulated summary of **Pep. 6, 12, 25**, showing their HPLC T_R, the amount of crude product obtained, the purification conditions, and the amounts of pure products obtained after HPLC runs.

No.	MW ($gmol^{-1}$)	RT (min)	Crude pdt (mg)	Purification conditions	Pure pdt (mg)
Pep. 6	1819.36	14.9	137.0	0-100% B; 2.0 mL/min; 60 min; 235 nm	22.6
Pep. 12	1594.93	16.7	150.0	0-100% B; 2.0 mL/min; 60 min; 240 nm	10.2
Pep. 25	1818.38	19.3	140.0	0-100% B; 2.0 mL/min; 60 mins; 230 nm	11.2

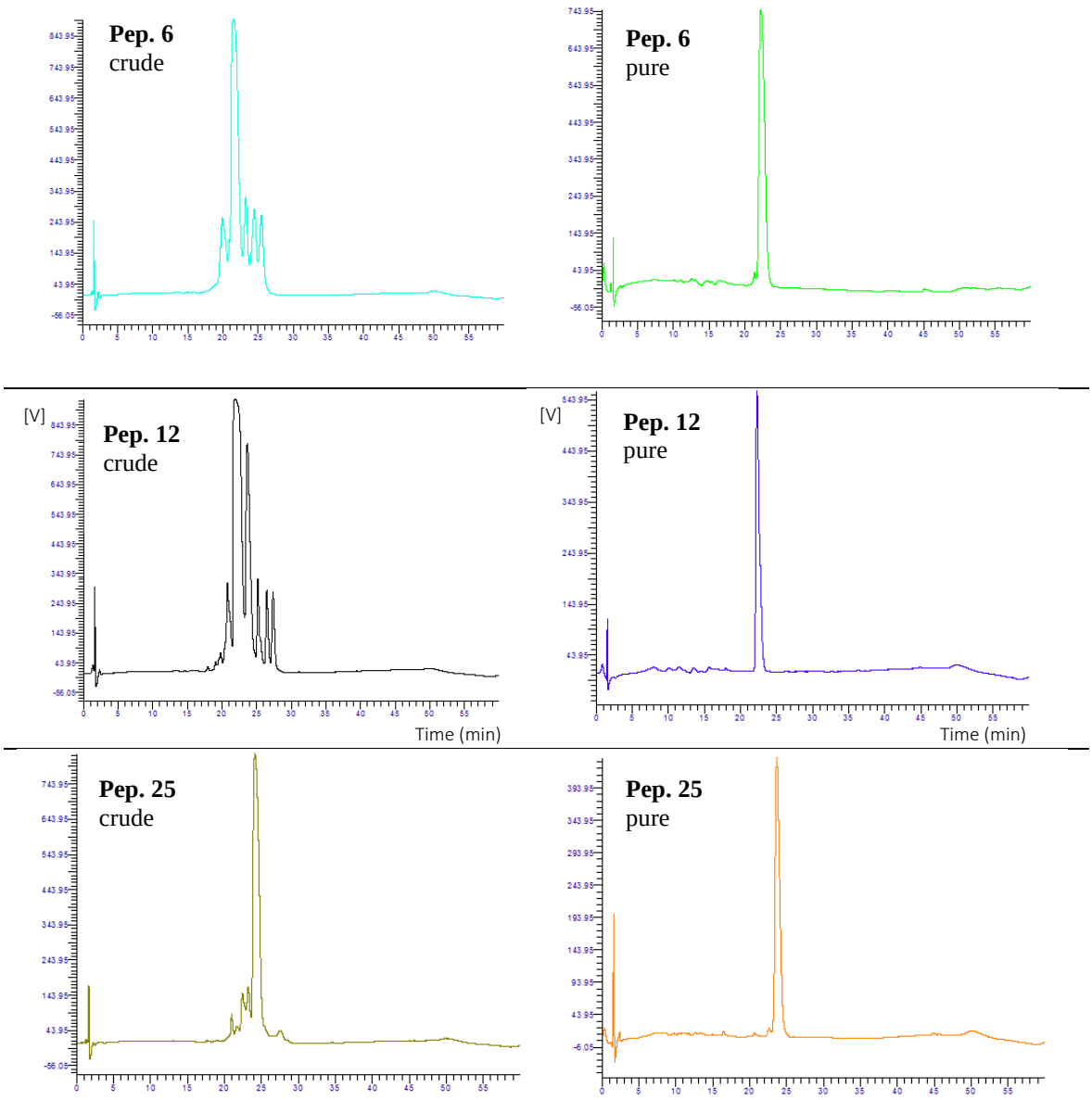

Figure 2.14. Analytical HPLC traces of crude and pure **Pep. 6**, **12** and **25**.

2.3.3. Synthesis of quaternary ammonium peptoid monomers

Further to the exploration of the *cis*-inducting fluorinated building blocks in peptoid synthesis, we endeavoured to incorporate monomers bearing cationic ammonium monomers: *N*et$_3$ae **49**, *N*et$_2$pgae **50** and *N*bnet$_3$ae **51**, (**Scheme 2.5**) which have been shown by Zuckermann (**Chapter 3**, **Section 3.2.2**) to have the ability to induce α-helices.[40]

The synthesis of the building blocks **49 – 51** to be used in the production of a library of 16 novel peptoids (**Section 2.3.4**) proceeded with the employment of commercially available *N*,*N*-diethylethylenediamine (**44**). The primary amine required protection to prevent over-alkylation of the molecule which would lead to side product formation. For this purpose, di-*tert*-butyl dicarbonate was used and the reaction was performed under basic conditions. The Boc-protection took place at ambient temperature and was completed after leaving the reaction to stir overnight. Subsequently, an acidic workup was performed to isolate the desired protected product from the remaining starting material. In this step, an aqueous solution of 1 M citric acid was used as opposed to a solution of 1 M hydrochloric acid to avoid the risk of Boc-deprotection. (**Scheme 3.5**)

The high stability of this Boc-protected tertiary amine in ambient conditions meant that the reaction could be performed on a multi-gram scale and the product could be safely stored even at room temperature without decomposition.

Ultimately, to produce the *N*-Boc protected quaternary ammonium species, 1.05 eq of the electrophile was used: iodoethane to produce **46**, propargyl bromide to produce **47**, and benzyl bromide to produce **48**. The desired cationic ammoniums were recovered as halogen salts. The cleavage of the Boc group was performed under standard conditions of TFA in DCM. This deprotection can also be performed in the presence of 4 M HCl in dioxane. This final step was fast and facile. The workup following this step required evaporation of DCM *in vacuo*, and the residual TFA was co-evaporated with the reaction solvent, and quantitatively yielded the desired unprotected amine (**49-51**). Both **49** and **50** were recovered as solids, following a crystallisation in toluene. **51**, was recovered as a thick oil and found to be hygroscopic – confirmed by a distinct water peak detected by NMR spectroscopy (**Figure 2.15**).

The quaternary amine monomers produced were subsequently used in the synthesis of antimicrobial peptoids in the **Section 2.3.4**, where they were used as cationic building blocks. (**Figure 2.17**)

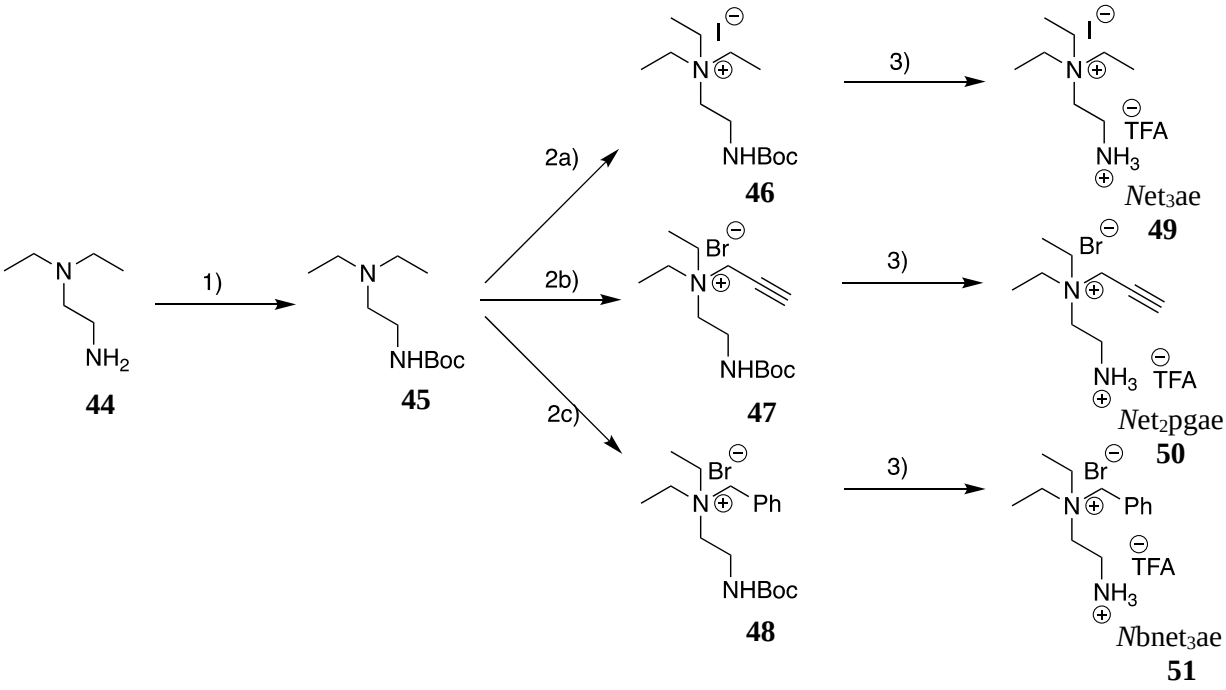

Scheme 2.5. Schematic representation of a three-step synthesis of *N*et$_3$ae (**49**), *N*et$_2$pgae (**50**), and *N*bnet$_3$ae (**51**) as TFA salts. 1) Boc$_2$O, TEA in DCM at RT o/n (avg. 84%); **2a)** EtI, DCM, reflux o/n (58%); **2b)** PrBr wt. 80% toluene at 40 ºC, 5 days*; **2c**) BzBr at 40ºC, 5 days (84%); **3)** TFA in DCM at RT, 2 h (quant.).
*Quantitative yield after Boc cleavage. The product is hygroscopic.

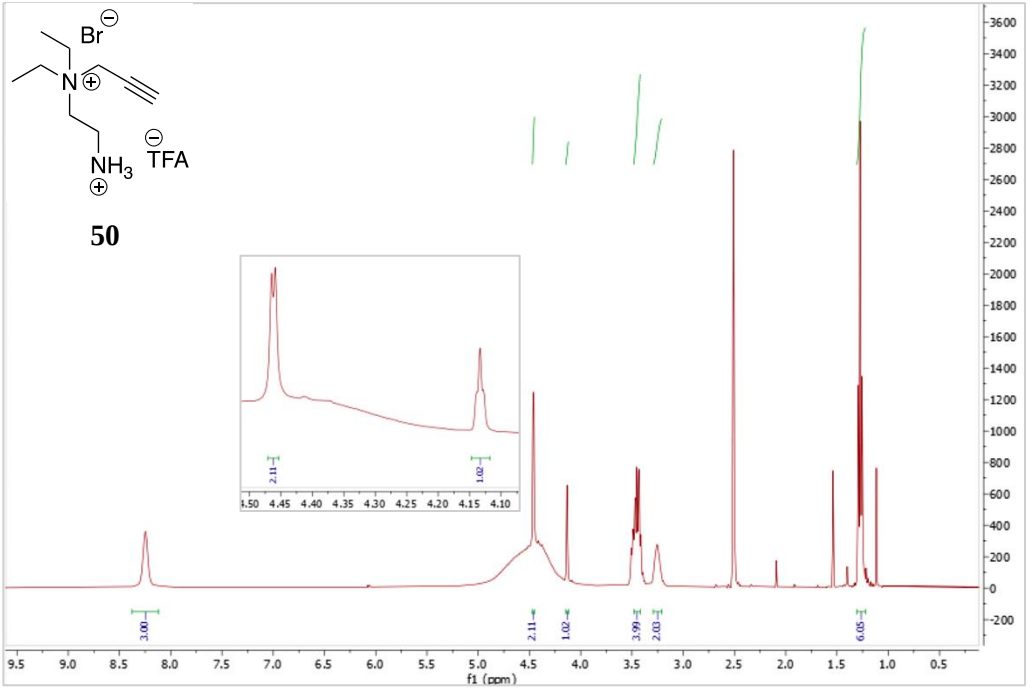

Figure 2.15. NMR (DMSO) spectrum of **50**, showing a broad water peak at 4.48 ppm.

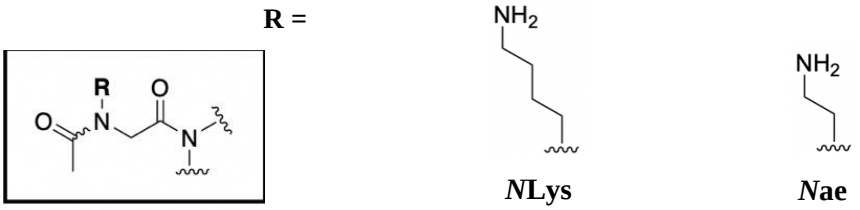

***N*Lys** **52** ***N*ae** **53**

Figure 2.16. *N*Lys and *N*ae monomers, commonly used as source of cationic charge in peptoids.

2.3.4. Synthesis of peptoids containing fluorinated and cationic monomers

Despite several studies pointing out the antibacterial potential of fluorine substitution into linear as well as macrocyclic peptoids, a 2020 study carried out by the Jensen group reported that in some cases inclusion of fluorinated monomers could significantly decrease peptoid antimicrobial activities.[41] The compounds synthesised in this study consisted of repeated short sequences of NSGs (*N*-substituted glycines) which compromised a selection of halogenated phenylethyls. Although these findings disfavour utilising fluorine in the synthesis of antimicrobial peptoids, it is imperative to focus on the significance of the sequence-specific nature of antimicrobial activity of peptoids.

The peptoid library prepared (**Figure 2.17**) was designed based on the *N*y*N*x*N*x repeating motif, and all the peptoid chains discussed in this section consisted of 12 peptoid building blocks. These sequences were based on the AMP magainin-2, wherein the *N*y monomer typically bore a hydrophilic cationic moiety (*N*Lys **52**); on the other hand, the *N*x monomer was a hydrophobic building block (*N*spe **2** or *N*Phe **40**). We desired to derivatise the *N*-terminal repeat unit by substituting the standard chiral aromatic monomers with novel fluorinated aliphatic building blocks first developed by the Cobb group.[33] It was envisaged that fluorine's unique properties could be utilised to mimic 'lipid tails' frequently used to improve antimicrobial properties of peptoids and peptides, by helping to target and penetrate the bacterial membranes.

Furthermore, in this library, more recently developed cationic ammonium building blocks were utilised to explore the effects of the *cis*-inducing *N*Lys derivatives on the amphiphilicity of antimicrobial peptoids. The use of the alkyl cationic ammonium monomers **49** – **51** has the potential to selectively target anionic bacterial membranes over the neutral mammalian membranes, and hence decrease the cytotoxicity of peptoids.

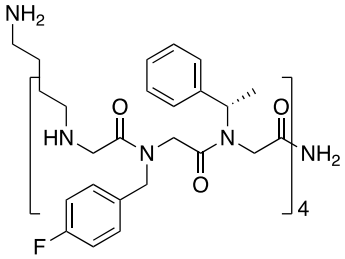

Pep. 23

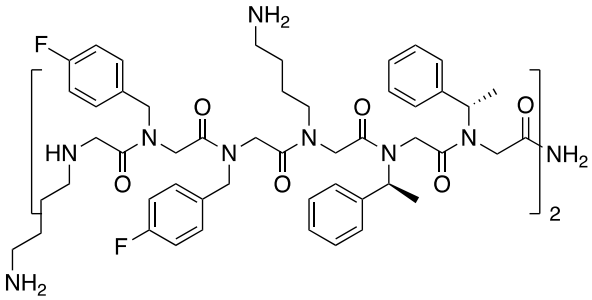

Pep. 24

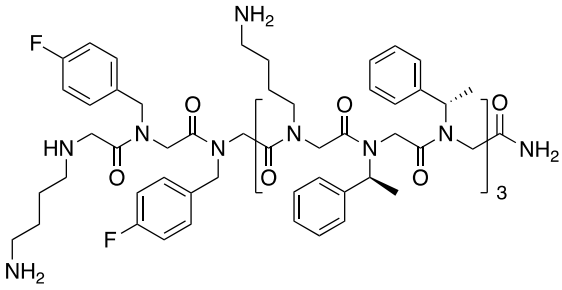

Pep. 26

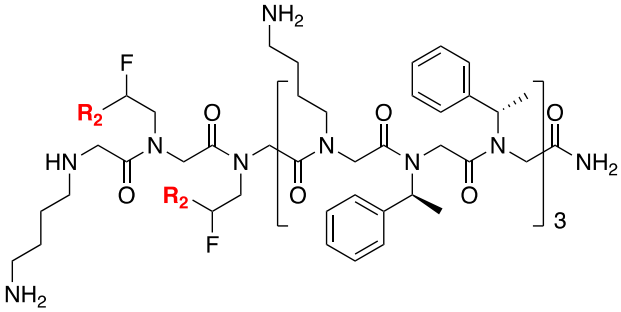

Pep.	R_2
27	H
28	F

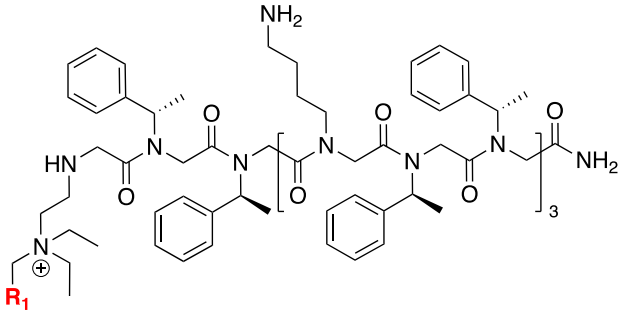

Pep.	R_1
29	H
30	Ph

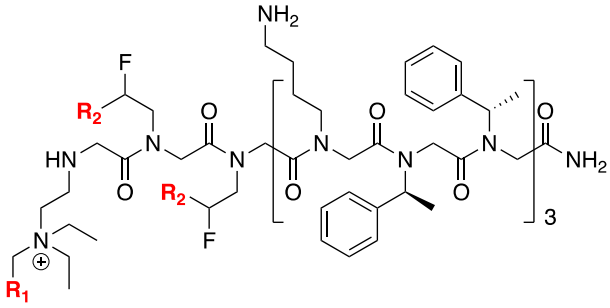

Pep.	R_1	R_2
31	H	H
32	Ph	H
33	Ph	F
34	$H_2C{\equiv}CH$	F

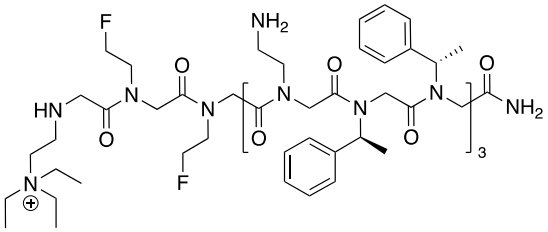

Pep. 35

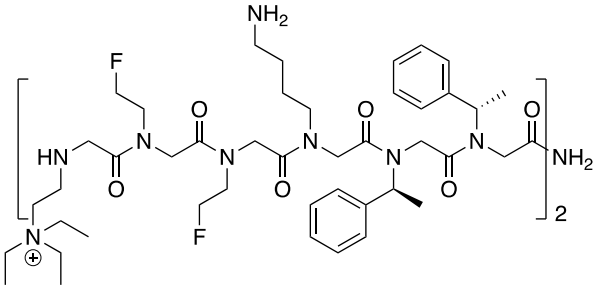

Pep. 36

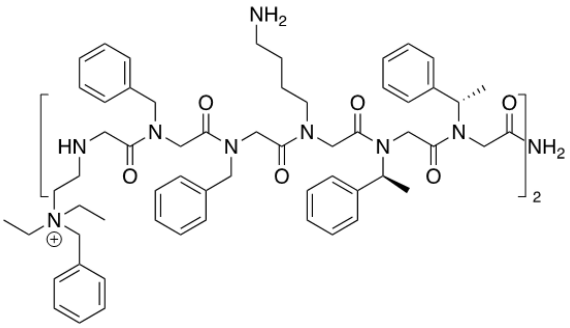

Pep. 37

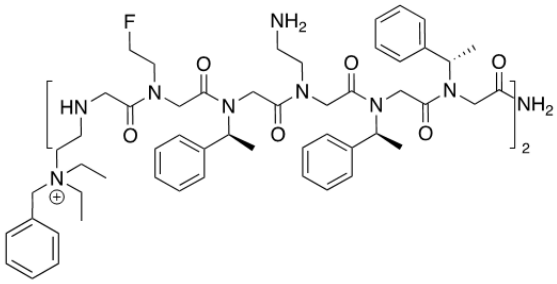

Pep. 38

Figure 2.17. A library of 16 peptoids was designed to explore the potential of fluorinated and cationic quaternary ammonium monomers to improve the activities against biological targets. *All peptoids in this library have a C-terminal amide.

2.3.5. Gram-positive vs. Gram-negative bacteria

Classification of bacteria begins with the utilisation of the Gram stain which categorises bacterial species into two types, the Gram positive and Gram-negative species.[42] The cell envelope which affects the degree of staining of the cells can be correlated with cell properties, such as cell wall thickness and membranes present. The Gram-negative bacteria species will present a thin layer of cell wall accompanied by inner and outer membranes decorated with pores and appendices. The Gram-positive bacteria possess much thicker cell walls. The overall architecture of cell envelopes will present a scope of differences in bacterial response to environmental stresses such as temperature extremes, UV radiation and antimicrobial agents. The specificities of bacterial envelopes and the differences seen in the two varieties are depicted in **Figure 2.18**.

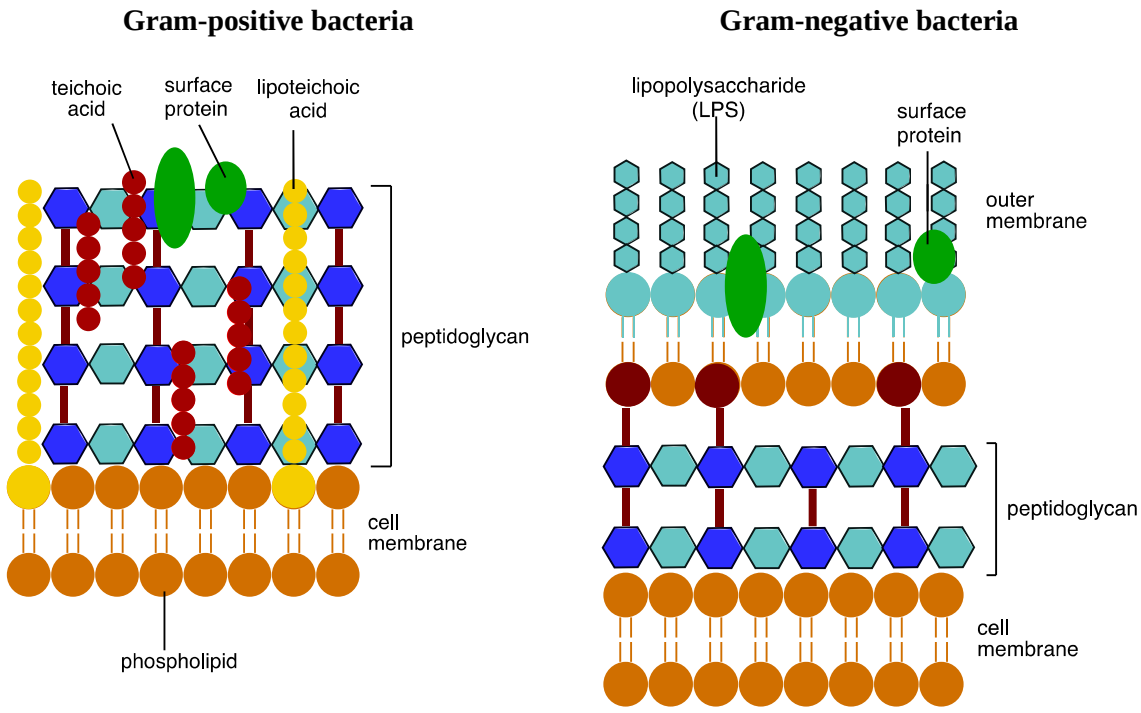

Figure 2.18. Diagrams showing Gram-positive and the Gram-negative cell membranes.

2.3.6. Minimum inhibitory concentration (MIC)

The MIC is the lowest concentration of an antibacterial agent which under strictly controlled *in vitro* conditions prevents visible growth of the test strain of an organism. Four different species of bacteria were used to investigate the antibacterial properties of the peptoids prepared: *E. coli* (Gram-negative), *S. aureus* (Gram-positive), *P. aeruginosa* (Gram-negative) and *B. subtilis* (Gram-positive). *E. coli* is commonly found in the lower intestine but can be a causative agent of blood-stream infections and UTIs (urinary tract infections); *S. aureus* is a clinically relevant pathogen which is responsible for toxic shock syndrome, postoperative wound infection, and food poisoning; *P. aeruginosa* is recognised for its biofilm formation and antibiotic resistance; *B. subtilis*, though non-pathogenic, is heat-resistant and causes bread spoilage.[43]

The Mueller-Hinton broth (MHB) used for the MIC assays was supplemented with metal ions (Mg^{2+} and Ca^{2+}) to better approximate the *in vivo* activities of our peptoids. It has been shown that these ions are vital for peptidoglycan synthesis, cell wall integrity and cell lysis prevention.[44,45] The mechanism of action of the peptoids against bacteria shows that these processes are specifically targeted, and so depriving bacteria of these elements would

invalidate the results. Detailed experimental procedures for the assays used can be found in **Chapter 7**.

In summary, the determination of the MIC values for each of the peptoids was carried out by applying MHB microdilution in 96 well plates. Three biological repeats in triplicates, reflecting three separate bacterial colonies, were used for each compound. Serial dilutions of 100 μM to 2 μM were carried out, wherein a negative control (DMSO only) was used, and wells containing medium only were used to correct for background absorption. This was followed by a subsequent overnight inoculation of the bacterial samples at 37 ^{o}C. The percentage growth within plates was determined and MIC values were calculated. MIC values are expressed as concentrations of peptoids at which at least 90% of bacteria were shown to be inviable. Interestingly, for most of the peptoids the increasing concentrations showed no effect on viability until MIC was reached and all of the bacterial cells were found to be killed.

Upon completion of the antibacterial screening, it was found that many of the peptoids in the library showed a substantial reduction in bacterial viability at low concentrations (**Table 2.8**).

Table 2.8. A tabulated summary of peptoids tested against four bacterial species, together with their ED_{50} values against HepG2, and SI values. All peptoids in this library have a C-terminal amide.

Entry	No.	Structure	ED_{50} (μM) HepG2	MIC (μM)				SI			
				E. coli	*P. aeruginosa*	*S. aureus*	*B. subtilis*	*E. coli*	*P. aeruginosa*	*S. aureus*	*B. subtilis*
1	**Pep. 15**	*N*Lys*N*2*f*et*N*spe[*N*Lys*N*2*f*et*N*et]$_4$	N/A	100	100	100	100	N/A	N/A	N/A	N/A
2	**Pep. 16**	*N*Lys*N*3*f*et*N*spe[*N*Lys*N*3*f*et*N*et]$_4$	N/A	100	100	100	50	N/A	N/A	N/A	N/A
3	**Pep. 17**	*N*Lys*N*1*f*et*N*spe[*N*Lys*N*1*f*et*N*1*f*et]$_4$	N/A	100	100	100	100	N/A	N/A	N/A	N/A
4	**Pep. 18**	*N*Lys*N*2*f*et*N*spe[*N*Lys*N*2*f*et*N*2*f*et]$_4$	N/A	100	100	100	25	N/A	N/A	N/A	N/A
5	**Pep. 6**	[*N*Lys*N*spe*N*spe]$_4$	16.3	6.25	12.5	3.13	1.56	2.6	1.3	5.2	10.4
6	**Pep. 12**	[*N*ae*N*spe*N*spe]$_4$	16.8	3.13	25	1.56	1.56	5.4	1	10.8	10.8
7	**Pep. 20**	[*N*Lys*N*Phe*N*Phe]$_4$	47.8	6.25	12.5	12.5	3.13	7.65	3.82	3.82	15.3
8	**Pep. 23**	[*N*Lys*N*pfb*N*spe]$_4$	24.5	3.13	12.5	3.13	1.56	7.8	2	7.8	15.6
9	**Pep. 24**	[*N*Lys*N*pfb*N*pfb*N*Lys*N*spe*N*spe]$_2$	19.6	3.13	12.5	3.13	1.56	6.3	1.5	6.3	12.6
10	**Pep. 25**	*N*amy*N*spe*N*spe[*N*Lys*N*spe*N*spe]$_3$	23.7	3.13	25	3.13	1.56	7.6	1	7.6	15.2
11	**Pep. 26**	*N*Lys*N*pfb*N*pfb[*N*Lys*N*spe*N*spe]$_3$	22.7	3.13	12.5	1.56	1.56	7.3	1.8	14.6	14.6
12	**Pep. 27**	*N*Lys*N*1*f*et*N*1*f*et[*N*Lys*N*spe*N*spe]$_3$	100	6.25	25	3.13	1.56	16	4	32	64
13	**Pep. 28**	*N*Lys*N*2*f*et*N*2*f*et[*N*Lys*N*spe*N*spe]$_3$	100	6.25	25	3.13	3.13	16	4	32	32
14	**Pep. 29**	*N*et$_3$ae*N*spe*N*spe[*N*Lys*N*spe*N*spe]$_3^+$	19.4	6.25	50	3.13	3.13	3.1	1	6.2	6.2
15	**Pep. 30**	*N*bnet$_2$ae*N*spe*N*spe[*N*Lys*N*spe*N*spe]$_3^+$	34.6	6.25	50	3.13	3.13	5.5	1	11.1	11.1
16	**Pep. 31**	*N*et$_3$ae*N*1*f*et*N*1*f*et[*N*Lys*N*spe*N*spe]$_3^+$	100	6.25	100	12.5	1.56	16	1	8	64
17	**Pep. 32**	*N*bnet$_3$ae*N*1*f*et*N*1*f*et[*N*Lys*N*spe*N*spe]$_3^+$	100	6.25	100	3.13	1.56	16	1	32	64
18	**Pep. 33**	*N*bnet$_3$ae*N*2*f*et*N*2*f*et[*N*Lys*N*spe*N*spe]$_3^+$	100	6.25	100	3.13	1.56	16	1	32	64
19	**Pep. 34**	*N*et$_2$pgae*N*2*f*et*N*2*f*et[*N*Lys*N*spe*N*spe]$_3^+$	100	6.25	100	3.13	1.56	16	1	32	64
20	**Pep. 35**	*N*et$_3$ae*N*1*f*et*N*1*f*et[*N*ae*N*spe*N*spe]$_3^+$	100	6.25	100	6.25	1.56	16	1	16	64
21	**Pep. 36**	[*N*et$_3$ae*N**f*et*N*1*f*et*N*Lys*N*spe*N*spe]$_2^{2+}$	100	100	100	100	25	1	1	1	4
22	**Pep. 37**	[*N*et$_2$bnae*N*Phe*N*Phe*N*Lys*N*spe*N*spe]$_2^{2+}$	52.5	6.25	50	3.13	3.13	8.40	1.04	16.8	16.8
23	**Pep. 38**	[*N*bnet$_3$ae*N*1*f*et*N*spe*N*ae*N*spe*N*spe]$_2^{2+}$	100	6.25	100	6.25	1.56	16	1	16	64

The desire to produce antibacterials selective for the Gram-negative pathogens remains the main goal of numerous researchers due to their high resistance to current antibiotics. It is evident that, as expected, none of the peptoid chains in this library show selective targeting for Gram-negative (*E. coli* and *P. aeruginosa*) species. It has been documented that peptoids target the outer membrane of Gram-negative bacteria, as they are initially attracted to the negatively charged lipopolysaccharides, which constitute a major part of the outer membrane. However, it is also the presence of these highly ordered structures which leads to the formation of a permeability barrier for antibacterial agents, including hydrophobic cationic peptoids.

Despite the challenges instigated by the Gram-negative outer membranes, it is valuable to point out that nearly all the peptoid MIC values against *E. coli* were lower than the AMP magainin-2. Per several studies, the *E. coli* MIC values of magainin-2 exceeded 10 μM.[46,47]

Meanwhile, the lowest MIC achieved in our *E. coli* assays was 3.13 μM, exhibited by several peptoids (**Table 2.8**, **Entries 12** and **23 – 26**). It is unsurprising that magainin-2 derivatives show increased antibiotic activities as peptoids show complete resistance to degradation by bacterial enzymes.[48] Whilst some of the peptoids have been previously screened against *E. coli* by the Cobb group, the MIC values reported in the past were not comparable to ours.[36] It can be suggested that the use of a different *E. coli* strain as well as the utilisation of MHB instead of LB media were both a contributing factor.

Pep. 6 (**Table 2.8**, **Entry 5**) and **Pep. 20** (**Table 2.8**, **Entry 7**) contain analogues of the amino acid phenylalanine (*N*Phe), and **Pep. 6** possesses a chirality factor introduced by the added C_α methyl. This affects the amide bond conformation, wherein the *N*spe monomer induces *cis* amide bond geometry to a greater extent. This leads to tighter alpha helices. It is evidenced by our MIC investigation that the helical character of peptoids does not significantly affect their antibiotic potency against Gram-negative bacterial species. Meanwhile, the substitution of the *N*spe monomers with *N*Phe in peptoids leads to a decreased activity of the peptoids against the Gram-positive bacteria, with the MIC values showing a four- and two-fold increase in *S. aureus* (3.13 μM for **Pep. 6** to 12.5 μM for **Pep. 20**, **Table 2.8**, **Entries 5** and **7**) and *B. subtilis* (1.56 μM for **Pep. 6** to 3.13 μM for **Pep. 20**, **Table 2.8**, **Entries 5** and **7**), respectively.

Initially, we wished to investigate the relationship between net charge and hydrophobicity of a peptoid and its biological activity, for which **Pep. 25** (**Table 2.8**, **Entry 10**), with an overall net charge of +2 was synthesised. Here, two of the *N*Lys **52** monomers

were replaced with the neutral alkyl *N*amy. This peptoid was previously reported in the literature to exhibit much lower antibiotic activity against both Gram-negative and Gram-positive bacteria, evidencing the importance of the overall positive charge on cell viability. In our investigation, we found that the *E. coli* strain that the peptoids were screened against showed a two-fold higher susceptibility to peptoid **Pep. 25** (3.13 μM, **Table 2.8**, **Entry 10**) relative to peptoid **Pep. 6** (6.25 μM, **Table 2.8**, **Entry 5**). The effect on *P. aeruginosa* was inverse, resulting in a two-fold higher MIC value for **Pep. 25** than **Pep. 6** (25 μM vs 12.5 μM, **Table 2.8**, **Entries 10** and **5**). Meanwhile, **Pep. 12** (*E. coli* MIC of 3.13 μM; *S. aureus* MIC of 1.56 μM, **Table 2.8**, **Entry 6**) wherein *N*Lys was replaced with a shorter *N*ae showed a two-fold increase in the MIC values for *E. coli* and *S. aureus* relative to **Pep. 6** (*E. coli* MIC of 6.25 μM; *S. aureus* MIC of 3.13 μM, **Table 2.8**, **Entry 5**). On the contrary, the *P. aeruginosa* cell viability for **Pep. 25** (*P. aeruginosa* MIC value of 25 μM) was increased two-fold relative to **Pep. 6** (*P. aeruginosa* MIC value of 12.5 μM).

In comparison to our control magainin mimic **Pep. 6** (**Table 2.8**, **Entry 5**), fluoroaryl-containing peptoids **Pep. 23** (**Table 2.8**, **Entry 8**), **Pep. 24** (**Table 2.8**, **Entry 9**), and **Pep. 26** (**Table 2.8**, **Entry 11**), all showed increased potency against *E. coli* whereby the MIC values decreased two-fold from 6.25 μM (**Pep. 6**) to 3.13 μM for all three peptoids (**Pep. 23**, **Pep. 24**, **Pep. 26**). For the Gram-positive *S. aureus*, the MIC value for **Pep. 26** saw a two-fold decrease to 1.56 μM compared to **Pep. 6** (3.13 μM), whilst the *S. aureus* cell viability values for **Pep. 23** (3.13 μM), and **Pep. 24** (3.13 μM) were unchanged. Evidently, this improvement in antibiotic properties of **Pep. 26** against *S. aureus* can be attributed to the incorporation of the monofluorinated monomers in the *N*-terminal *N*Lys*N*x*N*x motif, likely resulting in an overall increased lipophilicity and an enhanced targeting of the bacterial envelope. **Section 2.3.9** contains a detailed discussion of the log *D* study of this peptoid library. The increase in the overall antimicrobial effects could also be attributed to a decreased helicity of peptoids containing the *N*pfb **41** monomer, because this monomer has lesser *cis*-inducing effect on the amide bond than **2**.

Meanwhile, where the fluorinated aliphatic monomers *N*1*f*et **31** and *N*2*f*et **32** were used to substitute the *N*x building blocks in the *N*-terminal *N*y*N*x*N*x motif (**Pep. 28, Table 2.8**, **Entry 13** and **Pep. 27 Table 2.8**, **Entry 12**), the antibiotic activity against *E. coli* remained unchanged relative to **Pep. 6** (**Table 2.8**, **Entry 5**), at 6.25 μM. Additionally, in the case of these two peptoids, the cell viability for *P. aeruginosa* was two-fold higher relative to **Pep. 6**

(*P. aeruginosa* MIC for **Pep. 27** and **Pep. 28** = 25 μM; *P. aeruginosa* MIC for **Pep. 6** = 12.5 μM). Both **Pep. 27** and **Pep. 28** resulted in a two-fold increase in the MIC values for *B. subtilis*, relative to **Pep. 6** (*B. subtilis* MIC for **Pep. 27** and **Pep. 28** = 3.13 μM; *B. subtilis* MIC for **Pep. 6** = 1.56 μM). No effect was observed on the MIC values for *S. aureus* (*S. aureus* MIC for **Pep. 6**, **Pep. 27** and **Pep. 28** = 3.13 μM). Accounting for these results, it could be implied that in a membrane environment the global peptoid folding is not greatly affected by *N*1*f*et-containing **Pep. 27** and *N*2*f*et-containing **Pep. 28** as to produce a substantial change in the antibiotic properties of peptoids relative to **Pep. 6**. This is despite their effects on the local peptoid folding and their vastly different $K_{cis/trans}$ values reported in the literature.

Nonetheless, the 15-mer fluorine-rich peptoids (**Pep. 15 – Pep. 18**, **Table 2.8**, **Entries 1 – 4**) show no discernible antimicrobial properties against any of the bacterial species. It can hypothesised that, given their vastly different MIC values, the added degree of fluorous effect stemming from the fluorinated alkyl monomers leads to a decreased potency of these peptoids against all bacterial targets.

Peptoids containing cationic tertiary ammonium peptoid building blocks were found to show a considerably higher selectivity against *E. coli* compared to the Gram-negative *P. aeruginosa*. Within each species, **Pep. 35** (**Table 2.8**, **Entry 20**) and **Pep. 31 – Pep. 34** (**Table 2.8**, **Entry 16 – 19**) showed no difference in the MIC values (*E. coli* MIC = 6.25 μM, *P. aeruginosa* MIC = 100 μM, *S. aureus* MIC = 3.13 μM and *B. subtilis* MIC = 1.56 μM for **Pep. 35** and for **Pep. 31 – Pep. 34**), but the SI values for *E. coli* were 16-fold (*E. coli* SI = 16 for **Pep. 35** and **Pep. 31 – Pep. 34**) higher than the SI value found for *P. aeruginosa* (*P. aeruginosa* SI = 16 for **Pep. 35** and **Pep. 31 – Pep. 34**).

Meanwhile, *N*et$_3$ae-containing **Pep. 29** (**Table 2.8**, **Entry 14**) and **Pep. 30** *N*bnet$_3$ae-containing (**Table 2.8**, **Entry 15**) which both contained the chiral aromatic monomer *N*spe **2** in their *N*-terminal *N*y*N*x*N*x motifs allowed for a direct comparison of the *N*-terminal *N*Lys **52** substitutions in the magainin mimic **Pep. 6**. The introduction of the cationic quaternary ammonium monomers decreased the antibiotic potency **Pep. 29** and **Pep. 30** showed a four-fold increase in the MIC values for *P. aeruginosa*, relative to **Pep. 6** (*P. aeruginosa* MIC for **Pep. 29** and **Pep. 30** = 50 μM; for **Pep. 6** = 12.5 μM). These variable antibiotic effects of these peptoids on the two species can be attributed to the intrinsic ability of *P. aeruginosa* to form biofilms in the assay wells. Indeed, upon closer inspection, the formation of a surface film was noticed. Hancock[49] and co-workers reported that cationic AMPs lead to upregulation of genes

responsible for outer membrane permeability and biofilm formation in *P. aeruginosa*. Perhaps, the added cationic character in peptoids is likely to trigger this response rendering them ineffective as antibiotic agents against this species.

Interestingly, considering the sequences **Pep. 36 - 38** (**Table 2.8**, **Entries 21 – 23**) where the *N*y*N*x*N*x motifs containing the cationic ammonium and fluorinated aliphatic monomers were inserted into these peptoids twice, the overall antibacterial effect is strikingly different, when compared to **Pep. 6** (**Table 2.8**, **Entry 5**). The added cationic change would, in theory, imply an increased bacterial membrane targeting. Relative to the *N*et$_3$ae -containing **Pep. 36** (*E. coli* MIC of 100 μM, *P. aeruginosa* MIC of 100 μM, **Table 2.8**, **Entry 21**), the incorporation of a terminal *N*bnet$_3$ae into **Pep. 38** (*E. coli* MIC of 6.25 μM, *P. aeruginosa* MIC of 100 μM, **Table 2.8**, **Entry 23**), showed a 16-fold enhancement in the antibiotic potency against *E. coli* whilst showing no change in the MIC value for *P. aeruginosa*. Furthermore, replacing the *N*x in the terminal *N*y*N*x*N*x motif with the achiral aromatic *N*Phe to produce **Pep. 37** (*P. aeruginosa* MIC of 50 μM) yielded a two-fold decrease in the MIC value for *P. aeruginosa*. **Pep. 36** showed no significant efficacy against *S. aureus* (MIC = 100 μM) and the replacement of the *N*-terminal *N*et$_3$ae **Pep. 30** with *N*bnet$_3$ae showed a 16-fold decrease in the MIC value for **Pep. 38** (*S. aureus* MIC = 6.25 μM). The substitution of the terminal fluorinated achiral aliphatic monomers with *N*Phe, in the *N*y*N*x*N*x motif, yielded a two-fold increase in antibiotic potency for **Pep. 37** against *S. aureus* (MIC = 3.13 μM) compared to **Pep. 38**. Meanwhile, out of these three peptoids, **Pep. 38** exerted the highest antibiotic effect on *B. subtilis* (MIC value for **Pep. 38** = 1.56 μM vs 25 μM for **Pep. 36** and 3.13 μM for **Pep. 38**).

2.3.7. Cytotoxicity assays against liver cell line HepG2

In addition to the antimicrobial activity, low cytotoxicity is a required characteristic for novel antibiotic candidates. Based upon the cationic nature of AMPs, peptoids were designed in a similar fashion as to interact with bacterial membranes electrostatically. Nevertheless, due to structural ambiguities relating to cytotoxicity of antimicrobial peptoids, it was desired to evaluate the corresponding SI (selectivity index) values for each of the antimicrobial peptoids. SI is a simple parameter which quantifies the selectivity of compounds and describes the ratio of HepG2 ED_{50} to the bacterial MIC (ED_{50}/MIC). Importantly, the utilisation of SI values enables a simple predictor of a given peptoids potential off-target effects and hence cytotoxicity to host cells. Indeed, previous reports[36] suggest that on optimal combination of specific structural features favouring an improved selectivity without losing activity is not easily achieved. The incorporation of diverse peptoid monomers can result in considerable changes in global peptoid folding, and it can be detrimental to the SI values. In order to warrant further advancements in this area, rational design methods must be sought out to identify sequence specificities which ensure selective antimicrobial targeting.

A high throughput resazurin staining (alamarBlue®) assay was applied to investigate the cytotoxicity of peptoids to mammalian cells. The advantage of using this assay is that it provides a quantitative assessment of living cells in the sample. Upon entering viable cells, the weakly fluorescent blue stain turns fluorescent pink, and its emission intensity is correlated to cell viability. (**Scheme 2.6**)

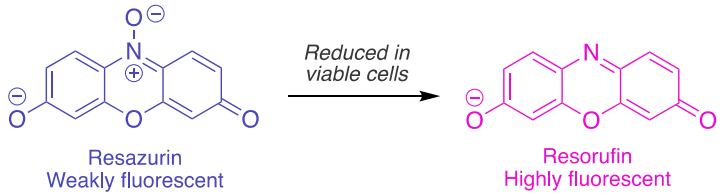

Scheme 2.6. Reduction of Resazurin, used in the alamarBlue® assay, to Resofurin which is highly fluorescent. The reduction takes place in mitochondria of the viable HepG2 cells.

The immortal liver cancer HepG2 cell line was utilised for the cytotoxicity assays. The immortal HepG2 liver carcinoma cells are often used in cytotoxicity studies to model toxicity to human liver cells. Immortal cell lines are used for cytotoxicity assays due to their high proliferation and reproducibility. A photograph of HepG2 cells is shown in **Figure 2.19**, and shows the formation of an epithelial tissue, characteristic for this cell line. It is important to

mention that in order to gather robust data, the biological repeats carried out for the cytotoxicity assays were within 4 passages, and none of the repeats were performed on passages >20.

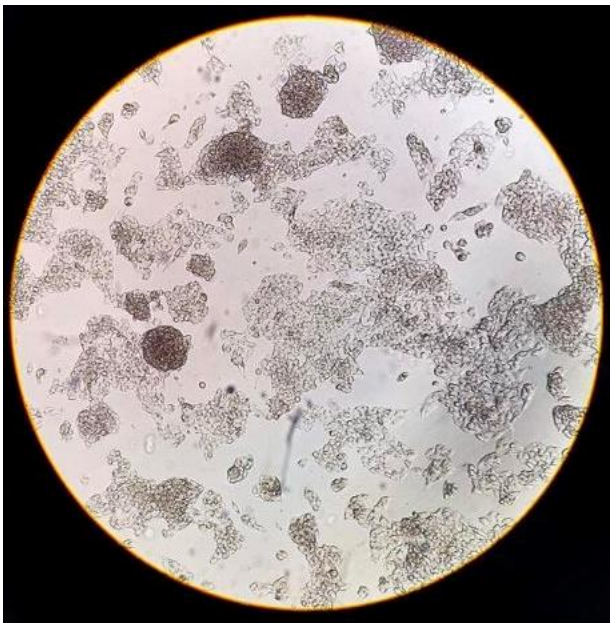

Figure 2.19. Photograph taken of HepG2 on the passage before cytotoxicity testing.

ED_{50} values (median effective dose/concentration values at which 50% of mammalian cells are found to be inviable) for the library were calculated. Similar to the MIC determination the assays were carried out in 96 well plates in triplicates on at least two occasions, using serial dilutions of 100 μM to 1.56 μM. The controls which were added to the plate were: amphotericin B (positive control), DMSO only (negative control) and wells containing medium only were used in order to correct for background fluorescence. HepG2 cells were incubated in wells overnight at 37 ^{o}C, the solutions were removed in the morning and new media containing various peptoid concentrations were added. After 20 hours of further incubation, alamarBlue® was added in order to measure cell viability by UV fluorescence.

Numerous compounds tested as antimicrobial agents were found to show potent bioactivities, and it was thus desired to investigate their toxicity to mammalian cells. The magainin-2 mimic **Pep. 6** (**Table 2.8**, **Entry 7**) showed the lowest ED_{50} of 16.3 μM and comparing its SI values to its achiral counterpart **Pep. 20**, it is apparent that chirality results in higher cytotoxicity, with the ED_{50} value being almost three-fold lower for **Pep. 6** compared to **Pep. 20** (ED_{50} of 47.8 μM, **Table 2.8**, **Entry 23**). Likewise, the inclusion of the achiral aromatic *N*pfb showed decreased cytotoxicity, with ED_{50} values for **Pep. 23** (ED_{50} of 24.5 μM,

Table 2.8, **Entry 5**), **Pep. 24** (ED_{50} of 19.6 μM, **Table 2.8**, **Entry 12**) and **Pep. 26** (ED_{50} of 22.7 μM, **Table 2.8**, **Entry 13**) being 1.2 to 1.5 higher. The effect of chirality on increased mammalian toxicity has been previously briefly documented by the Cobb group.[36] Furthermore, tightly folded α-helical AMPs have also shown increased cytotoxicity and increased haemolytic effects.[36]

The inclusion of cationic quaternary ammonium monomers had a less substantial effect on the HepG2 ED_{50}. It was found that the added aromaticity of the *N*bnet$_2$ae monomer (**Pep. 30**, ED_{50} 34.6 μM, **Table 2.8**, **Entry 14**) resulted in a two-fold increase in cell viability, but the substitution of the *N*-terminal *N*Lys with *N*et$_3$ae (**Pep. 29**, ED_{50} 19.4 μM, **Table 2.8**, **Entry 9**) showed only a marginal improvement compared to the magainin mimic **Pep. 6** (ED_{50} = 16.3 μM, **Table 2.8**, **Entry 7**)

Numerous peptoids which showed no toxicity to the HepG2 cell line were identified. Notably, the inclusion of the fluorinated achiral aliphatic submonomers led to no noticeable effect on the HepG2 cell viability (ED_{50} values for **Pep. 27**, **Pep. 28**, **Pep. 31 – 36** and **Pep. 38** were 100 μM, **Table 2.8**, **Entries 10**, **11**, **15**, **16** and **18 – 22**), even where a relatively high degree of chiral aromatic monomers was used (**Pep. 31 – 34**, **Pep. 38**). In turn, this resulted in impressive SI values measured for for **Pep. 27**, **Pep. 28**, **Pep. 31 – 36** and **Pep. 38**, wherein SI >10 for three out of four bacterial species (excluding *P. aeruginosa*), with the Gram-negative *E. coli* showing SI of 16 for all these peptoids except for **Pep. 36**. Interestingly, **Pep. 28** (**Table 2.8**, **Entry 10**) and **Pep. 27** (**Table 2.8**, **Entry 11**) both showed SI of 4 against the Gram-negative *P. aeruginosa* which was the highest value out of all the peptoids screened in this chapter. Whilst decreased cytotoxicity typically leads to compromised antibacterial activity, peptoids **Pep. 27** and **Pep. 28** showed a marginal reduction in the bacterial MIC values but they were completely non-toxic to HepG2.

2.3.8. Relationship between HPLC t_R and peptoid antimicrobial activity and cytotoxicity

As an important Lipinski's Rule of 5 component, hydrophobicity of a molecule is possibly the most important physicochemical property of drug candidates. As well as determining drug solubility, absorption, and membrane penetration, it plays a crucial role in drug partitioning into organs and tissues. Drug elimination from the body is also heavily dependent on its hydrophobicity.

Correlations between HPLC t_R and antimicrobial activities were investigated. In our data, peptoids eluting at more than 20 minutes were found to result in very low MIC values, whilst polar peptoids resulted in higher MIC values, for both Gram-positive species and *E. coli*. *P. aeruginosa* MIC values showed lower susceptibility to the antimicrobial action of polar peptoids. However, hydrophobic peptoids showed significant activity against all species. These relationships are shown in **Figure 2.20**. This suggests that peptoids with higher lipophilicity (as indicated by greater retention times in the RP C18 HPLC column) exhibit enhanced antimicrobial activity. In the previous study,[50] the cut-off point for t_R was approximately 22 minutes. Notably, almost all the peptoids investigated in this chapter that eluted at more than 20 minutes demonstrated lower MIC values. The exact mechanism underlying this relationship between lipophilicity and antimicrobial activity would require further investigation, but the data suggests a definite trend.

Peptoids which showed no considerable reduction in bacterial cell viability were not subjected to the cytotoxicity screening. (**Figure 2.21**) The scope of t_R covered by our antimicrobial peptoids is limited. When comparing the toxicity (HepG2 ED_{50} values) of the library to the t_R, no relationship between the two is seen. However, numerous compounds show no cytotoxic properties and could have the potential to positively contribute to the production of new antibiotics.

Based on this analysis, whilst hydrophobic peptoids do show enhanced efficacy against the four species of bacteria used, they can also lead to undesirable toxicity against mammalian cells. In addition, HPLC t_R offers some utility, it is not an ideal metric for achieving rational peptoid design. The ultimate goal is to develop tools to predict and understand peptoid behaviour both *in vitro* and *in vivo*.

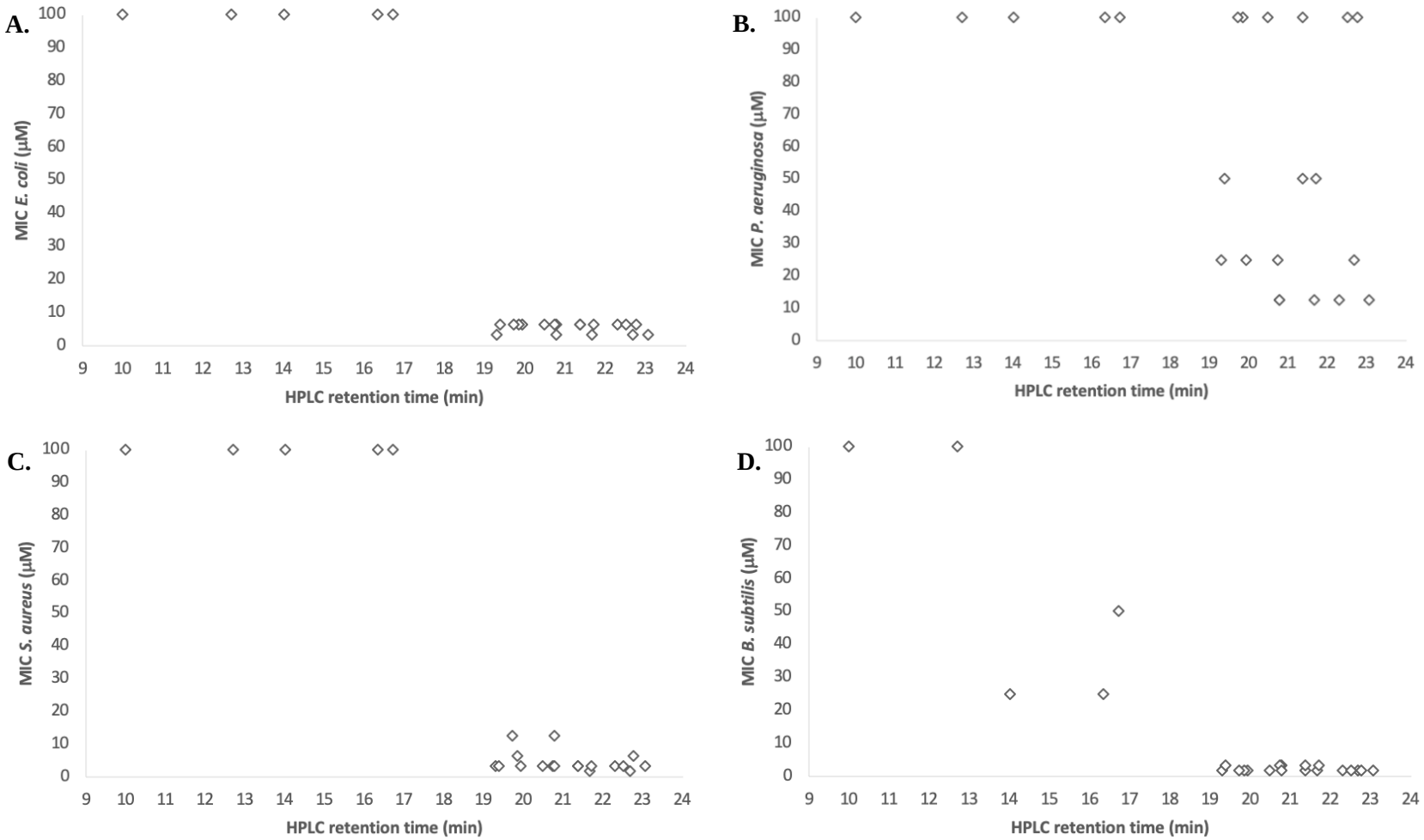

Figure 2.20. Relationships between the HPLC t_R and MIC values for pathogens screened against **A.** *E. coli*, **B.** *P.aeruginosa*, **C.** *S. aureus* and **D.** *B. subtilis*.

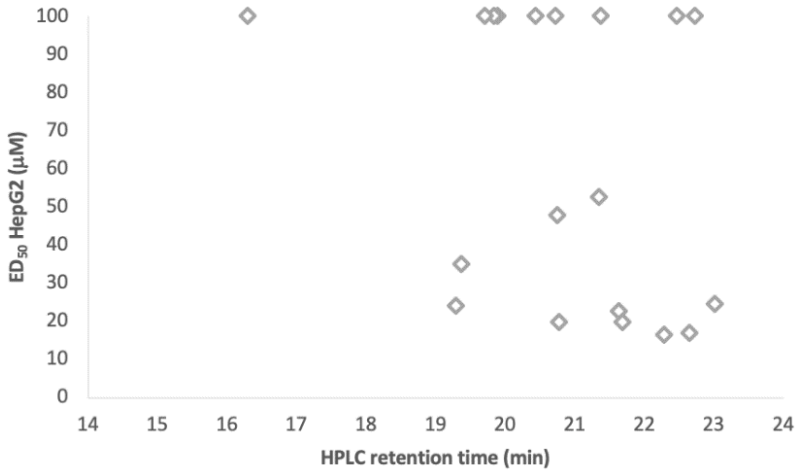

Figure 2.21. Relationship between the HPLC t_R and HepG2 ED_{50} values.

2.3.9 Log *D* measurements vs. HPLC-derived t_R: measure of peptoid lipophilicity

In many cases, it is not practical to determine the log *D* of every compound made in a library, especially where high throughput screening is involved, and where libraries can be very large. It is far more practical to utilise software tools which have access to large datasets of known values which can be used to determine functional group substitutions for each potential drug candidate. Nevertheless, due to global peptoid folding not being completely understood, such databases are not applicable in predicting peptoid log *D* values.

Prior to the study conducted by the Cobb group in 2017,[50] the utilisation of log *D* values, or partitioning experiments, had not been documented for peptoids. In order to expand on this work, it was decided that log *D* values of all of the peptoids which showed promising antimicrobial properties would be investigated.

To measure log *D* values for our peptoids, we utilised PBS buffer solution due to its neutral pH 7.4 and its ion concentrations which make it isotonic with blood plasma. Octanol was chosen as the organic phase in the experiments as its alkyl chain and polar hydroxyl moieties make it comparable to the phospholipid bilayer present in the cell membranes. Log *D* experiments are more representative of a biological system than RP HPLC t_R. To calculate the logarithmic ratio of the distribution coefficient (*D*), the equilibrium ratios of peptoid concentrations in PBS and octanol are used. It follows that a positive log *D* value indicates that the compound partitions in PBS more preferentially than in octanol, and vice versa. Hence, a higher value for the partitioning experiments signifies that the peptoid will be more hydrophilic than hydrophobic.

A detailed protocol for the partitioning experiments carried out in this thesis is described in **Chapter 7**. In summary, 300 mM solution of peptoid in PBS was added to an equal volume of octanol (500 μL) and left to agitate gently for 8 full days in order to reach equilibrium. For each peptoid, three repeats were carried out, and the absorption of each phase was measured by UV-Vis spectroscopy; and the Beer-Lambert law was utilised in order to calculate the accurate peptoid concentrations in each phase. Subsequently, peptoid hydrophobicity was determined using the log *D* equation shown in **Figure 2.22**. The log *D* values calculated for our antimicrobial peptoids are summarised in **Table 2.9**.

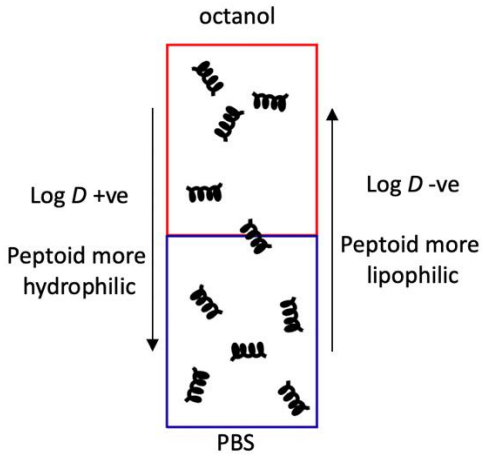

Log *D* = log ([PBS]/[octanol])

Figure 2.22. A diagram depicting the experimental set-up for hydrophobicity experiments. The equation representing the distribution coefficient *D* as a logarithm of the ratio between peptoid concentrations in PBS and octanol is also shown.

Table 2.9. A summary of peptoids tested against four bacterial species, together with their HPLC t_R and log *D* values. (nd = no data recorded)

Entry	No.	Structure	HPLC t_R (min)	Log *D*
1	**Pep. 13**	*N*LysNetNspe[*N*Lys*N*et*N*et]$_4$	12.50	nd
2	**Pep. 14**	*N*Lys*N*1*f*et*N*spe[*N*Lys*N*1*f*et*N*et]$_4$	10.50	nd
3	**Pep. 15**	*N*Lys*N*2*f*et*N*spe[*N*Lys*N*2*f*et*N*et]$_4$	12.70	nd
4	**Pep. 16**	*N*Lys*N*3*f*et*N*spe[*N*Lys*N*3*f*et*N*et]$_4$	16.70	nd
5	**Pep. 17**	NLysN1*f*etNspe[*N*Lys*N*1*f*et*N*1*f*et]$_4$	10.00	nd
6	**Pep. 18**	NLysN2*f*etNspe[*N*Lys*N*2*f*et*N*2*f*et]$_4$	14.00	nd
7	**Pep. 19**	*N*Lys*N*3*f*et*N*spe[*N*Lys*N*3*f*et*N*3*f*et]$_4$	17.40	nd
8	**Pep. 6**	[*N*Lys*N*spe*N*spe]$_4$	22.30	1.22
9	**Pep. 12**	[*N*ae*N*spe*N*spe]$_4$	22.67	-2.03
10	**Pep. 20**	[*N*Lys*N*Phe*N*Phe]$_4$	20.77	-0.08
11	**Pep. 23**	[*N*Lys*N*pfb*N*spe]$_4$	23.04	-0.36
12	**Pep. 24**	[*N*Lys*N*pfb*N*pfb*N*Lys*N*spe*N*spe]$_2$	20.78	0.96
13	**Pep. 25**	*N*amy*N*spe*N*spe[*N*Lys*N*spe*N*spe]$_3$	19.30	-1.26
14	**Pep. 26**	*N*Lys*N*pfb*N*pfb[*N*Lys*N*spe*N*spe]$_3$	21.65	0.07
15	**Pep. 27**	*N*Lys*N*1*f*et*N*1*f*et[*N*Lys*N*spe*N*spe]$_3$	19.91	1.18
16	**Pep. 28**	*N*Lys*N*2*f*et*N*2*f*et[*N*Lys*N*spe*N*spe]$_3$	20.73	0.00
17	**Pep. 29**	*N*et$_3$ae*N*spe*N*spe[*N*Lys*N*spe*N*spe]$_3^+$	21.70	-0.17
18	**Pep. 30**	*N*bnet$_2$ae*N*spe*N*spe[*N*Lys*N*spe*N*spe]$_3^+$	19.38	-0.80
19	**Pep. 31**	*N*et$_3$ae*N*1*f*et*N*1*f*et[*N*Lys*N*spe*N*spe]$_3^+$	19.73	-1.25
20	**Pep. 32**	*N*bnet$_3$ae*N*1*f*et*N*1*f*et[*N*Lys*N*spe*N*spe]$_3^+$	21.38	0.06
21	**Pep. 33**	*N*bnet$_3$ae*N*2*f*et*N*2*f*et[*N*Lys*N*spe*N*spe]$_3^+$	20.46	1.00
22	**Pep. 34**	*N*et$_2$pgae*N*2*f*et*N*2*f*et[*N*Lys*N*spe*N*spe]$_3^+$	22.49	-0.04
23	**Pep. 35**	*N*et$_3$ae*N*1*f*et*N*1*f*et[*N*ae*N*spe*N*spe]$_3^+$	19.85	1.66
24	**Pep. 36**	[*N*et$_3$ae*N*f*et*N*1*f*et*N*Lys*N*spe*N*spe]$_2^{2+}$	16.32	-0.85
25	**Pep. 37**	[*N*et$_2$bnae*N*Phe*N*Phe*N*Lys*N*spe*N*spe]$_2^{2+}$	21.36	-0.45
26	**Pep. 38**	[*N*bnet$_3$ae*N*1*f*et*N*spe*N*ae*N*spe*N*spe]$_2^{2+}$	22.74	0.38

It was endeavoured to explore how the HPLC t_R of the peptoids correlated with the hydrophobicity values (log *D*) (**Table 2.9**). **Figure 2.23** depicts the relationship between the HPLC t_R and the log *D* values and at first glance it shows no obvious correlation between the two.

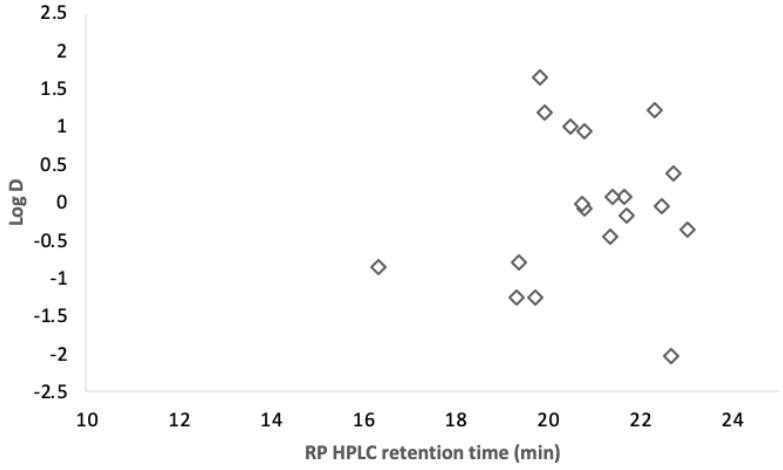

Figure 2.23. A graphical depiction of the relationship between RP HPLC t_R. and log *D* values of peptoids shown in **Table 2.9**. Notably, peptoids exhibiting the same HPLC t_R can have considerably different log *D* values.

An interesting situation arises where the terminal *N*y*N*x*N*x motif of peptoids **Pep. 6** ([*N*Lys*N*spe*N*spe]$_4$, **Table 2.9**, **Entry 8**) and **Pep. 12** ([*N*ae*N*spe*N*spe]$_4$, **Table 2.9**, **Entry 9**) is replaced with *N*et$_3$ae*N*1*f*et*N*1*f*et to give **Pep. 35** (*N*et$_3$ae*N*1*f*et*N*1*f*et[*N*ae*N*spe*N*spe]$_3$, **Table 2.9**, **Entry 23**) and **Pep. 31** (*N*et$_3$ae*N*1*f*et*N*1*f*et[*N*ae*N*spe*N*spe]$_3$, **Table 2.9**, **Entry 19**). The longer *N*Lys monomer, compared to *N*ae, confers a higher accessibility of the hydrogen-bonding primary amine; and therefore, one would expect peptoids containing longer-chain catonic monomers to show a higher preference for PBS in all instances. Comparing the log *D* values of the four peptoids (**Pep. 6**, **Pep. 12**, **Pep. 35**, **Pep. 31**), it was noticed that the partitioning pattern was reversed. **Pep. 6** (log $D_{(\textbf{Pep. 6})}$ = 1.22, **Table 2.9**, **Entry 8**) showed a switch in its partitioning preference from aqueous to organic (log $D_{(\textbf{Pep. 31})}$ = -1.24, **Table 2.9**, **Entry 19**); meanwhile, replacing the terminal repeating motif of **Pep. 12** (**Table 2.9**, **Entry 9**, log $D_{(\textbf{Pep. 12})}$ = -2.03) resulted in **Pep. 35** (**Table 2.9**, **Entry 23**, log $D_{(\textbf{Pep. 35})}$ value = 1.66) preferentially partitioning into the aqueous phase. The trend of preferential partitioning of peptoids into octanol, wherein the building blocks in the terminal motif are replaced with a cationic quaternary ammonium side chain or/and a fluorinated aliphatic side chain, prevails in this peptoid library.

Comparatively, as predicted, it was found that *N*2*f*et-containing **Pep. 28** (log $D_{(\textbf{Pep. 28})}$ = -0.01, **Table 2.9**, **Entry 16**) showed a greater preference for partitioning into octanol than *N*1*f*et-containing **Pep. 27** (log $D_{(\textbf{Pep. 27})}$ = 1.18, **Table 2.9**, **Entry 15**). This conforms to the previously reported studies[11,12] and can be explained by an increased dipole moment present within the *N*2*f*et monomer (**33**), compared to the *N*1*f*et (**32**) leading to an increased

hydrophobic surface.[35] Meanwhile, the *N*1*f*et-containing **Pep.27** (log $D_{(\mathbf{Pep.\ 27})}$ = 1.18, **Table 2.9**, **Entry 15**), resulted in a similar preference for PBS as the magainin mimic **Pep. 6** (log $D_{(\mathbf{Pep.\ 6})}$ = 1.23, **Table 2.9**, **Entry 8**). Henceforth, it can be postulated that the greater propensity for α-helical formation by *N*2*f*et compared to *N*1*f*et[33] resulted in a reduced availability of the cationic monomers to form intermolecular hydrogen bonds with its environment, rendering the peptoid containing this monomer much more lipophilic.

The HPLC t_R of **Pep. 36** ([*N*et$_3$ae*N*1*f*Et*N*1*f*Et*N*Lys*N*spe*N*spe]$_2^{2+}$, **Table 2.9**, **Entry 24**) was the shortest of all at 16.32 min, implying that it has the highest overall polarity, but it appeared to have fourth lowest log *D* value (-0.85), as it preferentially partitioned into octanol. This was likely caused by intermolecular interactions such as hydrogen bonding responsible for peptoid retention on the chromatography column, which cannot be considered an accurate measure of its preference for lipophobic environments. Certainly, the propensity of the *N*1*f*et and *N*et$_3$ae (**49**) monomers to encourage tightly bound helices rendered the peptoid unavailable for intermolecular bond formation with the silica column. This is corroborated by the log *D* value and HPLC t_R of peptoid **Pep. 37** ([*N*et$_2$bnae*N*Phe*N*Phe*N*Lys*N*spe*N*spe]$_2^{2+}$, -0.45 and 21.36 mins, respectively (**Table 2.9**, **Entry 25**). The achiral *N*Phe (**40**) (**Pep. 20**, **Table 2.9**, **Entry 10**) has a lesser predisposition to form *cis* amide bonds, which is reflected in its higher HPLC t_R, and a lower log *D* value compared to **Pep. 36** (**Table 2.9, Entry 24**). This result was opposite to that found for **Pep. 20** (wherein *N*x = *N*Phe), which was found to be more lipophilic than **Pep. 20** (log $D_{(\mathbf{Pep.\ 20})}$ = -0.08, **Table 2.9**, **Entry 10**; log $D_{(\mathbf{Pep.\ 6})}$ = 1.22, **Table 2.9**, **Entry 8**). Interestingly, peptoid **Pep. 38** showed preferential partitioning into PBS (log $D_{(\mathbf{Pep.\ 38})}$ = 0.38, **Table 2.9**, **Entry 26**), whilst its HPLC t_R was higher than the other two doubly charged cationic peptoids **Pep. 36** and **Pep. 37** (HPLC $t_{R(\mathbf{Pep.\ 38})}$ = 22.74 min, **Table 2.9**, **Entry 26**; HPLC $t_{R(\mathbf{Pep.\ 36})}$ = 16.32 min, **Table 2.9**, **Entry 24**; HPLC $t_{R(\mathbf{Pep.\ 37})}$ = 21.36 min, **Table 2.9**, **Entry 25**).

The relationship between log *D* and MIC values was investigated to determine if log *D* could serve as a reliable predictor of peptoid antimicrobial activity. The peptoids in our library covered a wide range of log *D* values, ranging from -2.02 (**Pep. 12**, **Table 2.9**, **Entry 9**) to 1.65 (**Pep. 35**, **Table 2.9**, **Entry 23**). **Figure 2.24** shows the graphs obtained for the two variables in all the bacterial species investigated in this chapter. While no definitive correlation between log *D* and MIC values can be easily seen for any of the bacteria studied an interesting observation emerges: the log *D* values for most efficacious peptoids tend to hover around 0 (interestingly, peptoids screened against bacterial targets in **Chapters 4** and **5** show a similar

pattern). Nevertheless, a more in-depth investigation is required to elucidate the underlying factors and relationships between log *D* values and antibacterial efficacy, as the current observations provide a basis for further exploration and understanding.

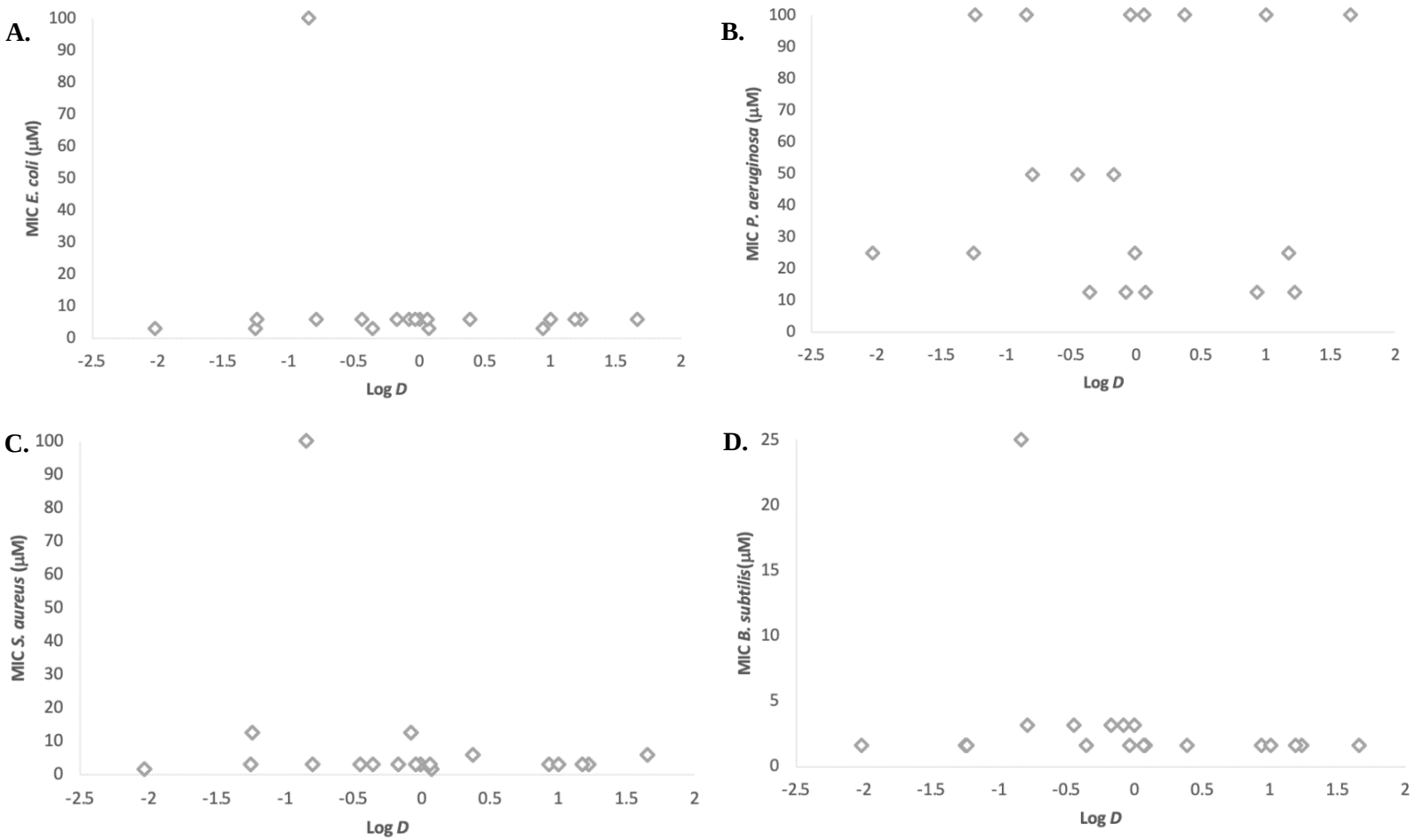

Figure 2.24. Charts depicting the relationship between log *D* values found for antimicrobial peptoids and their MIC values against **A.** *E. coli*, **B.** *P.aeruginosa*, **C.** *S. aureus* and **D.** *B. subtilis*.6fc

A different effect was noted for the ED_{50} HepG2/log *D* plot, wherein peptoids which displayed a preference for partitioning into PBS seemed to be less toxic to HepG2. This is an unsurprising result as numerous hydrophilic compounds have been previously reported to result in a lower overall cytotoxicity.[51,52] (**Figure 2.25**)

Low hydrophobicity reduces binding to the zwitterionic mammalian membranes, resulting in reduced cytotoxicity. Meanwhile, interactions with fatty acyl chains present within membranes are promoted by high hydrophobicity and are required for bacterial membrane permeabilisation. Glukhov[53] documented that breaching the optimal hydrophobicity will result in a loss of antimicrobial activity and an increase in mammalian cell toxicity. In this library, it was found that some peptoids with very similar log *D* values resulted in different in vitro activities. For example, peptoid **Pep. 27** had a comparable log *D* value to **Pep. 6**, but it displayed extremely low toxicity to HepG2 (100 μM) while maintaining very respectable efficacies against three of four pathogens (*E. coli* 6.25 μM; *S. aureus* 3.13 μM; *B. subtilis* 1.56 μM).

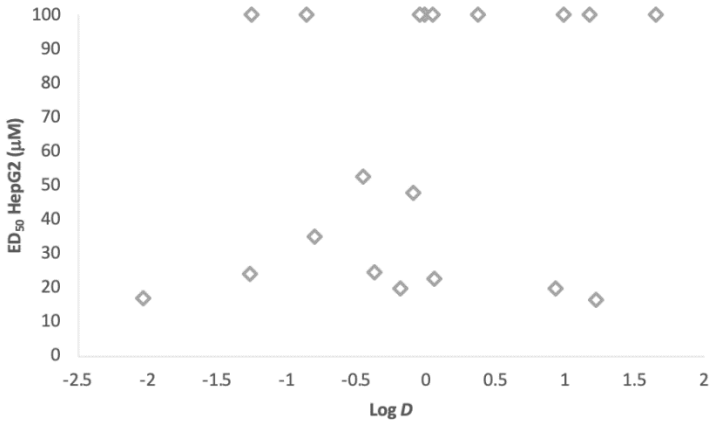

Figure 2.25. Relationship between the log *D* values found for antimicrobial peptoids and their HepG2 ED_{50} values.

2.4. Summary of Chapter 2

Being the most electronegative element, fluorine can have a strong effect on the basicity or acidity of nearby functional groups. The incorporation of fluorine into a compound can lead to its increased biding to the target active site due to fluoride's basic nature. A number of studies have also demonstrated that fluorine can aid physicochemical properties of peptides in biological systems.[1,5,6]

In the first part of this chapter, seven model 15-mer peptoids were produced, using the general peptoid synthesis (**Scheme 2.1**). Challenges arose during synthesis and purification due to the strongly electron-withdrawing properties of fluorine and the fluorous effect, impeding purification via RP HPLC. Consequently, significant optimisation efforts were necessary. However, due to minimal yield and inadequate antimicrobial activity (**Table 2.5**, **Table 2.8**, **Entries 1 – 4**), biophysical analysis of these peptoids was not carried out.

The second part of this chapter described the preparation of a library of peptoids (**Table 2.7**) which showed promising biological activities against a range of organisms (**Table 2.7**). In addition, a selection of fluorinated cationic peptoid dodecamers was obtained (**Figure 2.17**). The synthesis of these peptoids was not only less laborious but also much more time efficient compared to those initially investigated. This was also the case for their purification, whereby larger amounts of crude material were injected in each HPLC run. In turn, this enabled a quicker recovery of pure products, and higher yields. All the peptoids which have been successfully synthesised and purified, were obtained in >95% purities, as determined by analytical HPLC. In addition, optimisation of the cleavage step has been proposed, when working with peptoids containing a high degree of aromaticity.

Upon successful production of the peptoid dodecamers described in this chapter, they were employed in lipophilicity measurements, antibacterial and cytotoxicity assays. The experiments generated a range of interesting results. Notably, replacing the chiral aromatic *N*spe (**2**) monomers in the terminal repeat with fluoroalkyl building blocks *N*1*f*et (**32**) and *N*2*f*et (**33**) generated peptoids with greatly enhanced SI values for all the bacterial species tested. Moreover, the incorporation of achiral fluoroaromatic monomers (**32** and **33**) resulted in enhanced activities against the Gram-negative *E. coli*. The inclusion of *N*-terminal cationic quaternary ammonium monomers was found to have a less substantial effect on peptoid antimicrobial activities, and where two such monomers were involved, resulting in the overall peptoid charge 2+, it rendered **Pep. 36** (**Table 2.8**, **Entry 21**) and **Pep. 37** (**Table 2.8**, **Entry**

22) less efficacious compared to the magainin mimic **Pep. 6** (**Table 2.8**, **Entry 5**). In fact, peptoid **Pep. 36** was rendered completely inactive against both Gram-negative species and the Gram-positive *S. aureus*.

In the analysis of the log *D* values (**Table 2.9**), it was observed an interesting pattern. The inclusion of *N*-terminal *N*et$_3$ae*N*1*f*Et*N*1*f*Et motif exerted differing effects on peptoids containing *N*Lys monomers compared to those containing *N*ae monomers. Specifically, **Pep. 31**, log $D_{(\textbf{Pep. 31})}$ = -1.25, **Table 2.9**, **Entry 19,** (the counterpart of **Pep. 6**, log $D_{(\textbf{Pep. 6})}$ = 1.23, **Table 2.9**, **Entry 8**) demonstrated a shift in partitioning preference from aqueous to organic, whereas peptoid **Pep. 35**, log $D_{(\textbf{Pep. 35})}$ = -1.66, **Table 2.9**, **Entry 23**, (the counterpart of **Pep. 12**, log $D_{(\textbf{Pep. 12})}$ = 1.23, **Table 2.9**, **Entry 9**) showed the opposite shift from organic to aqueous partitioning preference. Notably, although peptoids with higher HPLC t_R values tended to exhibit increased antimicrobial properties, we did not find a direct correlation between the biological activities (both antimicrobial and cytotoxicity) of peptoids and their log *D* values. However, peptoids with log *D* values indicative of equal partitioning between octanol and PBS (log *D* = ~0) appeared to exhibit enhanced antimicrobial efficacies.

Whilst some general trends have been identified, we can report that log *D* might not be an ideal tool to predict suitability of a peptoid as an antibiotic. Whilst decreasing peptoid hydrophobicity will likely yield non-toxic peptoids, it seemingly has no effect on antimicrobial efficacy, and where it does have an effect, it is subtle. Therefore, the community's efforts to establish techniques for the rational design of antimicrobial peptoids should persist and expand beyond the current scope of investigation.

2.5. References for Chapter 2

[1] Fried, J., Sabo, E. F., 1954, *J. Am. Chem. Soc.,* **76**, 1455-1456.
[2] Park, B. K., Kitteringham, N. R., O'Neill, P. M., 2001, **41**, 443-470.
[3] Shah, P., Westwell, A. D., 2007, *J. Enzyme Inhib. Med. Chem.,* **22**, 527-540.
[4] Qiu, J., Stevenson, S. H., O'Beirn, M. J., Silverman, R. B., 1999, *J. Med. Chem.,* **42**, 329-332.
[5] Stefanidis, D., Cho, S., Dhe-Paganon, S., Jencks, W. P., 1993, *J. Am. Chem. Soc.,* **115**, 1650-1656.
[6] DeBernardis, J. F., Kerkman, D. J., Winn, M., Bush, E. N., Arendsen, D. L., McClellan, W. J., Basha, F. Z.,1985, *J. Med. Chem.,* **28**, 1398-1404.
[7] Böhm, H., J, Banner, D., Bendels, S., Kansy, M., Kuhn, B., Müller, K., Obst-Sander, U., Stahl, M., 2004, *ChemBioChem*, **5**, 637-643.
[8] Ichikawa, J., Kobayashi, M., Noda, Y., Yokota, N., Amano, K., Minami, T., 1996, *J. Org. Chem.,* **61**(8), 2763-2769.
[9] Cousins, D.L., Lim, Y.H., Harrity, J.P., 2022, *J. Org. Chem.,* **87**(15), 9764-9768.
[10] Buer, B.C., Meagher, J.L., Stuckey, J.A., Marsh, E.N.G., 2012, *Proc. Natl. Acad. Sci.,* **109**(13), 4810-4815
[11] Bhal, S.K., Kassam, K., Peirson, I.G., Pearl, G.M., 2007, *Mol. Pharm.,* **4**(4), 556-560.
[12] Jeffries, B., Wang, Z., Felstead, H.R., Le Questel, J.Y., Scott, J.S., Chiarparin, E., Graton, J., Linclau, B., 2020, *J. Med. Chem.,* **63**(3), 1002-1031.
[13] Huchet, Q.A., Kuhn, B., Wagner, B., Fischer, H., Kansy, M., Zimmerli, D., Carreira, E.M., Müller, K., 2013, *J. Fluorine Chem.,* **152**, 119-128.
[14] Clift, M.D., Ji, H., Deniau, G.P., O'Hagan, D., Silverman, R.B., 2007, *Biochemistry*, **46**(48), 13819-13828.
[15] Koide, H., Oishi, M., Oka, T., Miyake, T., Fuwa, T., Yokoyama, S., Miyazawa, T., 1990, Amino Acids (pp. 193-200). Springer, Dordrecht.
[16] Chaiken, I. M., Freedman, M. H., Lyerla, J. R., Cohen, J. S., 1973, *J. Biol. Chem.,* **248**, 884-891.
[17] Bilgiçer, B., Fichera, A., Kumar, K., 2001, *J. Am. Chem. Soc.,* **123**, 4393-4399.
[18] Tang, Y., Tirrell, D. A., 2001, *J. Am. Chem. Soc.,* **123**, 11089-11090.
[19] Buer, B. C., Marsh, E. N. G., 2012, Fluorine: a new element in protein design. Protein Sci., **21**, 453-462.
[20] Resnati, G., 1993, *Tetrahedron*, **49**, 9385-9445.
[21] Horváth, I. T., Rábai, J., 1994, *Science*, **266**, 72-75.
[22] Bilgiçer, B., Xing, X., Kumar, K., 2001, *J. Am. Chem. Soc.,* **123**, 11815-11816.
[23] Naarmann, N., Bilgiçer, B., Meng, H., Kumar, K., Steinem, C., 2006, *Angew. Chem. Int. Ed.,* **118**, 2650-2653.
[24] Lee, K. H., Lee, H. Y., Slutsky, M. M., Anderson, J. T., Marsh, E. N. G., 2004. *Biochemistry*, **43**, 16277-16284.
[25] Gottler, L. M., Lee, H. Y., Shelburne, C. E., Ramamoorthy, A., Marsh, E. N. G., 2008, *ChemBioChem*, **9**, 370-373.
[26] Gottler, L. M., de la Salud Bea, R., Shelburne, C. E., Ramamoorthy, A., Marsh, E. N. G., 2008, *Biochemistry*, **47**, 9243-9250.
[27] Buer, B. C., de la Salud-Bea, R., Al Hashimi, H. M., Marsh, E. N. G., 2009, *Biochemistry*, **48**, 10810-10817.
[28] Chiu, H. P., Suzuki, Y., Gullickson, D., Ahmad, R., Kokona, B., Fairman, R., Cheng, R. P., 2006, *J. Am. Chem. Soc.,* **128**, 15556-15557.
[29] Wang, Z., Felstead, H. R., Troup, R. I., Linclau, B., Williamson, P. T., 2023, *Angew. Chem. Int. Ed.,* **62**, e202301077.

[30] Wu, C. W., Kirshenbaum, K., Sanborn, T. J., Patch, J. A., Huang, K., Dill, K. A., Barron, A. E., 2003, *J. Am. Chem. Soc.*, **125**, 13525-13530.
[31] Gorske, B. C., Bastian, B. L., Geske, G. D., Blackwell, H. E., 2007, *J. Am. Chem. Soc.*, **129**, 8928-8929.
[32] Gorske, B. C., Blackwell, H. E., 2006, *J. Am. Chem. Soc.*, **128**, 14378-14387.
[33] Gimenez, D., Aguilar, J. A., Bromley, E. H., Cobb, S. L., 2018, *Chem. Int. Ed.*, **57**, 10549-10553.
[34] Gimenez, D., Zhou, G., Hurley, M. F., Aguilar, J. A., Voelz, V. A., Cobb, S. L., 2019, *J. Am. Chem. Soc.*, **141**, 3430-3434.
[35] Banks, J. W., Batsanov, A. S., Howard, J. A. K., 1999, O, Hagan, D.; Rzepa, HS; Martin-Santamaria, S. J. *Chem. Soc., Perkin Trans*. II, 2409-2411.
[36] Bolt, H. L., Eggimann, G. A., Jahoda, C. A., Zuckermann, R. N., Sharples, G. J., Cobb, S. L., 2017, *MedChemComm*, **8**, 886-896.
[37] Chongsiriwatana, N. P., Patch, J. A., Czyzewski, A. M., Dohm, M. T., Ivankin, A., Gidalevitz, D., Barron, A. E., 2008, *Proc. Natl. Acad. Sci.*, **105**, 2794-2799.
[38] Eggimann, G. A., Bolt, H. L., Denny, P. W., Cobb, S. L., 2015, *ChemMedChem*, **10**, 233-237.
[39] Davern, C. M., Lowe, B. D., Rosfi, A., Ison, E. A., Proulx, C., 2021, *Chem. Sci*., **12**(24), pp.8401-8410.
[40] Wijaya, A. W., Nguyen, A. I., Roe, L. T., Butterfoss, G. L., Spencer, R. K., Li, N. K., Zuckermann, R. N., 2019, *J. Am. Chem. Soc.*, **141**, 19436-19447.
[41] Molchanova N., Nielsen J., E., Sørensen K., B., Prabhala B., K., Hansen P., R., Lund R., Barron A., E., Jenssen., H., 2020, *Sci. Rep.*, **9**, 1-0.
[42] Silhavy, T. J., Kahne, D., Walker, S., 2010, *Cold Spring Harb. Perspect. Biol.*, **2**(5), p.a000414.
[43] Khan, H. A., Ahmad, A., Mehboob, R., 2015, *Asian Pac. J. Trop. Biomed.*, **5**(7), pp.509-514.
[44] Van Nhieu, G. T., Clair, C., Grompone, G., Sansonetti, P., 2004, *Biol. Cell*, **96**(1), pp.93-101.
[45] Rayman, M. K., MacLeod, R. A., 1975, *J. Bacteriol*., **122**(2), pp.650-659.
[46] Denardi, L. B., de Arruda Trindade, P., Weiblen, C., Ianiski, L. B., Stibbe, P. C., Pinto, S. C., Santurio, J. M., 2022, Braz. J. *Microbiol.*, pp.1-7.
[47] Choi, H., Chakraborty, S., Liu, R., Gellman, S. H., Weisshaar, J. C., 2014, *PLoS One*, **9**(8), p.e104500.
[48] Miller, S. M., Simon, R. J., Ng, S., Zuckermann, R. N., Kerr, J. M., Moos, W. H., 1995, *Drug Dev. Res*., **35**, 20-32.
[49] Gooderham, W. J., Bains, M., McPhee, J. B., Wiegand, I., Hancock, R. E., 2008, *J. of Bacteriol.*, **190**(16), pp.5624-5634.
[50] Bolt, H. L., Williams, C. E. J., Brooks, R. V., Zuckermann, R. N., Cobb, S. L., Bromley, E. H. C., 2017, *Pept. Sci.*, **108**(4), p.e23014.
[51] Asgari, S., Ziarani, G. M., Badiei, A., Rostami, M., Kiani, M., 2022, *Mater. Today Commun.*, **33**, p.104393
[52] Edwards, I. A., Elliott, A. G., Kavanagh, A. M., Zuegg, J., Blaskovich, M. A., Cooper, M. A., 2016, *ACS Infect. Dis.*, **2**(6), pp.442-450.
[53] Glukhov, E., Burrows, L. L., Deber, C. M., 2008, *Biopolymers*, **89**(5), pp.360-371.

Chapter 3: Control of Peptoid Secondary Structure

3.1 Determination of *cis*/*trans* amide bond equilibrium in peptoids: development of the acetamide model system

In peptides, hydrophobic effects and hydrogen bonding exert an effect on polypeptide folding. Raines[1] suggested that in the PPI-I and PPI-II helix the backbone carbonyl oxygen (O_{i-1} HOMO) donates electron density to the unoccupied antibonding orbital (LUMO) of the carbon in the preceding amide bond (C_i=O_i). The n → π* interactions were found to be strongest when O_{i-1} was in close proximity to C_i=O_i and was positioned along the Bürgi-Dunitz[2] trajectory ($\theta \cong 107^o$). Furthermore, for this favourable orbital overlap to be facilitated, it is imperative that the amide bond is in a *trans* conformation as supposed to a *cis* conformation.

In order to probe this interaction, Raines[1] used a library of derivatised *para*-phenyl esters of *N*-formyl-*L*-proline. NMR analysis of these model systems revealed that the peptide amide bond existed as a mixture of isomers, and this was shown by two sets of NMR signals – each corresponding to a different isomer. Indeed, by careful investigation of the formyl proton peaks, it was noted that the *trans*-isomer produced an upfield (shielded) shielded ^{1}H NMR signal. The authors plotted the relationship between $K_{trans/cis}$ against the substituent Hammett parameter (σ_ρ) as a straight line. (**Figure 3.1**)

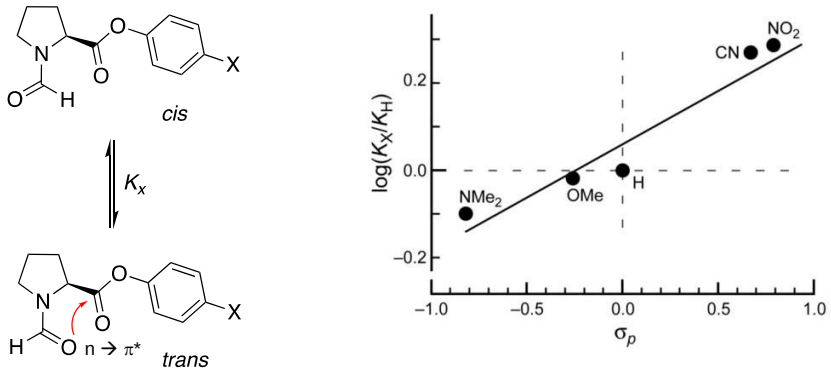

Figure 3.1. A) Equilibrium between the *cis* and *trans* amide bond conformations existing in the *N*-formyl-*L*-Pro phenyl esters used in this study. **B)** A logarithmic plot depicting the correlation between $K_{cis/trans}$ values and the electron-withdrawing ability of X substituent, calculated from experimental data.[1] (Figure adapted from Raines, 2009)

In peptoids, both *cis* and *trans* amide bonds can be stabilised by such backbone-to-backbone n → π * interactions, as these satisfy the requirement of the Bürgi-Dunitz angle. [2] Meanwhile, the backbone-to-side-chain n → π * interactions in peptoids were first investigated by the Blackwell group,[3] who in a similar fashion to Raines probed the interactions between the backbone carbonyl (O_{i-1}) and aromatic side chains of peptoid monomers. The effects of several side chains on the *cis*/*trans* amide bond equilibrium were assessed by 1D and 2D NMR spectroscopy. For this purpose, dipeptoids model systems were used, and the effects of different *C*-terminal caps were also investigated.[1,4]

The nature of the *C*-terminal capping group was found to have a considerable impact on the n → π_{Ar}* and n → $\pi_{Ci=Oi}$ interactions in the acetamides investigated by Blackwell and resulted in vastly different tautomerism of the amide bonds. [3] The applications of ester and methyl capping groups in the model peptoids resulted in environments which were less electronically and sterically realistic when compared to peptoid oligomers. The utilisation of a *dma* capping group resulted in a conformational bias. This is because the reduction in π-electron delocalisation lowers the C_i=O_i LUMO and participates in the n → $\pi_{Ci=Oi}$ interactions. Conversely, the *pip* capping group stabilises the positive charge on the nitrogen atom and minimises the n → $\pi_{Ci=Oi}$ bias and therefore it is more appropriate to use it in the synthesis of model peptoid systems. (Comparable $K_{cis/trans}$ values in $CDCl_3$ for two representative peptoid *C*-terminal caps are shown in **Table 3.1**)

Table 3.1. A summary of model peptoids**.** Two C-terminal caps (*pip* & *dma*) representative of peptoids, together with side chains used. Their corresponding $K_{cis/trans}$ values in $CDCl_3$ show a higher *trans* bias for acetamides containing the *dma* cap.[3]

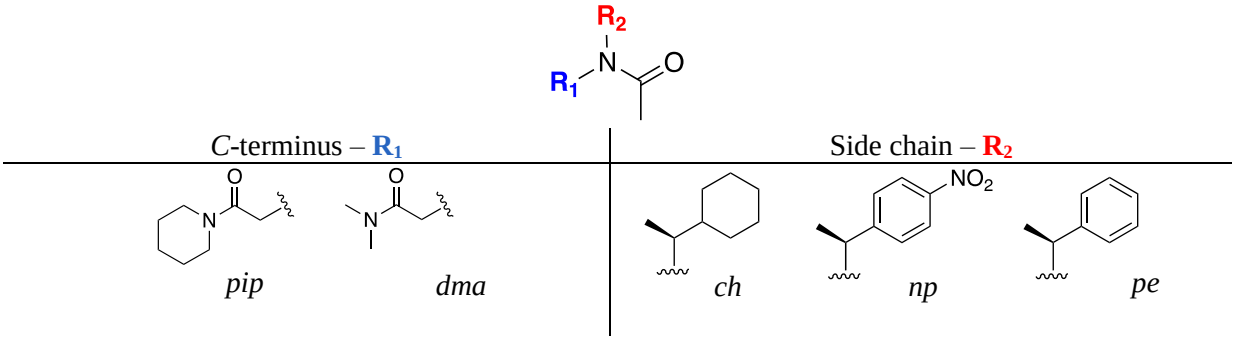

R_1	R_2	$K_{cis/trans}$ ($CDCl_3$)
pip	*ch*	0.31
dma	*ch*	0.25
pip	*np*	1.53
dma	*np*	1.12
pip	*pe*	0.70
dma	*pe*	0.54

The diastereomeric behaviour of the *N*-terminal acetyl group within the acetamides investigated by Blackwell[3] gives rise to distinguishable chemical shifts for the *cis* and *trans* amide bond isomers. Therefore, the elucidation of the $K_{cis/trans}$ values for these dipeptoid systems can be unequivocally achieved by ^{1}H-^{1}H NOESY NMR spectroscopy. $K_{cis/trans}$ constants are calculated by the ratios between the ^{1}H NMR *cis*/*trans* signals for each isomer.[4]

3.2. Peptoid side chains modulating peptoid secondary structures

3.2.1. Monomers inducing *trans* amide bond conformation in peptoids

The incorporation of a covalent macrocyclic constraint in a peptoid reduces its conformational heterogeneity and is often used as a means to encourage β-turn structures.[5] Moreover, introducing a triazole moiety into a peptoid chain encourages β-hairpin formation.[6,7] Alternatively, peptoid *N*-aryl side chains have been used to induce *trans* amide helices that can mimic PPII structure.[8] There exist a variety of *N*-aryl side chains which have been utilised to stabilise the *trans* amide conformation within peptoids, shown in **Figure 3.2**.

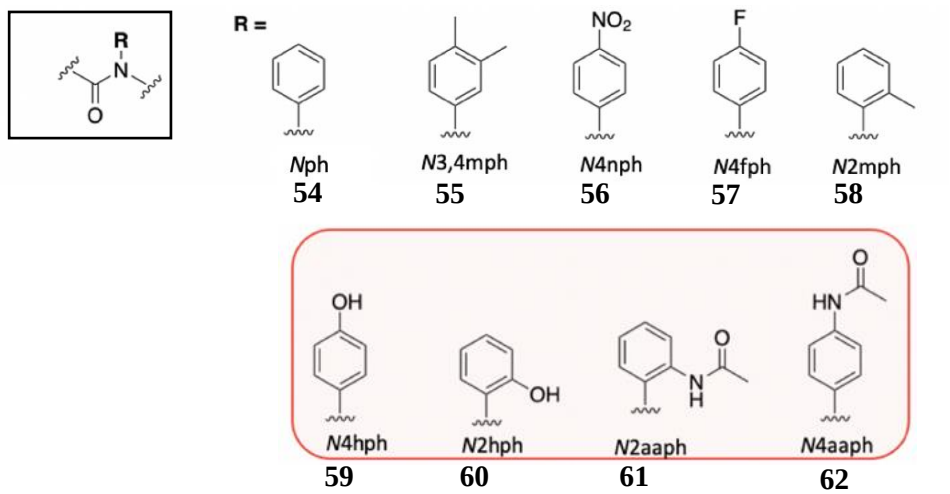

Figure 3.2. A selection of *trans*-stabilising *N*-aryl peptoid monomers. Monomers containing hydrogen-bond donating side chains are highlighted.

Kirshenbaum suggested that the peptoid turn structure showed a conformational stabilisation caused by the n → $\pi^*_{C=O}$ interaction taking place within the peptoid backbone.[9] Moreover, Blackwell installed hydrogen-bonding groups on the *N*-aryl moieties and investigated their effect on the stabilisation of *trans* amide bond configuration.[8] Indeed, it was shown that these non-covalent interactions occurred between the backbone carbonyls and the

o-hydroxyl and *o*-acetamide hydrogen-bond donors (**60**) (**Figure 3.3**). Furthermore, the use of *p*-hydrogen-bond donors was shown to lead to the formation of stabilising intrachain hydrogen bonding.

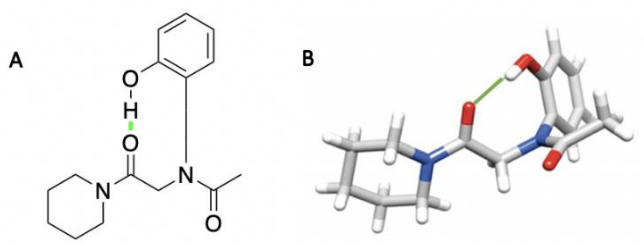

60

Figure 3.3. A. Intrachain hydrogen bonding occurring between the backbone C=O and the hydroxyl group located on the aryl side chain. **B**. Crystal structure of the *trans* amide bond conformation in a monomeric model peptoid (**60**). The hydrogen bond is shown as a green line.[3] (Figure adapted from Blackwell *et al*., 2007)

3.2.2. Monomers inducing *cis* amide bond conformation in peptoids

Since the pioneering work reported by Barron, [10] which led to the discovery of PPI-mimic 12-mer peptoid chain, research groups around the world have focussed their efforts on establishing *cis*-enhancing peptoid monomer libraries in the quest of designing peptoids with stable folded structures.[11-13] The work in this field led to achieving a collection of monomers based primarily on sterically bulky α-chiral aromatic *N*-side chains, which led to the formation of helical structures thanks to the n → $\pi_{C=O}$* and n → π_{Ar}* electronic interactions.[9] (**Figure 3.4**)

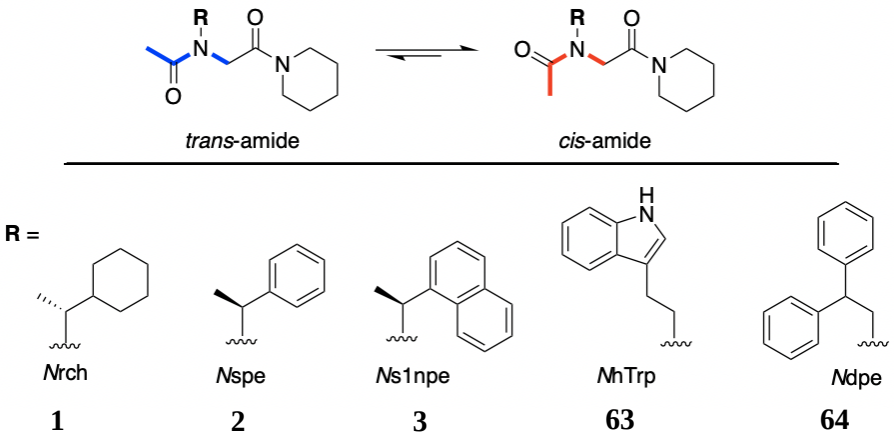

Figure 3.4. An equilibrium between the *cis* and *trans* amide bond conformation favouring the *cis* configuration, together with a selection of *cis* amide bond inducing monomers. The *cis* conformation is stabilised by steric and n → π* effects, except in the acetamides containing **1**.

Although these sterically demanding *N*-substituted monomers[3,12] allow for the control of peptoid secondary structure by locking the amide bond in its *cis* conformation, there has been a rise in demand for monomers of lower hydrophobicity which would aid in decreasing peptoid toxicity without losing the ability to reduce amide bond heterogeneity.[14] In the past decade, studies have emerged which focused on achieving this by exploiting the electronic and steric interactions and developing peptoid monomers which would enlarge the chemical space of this library.

Meanwhile, installation of a ^{t}Bu group on C^{α} of a side chain studied in the monomeric peptoid model capped with an acetyl and a piperidinyl group was reported in 2013 by Faure and co-workers.[15] Remarkably, incorporation of this moiety into Blackwell's model peptoid system[3] showed an exclusive preference for the *cis* amide isomer in all solvent systems used for the NMR analysis, where the $K_{cis/trans} > 19$. This stabilisation is achieved by steric effects.

Unfortunately, due to being acid-labile, incorporation of a ^{t}Bu sidechain into peptoid oligomers synthesised on a solid support is not practical. Nevertheless, the group reported solution synthesis of a peptoid chain consisting entirely of *Ngh*Ala (**65**) monomers, and the amide bonds within this oligomer were found to be 100% *cis*. Furthermore, alternating incorporation of *cis* inducing **65** and *N*Phe (**40**) resulted in a peptoid oligomer with a fully defined α-helical structure.

Impressively, the overall yield for the solution phase synthesis of the *cis/trans* alternating 6-mer was 66%, after 11 steps. While successful in this case, the solution phase synthesis of peptoids is not feasible in most cases due to it being very time consuming because of the need for purification by flash chromatography after each bromoacetylation step. The *cis*-inducing properties of a ^{t}Bu functional groups have led Faure's group to design a library of α,α-gem-dimethylated peptoid model trimers (**Figure 3.5**).[16]

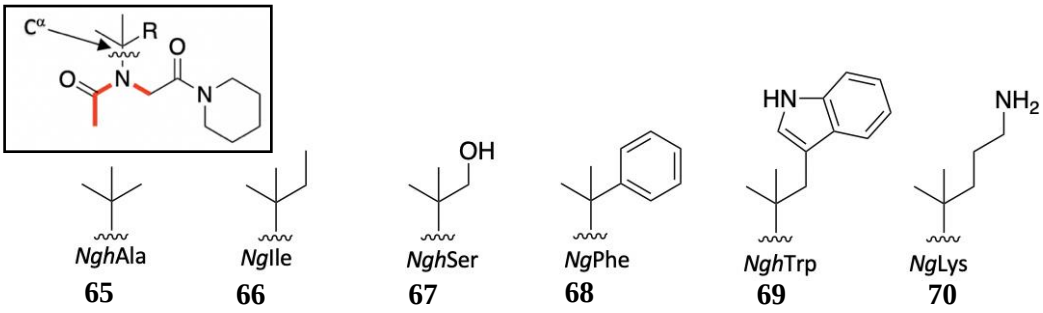

Figure 3.5. Structures of seven α,α-gem-dimethylated peptoid monomers bearing functionalities designed to mimic proteogenic amino acid side chains. The library contains aromatic, aliphatic and charges groups.[15,16]

Unsurprisingly, given the result of the previous study reporting the *cis*-inducing **65**, the NMR study of the peptoid models indicated that the majority of the submonomers, studied by Faure,[16] (including **65-70**) shows a strong preference of *cis* amide bond formation, and they all showed impressively high $K_{cis/trans}$ values of >19. The incorporation of cationic moieties is necessary for antibacterial properties of peptoids. The chemical diversity of cationic pendant groups has been limited to those that mimic proteogenic amino acid side chains (**Figure 3.6**): ammonium (**52** and **53**), guanidium (**70**) and imidazolium (**71**) functionalities.

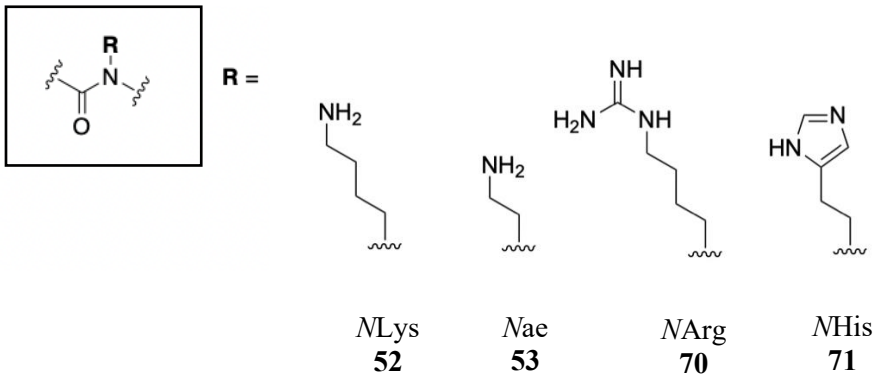

Figure 3.6. Proteogenic amino acid mimicking cationic peptoid submonomers.

The use of these monomers meets the need of incorporating a positive charge on a peptoid, however, it has no effect on the control of the *cis/trans* equilibrium. In 2012, the Faure group reported the use of triazolium side chains in the quest of inducing the *cis*-isomer.[17] The synthesis the of triazolium type monomers is carried out using Cu-catalysed cycloaddition (CuAAC) via click-chemistry. The reaction takes place between the *N*-propargyl side chain

and an organic azide, R-N_3. Following this, the group reported an in-situ methylation of the triazole, using iodomethane to generate a triazolium (**Figure 3.7**).[17]

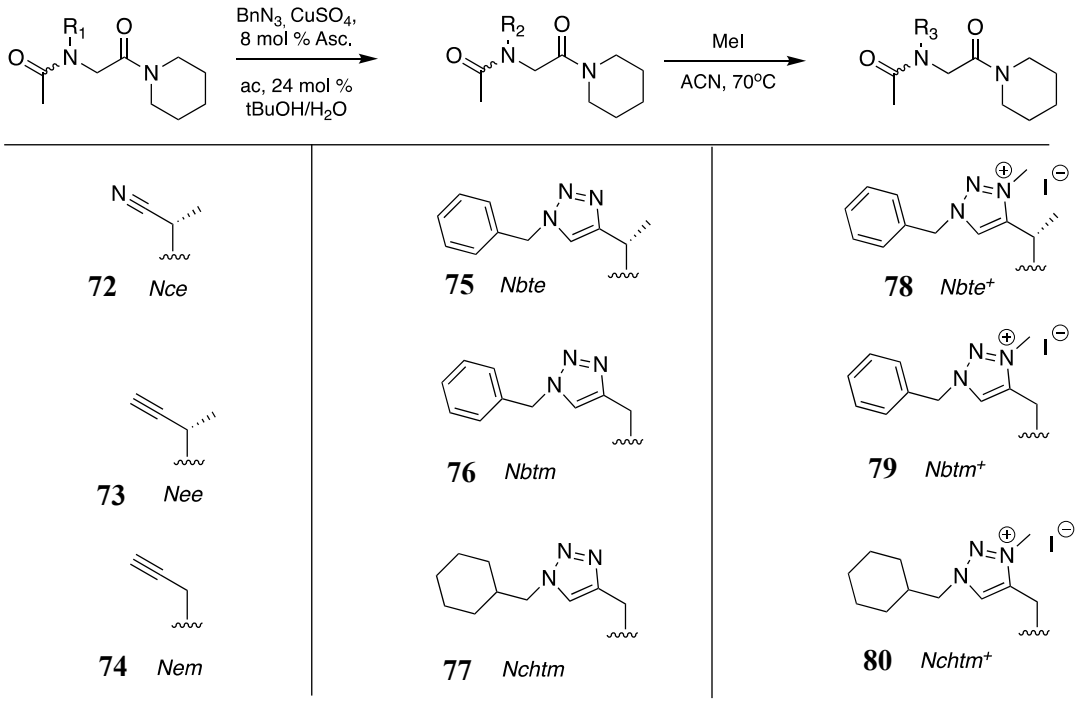

Figure 3.7. A schematic representation of Cu-catalysed azide-alkyl (CuAA) reaction and a subsequent methylation of the triazole to form a triazolium salt. A selection of pendant alkyne, triazole, and triazolium side chains is also included.[17]

The α-peptoid models (**Figure 3.7**) were subjected to *cis/trans* equilibrium analysis by ^{1}H NMR spectroscopy (**Table 3.2**). The charged triazolium monomers showed remarkable *cis* amide preference, with $K_{cis/trans}$ values exceeding 19 in $CDCl_3$. The triazolium pendant side chains supressed the *trans*-isomer to a great extent in all solvents, and the average $K_{cis/trans}$ values reported are comparable to *Ngh*Ala (**65**).[17] They allow for precise control of peptoid secondary structure, which conformationally locks it in place, and is compatible with solid-phase synthesis, on top of enhancing bacterial membrane targeting. (**Table 3.2**) Relative to their triazolium counterparts, the triazole moieties favoured the *cis* amide conformation to a much lesser extent. The *cis*-favouring nature of both systems can be attributed to the n → π_{Ar}* electronic interactions (**Figure 3.8**), and the electron deficient aryl rings present in the triazolium systems which will lead to much stronger interactions. In addition, the highest average $K_{cis/trans}$ value seen for *Nbte*$^+$ (**78**) is attributed to its *N*-C^α-chiral structure and steric effects.

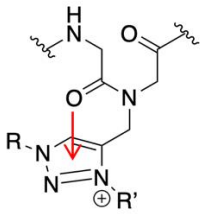

Figure 3.8. A depiction of triazolium monomer being locked in a *cis* conformation, stabilised by n → π_{Ar}* electronic effects (shown as a red arrow).

Table 3.2 $K_{cis/trans}$ values and the corresponding $\Delta G_{cis/trans}$ (kcal/mol) for compounds **72** – **80**, where $\Delta G_{cis/trans}$ = *-RT* ln $K_{cis/trans}$. **trans* amide rotamers not present; ΔG cannot be calculated.[17]

		$CDCl_3$		**CD_3CN**		**MeOD**		**D_2O**	
No.	**Side chain**	$K_{cis/trans}$	$\Delta G_{cis/trans}$	$K_{cis/trans}$	$\Delta G_{cis/trans}$	$K_{cis/trans}$	$\Delta G_{cis/trans}$	$K_{cis/trans}$	$\Delta G_{cis/trans}$
72	*Nce*	4.34	-0.87	8.22	-1.24	3.71	-0.77	2.92	-0.63
73	*Nee*	1.55	-0.26	3.04	-0.66	1.90	-0.38	1.36	-0.18
74	*Nem*	0.54	0.36	1.31	-0.16	0.78	0.15	1.00	0.00
75	*Nbte*	2.06	-0.43	1.99	-0.41	1.45	-0.22	1.34	-0.17
76	*Nbte*$^+$	>19	–*	11.73	-1.46	11.12	-1.42	5.52	-1.01
77	*Nbtm*	1.10	-0.06	1.11	-0.06	1.03	-0.02	1.07	-0.04
78	*Nbtm*$^+$	>19	–*	10.92	-1.41	8.67	-1.27	5.86	-1.04
79	*Nchtm*	1.12	-0.07	1.09	-0.05	1.00	00	1.06	-0.03
80	*Nchtm*$^+$	>19	–*	10.54	-1.39	9.02	-1.30	4.94	-0.94

Steric effects were proposed to be responsible for the different average $K_{cis/trans}$ values seen between **73** and **74**, whereby the $K_{cis/trans}$ value is almost three-fold higher for **73** than **74**. (The same applies for monomers **75** and **76**). Electronic effects are suspected where the interaction between the HOMO of the amide carbonyl and the LUMO of the alkyne takes place (compounds **72 – 74**). This is further reinforced by the relatively high $K_{cis/trans}$ value where a nitrile group was employed (**72** avg. $K_{cis/trans}$ = 5.37). (**Table 3.2**)

While impressive, the drawback of incorporating triazolium-type monomers into peptoid chains is that it adds two extra synthesis step per monomer incorporation. In addition, the inclusion of a permanent cation may not be desired within a given peptoid sequence.

In 2019, the Zuckermann's group explored the incorporation of cationic side chains which induced *cis* amide bond conformation via hydrogen bonds.[18] The group synthesised a library of α-peptoid models and thoroughly analysed their *cis* forming preferences in different solvents. In this thesis, due to the relevance to the presented results, only the cationic submonomers will be discussed. (**Figure 3.9**)

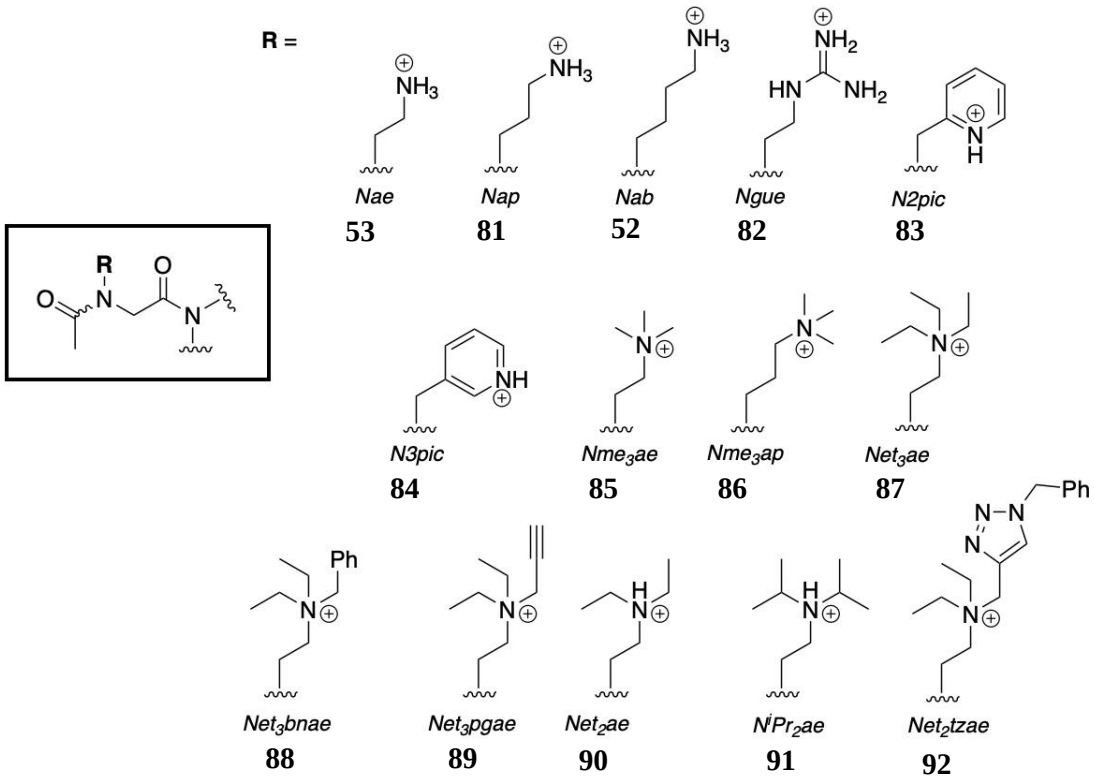

Figure 3.9. Library of cationic submonomers as TFA salts.[18]

It has been found that compared to its neutral amine counterpart, the cationic acetamide **81** showed an increased preference for a *cis* amide bond conformation, which was caused by hydrogen bond formation between the backbone $C{=}O_{i-1}$ and the N-H of the pendant side chain. This hydrogen bonding was found to occur in both the *cis* and *trans* amide bond conformations, which were almost isoenergetic.[18] (**Figure 3.10**) Furthermore, the $K_{cis/trans}$ values for **83** and **84** are much higher and are caused by the $n \rightarrow \pi_{Ar}^*$ electronic interactions between the backbone *i – 1* carbonyl and the electron poor pyridyl group.

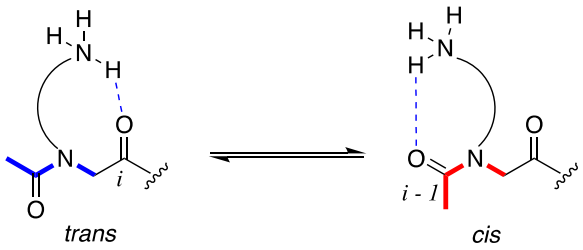

Figure 3.10. Hydrogen bonding hypothesis for *N*ae (**53**), based upon work reported by Blackwell[8] and Zuckermann[18]. Hydrogen bond is represented as a blue dotted line. The system is in a near equilibrium.

Peptoid monomers, bearing quaternary ammonium moieties in their pendant *N*-side chains have led to some of the highest $K_{cis/trans}$ values reported in literature.[18] For instance, the $K_{cis/trans}$ value for **85** increased 10-fold in aprotic solvent ($K_{cis/trans}$ = 22), compared to its non-substituted analogue **53** ($K_{cis/trans}$ = 1.9). Its dominant *cis* preference is also seen in protic solvents. Furthermore, the *cis* preference also increases with decreasing chain length (see **85** vs. **86**). (**Table 3.3**)

The vast increase in the $K_{cis/trans}$ values obtained can be attributed to the electronic effects of the positively charged cationic moiety, rather than to steric effects. This electronic effect is further enhanced in monomers bearing more electron deficient pendant *N*-side chains, particularly *N*et$_3$ae (**87**) and *N*et$_2$bnae (**88**) ($K_{cis/trans}$ = 70 in $CDCl_3$).

Table 3.3. $K_{cis/trans}$ values and the corresponding $\Delta G_{cis/trans}$ (kcal/mol) for compounds **52**, **53**, **81** – **92**, where $\Delta G_{cis/trans} = -RT \ln K_{cis/trans}$.[18]

No.	Side chain	$CDCl_3$		MeOD		D_2O	
		$K_{cis/trans}$	$\Delta G_{cis/trans}$	$K_{cis/trans}$	$\Delta G_{cis/trans}$	$K_{cis/trans}$	$\Delta G_{cis/trans}$
53	*Nae*	1.9	-0.38	2.4	-0.52	2.2	-0.47
81	*Nap*	3.1	-0.67	3.0	-0.65	2.1	-0.44
52	*Nab*	1.00	0.00	1.0	0.00	1.0	0.00
82	*Ngue*	2.0	-0.41	1.5	-0.24	1.2	-0.11
83	*N2pic*	5.4	-1.00	4.2	-0.85	3.2	-0.69
84	*N3pic*	4.3	-0.86	3.7	-0.77	2.2	-0.47
85	*Nme$_3$ae*	22	-1.83	6.1	-1.07	4.1	-0.84
86	*Nme$_3$ap*	4.7	-0.92	2.1	-0.44	1.7	-0.31
87	*Net$_3$ae*	70	-2.52	14	-1.56	5.8	-1.04
88	*Net$_2$bnae*	70	-2.52	15	-1.60	6.1	-1.07
89	*Net$_2$pgae*	40	-2.32	8.8	-1.29	4.4	-0.88
90	*Net$_2$ae*	13	-1.52	9.4	-1.33	5.4	-1.00
91	*N^{i}Pr$_2$ae*	30	-2.01	16	-1.64	8.1	-1.24
92	*Net$_2$tzae*	60	-2.42	8.5	-1.27	4.9	-0.94

3.2.3. Expanding the peptoid chemical space: phenolic building blocks

In the literature, there are a limited number of studies involving peptoids whereby phenolic monomers have been utilised in their synthesis. In the paper published by Blackwell,[8] the group involved unprotected aminophenols in the synthesis of peptoid models. While this approach proves successful in the synthesis of acetamide peptoid models, it is not encouraged in the synthesis of longer peptoids by the submonomer method due to the reactive nature of phenols and their proneness to undergo acylation and alkylation reactions.[19]

There exist orthogonal protection strategies which have assisted with a successful synthesis of phenolic peptoids on resin. The ^{t}Bu-protection of a hydroxy moiety on an aminophenol can be troublesome due to the non-selective nature of this reaction. Back in 1998, Liskamp reported *tert*-butylation of a 4-hydroxybenzonitrile (**93**) with *tert*-butyl trichloroacetimidate, to give **94**, which overcame this issue. The nitrile moiety was then reduced to form the desired primary amine **95**.[20] (**Scheme 3.1**)

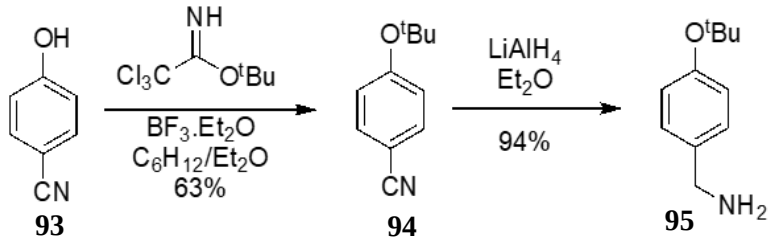

Scheme 3.1. A schematic representation of preparation of submonomers starting from a *p*-hydroxybenzonitrile.[20]

In 2014, the Cavelier[21] group reported the synthesis of *N*-homotyrosine building block **99** designed to be used in the monomer approach. The method utilises an orthogonal protection strategy and can be used to produce building blocks which are suitable for the submonomer method. Before the introduction of a ^{t}Bu to give **98**, the primary amine of **96** was protected with a Cbz group, to give **97**. The Cbz group was then cleaved to produce **99**, which was followed by Cbz cleavage using a Pd(0) catalyst. (**Scheme 3.2**)

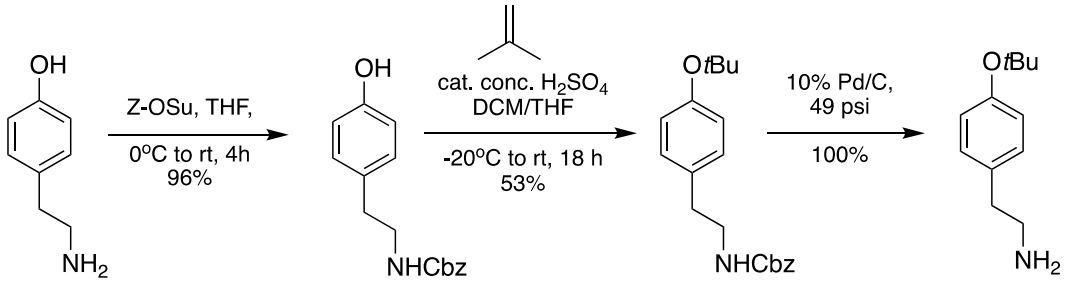

96 **97** **98** **99**

Scheme 3.2. A three step-synthesis generating a ^{t}Bu-protected tyramine.[21]

In short, at the present time, phenolic monomers that are well suited to submonomer peptoid synthesis are not readily available, and this helps to rationalise the absence of phenol-containing (i.e. Tyr-like) peptoids in literature. The use of an unmodified phenol group, with a free OH, is not practical given the risk of unwanted side reactions e.g. with the electrophilic bromoacetic acid that is used in the submonomer synthesis. Attempts to use the free phenol have been made via the use of a ring-deactivating functionality linked to the phenol ring. For instance, Kirshenbaum utilised 3-nitro-4-aminophenol in synthesis of peptoid models.[9] The use of such monomers has a potential to overcome the issue of unwanted side reactions by lowering the pKa of the phenol group.

3.2.4. Tetrafluoropyridyl: phenol protecting group

In 2019, the Cobb group reported the use of electron deficient heteroaryl halides in S_NAr reactions with phenols to access a new type of protecting group.[22] The reaction of phenols with pentafluoropyridyl (PFP) occurs via aromatic substitution at the 4'-position of the pyridine ring. Within the work carried out by Cobb,[22] the yields obtained for the reaction of various phenols with PFP exceeded 87%. The synthesis was straight forward with a 1:1 stoichiometric mixture of a phenol substrate and PFP (**100**) in the presence of a mild base. The removal of the TFP protecting group takes place in the presence of KF (source of fluoride ions) and a thiol (scavenger of the liberated **100**). TFP ethers are robust to a range of reactants including oxidants, strong acids, bases, and coupling reagents. (**Scheme 3.3**)

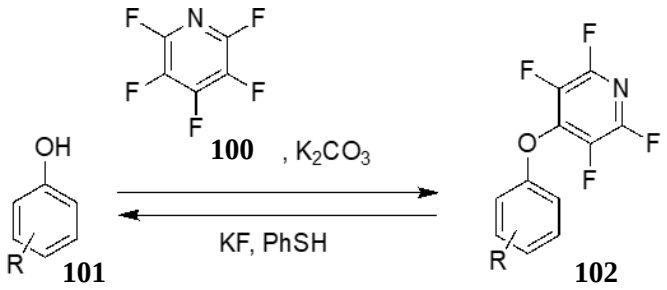

Scheme 3.3. A schematic representation of phenol substrate (**101**) TFP-protection with a PFP (**100**) to produce **102**. The successive phenol liberation is performed using KF as a source of fluoride ions, and thiophenol as an organosulphur. This phenolic substrate was employed in the library designed in the 2019 study and showed a clean synthesis of the protected phenol (**102**).[22]

3.3. Objectives for Chapter 3

Expansion of the chemical space of peptoid monomers provides an exciting path to follow as we seek to grow the antimicrobial peptoid library. Of interest was synthesis of a peptoid monomer library containing neutral monomers capable of stabilising the *cisoid* acetamide conformation by the means of both intra- and intermolecular hydrogen bonding. Herein, a library of model peptoids containing aminophenols and aminomethyl phenols will be synthesised and analysed.

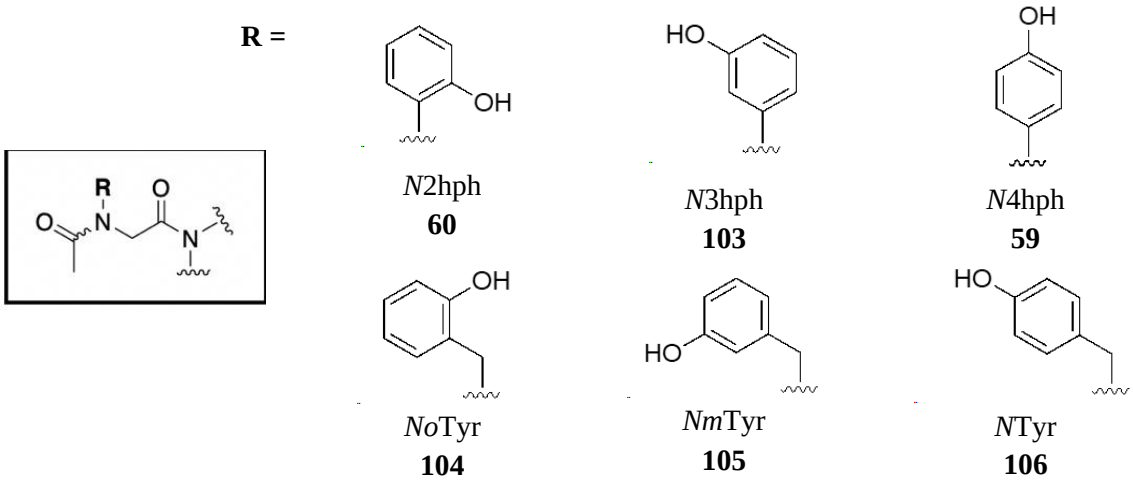

Figure 3.11. Six model peptoids containing the hydroxy aryls to be synthesised in this chapter.

Although aminophenols have been documented in the literature, and shown to favour a *trans* amide bond conformation, there exists no investigation of aminomethyl phenols. In addition to the stabilisation of secondary structure by hydrogen bonding, it is anticipated that π-stacking will also contribute to secondary structure stabilisation.

Previously, the Blackwell group reported that *o*-hydroxy anilines induced *trans* amide bond conformations by the formation of intramolecular hydrogen-bonding between the hydroxyl moiety and the backbone *i* carbonyl.[3] (**Figure 3.2)** It was anticipated that the incorporation of a methyl moiety and hence elongation of the distance between the peptoid backbone and the aryl hydroxyl would aid the hydrogen-bond formation between the side chain and the *i-1* carbonyl, resulting in the induction of *cis* amide bond conformation. (**Figure 3.12**)

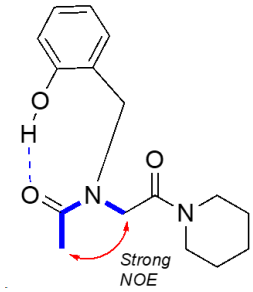

104

Figure 3.12. Postulated H-bonding between aryl hydroxyl and backbone C=O_{i-1} in **104**.

In order to obtain tyrosine-derivatives compatible with the submonomer approach the TFP-protection strategy will be applied and optimised where applicable. It is planned that all model peptoids synthesised in this thesis are to be investigated for the $K_{cis/trans}$ ratios by 1D and 2D NMR spectroscopic techniques.[1,4] Furthermore, to elucidate intermolecular forces which may occur between the acetamides, X-ray crystallography is to be used in order to obtain their crystal structures.

3.4. Chapter 3: Results and discussion

3.4.1. Synthesis of *O*-TFP tyrosine-type submonomers

The installation of non-terminal phenolic submonomers in antibacterial peptoids has, to date, not been explored. As seen in the literature, the use of TFP as a protecting group for phenols is not only fast but also highly selective to hydroxyls, demonstrated in the case of *m*-aminophenol.[22]

This part of the project commenced by obtaining TFP-protected aminophenol and hydroxy benzylamine derivatives (**Figure 3.13**).

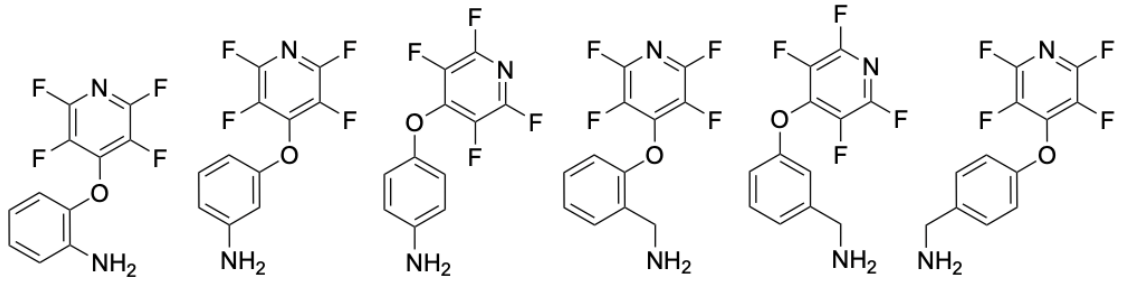

107 **108** **109** **110** **111** **112**

Figure 3.13. TFP-protected tyrosine derivatives initially planned to be synthesised in this library.

The TFP-protection of *o*- and *m*-aminophenol to produce **107** and **108** was performed in one step employing pentafluoropyridine (PFP) and a mild base (**Scheme 3.4**), at ambient temperature. Upon reaction completion, the relatively low boiling point of PFP (on par with H_2O) allowed for the excess reagent to be removed *in vacuo*. The protected products were recovered in high yields as light-yellow solids.

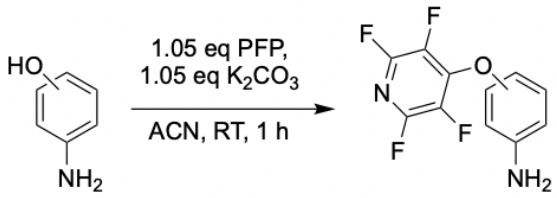

No.	Isomer
113	*ortho*
114	*meta*

No.	Isomer	Yield
107	*ortho*	93%
108	*meta*	95%

Scheme 3.4. A one step reaction scheme used to generate *O*-TFP *o*-aminophenol (**107**) and *O*-TFP *m*-aminophenol (**108**).

The one-step protection of these regioisomers was achievable due to the positioning of the primary amine on the phenol ring. In the case of *p*-aminophenol (**115**) an orthogonal protection strategy, again, was necessary. For this purpose, a Boc-group was used. (**Scheme 3.5.A**) This reaction took place under basic conditions and used di-*tert*-butyl dicarboxylate (Boc_2O). Upon workup, the ^1H NMR spectrum, shown in **Figure 3.13**, revealed the crude material consisted of the desired, *mono*-protected aminophenol (**116**), and the *N, O-di*-^{t}Bu-carbonyl *p*-aminophenol (**118**) (**Scheme 3.5.B**). It was therefore necessary to separate the desired product from the impurities by flash column chromatography, resulting in the recovery of a white solid in the yield of 45%. The TFP-protection followed using PFP and K_2CO_3 as a base to produce **117**. The subsequent *N*-Boc cleavage was achieved by allowing the intermediate **117** to react with TFA. The overall yield for this 3-step synthesis was 44%.

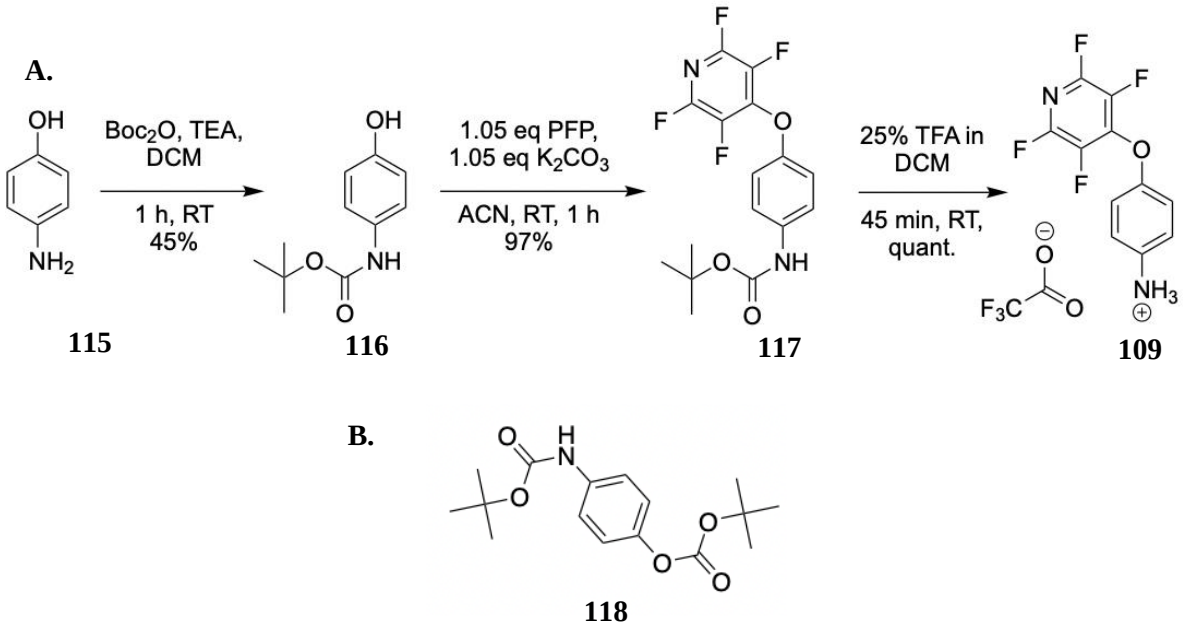

Scheme 3.5. A. Showing the synthesis of *O*-TFP *p*-aminophenol (**109**). **B**. *N, O*-Boc-protected side product (**118**).

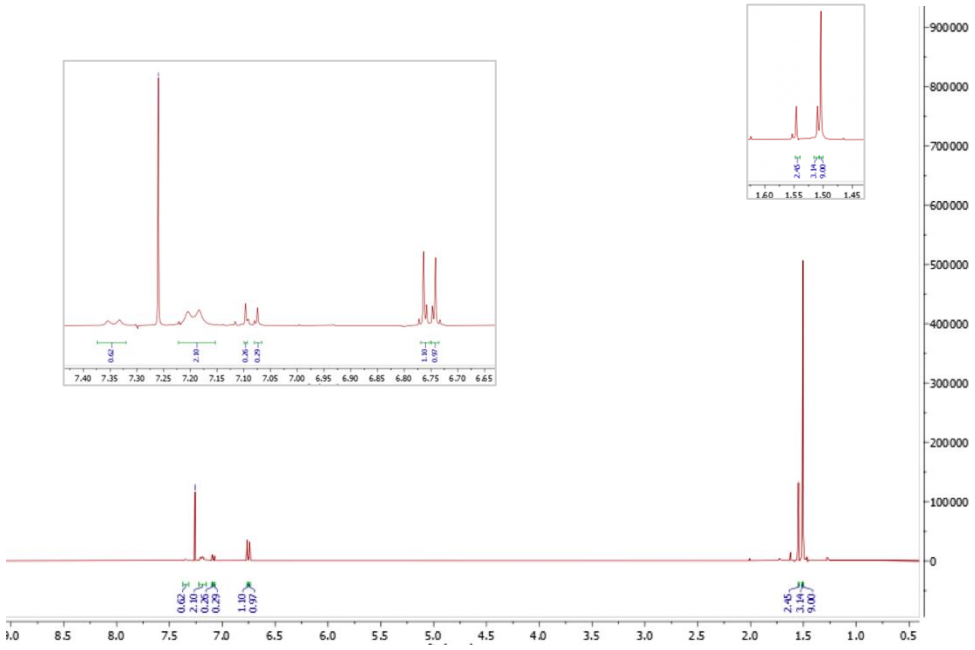

Figure 3.12. Crude ^{1}H NMR of **109** showing the presence **118** side-product; multiple singlets were detected in the *t*-Bu region, as well as in the aromatic region.

The synthesis of the *O*-TFP aminomethylphenols also proceeded with *N*-Boc protection (resulting in **122** – **124**). After alcohol protection with TFP under mild conditions to produce **125** – **127**, cleavage of the Boc group was performed using a solution of 25% TFA in DCM. This reaction was fast and facile, and the TFP group is resistant to these reaction conditions. The resulting TFP-protected compounds were obtained as TFA salts (**110** – **112**). (**Scheme 3.6**) A crystal structure obtained for **127** is shown in **Figure 3.14**.

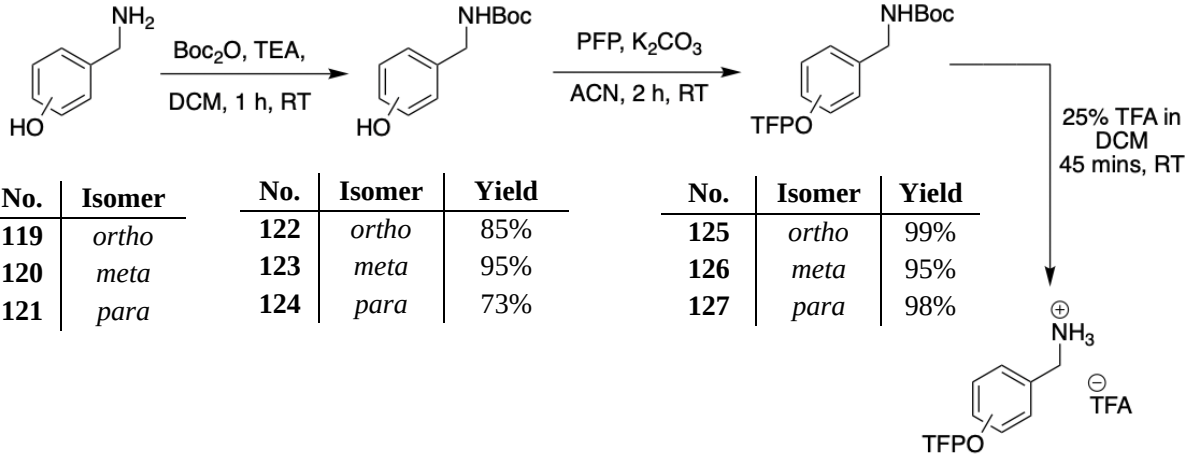

No.	Isomer
119	*ortho*
120	*meta*
121	*para*

No.	Isomer	Yield
122	*ortho*	85%
123	*meta*	95%
124	*para*	73%

No.	Isomer	Yield
125	*ortho*	99%
126	*meta*	95%
127	*para*	98%

No.	Isomer	Yield
110	*ortho*	quant.
111	*meta*	100%
112	*para*	quant.

Scheme 3.6. Synthesis of *O*-TFP aminomethylphenols as TFA salts.

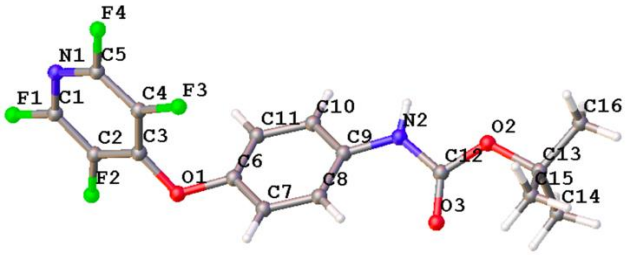

Figure 3.14. Ball-and-stick representation of *N*-Boc, *O*-TFP hydroxybenzylamine **127.** Carbon atoms are depicted in grey, hydrogen atoms in white, nitrogen in navy, oxygen in red, and fluorine in green. Structure was generated in Olex2 and is reported with a 50% thermal ellipsoid probability.

3.4.2. Synthesis of model peptoids containing protected tyrosine-type submonomers

The ability of hydroxyls to form intramolecular hydrogen bonding with the *i* and *i-1* carbonyls present in peptoid sequences provides an attractive avenue to explore their impact on the *cis/trans* ratios of peptoid amide bonds.[8,18] Furthermore, the strong electron withdrawing property as well as the steric bulk of the tetrafluorpyridine (TFP) bound to the hydroxyl moiety could serve as a *cis*-enhancing group. It was planned that model peptoids containing peptoid monomers **107** – **112**, and their deprotected derivatives, would be synthesised in order to

determine the ratio of *cis*/*trans* equilibrium in model peptoids containing aromatic alcohols and *O*-TFP-protected aromatic alcohols.

The syntheses of these model peptoids proceeded with a common intermediate, 2-bromo-1-piperidinyl ethanone (**129**), which was produced via an S_N2 reaction under basic conditions, which employed piperidine and bromoacetylbromide (**128**) while generating HBr as a by-product. **129** was recovered in good yield of as a yellow oil, and the crude product was not purified. (**Scheme 3.7**)

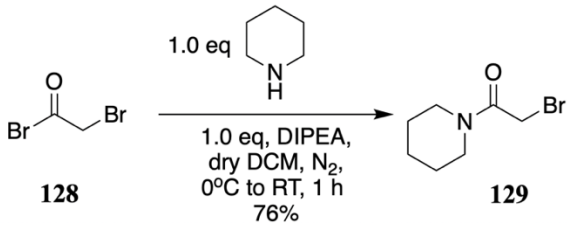

Scheme 3.7. Showing nucleophilic substitution reaction between bromoacetylbromide and piperidine under inert conditions to produce 2-piperidinyl-1-bromo ethanone.

Prior to the synthesis of the model peptoid library containing novel peptoid monomers, two control peptoid model systems were produced comprising of an aniline-containing **130** and a benzylamine-containing **40**. The most common procedure used to synthesise model peptoids in literature involves direct alkylation of the primary amine by an S_N2 mechanism under basic conditions. Due to their reactivity being lower than secondary amines, primary amines are typically employed in excess compared to the alkylating agent in order to encourage formation of monoalkylated product exclusively, and to decrease the rate of the second substitution following the production of the much more nucleophilic secondary amine. The two-step pathway which was utilised to produce these compounds is shown in **Scheme 3.8**. The first step of the synthesis employed **129** and four equivalents of a primary amine. After 20 minutes the reaction mixture was concentrated and the crude was employed in the second step of the synthesis, where it was subjected to acetylation under basic conditions. After acidic workup, the crude was purified by flash column chromatography yielding two model peptoids **130** and **40** in high yields. The crystal structure of a side-product **131** produced in the synthesis of **130** is shown in **Figure 3.15**.

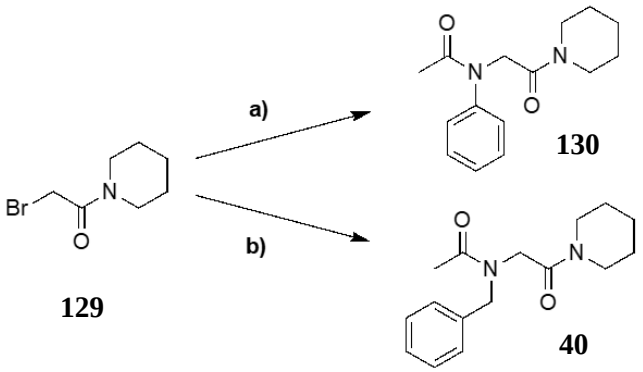

Scheme 3.8. Showing a two-step reaction pathway employed in the synthesis of the two control peptoids: **a**) 4.0 eq of aniline, THF at 0°C to RT, 20 mins; 4.0 eq of AcCl, 4.0 eq of DIPEA, DCM, RT to form **130** (overall yield of 68%) and **b**) 4.0 eq of aniline, THF at 0 °C to RT, 20 mins; 4.0 eq of AcCl, 4.0 eq of DIPEA, DCM, RT to form **40** (overall yield of 99%).

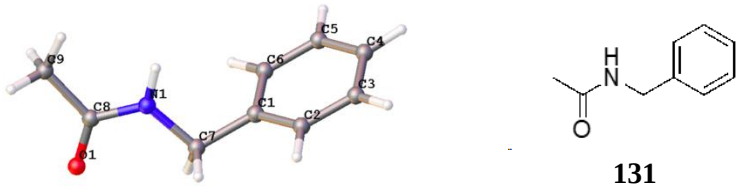

Figure 3.15. Ball-and-stick representation of a novel polymorph of *N*-benzylacetamide **131,** isolated from the crude mixture of **40**. Carbon atoms are depicted in grey, hydrogen atoms in white, nitrogen in navy and oxygen in red. Structure was generated in Olex2 and is reported with a 50% thermal ellipsoid probability.

The synthesis of model peptoid **123** containing the *O*-TFP *o*-aminophenol (**107**) was first attempted by reacting 2-bromo-1-piperidinylethanone with 4 equivalents of the amine at 50 °C overnight. However, no conversion was observed either by NMR or LC-MS. Subsequently, the number of equivalents of the amine used was decreased to 1.2, excess DIPEA was added, and the scale of the reaction was increased 6-fold. The reaction mixture was, again, heated overnight. Then, following a workup, the crude material was directly used in the acetylation step to produce the model peptoid **135**. This step was fast and facile, employing acetyl chloride, and a base. Following purification by flash column chromatography, traces of the desired product were recovered. The same synthesis route was used to produce the model peptoids containing *m*- and *p*-isomers, compounds **136** and **137** respectively. The overall yields for the syntheses of these compounds were very poor compared to the yields acquired in the synthesis of the control peptoids. (**Scheme 3.9**)

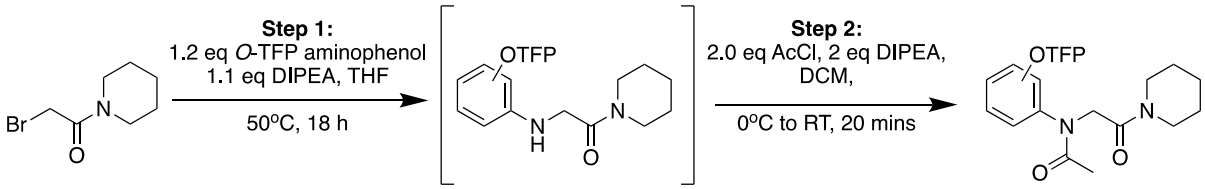

129

No.	Isomer*
132	*ortho*
133	*meta*
134	*para*

No.	Isomer	Overall yield
135	*ortho*	5%
136	*meta*	7%
137	*para*	6%

Scheme 3.9. A two-step reaction route to produce the model peptoid containing *O*-TFP aminophenols (**135** – **137**). Alkylation which involved bromine displacement by the amine derivative was followed by *N*-acetylation using acetyl chloride and DIPEA.
*Intermediate not isolated. Crude engaged in the next step without purification.

The low yields observed were initially attributed to the strong electron-withdrawing nature of the TFP-protecting group, which likely caused a general deactivation of the amino group. Originally, it was thought that the location, on the ring of the TFP group in the *o*-aminophenol derivative was responsible for this low reactivity. However, upon utilising the *m*- and *p*-isomers, it became evident that the TFP group decreased the reactivity of the amine group in all cases.

The syntheses of the model peptoids containing *O*-TFP aminomethylphenols commenced utilising the same reaction conditions. It was apparent that in addition to the poor reactivities of *O*-TFP aminomethylphenols excess alkylation during the first step of the synthesis was cumbersome. While the first alkylation of the primary amine had taken place at a much faster rate compared to the *O*-TFP aminophenols and no heating was required, the second alkylation followed almost immediately, resulting in tertiary amine side products **141** – **143** (**Scheme 3.10**). Although the presence of the desired monoalkylated product **137** – **139** was visible by the qualitative LC-MS measurements (**Figure 3.16A**) and its traces were detected by NMR spectroscopy, no product was recovered. (**Figure 3.16B and C**)

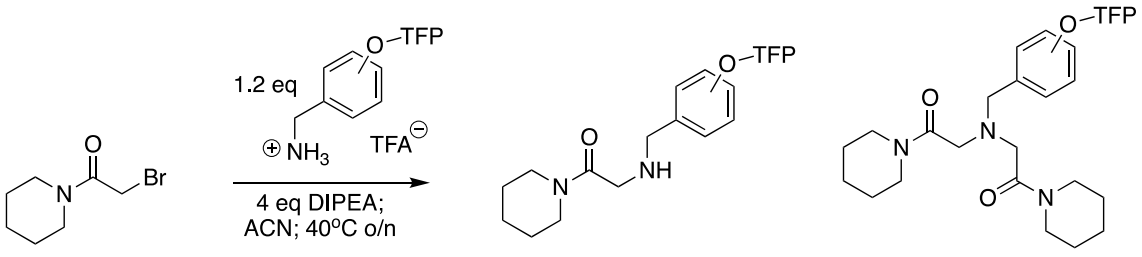

Minor

No.	Isomer
138	*ortho*
139	*meta*
140	*para*

Major

No.	Isomer
141	*ortho*
142	*meta*
143	*para*

Scheme 3.10. Attempted *N*-alkylation of *O*-TFP aminomethylphenol derivatives led to the production of the over-alkylated side product. The scheme portrays utilisation of 1.2 M of amine; however, this had also been the case where 3-5 equivalents of amine were used (see text). *Minor and Major products as determined by LC-MS analysis of crude reaction mixtures.

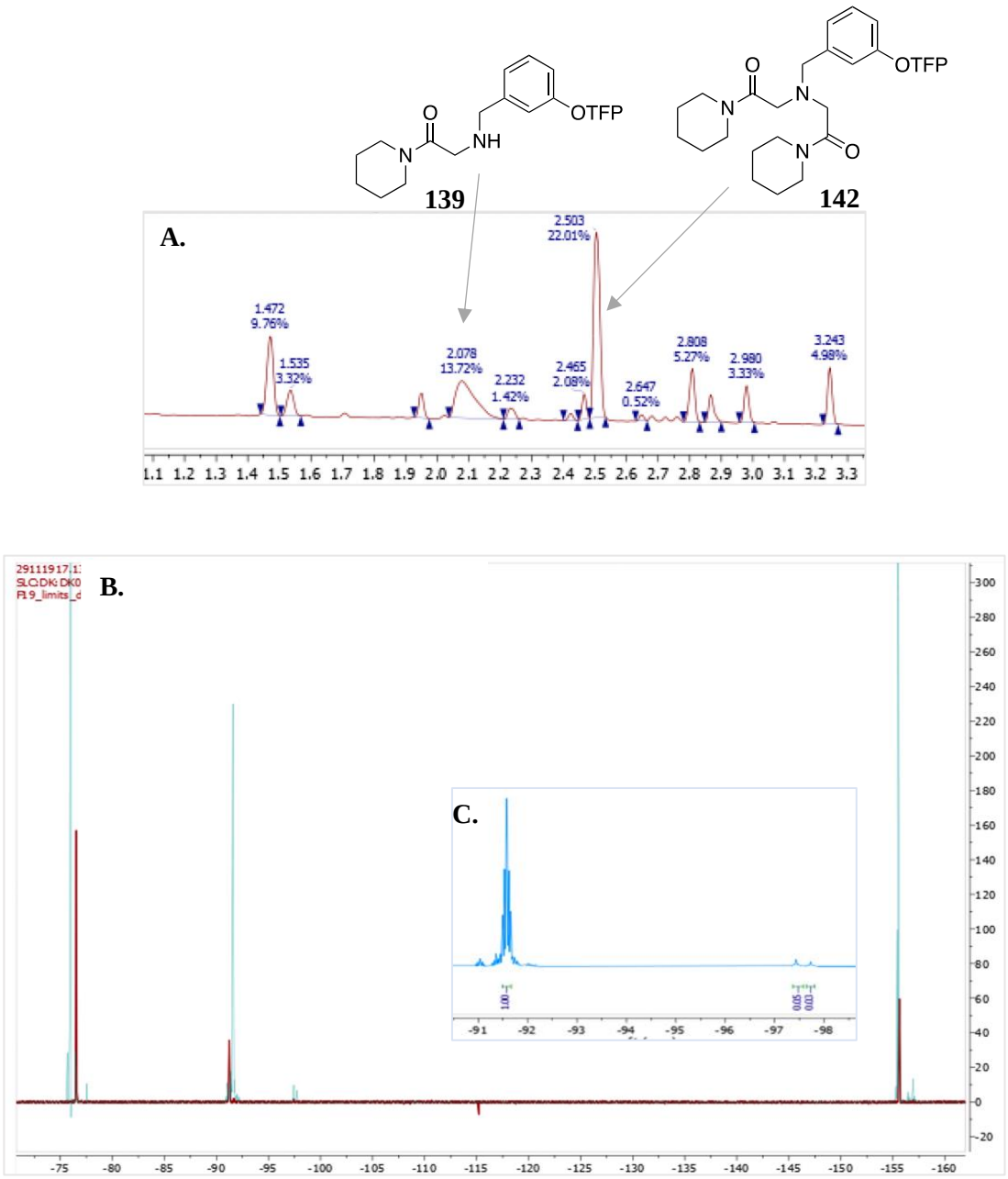

Figure 3.16. Analysis of the reaction mixture containing *O*-TFP *o*-aminomethylphenol **(119)** and the electrophile **129** (see text). **A.** LC-MS trace (qualitative measurement) showing traces of the desired intermediate **139** and the di-alkylated side product **141** as well as the starting material **110**. **B.** ^{19}F NMR signals (quantitative measurement) of pure **110** are shown as **maroon** peaks, and the crude reaction mixture (measured in CD_3CN) is shown as a **blue** signal. **C.** The ratio of mono- and di-substituted species to the starting material is 1:0.08 (7.4%).

Attempts were made to optimise the alkylation reaction, and various conditions which were employed for this purpose (summarised in **Table 3.4**, **Entry 4 – 11**). Previously, the number of equivalents of amine used was 1.2 eq w.r.t. the electrophile. Following this, the number of equivalents of O-TFP aminomethylphenol derivatives was increased. This adjustment was made under the suspicion that the over-alkylation was driven by the formation

of secondary amines in the reaction. This attempt, however, was unsuccessful and resulted in no significant reaction progression by $^{1}H/^{19}F$ NMR analysis.

Table 3.4. A summary of conditions used to test the nucleophilic substitution reaction between 2-bromo-1-piperidyl ethanone and phenolic amine derivatives. *The reaction took place in the presence of KI. (See text for details). As determined by LC-MS.

Entry	No. (equiv.)	Base (equiv.)	Solvent	Temperature and time	Reaction outcome[#]
1	**107**, **108**, **109** (1.2)	DIPEA (4.0)	THF	50°C, 5 days	Traces of product recovered
2	**110, 111, 112** (1.2)	DIPEA (4.0)	THF/ACN	50°C, 5 days	Overalkylation
3	**110, 111, 112** (3.0 or 4.0)	DIPEA (4.0)	THF	RT o/n & 50°C o/n	Overalkylation
4	**111** (4.0)	K_2CO_3*	ACN	6 h reflux	No reaction.
5	**127** (1.0)	NaH (2.2)	THF	RT for 2 h followed by 40°C for 2 h	Traces of product seen by LC-MS (degradation)
6	**127** (1.0)	NaH (2.2)	DMF	RT; 45 mins	No reaction (degradation)
7	**127** (1.0)	DIPEA (4.0)	ACN	RT o/n, followed by 6 h reflux	No reaction
8	**127** (1.0)	Cs_2CO_3 (2.0)	DMF	80°C; o/n	No reaction.
9	**110, 111, 112** (2.0)	$AgClO_4$ (3.0)	ACN	RT, o/n	No pdt recovered
10	**110** (2.0)	Cs_2CO_3 (2.0)	DMF	80°C; o/n	21% yield (*o*-)
11	**111**, **112** (2.0)	Cs_2CO_3 (2.0)	DMF	1 hr; RT	Over-substitution
12	**109** (2.0)	Cs_2CO_3 (2.0)	DMF	80°C; o/n	No reaction

Due to the poor reactivity of the *O*-TFP aminomethylphenol derivatives, an *in-situ* Finkelstein reaction was attempted, shown in **Scheme 3.11**. The aim of this step was to substitute the bromide located on **40** with iodide and aid the attack of the electrophile by the nucleophile. The reaction was performed in ACN and refluxed for ca. 6 hours. However, no reaction progression had occurred. (**Table 3.4, Entry 4**)

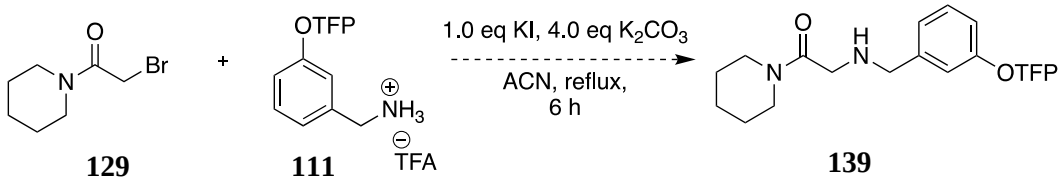

129 **111** **139**

Scheme 3.11. Attempted one-step synthesis showing the *in-situ* Finkelstein reaction. Here, 2 eq of *O*-TFP *m*-aminomethylphenol (**111**) potassium iodide and potassium carbonate in acetonitrile were used.

A different approach was undertaken, whereby the alkylation was performed on *N*-Boc, *O*-TFP *p*-aminomethylphenol (**127**), using different basic reagents as well as different solvents (**Scheme 3.12**, **Table 3.4 Entry 5 – 8**). Here, NaH was employed in order to deprotonate the secondary amine. The pKa of sodium hydride is 40, and whilst numerous studies[23-25] document its effective use in the alkylation of amides, including Boc-protected amines, it was deemed too strong of a base (in both solvents: in THF and DMF) and had likely led to TFP cleavage or molecule degradation in the solvents used. **127** and two different bases with pKa <40, DIPEA and Cs_2CO_3, were investigated in ACN and DMF. Albeit, even after refluxing, these reagents were found to not be sufficiently basic to deprotonate the carbamate.

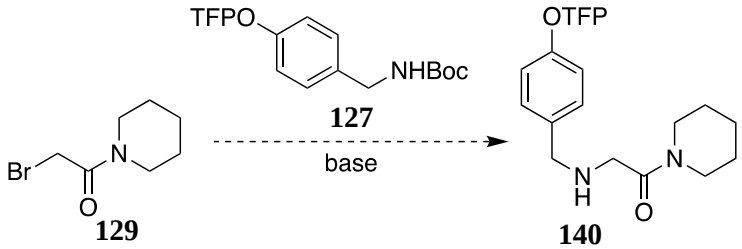

Scheme 3.12. Attempted one-step synthesis showing *N*-alkylation reaction between the electrophile **129** and nucleophile **127**.

Due to the low amine nucleophilicity, caused by TFP group deactivation, the next step in these optimisation efforts was to encourage the abstraction of the bromine through utilisation of silver perchlorate ($AgClO_4$, **Table 3.4 Entry 9**). Previously, the utilisation of silver salts had been successful employed in the resin-bound synthesis of peptoids containing electron poor anilines.[26] The high affinity of silver to form insoluble salts is the driving factor in the reaction. Here, 2 equivalents of the *O*-TFP aminomethylphenol derivative, neutralised with a base, were reacted with 3 equivalents of $AgClO_4$ in acetonitrile. (**Scheme 3.13**) After stirring for ca. 4 hours, no improved reaction outcome was recorded, as only traces of the desired product were detected by LC-MS, again dominated by the di-substituted side-product, and no product spot was detected by TLC.

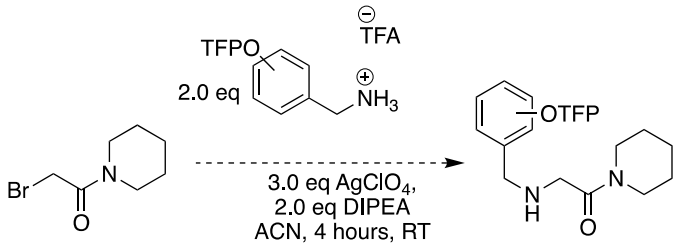

129

No.	Isomer
138	*ortho*
139	*meta*
140	*para*

Scheme 3.13. Attempted one-step synthesis showing *N*-alkylation reaction between the electrophile **129** and the O-TFP benzylamine derivates, with the aid of silver perchlorate ($AgClO_4$)

In 2016, Castillo and co-workers[27] reported Cs_2CO_3-promoted alkylation of aromatic and aliphatic amines. It has been hypothesised that this is achieved via the formation of a complex comprising of the primary amine and caesium which leads to an increased acidity of the amine. This in turn results in an enhanced nucleophilic property of the amine which surpasses the reactivity of the secondary amine. This is shown in **Scheme 3.14**, which suggests that the second alkylation does not occur due to steric hindrance imposed by the di-alkylated species.

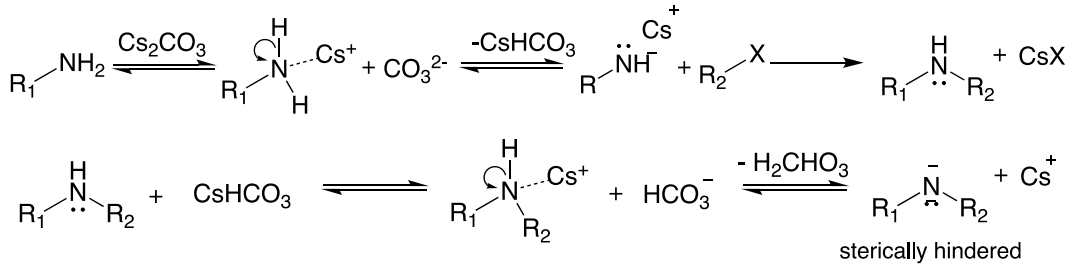

Scheme 3.14. A proposed mechanistic representation of nucleophilic substitution reaction taking place between the primary amine and electrophile. Second alkylation is averted by the steric hindrance of the secondary amine.[26]

Cs_2CO_3 was employed in the alkylation of **101** (**Table 3.4**, **Entry 10**). For this purpose, the electrophile **129**, 2 equivalents of the amine and Cs_2CO_3 were employed. The reaction was allowed to stir at 80 ^oC for 2 hours (**Scheme 3.15**). After this time, a TLC monitoring revealed the formation of **137**. After flash column chromatography, the desired product was recovered in a satisfactory yield. Subsequently, **138** was acetylated, giving rise to **129**. Encouraged by this result, the same reaction conditions were applied in the alkylation of **89** (**Table 3.4**, **Entry 12**). In this case no product was recovered. Surprisingly, the employment of **102** and **103** in the

Cs_2CO_3-mediated *N*-alkylation resulted in over-substitution, after being left to stir at RT for 1 hour. (**Table 3.4**, **Entry 11**)

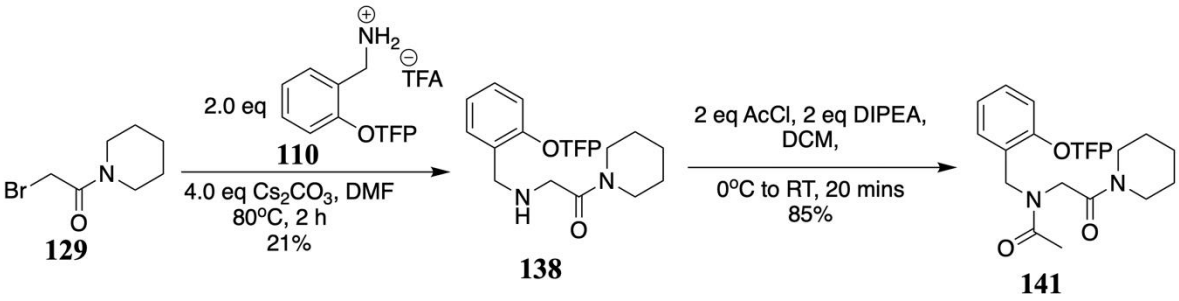

Scheme 3.15. A one step synthesis of a nucleophilic substitution taking place between **110** and **129** leading to the synthesis of mono-alkylated product **141**. Here, 2 eq of amine and 4 eq of Cs_2CO_3 in DMF were employed. The reaction was stirred overnight at 80 °C.

Thus far, the utilisation of the typical conditions and their subsequent optimisation to acquire the model peptoid library designed in order to investigate the effects of phenolic monomers on the *cis/trans* equilibrium of peptoids, had been successful in the synthesis of four model peptoids containing tyrosine derivatives **135** – **137** and **141**. A different synthetic approach was utilised to obtain the *O*-TFP *m*- and *p*-aminomethyl phenol (**111** and **112**) containing acetamides, wherein the TFP-protected amine derivative was to be reacted with 2-hydroxy-1-piperidyl ethanone (**145**), in a Mitsunobu reaction.

To obtain **144**, the commercially available benzyloxyacetyl chloride (**142**) underwent an S_N2 reaction with a piperidine in basic conditions. The reaction resulted in 49% yield after purification, giving the intermediate **143** which was engaged in the high yielding (98%) hydrogenolysis reaction using H_2 atmosphere and 10% palladium on activated carbon as a catalyst. (**Scheme 3.16**)

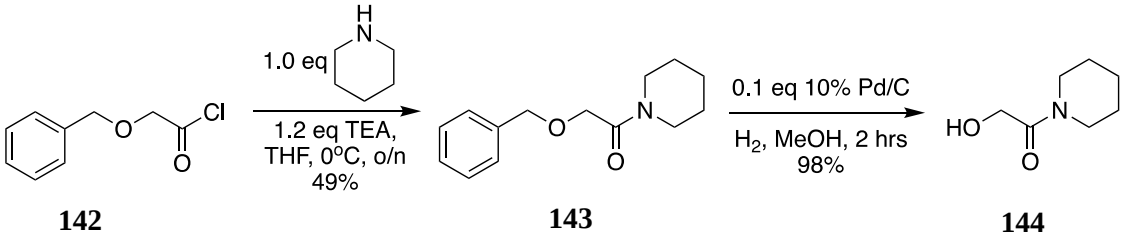

Scheme 3.16. A two-step synthetic route used to obtain 2-hydroxy-1-piperidyl ethanone (**144**) which served as the electrophile for the Mitsunobu reaction.

Subsequently, **144** was engaged in a Mitsunobu reaction with the TFP-protected *p*-aminomethylphenol (**103**). It was hypothesised that the bulkiness of the intermediate in this reaction would result in the formation **140**. The reaction took place under an inert atmosphere, and at 0 ^{o}C DIAD was carefully added. However, this reaction was unsuccessful, akin to previously attempted alkylation (**Scheme 3.17**)

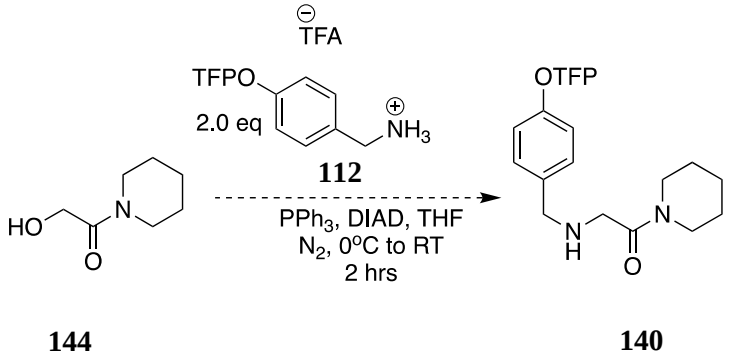

144 **140**

Scheme 3.17. An overview of the attempted Mitsunobu reaction which was used to react 2-hydroxy-1-piperidinyl ethanone **144** and *O*-TFP *p*-aminomethylphenol **112**.

Finally, a three-step reaction route was investigated (**Scheme 3.18**), wherein the amine derivative **112** engaged in an S_N2 reaction with nitrobenzenesulfonyl chloride.[28] It was postulated that the nosyl (Ns) group would be less deactivating than a Boc-group and hence would allow the attack of **129** under mild basic conditions. By utilising an organosulfur material, Ns can be removed without interfering with the rest of the molecule. Denosylation proceeds via the formation of a Mesenheimer complex (**148**) and liberates 1 eq of SO_2 gas.

The first step of the four-step synthetic route resulted in the formation of **146** (Crystal structure obtained is shown in **Figure 3.17**), in an 88% yield after flash column chromatography, whereas the second substitution took place at 50 ^{o}C using **129** in the presence of DIPEA in THF. The desired *di*-substituted intermediate **147** was collected as a colourless oil in a good yield (49%). **147** was engaged in the cleavage of the nitrobenzylsulfonyl as an attempt to form **140** in the presence of thiophenol and a mild base. After 2 hours, the LC-MS monitoring of the reaction mixture revealed no presence of the desired product, and no product was recovered during purification.

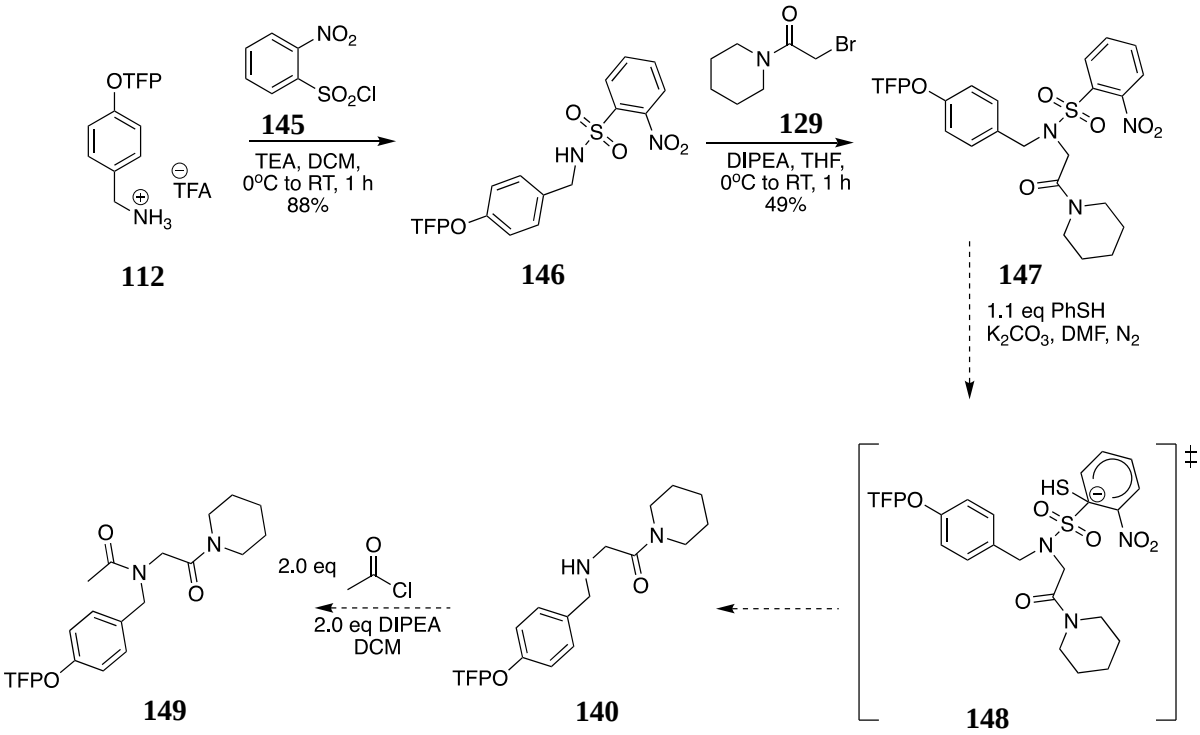

Scheme 3.18. Attempted four-step reaction pathway to obtain the model peptoid containing *O*-TPF *p*-aminomethylphenol (**149**).

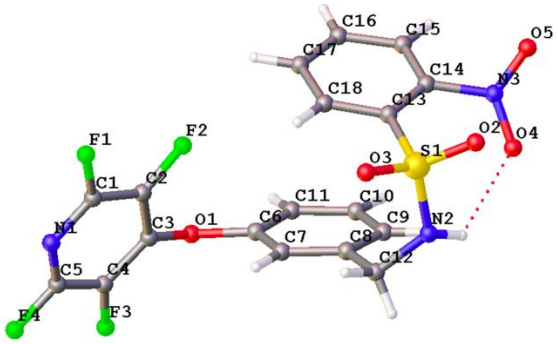

Figure 3.17. Ball-and-stick representation of the *N*-Ns, *O*-TFP *p*-aminomethylphenol **146.** Carbon atoms are depicted in grey, hydrogen atoms in white, nitrogen atoms in navy, oxygen atoms in red, and fluorine atoms in green. Presence of a H-bond between the amide proton and the oxygen of the nitro group seen as a red dotted line. Structure was generated in Olex2 and is reported with a 50% thermal ellipsoid probability.

It was decided that the protection strategy for the synthesis of the complete desired model peptoid library would be changed. Evidently, the extremely electron-withdrawing nature of the TFP protecting group hampered the obtainment of peptoids containing *m*- and *p*-aminomethylphenol monomers (**111** and **112**, respectively). The crucial step of this optimisation was to utilise an *O*-protecting group which would be orthogonal to the Boc group,

allowing the more reactive amine to be Boc-protected prior to the protection of the alcohol. The removal of the chosen protecting functionality attached to the free amine could not interfere with the protected phenol.

In addition, given that the electron withdrawing property of the aromatic ring can be explored to achieve a discreetly folded peptoid chain, we sought to explore the effect of different protecting groups on the *cis*/*trans* equilibrium in model peptoids containing aminomethylphenol derivatives. Notably, substitution of the sp^2 hydrogens with electron withdrawing species, such as TFP ethers, could have a potential to result in a profound effect on the *cis*/*trans* equilibrium of the backbone amide by exploiting the n → π* interactions. This proceeded with a synthesis of a model peptoid containing *o*-aminomethylphenol protected with a group other than TFP.

The three-step syntheses, shown in **Scheme 3.19**, was undertaken in order to produce *O*-Bnz aminomethylphenol monomers (**122** – **124**) which were to be incorporated into model peptoids. The *N*-Boc protected aminomethylphenol derivatives were reacted with benzylbromide under reflux, using K_2CO_3 as a base. After 8 hours, the solids were filtered off and the desired products were recovered in good yields after purification. The cleavage of the Boc-protecting group was performed under acidic conditions. The desired *O*-Bnz aminomethylphenol salts (**153** – **155**) were obtained in quantitative yields.

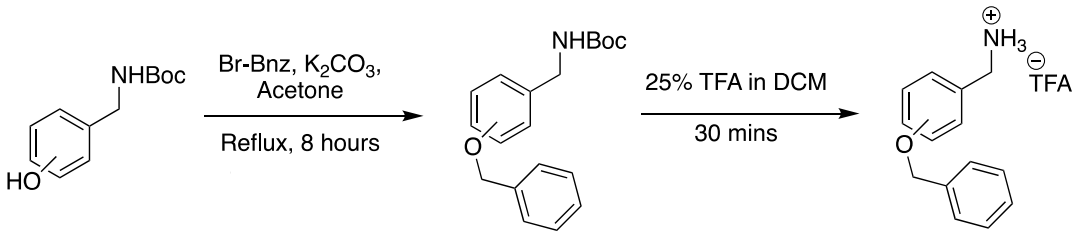

No.	Isomer
122	*ortho*
123	*meta*
124	*para*

No.	Isomer	Yield
150	*ortho*	92%
151	*meta*	84%
152	*para*	69%

No.	Isomer	Yield
153	*ortho*	quant.
154	*meta*	quant.
155	*para*	quant.

Scheme 3.19. Showing the three-step synthesis of the *O*-Bnz *m*- and *p*-aminomethylphenols.

The original conditions used in the synthesis of the control model peptoids were applied in the synthesis of model peptoids containing the monomers bearing *O*-Bnz aminomethylphenols. The electrophile **129** was dropwise added to a solution of the primary amine (4.0 eq) and DIPEA. Subsequently, the crude material was acetylated. After acidic

workup and purification, the two model peptoids were obtained in satisfying yields. The synthesis of the model peptoids containing the *O*-Bnz aminomethylphenols is shown in **Scheme 3.20**.

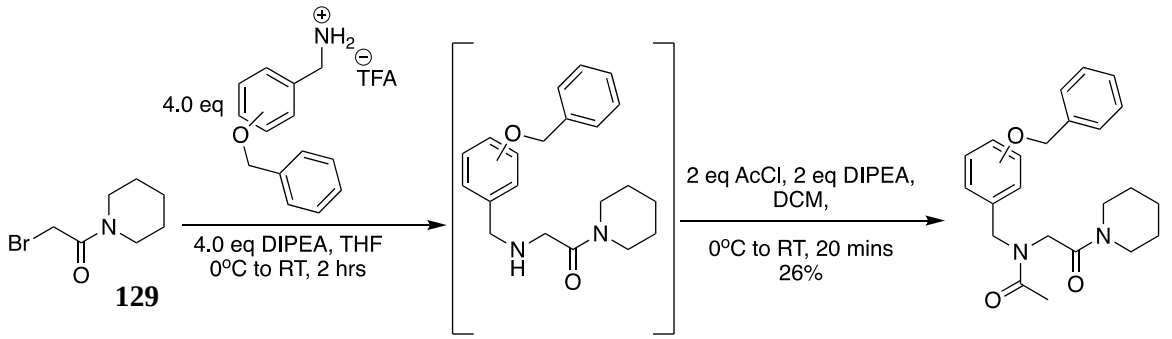

No.	Isomer
156	*ortho*
157	*meta*
158	*para*

No.	Isomer	Yield
159	*ortho*	28%
160	*meta*	26%
161	*para*	23%

Scheme 3.20. A two-step synthetic route used in the synthesis of model peptoids containing *O*-Bnz aminomethylphenols. The second step of this route was undertaken without isolation of the intermediate.

3.4.3. Synthesis of model peptoids containing unprotected hydroxyaniline derivatives

The production of model peptoids containing unprotected hydroxyaniline derivatives proceeded with the employment of potassium fluoride (KF), acting as a source of F^- ions, as well as thiophenol, and both reagents were used in excess. (**Scheme 3.21**) The LC-MS monitoring (**Figure 3.18**) of the synthesis of **103** after 3 hours showed full conversion of the substrate into the liberated phenol as well as the formation of a *tri*-substituted PFP by-product (**162**). After purification the phenols were obtained in good yields.

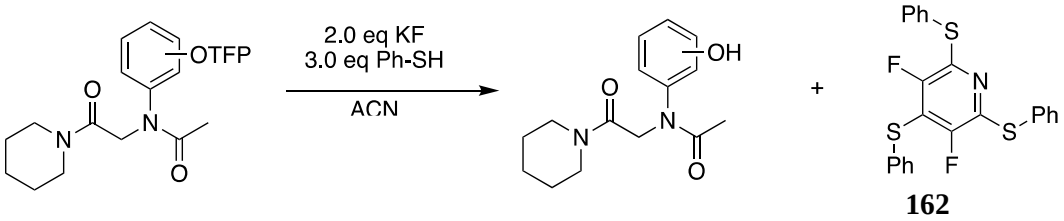

No.	Isomer
135	*ortho*
136	*meta*
137	*para*

No.	Isomer	Yield
60	*ortho*	74%
103	*meta*	74%
59	*para*	88%

Scheme 3.21. One step synthesis used to cleave the TFP-group yielding model peptoids containing *o*-, *m*- and *p*-aminophenols (**60**, **103**, **59**).

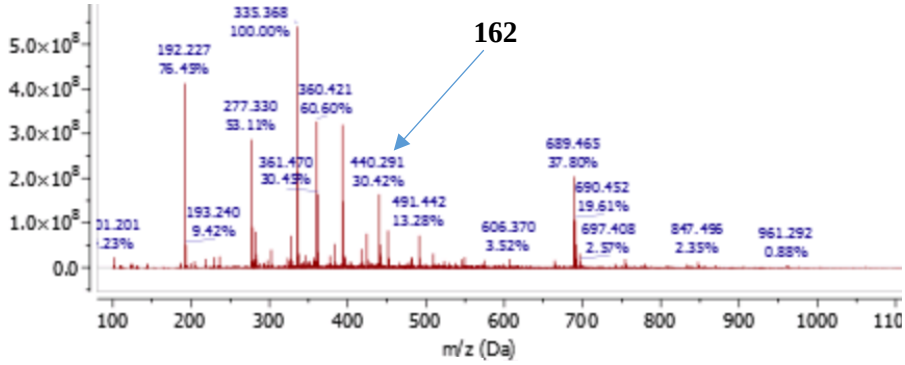

Figure 3.18. MS/MS trace of the crude peptoid **103** showing the *tri*-substituted PFP side product **162** (*m*/*z* = 440).

3.4.4. Synthesis of model peptoids containing unprotected aminomethylphenol derivatives

Hydrogenolysis produced model peptoids containing unprotected hydroxy benzylamine residues. Standard conditions of hydrogen atmosphere and 10% Pd/C catalyst were used for the cleavage of the benzyl phenyl ethers and such conditions produced the desired products in very high yields thanks to clean conversions. (**Scheme 3.22**)

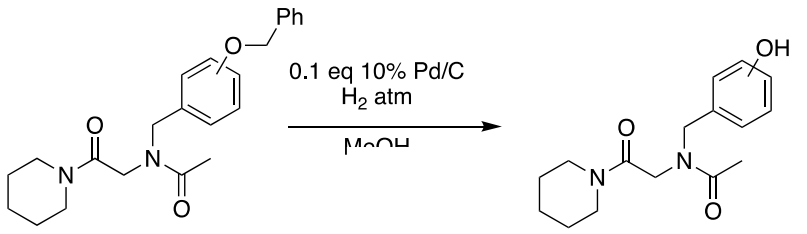

No.	Isomer
159	*ortho*
160	*meta*
161	*para*

No.	Isomer	Yield
104	*ortho*	97%
105	*meta*	76%
106	*para*	98%

Scheme 3.22. One-step synthesis used to cleave the benzyl phenyl ethers yielding model peptoids containing hydroxy benzylamines.

3.4.5. NMR analysis: The effect of tyrosine-type submonomers on the peptoid amide bond *cis/trans* conformational equilibrium

The impact of the hydroxy aryl-based side chains on the peptoid amide bond *cis/trans* equilibrium was analysed using NMR spectroscopic techniques as documented in the literature.[29] The effect of these side chains was assessed by direct comparison to **130** and **40** which were used as controls. The experimental procedures used for the obtainment of the $K_{cis/trans}$ and $\Delta G_{cis/trans}$ are described in detail in **Chapter 7**, **Section 7.6.50**.

In order to determine the population ratios between the *cis*- and *trans*-isomers in solution for each of the model peptoids in this study, ^{1}H NMR resonances of peptoids were measured in three different solvents: $CDCl_3$, CD_3CN and CD_3OD. The use of a protic solvent probed the effects of polar environments on the proton donating hydroxy moieties located on the aryl rings. In addition to the 1D ^{1}H NMR, the nuclear Overhauser effect spectroscopy (NOESY) was employed to distinguish between the *cis*- and *trans*-isomers. Furthermore, ^{1}H-^{13}C 2D NMR techniques HMBC (the heteronuclear multiple bond correlation) and HSQC (the heteronuclear single quantum coherence) were used to accurately assign each proton peak to aid $K_{cis/trans}$ determination.

It was imperative to complete NMR inversion experiments in order to extract T_1 data (the spin-lattice relaxation time constants), for the three main proton groups used in the determination of $K_{cis/trans}$ values for the model peptoids synthesised in this thesis. Importantly, each nucleus in a molecule has a different T_1 value which will affect the relative integration between signals. For quantitative purposes it is mandatory to allow the relaxation time of the

NMR to be at least five times greater than the longest T_1. The inversion experiments were carried out on model peptoids **60** and **104** in $CDCl_3$, CD_3CN and CD_3OD. The $K_{cis/trans}$ values reported were calculated from ^1H NMR experiments with relaxation time of 13.9 s (wherein delay period = 10 s, and acquisition period = 3.9 s). Consequently, the T_1 value for each of the nucleus involved in the determination of the $K_{cis/trans}$ value must not have exceeded 2.78 s (the relaxation time must be at least five times greater than T_1). The T_1 values calculated for chosen peptoids are shown in **Table 3.5**. These values were extracted from ^1H NMR inversion experiments (**Figure 3.19**). Meanwhile, the T_1 relaxation curve for **104** together with the three-parameter exponential fit equations for this model system are shown in **Figure 3.20**.

Table 3.5. Example of two peptoids showing T_1 values extracted from the ^1H NMR inversion experiments.

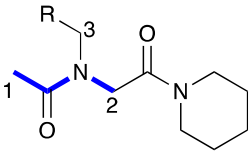

Model peptoid	NMR solvent	T_1 (s)					
		1 *cis*	**1 *trans***	**2 *cis***	**2 *trans***	**3 *cis***	**3 *trans***
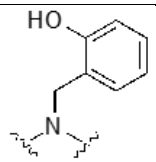 **104**	**$CDCl_3$**	1.32	1.26	0.63	0.74	0.72	0.71
	CD_3CN	2.32	2.20	1.12	1.09	1.30	1.25
	CD_3OD	1.25	1.24	0.61	0.64	0.78	0.76
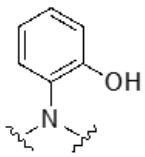 **60**	**$CDCl_3$**	nd	1.71	nd	0.85[a]	nd	nd
	CD_3CN	nd	2.57	nd	1.44[a]	nd	nd
	CD_3OD	nd	*	nd	0.95[a]	nd	nd

nd (no data recorded) = absence of protons
*proton signals overlap with the solvent peak
[a]average of two ^1H NMR signals corresponding to atropisomeric backbone methylene protons

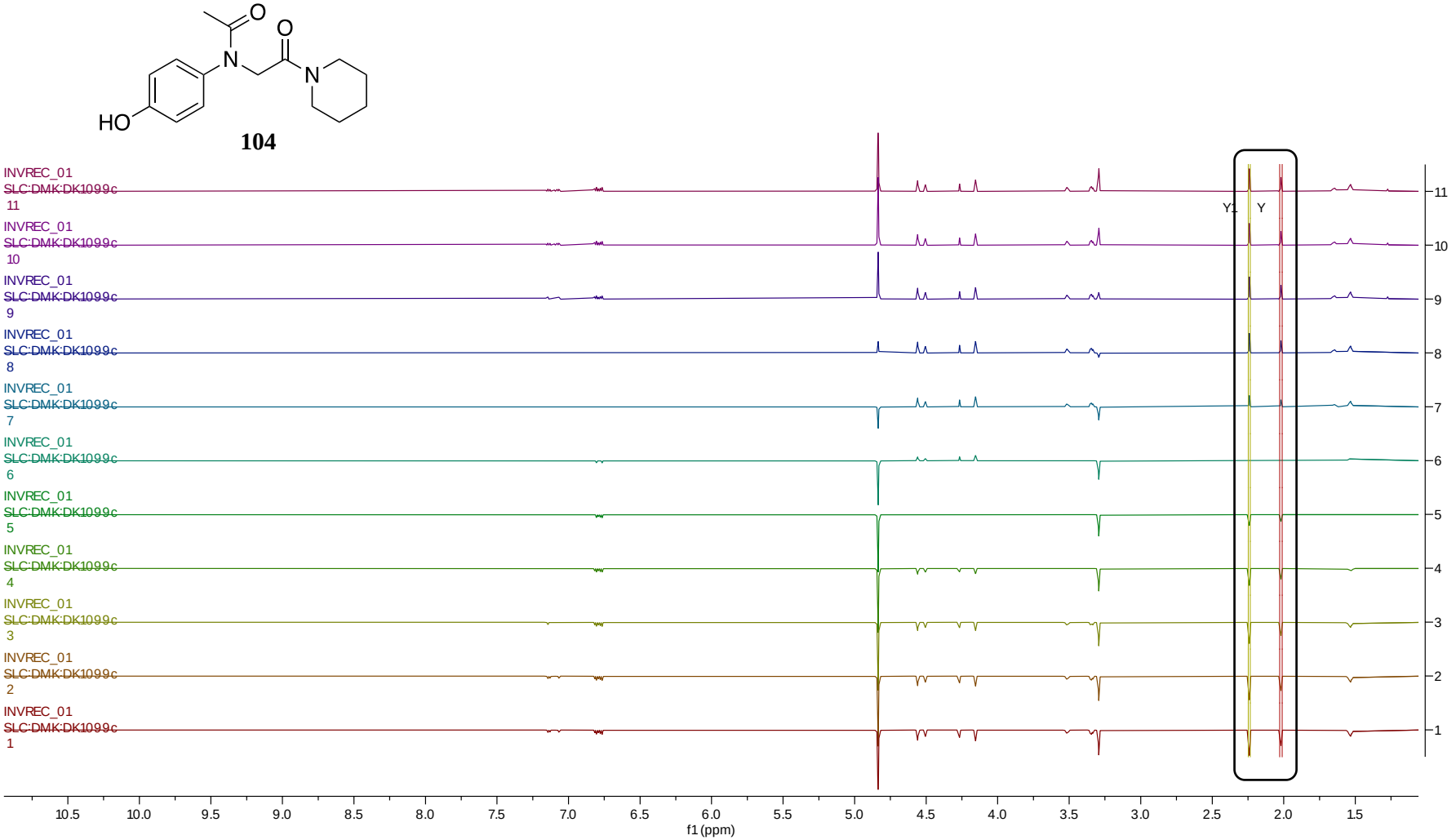

Figure 3.19. Data extracted from inversion experiments carried out for **104** in CD_3OD. Example T_1 calculations and values for the terminal acetal protons shown.

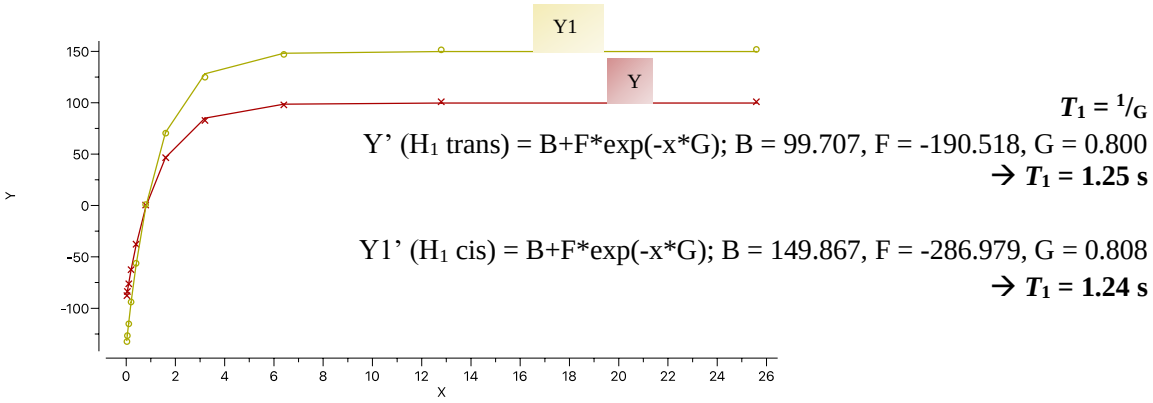

Figure 3.20. T_1 relaxation (longitudinal relaxation) curve of the terminal acetyl protons of the model peptoid **104**.

Assignment of the NMR spectra for the two model systems (**60** and **104**) and the subsequent determination of the *cis*/*trans*-isomer ratio is vastly affected by the relaxation periods of the nuclei. Whilst all of the protons in the molecule can be assigned to either *cis* or *trans*-isomers, the rapid motion of the freely spinning acetyl protons offers less effective relaxation mechanisms compared to other protons in the model peptoids. Likewise, rapid relaxation results in broad or even undetectable NMR signals, as well as unresolvable *J*-couplings. Still, it was ensured that enough time was allocated for the terminal methyl protons to reach nuclei relaxation at 298 K. The T_1 data collected for the two model systems showed that our ^{1}H NMR experimental setup allowed for unequivocal assignment of *cis*- and *trans*-isomers for all of the dipeptoids.

$K_{cis/trans}$ value determination studies were commenced by subjecting the model systems containing the more extended aromatic systems to NMR analysis. Peptoid **40** was used as the reference compound, and the aniline (**130**) monomer induced fully homogeneous trans amide geometry within the system. ^{19}F NMR spectroscopic analysis confirmed the predicted position of the TFP substitution pattern seen in *O*-TFP containing model systems as para to the nitrogen in the heteroaromatic. Summary of the NMR findings for peptoids in this chapter is shown in **Table 3.6**, and the experimental procedure is described in **Chapter 7**, **Section 7.6.50**.

Table 3.6. $K_{cis/trans}$ values in different solvents (CD_3OD, CD_3CN, $CDCl_3$) and their corresponding Gibbs free energy differences (ΔG in kcal mol^{-1}) of model peptoids containing different monomers. $K_{cis/trans}$ values are calculated using three sets of ^1H NMR resonances and are rounded to two decimal places.

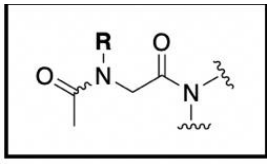

R =

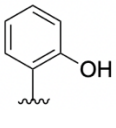

*N*2hph **60**

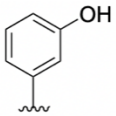

*N*3hph **103**

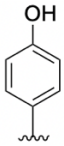

*N*4hph **59**

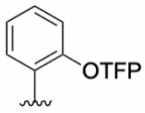

*N*2h(TFP)ph **135**

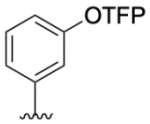

*N*3h(TFP)ph **136**

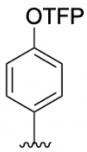

*N*4h(TFP)ph **137**

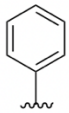

*N*ph **130**

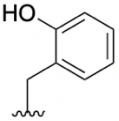

*No*Tyr **104**

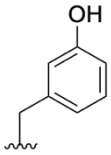

*Nm*Tyr **105**

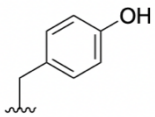

*N*Tyr **106**

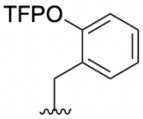

*No*Tyr(TFP) **141**

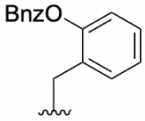

*No*Tyr(Bnz) **159**

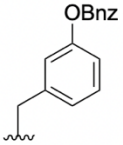

*Nm*Tyr(Bnz) **160**

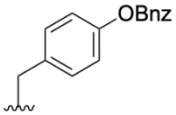

*N*Tyr(Bnz) **161**

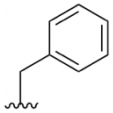

*N*Phe **40**

Entry	No.	$CDCl_3$			CD_3CN			CD_3OD		
		$K_{cis/trans}$	ΔG (kcal mol^{-1})[a]	^{19}F $K_{cis/trans}$	$K_{cis/trans}$	ΔG (kcal mol^{-1})	^{19}F $K_{cis/trans}$	$K_{cis/trans}$	ΔG (kcal mol^{-1})	^{19}F $K_{cis/trans}$
1	**60**	-*	-	-	-*	-	-	-*	-	-
2	**103**	-*	-	-	-*	-	-	-*	-	-
3	**59**	0.05	1.77	-	0.05	1.77	-	0.04	1.91	-
4	**135**	-*	-	-	0.11	1.31	0.1	0.06	1.67	0.07
5	**136**	-*	-	-	-*	-		-*	-	-
6	**137**	0.04	1.91	0.02	0.18	1.02	0.03	0.04	1.91	0.3
7	**130**	-*	-	-	-*	-	-	-*	-	-
8	**104**	7.13	-1.16	-	8.70	-1.28	-	0.65	0.26	-
9	**105**	0.27	0.78	-	0.99	0.00	-	0.62	0.28	-
10	**106**	0.19	0.98	-	1.04	-0.02	-	0.75	0.17	-
11	**141**	0.35	0.62	0.33	1.40	-0.20	1.37	0.80	0.13	0.80
12	**159**	0.18	1.02	-	1.11	-0.06	-	0.49	0.42	-
13	**160**	0.26	0.80	-	1.13	-0.07	-	0.69	0.22	-
14	**161**	0.26	0.80	-	1.14	-0.08	-	0.69	0.22	-
15	**40**	0.26	0.80	-	1.15	-0.08	-	0.04	1.91	-

[a] The value was calculated using the Gibbs Free Energy equation $\Delta G^o = -RT \ln(K_{eq})$ at 298 K, where $R = 1.987 \times 10^{-3}$ kcal $K^{-1}mol^{-1}$.

* Presence of only one isomer (*trans*). NMR signals corresponding to the *cis*-isomer were not detected.

3.4.6. The effect of tyrosine-type submonomers on $K_{cis/trans}$ values: solution state analysis: 59, 60, 103, 130, 135 – 137.

It was anticipated that the bulky, electron withdrawing TFP group would induce *cis* amide bonds, especially in the case of **135** (**Table 3.6**, **Entry 4**), and to a lesser extent **136** (**Table 3.6**, **Entry 5**), where the steric bulk sits closer to the peptoid backbone. Furthermore, it was postulated that the high electronegativity of fluorine could induce hydrogen bonding between the model systems found in literature document such structures encourage more restriction to the rotation of the side chain relative to the amide centre resulting in *cis* acetamide formation.[29]

The high Gibbs free energy ($\Delta G_{cis/trans}$) values obtained, for the hydroxyaniline-based peptoids, in all solvents are characteristic for the *trans* amide bond geometry. The *trans* acetamides exhibit increased stabilisation in chloroform for all the hydroxyaniline-containing dipeptoids (**Table 3.6**, **Entries 1 – 7**). Generally, decreased $K_{cis/trans}$ values for model systems in $CDCl_3$ have been reported in the literature.[3,17,18] The NOESY spectra collected for these model systems revealed strong *NOE* signals between the *o*-aryl protons and the terminal acetyl methyl protons (**Figures 3.21** and **3.22** show NOESY spectra evidencing the predominance of *trans* geometry within the acetamides **135**, **60** and **103**, in $CDCl_3$).

Initially, it was expected that the protection of the hydroxy functionality with a TFP group (**135** – **137**, **Table 3.6**, **Entries 4 – 6**) would potentially induce *cis*-isomer preference. This proved not to be the case and an enhancement in the *cis*/*trans* preferences for the TFP containing model peptoids, relative to **130**, **59**, **60** and **103**, was not observed. This implies that the strength of the $n \rightarrow \pi_{C=O}^*$ forces in these dipeptoids overshadow the *cis*-inducing $n \rightarrow \pi_{Ar}^*$ electronic interactions. The increase of the $K_{cis/trans}$ values in acetonitrile occurs in both **137** (**Table 3.6**, **Entry 6**) and **135** (**Table 3.6**, **Entry 4**), amounting to 0.18 and 0.11 respectively. This data is consistent with the early studies in the Blackwell group,[3] where the preference for *cis* amide bond formation was found to be favoured in acetonitrile. Meanwhile, **136** amide bond geometry isomerisation was found to be 100% *trans* in all of the solvents, evidenced by the lack of NMR resonances attributed to *cis*-isomerisation.

Characteristic for the *trans* amide bond geometry, the NOESY spectrum collected for compound **135** revealed a strong *NOE* signal between the aryl proton and the terminal acetyl methyl protons, shown in **Figure 3.21**. Interestingly, the NMR analysis revealed that peptoid **135** displayed an atropoisomeric effect on the backbone methylene protons, which can explain

the enhancement of the *trans* character of the amide bond population present in the sample. The presence of the two non-equivalent protons revealed two doublets ($J_{HH,123}$ = 16.0 Hz) in the ^{1}H NMR analysis, each integrating to one proton. **Figure 3.21** shows the H-bonding stabilising the *trans-(M*) isomer of compound **135**. To this end, we have shown that placing the *O*-TFP moiety in the *ortho* position of the *N*-aryl side chain will create a large degree of hindrance to rotation in the model peptoid **135** ($K_{cis/trans}$ = 0.11, $\Delta G_{cis/trans}$ = 1.31). The steric barrier causes a conformational interconversion to be slow enough to allow the two backbone protons to fully resolve their non-equivalencies which can be seen in the ^{1}H NMR spectrum as two characteristic NMR resonances. Notably, the effect of the steric strain not present in the *m*- or *p*-regioisomers (dipeptoids **136** and **137**, respectively).

In line with Blackwell's report,[3] and similar to the behaviour of geminal protons in **135**, the presence of the liberated *ortho*-hydroxy moiety in **60** (**Table 3.6**, **Entry 1**) restricted the rotation of the *N*-aryl side chain. The observable non-equivalence in **60** can be attributed to a high order of dissymmetry. (**Figure 3.22**) The non-equivalence around the trivalent *N*-centre is therefore not attributed to the presence of different substituents, as evidenced by the library of model peptoids containing *N*-hydroxyaryls synthesised in this thesis. This is in an agreement with Siddal's research findings[30], which concluded that trivalent nitrogen centres would produce non-equivalent geminal protons (H_a and H_b) when $R \neq R_1$, which is caused by their identities being determined by the orientation of the *ortho* groups R and R_1. ^{1}H-^{1}H NOESY NMR spectrum showing the presence of non-equivalent geminal protons in **60** and **103** can be seen in **Figure 3.22**.

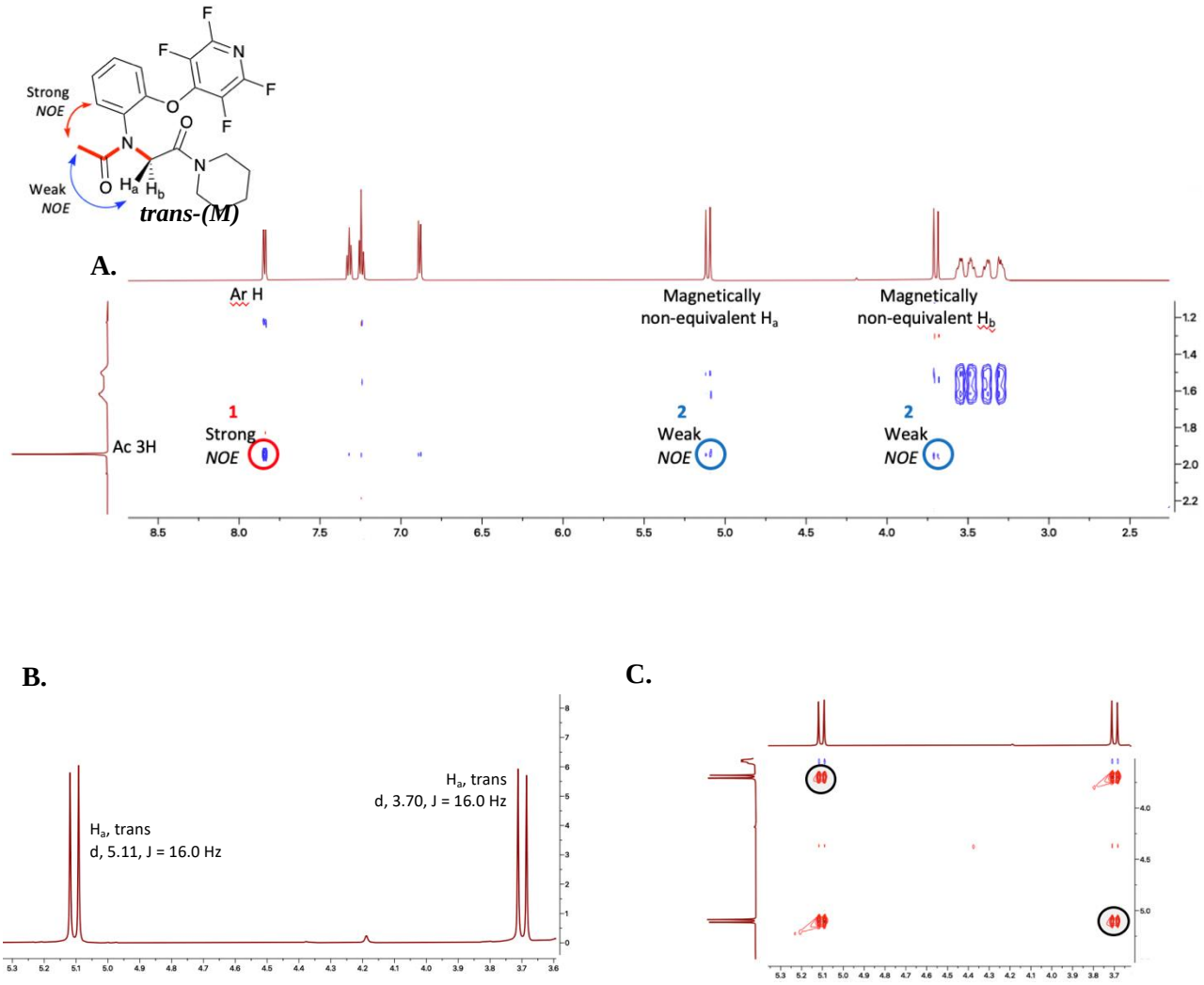

Figure 3.21. A. ^{1}H-^{1}H NOESY spectrum of **135** in $CDCl_3$ showing spatial correlation between **1**) the terminal acetyl protons and the aromatic proton in the *ortho* position; **2**) the terminal protons and the atropoisomeric backbone methylene protons H_a and H_b; **B**. ^{1}H NMR showing the presence of non-equivalent protons; **C.** ^{1}H-^{1}H NOESY spectrum showing the discreet spatial correlation between the two backbone methylene protons.

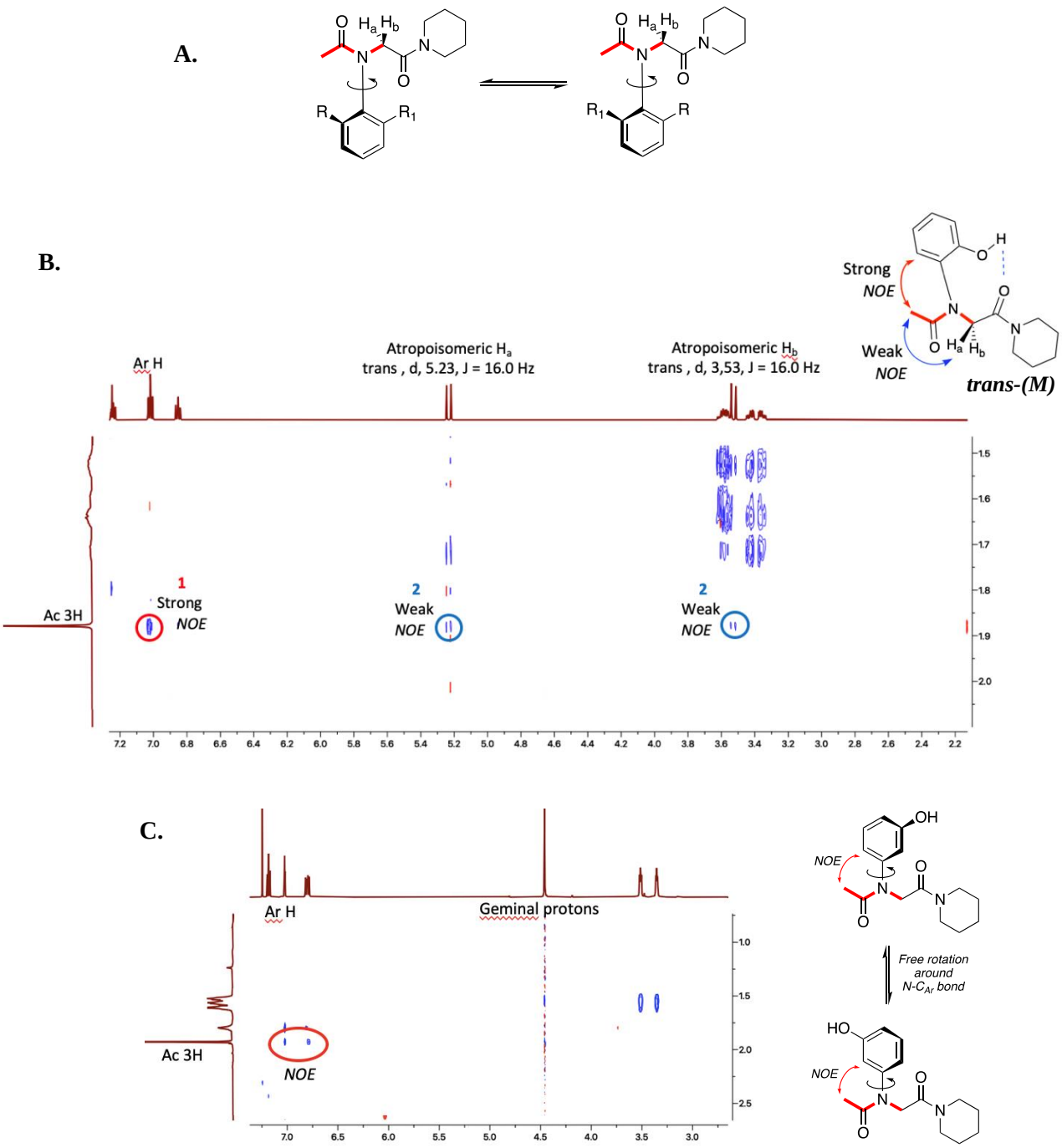

Figure 3.22. A. A schematic depiction of interchanging identities of H_a and H_b with respect to R and R_1. **B.** Structure of **60** showing *NOE* signals associated with the terminal acetal protons & H-bonding between the aryl hydroxyl and O_i; ^{1}H-^{1}H NOESY spectrum of **60** in $CDCl_3$ showing spatial correlation between **1**) the terminal acetyl protons and the aromatic proton in the *ortho* position; **2**) the terminal protons and the atropoisomeric geminal protons H_a and H_b. **C.** Structure of **103** showing NOE signals w.r.t. terminal acetal protons; ^{1}H-^{1}H NOESY spectrum of **103** in $CDCl_3$ showing spatial correlation between the terminal acetyl protons and the aromatic protons in the *ortho* position.

The non-covalent intermolecular forces stabilising the *trans* amide conformation in **60** can further be identified from the ^{1}H NMR spectroscopic analysis of **59**, **60** and **103** model systems. The formation of the intramolecular eight-membered-ring hydrogen bonding (shown in **Figure 22.B.**) between the side chain hydroxyl proton donor and the C=O$_i$ can be evidenced by the downfield chemical shift of the alcohol peak of **60** relative to the upfield shifts of **59** (**Table 3.6**, **Entry 3**) and **103** (**Table 3.6**, **Entry 2**). (**Figure 3.23**) In addition, it had been demonstrated that modulating the concentrations of model systems containing *m*- and *p*-hydroxyanilines will result in the formation of intermolecular hydrogen bonding.[3]

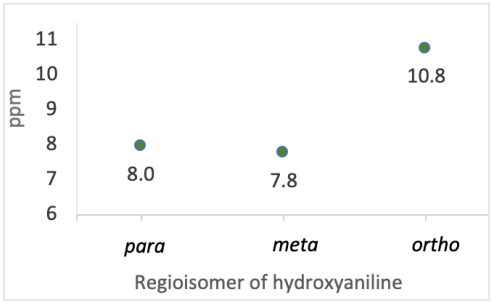

Figure 3.23. A chart showing chemical shifts of the aromatic -O**H** seen in the ^{1}H NMR spectra of model systems **59**, **60** and **103** in $CDCl_3$. The ppm values correlate with the type of hydrogen bonding present in the mixing samples of the acetamides.

3.4.7. The effect of tyrosine-type submonomers on $K_{cis/trans}$ values: solution state analysis: 40, 104 – 106, 141, 159 – 161

It has been demonstrated that the hydroxyaryl monomers in the previous set of model peptoids induce *trans* amide bonds. Indeed, even the extremely bulky and electron-withdrawing nature of the TFP-group did not generate *cis*-isomerism. As evidenced by previous studies, the enhancement of *cis* geometry is desired when designing antimicrobial peptoids.

The introduction of hydrogen bond donors can lead to the stabilisation of peptoid secondary structures. In model systems containing hydroxy benzylamines, it was postulated that the addition of a spacer (CH_2) in between the amine and the aryl side chain could aid us to facilitate the formation of hydrogen bonding between the hydroxy moiety and O$_{i-1}$, resulting in

a direct effect on local conformations of these acetamides. Addition of a spacer also enabled to directly compare the introduction of aryl ring substituents to **40** (**Table 3.6**, **Entry 15**) which was used as an achiral aromatic reference compound.

The analysis of **40** ^{1}H NMR spectrum revealed equilibrium values consistent with previously reported data.[3] While the *trans*-isomerism of **40** was most prevalent in the non-polar $CDCl_3$ ($K_{cis/trans}$ = 0.26), the solvent-dependent peptoid secondary structure generation led to its decreased $\Delta G_{cis/trans}$ value in CD_3CN, signifying stabilisation of *cis* amide bond geometry. The energetical favouritism of *cis*-isomerisation for the reference compound **40** showed a decrease in $\Delta G_{cis/trans}$ of 0.88 kcal mol^{-1} in CD_3CN when compared to $CDCl_3$.

The *O*-Bnz-containing acetanilide $K_{cis/trans}$ values showed no substantial variation for the model systems **159** – **161** (**Table 3.6**, **Entries 12 – 14**), relative to **40**. The three dipeptoids exhibited the formation of *trans* amide bonds only (**Table 3.6**). Additionally, the general trend of secondary structure generation follows the observations from the ^{1}H NMR spectroscopic analysis of hydroxyanilines, discussed in **Section 3.3.4.2**. Notably, **159** (**Table 3.6**, **Entry 12**) showed an increased *trans*-isomerism compared to **160** and **161** (**Table 3.6**, **Entries 13** and **14**). In this instance, the *o*-substituent in **159** contributed to a marginal increase in *trans* geometry ($\Delta[\Delta G_{cis/trans}\ (CD_3OD)]_{\mathbf{160\ \&\ 159}}$ = 0.20 kcal mol^{-1}; $\Delta[\Delta G_{cis/trans}\ (CD_3CN)]_{\mathbf{160\ \&\ 159}}$ = 0.01 kcal mol^{-1}) possibly arising from dissymmetry caused by the non-identical R and R_1 groups (**Figure 3.22.A**.). This could have been achieved in absence of detectable atropoisomerism at 298 K, due to the inversion rate of backbone geminal protons being significantly greater than in model systems **60** and **107**.

Meanwhile, introduction of the *O*-TFP *o*-hydroxybenzylamine **110** present in **141** (**Table 3.6**, **Entry 11**) resulted in the generation of a slight increase in the *cis*/*trans* ratios produced, relative to the reference peptoid **40** (**Table 3.6**, **Entry 15**), in all the solvents in the range of $\Delta K_{cis/trans}$ = 0.09 to 0.25. The increase in the *cis* bias in **141** compared to **40** was highest in $CDCl_3$ (35%) and lowest in CD_3OD (16%). This implies that the *cis* configuration of **141** is more lipophilic than its *trans* configuration. Regardless, the $\Delta G_{cis/trans}$ values calculated for **141** indicate that peptoid monomer **110** does not induce a considerable *cis* bias. Contrary to our initial speculations of the ability of the sterically bulky TFP to induce *cis* amide bonds, these findings led us to believe that there exists electronic repulsion between O_{i-1} and the *O*-TFP. This causes the n $\rightarrow$ $\pi_{C=O}$* forces to dominate, resulting in the enhancement in *trans* amide bond isomerism. (**Scheme 3.23**)

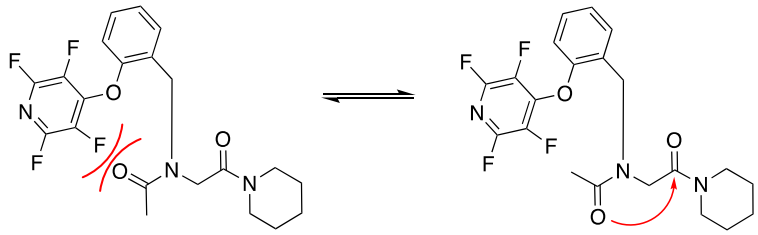

Scheme 3.23. Schematic depiction of the electronic repulsion interactions in **141** leading to a *trans* bias in amide bond populations. The n → $\pi_{C=O}$* forces are also shown (red arrow).

The removal of the TFP group and liberation of the hydroxyl groups in **106** and **105** yielded acetamides with *cis*/*trans* equilibrium systems displaced to the *trans*-isomer (**Table 3.6**, **Entry 9** and **10**). Moreover, **106** ($K_{cis/trans}$ = 1.04) resulted in marginally greater population of *cis* amides than **105** ($K_{cis/trans}$ = 0.99) in CD_3CN. While noticeable, it did not produce an energetically significant change. In contrast, **104** (**Table 3.6**, **Entry 8**), bearing the *o*-hydroxy aryl monomer **119**, saw significant enhancement in the *cis* amide preference. Indeed, even in $CDCl_3$, ($K_{cis/trans}$ = 7.05) **104** saw a 9-fold increase in the $K_{cis/trans}$ value compared to the aryl reference **40** ($K_{cis/trans}$ = 0.80). The favoured *trans* geometry of this acetanilide in the protic CD_3OD ($K_{cis/trans}$ = 0.65) was indicative of a switch in isomer populations caused by intermolecular hydrogen bonding. The presence of hydrogen bond acceptors in methanol lead to hydrogen bond formation between the solvent and **104** which outcompeted the intramolecular hydrogen bonding resulting in higher $\Delta G_{cis/trans}$. In CD_3CN, $K_{cis/trans}$ value of **104** increased by 22% (90% *cis* amide population) compared to $CDCl_3$. As expected, the solvent nature influenced the local confirmation of the amide bond in **104**. This was evidenced by very intense NOE signals between the terminal acetyl protons and the backbone methylene protons and indicated their increased spatial proximity in CD_3CN. Further analysis of ^1H NMR spectral data gave an even stronger indication of hydrogen bonding present in **104**, wherein the chemical shift of the alcohol moiety for the *cis*-isomer showed high deshielding relative to the *trans*-isomer. **Figure 3.24** depicts formation of the eight-membered-ring hydrogen bonding between the *o*-hydroxy aryl side chain and the O_i in **104**, as well as detailed ^1H-^1H NOESY NMR analysis of the system.

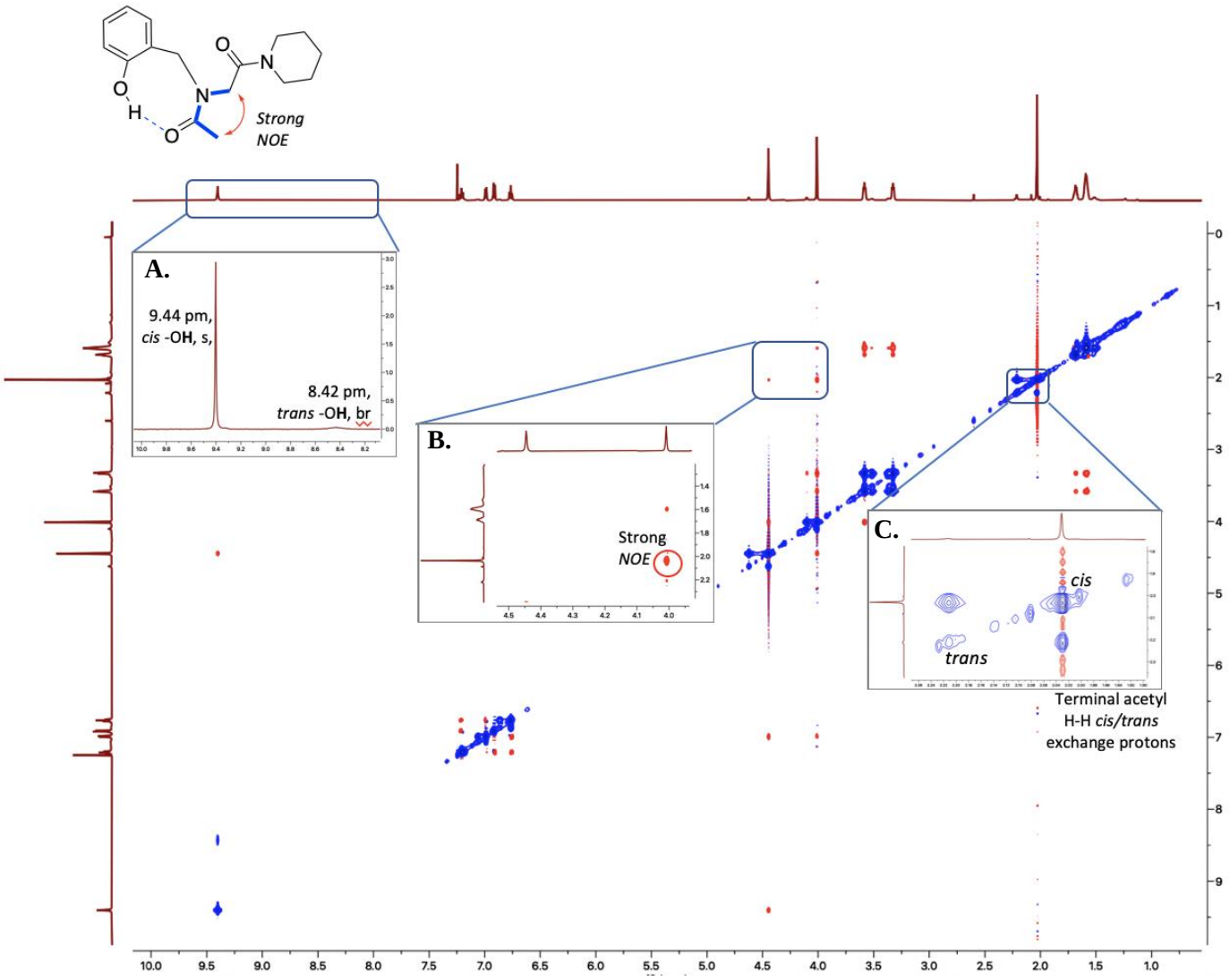

Figure 3.24 Structure of **126** showing H-bonding between the side chain hydroxyl H-bond donor and the terminal carbonyl & ^{1}H-^{1}H NOESY NMR spectrum of **104** in $CDCl_3$. **A.** Hydroxyl proton chemical shifts in both *cis*- and *trans*-isomers; **B.** NOE peaks showing spatial correlation between terminal acetyl protons and backbone methylene protons; **C.** Spatial correlation between terminal acetyl exchange protons of the *cis*- and *trans*-isomers of **104**.

3.4.8. Characterisation of acetamides 59, 60, 130 and 136 in the solid state

We endeavoured to provide supporting evidence that the peptoid monomers discussed in this thesis have the potential to give rise to distinct local amide conformations. Despite efforts to obtain crystal structures of all the model systems, the vast majority of these attempts were unsuccessful due to the materials being yielded as oils, particularly for acetamides containing benzylamine monomers, which prevented us from obtaining crystals suitable for single crystal X-ray crystallography. Crystals of the peptoids for which X-ray data were obtained were grown by slow evaporation at room temperature from saturated mixtures of polar

and non-polar solvents, such as chloroform and *n*-hexanes. The torsion angles observed in the X-ray crystal structures of five model peptoids are shown in **Table 3.7**. In all the model peptoids containing anilines, the dihedral angles found corroborated the NMR data which is discussed in **Sections 3.4.6** and **3.4.7**.

Table 3.7. Dihedral angles of model peptoids **59**, **60**, **130** and **136** observed by X-ray crystallography.

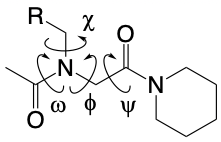

Entry	No.	ω (deg) C8-C7-N1-C9	ϕ (deg) C7-N1-C9-C10	ψ (deg) N1-C9-C10-N2	χ (deg) C2-C1-N1-C9
1	**59**	-178.63	92.19	178.44	116.66
2	**60**[a]	179.58/-179.43	-74.88/76.7	165.25/-168.59	-98.98/98.44
3	**130**	178.70	101.20	168.18	64.60
4	**136**	-173.22	-96.80	-175.73	73.60

[a] presence of two non-identical structures found in the unit cell.

As predicted, for all of the previously reported model systems **130**, **59** and **60**,[3] the amide bond dihedral angles (ω) demonstrated amide bond planarity, with their values being close to 180°. This is consistent with the *trans* amide bond conformation being preferred. This discrete conformation allows the steric bulk in the model peptoids to be distributed around the sp^2 hybridised amide nitrogen atoms as to disallow steric pressures leading to the establishment of the energetic minimum. In these instances, the n → $\pi_{C=Oi}$* interactions are favoured. Such orientations are caused by the repulsive interactions between the aryl ring and O_{i-1}. In the case of the model peptoid **60**, two independent motifs were shown to constitute the unit cell and they were found to be mirror images of each other. This is shown by the angle values being almost exact for both structures but orientated in opposite directions. Likewise, the hydrogen bond lengths measured were also virtually *idem* (**2.654 Å and 2.663 Å**).

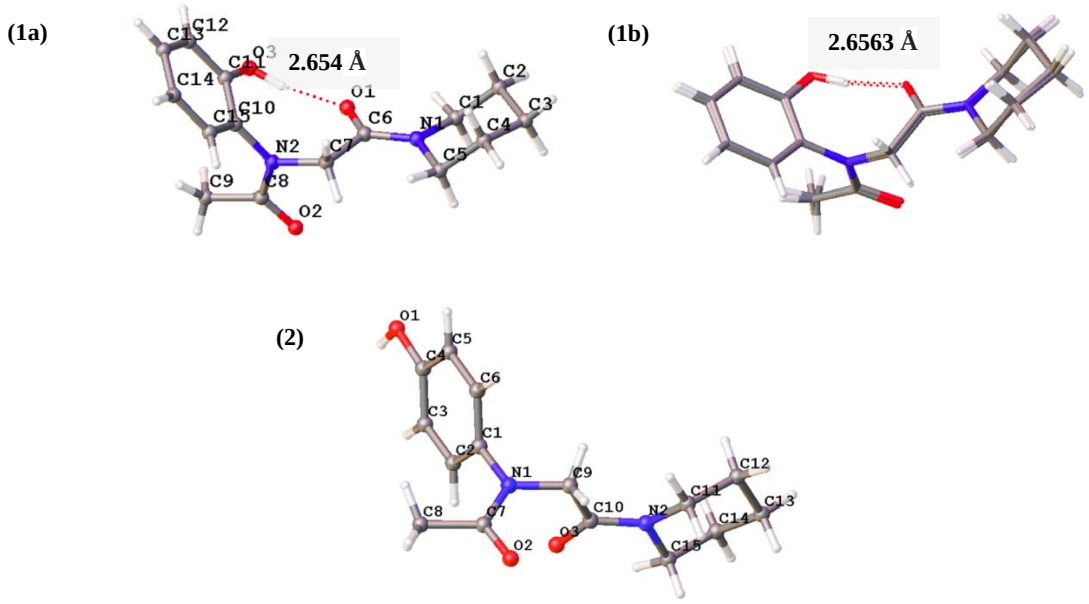

Figure 3.25. Ball-and-stick representations of the *trans* amide model systems **60 (1a)** & **59 (2)**, Together with the superimposition of two independent virtually identical structures of **60 (1b)**, found in the unit cell. Carbon atoms are depicted in grey, hydrogen atoms in white, nitrogen atoms in navy and oxygen atoms in red. The presence of the eight-membered-ring H-bonding is depicted as red dotted lines seen in **(1)**. Structure was generated in Olex2 and is reported with a 50% thermal ellipsoid probability.

The *O*-TFP containing **136** showed no substantial deviation from the three model peptoid systems, with the ω angle value of 179.58º (**Table 3.7**, **Entry 4**) being most planar. The ψ angles for the four peptoids were comparable to ω (range of 165.25 º to 178.44º). Meanwhile, the ϕ angle values in **60** differed from the achiral **130**, showing a decrese to 74.88/76.7º, shown in **Table 3.7**, **Entry 2** (vs 101.2º, **Table 3.7**, **Entry 3**). The ϕ angle values for the other three peptoids did not differ substantially relative to **130**. (**Figure 3.26**)

A. **B.**

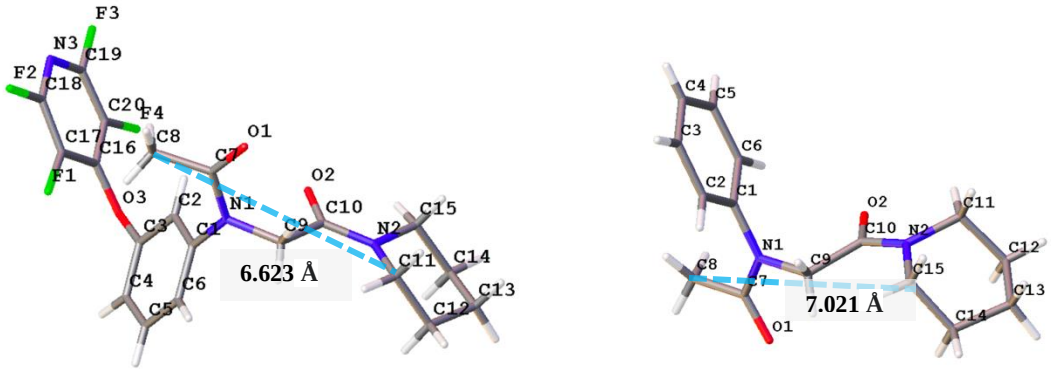

Figure 3.26. A. Stick representation of the model system **136 (A.)** & **130 (B.)** The interatomic distances between the *N*-terminal acetyl Cα and the *C*-terminal piperidyl Cα are shown as blue dotted lines. Carbon atoms are depicted in grey, hydrogen atoms in white, nitrogen atoms in navy and oxygen atoms in red. Structure was generated in Olex2 and is reported with a 50% thermal ellipsoid probability.

Further inspection of the X-ray crystal structures and their χ angle values provided insight to the stabilisation of the the *cis*/*trans* isomerism in **136**. From the NMR analysis, it was shown that the *O*-TFP *m*-hydroxylaniline monomer **136** induces a *trans* amide bias, evidenced by the *cis*/*trans* equilibrium being completely displaced to the *trans*-isomer (**Table 3.6**, **Entry 5**). Meanwhile, the heteroaromatic side chain showed a deviated perpedicular orientation with respect to the amide bond plane, whereby χ = 73.6°. Although it is not substantially different from χ observed in **130** (χ = 64.6°, **Table 3.7**, **Entry 3**), it is significantly greater than χ angle values of **59** and **60** (χ = 116.66° and 98.98°, respectively, (**Table 3.7**, **Entries 1** and **2**). (**Figure 3.25** This was found to be the most energetically minimised configuration of **136** in the solid state, accounting for the sterically restrictive and electrically repulsive nature of **108**.

Next, the analysis focused on the potential of **130** to induce the formation of β-turns, which in peptides are determined by the distance between the Cα atoms of residues *i* and *i+3*, found to be 7 Å. Indeed, the distance between the *N*-terminal acetyl Cα and the *C*-terminal piperidyl Cα was found to be 6.623 Å which is less than that required for the formation of the reverse-turn structures. Comparatively, the distance between the two Cα atoms exceeds 7 Å in **130** (C11… C8 = 7.021 Å). (**Figure 3.26.B**)

3.4.9. Characterisation of acetamide 105 in solid state

The data collected from single crystal X-ray crystallography for **105** revealed one independent structure in the unit cell corresponding to the target molecule. As discussed earlier, in the solution state the $K_{cis/trans}$ value obtained for this system showed a high *trans* content (60%). Remarkably, the solid-state structure of **105** revealed characteristic for *cisoid* geometry ω angle value (ω = 2.69 °). This deviation can be assigned to the presence of forces which render this twisting of the amide to produce the best packing motif in a unit cell. Indeed, upon further inspection of the X-ray crystallography data, the centrosymmetric hydrogen bonding, between the aryl *m*-hydroxyl of one molecule and O_{i-1} of the other, resulting in dimer formation in the sample of **105** is deemed responsible for this isomeric switch between solution and solid states. Moreover, the presence of the intermolecular hydrogen bonds led to a deviation of the orthogonal orientation of the *m*-hydroxy aryl group (χ = -69.11 °). This contributed to a more optimal orbital overlap resulting in dominating n → π_{Ar}* electrostatic forces. These findings suggest that in oligomeric systems, the incorporation of multiple *m*-hydroxybenzylamine monomers (**111**) could potentially yield discrete α-helical foldamers.

A.

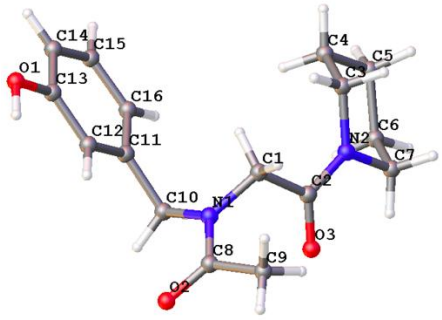

B.

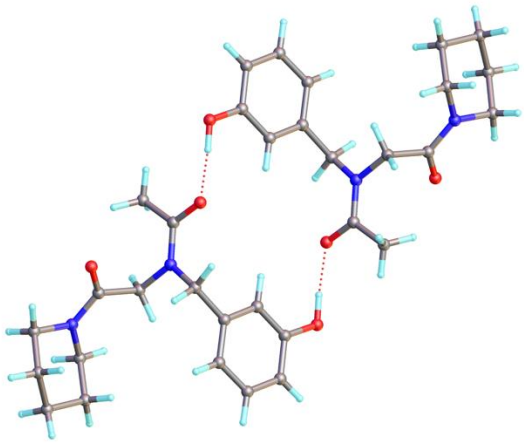

C.	ω (deg)	ϕ (deg)	ψ (deg)	χ (deg)
105	2.69	86.40	160.83	-69.11

Figure 3.27. Ball-and-stick representations of **105. A.** Depiction of a single structure of the *cis* **105**; **B.** Dimer of two identical structures of **105** connected by intermolecular hydrogen bonding; **C.** Torsion angles observed by X-ray crystallography. Carbon atoms are depicted in grey, hydrogen atoms in white, nitrogen atoms in navy and oxygen atoms in red. Structure was generated in Olex2 and is reported with a 50% thermal ellipsoid probability.

3.4.10. Further exploiting the aryl ortho-position to establish hydrogen-bonding-induced *cis* amide geometry

3.4.10.1. Synthesis of model peptoids containing amino(aryls)

Motivated by the ability of the *o*-hydroxybenzylamine monomer (**119**) to strongly induce *cisoid* geometry in the model system **104** (**Table 3.6**, **Entry 8**), we sought to explore this aromatic position further by utilising amine hydrogen bond donors. Previously, it has been shown that sp^2 hybridisation, which leads to trigonal planar geometry of amines, puts a strain on the hydrogen-bonding ring structure.[31] It was therefore envisaged to include sp^3 hybridised amine groups in our investigation. For this purpose, we began the synthesis of a model peptoid containing *o*-aminobenzylamine **163** by subjecting the commercially available starting material to Boc-protection in basic conditions. The desired product **164** was isolated from the crude mixture as a white solid, yielding crystals suitable for single crystal X-ray crystallography. (**Figure 3.28.A**) Subsequent Cbz-protection of the aniline amine was performed using benzyl chloroformate, which was allowed to stir at ambient conditions overnight. In order to liberate the aliphatic amine of **165** to produce *N*-Cbz *o*-aminobenzylamine monomer **166**, 25% TFA in DCM was used to yield the desired product as a crystalline solid shown in **Figure 3.28.B**. The displacement of the bromide from bromopiperidyl ethanone took place in the presence of caesium carbonate, in order to minimise over-substitution of the primary amine. Acetyl chloride was used to yield the desired peptoid **167** containing a *N*-Cbz protecting group, which was cleanly and conveniently deprotected using a Pd(0) catalyst and hydrogen atmosphere, resulting in **168**. (**Scheme 3.24**)

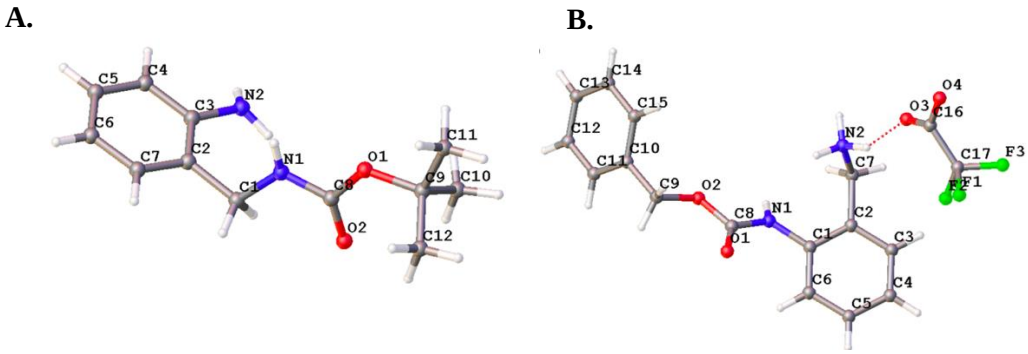

Figure 3.28. Ball-and-stick representations of **164 (A.)** and **166 (B.).** Carbon atoms are depicted in grey, hydrogen atoms in white, nitrogen atoms in navy, oxygen atoms in red and fluorine atoms in green. Structures were generated in Olex2 and are reported with a 50% thermal ellipsoid probability.

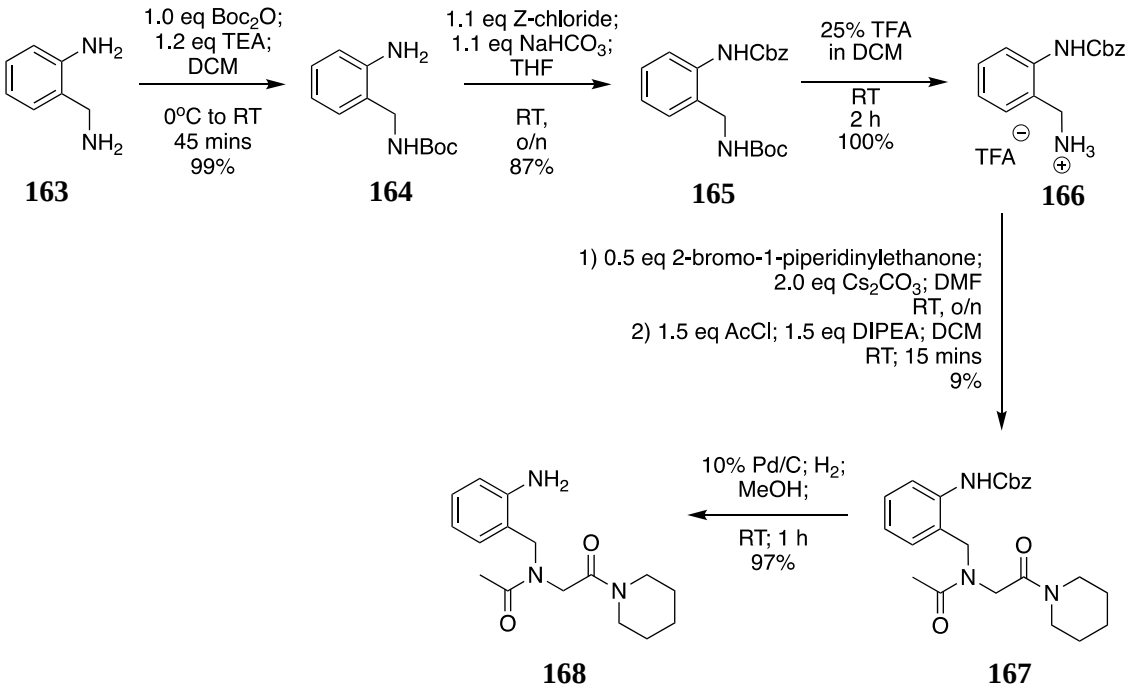

Scheme 3.24. Schematic depiction of a six-step synthesis to generate **168.** No isolation of the intermediate was performed after the fourth step. The overall yield for this synthesis was 8%.

In addition to the synthesis of **168** containing the *o*-amino(aryl) **163**, a model peptoid system containing the same monomer incorporated at the aryl amine was also prepared (**Scheme 3.25**). **164** was converted in 2 steps to the Boc-protected *o*-aminomethyl aniline containing **169**, which was then Boc-deprotected in acidic conditions to yield **170**.

Single crystals of the deacetylated **169** (**Figure 3.29**) were isolated and deemed suitable for X-ray crystallography and showed the presence of intermolecular hydrogen bonding present between two virtually equivalent molecules.

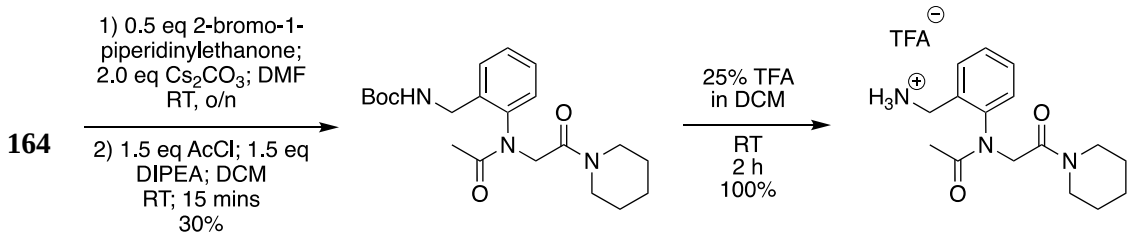

169 **170**

Scheme 3.25. Schematic depiction of the three-step synthesis to generate the model peptoid **170.** No isolation of the intermediate was performed after the second step. The overall yield for this synthesis was 30%.

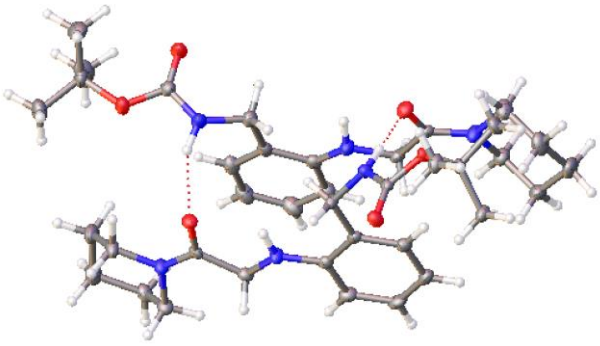

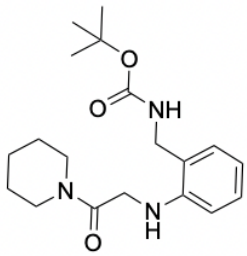

171

Figure 3.29. Ball-and-stick representation of deacetylated **171** dimer present in the unit cell. Carbon atoms are depicted in grey, hydrogen atoms in white, nitrogen in navy and oxygen in red. Structure was generated in Olex2 and is reported with a 50% thermal ellipsoid probability.

3.4.10.2. The effect of amino(aryls) on $K_{cis/trans}$ values: solution state analysis

A previous study by Zuckermann[18] used peptoid monomers with cationic ammonium side chains and showed they strongly induce *cisoid* geometry in peptoids by forming H-bonds. It was demonstrated that, indeed, strategic placement of aryl substituents can not only modulate the *cis*/*trans* equilibrium but can also induce intermolecular interactions which effectively switch the amide bond isomerism (**Table 3.6**). Initially, the $K_{cis/trans}$ values of peptoids **168** and **170** were to be to investigated in order to determine how each regioisomer impacted the rotation around the ω angle. It was also sought to examine how the hydrogen bond donor deactivation would impact the system. Therefore, the $K_{cis/trans}$ and $\Delta G_{cis/trans}$ values of protected model peptoids **167** and **169** were also determined. The impact of the amino(aryl) acetamides (**167** – **170**) on the *cis*/*trans* equilibrium was analysed by NMR spectroscopic techniques. The results of the study presented unprecedented effects of these novel monomers and their protected derivatives on the amide bond isomerism. (**Table 3.8**)

Table 3.8. $K_{cis/trans}$ and $\Delta G_{cis/trans}$ values for the model peptoids synthesised in **Section 3.4.10.1** in $CDCl_3$, CD_3OD and CD_3CN.

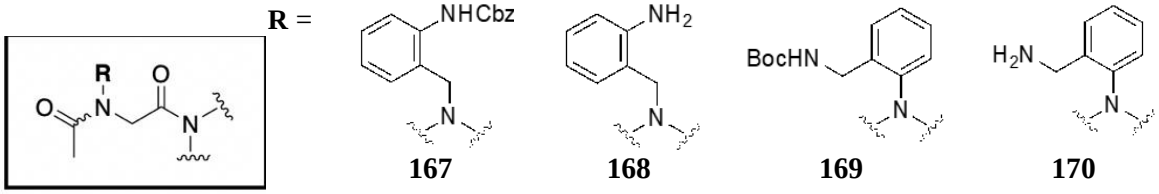

Entry	No.	$CDCl_3$		CD_3CN		CD_3OD	
		$K_{cis/trans}$	$\Delta G_{cis/trans}$ (kcal mol^{-1})[a]	$K_{cis/trans}$	$\Delta G_{cis/trans}$ (kcal mol^{-1})	$K_{cis/trans}$	ΔG (kcal mol^{-1})
1	**167**	3.92	-0.81	7.38	-1.18	1.44	-0.22
2	**168**	2.35	-0.51	4.97	-0.95	1.93	-0.39
3	**169**	0.13	1.21	0.24	0.85	-	-
4	**170**	-*	-	-	-	-	-

[a] The value was calculated using the Gibbs Free Energy equation $\Delta G^o = -RT \ln(K_{eq})$ at 298 K, where R = 1.987 x 10^{-3} kcal $K^{-1}mol^{-1}$.

*Indicating the presence of just the *cis*-isomer. NMR signals corresponding to the *trans*-isomer were not detected.

As observed in peptoids containing *N*-hydroxyaryl side chains (**Table 3.6**) the presence of *cisoid* amide bonds will lead to formation of interatomic spatial *NOE* signals between the backbone methylene protons and *N*-terminal acetyl protons. On the other hand, a strong

correlation between the *N*-terminal methyl protons and the side chain methylene signifies a *trans* amide conformation.

When the *N*-Cbz *o*-aminobenzylamine containing acetamide **167** (**Table 3.8**, **Entry 1**) was analysed by ^{1}H NMR spectroscopy in $CDCl_3$ it showed the presence of two isomers, deduced from a set of two *N*-terminal acetyl proton peaks and three sets of two methylene proton peaks. However, the ^{1}H-^{1}H NOESY analysis showed that both of the *cis* and *trans* acetyl peaks correlated to both *cis* and *trans* backbone and side chain methylene protons to varying degrees, which was caused by the spatial vicinity of *cis*/*trans* protons. (**Figure 3.30**) It was postulated that the presence of NOE signals between different protons in *cis* and *trans*-isomers was a consequence of fast interconversion of resonances in the NOESY experiment. The rapid exchange of the isomers in the sample led to the dynamic NOE effect, and varied intensities of the NOE contacts were solvent dependent. We observed that in polar and more viscous solvents, the slower interconversion rate of the resonances allowed for the unequivocal assignment of the amide bond isomerism, as the *NOE* signal between the *cis* acetyl signal (assigned as the more intense peak in the ^{1}H NMR spectrum) and the backbone methylene proton signal was most intense. This was evidential of equilibrium displacement to the *cis*-isomer of the amide bond of **167**, in CD_3OD and CD_3CN. Furthermore, the definite assignment of the chemical shifts in CD_3OD and CD_3CN aided the assignment of **167** in $CDCl_3$, where the *cis*-isomer was dominant.

In $CDCl_3$, the *trans* ^{1}H NMR signals were not only w but also exhibited a considerable broadness, which also gave rise to substantial broadening in the NOESY NMR spectrum, shown in **Figure 3.30.A.** Therefore, despite the apparent presence of two isomers in, the integration of signal peaks of **167**, this may not have been accurate. This is because the intensity of the ^{1}H NMR peaks depends not only on the concentration of the two isomers relative to each other, but also the rate of exchange and the relaxation properties of protons.

The general trend seen for the isomer ratios in the solvents employed was characteristic to isomerism determined by intramolecular H-bonding. The acetyl proton peak correlated with the *cis*-isomer showed a decreased intensity in CD_3OD, signifying the presence of eight-membered ring hydrogen bonding (**Figure 3.30.B.**), likely taking place between the oxygen belonging to the *N*-terminal carbonyl and the *ortho* aromatic amino group. Regardless, the $K_{cis/trans}$ values revealed that even in methanol, the *cis*-isomer population was dominant ($K_{cis/trans}$ = 1.44). As expected, in the *cis*-favouring acetonitrile, this preference increased 5-fold compared to chloroform.

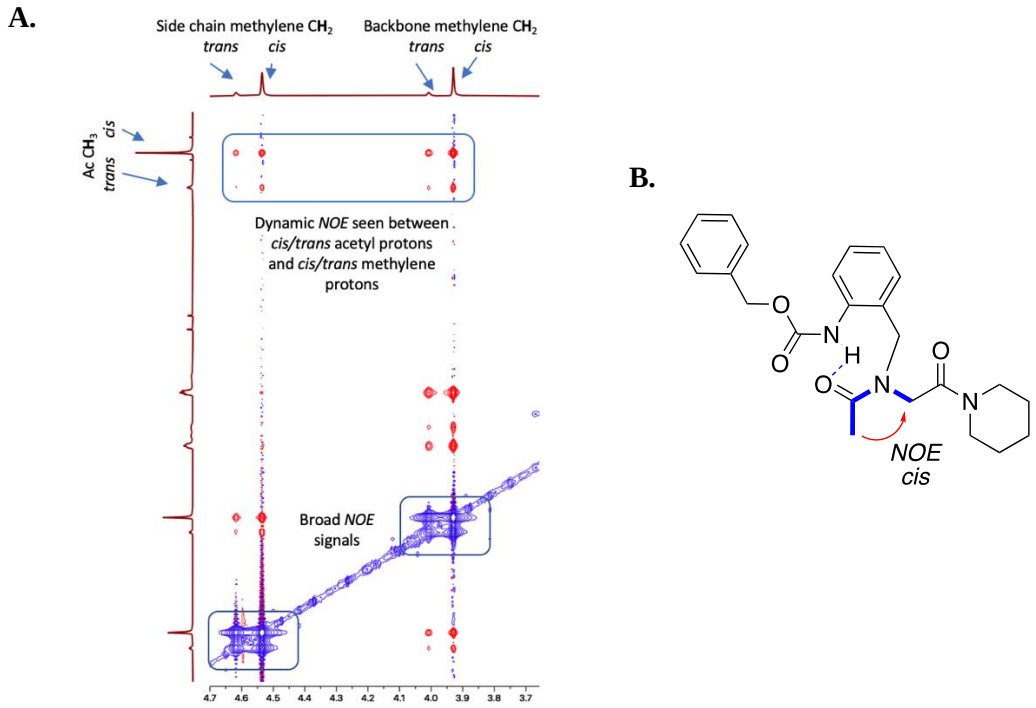

Figure 3.30. A. A segment of the ^{1}H-^{1}H NOESY spectrum of **167** in $CDCl_3$ showing *NOE* contacts between the *N*-terminal *cis*/*trans* acetyl protons and the *cis*/*trans* side chain and backbone methylene protons. These correlations arose from close vicinity of the isomers in the mixing sample. **B**. A depiction of the H-bond formation between the aromatic amine and the *N*-terminal O_{i-1} (shown as a blue dotted line), and the resulting *NOE* signal between the acetyl protons and backbone protons.

Liberation of the aromatic amine resulted in decreased $K_{cis/trans}$ values for **168** in polar aprotic ($\Delta[K_{cis/trans}(CD_3CN)]_{167-168} = 2.41$) and apolar aprotic ($\Delta[K_{cis/trans}CDCl_3]_{167-168} = 1.42$) solvents relative to **167**. (**Table 3.8**, **Entries 1** and **2**) It was postulated that this was caused by the abstraction of the bulkiness of Cbz group which influenced the conformation of the acetamide. This favoured intramolecular hydrogen bonding took place between the aromatic amine proton and O_{i-1} due to the proximity of the two. Contrarily, in the polar protic environment of CD_3OD, the *cis* content of **168** increased by 34% relative to **167**. This suggests that the polar Cbz group can effectively 'shield' the hydrophobic regions of **167** in CD_3OD, making the aromatic amine and the O_{i-1} more accessible for intermolecular hydrogen bonding. These forces will compete with the intramolecular hydrogen bonding which stabilises the *cis* conformation of peptoids. In turn, this will lead to a more extended and flexible peptoid structure. Still, in CD_3OD, the *cis* conformation of the amide bond dominated in **168** ($\Delta G_{cis/trans}(CD_3OD)]_{168} = -0.22$ kcal mol^{-1}).

Relative to the $K_{cis/trans}$ value of 8.70 found for **104** in acetonitrile (**Table 3.6**, **Entry 8**), **168** showed a 43% decrease in the *cis* amide bond population. This can be attributed to the planarity of the amino group which evidently decreased the stabilisation of the *cisoid* geometry of the acetamide by hindering the formation of intramolecular hydrogen bonding between the aryl *ortho* substituent and O_{i-1}.

We turned our attention to the model peptoids **169** and **170**. The Boc-protected model peptoid **169** showed *trans* geometry in all tested solvents (**Table 3.8**, **Entry 3**), with the aprotic solvents showing a greater bias towards *cis*-isomerism (2-fold increase in *cis* population in CD_3CN, and 3.5-fold increase in $CDCl_3$), relative to CD_3OD ($K_{cis/trans} = 0.07$). Further analysis of the ^1H NMR spectrum revealed characteristic doublets corresponding to atropoisomerism, within each *cis*- and *trans*-isomer, caused by the asymmetric nature of the Boc-protected aniline monomer **164**, which resulted in restricted rotation of the aromatic side chain group around the *N*–C_{Ar} bond. The backbone geminal methylene protons of **169** appeared as two sets of coupled doublets ($^2J_{HH,cis} = 17.9$ Hz, $^2J_{HH,cis} = 17.9$ Hz & $^2J_{HH,trans} = 15.7$ Hz, $^2J_{HH,trans} = 16.2$ Hz). In addition, within each isomer, the backbone geminal protons showed a spatial contact in ^1H-^1H NOESY NMR spectrum. (**Figure 3.31**)

An interesting result of the analysis was obtained for the unprotected model system **170** (**Table 3.8**, **Entry 4**), in all of the solvents employed for the $K_{cis/trans}$ value determination. Evidenced by ^1H NMR analysis, the *cis/trans* equilibrium for the acetamide **170** was completely displaced to the *cis*-isomer (**Table 3.8**, **Entry 4**). Remarkably, full displacement of the equilibrium to the *cis*-isomer was present even in polar protic CD_3OD. Further analysis of the ^1H–^{13}C HMBC NMR spectrum revealed a lack of 2-, 3- and 4-bond correlations between the methylene ^1H NMR peak which was partaking in the NOE signal, and aromatic ^{13}C peaks in ^1H–^{13}C HMBC, and therefore this confirmed the presence of the *cis*-isomer. (**Figure 3.32**) The *ortho* aromatic methyl amine proton signals were found to be very deshielded, found at >11 ppm in CD_3CN and $CDCl_3$ respectively. Such high chemical shift values are consistent with alcohol-based model systems within which the amide bond geometry is determined by the formation of intramolecular hydrogen bonding. This provides evidence for the formation of the eight-membered ring shown in **Figure 3.32**.

Moreover, relative to its protected parent model peptoid **169** (**Table 3.8**, **Entry 3**), the acetyl methyl proton peak in **170** (**Table 3.8**, **Entry 4**) was found at a higher chemical shift of 2.34 – 2.47 ppm in all of the solvents employed. Such pronounced deshielding of the *N*-

terminal protons can be assigned to the model peptoid backbone adopting a non-linear conformation. The anisotropic effect of the amide bond, caused by deviation of the plane of the acetyl group, resulted in a dipole moment which gave rise to the downfield shift of the *N*-terminal acetyl protons.

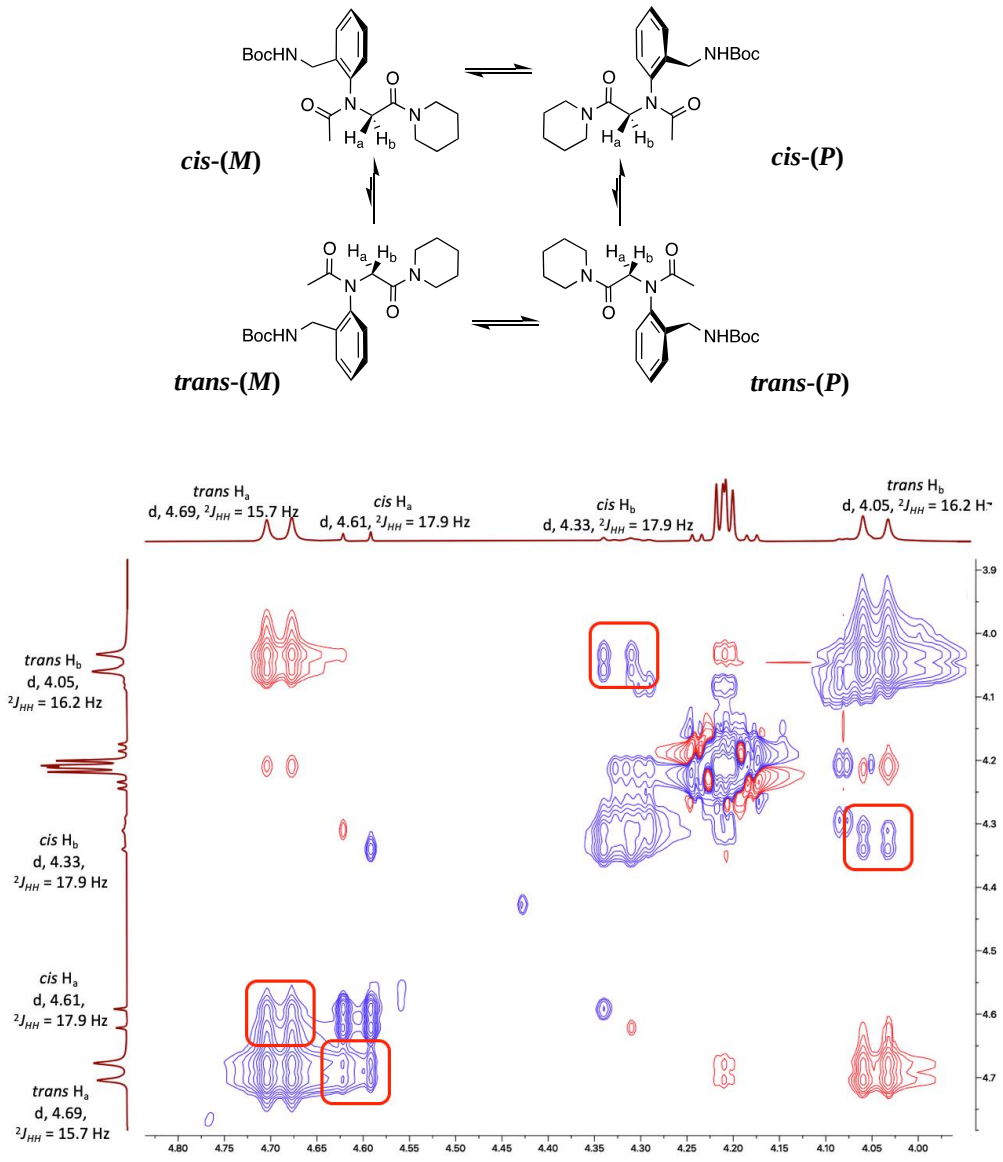

Figure 3.31. A schematic representation of the acetamide **169** showing equilibrium between the *cis/trans (M/P)*-isomers, together with the chemical shifts and coupling constants calculated for these protons. Included here is also the ^{1}H-^{1}H NOESY NMR spectrum of **169** in CD_3CN showing *NOE* spatial (red bubbles) contacts between the magnetically non-equivalent *cis*/*trans* geminal protons.

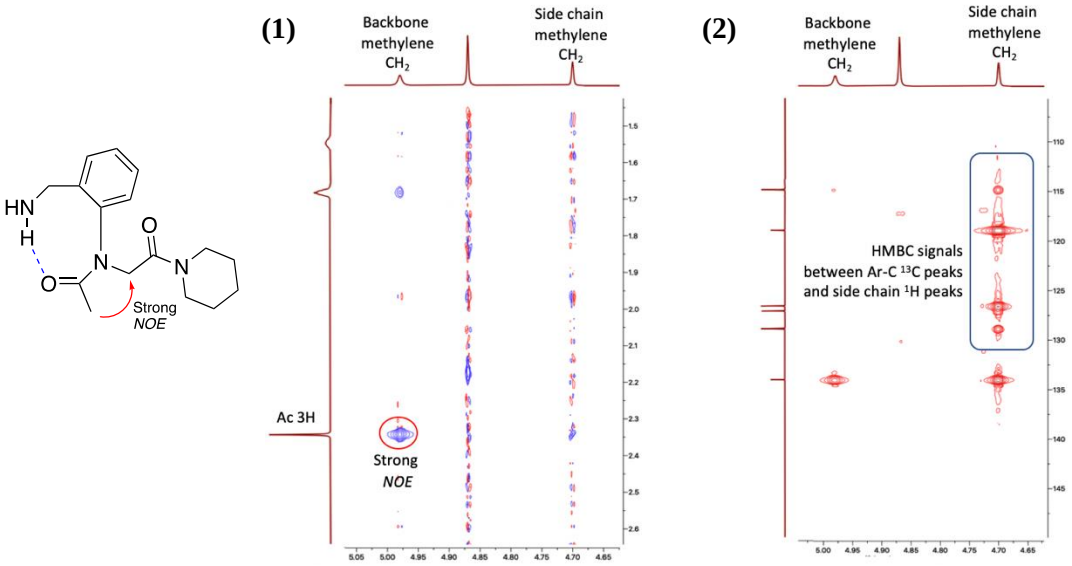

Figure 3.32. Structure of **170** showing the intramolecular hydrogen bonding stabilising the *cis* amide bond geometry exhibited by this acetamide. **(1)** NOESY NMR spectrum showing the spatial correlation between the acetyl methyl ^{1}H peak and the assigned backbone methylene ^{1}H signal. **(2)** ^{1}H-^{13}C HMBC NMR spectrum showing the characteristic multiple-bond correlation between ^{1}H NMR resonance and ^{13}C NMR resonances.

3.4.10.3. The effect of acetamide 169 on $K_{cis/trans}$ values: solid state analysis

It was sought to gain a further understanding of the effects of amino(aryls) on the *cis/trans*-isomer equilibrium in the model peptoid systems. We were particularly keen to gather more insight about the mechanisms involved in *cis* amide bond induction in these acetamides. Unfortunately, it was only possible to gain an X-ray structure for one of the four model peptoids.

Single crystals of the *trans* model peptoid **169** which were isolated from the sample were deemed suitable for single crystal X-ray crystallography and the crystal structure which was obtained corroborated the solution state analysis. One independent motif was found to constitute the unit cell corresponding to the target molecule. (**Figure 3.33**) The crystal structure of **169** exhibited a ω angle value which only deviated 3° from the trigonal planar 180°. The planarity of the *N*-C_{Ar} bond also aligned with the sp^2 hybridisation of the *N*-atom (χ = 85.4°), which has been discussed in detail in other *trans*-inducing peptoid model systems (**Section 3.4.8**). Indubitably, the orthogonality of the π-system in **169** allowed it to adopt a conformation which minimised the steric pressure in the model peptoid and achieved good orbital overlap,

stabilising of the n → $\pi_{C=Oi}$* interactions favouring *trans*-isomerism. Upon further analysis, the distance between the *N*-terminal carbon and the piperidyl C_α revealed that the Boc-protected building block **164** has the ability to form reverse turn structures in peptoids (6.605 Å).

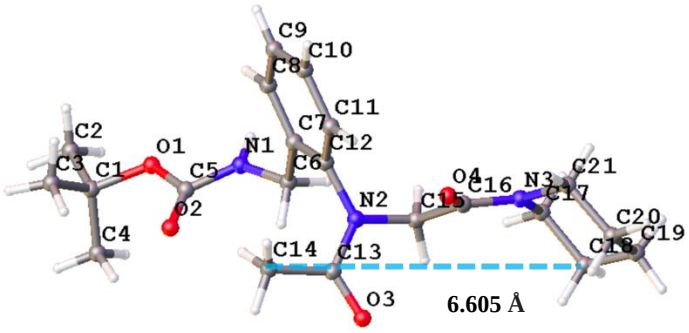

No.	ω (deg) C8-C7-N1-C9	ϕ (deg) C7-N1-C9-C10	ψ (deg) N1-C9-C10-N2	χ (deg) C2-C1-N1-C9
169	-177.0	-91.3	-175.3	85.4

Figure 3.33. Ball-and-stick representation of the model system **169** together with its dihedral angles observed by X-ray crystallography. The interatomic distance between the *N*-terminal acetyl C_α and the *C*-terminal piperidyl C_α is shown as a blue dotted line. Carbon atoms are depicted in grey, hydrogen atoms in white, nitrogen atoms in navy and oxygen atoms in red. Structure was generated in Olex2 and is reported with a 50% thermal ellipsoid probability.

3.5. Summary of Chapter 3

The control of peptoid secondary structure remains a major challenge in the field, and despite recent advances, rational peptoid design remains the key objective of numerous research groups. In the past decade, *cis*- and *trans*-directing peptoid monomers have been designed in the quest of modulating peptoid amide bond geometry. Up until 2019, no reliable protecting groups existed to effectively explore the use of aromatic alcohols (phenols) in peptoid synthesis. Hence, the TFP phenol protecting group, first documented in the Cobb group, was proposed as a potential protecting group for accessing phenol containing monomers that could be used in peptoid synthesis performed via a submonomer approach. However, due to its highly deactivating nature the TFP group proved troublesome to incorporate into model peptoids in solution. Hence, a different orthogonal protection strategy, *O*-Bnz, had been proposed and executed, resulting in the formation of the desired library of model peptoids containing liberated phenolic peptoid submonomers.

All of the hydroxybenzylamine-containing model peptoids), both protected (**141**, **159 – 161**) and unprotected (**104 – 106)**, were subjected to extensive NMR analysis in order to determine their amide *cis/trans*-isomerisation preferences (**Table 3.6**). Remarkably, the neutral model peptoid **104** which contained the *o*-hydroxybenzylamine was found to largely displace the amide bond equilibrium to the *cis*-isomer (**Table 3.6**, **Entry 8**). It was proposed that this occurs due to this isomer being stabilised by the formation of 8-membered intramolecular hydrogen bonding ring between the aryl hydroxy moiety and the *N*-terminal carbonyl. The $K_{cis/trans}$ value found for this peptoid in acetonitrile was 8.70 (**Table 3.6**, **Entry 8**). Conversely, the NMR data collected for the *o*-hydroxyaniline-containing model peptoid **60** (**Table 3.6**, **Entry 1**) was consistent with earlier studies in the Blackwell group[3] which reported the stabilisation of the *trans* amide geometry by the formation of intramolecular hydrogen bonding between the aryl hydroxyl and O_i, which gave rise to a 100% *trans* amide bond geometry.

Encouraged by the *cis*-inducing *o*-hydroxy benzylamine, it was decided to explore this position by substituting it with another well-known hydrogen bond donor $–NH_2$. Compound **167**, which contained the Cbz-protected aminobenzylamine **166** and resulted in a higher $K_{cis/trans}$ value than its liberated counterpart **168** (**Table 3.8**, **Entries 1** and **2**), which showed a 33% decrease in the *cis* amide content. Interestingly, the introduction of *o*-aminomethyl aniline to form **170** (**Table 3.8**, **Entry 4**) resulted in the amide bond equilibrium being completely displaced to the *cis*-isomer.

Crystal structures collected for the model peptoids (**Sections 3.4.8**, **3.4.9** and **3.4.10.3**) corroborated the NMR results obtained for all of the acetanilides, with the exception of model peptoid **105**, shown in **Figure 3.27**, which showed the presence of two virtually identical *cis* acetamides in the unit cell which were found to form a dimer linked by intermolecular hydrogen bonds taking place between the aryl hydroxide and the O_{i-1}.

Peptoid oligomers containing the novel monomers investigated in this chapter were designed and synthesised in **Chapter 4**. The biophysical analyses together with the biological evaluations are also reported in **Chapter 4**.

3.6. References for Chapter 3

[1] Hodges, J.A., Raines, R.T., 2006, *Org. Lett.*, **8**(21), 4695-4697.

[2] Bürgi, H.B., Lehn, J.M., Wipff, G., 1974, *J. Am. Chem. Soc*., **96**(6), 1956-1957.

[3] Gorske, B.C., Bastian, B.L., Geske, G.D., Blackwell, H.E., 2007, *J. Am. Chem. Soc*., **129**(29), 8928-8929.

[4] Kümin, M., Sonntag, L.S., Wennemers, H., 2007, *J. Am. Chem. Soc*., **129**(3), 466-467.

[5] Nnanabu, E., Burgess, K., 2006, *Org. Lett*., **8**, 1259-1262.

[6] Pokorski, J.K., Miller Jenkins, L.M., Feng, H., Durell, S.R., Bai, Y., Appella, D.H., 2007, *Org. Lett*., **8**, 2381-2383.

[7] Shin, S.B.Y., Yoo, B., Todaro, L.J., Kirshenbaum, K., 2007, *J. Am. Chem. Soc*., **129**, 3218-3225.

[8] Stringer, J.R., Crapster, J.A., Guzei, I.A., Blackwell, H.E., 2010, *J. Org. Chem*., **75**, 6068-6078.

[9] Shah, N.H., Butterfoss, G.L., Nguyen, K., Yoo, B., Bonneau, R., Rabenstein, D.L., Kirshenbaum, K., 2008, *J. Am. Chem. Soc*., **130**, 16622-16632.

[10] Patch, J.A., Barron, A.E., 2003, *J. Am. Chem. Soc*., **125**, 12092-12093.

[11] Paul, B., Butterfoss, G.L., Boswell, M.G., Huang, M.L., Bonneau, R., Wolf, C., Kirshenbaum, K., 2012, *Org. Lett*., **14**, 926-929.

[12] Gorske, B.C., Stringer, J.R., Bastian, B.L., Fowler, S.A., Blackwell, H.E., 2009, *J. Am. Chem. Soc*., **131**, 16555-16567.

[13] Stringer, J.R., Crapster, J.A., Guzei, I.A., Blackwell, H.E., 2011, *J. Am. Chem. Soc*., **133**, 15559-15567.

[14] Bolt, H.L., Eggimann, G.A., Jahoda, C.A., Zuckermann, R.N., Sharples, G.J., Cobb, S.L., 2017, *MedChemComm*, 8(5), 886-896.

[15] Roy, O., Caumes, C., Esvan, Y., Didierjean, C., Faure, S., Taillefumier, C., 2013, *Org. Lett*., 15, 2246-2249.

[16] Shyam, R., Nauton, L., Angelici, G., Roy, O., Taillefumier, C., Faure, S., 2019, *Biopolymers*, **110**, e23273.

[17] Caumes, C., Roy, O., Faure, S., Taillefumier, C., 2012, *J. Am. Chem. Soc*., **134**, 9553-9556.

[18] Wijaya, A.W., Nguyen, A.I., Roe, L.T., Butterfoss, G.L., Spencer, R.K., Li, N.K., Zuckermann, R.N., 2019, *J. Am. Chem. Soc*., **141**, 19436-19447.

[19] Zuckermann, R.N., Kerr, J.M., Kent, S.B., Moos, W.H., 1992, *J. Am. Chem. Soc*., **114**, 10646-10647.

[20] Kruijtzer, J.A., Hofmeyer, L.J., Heerma, W., Versluis, C., Liskamp, R.M., 1998, *Chem. Eur. J*., **4**, 1570-1580.

[21] René, A., Martinez, J., Cavelier, F., 2014, Eur. *J. Org. Chem*., **36**, 8142-8147.

[22] Brittain, W.D., Cobb, S.L., 2019, *Org. Biomol. Chem*., **17**, 2110-2115.

[23] FONES, W.S., 1949, *J. Org. Chem*., **14**(6), 1099-1102.

[24] Malkov, A.V., Vranková, K., Černý, M., Kočovský, P., 2009, *J. Org. Chem*., **74**, 8425-8427.

[25] Bogdal, D., 1999, Molecules, **4**, 333-337.

[26] Proulx, C., Yoo, S., Connolly, M.D., Zuckermann, R.N., 2015, *J. Org. Chem*., **80**, 10490-10497.

[27] Castillo, J.C., Orrego-Hernández, J., Portilla, J., 2016, *Eur. J. Org. Chem*., 2016, 3824-3835.

[28] Kan, T., Fukuyama, T., 2004, *Chem. Commun*., **4**, 353-359.

[29] Wu, C.W., Sanborn, T.J., Huang, K., Zuckermann, R.N., Barron, A.E., 2001, *J. Am. Chem. Soc*., **123**(28), 6778-6784.

[30] Stewart, W.E., Siddall, T.H., 1970, *Chem. Rev.*, **70**(5), 517-551.

[31] Scheiner, S., Grabowski, S.J., Kar, T., 2001, *J. Phys. Chem. A*, **105**(46), 10607-10612.

Chapter 4: Hydrogen-Bonding-Induced Peptoid Helices

4.1. Tyrosine-based antimicrobials

Tyrosine (Tyr) is present in numerous antimicrobial peptides (AMPs), and its incorporation into synthetic macromolecules offers an attractive avenue to make them biologically efficacious. The literature extensively documents the incorporation of Tyr into synthetic macromolecules, primarily focusing on their involvement in the formation of self-assembled amphiphilic conformations.[1,2] This process facilitates the segregation of cationic charges on the surfaces of these macromolecules, a key factor in their antimicrobial activity.[3] Moreover, the incorporation of a phenolic functionality into synthetic antimicrobials offers antioxidant properties[4] and therefore, has a further capability to enhance the antimicrobial properties of a molecule. An important feature of peptides is their relative hydrophobicity which enables them to interact with the hydrophobic regions of bacterial inner membrane. The charge to hydrophobicity balance within an antimicrobial is crucial to reduce its cytotoxic effects.[5] Tyr stands out due to its distinct combination of hydrophobic and polar properties, making it particularly noteworthy in this context.

Protegrin-1 (**Pep. 40**, **Figure 4.1.A**) showcases an ability to readily insert into anionic phospholipids and zwitterionic monolayers, which are more commonly found in mammals.[6] Protegrin-1 (**Pep. 40**) exemplifies this with its 'imperfect' amphipathicity. The presence of disulfide bonds in protegrin-1 facilitates the formation of β-hairpin structures, causing the polar groups to orient outwards, leading to the disruption of the polar lipid heads at the amphipathic interface, ultimately resulting in membrane disruption and cell death. Although **Pep. 40** exhibits modest cytotoxicity, it has been demonstrated that reducing the membrane's overall anionic character can decrease cytotoxicity even further.[7,8]

An interesting observation was documented by Porto and co-workers who focused on the design of a peptide library derived from the plant antimicrobial peptide guavanin (**Pep. 41**, **Figure 4.1.B**). **Pep. 41**, a 20-amino-acid-long peptide, is comprised of cationic arginine (Arg) residues, as well as Tyr residues which provides an amphiphilic feature and unusual hydrophobic complement. As a result, it leads to hyperpolarisation of the *E. coli* cell membrane, suggesting it acts as a selective ionophore.[9] This bactericidal mechanism of action is also assigned to valinomycin,[10] but does differentiate **Pep. 41** from other AMPs, which naturally cause cell lysis by mechanisms outlined in detail in **Chapter 1**.

Tyrocidine A (**Pep. 42**, **Figure 4.1.C**) is a Tyr-containing antimicrobial macrocyclic peptide produced by *B. brevis*.[11] Structural investigation carried out by Loll and coworkers revealed that it forms a symmetric amphipathic homodimer, resembling β-sheets.[12] In this configuration, the Tyr side chains face away from the membrane, meaning that the polar Tyr residues are in direct contact with the aqueous environment. Consequently, the hydroxyl group of tyrosine enhances bacterial membrane targeting, disrupting its integrity, and thereby conferring high efficacy of tyrocidine against Gram-positive organisms.

Cell-membrane-targeting AMPs have been introduced by nature as the first line of defence but are particularly susceptible to proteolytic degradation which leads to them becoming ineffective. Nature-inspired mimetics offer an avenue to circumvent this issue. The effects of L-Tyr utilisation in antimicrobial polyacrylates (**172**, **Figure 4.1D**) has been documented by Datta and co-workers.[13] The compounds were found to be efficacious against fungal and Gram-negative bacterial targets, including methicillin-resistant *S. aureus* (MRSA, MIC = 85 μg mL^{-1}), yet they displayed no cytotoxicity against HaCaT at maximum MIC used in the assays (100 μg mL^{-1}).

A.

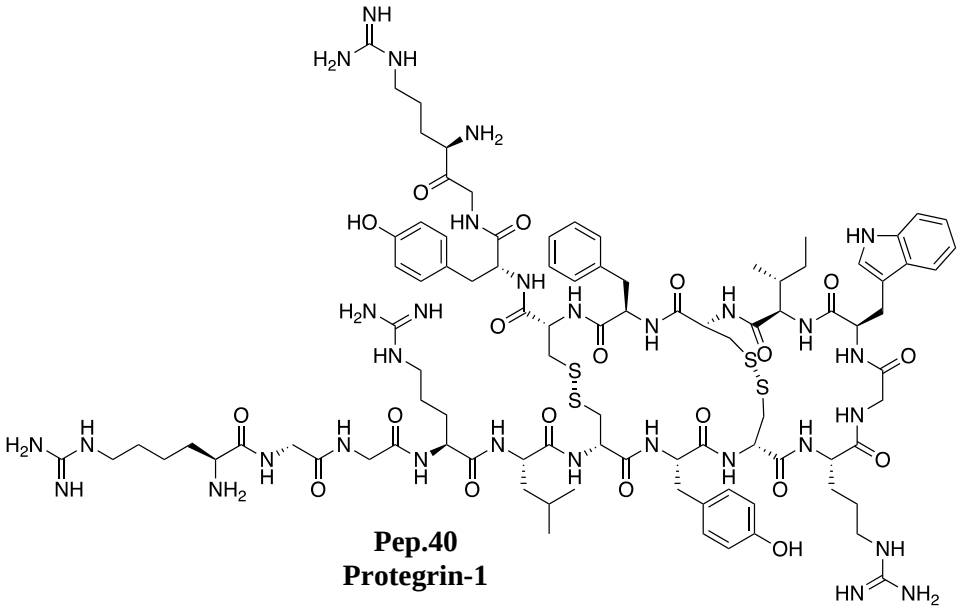

Pep.40
Protegrin-1

B.

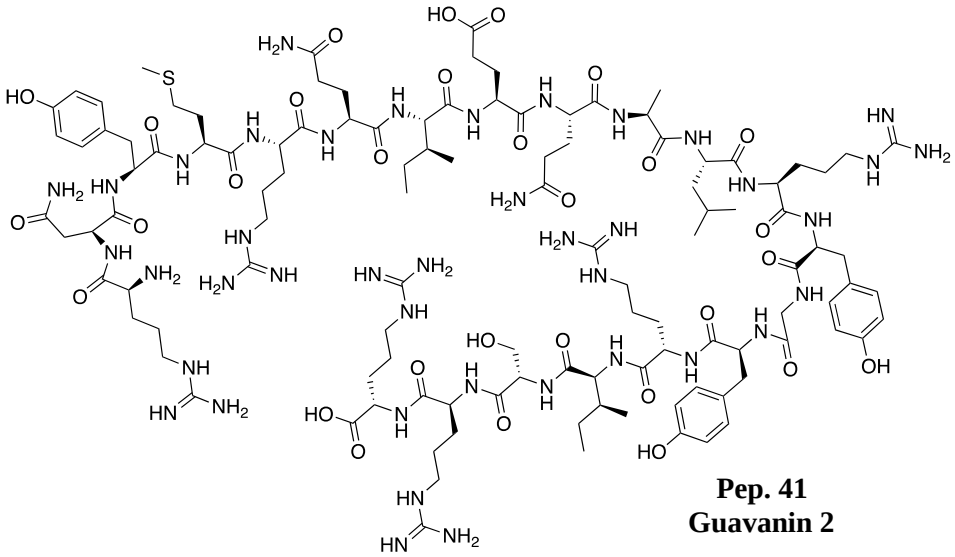

Pep. 41
Guavanin 2

C.

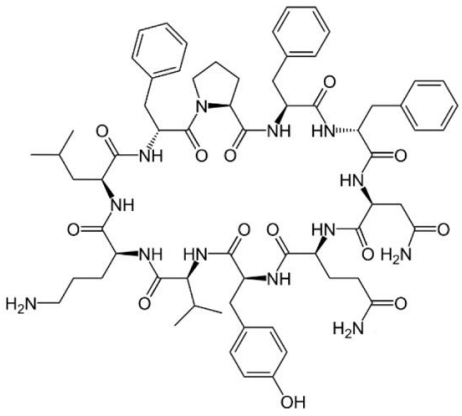

Pep. 42
Tyrocidine A

D.

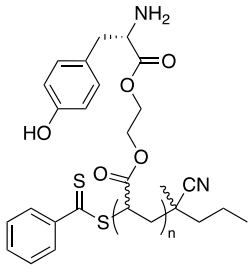

172
L-Tyr containing polyacrylate

Figure 4.1. A selection of tyrosine-containing antimicrobials.

4.2. Objectives for Chapter 4

Chapter 3 studied in detail the incorporation of tyrosine-type building blocks into model dipeptoids, and their effects on peptoid amide bond conformation. Whilst the *No*Tyr (**104**) was found to form intramolecular hydrogen bonding facilitating a *cis* amide bond preference, the crystal structure of its *meta*-counterpart (**105**) revealed intermolecular hydrogen bond formation, and hence, *cis* amide bond induction in the solid state. Building on the work outlined in **Chapter 3**, exploration of the properties, structure, and biological activity of a series of peptoid oligomers containing tyrosine-type monomers. In addition, as highlighted in **Chapter 3** a lack of tractable synthetic approaches to incorporate tyrosine-type monomers has meant that very little work has been reported on peptoid oligomers that contain such monomers. We set out to design and prepare a library of peptoid nonamers mainly comprised of *N*Tyr monomers. With this library in hand, it was planned to study their secondary structure (by CD analysis), physicochemical properties (lipophilicity as determination using the log *D* procedure outlined in **Chapter 2**) and their antimicrobial properties.

4.3. Chapter 4: Results and discussion

4.3.1. Application of tyrosine-type monomers in the synthesis of peptoids

In order to facilitate the synthesis of peptoid oligomers containing *N*Tyr residues, we initially envisioned their syntheses through a route that utilised the *O*-TFP-protection strategy pioneered by the Cobb group.[14] However, given the deactivating nature of the TFP protecting group,[15] we wished to compare its suitability for solid-phase synthesis of peptoids to the *O*-Bnz containing derivatives. The synthesis of these building blocks is discussed in **Section 3.4.1**, **Chapter 3**.

The *N*Phe-rich pentameric peptoid precursor **Pep. 43** (**Figure 4.2**) was synthesised on Rink Amide resin, using the standard submonomer approach conditions, discussed in **Chapter 2**. The TFA salt of TFP-protected *p*-hydroxy benzylamine **112** was first basified with DIPEA, so as to counteract the TFA content of the substrate, and it was allowed to react with the growing peptoid chains for 1 hour. The reaction was then monitored by LC-MS and **112** was revealed to have fully displaced the bromide. However, the MS/MS fragmentation pattern obtained upon *N*Lys (**52**) coupling was not that of the expected peptoid **Pep. 44**. (**Figure 4.3**) The fragmentation pattern and MS data implied the formation of **Pep. 45**. (**Figure 4.4**)

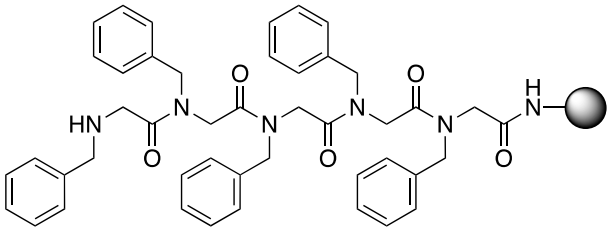

Pep. 43

Figure 4.2. Pentameric, *N*Phe (**40**)-rich peptoid precursor **Pep. 43**.

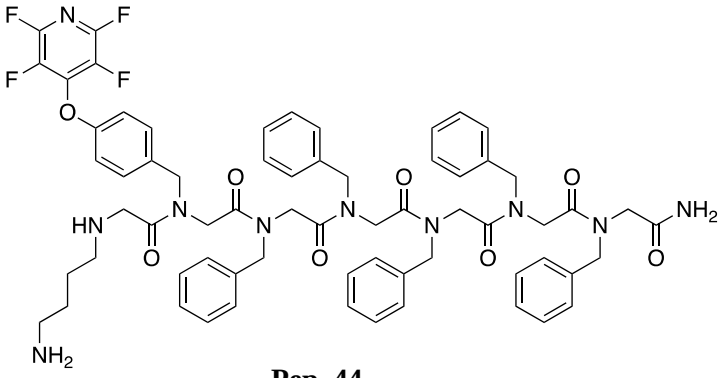

Pep. 44
Calculated *m/z* = 1193.516

Figure 4.3. Structure of target heptameric peptoid **Pep. 44**, showing its expected *m/z*.

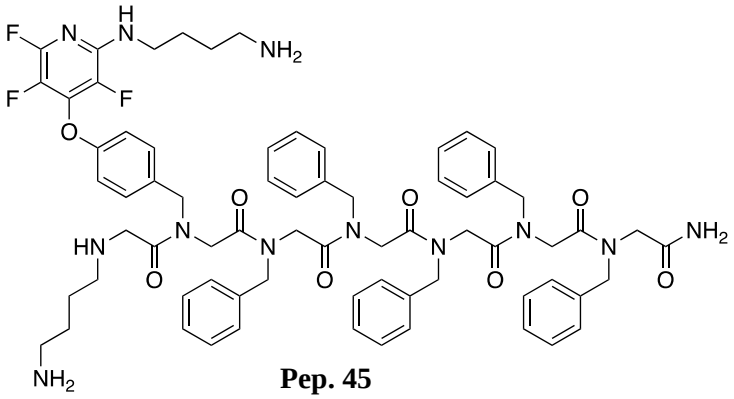

Pep. 45
Calculated *m/z* = 1261.601; found *m/z* = 1261.734

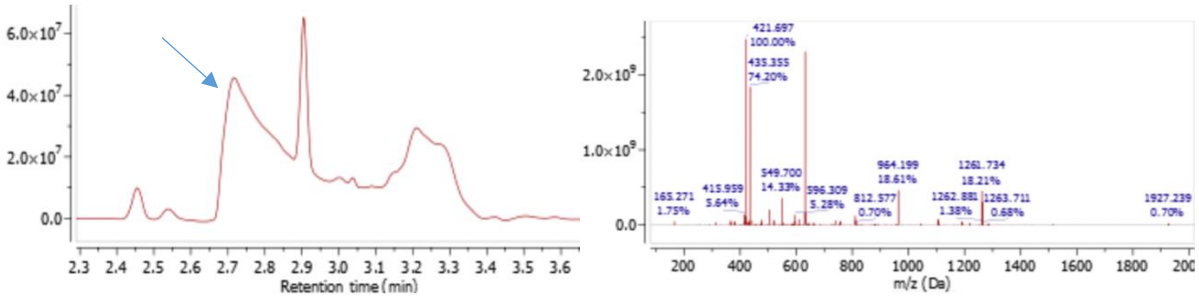

Figure 4.4. LC-MS trace collected for **Pep. 45**, showing the formation of the heptamer containing the di-substituted TFP. No mass corresponding to the desired **Pep. 44** (m/z = 1193.516) was found.

It was hypothesised that an S_NAr reaction took place resulting in 2'-substitution on the TFP ring, because the *m/z* fragmentation patterns matched that of a **Pep. 45**. In addition, upon ^{19}F spectroscopic analysis, three ^{19}F NMR signals, as opposed to two ^{19}F NMR peaks which were present in the TFP-containing starting material were seen. The ^{19}F NMR data supported the formation of **Pep. 45**. Subsequently, the addition of monomers to **Pep. 45** was continued,

with *N*Phe (**40**) being added. Indeed, both the bromoacetylation and bromo-displacement steps were successful, resulting in the obtainment of octamer **Pep. 46**, confirmed by the mass fragmentation pattern, attained by LC-MS. (**Figure 4.5** and **Figure 4.6**)

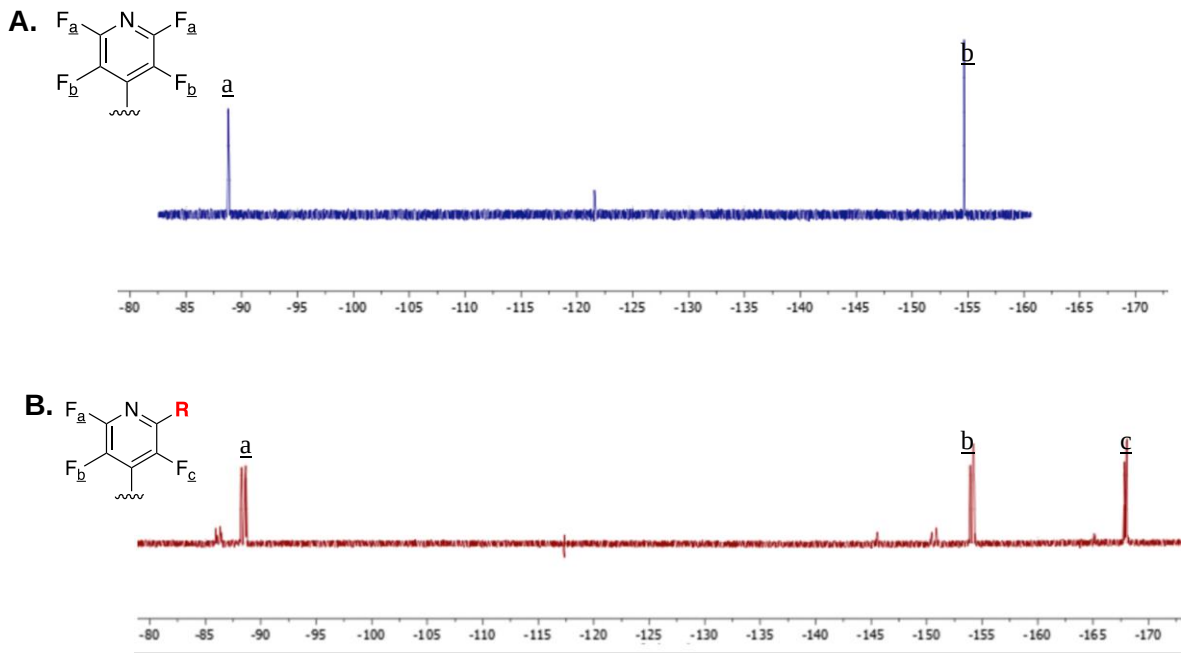

Figure 4.5. ^{19}F NMR patterns acquired for: **A**. O-TFP *p*-aminomethylphenol (**112**), showing two ^{19}F signals characteristic for 4'-substituted PFP ring; **B**. **Pep. 45** crude material, showing three characteristic ^{19}F signals corresponding to a 2'-,4'-di-substituted PFP ring.

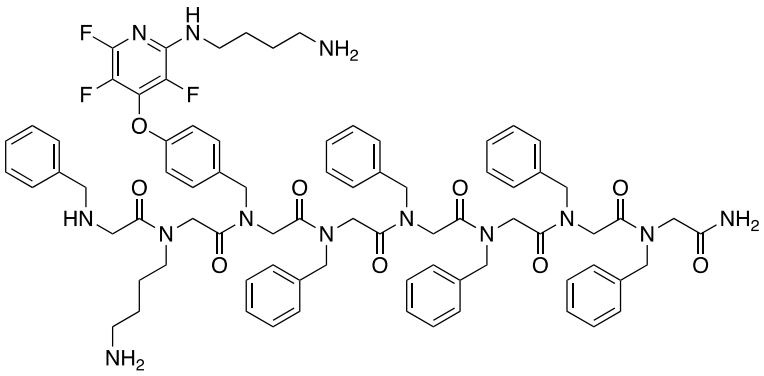

Pep. 46

Calculated *m/z* = 1408.678; found $[M+1]^{+}$ = 1408.875; $[M+2]^{2+}$ = 705.433

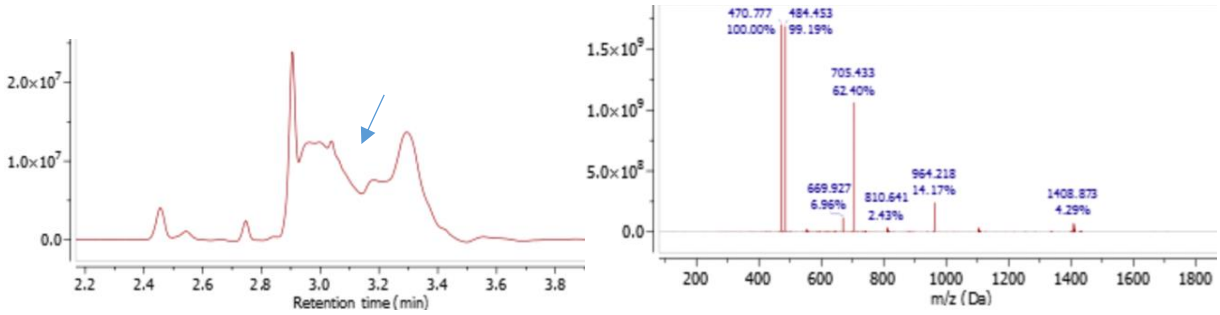

Figure 4.6. LC-MS trace found for **Pep. 46** showing successful incorporation of *N*Phe peptoid monomer.

Meanwhile, the synthesis of the test peptoid containing **155** (**Pep. 47**), which contained the Bu protecting group was successful as determined by the LC-MS monitoring, both the UV and *m/z* traces showed the presence of the desired compound(**Figure 4.7**).

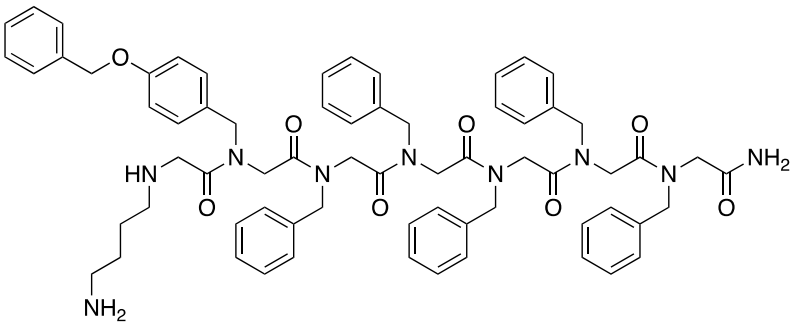

Pep. 47
Calculated *m/z* = 1134.573; found $[M+1]^+$ = 1134.786; $[M+2]^{2+}$ = 568.460

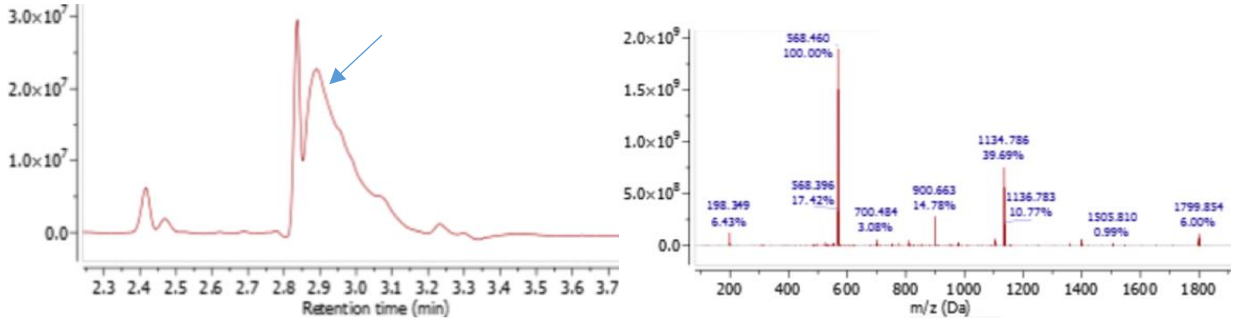

Figure 4.7. Structure of **Pep. 47** and the LC-MS trace found for **Pep. 47**, showing the *m/z* of the desired product containing *O*-Bnz *p*-aminomethylphenol.

As reported by the Cobb group, the cleavage of the 2'-substituted TFP protecting group can still occur in the presence KF and thiophenol.[14] Hence, we wished to compare the deprotected reaction outcomes for the two peptoids. Consequently, both **Pep. 46** and **Pep. 47** were cleaved from the resin in the presence of a cleavage cocktail constituting of TFA/TIPS/H_2O (95:2.5:2.5). The mother liquors were collected, and the resin beads were washed with DCM. Upon concentration, the crude residue was were suspended in water and lyophilised resulting in the obtainment of white powders. The two peptoid chains **Pep. 46** and **Pep. 47** were then subjected to test reactions aiming for alcohol deprotection.

The TFP group in **Pep. 46** was cleaved using excess KF and thiophenol, and after stirring at ambient conditions overnight no more starting material was detected. Instead, the intense presence of a UV signal eluting at t_R = 3.98 min, corresponding to the tri substituted PFP by-product (**162**) formed by the S_NAr reaction between the pyridine ring and the excess thiophenol, was detected. Due to its high lipophilicity compared to the product (*m/z* 1191, t_R = 2.34 min) the isolation of the desired **Pep. 48** would not be deemed cumbersome (**Figure 4.8**) However, depending on the hydrophobicity of dodecameric peptoids (12-mers have been shown to present high antimicrobial properties) synthesised, this side product could interfere

with successful elucidation of the desired products. Instead, the use of methyl thioglycolate could be more appropriate in such cases.[14] Probing of the crude mixture by ^{19}F NMR spectroscopy revealed one ^{19}F NMR signal at δ -116.75 ppm (**Figure 4.8B**). Comparison of ^{19}F NMR signals reported for different PFP substitution patterns obtained in this chapter (for **112**, **Pep. 45** and **162**) is shown in **Table 4.1**.

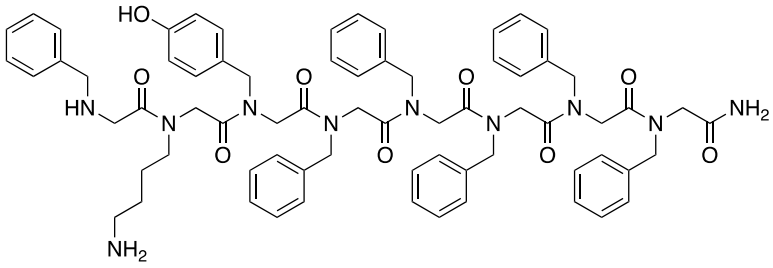

Pep. 48

Calculated m/z = 1191.560; found $[M+1]^+$ = 1191.714; $[M+2]^{2+}$ = 546.203

A.

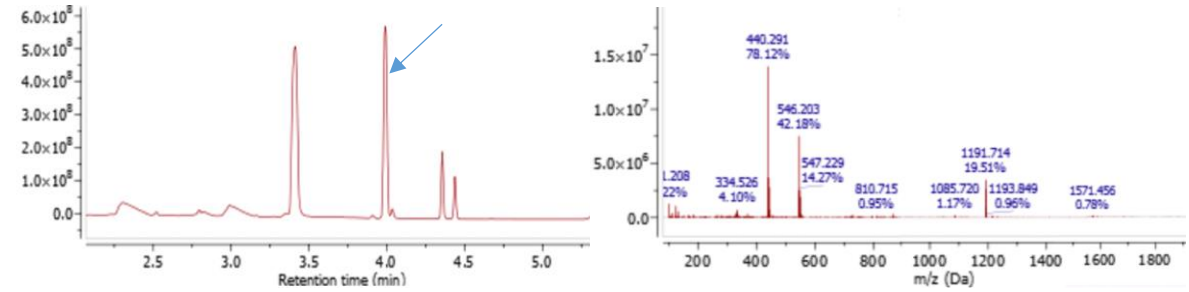

B.

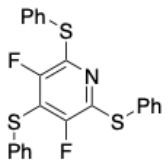

162

Figure 4.8. Structure of peptoid **Pep. 48**, produced via TFP-cleavage as described in the text. **A.** LC-MS trace obtained for **Pep. 48**, showing the *m/z* of the desired product. **B.** ^{19}F NMR spectrum of **Pep. 48**, showing one distinct ^{19}F signal at -116.75 ppm corresponding to the tri-substituted PFP side-product **162**.

Table 4.1. Assigned ^{19}F signals arising from different patterns of substitution on the PFP ring of **112**, and the compound numbers these substitutions correspond to.

No.	Substitution pattern on PFP ring	Observed ^{19}F NMR chemical shifts δ(ppm)
112	4'-substitution	δF1 = -88.85, δF2 = -154.48
Pep. 45	2'-4'-di-substitution	δF1 = -88.56, δF2 = -154.19, δF3 = 169.98
162	2'-2'-4'-tri-substitution	δF1, 2 = -116.75

Concurrently, the hydrogenolysis reaction employing hydrogen and 10% Pd/C catalyst was used to cleave the benzyl ether to liberate the alcohol and give **Pep. 49**. Initially, the reaction was stirred at ambient temperature for two hours. The LC-MS monitoring of the mixture revealed that it mostly contained unreacted starting material. Henceforth, the reaction was brought to reflux and stirred for a further two hours, and after this time the benzyl ether cleavage was complete and produced **Pep. 49**. (**Figure 4.9**)

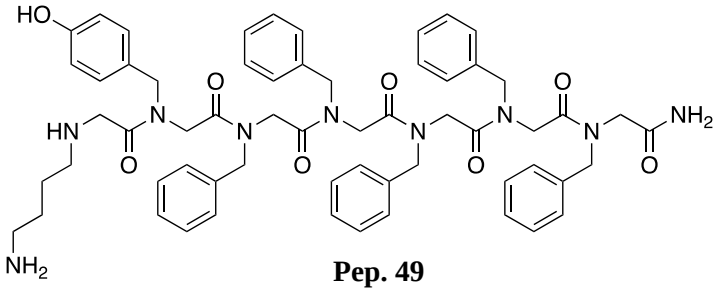

Pep. 49

Calculated *m/z* = 1044.527; found $[M+1]^+$ =1044.687; $[M+2]^{2+}$ = 523.216

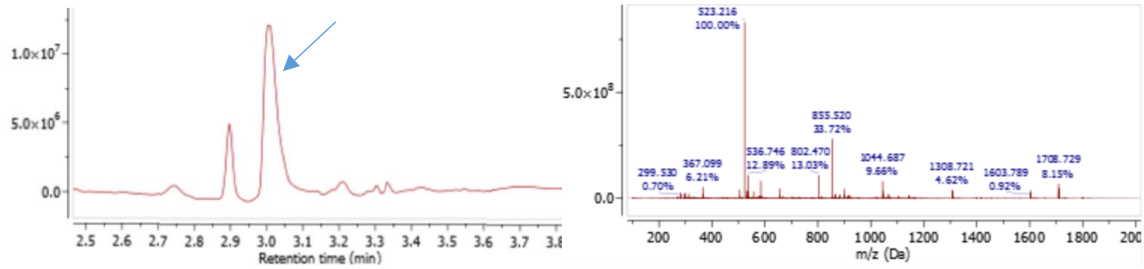

Figure 4.9. LC-MS trace found for **Pep. 49**, showing the m/z of the desired product, together with its structure.

This initial work demonstrated that either of the protecting strategies, TFP or Benzyl can be utilised, with varying degrees of success, to produce peptoids bearing *N*Tyr monomers. It was noted that the choice of the protecting group needs to be made whilst considering the

stability of other potential side chain moieties used within the peptoid sequence. For instance, if the *O*-Bnz protecting group approach was used then the deprotection conditions, could make the use of alkene containing monomers problematic Likewise, the *cis*-inducing electron-withdrawing nitrobenzylamine monomer (**173**)[16] could get reduced by such conditions and would result in the formation of aminobenzylamine (**174**), which would potentially alter both the secondary structure and peptoid antimicrobial properties. (**Scheme 4.1**)

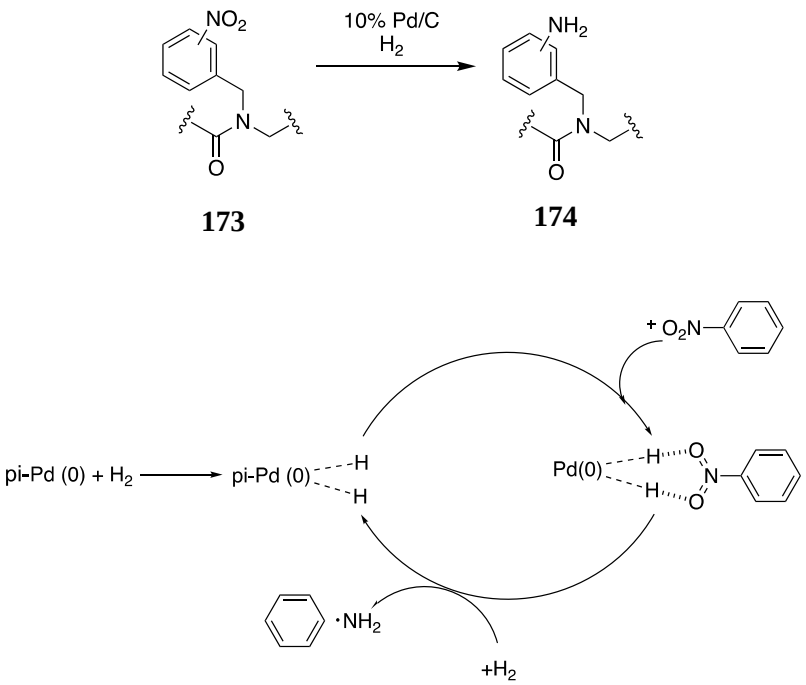

Scheme 4.1. Pd(0)-catalysed reduction of nitro groups in **173** to amino groups, giving rise to **174**, together with the catalytic cycle for this reaction.

It was therefore desirable to establish a protecting group strategy wherein the liberation of the alcohol moiety would be mild enough as to not interact with other monomer side chains, and wherein the elimination of the side product would be simple enough as to not interfere with product purification. Furthermore, establishing a strategy which would enable us to selectively tag the phenol moieties in peptoids would serve as an additional advantage. Specifically, we endeavoured to establish a novel synthetic route to a selective TFP-tagging of peptoids on resin.

The utilisation of the Allyl-protecting group strategy became an attractive avenue to pursue in order to tackle this setback due to mild aprotic conditions of $Pd(PPh_3)_4$ required to cleave Allyl ethers.[17] In addition, the Allyl ether cleavage is compatible with solid phase synthesis, and any side products or unreacted reagents can be easily washed off.

The *N*-Boc aminomethylphenols (**122** – **124**) previously made *in-house* (**Section 3.4.1**) were reacted with allyl bromide under reflux and in the presence of a mild base. Upon purification, the *O*-allyl protected products were recovered in good yields. (**Scheme 4.2**, first step)

Previously, Parker and Svanholm[18] reported TFA-catalysed *o*-Claisen rearrangement of aryl ethers. With this in mind, a test reaction was executed using a 25% solution of TFA in DCM to deprotect the *N*-Boc *p*-aminomethylphenol (**124**). (**Scheme 4.3**) ^{1}H NMR was used to probe this reaction mixture and revealed no *o*-Claisen rearrangement had taken place, corroborated by the ^{1}H NMR signals in the aromatic region, distinct for the *p*-regioisomer (**177**). (**Figure 4.10**) The crystal structure obtained for **180** is shown in **Figure 4.11**. Encouraged by this result a scale up of the reaction was performed, followed by the deprotection of *N*-Boc, *O*-Allyl *o*- and *m*-aminomethylphenols (**175** and **176**) to generate *O*-allyl aminomethylphenol derivatives as trifluoroacetate salts (**178** and **167**) to be used in the synthesis of peptoids. The mechanism showing potential *O*-Claisen rearrangement is shown in **Scheme 4.3**.

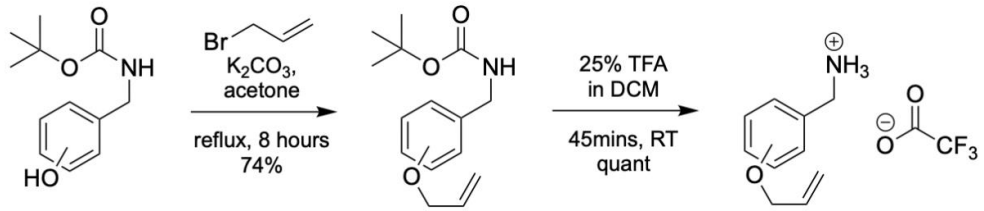

No.	Isomer
122	*ortho*
123	*meta*
124	*para*

No.	Isomer	Yield
175	*ortho*	94%
176	*meta*	90%
177	*para*	79%

No.	Isomer	Yield
178	*ortho*	quant.
179	*meta*	quant.
180	*para*	quant.

Scheme 4.2. A two-step synthesis used to produce *O*-allyl aminomethylphenols as TFA-salts.

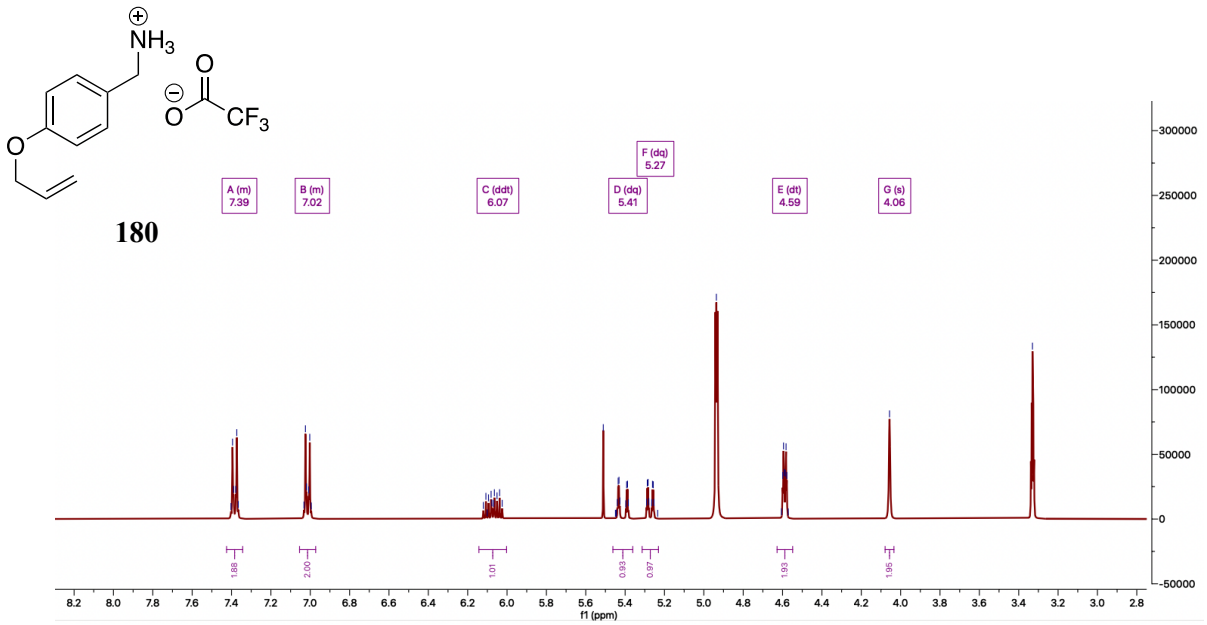

Figure 4.10. ^{1}H NMR spectra of *O*-Allyl *p*-aminomethylphenol **180**, confirming no *o*-Claisen rearrangement had taken place.

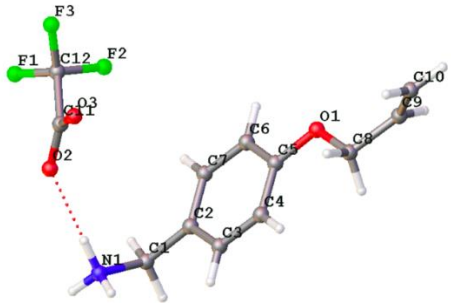

Figure 4.11. Ball -and-stick representation of **180** present in the unit cell. Hydrogen bonding is represented by red dotted lines. Carbon atoms are depicted in grey, hydrogen atoms in white, nitrogen atoms in navy, oxygen atoms in red, and fluorine atoms in green. Structure was generated in Olex2 and is reported with a 50% thermal ellipsoid probability.

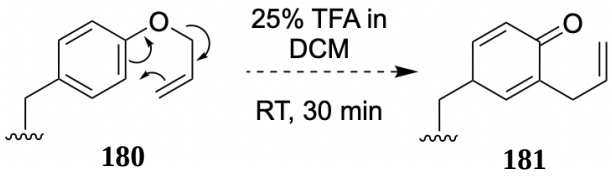

Scheme 4.3. Curly arrow mechanism showing the potential *o*-Claisen rearrangement in **180** in the presence of TFA, as reported by Parker and Svanholm.[18]

4.3.2. Synthesis of a series of nonamer peptoids containing tyrosine-type monomers

A library of seven nonamer peptoid chains containing the *O*-allyl submonomers **168** – **170** was designed and synthesised on Rink Amide resin (0.77 mmol/g), by the submonomer approach (**Scheme 4.4).** The Allyl protecting group was found to be compatible with the synthesis and it was conveniently removed *in-situ* by the utilisation of a Pd(II) catalyst in the presence of an activator (PhSiH). The library of peptoids constituted of oligomers, each containing a chiral reporter *N*spe (**2**) in order to yield chirally homogenous mixtures. **Pep. 50** was designed as a control peptoid, containing no *N*Tyr monomers. **Pep. 51 – 53** and **Pep. 54 – 56** contained phenolic monomers wherein the hydroxyl group was located at different positions around the aryl ring (**Figure 4.10**). The purpose was to investigate whether increasing the number of hydroxy-containing aryls would have a cooperative effect on the alpha helicity of the peptoids and to determine whether the varying geometries of the hydroxy aryls would affect the overall secondary structures of long peptoids.

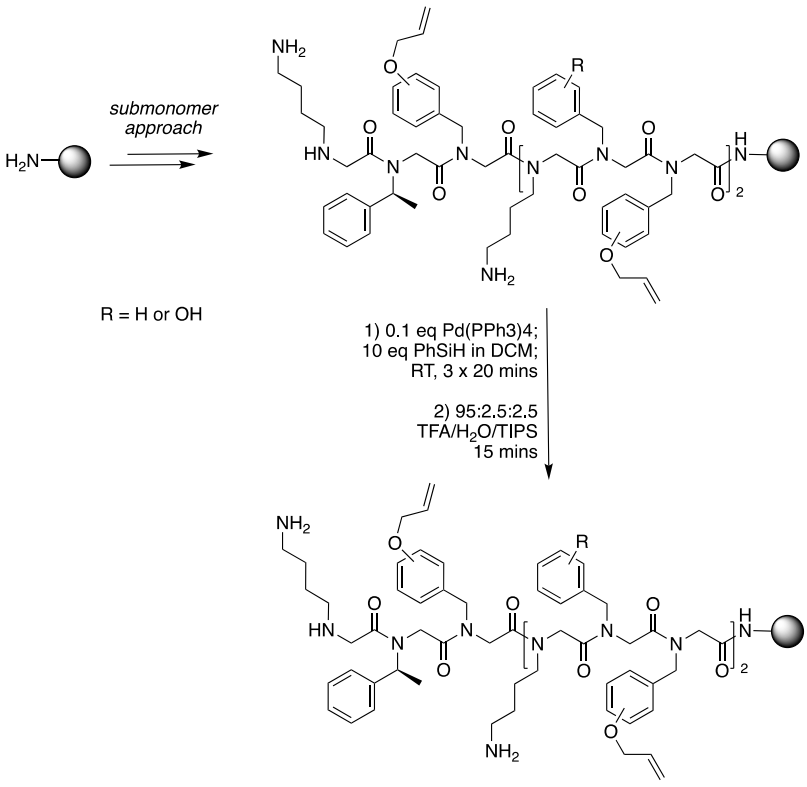

Scheme 4.4. A schematic representation of the synthetic approach used to produce six *N*Tyr-containing peptoid chains (**Pep. 51** – **56, Figure 4.11**), bearing liberated hydroxy moieties. For a detailed description of the submonomer method, see **Chapter 2**.

Due to their extremely polar nature, the peptoids were poorly soluble in aprotic solvents. Moreover, it was observed that as the degree of hydroxyl groups within the peptoids increased, their solubility in water decreased. This solubility issue posed significant challenges, particularly for **Pep. 54– 56**, which had a higher number of hydroxyl groups, compared to **Pep. 51 – 53**. As a result of this poor solubility, the yields obtained for these particular peptoids were low. (**Figure 4.12**)

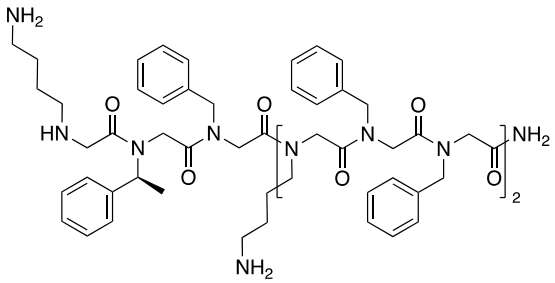

Pep. 50 *N*Lys*N*spe*N*Phe[*N*Lys*N*Phe*N*Phe]$_2$; **Yield** = 12%

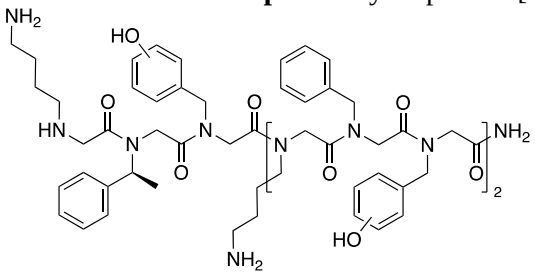

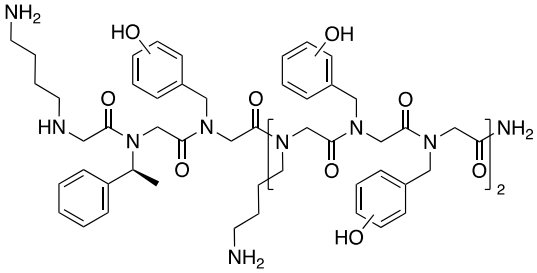

No.	Sequence	Yield
Pep. 51	*N*Lys*N*spe*No*Tyr [*N*Lys*N*Phe*No*Tyr]$_2$	2%
Pep. 52	*N*Lys*N*spe*Nm*Tyr [*N*Lys*N*Phe*Nm*Tyr]$_2$	2%
Pep. 53	*N*Lys*N*spe*N*Tyr [*N*Lys*N*Phe*N*Tyr]$_2$	9%

No.	Sequence	Yield
Pep. 54	*N*Lys*N*spe*No*Tyr [*N*Lys*No*Tyr*No*Tyr]$_2$	2%
Pep. 55	*N*Lys*N*spe*Nm*Tyr [*N*Lys*Nm*Tyr*Nm*Tyr]$_2$	1%
Pep. 56	*N*Lys*N*spe*N*Tyr [*N*Lys*N*Tyr*N*Tyr]$_2$	<1%

Figure 4.12. Seven nonamer (**Pep. 50** – **56**) peptoids designed and synthesised for their biophysical and biological evaluation. (All peptoids synthesised in this library have a C-terminal amide)

4.3.3. Crystal structure of 178: occurrence of C–F…H–N bonding

In 1996, upon their analysis of the Cambridge Structural Database System (CSDS), O'Hagan and co-workers[19] concluded that, in the light of rare optimal C–F…H contacts, fluorine is a poor hydrogen bond acceptor. Since then, a greater deal of evidence supporting organic fluorine as a hydrogen bond acceptor has been reported. In particular, the presence of hydrogen bonds with fluorine in the gaseous state and in solution has been recognised.[20] Meanwhile, stronger intermolecular interactions present within a solid state dominate weaker

interactions with organic fluorine, and thus have a more prominent effect on molecular arrangement. This area continues to be widely debated, as the published evidence supports the existence of hydrogen bonding with fluorine; however, it is generally accepted that these interactions are unlikely to be energetically significant in all systems.[21-23]

Upon the treatment of **177** with TFA, we were able to isolate single crystals of **178** as a TFA salt, suitable for X-ray crystallography. The unit cell revealed the presence of two molecules of **178** connected by a series of hydrogen bonds between the TFA C=O and **178** NH_3. In addition, the presence of a hydrogen bond between the fluorine located within the TFA molecule and the NH_3 moiety was noted. Jeffrey categorised the hydrogen bond acceptor-donor distances within the range of 2.2 to 2.5 Å to be strong in nature.[24] Interestingly, the mean distance between donor and acceptor in peptide secondary structures was close to 3 Å, which classifies their strength as moderate. In addition, IUPAC set the hydrogen bond criterium in X–H…Y systems whereby the X–H…Y angle is to be as close as possible to 180°, and usually is in the range of 110-180°.[25] Hence, considering these criteria for hydrogen bonding, it can be established that, indeed, the presence of the N–H…F interaction is evidenced (**Figure 4.13**); and comparing the interatomic distances of N–H…F and N–H…O, it can be deduced that the dominating interactions dictating the arrangement of the motifs within the unit cell are hydrogen bonds linking N–H…O.

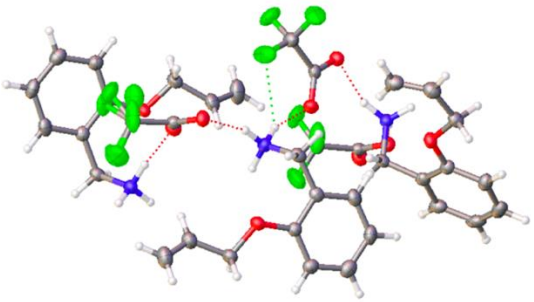

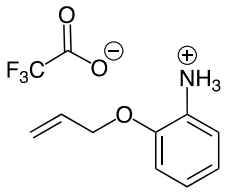

178

F…H–N distance (Å)	O…H–N distance (Å)	F…H–N angle	O…H–N angle
2.48	1.84 – 1.96	123°	158 – 168°

Figure 4.13. Ellipse-and-stick representation of **178** dimer present in the unit cell (structural formula of **178** as a TFA salt is depicted on the right). It evidences the existence of hydrogen bonding between the amine proton and the TFA fluorine atom. The occurrence of F…H–N bonding is represented by a green dotted line. O…H–N bonding is represented by red dotted lines. Carbon atoms are depicted in grey, hydrogen atoms in white, nitrogen atoms in navy, oxygen atoms in red, and fluorine atoms in green. Structure was generated in Olex2 and is reported with a 50% thermal ellipsoid probability.

4.3.4. Synthesis of peptoid nonamers containing amino(aryl) derivatives

In order to probe the incorporation of *o*-amino(aryl) derivatives (investigated for their *cis*-inducing properties in **Chapter 3**), a strategy was devised to synthesise two peptoid nonamers, wherein the cationic *N*Lys monomers were to be replaced by the novel amine containing aromatic building blocks to form **Pep. 57** and **Pep. 58**. (**Figure 4.14**)

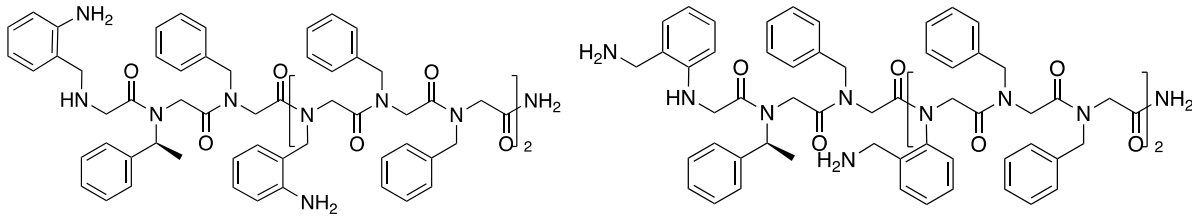

Pep. 57 **Pep. 58**

Figure 4.14. Aryl amine derivatives of **163** were investigated for their incorporation into peptoid oligomers, resulting in the production of **Pep. 54** and **Pep. 55**.

As previously outlines, cleaving peptoid protecting groups using H_2 and a Pd/C catalyst is impractical due to potential side reactions. Consequently, it was imperative to develop a new building block (**183**), to facilitate the synthesis of **Pep. 57**, in which the aromatic amine of compound **182** was protected with a suitable protecting group, one that could be employed in the solid-phase synthesis of peptoids containing a diverse range of functional groups. The alloc protecting group was selected for its highly efficient installation and compatibility with solid-phase synthesis. Thereafter, **183** was Boc-deprotected using acidic conditions, resulting in **184** obtained in quantitative yield. This synthetic approach is outlined in **Scheme 4.5**. Crystal structure of **184** as a TFA salt is shown in **Figure 4.15**.

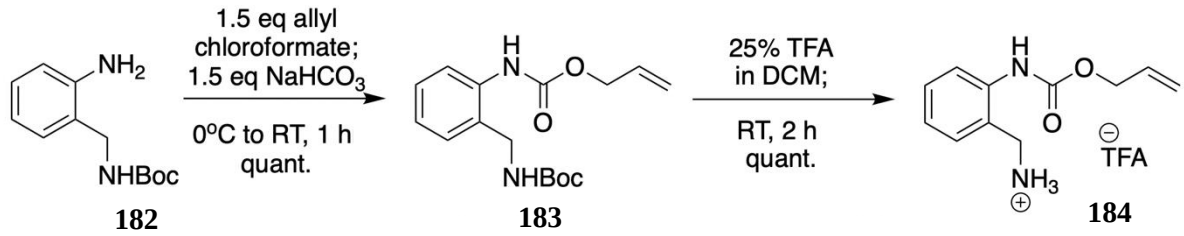

182 **183** **184**

Scheme 4.5. A two-step synthetic route used to produce alloc-protected aminobenzylamine **183**, suitable for solid-phase peptoid synthesis.

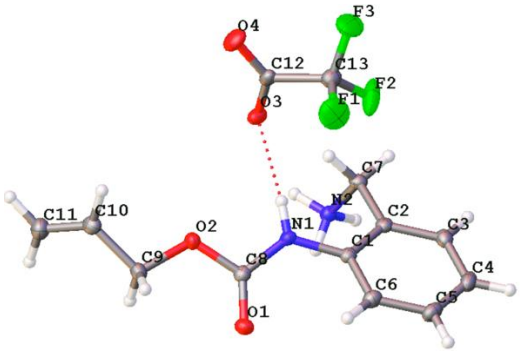

Figure 4.15. Ellipse-and-stick representation of **184** present in the unit cell. C=O…H–N bonding is shown as red dotted lines. Carbon atoms are depicted in grey, hydrogen atoms in white, nitrogen atoms in navy, oxygen atoms in red, and fluorine atoms in green. Structure was generated in Olex2 and is reported with a 50% thermal ellipsoid probability.

The synthesis of alloc-protected **Pep. 59** was carried out on Rink Amide resin (0.77 mmol/g), using the submonomer approach and utilising *N*spe **2**, *N*Phe **40** and **184**. In order to liberate the aromatic amine functionalities, the alloc protecting group was removed *in-situ* in the presence of a Pd(II) catalyst and an activator (PhSiH), and the side products were washed off the resin. (**Scheme 4.6**) **Pep. 57** was subsequently engaged in the biophysical and biological evaluation, discussed in **Sections 4.3.5** and **4.3.6**.

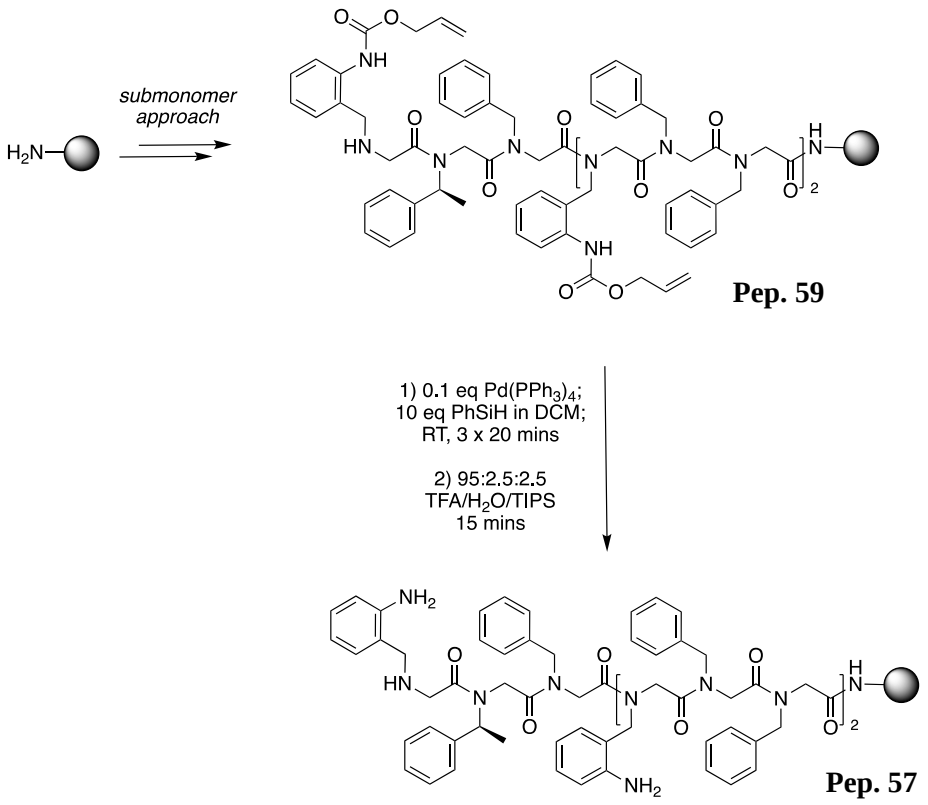

Scheme 4.6. A schematic representation of the synthetic approach used to produce **Pep. 57**. For a detailed description of the submonomer method, see **Chapter 2**.

A different situation arose when the synthesis of **Pep. 58** (**Scheme 4.7**) was attempted. The progression of the synthesis of **Pep. 60**, using the standard conditions of the submonomer method, was monitored by LC-MS after the coupling of the third (**Figure 4.16 A. Pep. 61**), fifth (**Figure 4.16 B. Pep. 62**) and ninth amine (**Figure 4.16 C. Pep. 63** and **Pep. 64)**. It was found that after the synthesis of the second repeat motif, the coupling of the subsequent chiral aromatic *N*spe (**2**) was cumbersome. It was suspected that the incorporation of **2** was hindered by its bulky nature, as the coupling of the bromoacetate proceeding this amine was not affected. A double coupling of this amine and heating the reaction vessel to 50 ^{o}C were attempted but did not yield a positive result. Similarly, the incorporation of the terminal Boc-protected aryl amine **182** was not successful. This synthesis was not explored further due to time constraints. Likewise, the introduction of chirality at the side chain Cα should be further explored in order to investigate its compatibility with the synthesis of peptoids containing **182**. There also exists a possibility that the Boc-protecting group located *ortho* to the aniline amine of **182** could impose a steric constrain on the peptoid backbone, which interferes with the incorporation of

bulky amines. Detailed LC-MS analyses together with the structures corresponding to fragments of **Pep. 48** can be seen in **Figure 4.16**.

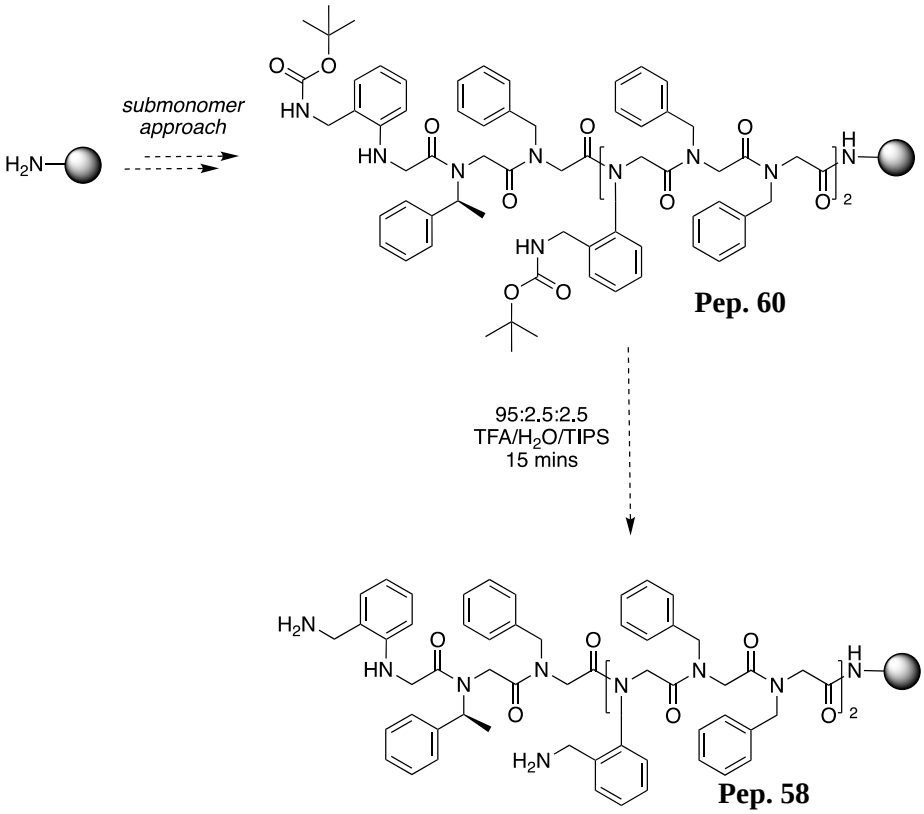

Scheme 4.7 An attempted synthesis of **Pep. 58**. For a detailed description of the submonomer method, see **Chapter 2**.

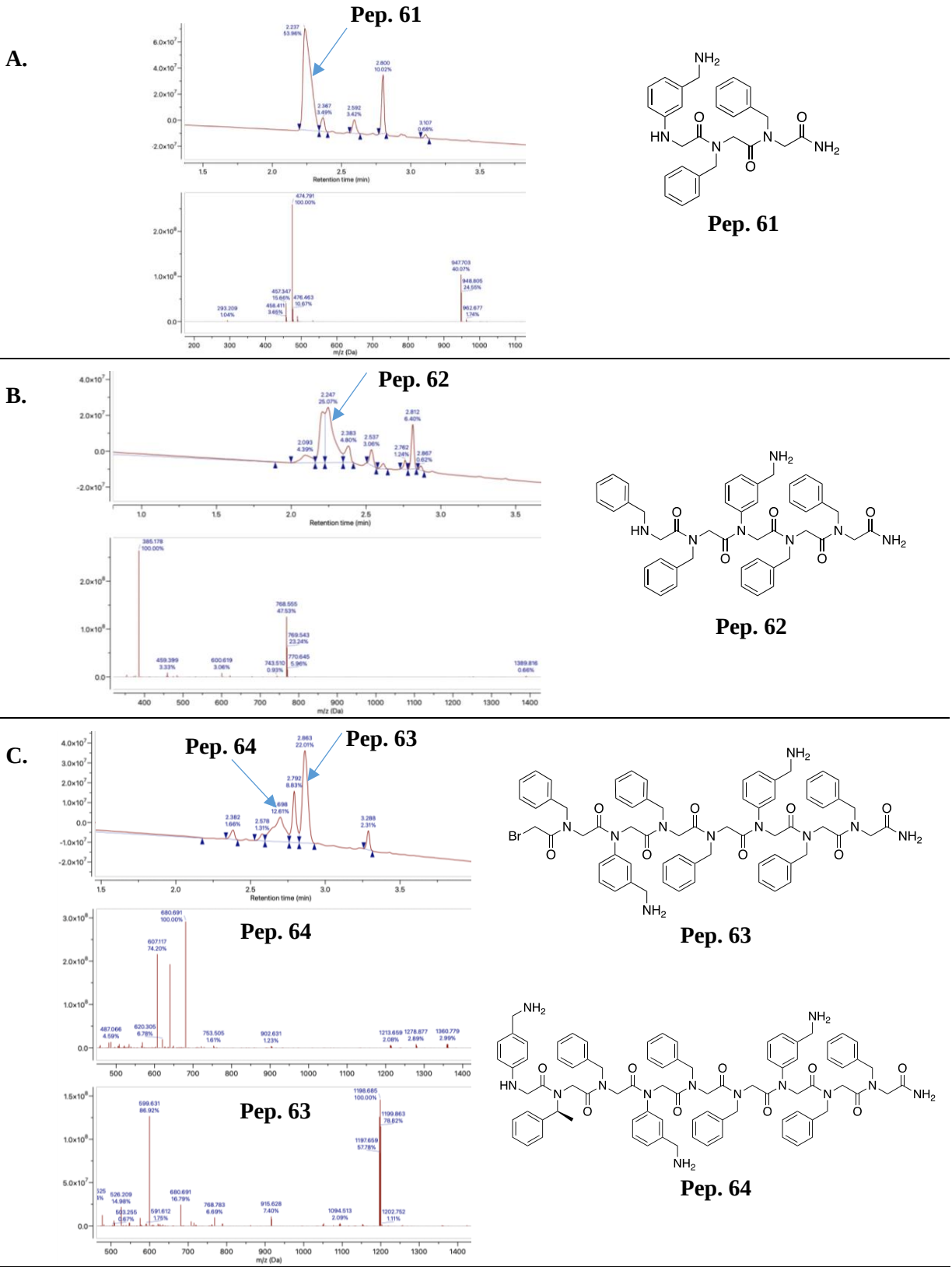

Figure 4.16. Three panels showing detailed LC-MS analyses of **Pep. 58** synthesis progress after the coupling of: **A.** 3 monomers, **Pep. 60**, t_R = 2.247 min, $[M+1]^+$ = 474.791, $[2M+1]^+$ = 947.703; **B.** 5 monomers, **Pep. 61**, t_R = 2.249 min, $[M+1]^+$ = 768.555, $[2M+1]^+$ = 1389.816; **C. Pep. 63**, t_R = 2.863 min, $[M+1]^+$ = 1198.685, $[M+2]^+$ = 599.631; **Pep. 64**, t_R = 2.698 min, $[M+1]^+$ = 1360.779, $[M+2]^+$ = 680.691.

4.3.5. Minimum inhibitory concentration (MIC) and cytotoxicity assays

For the determination of the antibacterial MICs of the peptoids synthesised in this chapter, the protocol summarised in **Chapter 2**, **Section 2.3.6** was used. In addition, similarly to the peptoids investigated in **Chapter 2**, **Pep. 50 – 56** were screened against HepG2 cells to investigate their toxicity against liver cells, using the protocol described in **Chapter 2**, **Section 2.3.7**. In addition, the selectivity index (SI) values were calculated (**Table 4.2**)

Table 4.2. A summary of peptoids tested against four bacterial species, together with their ED_{50} values against HepG2, and SI values. (nd = no data recorded)

No.	Sequence
Pep. 50	*N*Lys*N*spe*N*Phe[*N*Lys*N*Phe*N*Phe]$_2$
Pep. 51	*N*Lys*N*spe*No*Tyr[*N*Lys*N*Phe*No*Tyr]$_2$
Pep. 54	*N*Lys*N*spe*No*Tyr[*N*Lys*No*Tyr*No*Tyr]$_2$
Pep. 52	*N*Lys*N*spe*Nm*Tyr[*N*Lys*N*Phe*Nm*Tyr]$_2$
Pep. 55	*N*Lys*N*spe*Nm*Tyr[*N*Lys*Nm*Tyr*Nm*Tyr]$_2$
Pep. 53	*N*Lys*N*spe*N*Tyr[*N*Lys*N*Phe*N*Tyr]$_2$
Pep. 56	*N*Lys*N*spe*N*Tyr[*N*Lys*N*Tyr*N*Tyr]$_2$
Pep. 57	*N*2aPhe*N*spe*N*Phe[*N*2aPhe*N*Phe*N*Phe]$_2$

Entry	No.	ED_{50} (μM)	MIC (μM)				SI			
		HepG2	*E. coli*	*P. aeruginosa*	*S. aureus*	*B. subtilis*	*E. coli*	*P. aeruginosa*	*S. aureus*	*B. subtilis*
1	**Pep. 50**	100	12.5	100	12.5	3.13	8	1	8	32
2	**Pep. 51**	100	12.5	100	12.5	3.13	8	1	8	32
3	**Pep. 54**	100	6.25	50	1.56	1.56	16	2	64	64
4	**Pep. 52**	100	50	100	6.25	6.25	2	1	16	16
5	**Pep. 55**	nd	100	nd	100	100	nd	nd	nd	nd
6	**Pep. 53**	100	50	100	100	6.25	2	1	1	16
7	**Pep. 56**	nd	100	nd	100	nd	nd	nd	nd	nd
8	**Pep. 57**	100	100	nd	100	nd	1	nd	1	nd

The exploration of the *N*Tyr monomer in peptoids has not been previously reported, and we wished to design and synthesise peptoid oligomers which would thoroughly explore the effects their incorporation would have in biological systems. The library in this chapter consisted of six *N*Tyr-based peptoid nonamers (**Pep. 51** – **Pep. 56**), and a control peptoid **Pep.**

50. These oligomers were based on the *N*y*N*x*N*x repeating motif, and each peptoid bared a chiral *N*spe (**2**) monomer to induce a specific helical chirality.

What was interesting to note was that the overall toxicity of peptoids in this library showed no significant effects on the HepG2, as even at the highest compound concentrations used, the HepG2 population reduction was not considerable.

Pep. 50 (**Table 4.2**, **Entry 1**) was found to show promising MIC values against *E. coli*, and due to its ED_{50} value of 100, the SI calculated for this species was 8. Unsurprisingly, due to its biofilm-forming properties, *P. aeruginosa* showed no susceptibility to this peptoid at any of the concentrations used. Improved activities of **Pep. 50** were seen against the Gram-positive species, with *S. aureus* showing considerable population reductions at 12.5 μM, and *B. substilis* showing susceptibility to this peptoid at 3.13 μM.

The complete replacement of *N*Phe (**40**) monomers (**Pep. 50**, **Table 4.2**, **Entry 1**) to *No*Tyr in **Pep. 51** (**Table 4.2**, **Entry 2**) resulted in a 2-fold increase in the susceptibility of both *E. coli* (6.25 μM) and *B. subtilis* (1.56 μM) to the antimicrobial effects of this peptoid. A more notable activity enhancement was seen for *S. aureus* which showed an eight-fold reduction in the MIC value (1.56 μM) relative to **Pep. 50** (12.5 μM). Considering the α-helix-inducing properties of *No*Tyr, it can be suggested that the formation of a tight-helix encourages bacterial-membrane targeting, whereby membrane interaction with the cationic *N*Lys would be more accessible. In addition, there was a suspicion that the creation of tight helices would led to lower polarities of peptoids, which was contrary to what one might expect based on the inherent polar nature of hydroxyls. This would, in turn, result in enhanced interactions with the bacterial membranes, increasing bacterial susceptibility to **Pep. 54**. (**Table 4.2**, **Entry 3**) On the other hand, partial *N*Phe replacement with *No*Tyr to form **Pep. 51**, resulted in no significant change in activities against the bacterial species in this assay, compared to **Pep. 50** (**Table 4.2**, **Entry 1)** with the exception for the MIC value found for *P. aeruginosa*, which showed complete eradication of bacterial populations, at the highest peptoid concentration used (100 μM).

Interestingly, the incorporation of both *Nm*Tyr and *N*Tyr (**Pep. 52**, **Pep, 55**, **Pep. 56**, **Pep. 53**, **Table 4.2**, **Entries 4 – 7**) resulted in decreased efficacy against all of the bacterial species used, relative to *No*Tyr (**Pep. 51** and **Pep. 54**, **Table 4.2**, **Entries 2** and **Entry 3**). This implied that there is a correlation between the position of the hydroxyl on the aryl ring and the antibacterial potency of the peptoid nonamers. We would consider the *ortho*- substituent yielding most efficacious peptoids, followed by *meta*-, and *para*- substituents which rendered

the peptoid nonamers least active. However, this effect is different for *S. aureus*. Specifically, where partial replacement of *N*Phe monomers of **Pep. 50** (**Table 4.2**, **Entry 1**) is considered, compared to *Nm*Tyr, there is a two- and 16-fold decrease in peptoid efficacy against *S. aureus* for *No*Tyr and *N*Tyr, respectively. (**Table 4.2**, **Entries 2**, **4** and **6**).

4.3.6. Log *D* measurements vs. HPLC-derived t_R: measure of peptoid lipophilicity

To obtain log *D* values of the nonamer peptoids, the protocol described in **Chapter 2**, **Section 2.3.9** was used. **Figure 4.17** shows the relationship between the HPLC t_R and the log *D* values of the nonamer peptoids investigated in this chapter. The HPLC t_R and log *D* values are shown in **Table 4.3**. No obvious trend between the two was observed.

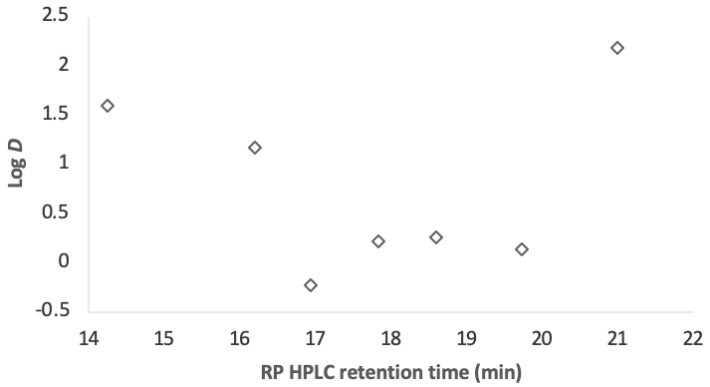

Figure 4.17. A graphical depiction of the relationship between RP HPLC t_R. and Log *D* values of peptoids shown in **Table 4.6.**

Table 4.3. A tabulated summary of phenolic peptoids (**Pep. 50** – **57**) tested against four bacterial species, together with their HPLC t_R and log *D* values.

Entry	No.	Sequence	HPLC t_R	Log *D*
1	**Pep. 50**	*N*Lys*N*spe*N*Phe[*N*Lys*N*Phe*N*Phe]$_2$	21.00	2.18
2	**Pep. 51**	*N*Lys*N*spe*No*Tyr[*N*Lys*N*Phe*No*Tyr]$_2$	19.73	0.13
3	**Pep. 54**	*N*Lys*N*spe*No*Tyr[*N*Lys*No*Tyr*No*Tyr]$_2$	17.82	0.22
4	**Pep. 52**	*N*Lys*N*spe*Nm*Tyr[*N*Lys*N*Phe*Nm*Tyr]$_2$	18.60	0.25
5	**Pep. 55**	*N*Lys*N*spe*Nm*Tyr[*N*Lys*Nm*Tyr*Nm*Tyr]$_2$	16.20	1.17
6	**Pep. 53**	*N*Lys*N*spe*N*Tyr[*N*Lys*N*Phe*N*Tyr]$_2$	16.94	-0.24
7	**Pep. 56**	*N*Lys*N*spe*N*Tyr[*N*Lys*N*Tyr*N*Tyr]$_2$	14.24	1.60
8	**Pep. 57**	*N*2aPhe*N*spe*N*Phe[*N*2aPhe*N*Phe*N*Phe]$_2$	29.41	-2.20

The HPLC t_R values, shown in **Table 4.3**, observed for the peptoids show increasing polarity as the aryl hydroxide moves from the *ortho-* to *para-* position, which can be assigned to the hydroxyls becoming increasingly accessible to form hydrogen bonds with the solvents present in the HPLC system. It is suggested that the hydroxyls in **Pep. 51** (**Table 4.3**, **Entry 2**) and **Pep. 54** (**Table 4.3**, **Entry 3**) would much less likely interact with the hydrogen-bond-forming solvents, which leads to slower elution of these peptoids. Hence, it was not surprising that **Pep. 53** (**Table 4.3**, **Entry 6**) was found to have the lowest HPLC t_R of 14.24 min.

It was aimed to establish correlations between the HPLC t_R and the antimicrobial properties of the nonamers synthesised in this section, as illustrated in **Figure 4.18**. Within this library of peptoids, no substantial biocidal effects were observed against *P. aeruginosa*. Consequently, a correlation plot between the MIC values against *P. aeruginosa* and the HPLC t_R was not constructed. Nonetheless, the impact of increasing HPLC t_R values was notable across the three bacterial species. This observation strongly suggested that the antimicrobial potency of these particular peptoids was directly related to their lipophilicity as determined by RP HPLC t_R. This trend was particularly evident in the context of Gram-positive bacteria, where shifts in antimicrobial efficacy were most pronounced. In contrast, Gram-negative *E. coli* exhibited a more gradual transition from 'inactive' to 'active' state. However, **Pep. 54** (HPLC t_R = 17.82 min; **Table 4.3**, **Entry 3**) exhibited substantial activity against *E. coli* (6.25 μM) despite its deviation from the typical pattern.

Moving forward, it was aimed to uncover any trends that could potentially link antibacterial MIC values to the log *D* values (log *D* values for this library of peptoids are shown in **Table 4.3**). Interestingly, the hydroxyl-containing peptoid nonamers which exhibited the highest levels of biocidal activity demonstrated log *D* values within the range of approximately 0 – 0.5 (**Pep. 51** log *D* of 0.13, **Pep. 54** log *D* of 0.22, **Pep. 52** log *D* of 0.25, **Table 4.3**, **Entries 2-4**). Though, **Pep. 50** (**Table 4.3**, **Entry 1**), which contained the *N*Phe (**40**) and *N*spe (**2**) monomers exclusively, did not follow this trend as its log *D* value was found to be the highest in this library and it showed respectable antimicrobial efficacies of 3.13 – 6.25 μM. The log *D* measurements collected for this library suggest that the correlation between the antimicrobial activities and log *D* values is sequence specific. (**Figure 4.19**)

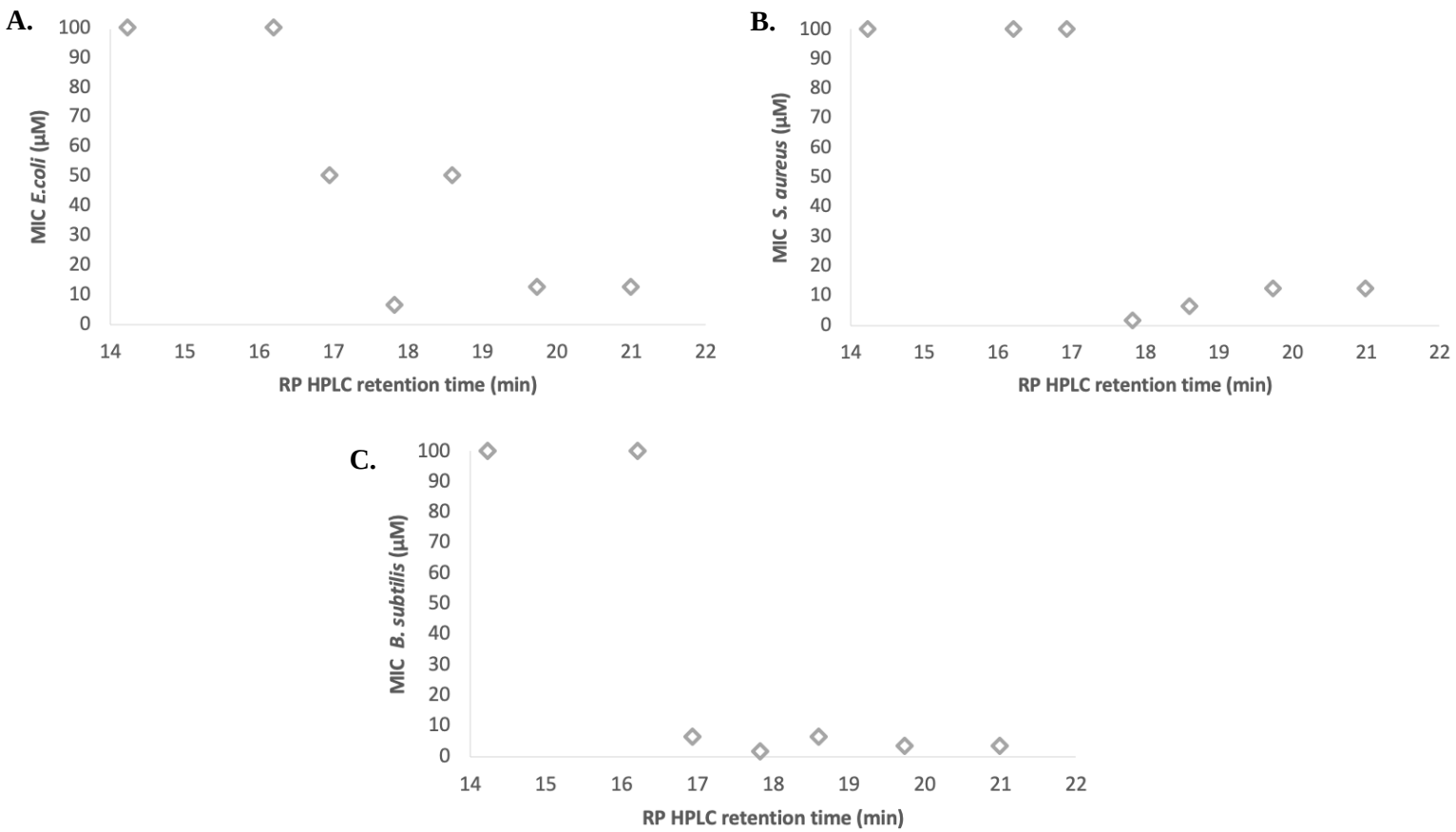

Figure 4.18. Relationships between the HPLC t_R and MIC values for **A**. *E. coli*, **B**. *S. aureus* and **C**. *B. subtilis*.

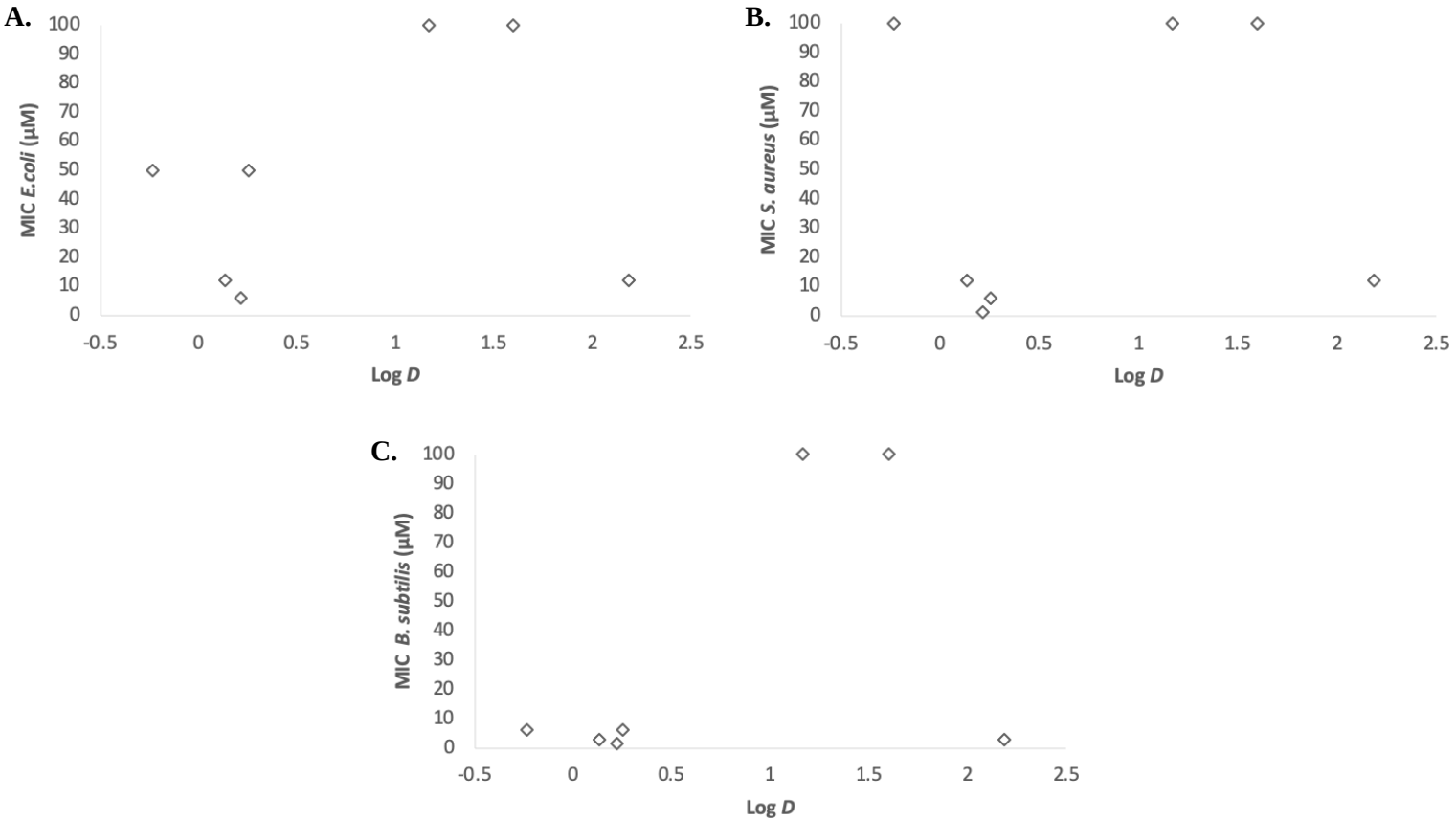

Figure 4.19. Charts depicting the relationship between log *D* values found for antimicrobial peptoids and their MIC values for **A**. *E. coli*, **B**. *S. aureus* and **C**. *B. subtilis*.

4.4. Summary of Chapter 4

Widely underappreciated in drug discovery, the hydroxyl moiety has the potential to modulate physicochemical properties of molecules, whilst exerting a positive effect on the interactions between antimicrobials and bacterial membranes. In this chapter, the tyrosine-monomer derivatives studied in **Chapter 3** were incorporated into peptoids and investigated their properties. The utilisation of the amino(aryl)-containing **163** monomer derivatives in the production of peptoids was also explored.

The synthesis of a library of seven peptoid nonamers containing *N*Tyr derivatives, was performed using the general submonomer peptoid synthesis approach. To achieve this, the synthesis of *N*Tyr peptoid monomers bearing protecting groups compatible with submonomer peptoid synthesis on solid phase was carried out. The hydroxyl group in the monomer building blocks were protected with an allyl group which was conveniently removed *in-situ* via a Pd(II)-catalysed reduction. Full synthesis of the Allyl-protected building blocks is shown in **Scheme 4.2**.

Subsequently, the peptoids prepared, **Pep. 50 – 56**, were subjected to antimicrobial assays (**Table 4.2**), wherein they were tested against a range of Gram-positive and Gram-negative bacteria. A clear correlation between the position of the hydroxyl on the aromatic ring and the efficacy against the bacteria used in this study was noticed. **Pep. 54** (**Table 4.2**, **Entry 3**) revealed lowest MIC values for all of the species, attributed to the alpha-helix inducing the *ortho*- monomer **104**, which is discussed in detail in **Chapter 3**. It is also worth noting, particularly for future therapeutic applications, that all of the nonamer peptoids in this chapter which were screened against HepG2 cells showed no toxicity.

Hydrophobicity measurements for the hydroxyl-containing nonamer peptoids were also investigated. Firstly, a positive correlation was determined between HPLC t_R and antibacterial potency. However, no correlation was noted between HPLC t_R and log *D* values. Interestingly, peptoids which showed the lowest MIC values exhibited log *D* measurements in the rage of 0-0.5. This was the case for all of the bacteria screened against in this chapter.

Moreover, a clear link can be established between the position of the hydroxyl on the aryl ring and the hydrophobicity as determined by the HPLC t_R. Indeed, the incorporation of the *Np*Tyr yielded very polar peptoids, as in the case of **Pep. 56** (t_R = 14.24 min). (**Table 4.3**, **Entry 7**) No trends were established between **Pep. 51** – **56** and log *D* values.

In addition, two peptoids containing derivatives of the compound **182** (amine containing monomer) were designed. It was necessary to establish a protection strategy to incorporate this monomer into peptoid chains. The production of **Pep. 57**, proceeded by the protection of the aryl amine with an Alloc group (synthesis of **184**, **Scheme 4.5**). **Pep. 57** was then engaged in antimicrobial and cytotoxicity assays as well as log *D* analysis. However, **Pep. 57** it was not efficacious against either Gram-positive or Gram-negative bacteria. Pleasingly, it showed no toxic effects against the HepG2 cells. (**Table 4.2**, **Entry 8**) The synthesis of **Pep. 58** was unsuccessful. It was hypothesised that the bulky nature of the Boc-protected *o*-aminomethyl(aryl) (**182**), together with its close proximity to the peptoid backbone, hindered peptoid elongation.

4.5. References for Chapter 4

[1] Drin G., Antonny B., 2010, *FEBS Lett*., **584**, 1840–1847.
[2] Cornell R.B., Taneva S.G., 2006, *Curr. Protein Pept.,* **7**, 539–552.
[3] Giménez-Andrés, M., Čopič, A. and Antonny, B., 2018, *Biomolecules*, **8**(3), 45.
[4] Platzer, M., Kiese, S., Tybussek, T., Herfellner, T., Schneider, F., Schweiggert-Weisz, U., Eisner, *P.*, 2022, *Front. Nutr*., **9**, 882458.
[5] Chongsiriwatana, N. P., Patch, J. A., Czyzewski, A. M., Dohm, M. T., Ivankin, A., Gidalevitz, D., Barron, A. E., 2008, *Proc. Natl. Acad. Sci*., **105**, 2794-2799.
[6] Lazaridis, T., He, Y. and Prieto, L., 2013, *Biophys. J*., **104**(3), 633-642.
[7] Gidalevitz, D., Ishitsuka, Y., Muresan, A.S., Konovalov, O., Waring, A.J., Lehrer, R.I., Lee, K.Y.C., 2003, *Proc. Natl. Acad. Sci*., **100**(11), 6302-6307.
[8] Jang, H., Ma, B., Woolf, T.B. and Nussinov, R., 2006, *Biophys. J*., **91**(8), 2848-2859.
[9] Porto, W.F., Irazazabal, L., Alves, E.S., Ribeiro, S.M., Matos, C.O., Pires, Á.S., Fensterseifer, I.C., Miranda, V.J., Haney, E.F., Humblot, V., Torres, M.D., 2018, *Nat. Commun*., **9**(1), 1490.
[10] Schiefer HG, Schummer U, Gerhardt U., 1979, *Curr. Microbiol*., **3**, 85–88.
[11] Mootz, H.D. and Marahiel, M.A., 1997, *J. Bacteriol*., **179**(21), 6843-6850.
[12] Loll, P.J., Upton, E.C., Nahoum, V., Economou, N.J. and Cocklin, S., 2014, *Biochim. Biophys. Acta (BBA)-Biomembr*., **1838**(5), 1199-1207.
[13] Datta, L.P., Dutta, D., Chakraborty, A. and Das, T.K., 2019, *Biomater. Sci.*, **7**(6), 2611-2622.
[14] Brittain, W.D. and Cobb, S.L., 2019, *Org. Biomol. Chem.*, **17**(8), 2110-2115.
[15] Brittain, W.D. and Coxon, C.R., 2022, *Chem.–Eur. J*., **28**(7), e202103305.
[16] Gorske, B.C., Jewell, S.A., Guerard, E.J. and Blackwell, H.E., 2005, *Org. Lett*., **7**(8), 1521-1524.
[17] Vutukuri, D.R., Bharathi, P., Yu, Z., Rajasekaran, K., Tran, M.H. and Thayumanavan, S., 2003, *J. Org. Chem.*, **68**(3), 1146-1149.
[18] Svanholm, U. and Parker, V.D., 1972, *J. Chem. Soc., Chem. Commun*., (11), 645-646.
[19] Howard, J.A., Hoy, V.J., O'Hagan, D. and Smith, G.T. ,1996, *Tetrahedron*., **52**(38), 12613-12622.
[20] Schneider, H.J., 2012, *Chem. Sci.*, **3**(5), 1381-1394.
[21] Pietruś, W., Kafel, R., Bojarski, A.J. and Kurczab, R., 2022, *Molecules*., **27**(3), 1005.
[22] Dalvit, C., Invernizzi, C. and Vulpetti, A., 2014, *Chem.–Eur*. J., **20**(35), 11058-11068.
[23] Dalvit, C. and Vulpetti, A., 2016, *Chem.–Eur. J*., **22**(22), 7592-7601.
[24] Jeffrey, G. A., 1997, *An Introduction to Hydrogen Bonding*, Oxford University Press.
[25] Arunan, E., Desiraju, G.R., Klein, R.A., Sadlej, J., Scheiner, S., Alkorta, I., Clary, D.C., Crabtree, R.H., Dannenberg, J.J., Hobza, P. and Kjaergaard, H.G., 2011, *Pure Appl. Chem.*, **83**(8), 1637-1641.

Chapter 5: Cyclic Peptoids

5.1. Biopolymer cyclisation

5.1.1. Cyclic peptides: a class of peptidomimetics

In peptides, the utilisation of macrocyclisation to provide improved proteolytic resistance,[1,2] maintain stability under harsh conditions[3] and enhance biological functions, has been well established.[4-7]

In nature, numerous peptides are cyclic, and this structural feature is not only associated with peptide kinetics but also with their biological functions.[8] A notable example of cyclisation in a polypeptide is the formation of intramolecular disulphide bridges between side chains bearing thiol moieties. It is the most commonly occurring staple in nature, whereby ca. 30% of eukaryotic proteins present this type of linkage. Approximately half of cysteines within peptides exist as disulphide bonds. The instability of thiol groups in cysteines which leads to a spontaneous formation of such staples and is therefore most energetically efficient.[7] The cyclisation of insulin (**Pep. 68**) via disulphide bridges helps to maintain its stable three-dimensional structure, which is crucial for its interaction with its target receptors.[9] (**Figure 5.1**) Furthermore, due to its high susceptibility to redox transformations, which lead to the formation of highly nucleophilic thiolate (RS-) under basic conditions, thiol-based side chains are most commonly utilised in the development of new stapling techniques. For this reason, its use in macrocyclisation is much more favoured than the use of amino and hydroxy moieties.[9]

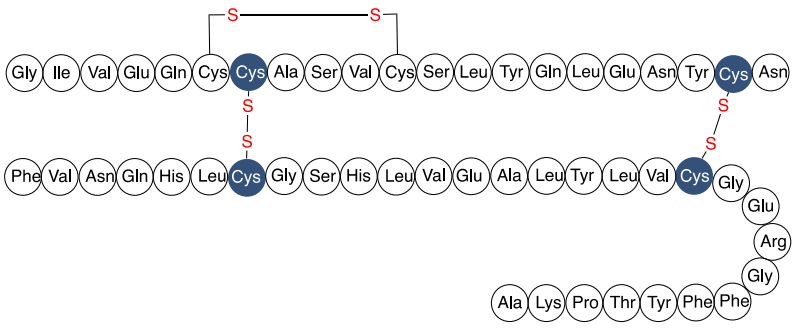

Pep. 68

Figure 5.1. A diagram depicting insulin (**Pep. 68**) as a polypeptide comprised of two peptide chains (21- and 30-amino-acid long), linked together by two disulphide bonds. The three disulphide bonds linking the thiol moieties (red) are also shown.[9]

Macrocyclisation has also been markedly utilised in the development of peptide-based therapeutics. Firstly, peptide chains are the middle ground between small molecules and larger therapeutic agents, such as antibodies. Hence, the scope of target binding of peptides has made them an attractive scaffold for drug development.[10] This attribute gains prominence when the target is the intricate domain of protein-protein interactions. The decreased conformational flexibility of macrocycles, which in turn leads to a higher rigidity, results in an enhanced target binding and hence increases potency.

Secondly, peptide macrocyclisation can aid membrane permeability[11] by satisfying the intramolecular hydrogen bonding requirements and by reducing the number of effective rotatable bonds (dictated by Lipinski's Rule of 5). Cyclic peptides that are most permeable arrange themselves to form intramolecular hydrogen bonds on the inner surface of the molecules. Conversely, cyclic peptides with hydrogen-bond donors facing the solvent tend to exhibit lower membrane permeability. An illustrative case is that of cyclosporin (**Pep. 69**).[12] In polar environments it can non-covalently bind to its receptor as it exposes its hydrogen atoms; in apolar environments, it shows a degree of intramolecular hydrogen bonding which in turn increases its lipophilicity aiding its permeability through cell membranes. (**Figure 5.2**) In addition, the head-to-tail cyclisation eliminates free amine and carboxylate termini which often serve as the site of cleavage for exopeptidases.[13]

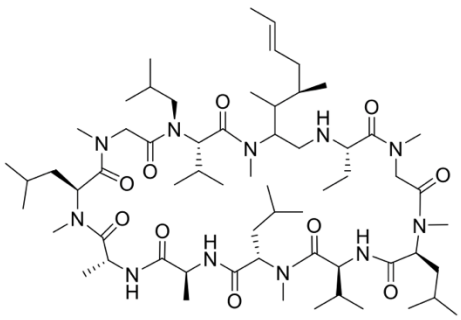

Pep. 69

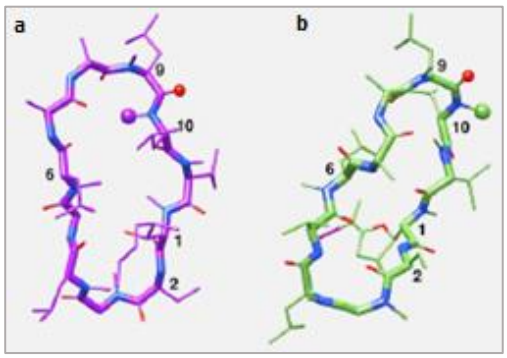

Figure 5.2. Cyclosporin (**Pep. 69**) in its (**a**) unbound and (**b**) bound conformations. The secondary structures have been generated by NMR spectroscopy, revealing the formation of intramolecular hydrogen bonding when bound.[12] (Figure adapted from Borel *et al.*)

Due to high rates of peptide degradation *in vivo*, cyclisation has been extensively employed as a method to overcome this shortcoming. Cyclisation in proteins can lead to an

enhanced enzyme function which can occur at conditions which deviate from their native state, including variations in temperatures and fluctuating pH levels.[3]

5.1.2. Cyclic peptoids

As previously discussed, (**Chapter 1**) the tertiary amide backbone in peptoids allows this class of peptidomimetic to overcome the limitations of peptides such as a high susceptibility towards proteolysis. Nonetheless, due to the absence of hydrogen bonding within peptoid backbones, their conformational heterogeneity hinders the development of structures with well-defined geometry. This lack of conformational stability, in addition to high lipophilicity induced by the substantial use of aromatic monomers, can lead to off-target effects of peptoids when screened against active sites. The importance of conformational rigidity and its application in precise active site targeting, especially in the context of drug design and molecular recognition, is well known. A well-defined conformation which is complementary to the target site allows for optimal binding and specificity. Due to the intrinsic amide bond heterogeneity within peptoid backbones, this control is difficult to achieve, and can result in reduced binding affinity. Cyclisation of linear peptoids offers a straightforward route to overcome amide bond heterogeneity within peptoid backbones.

There are four key methods of peptoid cyclisation, i) head to tail; ii) side chain to side chain; iii) head to side chain; iv) side chain to tail.

Pioneered by Kirschenbaum, in 2007,[14] cyclisation via amide bond formation is the most routinely applied approach in the formation of head-to-tail type structures (**Pep. 71**). Despite the potential for forming these structures through exposure to high temperatures and microwave conditions due to peptoids' thermal stability, the preference lies in utilising coupling reagents. This method mirrors the classic approach used in peptide cyclisation, but renders the use of uranium/guanidium-type coupling reagents unnecessary due to the absence of chiral centres in peptoid backbones. (**Scheme 5.1A.**)

The synthesis of smaller peptoid cycles is receiving considerable attention due to their demonstrated efficacy in epilepsy treatment and mood stabilisation applications.[15] Culf optimized the synthesis of cyclic tri-, tetra-, and penta-peptoids (**Pep. 72, Scheme 5.1.B.**) using EDC and HOAt, achieving high yields of up to 97%.[15] Building on this research, Caumes[16] found that employing a chiral peptoid monomer like *N*spe facilitated the cyclisation of small peptoids, such as **Pep. 73**. Tetracyclic peptoids composed of *N*spe and propargylglycine

monomers yielded >20% higher than those consisting solely of propargylglycines (>10%). (**Figure 5.3.A.**) The group obtained a crystal structure of this small peptoid cycle, shown in **Figure 5.3.B**.

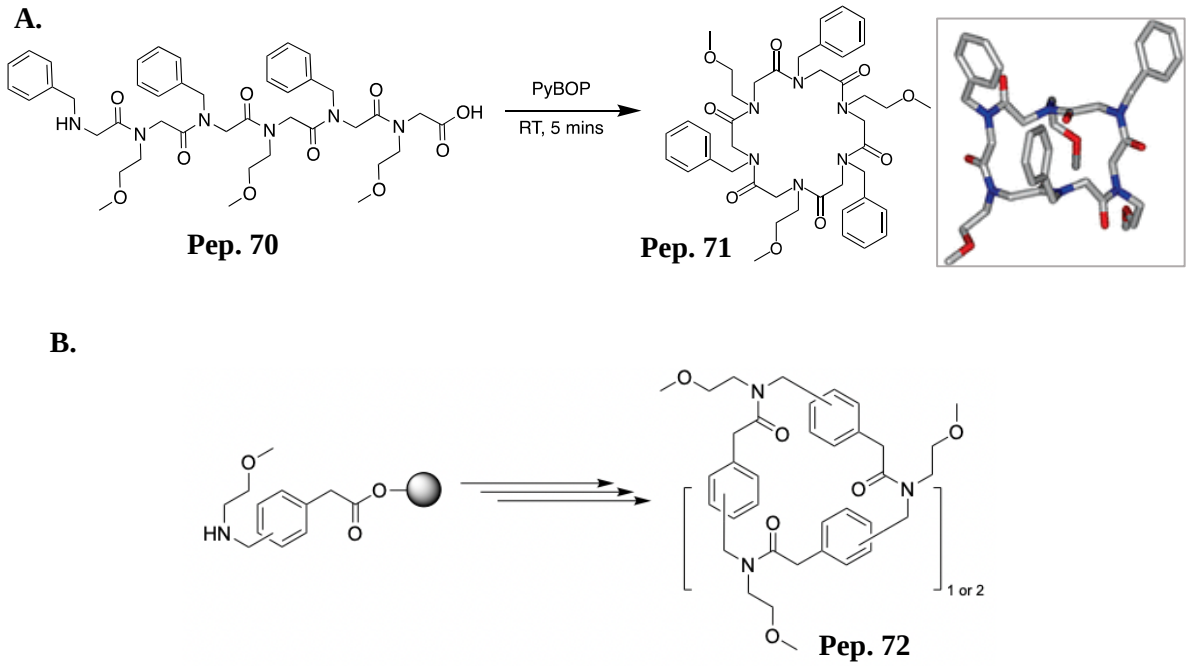

Scheme 5.1. A. A one-step synthesis of a cyclic peptoid via a head-to-tail cyclisation, resulting in a lactam.[14] **B.** Synthesis of small peptoid cycles, using EDC and HOAt as coupling reagents.[15] (Figure adapted from Culf *et al.*)

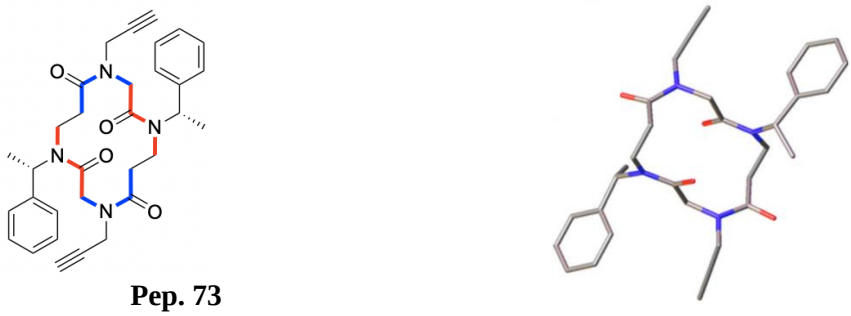

Figure 5.3.A. A depiction of tetracyclic peptoids composed of *N*spe and propargylglycine monomers synthesised by Caumes. **B.** Crystal structure of the same cycle.[16] (Figure adapted from Caumes *et al.*)

Meanwhile, Kaniraj reported a novel cyclisation strategy employing a linear peptoid precursor (**Pep. 73**), which incorporates a nucleophilic side chain. This method facilitates side-chain-to-tail peptoid cyclisation, which operates via an S_N2 mechanism. It is compatible with

solid-phase synthesis, occurring efficiently on resin. Notably, this methodology yields the cyclized product (**Pep. 74**) in high yields.[17]

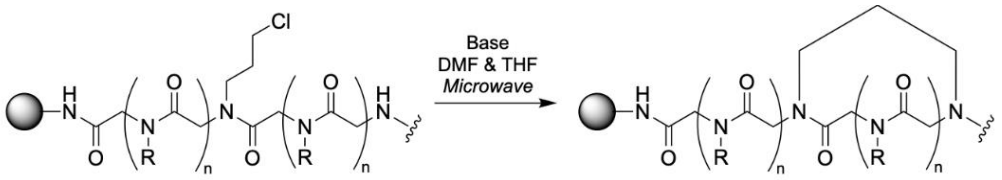

Pep. 73 **Pep. 74**

Scheme 5.2. A one-step cyclisation reaction, via S_N2, yielding a side-chain-to-tail type peptoid cycle.[17]

There exists a range of methods that have been reported to access peptoid macrocycles in which cyclisation can occurr via side-chain-to-side-chain linkage. One illustrative example is the cyclisation approach which involves a CuAAC reaction.[18] (**Scheme 5.3**) The incorporation of monomers bearing an azide and an alkyne will yield a triazole linkage (**Pep. 76**) which electronically and topologically mimics the *trans* amide bond geometry in a peptide (the triazole-type linkage will also result in the increased rigidity and the formation of a trans amide bond in peptoids, as discussed in **Chapter 1**). Moreover, the high scope in pH and solvent compatibility in this reaction means that the reaction can be carried out in aqueous conditions, at a pH which would not lead to peptide/peptoid denaturation.

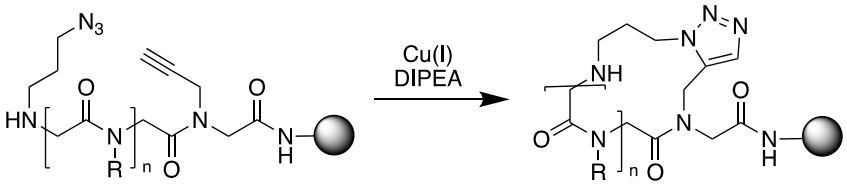

Pep. 75 **Pep. 76**

Scheme 5.3. General approach for the production of a triazole staple in a one-step Cu-catalysed azide-alkyne cycloaddition.[18]

Another example is olefin metathesis, pioneered by Grubbs,[19] a ring-closing methathesis (RCM) that involves two alkene-containing side chains to form a carbon-carbon bond. Khan[20] and co-workers explored in detail this cyclisation reaction of peptoids containing butyl-1-ene side chains, on a solid phase. In this investigation, various ruthenium catalysts were

explored, and the Hoveyda-Grubbs Catalyst (HG2) **185** (**Scheme 5.3**) was found to be versatile in terms of its compatibility with a diversity of peptoid monomer functionalities. Furthermore, the compatibility of RCM with solid-phase synthesis means that the side and by-products of this reaction can be easily washed away. Initial efforts focused on synthesising cyclic peptoid libraries under microwave conditions; however, due to the formation of dimers, the syntheses were conducted at 40 ^{o}C. These milder conditions yielded the desired cyclic peptoids of various sizes in satisfying (70-95%) yields, with minimal dimer formation (<5%). The schematic representation of this reaction is shown in **Scheme 5.4**.

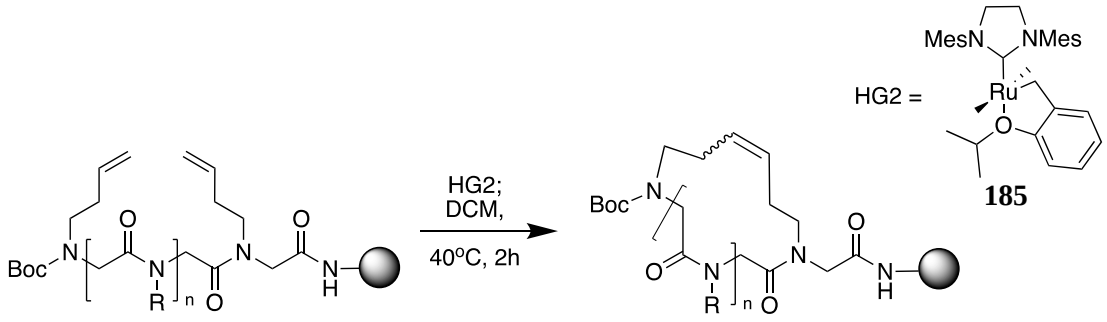

Pep. 77 **Pep. 78**

Scheme 5.4. One-step synthesis of a peptoid cycle bearing an alkylene staple, via RCM.[20]

5.1.3. Cyclic peptoids as antimicrobials

Similar to cyclic peptides, cyclic peptoids are of a great interest as an important class of peptidomimetics due to their preorganisation and increased rigidity, which means that they can potentially bind more tightly to target active sites. As is the case with peptide cyclisation, peptoid macrocyclisation can enhance membrane permeability and its selectivity is regulated by modulating hydrophobicity which aids peptoid intercalation into phospholipid-rich membranes.

An earlier investigation, carried out in the Riccardis group,[21] showed that peptoid cyclisation resulted in enhanced antibacterial and antifungal efficacy when compared to their linear counterparts. Later, Kirshenbaum[22] explored the effects of head-to-tail cyclisation of amphipathic peptoids on antibacterial activity. Not only did these compounds showed potencies against both the Gram-positive and Gram-negative bacteria, but they also exhibited impressively low hemolytic activities. The cyclic peptoid **Pep. 79** showed a remarkable SI value against *E. coli* and *S. aureus* of over 32. A later study by the same research group illustrated macrocyclic peptoids formed membrane pores, resulting in MRSA cell death. The

cyclic peptoid **Pep. 80**,[23] with its MIC value of 3.9 μg/mL and LC_{50} (lethal concentration 50) value of 180, proved particularly efficacious and selective for MRSA over HeLa cells. (**Figure 5.4**)

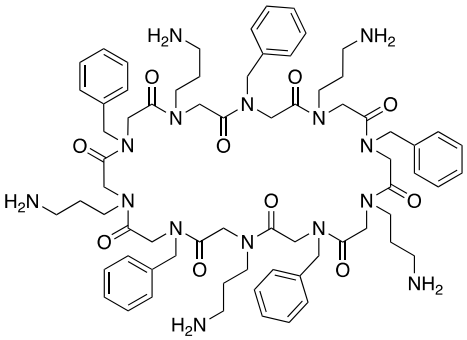

Pep. 79

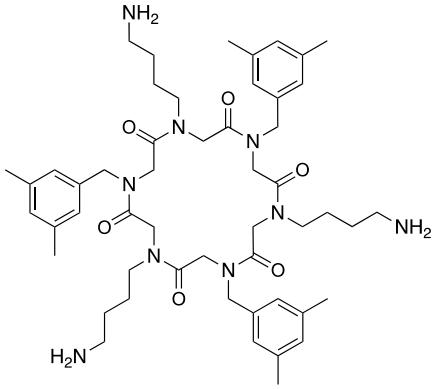

Pep. 80

Figure 5.4. Two cyclic peptoids investigated by Kirshenbaum for their antibacterial properties.[22,23]

5.1.4. Modification of biopolymers: the application of perfluoroaromatics

Perfluoroaromatics can react via sequential S_NAr substitution reactions, an application of this has been explored by the Pentelute group in the formation of macrocyclic peptides (**Scheme 5.4**).[24] The addition of a perfluoroaromatic reagent (e.g. hexafluorobenzene **186**), in the presence of a base to a polypeptide bearing two cysteines (**Pep. 81**) three residues apart led to the formation of stapled structures. Moreover, the *di*-substitution of **186** was found to be regioselective, wherein the ring was *di*-substituted in the 1- and 4-positions, which can be rationalised by *para*-activation. Remarkably, this activation led to the formation of cyclic structures (**Pep. 82**) exclusively, even in the presence of a large excess of **186** (10 eq). This was also the case where decafluorobiphenyl **187** was used instead of **186**, leading to a disubstitution in the 1- and 8-positions (**Pep. 83**). (**Scheme 5.5**)

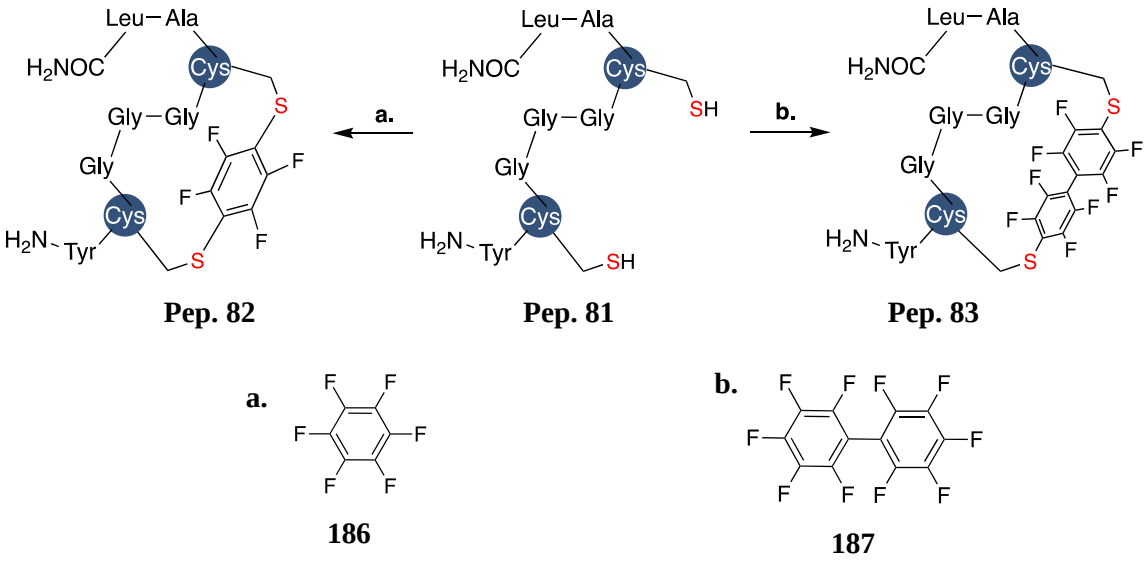

Scheme 5.5. A scheme illustrating the stapling of unprotected cysteines by perfluoroaromatic agents, using **a.** hexaflyorobenzene & **b.** decafluorobiphenyl.[24]

5.2. Susceptibility of pentafluoropyridine (PFP) to S_NAr

The susceptibility of pentafluoropyridine (PFP) to S_NAr reactions has been widely documented. Highly nucleophilic species including thiols, amines and alcohols have been shown to displace the fluorine moiety in the 4'-position of the pentafluoropyridine ring. Due to its electron-deficient nature, the resulting tetrafluoropyridine ring can subsequently undergo further substitutions resulting in, potentially, all of its fluorine moieties being displaced by the more reactive nucleophilic species.[25-27]

Previously, it has been reported that second substitutions of 2'-moieties required lengthy reflux conditions, complemented by an alkaline base.[28] As discussed in **Chapter 3**, the unprecedented susceptibility of TFP to 2'-substitution with species of highly nucleophilic nature, such as amines, can be carried out in mild conditions. Indeed, the displacement of the fluorine moiety occurs in a clean, fast, and facile manner, as confirmed by the ^{19}F NMR signal patterns, shown in **Chapter 4**. However, the scope of nucleophiles that can be used for this purpose is not limited to amines. The Cobb group applied the propensity of the PFP ring for 4'-S_NAr to access TFP-tagged peptides via the nucleophilic side chains of amino acid residues such as cysteine, lysine, tyrosine and serine.[29]

While the *ortho* position (2') of the PFP ring undergoes thermodynamically favoured substitutions, it has been documented that under certain conditions, the kinetic *meta*-moiety (3') can be selectively substituted. Explicitly, Sanford and co-workers[30] showed that due to

geometric constraints, bifunctional nucleophiles, such as **188**, could be used to change this substitution order. Thanks to its less thermodynamically favoured nature, the *meta*-substitution to form **189** required refluxing over extended periods of time. (**Scheme 5.6**)

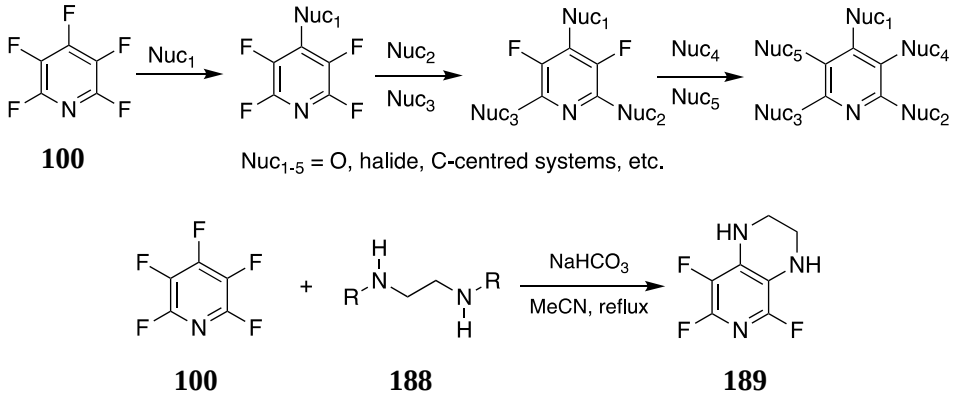

Scheme 5.6. A. Showing a sequential PFP-substitution by nucleophiles. **B**. showing a selective substitution of the *meta*-position of **100** by **188**.[30]

5.3. Objectives for Chapter 5

Macrocyclisation of peptoids offers advantages over linear peptoid chains by providing rigidity and optimising hydrophobicity, potentially improving peptoid selectivity for biological targets. Whilst head-to-tail cyclisation is the most explored within the field of peptoid science with respect to biological applications, the increased scope of scaffolds that can be accessed via cyclisation reactions involving side chains has meant that this approach has gained interest in recent years.

The work described in **Chapter 4** relating to the susceptibility of the TFP group to 2'-S_NAr reactions with aliphatic amines opens up possibilities for the synthesis of new peptoid and peptide cyclic structures. Therefore, establishing a route for synthesis of biopolymers bearing a TFP-based staple became of interest. In addition, reviewing the literature on peptide/peptoid macrocyclisation, there is a gap in the cyclisation strategies which involve residues bearing hydroxy and amine moieties.

In this chapter, peptide and peptoid cyclisation was to be explored, utilising tyrosine and lysine (*N*Lys and *N*Tyr in peptoids) residues in the cyclisation reaction. By harnessing the susceptibility of a TFP group to 2'-substitution reactions, it was predicted that macrocyclic peptoids could be yielded in a more controlled fashion, involving nucleophiles other than thiols.

This chapter investigates peptide and peptoid cyclisation, employing Tyr and Lys amino acids alongside peptoid *N*Lys and *N*Tyr building blocks. The focus lies in exploiting the reactivity of a TFP group towards 2'-substitution reactions to facilitate a controlled synthesis of macrocyclic peptoids. In addition to establishing a synthetic route to reach novel macrocyclic architectures, investigating the versatility of this cyclisation method was desired. Thus, the plan was to maximise the compatibility of the cyclisation reaction with a variety of different side chains and different ring sizes. For this purpose, the *O*-TFP *N*Tyr derivative (**112**), developed in **Chapter 3**, was to be reacted with *N*Lys in order to close the cycles. Furthermore, to examine the compatibility of this method with peptide cyclisation, amino acid counterparts were to be synthesisted and used as building blocks. The target asymmetric macrocycles **Pep. 84** and **Pep. 85** are shown in **Figure 5.5**. The incorporation of **112** was necessary to be followed by the 2'-S_NAr reaction in order to avoid side reactions with the nucleophiles, as explained in depth in **Chapter 4**. These macrocycles were to be examined for

their biological activity to investigate their potential for downstream application as antimicrobials. Their log *D* values are also to be measured.

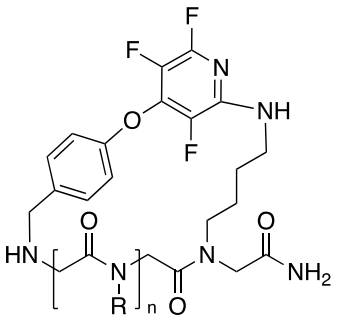

Pep. 84

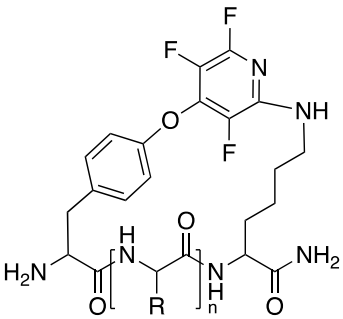

Pep. 85

Figure 5.5. The proposed asymmetric macrocyclic peptoid and peptide targets, whereby the Lys and Tyr moieties are linked via a TFP staple (n = 1-6).

5.4. Chapter 5: Results and discussion

5.4.1. Synthesis of Alloc-protected *N*Lys

In order to proceed with the synthesis of the asymmetric cyclic peptoids, it was necessary to establish a protection group strategy for the *N*Lys building block which would be compatible with this cyclisation reaction. Initially, we explored the idea of Fmoc-protection of the commercially available Boc-1,4-diaminobutane due to its compatibility with solid synthesis and ease of Fmoc-deprotection which requires the use of piperidine. It had been reported that TFP is prone to 2'-S_NAr by piperidine, but the literature indicates that heating to reflux is necessary for the reaction to occurr.[28] However, as illustrated in **Chapter 4**, the TFP group readily reacts with primary amines at room temperature. A test reaction was conducted to investigate if piperidine was capable of displacing the fluorine moiety at 2'-position within the TFP ring. After 20 minutes, three peaks corresponding to three fluorine environments of **190** appeared in the ^{19}F NMR spectrum (**Table 5.1**). The results provided clear evidence of the potential issue arising during the cyclisation process, in the presence of piperidine.

Table 5.1. Assigned ^{19}F NMR signals arising from different patterns of substitution on the TFP ring, and the compound numbers these substitutions correspond to.

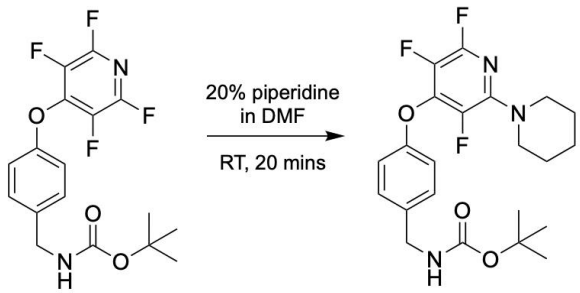

127 **190**

Compound number	Substitution pattern on PFP ring	Observed ^{19}F NMR chemical shifts δ (ppm)
127	4'-substitution	δF1 = -88.85, δF2 = -154.48
189	2'-4'-di-substitution	δF1 = -91.16, δF2 = -147.64, δF3 = 168.18

It was therefore decided that an alternative amine-protecting group strategy to produce a building block compatible with the cyclisation reaction would be needed. The alloc-protecting group, where a Pd(II) catalyst is required to liberate the amine, was deemed a suitable candidate. **Scheme 5.7** illustrates two-step synthesis to produce alloc-protected *N*Lys

193. Alloc protection utilised allyl chloroformate in basic conditions to produce **192** from **191**, and Boc cleavage occurred in acidic conditions to produce **193** in quantitative yield.

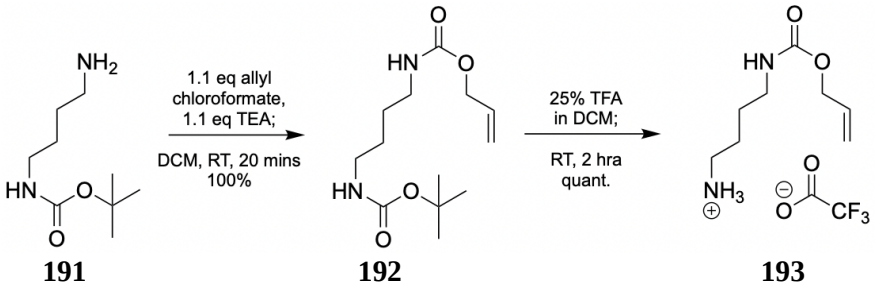

191 **192** **193**

Scheme 5.7. A two-step synthesis to produce *N*-Aloc-1,4-diaminobutane **193** as a TFA salt.

5.4.2. Synthesis of TFP-stapled peptoid cycles

Preliminary work was undertaken to determine the most suitable reaction conditions to produce the asymmetric peptoid cycle consisting of two *N*Phe **40** monomers in between *N*Lys **52** and **112**. It was envisaged that if the reaction were to be successful, two monomers in between the monomers involved in forming peptoid cycles would most efficiently yield the desired macrocycles. This is because there are *i+3* peptoid monomers per turn in a peptoid α-helix, and hence such sequences would most likely facilitate peptoid stapling. Whilst the *N*-terminal secondary amine is nucleophilic and would typically react with the 2'-S_NAr-prone TFP moiety, it is normally necessary to protect or acetylate it to prevent any side reactions. However, the pseudo-dilution conditions which are attained by the utilisation of a solid support overcome this issue. For our synthesis, we used the Rink Amide MBHA resin due to its low loading of 0.516 mmol/g.

The synthesis commenced with the loading of the resin with the Alloc-protected *N*Lys monomer **192** in the presence of DIPEA to basify the nucleophile. Subsequently, the loading of the two aromatic monomers ensued. *N*Phe (**40**) was selected for this purpose due to its UV-active aryl ring, ensuring even traces of the peptoids would be detectable in the LC-MS monitoring of this reaction. Following this, O-TFP *Np*-Tyr was coupled to the growing peptoid chain. Once the desired linear peptoid was synthesised, the next step involved alloc-deprotection, carried out using $Pd(PPh_3)_4$ catalyst in the presence of PhSiH. Subsequently, the resin was allowed to shake in DMF overnight, and LC-MS monitoring revealed complete cyclisation of **Pep. 87**, confirming a spontaneous S_NAr on the TFP ring by the nucleophilic *N*Lys (**Scheme 5.8**, **Figure 5.6**).

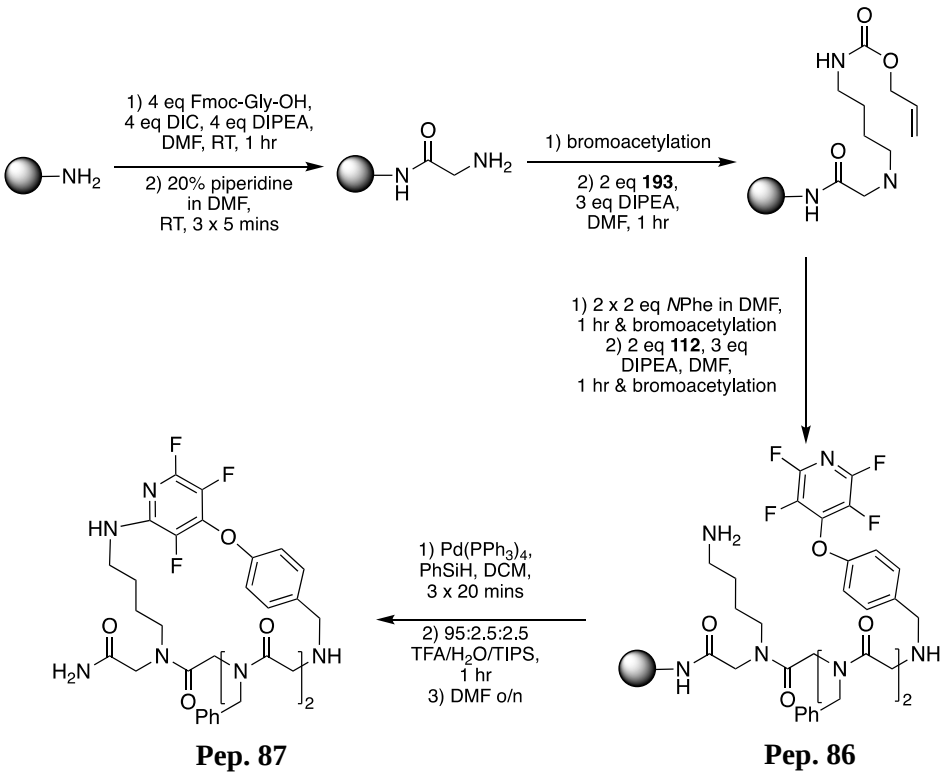

Scheme 5.8. A schematic representation of the synthesis of the 4-membered peptoid cycle **Pep. 87**, illustrating the cyclisation reaction which utilises the susceptibility of the TFP-ring to 2'-S_NAr. Bromoacetylation requires the use of bromoacetic acid and DIPEA in DMF, as outlined in **Chapter 2**.

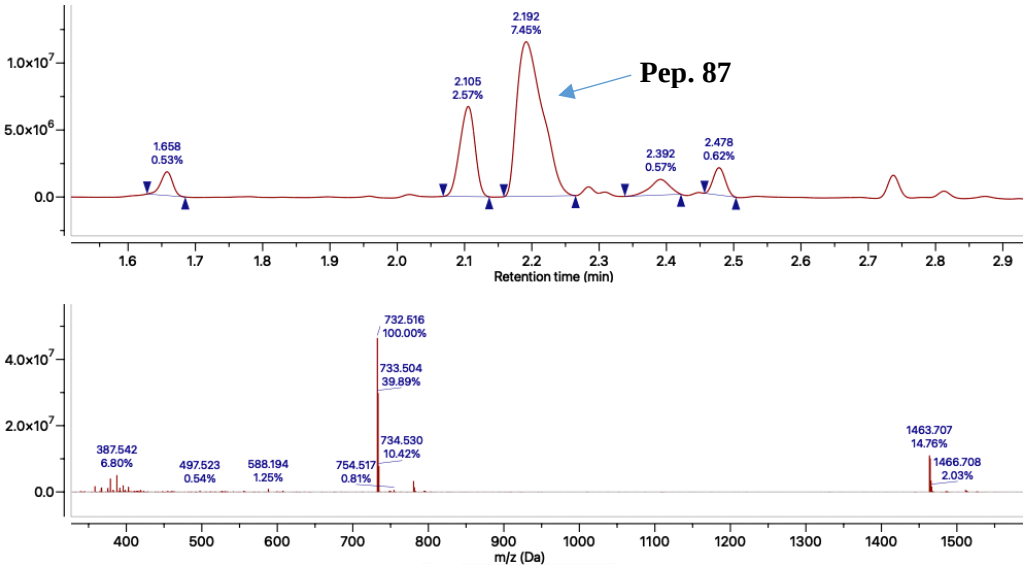

Figure 5.6. LC-MS trace showing the cyclised product **Pep. 87** as the main peak: [M+1] = 732.516, [(M+MeCN)/2] = 387.542, [M+2] = 1463.707.

The cyclisation reaction and production of **Pep. 87** demonstrated the compatibility of its conditions with submonomer solid phase peptoid synthesis. In addition, it was gratifying to

see that the cyclisation reaction onto the TFP moiety proceeded spontaneously without the requirement for basic conditions or heating. To further elucidate the extent of applicability of this reaction, the next aim was to investigate its adaptability to a diverse range of ring sizes. The smallest ring size investigated bore one peptoid monomer (n = 1) in between the two monomers participating in ring closure, and the largest ring bore six monomers (n = 6) in between *N*Lys and *O*-TFP *Np*-Tyr. This library of peptoids comprised *N*Phe monomers. Remarkably, ring closure occurred spontaneously for all the investigated peptoids. **Figure 5.7** illustrates the compatibility of this reaction with the largest ring size which was formed (eight monomers, **Pep. 88**) and shows clean conversion of the linear peptoid precursor to the cyclised form.

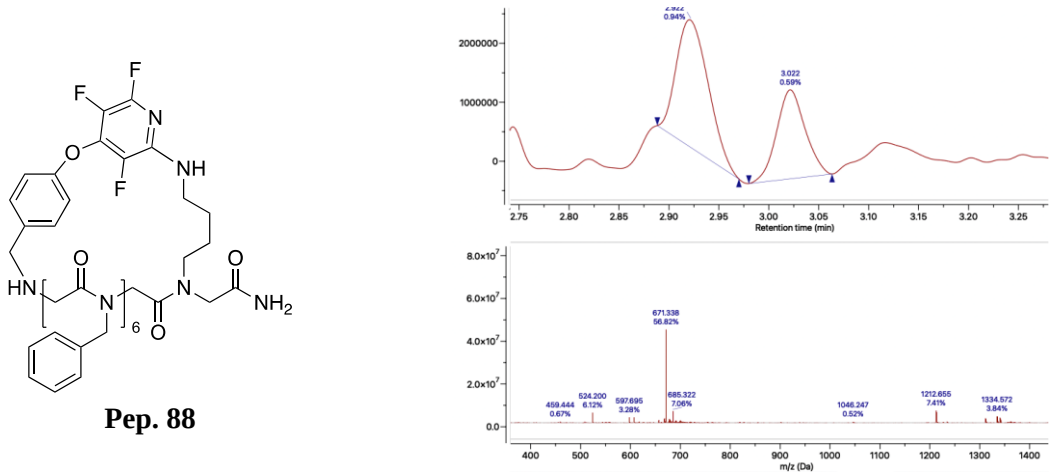

Figure 5.7. LC-MS trace showing the cyclized product **Pep. 88**. The relatively low intensity of the cyclised peptoid peak is explained in the text.

Having completed the synthesis of six cycles, the objective was to purify them to investigate the yields obtained for each ring size. The final cleavage from the resin utilised the standard cleavage solution of TFA/TIPS/H_2O and was allowed to proceed at room temperature for 30 mins. However, upon recovering the crude products, we observed exceptionally low crude yields relative to the expected values. Each peptoid was synthesised on a 0.2 mmol scale, and based on this the expected crude yields should have exceeded 150 mg. Nevertheless, the recovered crude yields ranged from 3-15 mg. While the recovered crude yields for larger cycles were higher than those recovered for smaller cycles, purification of the compounds synthesized in the preliminary screening was not carried out due to the anticipated low yields of the pure produces which would not be sufficient to complete the planned analyses.

This observation suggested that the cycles hindered the cleavage site (**Figure 5.8**, shown in red), especially during cleavage of the smaller members of this library. Although cleavage could occur at three other sites within the MBHA linker (**Figure 5.8**, shown in blue), no side products were detected for this reaction.

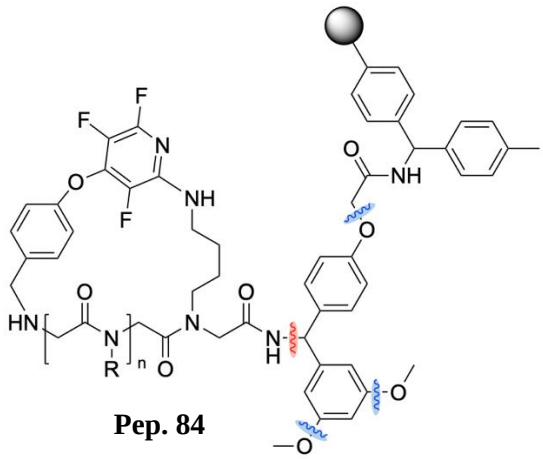

Pep. 84

Figure 5.8. A TFP-stapled peptoid cycle (**Pep. 84**) attached to the MBHA resin, where R = –CH_2Ph and n = 1–6. The cleavage site (red) is hindered by the bulkiness of the macrocycle. Other possible cleavage sites within the MBHA resin are shown in blue.

It was hypothesised that insertion of a "spacer" in the form of a peptide/peptoid monomer would circumvent this issue. For this purpose, it was decided to use a Gly/*N*rpe residue and began the synthesis of linear precursors by employing the standard monomer synthesis, commonly used in the solid-phase peptide synthesis (SPPS). The monomer and submonomer methods can be used together to form peptide/peptoid hybrids on resin, and numerous research groups have used the two approaches to successfully synthesise such molecules.[31,32] A scheme used to produce peptoid cycles including a Gly spacer (**Pep. 89**) is shown in **Scheme 5.9**. Whilst typically HOBt is used in order to prevent amino acid epimerisation, it was not required in the case of Gly coupling because Gly does not contain a chiral centre.

Scheme 5.9 was used to synthesise cyclic peptoids consisting of a variety of monomers. Examining the compatibility of this cyclisation reaction with peptoid monomers bearing a diversity of side chains was crucial, particularly as the objective was to assess the biological activities of these cycles against both Gram-positive and Gram-negative bacteria.

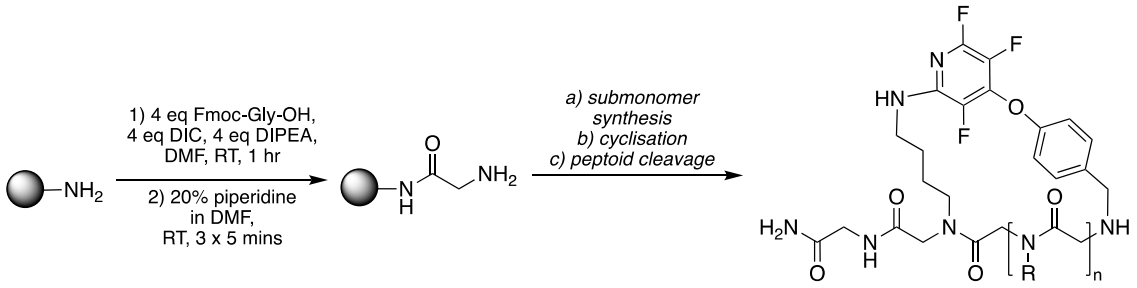

Pep. 89

Scheme 5.9. The synthetic route used to produce cyclic peptoids (**Pep. 89**) which included a Gly residue used a "spacer" to accommodate for the steric hindrance of the cleavage site within the MBHA resin. Steps a) b) and c) are shown in detail in **Scheme 5.7**.

In particular, the introduction of cationic peptoid monomers, such as *N*Lys, and the chiral aromatic *N*spe were of interest because peptoid oligomers containing a combination of these building blocks have been found to be particularly efficacious against pathogens.[33,34] In addition, heteroaromatics and side chains containing polar moieties, as well as fluorinated moieties were also desirable to investigated. Introduction of polar moieties aids compound solubility in aqueous environments, and fluorinated groups can have interesting effects on physicochemical properties of compounds.[35-37] (**Chapter 2**, **Sections 2.1.1**, **2.1.2**) Six cyclic peptoids of various ring sizes were produced in this library, shown in **Figure 5.9**. The recovered crude yields of peptoids (**Pep. 90 – 95**) synthesised using **Scheme 5.9** were significantly higher than those obtained from peptoids synthesised using **Scheme 5.8**. The purification of these peptoids was possible and enough material (between 3.0 and 6.7 mg; 3-11%) was recovered to engage the peptoids in biological and biophysical evaluation (**Sections 5.4.5** and **5.4.6**).

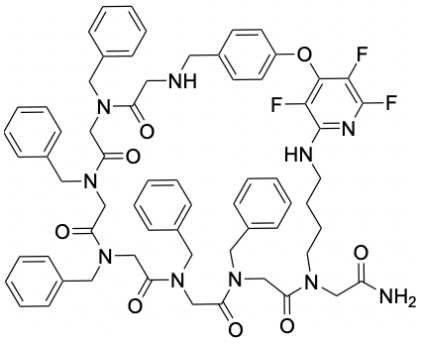

Pep. 90, 3%

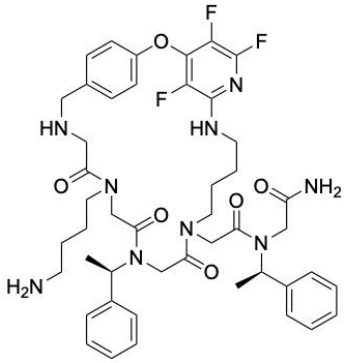

Pep. 91, 9%

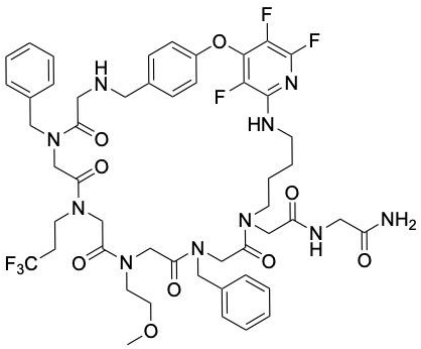

Pep. 92, 4%

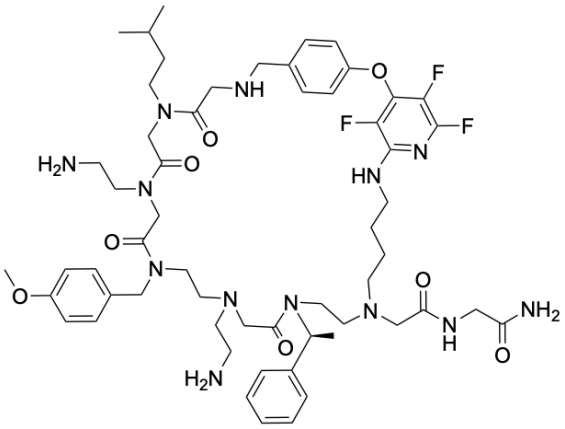

Pep. 93, 7%

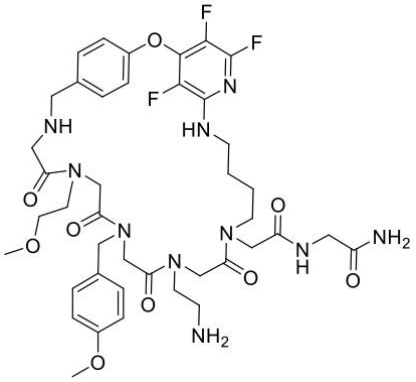

Pep. 94, 7%

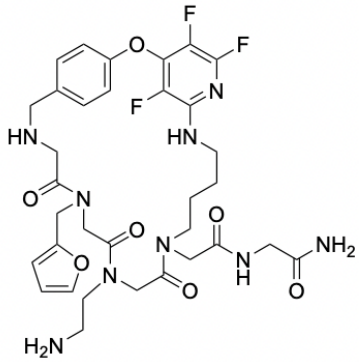

Pep. 95, 11%

Figure 5.9. Six peptoids of varying ring sizes produced in this study. The peptoids constitute a variety of different submonomers, such as aromatic, aliphatic, chiral and submonomers bearing electronegative moieties.

5.4.3. Attempted synthesis of of Trt- and Mmt-protected *N*Lys

Alkyne- and halogen-containing peptoid monomers were also of interest, but it was anticipated that the utilisation of a Pd(II) catalyst could lead to cross-coupling reactions between the liberated amine and the halogen-containing or unsaturated side chain.

A protecting group was sounght that could be employed to generate a protected *N*Lys without requiring a metal catalyst for deprotection, thereby reducing the risk of side reactions. For this purpose, a trityl (Trt) group was proposed to protect the amine. Trt requires mild acidic conditions to be cleaved off, which potentially would not result in peptoid cleavage from the resin.[38] **Scheme 5.10** illustrates the two-step synthesis used to produce the Trt-protected *N*Lys monomer **195**. The first step involved the employment of **193** as a TFA salt, which was basified and engaged in a S_N2 reaction to produce **194**. Then, the alloc was cleaved using a palladium catalyst under an inert atmosphere to produce the desired final product which was to be engaged in the synthesis of a linear peptoid bearing the Trt-protected *N*Lys **195**. The crystal structure obtained for **195** is shown in **Figure 5.10**.

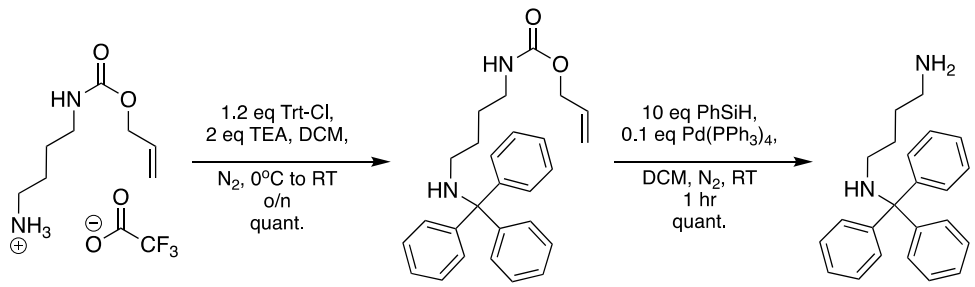

193 **194** **195**

Scheme 5.10. A two-step synthesis used to produce **195**.

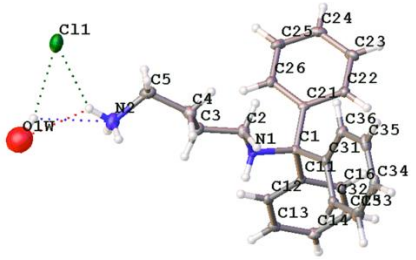

Figure 5.10. Ellipse-and-stick representation of **195** dimer present in the unit cell. As well as Cl, 1/3 of H_2O molecule is present in the structure. The water molecule is sitting in the channels and is disordered over three positions. Carbon atoms are depicted in grey, hydrogen atoms in white, nitrogen atoms in navy, oxygen atoms in red, and chlorine atoms in dark green. Structure was generated in Olex2 and is reported with a 50% thermal ellipsoid probability.

In order to investigate the compatibility of the Trt group with the synthesis of our macrocycles on resin, we conducted a preliminary screening whereby we synthesised **Pep. 96**, incorporating the Trt-protected *N*Lys to participate in the cyclisation. The synthesis of the linear precursor proceeded via the submonomer approach, and the linear peptoid was analysed by LC-MS to ensure that **195** was coupled onto the growing peptoid chain and the Trt did not sterically hinder the coupling of the proceeding monomer, and synthesis of the parent peptoid was completed. The LC-MS trace showing presence of the desired linear precursor is shown in **Figure 5.11**.

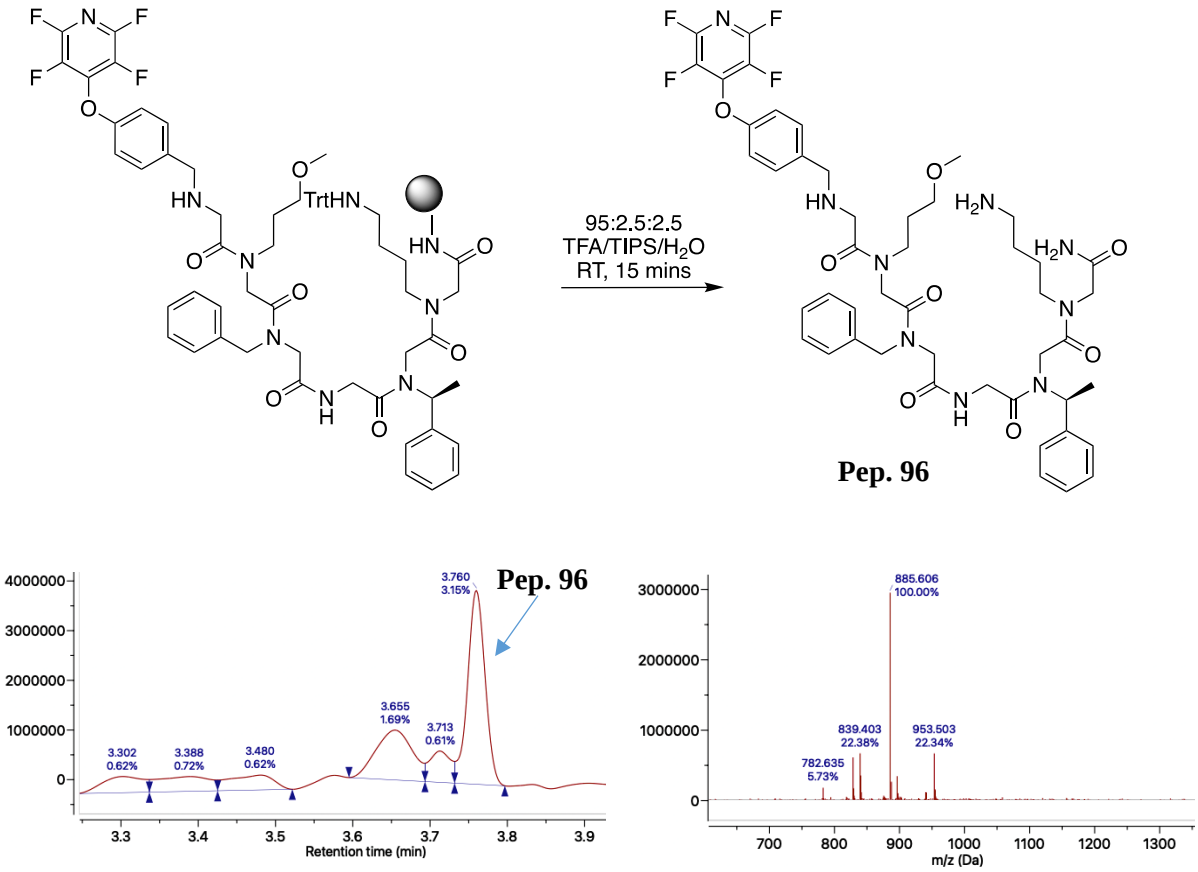

Figure 5.11. LC-MS trace of the text cleavage, showing presence of **Pep. 96** (MW = 951; *m*/*z* = 953.503).

The stability of the Trt group varies among different residues. For instance, Trt-protected Ser residue displays extreme susceptibility to mild acidic conditions, while the Trt group protecting the Cys thiol is highly stable. We used a cleavage solution consisting of 1% TFA (1:94:2.5:2.5, TFA/DCM/TIPS/H_2O) to treat the resin-bound peptoid precursor. Upon *N*Lys deprotection, the solution turned yellow due to the formation of a stable Trt carbocation

196, indicating at least partial Trt cleavage (**Scheme 5.11**). However, when a small portion of the resin containing the peptoid was treated with a cleavage cocktail containing 95% TFA, the solution turned an intense yellow color. This indicated that the *N*Lys monomers were still Trt-protected. The TFA content in the cleavage solution was increased to 10% and repeated the test. The cleavage cocktail still turned bright yellow. Nonetheless, a cyclisation reaction was carried out in the presence of DIPEA to ensure neutralisation of any residual TFA. Unfortunately, no desired cyclised product was detected in the LC-MS trace obtained for this reaction.

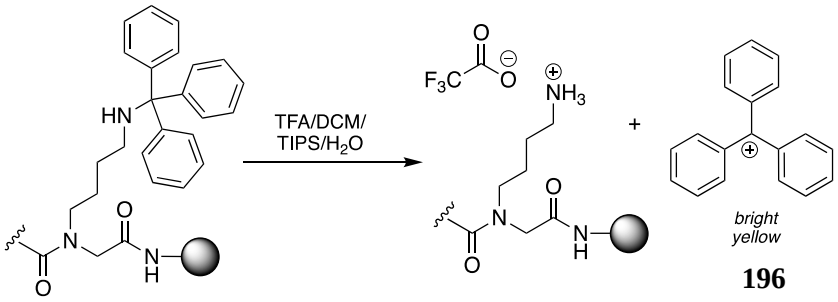

196

Scheme 5.11. Deprotection of the *N*Lys side chain results in the formation of a stable Trt carbocation **196**, which turns the cleavage solution bright yellow.

Due to the stability of the Trt-protected *N*Lys monomer, an alternative protecting group strategy was considered to enable a more compatible deprotection procedure, ensuring that the linear peptoid remained securely attached to the Rink Amide Resin. The goal was to switch the protecting group to one that would be more unstable in very mild acidic conditions.

*N*Lys(Mmt)-containing linker compounds were reported by Dubochwik to require very mild acidic conditions (1% TFA) to be deprotected, liberating the aliphatic amine.[39] Due to it's the structural similarity between the Lys residue and *N*Lys monomer, Mmt was selected as the protection group strategy to be investigated in the synthesis of peptoid cycles. The extremely mild acidic conditions required to cleave the protecting group from the resin were to ensure that no side reactions would occur and the peptoid would remain attached to the resin.

The synthesis of the *N*Lys(Mmt) proceeded with the employment of **192**, which was Mmt protected using Mmt-Cl under basic conditions (**Scheme 5.12**). However, it was observed that the intermediate **197** was unstable on silica gel, which is mildly acidic, resulting in an inadvertent Mmt cleavage. To resolve this, the reaction mixture underwent a water wash, followed by evaporation of volatiles to produce **197** as an amber oil. Then, **198** was engaged

in alloc-deprotection in the presence of Pd(II) and an activator. Due to the extreme instability of Mmt-protected amines under acidic conditions, the monitoring of the reaction progress was not possible by LC-MS. The reaction was monitored by TLC after adding TEA in order to neutralise the silica gel. Unfortunately, the starting material, the product and any by- and side products appeared to elute very close together and were not possible to separate. Therefore, this two-step synthesis was abandoned.

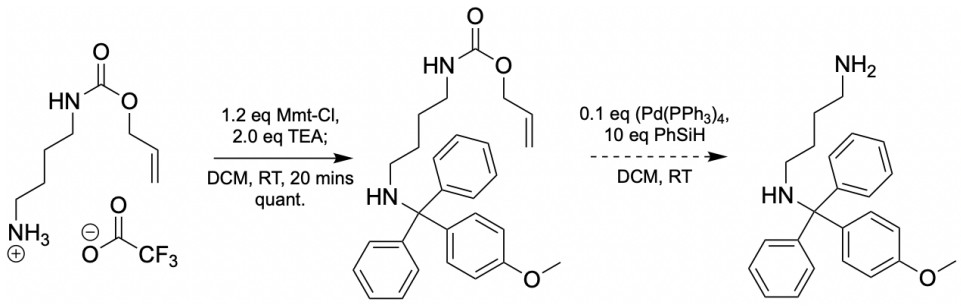

192 **197** **198**

Scheme 5.12. Attempted two-step synthesis to produce **198**.

It was hypothesised that an Fmoc group could serve as an alternative to Alloc. The synthesis, depicted in **Scheme 5.13**, involved the Fmoc-protection of commercially available *N*-Boc-1,4-diaminobutane **191** under basic conditions, resulting in the formation of **199** as a white solid. Boc-deprotection was then carried out using 25% TFA in DCM, yielding **199**. Subsequently, Mmt-protection was performed using the conditions shown in the first step of **Scheme 5.11** to produce **201**. The instability of Mmt under acidic conditions made it challenging to confirm the success of deprotection; however, Fmoc cleavage is known for being fast and facile. In many cases, the dibenzofulvene-piperidine adduct **203** by-product of Fmoc-deprotection elutes early during normal phase column chromatography purifications due to its high lipophilicity. Unfortunately, the spots on the TLC plate were indistinguishable, and the purification of the desired product **202** was unsuccessful. Consequently, due to time constraints, we opted not to continue exploring the Mmt-attachment on the *N*Lys **52** monomer.

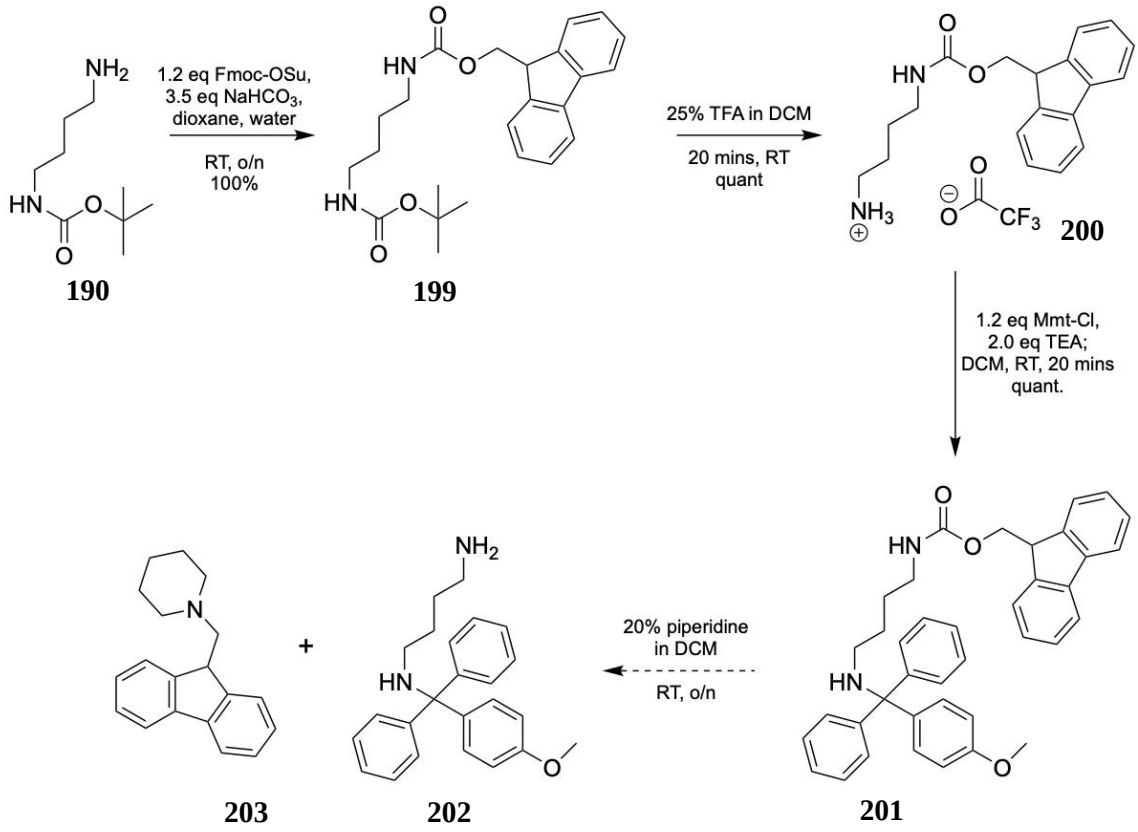

Scheme 5.13. Attempted four-step synthesis to produce **202**.

5.4.4. Synthesis of *O*-TFP Tyr amino acid

With the formation of cyclic peptoids achieved, attention turned to investigating the compatibility of this stapling technique in peptide cyclisation. The process began by establishing a reliable synthetic route to produce *O*-TFP *N*-Boc Tyr (**205**). The two-step synthesis of **206**, depicted in **Scheme 5.14**, served as a convenient starting point for our study. TFP protection was carried out on the commercially available Boc-Tyr-OMe **204** under basic conditions, yielding **205**. The crystal structure of **205** is presented in **Figure 5.12**. Subsequent saponification to liberate the carboxyl group employed $LiOH.H_2O$, resulting in the formation of **206**.

The analysis of the reaction mixture by LC-MS revealed the presence of side products **207** and **208** (**Figure 5.13**). The formation of these side products arose from the liberated –OMe attacking the TFP group, and this reaction could not be controlled; nucleophilic substitution and saponification appeared to take place in tandem. Following this, the reaction mixture underwent purification in the attempt to separate the desired TFP-protected **205** from the side products. Unfortunately, **208** co-eluted with the desired product. Despite repeated

purification attempts on the residue containing **206** and **208**, their separation was not successful. **207** was successfully separated and analysed to confirm the –OH substitution on the TFP ring. The ^{19}F NMR signals found for all three compounds are presented in **Table 5.2**.

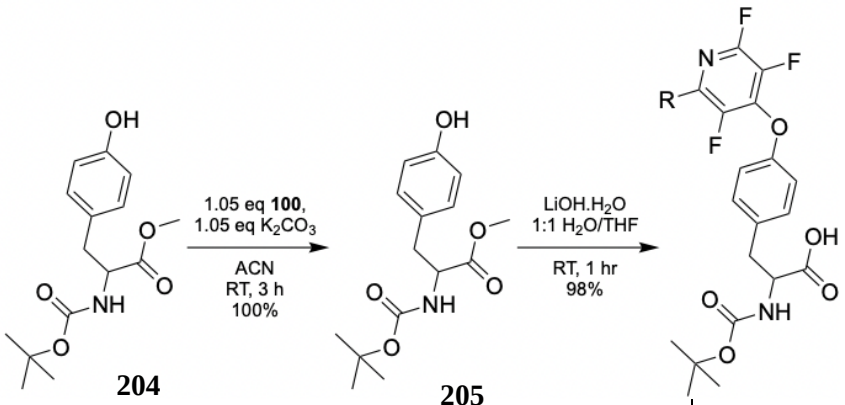

No.	R	
206	F	*(desired)*
207	OH	*(side*
208	OMe	*products)*

Scheme 5.14. A two-step synthesis employed to produce **206**, the side products **207** and **208** are identified.

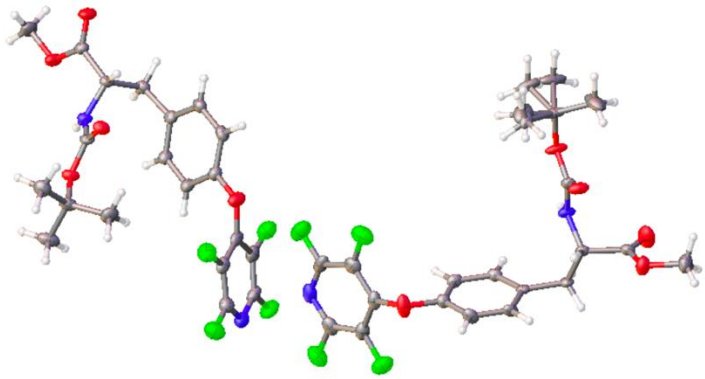

Figure 5.12. Ellipse-and-stick representation of **205** in the unit cell. Two molecules in the asymmetric unit are present. Carbon atoms are depicted in grey, hydrogen atoms in white, nitrogen atoms in navy, oxygen atoms in red, and fluorine atoms in green. Structure was generated in Olex2 and is reported with a 50% thermal ellipsoid probability.

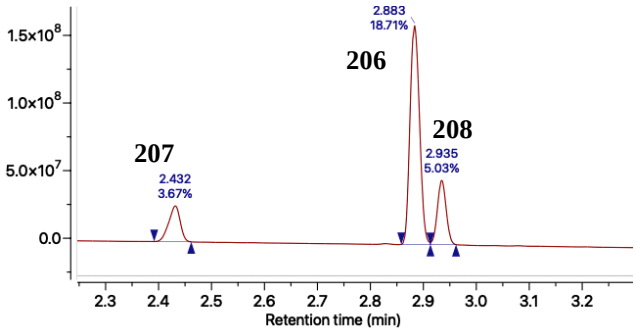

Figure 5.13. LC-MS trace showing the crude mixture containing **206**, **207** and **208**. **207** [M-1] = 427.294; **206** 429.270; **208** 441.355

Table 5.2. Assigned ^{19}F signals arising from different patterns of substitution on the PFP ring, and the compound numbers these substitutions correspond to.

Compound number	Substitution pattern on PFP ring	Observed ^{19}F NMR chemical shifts δ (ppm)
206	4'-substitution	δF1 = -92.34, δF2 = -157.15
207	2'-4'-di-substitution	δF1 = -94.26, δF2 = -155.19, δF3 = 163.71
208	2'-4'-di-substitution	δF1 = -94.80, δF2 = -157.93, δF3 = 166.15

Despite the desired product **206** still containing traces of **208**, it was employed in the synthesis of cyclic peptides (**Pep. 85**) by stapling peptide precursors **Pep. 97**, shown in **Scheme 5.15**. It was hoped that the peptide oligomers containing the side product **208** would be relatively easy to isolate from the desired peptide cycles. Preliminary screening was conducted to investigate the compatibility of this method with peptide cyclisation using the commercially available Fmoc-Lys(Alloc)-OH (**209**); Phe residues were incorporated between the two amino acids involved in the cyclisation. The initial goal was to synthesise a four-membered cycle, as the typical α-turn in peptides consists of *i+3* amino acids. However, the stapling of the linear peptide was unsuccessful. It was hypothesised that the bulkiness of the phenyl moieties hindered the stapling due to added rigidity. Cyclic peptides of other sizes were also not successfully synthesised.

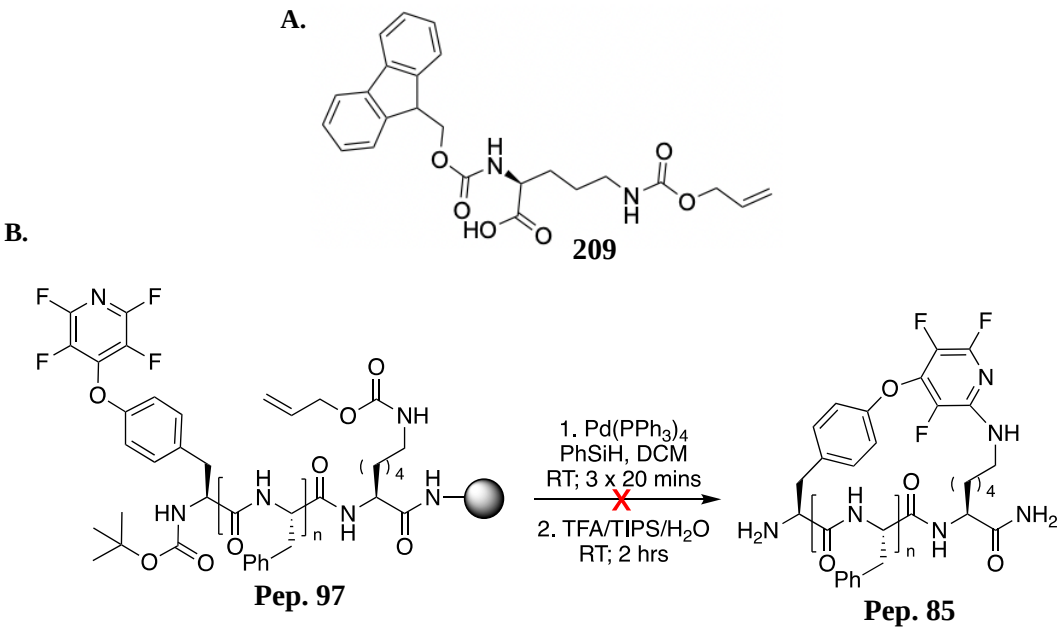

Scheme 5.15. A. Structure of the commercially available Fmoc-Lys(Alloc)-OH **208**. **B.** Attempted synthesis of Phe-containing **Pep. 85** of various sizes.

It was intended to employ amino acids bearing less bulky side chains in order to investigate if we would be able to use this stapling technique to successfully cyclise peptides. For this purpose, Ala was used in place of Phe residues, and like before we commenced the synthesis of a 4-membered ring. (**Scheme 5.16**) Indeed, upon alloc-cleavage and subsequent shaking of the resin in DMF, the peptide cycle (**Pep. 99**) was successfully formed. Contrastingly to the synthesis of cyclic peptoids, the stapling of the cyclic 4-monomer peptide was successful without a Gly spacer. Encouraged by this result, it was desired to increase the ring size to examine the scope of this reaction further; however, to no avail.

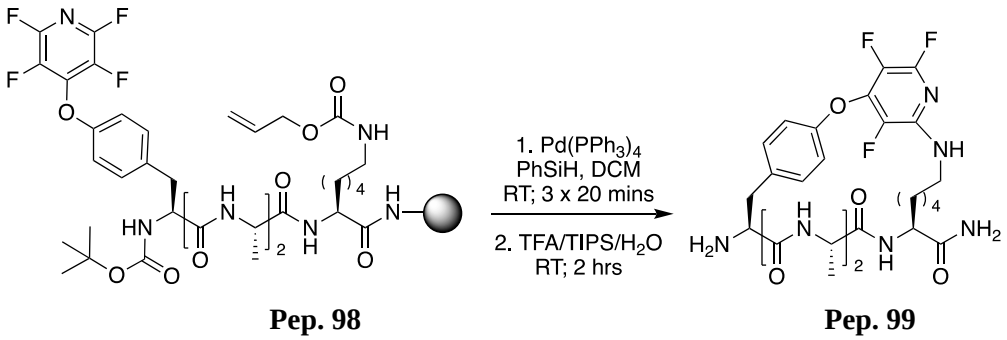

Scheme 5.16. A scheme depicting the synthesis of Ala-containing 4-membered cyclic peptide.

Further to the demonstration that this stapling reaction was successful, it was noted that the uncyclised side product **Pep. 100** eluted very closely to the cyclised desired **Pep. 99**. (**Figure 5.14**) Purification of the crude material would most certainly be very tricky.

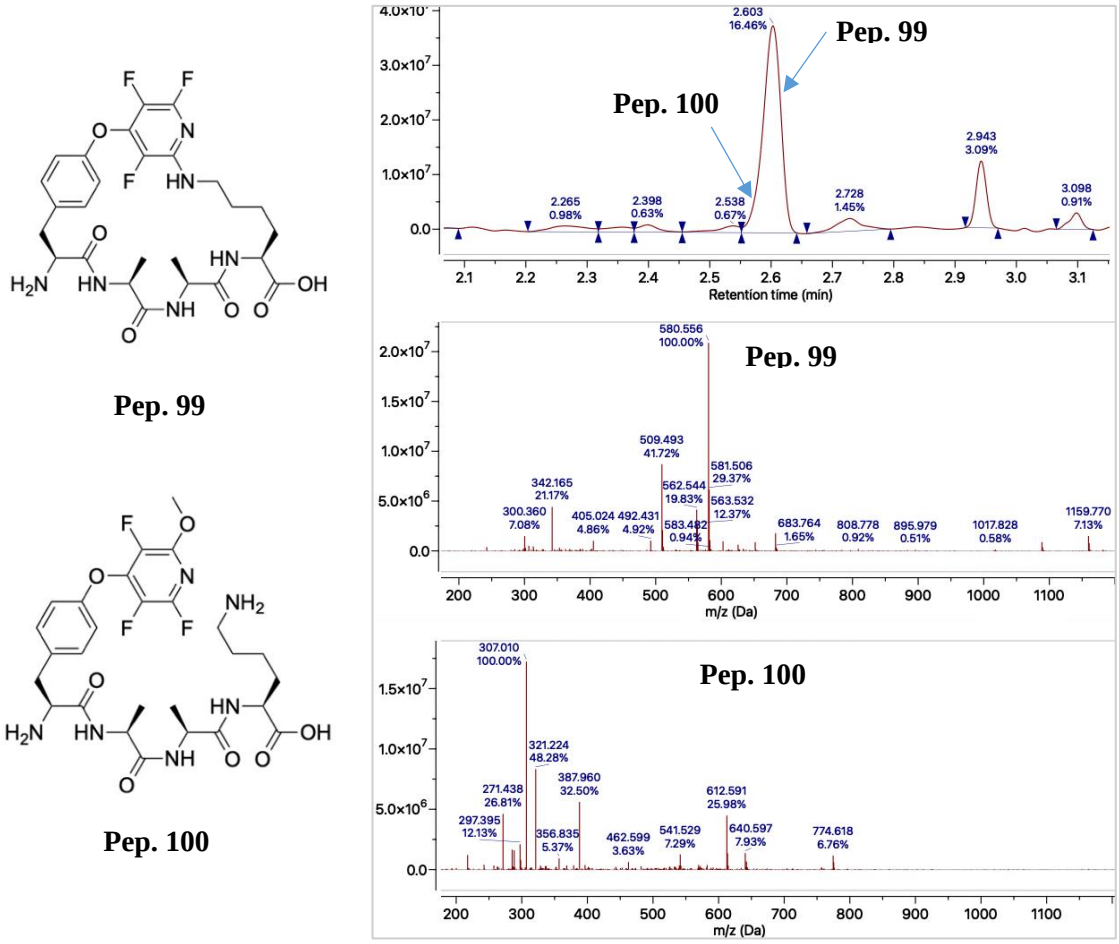

Figure 5.14. Left: Structures of the cyclised desired product **Pep. 99** and the linear side product **Pep. 100**. **Right:** LC-MS analysis of the crude mixture of **Pep. 99**

A different route was to be established to produce the TFP-protected *N*Tyr building block, as it was intended to avoid the production of the side product **208**. (**Scheme 5.17**) The synthesis employed commercially available Fmoc-Tyr(^{t}Bu)-OH (**214**) which underwent allyl-protection using allyl bromide in basic conditions to produce **211**. Subsequent ^{t}Bu deprotection followed in the presence of 25% TFA in DCM to produce **212**. The crude **212** was directly engaged in *O*-TFP protection to produce **213**. Allyl-deprotection in the presence of Pd(II) catalyst yielded **214** as a white solid. The overall yield for this reaction scheme was a very satisfying 89%.

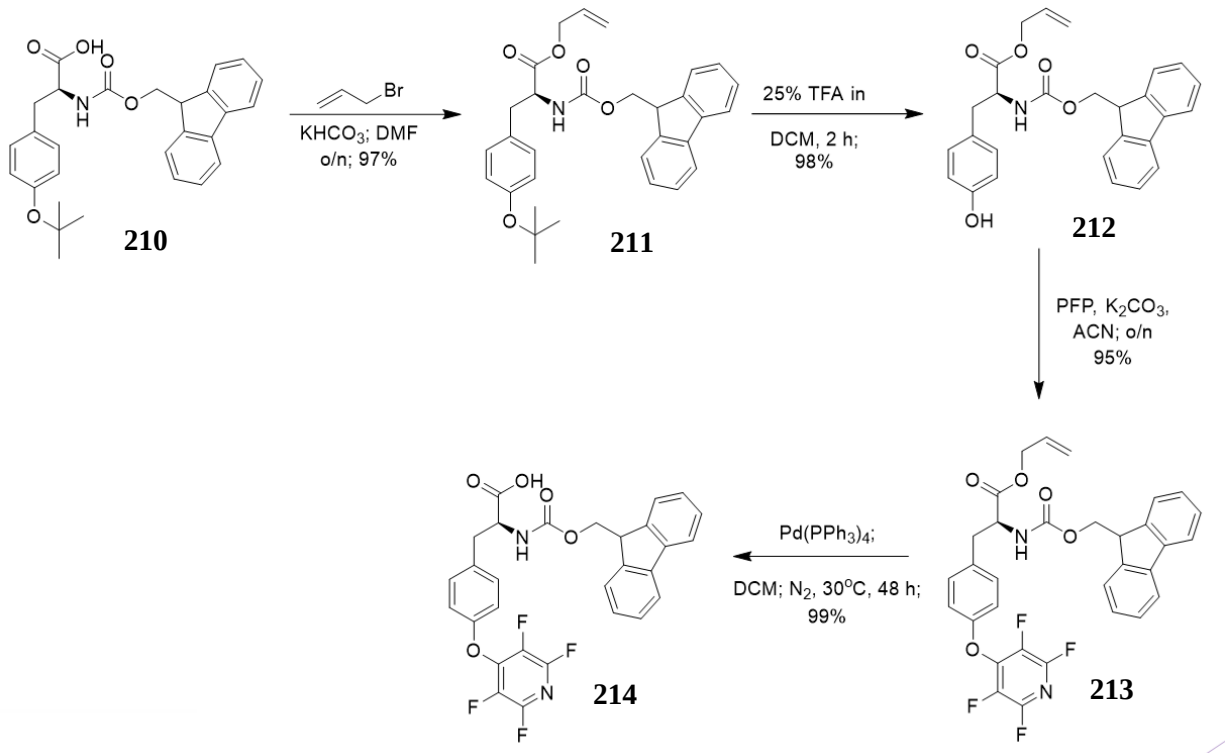

Scheme 5.17. A scheme illustrating a four-step synthesis to produce Fmoc-Tyr(TFP)-OH **214**.

Antimicrobial biopolymers are characterised by their cationic nature, so that they can selectively target anionic bacterial cell membranes. Therefore, incorporation of an amino acid bearing a cationic side chain such as an amine, as in the case of Lys, was planned. Here, a four-membered cyclic peptide **Pep. 101**, bearing Lys and Ala residues, was synthesised, using **Scheme 5.15**. The yield recovered for this peptide was very low (3.0 mg, 4%). Nevertheless, the material recovered for this synthesis was deemed enough for evaluation of **Pep. 101**'s (**Figure 5.15**) antimicrobial and cytotoxic activities. Log *D* measurements on this peptide were also carried out (**Section 5.4.6**)

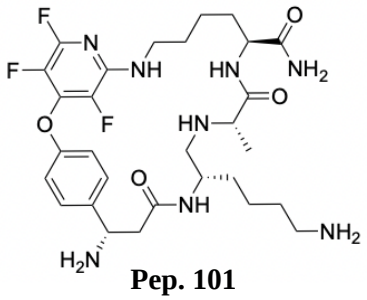

Pep. 101

Figure 5.15. A four-membered cyclic peptide **Pep. 101** containing Ala and Lys produced in this study.

5.4.5. Minimum inhibitory concentration (MIC) and cytotoxicity assays

For the MIC analysis of the cyclic peptoids and peptide synthesised in this chapter, the protocol summarised in **Section 2.3.4.2** was used. In addition, similarly to the peptoids in **Chapter 2**, **Table 5.3**, **Entries 1-7** were screened against HepG2 cells to investigate their toxicity against liver cells, using the protocol described in **Section 2.3.4.3**. In addition, the selectivity index (SI) values were calculated (**Table 5.3**).

Table 5.3. A tabulated summary of six cyclic peptoids and one cyclic peptide tested against four bacterial species, together with their ED_{50} values against HepG2, and SI values. (nd = no data recorded)

		ED_{50} (μM)	**MIC (μM)**				**SI**			
Entry	**No.**	**HepG2**	***E. coli***	***P. aeruginosa***	***S. aureus***	***B. subtilis***	***E. coli***	***P. aeruginosa***	***S. aureus***	***B. subtilis***
1	**Pep. 90**	N/A	100	100	100	100	nd	nd	nd	nd
2	**Pep. 91**	100	50	100	50	12.5	2	1	2	8
3	**Pep. 92**	N/A	100	100	50	50	nd	nd	nd	nd
4	**Pep. 93**	100	25	50	12.5	3.13	4	2	8	32
5	**Pep. 94**	N/A	100	100	100	100	nd	nd	nd	nd
6	**Pep. 95**	N/A	100	100	100	50	nd	nd	nd	nd
7	**Pep. 101**	100	100	100	100	100	1	1	1	1

Amongst the peptoids screened against the tested antibacterial targets, **Pep. 93** shows the most promising antibacterial potencies (**Table 5.3, Entry 4**). Whilst moderately effective against the Gram-negative *E. coli* and *P. aeruginosa* (MICs of 50 μM and 25 μM, respectively), it shows much more enhanced efficacies against *S. aureus* and *B. subtilis* (MICs of 12.5 μM and 3.13 μM). This cyclic peptoid also exhibits no cytotoxic properties, and the SI value found for *B. subtilis* is 32. **Pep. 93** is an 8-membered peptoid ring which has a double positive charge owing to the presence of two *N*ae building blocks. Furthermore, this molecule contains a chiral center derived from *N*spe. The presence of both the 2+ charge and the α-helical-inducing component in **Pep. 93** potentially contribute to its antibacterial potency. However, a more thorough investigation involving a wider range of peptoid building blocks is needed to fully understand the specific effects of these building blocks.

Several cyclic compounds in this library demonstrated no significant bactericidal effects, including the only peptide screened, **Pep. 101 (Table 5.3, Entry 7)**. **Pep. 91** (**Table 5.3, Entry 2**) and **Pep. 92** (**Table 5.3, Entry 3**) exhibited some efficacy against Gram-positive species, and **Pep. 91** displayed an *E. coli* MIC value of 50 μM. These findings suggest that TFP-stapled cyclic biopolymers hold potential for downstream applications. By fine-tuning monomer incorporation, particularly by incorporating a higher proportion of monomers bearing cationic functionalities, it may be feasible to develop molecules with more robust antimicrobial effects. This gains further support from the observation that none of the cyclic biopolymers screened against HepG2 exhibited cytotoxic properties.

5.4.6. Log *D* measurements vs. HPLC-derived t_R: measure of peptoid lipophilicity

In order to measure log *D* values of the macrocycles synthesised in this chapter, the protocol used was the same as the one described in **Chapter 2**, **Section 2.3.8**. **Table 5.4** shows HPLC t_R and log *D* values obtained for the macrocycles.

Table 5.4. A summary of six cyclic peptoids and one cyclic peptide tested against four bacterial species, together with their HPLC t_R and log *D* values. (nd = no data recorded)

Entry	No.	HPLC t_R	log *D*
1	**Pep. 90**	30.80	nd
2	**Pep. 91**	23.72	-0.94
3	**Pep. 92**	24.00	nd
4	**Pep. 93**	21.86	-0.08
5	**Pep. 94**	24.76	nd
6	**Pep. 95**	19.52	nd
7	**Pep. 101**	17.81	1.70

Log *D* values, shown in **Table 5.4**, were only measured for the cycles which showed antibacterial efficacies. The observed t_R value for **Pep. 101** (**Table 5.4, Entry 7**) (t_R = 17.81 min) was notably lower than those observed for the peptoids **Pep. 91** (**Table 5.4, Entry 2**) and **Pep. 93** (**Table 5.4, Entry 4**) (t_R = 23.72 min and 21.86 min, respectively). This outcome was anticipated, considering that hydrogen bonds can readily form between amides present within peptide bonds and the aqueous environment of the HPLC system. This interaction not only led

to **Pep. 101** having lower t_R values in HPLC analyses but also resulted in the log *D* value of **Pep. 101** (log *D* = 1.70) being considerably higher than those of peptoids (**Pep. 91** log *D* = -0.94; **Pep. 93** log *D* = -0.08).

Peptoids **Pep. 91** and **Pep. 93** (**Table 5.4, Entries 2** and **4**) exhibit similar HPLC t_R values, with only a 2-minute difference. Despite this proximity in t_R values, they display significantly different log *D* values. Specifically, **Pep. 93** demonstrates a log *D* value closer to zero (-0.08), indicating an even partitioning between water and octanol. This characteristic aligns with findings described in previous chapters, where peptoids displaying the most promising antibacterial potencies also exhibited an even partitioning between water and octanol. (**Sections 2.3.8** and **4.3.6**).

5.5. Summary of Chapter 5

Peptoids open new avenues for the development of therapeutics; in particular, targeting larger active sites, such as bacterial membranes, which small molecules have been proven to have difficulty achieving. It has been suggested that the conformational heterogeneity within peptoid structures plays a major role in off-target effects. Due to *cis/trans* amide bond isomerism, various research groups have focused their efforts on establishing additional degrees of rigidity which have been explored in addition to the diversity of peptoid submonomers which restrict the *cis* → *trans* isomer exchange.

The susceptibility of the TFP group to S_NAr reactions was explored and utilised it in the production of novel peptoid macrocycles. Indeed, the cyclisation reaction proved to be fast and facile and compatible with peptoid rings of a range of sizes. Furthermore, the compatibility of this method in the synthesis of peptide macrocycles was explored. Whilst, likely due to the backbone flexibility, the compatibility of this method with peptoid rings of a range of sizes was established, the constrained nature of peptide chains resulted in only four-membered peptide ring formation. (**Pep. 99** and **Pep. 101**; **Scheme 5.16** and **Figure 5.15**)

To facilitate the synthesis of an appropriate TFP containing building block in high purity, to be used in the synthesis of cyclic peptides, a 4-step synthesis of Fmoc-Tyr(TFP)-OH **213** was established, achieving an excellent overall yield of 89%. This approach followed initial attempts to synthesise Boc-Tyr(TFP)-OH **206** via a 2-step reaction route, which resulted in the production of methoxy and methyl 2'-substituted TFP side products **207** and **208**.

The antibacterial properties of the macrocycles synthesised in this chapter were evaluated and their log *D* values were recorded. A diversity of different peptoid monomers were used, and it was found that **Pep. 93**, an 8-membered cyclic peptoid with a double positive charge was particularly efficacious against the Gram-positive *S. aureus* and *B. subtilis* (MIC values of 12.5 μM and 3.13 μM respectively). Furthermore, **Pep. 93** was found to have minimal cytotoxicity which resulted in its SI value of 32 against *B. subtilis.* This highlights a potential downstream therapeutic application of the TFP-stapled peptoid macrocycles. **Pep. 93** was also found to demonstrate even partitioning between water and octanol, with its log *D* value being -0.82. This finding is consistent with earlier observations in **Chapter 4**, which indicated that compounds with log *D* values around 0 exhibited the highest potency against antibacterial targets.

Pep. 101 is the only peptide synthesised in this chapter, and it did not show antimicrobial properties against any of the bacterial species screened. Compared to the peptoid

macrocycles which were investigated for their log *D* values, **Pep. 91** showed a similar HPLC t_R (HPLC t_R = 23.72 mins) to **Pep. 93** (HPLC t_R = 21.86 min), but they were found to have vastly different log *D* values (-0.94 and -0.08, respectively) (**Table 5.4, Entries 1** and **4**)

In conclusion, the application of TFP containing moieties permitted rapid access to biopolymer macrocycles that display antimicrobial efficacy and promising SI's.

5.6. References for Chapter 5

[1] Mendive-Tapia, L., Preciado, S., García, J., Ramón, R., Kielland, N., Albericio, F., Lavilla, R., 2015, *Nat. Commun*., **6**, 7160.
[2] Walensky, L.D., Bird, G.H. J., 2014, *Med. Chem*., **57**, 6275–6288.
[3] Hayes, H.C., Luk, L.Y., Tsai, Y.H., 2021, *Org. Biomol. Chem*., **19**, 3983–4001.
[4] Vinogradov, A.A., Yin, Y., Suga, H., 2019, *J. Am. Chem. Soc*., **141**, 4167–4181.
[5] Passioura, T., 2019, *Biochemistry*., **59**, 139–145.
[6] Dougherty, P.G., Qian, Z., Pei, D., 2017, *Biochem. J*., **474**, 1109–1125.
[7] Bechtler, C., Lamers, C., 2021, *RSC Med. Chem.*, **12**, 1325–1351.
[8] Joo, S.H., 2012, *Biomolecules Ther*., **20**(1), 19.
[9] Bechtler, C., Lamers, C., 2021, *RSC Med. Chem.*, **12**, 1325–1351.
[10] Hummel, G., Reineke, U., Reimer, U., 2006, *Mol. BioSystems.*, **2**(10), 499-508.
[11] Frost, J.R., Scully, C.C., Yudin, A.K., 2016, *Nat. Chem*., **8**(12), 1105–1111.
[12] Borel, J.A., Feurer, C., Gubler, H.U., Stähelin, H., 1994, *Inflamm. Res.*, **43**(3), 179–186.
[13] Vazeux, G., Iturrioz, X., Corvol, P., Llorens-Cortes, C., 1998, *Biochem. J*., **334**(2), 407–413.
[14] Shin, S.B.Y., Yoo, B., Todaro, L.J., Kirshenbaum, K., 2007, *J. Am. Chem. Soc*., **129**, 3218–3225.
[15] Culf, A.S., Čuperlović-Culf, M., Léger, D.A., Decken, A., *Org. Lett.*, **16**, 2780–2783.
[16] Caumes, C., Fernandes, C., Roy, O., Hjelmgaard, T., Wenger, E., Didierjean, C., Taillefumier, C., Faure, S., 2013, *Org. Lett*., **15**, 3626–3629.
[17] Kaniraj, P.J., Maayan, G., 2015, *Org. Lett*., **17**, 2110–2113.
[18] Nilsson, C., Simpson, N., Malkoch, M., Johansson, M., Malmström, E., 2008, *J. Polym. Sci. Part A*., **46**, 1339–1348.
[19] Grubbs, R.H., 2004, *Tetrahedron*., **60**, 7117–7140.
[20] Khan, S.N., Kim, A., Grubbs, R.H., Kwon, Y.-U., 2011, *Org. Lett*., **13**, 1582–1585.
[21] Comegna, D., Benincasa, M., Gennaro, R., Izzo, I., De Riccardis, F., 2010, *Bioorg. Med. Chem*., **18**, 2010–2018.
[22] Huang, M.L., Shin, S.B.Y., Benson, M.A., Torres, V.J., Kirshenbaum, K., 2012, *ChemMedChem.*, **7**(1), 114–122.
[23] Huang, M.L., Benson, M.A., Shin, S.B.Y., Torres, V.J., Kirshenbaum, K., 2013, *Eur. J. Org. Chem.*, **17**, 3560–3566.
[24] Spokoyny, A.M., Zou, Y., Ling, J.J., Yu, H., Lin, Y.S., Pentelute, B.L., 2013, *J. Am. Chem. Soc*., **135**(16), 5946–5949.
[25] Amii, H., Uneyama, K., 2009, *Chem. Rev.*, **109**, 2119–2183.
[26] Wielgat, J., Domagala, Z. 1975, *Rocz. Chem.*, **49**, 1039–1041.
[27] Fuhrer, T.J., Houck, M., Corley, C.A., Iacono, S.T., 2019, *J. Phys. Chem. A.*, **123**, 9450–9455.
[28] Brittain, W.D., Cobb, S.L., 2019, *Org. Biomol. Chem*., **17**(8), 2110–2115.
[29] Gimenez, D., Mooney, C.A., Dose, A., Sandford, G., Coxon, C.R., Cobb, S.L., 2017, *Org. Biomol. Chem*., **15**(19), 4086–4095.
[30] Sandford, G., Slater, R., Yufit, D.S., Howard, J.A., Vong, A., 2005, *J. Org. Chem.*, **70**(18), 7208–7216.
[31] Olsen, C.A., Montero, A., Leman, L.J., Ghadiri, M.R., 2012, *ACS Med. Chem. Lett*., **3**, 749–753.
[32] Stawikowski, M.J., 2013, Peptoids and Peptide–Peptoid Hybrid Biopolymers as Peptidomimetics. *Peptide Modifications to Increase Metabolic Stability and Activity*. 47–60.
[33] Bolt, H. L., Eggimann, G. A., Jahoda, C. A., Zuckermann, R. N., Sharples, G. J., Cobb, S. L., 2017, *MedChemComm*, **8**, 886-896.
[34] Patch, J. A., Barron, A. E., 2003, *J. Am. Chem. Soc.*, **125**, 12092-12093.

[35] Stefanidis, D., Cho, S., Dhe-Paganon, S., Jencks, W.P., 1993, *J. Am. Chem. Soc*., **115**, 1650–1656.
[36] DeBernardis, J.F., Kerkman, D.J., Winn, M., Bush, E.N., Arendsen, D.L., McClellan, W.J., Basha, F.Z., 1985, *J. Med. Chem*., **28**, 1398–1404.
[37] Wang, Z., Felstead, H.R., Troup, R.I., Linclau, B., Williamson, P.T., 2023, *Angew. Chem. Int. Ed.*, **62,** e202301077.
[38] Krainer, E., Naider, F., Becker, 1993, *J. Tetrahedron Lett.*, **34**(11), 1713–1716.
[39] Dubowchik, G.M., Radia, S., 1997, *Tetrahedron Lett.*, **38**(30), 5257–5260.

Chapter 6: Conclusions and Future Work

Peptoids represent a class of peptidomimetics that offers significant advantages over peptides, such as proteolytic stability and enhanced biological function, all while maintaining the capability to target the complex domain of protein-proftein interactions. Previous studies have demonstrated that peptoids possess not only antimicrobial but also antifungal properties, and even specificity towards carcinoma cells.[1] The overarching aim of this thesis was to elucidate connections between peptoid structure, physical attributes and antimicrobial efficacy whilst minimising peptoid toxicity to mammalian cells. It was aimed to develop novel peptoid scaffolds and expand the chemical diversity of peptoids with therapeutic potential. The research in this thesis was to encompass a wide array of peptoid structures, including long chains and macrocycles. Additionally, novel monomers were to be synthesised to address the peptoid amide bond heterogeneity.

Chapter 2 describes the work that was carried out to explore the application of fluorine in peptoid synthesis, recognising its high electronegativity and consequential influence on the acidity of adjacent functional groups, which in turn affects binding affinity in target active sites.[2] Fluorine's impact on the peptoid amide bonds was initially explored by the Cobb group via the design of novel monomers. Herein, 15-mer and 12-mer peptoid oligomers were synthesised (**Figures 2.8**, **2.13** and **2.17**) and their biological activities were evaluated (**Table 2.8**).Among the peptoids synthesised, peptoids which contained fluorinated alkyl monomers, such as *N*1*f*et (**31**) and *N*2*f*et (**32**) replacing the chiral aromatic *N*spe (**2**), displayed enhanced antimicrobial activities and reduced cytotoxicity against Hep2G cells (**Table 2.8**, Entry **12**, **13** and **16** – **23**) giving rise to impressive SI values across all screened bacterial species, with **Pep. 27** and **Pep. 28** exhibiting exceptional results (SI of >16 for *E. coli*, >32 for *S. aureus* and >64 *B. subtilis*, **Table 2.8**, **Entries 12** and **13**). The incorporation of cationic ammonium monomers, such as *N*et$_3$ae (**49**) and *N*et$_2$bnae (**51**) (**Scheme 2.5**) resulted in decreased cytotoxicity when screened against HepG2 for **Pep. 29** and **Pep. 30** (HepG2 ED_{50} of 19.4 and 34.6; **Table 2.8**, **Entries 14** and **15** respectively). The results obtained in this chapter strongly suggest the therapeutic potential of combining fluorinated and cationic ammonium peptoid submonomers. Beyond the investigation of structure-activity relationships (SAR) of peptoids, the lipophilicities of the prepared materials were also studied using log *D* measurements (**Section 2.3.9**, **Table 2.9**). While some trends in the log *D* data were identified, such as log *D* values obtained for most efficacious peptoids which hovered around 0, it became apparent that log *D*

may not reliably predict antibiotic properties of peptoids. It was also noted that while reducing peptoid hydrophobicity (e.g. **Pep. 6** ED_{50} = 16.3 μM, **Table 2.8**, **Entry 5**, and log *D* = 1.23, **Table 2.9**, **Entry 8**; **Pep. 34** ED_{50} = 100 μM, **Table 2.8**, **Entry 19**, and log *D* = -0.04, **Table 2.9**, **Entry 23**) may decrease toxicity, its impact on antimicrobial efficacy appears to be minimal.

Building on from **Chapter 2**, wherein fluorinated peptoids exhibited notable activity and promising selectivity indices (SI), a deeper exploration into the use of these monomers is necessitated in the future. Specifically, it is proposed to reposition the *N*y*N*x*N*x motif composed of fluorinated monomers to the central region of the peptoid oligomers. This adjustment will aim to elucidate the significance of the fluorinated motif placement within the peptoid backbone (**Figure 6.1.A.**). Additionally, it is encouraged to integrate hydroxy aryl monomers, which were investigated in **Chapters 3** and **4**, into peptoids. The introduction of phenolic groups is anticipated to impart decreased peptoid hydrophobicity, potentially leading to reduced cytotoxicity (**Figure 6.1.B.**). An intriguing avenue for exploration also involves the incorporation of both phenolic and fluorinated monomers within the same sequences. Peptoids with this novel combination can be designed to examine if combining the fluorous effect and the polarity of hydroxyl groups could yield potent bioactive peptoid oligomers. (**Figure 6.1.C.**)

In addition to studying the bioactivity of the aforementioned sequence modifications, it is necessary to assess secondary structures of peptoid oligomers using circular dichroism (CD) spectroscopy and compared their log *D* values. Such investigations should be carried out to contribute to the collection of data that could ultimately be used in our overall aim to achieving a more rational design of bioactive peptoids.

A.

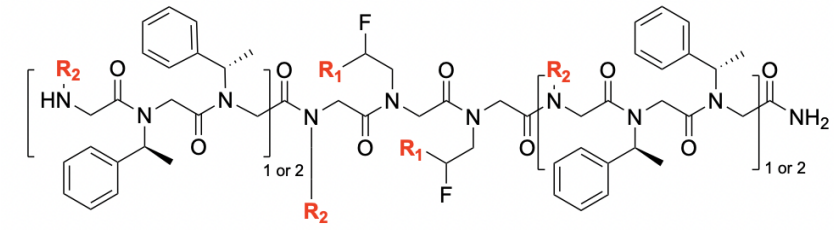

Pep. 102

B.

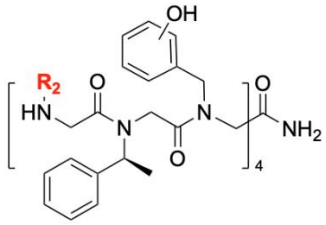

Pep. 103

C.

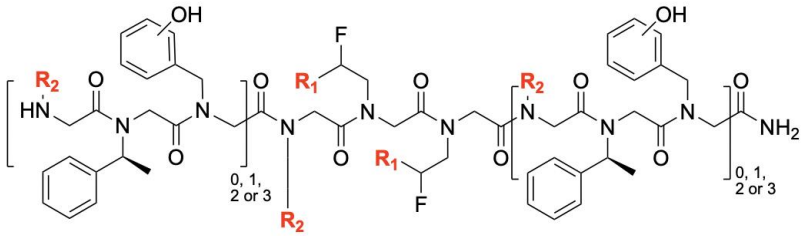

Pep. 104

R_1 = F or H

R_2 = any of **49** - **52**

Figure 6.1. Proposed dodecamer peptoid structures containing **A.** Fluorinated monomers; **B.** Hydroxy(aryl) monomers; **C.** A combination of fluorinated and hydroxy(aryl) monomers.

The focus of **Chapter 3** involved peptoid synthesis strategies, insights into amide bond isomerisation, and the structural characterisation of dipeptoid model systems. This included the development of hydroxyl-containing peptoid monomers and contributed to the ongoing quest for precise control over peptoid secondary structure. Initially, TFP-protected hydroxy aryl building blocks (**107** – **112**) were to be used to produce a library of model dipeptides; however, due to TFP's deactivating nature, Bnz was used as an alternative protecting group. The liberation of the hydroxyl moieties was performed by Pd(0)-catalysed *O*-Bnz cleavage (**Scheme 3.20**). The subsequent in-depth NMR analysis of the hydroxybenzylamine-containing model peptoids provided insights into the amide *cis/trans*-isomerisation of these systems. Notably, *No*Tyr **104** showed a pronounced preference for the *cis* amide configuration due to intramolecular hydrogen bonding, while the *o*-hydroxyaniline-containing acetamide **60** favoured a *trans* amide geometry. Furthermore, the substitution of the *ortho* position with another hydrogen bond donor, $–NH_2$, also resulted in *cis* amide bond geometry (acetamides

168 and **170**). Some of the other findings in **Chapter 3** include the elucidation of the crystal structure of dipeptide **105** which revealed dimer formation linked by intermolecular hydrogen bonding.

Expanding on the findings in **Chapter 3**, future investigation into the *ortho* position of the benzylamine moiety could be undertaken, and the substitution with other hydrogen-bond donors, such as a thiol group (see **Figure 6.2**) would be interesting. Performing molecular modeling analyses on acetamide **170**, which contains aminomethyl aniline (a derivative of compound **163**) and exclusively exhibits a *cis* amide bond configuration, would assist in uncovering the 3D arrangement of **170**. These studies would specifically contribute to comprehending the forces driving its preference for the *cis* amide configuration. Notably, this preference does not appear to be driven by hydrogen bonding between the -NH_2 group and the acetyl carbonyl group, thus necessitating further investigation through molecular modeling techniques.

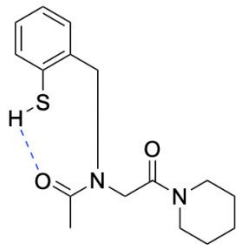

215

Figure 6.2. Proposed acetamide containing *o*-thiobenzylamine which could serve as a *cis*-inducing moiety. Hydrogen bonding is shown as a blue dotted line.

Chapter 4 discussed the synthesis of peptoid oligomers containing hydroxyl and amino aryl monomer, with their biological and biophysical evaluation being detailed therein. The chapter provides insights into synthesis strategies, structure-function relationships, and antimicrobial activity evaluations. The nonamer peptoids synthesised in **Chapter 4** contain aromatic and cationic monomers. Initially, the TFP-protecting group was intended to be used in the synthesis of the hydroxy aryl-containing monomers and the subsequent peptoid oligomers. However, due to its unprecedented susceptibility to 2'-S_NAr, the allyl protecting group approach was employed for these monomers, while the amino-aryls were protected with the alloc protecting group, both of which are cleavable in the presence of a Pd(II) catalyst.

The screened peptoids (**Table 4.2**) demonstrated significant correlations between the position of the hydroxyl on the aromatic ring and efficacy against bacteria. None of the peptoid

nonamers screened in **Chapter 4** showed toxicity against HepG2 cells (HepG2 ED_{50} of 100 μL, **Table 4.2**), resulting in impressive SI values. In particular **Pep. 54** showed exceptional selectivity for Gram-positive bacteria (SI of 64 for *S. aureus* and 64 for *B. subtilis*, **Table 4.2**, **Entry 3**). Moreover, a positive correlation was found between the peptoid HPLC t_R and their antibacterial activities. Furthermore, it was revealed that the position of the hydroxyl on the aryl ring influenced the hydrophobicity of peptoids, with the incorporation of *N*Tyr **118** yielding most polar peptoids (**Pep. 53** HPLC t_R = 16.94 min and **Pep. 57** HPLC t_R = 14.24 min).

For future investigations, employing harsher synthesis conditions for **Pep. 58**, which contains *N*-Boc aminomethyl aniline monomers (**168**), is proposed. Microwave-assisted synthesis is suggested, potentially yielding more efficient bromide displacement step in the submonomer peptoid synthesis. In addition, conducting CD analysis on amino(aryl)-rich **Pep. 57** and **Pep. 58**, could be used to establish comparative insights that would contribute to a more rational peptoid design approach in the future.

To elaborate on the investigation into antimicrobial efficacies of the nonamer peptoids discussed in **Chapter 4**, **Pep. 105** and **Pep. 106** (**Figure 6.3**) should be synthesised. Specifically, **Pep. 105** is a nonamer peptoid comprising alternating amino(aryl) (**168** or **170**) and *N*Spe (**2**) monomers, along with *N*Lys (**52**) in the *N*y*N*x*N*x motif. Conversely, **Pep. 106** is a nonamer composed of amino(aryl) (**168** or **170**) and **40** within the *N*y*N*x*N*x motif. Notably, in these sequences, the amino(aryl) monomers replace the aromatic achiral *N*Phe (**40**), serving to induce α-helices, while **52** imparts cationic character to the peptoids.

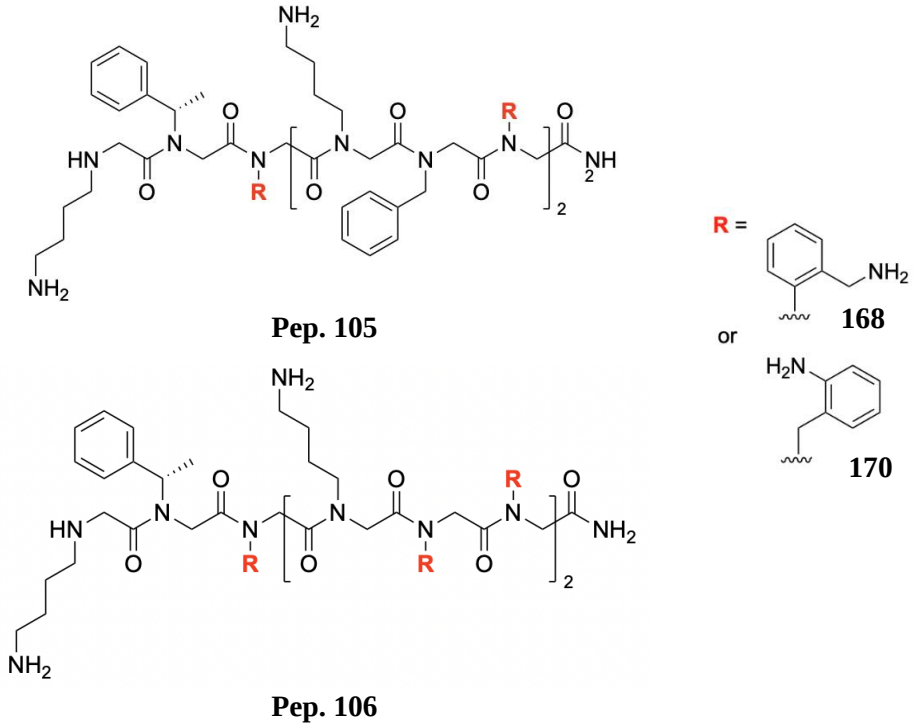

Figure 6.3. Proposed nonamer peptoids containing derivatives of *o*-amino benzylamine (**163**).

The exploration of TFP-tagging of hydroxy moieties on resin has begun, with *O*-allyl phenolic monomers being synthesised. Initially, the synthesis entailed obtaining hydroxy(aryl) monomers protected with the allyl group, ensuring cleavage compatibility with peptoid synthesis on resin. (**Scheme 6.1**) A crystal structure was obtained for **223** (**Figure 6.4)**. In the future, these monomers will be incorporated into peptoids, followed by deprotection and TFP-tagging under basic conditions, resulting in TFP-tagged peptoid chains, as shown in **Scheme 6.2**. As demonstrated in **Chapter 3**, *O*-TFP hydroxyanilines (**107** – **109**) led to *trans* amide geometry in acetamides **135** – **137** and could serve as inducers of β-turn formation in peptoids. This approach presents a promising avenue for tailored introduction of TFP-containing motifs into peptoid structures, potentially affording interesting structural motifs with novel biological applications.

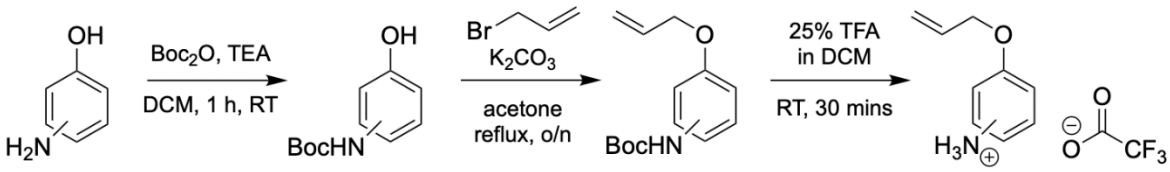

No.	Isomer
113	*ortho*
114	*meta*
115	*para*

No.	Isomer	Yield
216	*ortho*	51%
217	*meta*	49%
116	*para*	45%

No.	Isomer	Yield
218	*ortho*	64%
219	*meta*	64%
220	*para*	83%

No.	Isomer	Yield
221	*ortho*	quant.
222	*meta*	quant.
223	*para*	quant.

Scheme 6.1. Two-step synthesis of *O*-Allyl aminophenols as TFA salts (**221** – **223**).

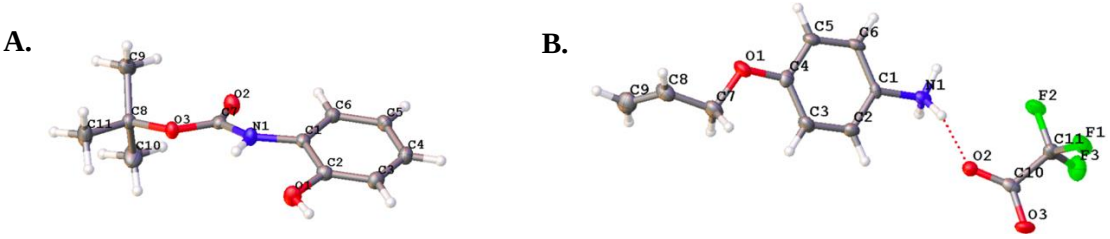

Figure 6.4. Ellipsoid-and-stick representations of **A**. *N*-Boc *o*-aminophenol **216** and **B**. *O*-Allyl aminophenol **223**. Carbon atoms are depicted in grey, hydrogen atoms in white, nitrogen in navy, oxygen in red, and fluorine in green. Structure was generated in Olex2 and is reported with a 50% thermal ellipsoid probability.

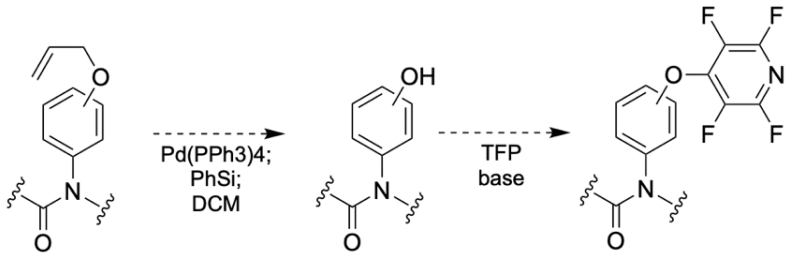

224 **225** **226**

Scheme 6.2. Proposed *O*-Allyl deprotection and subsequent TFP-protection on resin

In **Chapter 5**, the focus shifted to exploring cyclisation methods to establish conformational heterogeneity by restricting *cis/trans* amide bond isomerism. A novel stapling strategy involving the TFP group was sought. It was found that the TFP group gave ready access to be not only fast and facile but also compatible with peptoid rings of various sizes. However, limitations were observed in the formation of peptoid macrocycles (**Pep. 84**) due to backbone flexibility which was resolved by incorporating a "spacer" (**Pep. 89**), shown in

Scheme 5.9. Furthermore, a novel amino acid, Fmoc-Tyr(TFP)-OH **214**, was synthesised in a high overall yield (>80%, **Scheme 5.17**), via a 4-step synthetic route.

All of the macrocycles prepared were evaluated in antibacterial assays. Amongst the macrocycles screened, **Pep. 93** exhibited significant efficacies against Gram-positive bacteria with minimal cytotoxicity (*S. aureus* MIC = 12.5 μM; *B. subtilis* MIC = μM 3.13 μM; HepG2 ED_{50} = 100 μM, **Table 5.3, Entry 4**) indicating potential therapeutic applications for TFP-stapled structures. Moreover, **Pep. 93** exhibited equal partitioning between water and octanol (log *D* = -0.08, **Table 5.4**, **Entry 4**) which suggests that TFP-stapled cycled with log *D* values around 0 are bound to exhibit high potency against antibacterial targets. **Pep. 101**, which was the only peptide synthesised in **Chapter 5**, and demonstrated no antimicrobial properties. Comparative analysis with peptoids revealed differences in log *D* values despite similar HPLC t_R (**Pep. 91** HPLC t_R = 23.72, log *D* = -0.94, **Table 5.4**, **Entry 2**; **Pep. 93** HPLC t_R = 21.86; log *D* = -0.08 **Table 5.4**, **Entry 4**).

As demonstrated by **Pep. 93**, the increased cationic character and the incorporation of chiral aromatic monomers may contribute to amplified antimicrobial activities. Consequently, in the future an increased inclusion of *N*Lys (**52**) and *N*spe (**2**) monomers into the TFP-stapled peptoids (**Pep. 107**). (**Figure 6.4**) could be investigated. Additionally, integrating a hydroxy-bearing side chain into the stapling reaction to facilitate the synthesis of **Pep. 108** (**Figure 6.4)** could be attempted. **Pep. 108** utilizes 1-aminobutan-4-ol; however, the aliphatic chain length selected for this synthesis may vary. This broadening of nucleophilic options, to include nucleophiles such as thiols, would enhance the structural diversity and potentially the biological activity of the synthesised macrocycles. Similarly, the incorporation of two Lys amino acids into the TFP-stapled cyclic peptides (**Pep. 109**) could be probed to help bacterial membranes targeting, and thus potentially yielding more biologically active macrocyclic peptides. Moreover, we propose incorporating the Ser monomer in the synthesis of cyclic peptides. (**Pep. 110**) The range of nucleophiles utilised can be diversified, with amino acids such as Met being viable candidates for incorporation.

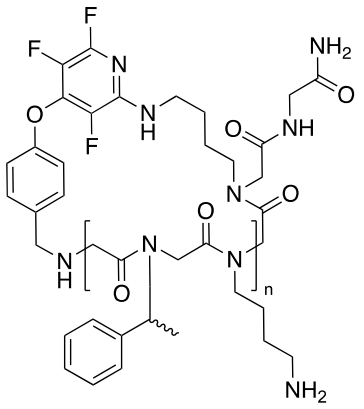

Pep. 107

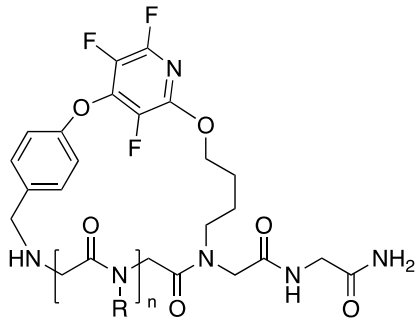

Pep. 108

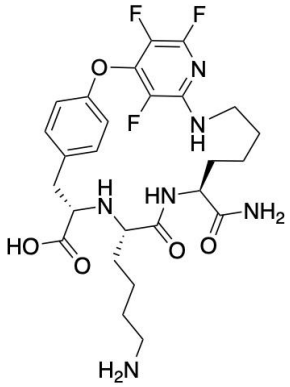

Pep. 109

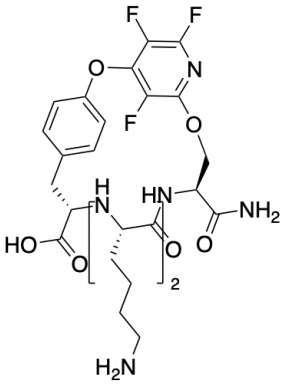

Pep. 110

Figure 6.4. Proposed cyclic peptoid and peptide structures containing higher degree of cationic groups (**Pep. 107** and **Pep. 109**); hydroxy-based nucleophile (**Pep. 108** and **Pep. 110**) used in the formation of the 2', 4'-substituted TFP staple.

Building upon the findings in **Chapter 5**, an interesting approach for cyclisation involves producing cyclic peptoids through Grubbs metathesis, employing *N*Tyr ether derivative **227**. Steps have been undertaken to produce this building block, shown in **Scheme 6.3.A**. The first step involved Boc-protection of the 4-aminomethylphenol **121** to produce **124**, followed by ether formation under basic conditions to produce **226**, Boc-deprotection took place under acidic conditions to yield **227**. Metathesis has previously been successfully employed by Khan and co-workers in the synthesis of peptoid macrocycles, using 3-buten-1-amine building blocks. (**Scheme 5.4**, **Section 5.1.2**) Future work involves the synthesis of the linear **Pep. 111**, followed by its cyclisation to form the target macrocyclic scaffold **Pep. 112**, both depicted in **Scheme 6.3.B**. This approach holds promise for expanding the repertoire of peptoid cyclisation methods, and potentially provide biologically active structures.

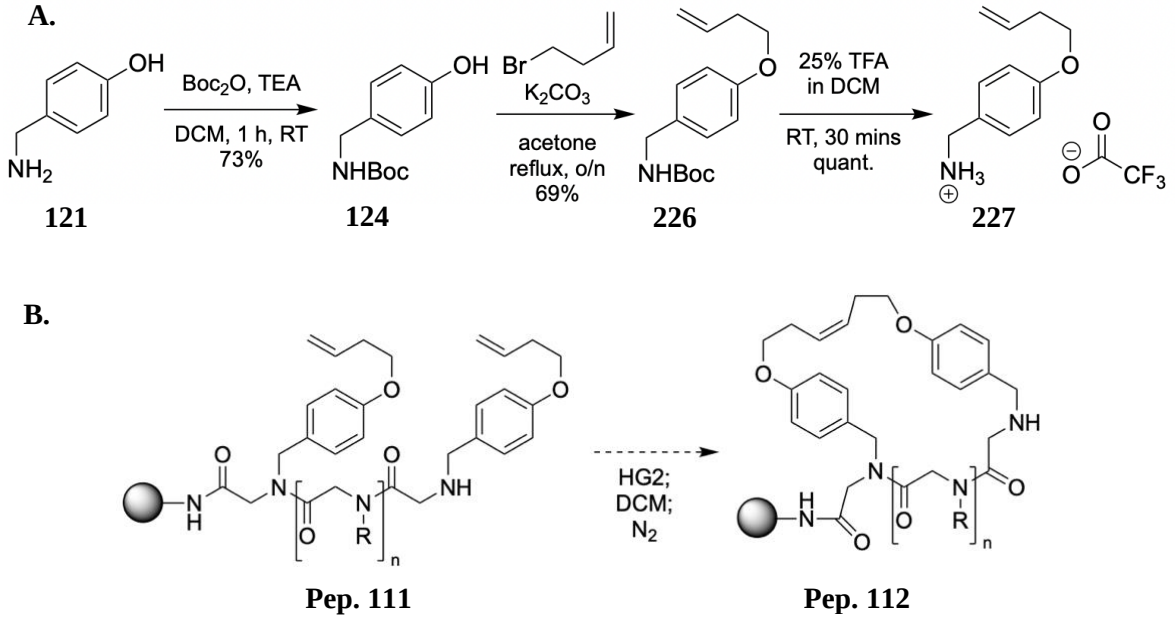

Scheme 6.3.A. A three-step synthetic route to form **227**. **B.** Proposed synthesis of macrocyclic peptoid target **Pep. 112**, which uses **227** to form a carbon-carbon bond which serves as a staple.

The primary objectives of this thesis, including developing new peptoid monomers, increasing our understanding of the connections between peptoid structure and hydrophobicity, and structure activity relationship (SAR), have been largely accomplished. In addition, novel polar peptoid monomers have been synthesised to successfully address both the issues peptoid hydrophobicity and amide bond heterogeneity within the field. Finally, the work has successfully designed and produced a variety of new peptoid scaffolds: both linear and macrocyclic with enhanced chemical diversity and therapeutic promise against a range of microbial targets.

References for Chapter 6

[1] Bolt, H. L., Eggimann, G. A., Jahoda, C. A., Zuckermann, R. N., Sharples, G. J., Cobb, S. L., 2017, *MedChemComm*, **8**, 886-896.
[2] Fried, J., Sabo, E. F., 1954, *J. Am. Chem. Soc.*, **76**, 1455-1456.

Chapter 7: Experimental Section

7.1. Materials and reagents

All reagents used in this project were purchased from commercial sources and used without further purification. Peptide synthesis grade DMF was obtained from AGTC Bioproducts (Hessle, UK), PyBOP from Apollo Scientific (Stockport, UK) and NMR solvents which were purchased from Cambridge Isotopes Inc., supplied by Goss Scientific (Crewe, UK). All resins and amino acids were purchased from Novabiochem by Merck (Darmstadt, Germany). Amines used in submonomer peptoid synthesis were obtained either from Sigma Aldrich (Gillingham, UK) or TCI Europe (Zwijndrecht, Belgium). These chemicals were used without further purification and stored under appropriate conditions, as detailed in the manufacturer's instructions. Bond Elut solid phase extraction cartridges (20 mL, polypropylene with two polypropylene frits) were purchased from Crawford Scientific and used as reaction vessels for solid phase synthesis.

Solvents were removed *in vacuo* using a Büchi Rotavapor R11. The following centrifuges were used: an Eppendorf centrifuge 5415D (for 1.5 mL tubes) or a Beckman-Coulter Allegra X-22R (for 15mL or 50 mL tubes). A Radleys Discovery Technology shaker was also used to mix solutions where indicated and aqueous solutions were lyophilised using a Christ Alpha 1-2 LD Plus freeze drier.

7.2. Purification and characterisation

7.2.1. General procedure for peptoid purification by preparative high-pressure liquid chromatography (prep HPLC)

Samples to be purified were dissolved in a mix of deionised H_2O/MeCN (ratio dependent on solubility), centrifuged or filtered (if necessary) and injected onto a Supelco Analytical Discovery B10 Wide Pore C18-5 column (25 cm x 10 mm, 5 μm) using a semi-preparative Perkin Elmer Series 200 LC pump and 785A UV-vis detector. A gradient of 0-100% solvent B in solvent A (solvent A = 95% H_2O, 5% MeCN, 0.1% TFA, solvent B = 95% MeCN, 5% H_2O, 0.1% TFA) over 40-60 minutes with a flow rate of 2.0 ml/min was used and absorbance data collected at 220 nm. Fractions were analysed by LC-MS (according to **Section 7.3.2**) and analytical HPLC (**Section 7.3.4**) and the fractions containing desired product were lyophilised.

7.2.2. Liquid chromatography electrospray ionisation mass spectrometry (LC-MS)

Analytical LC-MS data were obtained using a triple quadrupole mass spectrometer equipped with an Acquity UPLC (Waters Ltd, UK) and a photodiode array detector. Samples were injected onto the Acquity UPLC BEH C18 column (1.7 μm, 2.1 mm × 50 mm) with a flow rate of 0.6 mL min-1 and a linear gradient of 5–95 % of solvent B over 3.8 min (A = 0.1 % formic acid in H_2O, B = 0.1 % formic acid in acetonitrile). The flow was introduced into the electrospray ion source of the Aquity TQD mass spectrometer.

7.2.3. Quadrupole time-of-flight mass spectrometry (QToF)

Measurements were performed using a QToF Premier mass spectrometer with an Acquity ultra-performance liquid chromatography system (Waters Ltd, UK). Samples were injected to the Acquity UPLC BEH C18 column (1.7 μm, 2.1 mm x 100 mm) with a flow rate of 0.6 mL min-1 and a linear gradient of 0–99 % of solvent B over 6 min (A = 0.1 % formic acid in H_2O, B = 0.1 % formic acid in acetonitrile). The solvent flow from the UPLC was injected into a 0.2 mL/min flow of acetonitrile which was introduced into the electrospray ion source.

7.2.4. Analytical high-pressure liquid chromatography (HPLC)

Samples were dissolved in a mix of deionised H_2O/MeCN (ratio dependent on solubility) and 10-150 μl injected onto a Phenomenex Luna C18 LC column (25 cm x 4.6 mm, 5 μm, 100 Å) or an SB Analytical ODS-H optimal column (25 cm x 4.6 mm, 5 μm) using a Perkin Elmer Series 200 Autosampler and Perkin Elmer Series 200 LC Pump. Detection was achieved using a Series 200 UV-vis detector. A gradient of 0-100% solvent B in solvent A (solvent A = 95% H_2O, 5% MeCN, 0.05% TFA, solvent B = 95% MeCN, 5% H_2O, 0.03% TFA) over 40 minutes with a flow rate of 1.0 ml/min was used. Absorbance data was collected at 220 nm and processed using TotalChem software.

7.2.5. Nuclear magnetic resonance (NMR) spectroscopy

^{1}H, ^{19}F NMR spectra were obtained on the following machines: Varian Mercury-400 MHz, Varian VNMRS-600 MHz and Bruker Avance-400 MHz spectrometers.

Chemical shifts are reported in parts per million (δ ppm) and relative to residual solvent peaks. J couplings are reported in hertz (Hz). Multiplicities: s = singlet, d = doublet, dd = doublet of doublets, td = triplet of doublets, m = multiplet, q = quartet, t = triplet.

7.3. Biological and biophysical analysis

7.3.1. Bacterial culture preparation

Escherichia coli K-12 wild-type strain (BW25113), *Pseudomonas aeruginosa* (FDA204P) *Staphylococcus aureus* (3R7089 strain Oxford / ATCC9144) and *Bacillus subtilis* (laboratory strain from clinical isolate) were selected for bacteriological studies as representative Gram-negative (*E. coli* and *P. aeruginosa*) and Gram-positive (*S. aureus* and *B. subtilis*) species. Bacterial cultures were prepared by streaking bacterial strains onto LB agar plates with an inoculation loop and incubated overnight at 37 °C. A single colony was selected and placed in 5 mL of Iso-sensitest broth (Sigma Aldrich) and incubated with shaking for 16–18 h at 37 °C to provide liquid cultures for testing.

7.3.2. Antibacterial minimum inhibitory concentration (MIC) determination

MIC values were obtained according to the previously described protocol[5] and were conducted in 96-well plates (Sarsted, Fisher Scientific). Bacteria were grown from overnight cultures in Mueller-Hinton broth to an A650nm of 0.07 equivalent to a 0.5 MacFarland standard (240 μM $BaCl_2$ in 0.18 M H_2SO_4). This culture was diluted ten-fold with Mueller-Hinton broth before use. Peptoids were initially dissolved in DMSO (5 mM) and diluted further in Mueller-Hinton broth to achieve a concentration range of 4–200 μM using 2-fold serial dilutions. 50 μL of inoculum and 50 μL of peptoid solution were added to each test well (final concentration range of 2–100 μM). Experiments were performed in triplicate. A positive control for bacterial growth contained only the inoculum and Mueller-Hinton broth. Other controls contained the inoculum and serial dilutions of ampicillin (from 250 μg/mL to 2 μg/mL), serial dilutions of DMSO and the inoculum to confirm no inhibitory effect on bacterial growth, and Mueller-Hinton broth alone as a sterile control. The MIC was defined as the lowest concentration which completely inhibited bacterial growth after incubation at 37 °C for 16 h with shaking. Quantitative data was attained from absorbance values using a Biotek Synergy H4 plate reader.

7.3.3. Cytotoxicity assays with HepG2 epithelial cells

Cytotoxicity analyses were performed in 96-well plates (Costar, Fisher Scientific) using alamarBlue® (Invitrogen) for cell viability detection using a modified protocol as previously described.[9] The HepG2 cells were grown at 37 °C, 5 % CO_2 in $DMEM_{10}$ high glucose supplemented with heat-inactivated foetal bovine sera (FBS, 10 %; Biosera Ltd) and penicillin/streptomycin (P/S, 1 %). Cells were counted using a Neubauer Improved Hemocytometer. HepG2 cells were seeded 1 day prior to treatment in 96 well plates at a concentration of 2 x 10^5 cells mL^{-1} in 100 μL of medium (2 x 10^4 cells/well). After 24 hours, cells were incubated with the compounds in a dilution series in triplicate from 2–100 μM (5 mM stock solutions in DMSO; untreated cells with DMSO as a negative control) in 50 μL of the media for 1 hour. Afterwards, 40 μL of medium was removed from each well before the addition of 90 μL of the media, followed by incubation for 24 hours at 37 °C, 5 % CO_2. Then, 10 μL of alamarBlue® (Invitrogen) was added to each well before a 2 hour incubation prior to assessing cell viability using a fluorescent plate reader (Biotek; λ_{ex} 560 nm, λ_{em} 600 nm).

7.3.4. Partitioning experiments (log *D* determination)

Peptoids were dissolved at 1 mM in either Phosphate Buffered Saline (PBS) or 1-Octanol. Exact concentrations were measure using UV spectrometry (Shimadzu UV-3600) using the phenylalanine-like peak centred at 258 nm and a molar extinction coefficient of 195 M^{-1} cm^{-1} per residue. It was necessary to subtract baselines and the influence of the peptoid backbone absorption at lower wavelengths to get accurate concentration data.

Partition experiments were carried out by putting 450 μL of octanol in contact with 450 μL of PBS, which contained between 10 and 100 μL of peptoid. Each peptoid was measured in triplicate. The samples were allowed to equilibrate under gentle agitation for ~150 hours. After this point samples were taken from the PBS half and the octanol half and diluted to produce sufficient volume for spectroscopy (1 mL). The concentration of peptoid remaining in the PBS and the octanol was measured individually using the phenylalanine peak as before. From these concentrations the ratio K_v of concentration in PBS to concentration in octanol was calculated.

7.4. General procedures

7.4.1. General procedure for peptoid synthesis

Fmoc-protected Rink Amide resin (0.7 – 0.8 mmol, loading of 0.84 mol g^{-1}) was left to swell in DMF (1 mL) for 30 minutes at 400 rpm. The resin was drained and the Fmoc protecting group was removed with a solution of 20% piperidine in DMF (2 mL, 2 x 15 minutes). The left-over mixture was drained, and the resin was washed with DMF (4 x 2 mL). Then, a solution of bromoacetic acid (0.6 M in 1 mL in DMF) and DIC (0.2 mL) was added to the resin and left to shake for 15-20 minutes, at RT. Subsequently, the mixture was drained, and the resin was washed with DMF (4 x 2 mL). The bromine displacement was performed by adding a solution of 1.2 M of desired submonomer in DMF (1 mL). The resin was let to shake at RT for 1 hour. In the case of:

a) Fluorinated submonomers, the reaction times were extended to 2 hours per submonomer addition. The steps of bromoacetylation and bromine displacement were repeated until target sequences were reached;
b) Cationic submonomers, the building blocks were basified with DIPEA (2 eq) to aid the bromide displacement step;
c) Alloc/Allyl-protected submonomers, the building blocks were basified with DIPEA to aid the bromide displacement step. Upon completion of the peptoid sequences, the Alloc/Allyl protecting groups were cleaved using a solution of $Pd(PPh_3)_4$ (0.1 eq), PhSiH (10 eq) in DCM (2 mL).

7.4.2. General procedure for peptoid cleavage (acid-labile resin)

The cleavage of the final peptoids sequences from the resin was performed using 1 mL of a cleavage cocktail of TFA/TIPS/H_2O (95:2.5:2.5 *v/v/v*). The resin was left to shake for 15 minutes, before the cocktail was collected and the resin was washed with DCM (2 x 2 mL). This solution containing the crude peptoid was concentrated *in vacuo*, resulting in a formation of a viscous oil which turned into a white precipitate upon the addition of EtO_2. The mother liquor was decanted and the solid was dissolved in 1:1 H_2O/ACN and lyophilised.

7.4.3. General procedure for *N*-Boc protection

At 0 ºC, under an N_2 atmosphere, an amine derivative was dissolved in DCM and treated with TEA. Then, to this solution was added dropwise a solution of di-*tert*-butyl dicarbonate in DCM. The solution was allowed to warm up to RT and was stirred for 1 hour. The reaction mixture was then washed with a solution of 1 M citric acid and the aqueous layer was extracted twice with DCM. The organic extracts were combined, dried with $MgSO_4$, filtered, and concentrated *in vacuo*. Where required, the crude product was purified by flash column chromatography.

7.4.4. General procedure for *N*-Boc cleavage

At RT, under ambient atmosphere, to a flask charged with an amine derivative (1.00 eq) was added a solution of 25% of TFA in DCM. The resulting reaction mixture was left to stir for 45 minutes. Then, the volatiles were evaporated *in vacuo* and the residual TFA was co-evaporated with DCM thrice. Subsequently, the residual DCM was allowed to evaporate under high vacuum. No further purification was performed.

7.4.5. General procedure for hydrogenation using 10% Pd/C cat. and H_2

A flask charged with benzyl ether derivative (1.00 eq) in methanol was inertised before the addition of 10% Pd/C catalyst moist. with water (0.10 eq). H_2 atmosphere was introduced via balloon and the reaction mixture was allowed to stir for 2 hours at RT. The reaction mixture was filtered through a celite cake, which was then copiously washed with methanol. The filtrate was collected and concentrated *in vacuo*.

7.4.6. General procedure for *O*-TFP protection

To a stirred solution of an aminophenol derivative (1.00 eq) in ACN was added pentafluoropyridine **100** (1.05 eq) and K_2CO_3 (1.05 eq). The resulting reaction mixture was allowed to stir overnight at ambient conditions and was filtered. The filtrate was concentrated *in vacuo*, and dried under high vacuum. The desired product was collected as a solid.

7.4.7. General procedure for *O*-TFP deprotection

O-TFP protected substrate (1.0 eq) was dissolved in ACN and treated with 2.00 eq of KF and 3.00 eq of thiophenol. The resulting reaction mixture was stirred for ca. 2 hr. The reaction mixture was filtered, and the filtrate was concentrated *in vacuo*. The residue was directly purified by flash column chromatography and the fractions containing the desired product were combined and concentrated.

7.4.8. General procedure for the *O*-alkylation

N-Boc aminomethylphenol (1.00 eq) was dissolved in acetone and treated with K_2CO_3 (1.10 eq) and an alkyl bromide (1.10 eq). The resulting reaction mixture was refluxed for 7-8 hours. Then, the solids were filtered off and washed liberally with acetone, and the filtrate was evaporated *in vacuo*. The residue was washed through a silica plug, using a gradient of EtOAc in hexane as eluent.

7.4.9. General procedure for the synthesis of model peptoids containing amine derivatives

2-bromo-1-piperidinyl ethenone **129** (1.00 eq) and was dissolved in THF or DMF and, at 0ºC, under N_2 atmosphere, it was added to a solution of 1.20 or 4.00 eq amine, and 1.2, 2.0 or 4.00 eq of DIPEA/Cs_2CO_3 where the amine derivative was used as a TFA salt, in THF or DMF (dropwise addition). The reaction mixture was brought to RT, and concentrated in vacuo and the resulting residue was suspended in EtOAc. The solids were filtered and washed with EtOAc. Upon subsequent evaporation of volatiles, the crude was dissolved in DCM and treated with 2.00 eq of acetyl chloride and 2.00 eq of DIPEA. Then, it was stirred for 20 minutes, washed with a solution of 1 M citric acid; the phases were separated, and the aqueous phase was extracted with DCM thrice. The organics were combined, dried with $MgSO_4$, filtered and concentrated *in vacuo*. The crude product was purified by flash column chromatography.

7.4.10. General procedure for the synthesis of TFP-stapled peptoid cycles

Fmoc-protected MBHA Rink Amide resin (1 mmol, loading of 0.516 mol g^{-1}) was left to to swell in DMF (1 mL) for 30 minutes at 400 rpm. The resin was drained and the Fmoc protecting group was removed with a solution of 20% piperidine in DMF (2 mL, 2 x 15 minutes). The left-over mixture was drained, and the resin was washed with DMF (4 x 2 mL). Then, a solution of HO-Gly-Fmoc (4 mmol, 4 eq), DIC (4.0 mmol, 4.0 eq) and DIPEA (4.0 mmol, 4.0 eq) in DMF (2 mL) was added and the resin was shaken for 1 hour at RT. Subsequently, the mixture was drained, and the resin was washed with DMF (4 x 2 mL). The Fmoc protecting group was removed with a solution of 20% piperidine in DMF (2 mL, 2 x 15 minutes). The left-over mixture was drained, and the resin was washed with DMF (4 x 2 mL). Then, a solution of bromoacetic acid (0.6 M in 1 mL in DMF) and DIC (0.2 mL) was added to the resin and left to shake for 15-20 minutes, at RT. The mixture was drained, and the resin was washed with DMF (4 x 2 mL). Bromide displacement was performed by adding a *N*-Alloc 1,4-diaminobutane (2.0 eq) and DIPEA (3.0 eq) in DMF (1 mL). The steps of bromoacetylation and bromine displacement were repeated (see **Section 7.4.1**) until the desired linear precursors bearing the TFP-protected *N*Tyr were produced. The resin was thoroughly washed with DCM (4 x 2mL). Then, $Pd(PPh_3)_4$ (0.1 eq), PhSi (10 eq) in DCM (1.5 mL) was added to the resin (3 x 20 min). The resin was washed with DCM (x3) and DMF (2 mL) was added. The linear peptoids were left to cyclise with shaking on resin overnight.

7.4.11. General procedure for the synthesis of TFP-stapled peptide cycles

Fmoc-protected MBHA Rink Amide resin (1 mmol, loading of 0.516 mol g^{-1}) was let to swell in DMF (1 mL) for 30 minutes at 400 rpm. The resin was drained and the Fmoc protecting group was removed with a solution of 20% piperidine in DMF (2 mL, 2 x 15 minutes). The left-over mixture was drained, and the resin was washed with DMF (4 x 2 mL). Then, a solution of HO-Lys(Alloc)-Fmoc (4 mmol, 4 eq), DIC (4.0 mmol, 4.0 eq) and DIPEA (4.0 mmol, 4.0 eq) in DMF (2 mL) was added and the resin was shaken for 1 hour at RT. Subsequently, the mixture was drained, and the resin was washed with DMF (4 x 2 mL). The Fmoc protecting group was removed with a solution of 20% piperidine in DMF (2 mL, 2 x 15 minutes). The left-over mixture was drained, and the resin was washed with DMF (4 x 2 mL). Iterative AA addition and deprotection followed, until the desired linear peptoids were produced. Then, the resin was thoroughly washed with DCM (4 x 2mL). Then, $Pd(PPh_3)_4$ (0.10 eq), PhSi (10.00 eq) in DCM (1.5 mL) was added to the resin (3 x 20 min). The resin was

washed with DCM (x3) and DMF (2 mL) was added. The linear peptoids were left to cyclise on resin overnight.

7.5. Experimental data for Chapter 2

7.5.1. Synthesis of Boc-protected *N,N*-diethylethylenediamine (45)

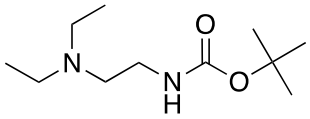

45

Using the general procedure described in **Section 7.4.3, 44** (12.1 mL, 86 mmol, 1.00 eq) was Boc-protected, yielding the desired product **45** as a yellow oil (15.1 g, 84%).

LRMS (TOF MS ES$^+$) calcd for $C_{11}H_{24}N_2O_2$: 217.33; found: 217.32.

^{1}H NMR (400 MHz, $CDCl_3$) δ 5.03 (br, 1H, N*H*), 3.18 (d, ^{3}J = 7.0 Hz, 2H, CH_2), 2.60 – 2.51 (m, 6H, CH_2), 1.44 (s, 9H, ^{t}Bu-CH_3), 0.99 (t, ^{3}J = 7.0 Hz, 6H, CH_2CH_3).

All physical and spectroscopic data match those previously reported.[1]

7.5.2. Synthesis of *N,N,N*-triethylethylenediamine (49)

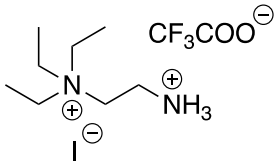

49

To a solution of **45** (7.90 g, 36.0 mmol, 1 eq) in DCM (70 mL) was carefully added idiodoethane (5 mL, excess). The reaction mixture was brought to reflux and stirred overnight. Volatiles were evaporated in vacuo, and the resulting white solid was suspended in Et_2O (100 mL), filtered, and engaged in a Boc-cleavage using the procedure in **Section 7.4.4** to yield the desired product (**49**) as an amber solid (8.10 g, quant).

HRMS (TOF MS ES$^+$) calcd for $C_8H_{22}N_2^{2+}$: 145.1705; found: 145.1728

^{1}H NMR (400 MHz, DMSO) δ 8.19 (br, 3H, NH_3), 3.36-3.28 (q, ^{3}J = 7.0 Hz, 6H, CH_2CH$_3$), 3.25 – 3.18 (m, 4H, CH_2), 1.20 (t, ^{3}J = 7.0 Hz, 9H, CH_3).

All physical and spectroscopic data match those previously reported.[1]

7.5.3. Synthesis of *N*-Boc protected *N,N,N*-benzyldiethylethylenediamine (48)

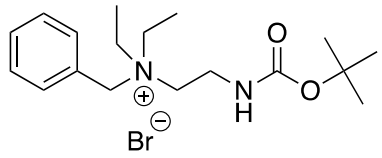

48

A tube was charged with **45** (3.00 g, 1.00 mmol, 1.00 eq) and benzyl bromide (1.81 mL, 1.10 mmol, 1.10 eq). The tube was sealed and the mixture was heated at 40°C for 5 days. Toluene was added to the thick gel and the resulting mixture was allowed to stir overnight at 60°C, resulting in precipitation. The solids were filtered and dried to yield the desired product **48** as a pale-yellow powder (4.60 g, 86%).

LRMS (TOF MS ES$^+$) calcd for $C_{18}H_{31}N_2O_2^+$: 307.458; found: 307.390

^{1}H NMR (400 MHz, DMSO) δ: 7.59-7.48 (m, 5H, Ar*H*), 4.55 (d, 2H, ^{3}J = 2.5 Hz, CH_2), 3.43 (q, 2H, ^{3}J = 7.1 Hz, CH_2), 3.21 (q, 4H, ^{3}J = 7.1 Hz, CH_2), 3.12 (m, 2H, CH_2), 1.41 (s, 9H, ^{t}Bu-CH_3), 1.35 (t, 6H, ^{3}J = 7.1 Hz, CH$_2$CH_3).

All physical and spectroscopic data match those previously reported.[1]

7.5.4. Synthesis of *N,N,N*-benzyldiethylethylenediamine (51)

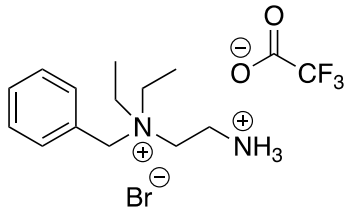

51

Using the general procedure described in **Section 7.4.4**, **45** (1.00 eq) was treated with the cleavage solution. The desired product **51** was collected as a yellow oil (quant).

LRMS (TOF MS ES+): calcd for $C_{13}H_{23}N_2^+$: 207.1851; found: 207.1861.

^{1}H NMR (400 MHz, CD_3CN) δ 7.63 – 7.50 (m, 5H, Ar*H*), 3.70 (m, 2H, CH_2), 3.51 (m, 2H, CH_2), 3.33 – 3.24 (m, 4H, CH_2), 3.09 (m, 2H, CH_2), 1.44 (t, 6H, ^{3}J = 7.2 Hz, CH$_2$CH_3).

All physical and spectroscopic data match those previously reported.[1]

7.5.5. Synthesis of *N,N,N*-diethylpropargylethylenediamine (50)

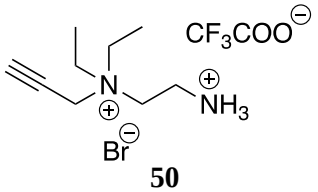

50

A tube was charged with **45** (3.00 g, 1.00 eq) and propargyl bromide 80% wt. in toluene (1.65 g, 1.10 eq). The tube was sealed, and the mixture was allowed to stir at 40 °C for 5 days. Toluene was decanted and the dark brown gel was dried and treated with a cleavage solution (**Section 7.4.4**) The mixture was concentrated in vacuo and the residual TFA was co-evaporated with DCM. The desired product **50** was collected as a viscous dark brown oil (5.10 g, quant).

HRMS (TOF MS ES+): calcd for $C_9H_{19}N_2$: 155.1548; found: 155.1546.

^{1}H NMR (400 MHz, DMSO) δ: 8.64 (br, 3H, N*H*$_3$), 4.49 (d, ^{4}J = 3.0 Hz, 2H, C*H*$_2$), 4.13 (t, ^{4}J = 2.0 Hz, 1H, C*H*), 3.61 – 3.56 (m, 2H, CH$_2$), 3.52 – 3.36 (q, ^{3}J = 7 Hz, 4H, C*H*$_2$), 3.29 – 3.07 (m, 2H, C*H*$_2$), 1.29 (t, ^{4}J = 7 Hz, 6H, C*H*$_3$).

All physical and spectroscopic data match those previously reported.[1]

7.5.6. Synthesis of dodecamer peptoids

The syntheses of a series of linear 12-mer and 15-mer peptoids (**Table 7.1**) were carried out using the general procedures outlined in **Section 7.4.1.**

Table 7.1. A tabulated summary of manually synthesised peptoid dodecamers. [a][M+2]$^{2+}$; [a]after HPLC purification

No.	Sequence	t_R (min)	Calc. mass [M]	Obs. Mass [M+H]$^+$	Pure pdt (mg)	Isolated Yield (%)[a]
Pep. 13	*N*Lys*N*et*N*spe[*N*Lys*N*et*N*et]$_4$	12.5	1585.06	1587.07	5.0	8
Pep. 14	*N*Lys*N*1*f*et*N*spe[*N*Lys*N*1*f*et*N*et]$_4$	10.5	1674.10	1676.67	4.6	7
Pep. 15	*N*Lys*N2f*et*N*spe[NLysN2fetNet]$_4$	12.7	1763.98	1765.12	18.9	20
Pep. 16	*N*Lys*N*3*f*et*N*spe[*N*Lys*N*3*f*et*N*et]$_4$	16.7	1854.92	1855.91	27.1	23
Pep. 17	*N*Lys*N*1*f*et*N*spe[*N*Lys*N*1*f*et*N*1*f*et]$_4$	10.0	1745.98	1748.00	11.1	11
Pep. 18	*N*Lys*N2f*et*N*spe[*N*Lys*N2f*et*N2f*et]$_4$	14.0	1908.89	1909.87	27.3	28
Pep. 19	*N*Lys*N*3*f*et*N*spe[*N*Lys*N*3*f*et*N*3*f*et]$_4$	17.4	2071.82	1035.90[a]	6.9	19
Pep. 6	[*N*Lys*N*spe*N*spe]$_4$	14.9	1819.36	1820.55	22.6	39
Pep. 12	[*N*ae*N*spe*N*spe]$_4$	16.7	1707.11	1707.96	10.2	33
Pep. 20	[*N*Lys*N*Phe*N*Phe]$_4$	20.77	1707.15	1707.86	10.4	28
Pep. 23	[*N*Lys*N*pfb*N*spe]$_4$	23.04	1835.22	1836.07	10.8	26
Pep. 24	[*N*Lys*N*pfbt*N*pfb*N*Lys*N*spe*N*spe]$_2$	20.78	1835.22	1836.26	7.5	26
Pep. 25	*N*amy*Ns*peNspe[*N*Lys*N*spe*N*spe]$_3$	19.3	1818.38	1819.64	11.2	34
Pep. 26	*N*Lys*N*pfbt*N*pfb[*N*Lys*N*spe*N*spe]$_3$	21.65	1827.29	1828.32	12.6	29
Pep. 27	*N*Lys*N*1*f*et*N*1*f*et[*N*Lys*N*spe*N*spe]$_3$	19.91	1702.16	1704.27	20.2	30
Pep. 28	*N*Lys*N*2fet*N*2fet[*N*Lys*N*spe*N*spe]$_3$	20.73	1738.14	1738.99	11.7	32

No.	Sequence	t_R (min)	Calc. mass [M]	Obs. Mass $[M+H]^+$	Pure pdt (mg)	Isolated Yield (%)
Pep. 29	*N*et$_3$ae*N*spe*N*spe[*N*Lys*N*spe*N*spe]$_3^+$	21.70	1876.48	1876.42	10.2	24
Pep. 30	*N*bnet$_2$ae*N*spe*N*spe[*N*Lys*N*spe*N*spe]$_3^+$	21.61	1938.55	1938.49	6.9	17
Pep. 31	*N*et$_3$ae*N*1*f*et*N*1*f*et[*N*Lys*N*spe*N*spe]$_3^+$	19.73	1760.26	1761.29	14.2	37
Pep. 32	*N*bnet$_3$ae*N*1*f*et*N*1*f*et[*N*Lys*N*spe*N*spe]$_3^+$	21.38	1822.33	1822.16	7.5	14
Pep. 33	*N*bnet$_3$ae*N*2*f*et*N*2*f*et[*N*Lys*N*spe*N*spe]$_3^+$	20.46	1858.32	1858.04	10.2	16
Pep. 34	*N*et$_2$pgae*N*2*f*et*N*2*f*et[*N*Lys*N*spe*N*spe]$_3^+$	22.49	1806.24	1806.12	9.2	41
Pep. 35	*N*et$_3$ae*N*1*f*et*N*1*f*et[*N*ae*N*speNspe]$_3^+$	19.85	1676.97	1676.02	16.6	57
Pep. 36	[*N*et$_3$ae*N*1*f*et*N*1*f*et*N*Lys*N*spe*N*spe]$_2^{2+}$	16.32	1700.16	850.61*	8.7	20
Pep. 37	[*N*et$_2$bnae*N*Phe*N*Phe*N*Lys*N*spe*N*spe]$_2^{2+}$	21.36	2000.19	1000.84	8.8	11
Pep. 38	[*N*bnet$_3$ae*N*1*f*et*N*spe*N*ae*N*spe*N*spe]$_2^{2+}$	22.74	1857.36	928.73*	8.3	19

7.6. Experimental data for Chapter 3

7.6.1. Synthesis of *O*-TFP *o*-aminophenol (107)

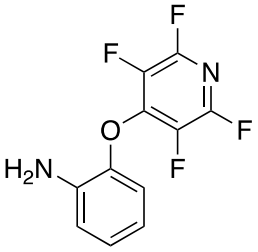

107

Using the general procedure described in **Section 7.4.6, 113** (2.00 g, 18.3 mmol, 1.00 eq) was TFP-protected, yielding the desired product **107** as a light-yellow solid (4.40 g, 93%).

HRMS (TOF MS ES+): calcd for $C_{11}H_7F_4N_2O$: 259.0495; found 259.0502.

^{1}H NMR (400 MHz, $CDCl_3$) δ 7.03 (td, ^{3}J = 8.0, ^{2}J = 1.2, 1H, Ar*H*), 6.86 (dd, ^{3}J = 8.0, ^{2}J = 1.8, 1H, Ar*H*), 6.77 (dd ^{3}J = 8.0, ^{2}J = 1.2, 1H, Ar*H*), 6.71 (td, ^{3}J = 8.0, ^{2}J = 1.4, 1H, Ar*H*).

^{19}F NMR (400 MHz, $CDCl_3$) δ -88.72 – -88.87 (m, 2F), 155.3 – -155.45 (m, 2F).

^{13}C NMR (101 MHz, $CDCl_3$): 157.0, 148.3, 145.6-145.1 (m), 143.1 –142.7 (m), 137.9 – 137.4 (m), 135.23 – 134.8 (m), 130.6, 111.8, 106.1, 103.3.

7.6.2. Synthesis of *O*-TFP *m*-aminophenol (108)

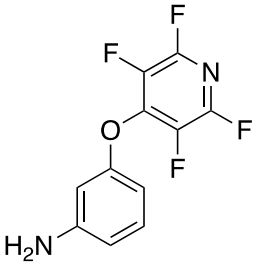

108

Using the general procedure described in **Section 7.4.6, 114** (2.00 g, 18.3 mmol, 1.00 eq) was TFP-protected, yielding the desired product **108** as an off-white solid (4.50 g, 95%).

HRMS (TOF MS ES+): calcd for $C_{11}H_7F_4N_2O$: 259.0495; found: 259.0496.

^{1}H NMR (400 MHz, $CDCl_3$) δ 7.16-7.10 (m, 1H, Ar*H*), 6.51-6.48 (m, 1H, Ar*H*), 6.39-6.34 (m, 2H, Ar*H*).

^{19}F NMR (400 MHz, $CDCl_3$) δ -88.80 – -89.04 (m, 2F), -154.24 – -154.46 (m, 2F).
^{13}C NMR (101 MHz, $CDCl_3$): 151.0, 143.6, 145.6-145.1 (m), 143.6, 143.2 –142.7 (m), 137.7 –137.1 (m), 137.0, 134.9 –134.4 (m), 126.2, 118.6, 117.0.

7.6.3. Synthesis of *N*-Boc *p*-aminophenol (105)

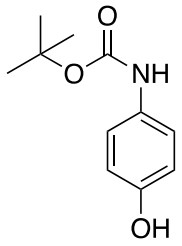

116

Using the general procedure described in **Section 7.4.3**, **115** (2.50 g, 23 mmol, 1.00 eq) was Boc-protected, yielding the desired product **116** as a white solid after flash column chromatography (2.30 g, 48%).

HRMS (TOF MS ES+): calcd for $C_{11}H_{15}NO_3$ = 210.1130; found: 210.1137.
^{1}H NMR (400 MHz, DMSO): 7.26 – 7.20 (m, 2H, Ar*H*), 6.81 – 6.75 (m, 2H, Ar*H*), 1.53 (s, 9H, ^{t}Bu-CH_3).
^{13}C NMR (101 MHz, $CDCl_3$): 152.7, 151.3, 135.7, 119.9, 117.6, 80.9, 28.3.
Physical and spectroscopic data match those previously reported.[2]

7.6.4. Synthesis of *N*-Boc, *O*-TFP *p*-aminophenol (117)

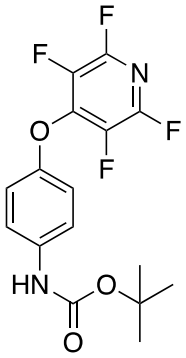

117

Using the general procedure described in **Section 7.4.6**, **116** (2.30 g, 11.0 mmol, 1.00 eq) was TFP-protected, yielding the desired product **117** as a white solid (3.70 g, 94%).

HRMS (TOF MS ES+): calcd for $C_{16}H_{15}F_4N_2O_3$: 359.1019; found: 359.1018.

^{1}H NMR (400 MHz, $CDCl_3$) δ 7.43 – 7.37 (m, 2H, Ar*H*), 7.06 – 7.00 (m, 2H, Ar*H*), 1.54 (s, 9H, ^{t}Bu-C*H*$_3$).

^{19}F NMR (400 MHz, $CDCl_3$) δ -88.59 – -88.87 (m), -155.24 – -155.43 (m)

^{13}C NMR (101 MHz, $CDCl_3$) δ 152.7, 151.3, 145.6 – 145.1 (m), 143.2 – 142.7 (m), 137.6 – 137.0 (m), 135.0 – 134.4 (m), 135.7, 119.9, 117.6, 80.9.

7.6.5. Synthesis of *O*-TFP *p*-aminophenol (109)

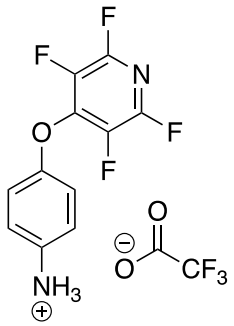

109

Using the general procedure described in **Section 7.4.4**, **117** (97 mg, 0.27 mmol, 1.00 eq) was treated with a cleavage solution to produce **109** as a white solid (113 mg, quant).

HRMS (TOF MS ES+): calcd for $C_{11}H_7F_4N_2O$: 259.0495; found: 259.0499.

^{1}H NMR (400 MHz, DMSO): 7.00 – 6.94 (m, 2H, Ar*H*), 6.59 – 6.53 (m, 2H, Ar*H*).

^{19}F NMR (400 MHz, DMSO): -91.47 – -91.74 (m, 2F), 156.07 – -156.31 (m, 2F).

^{13}C NMR (101 MHz, DMSO): 146.9, 146.8, 145.6 – 145.1 (m), 143.1 – 142.4 (m), 137.7 – 137.2 (m), 135.2 – 134.7 (m), 118.2, 114.8.

7.6.6. Synthesis of *N*-Boc *o*-aminomethylphenol (122)

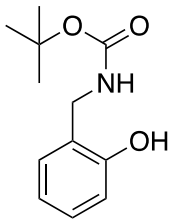

122

Using the general procedure described in **Section 7.4.3**, **119** (3.00 g, 24.4 mmol, 1.00 eq) was Boc-protected, yielding the desired product **122** as a white solid (4.70 g, 85%).

HRMS (TOF MS ES-): calcd for $C_{12}H_{16}NO_3$: 222.1130; found: 222.1126.

^{1}H NMR (400 MHz, $CDCl_3$) δ 8.92 (br, 1H, ArO*H*), 7.23 (td, 1H, ^{3}J = 7.2, ^{4}J = 1.6, Ar*H*), 7.08 (dd, 1H, ^{3}J = 7.2, ^{4}J = 1.7, Ar*H*), 6.97 (dd, 1H, ^{3}J = 8.2, ^{4}J = 1.2, Ar*H*), 6.85 (td, 1H, ^{3}J = 7.4, ^{4}J = 1.2, Ar*H*), 4.26 (d, 2H, ^{3}J = 6.8, CH_2), 1.47 (s, 9H, ^{t}Bu-CH_3).

^{13}C NMR (126 MHz, $CDCl_3$) δ 158.4, 155.8, 130.6, 129.9, 124.9, 119.8, 117.8, 81.3, 41.3, 28.3.

Physical and spectroscopic data match those previously reported.[3]

7.6.7. Synthesis of *N*-Boc, *O*-TFP *o*-aminomethylphenol (125)

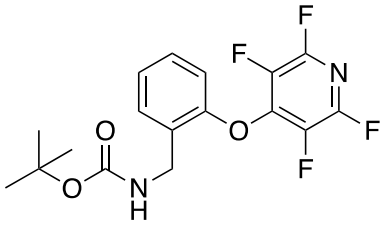

125

Using the general procedure described in **Section 7.4.6, 122** (0.68 g, 3.04 mmol, 1.00 eq) was TFP-protected using yielding the **125** as an off-white solid (1.12 g, 99%).

HRMS (TOF MS ES+): calcd for $C_{17}H_{17}F_4N_2O_3$: 373.1175; found: 373.1161.

^{1}H NMR (400 MHz, $CDCl_3$) δ 7.44 (dd, 1H, ^{3}J = 7.4 Hz, ^{2}J = 1.9 Hz, Ar*H*), 7.27 (m, 1H, Ar*H*), 7.21 (td, 1H, ^{3}J = 7.4 Hz, ^{2}J = 1.3 Hz, Ar*H*), 6.81 (dd, 1H, ^{3}J = 8.1 Hz, ^{2}J = 1.2 Hz, Ar*H*), 4.49 (d, 2H, ^{3}J = 6.2 Hz, CH_2), 1.44 (s, 9 H, ^{t}Bu-CH_3).

^{19}F NMR (400 MHz, $CDCl_3$) δ -88.50 – 88.76 (m, 2F), -154.80 – -155.09 (m, 2F).

^{13}C NMR (101 MHz, $CDCl_3$) δ 155.8, 153.9, 145.6 - 145.2 (m), 143.7 - 142.7 (m), 137.6 - 137.08 (m), 135.0 - 134.5 (m), 130.2, 128.9, 128.7, 125.5, 115.5, 79.7, 39.6, 28.3.

7.6.8. Synthesis of *O*-TFP *o*-aminomethylphenol (110)

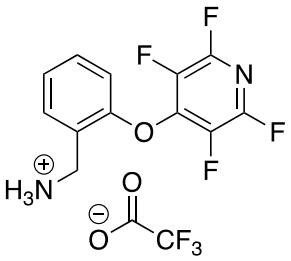

110

Using the general procedure described in **Section 7.4.4**, **125** (293 mg) was treated with a cleavage solution to produce **110** as a yellow wax (307 mg, quant).

HRMS (TOF MS ES+) calcd for $C_{12}H_9F_4N_2O$: 273.0651; found: 273.0655.

^{1}H NMR (400 MHz, DMSO) δ 8.46 (br, 3H, N*H*$_3$), 7.62 (dd, 1H, ^{3}J = 7.6 Hz, ^{4}J = 1.7 Hz, Ar*H*), 7.43 (td, 1H, ^{3}J = 7.6 Hz, ^{4}J = 1.1 Hz, Ar*H*), 7.37 – 7.25 (m, 2H, Ar*H*), 4.23 (q, 2H, ^{3}J = 5.8 Hz, C*H*$_2$).

^{19}F NMR (400 MHz, DMSO) δ -90.74 – -91.01 (m, 2F), -154.47 – 154.79 (m, 2F).

^{13}C NMR (101 MHz, DMSO) δ 154.0, 144.2 – 143.8 (m), 143.0 – 142.5 (m), 138.1 – 137.7 (m), 135.6 – 135.0 (m), 131.3, 131.0, 125.7, 123.63, 117.6, 116.3, 37.3.

7.6.9. Synthesis of *N*-Boc *m*-aminomethylphenol (123)

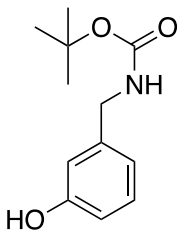

123

Using the general procedure described in **Section 7.4.3**, **120** (2.50 g, 20.3 mmol, 1.00 eq) was Boc-protected, yielding the desired product **123** as a pale-yellow oil after FC chromatography (gradient of EtOAc/hexane, 4.30 g, 95%).

HRMS (TOF MS ES-): calcd for $C_{12}H_{16}NO_3$ = 222.1130; found: 222.1133.

^{1}H NMR (400 MHz, $CDCl_3$) δ 7.19 (t, 1H, ^{3}J = 8.0 Hz, Ar*H*), 6.75-6.82 (m, 3H, Ar*H*), 4.62 (d, 2H, ^{3}J = 8.0 Hz, CH_2), 1.48 (s, 9H, ^{t}Bu-CH_3).

^{13}C NMR (126 MHz, $CDCl_3$) δ 156.3, 140.4, 129.8, 119.3, 114.5, 114.3, 79.9, 44.5, 28.5.

Physical and spectroscopic data match those previously reported.[4]

7.6.10. Synthesis of *N*-Boc, *O*-TFP *m*-aminomethylphenol (126)

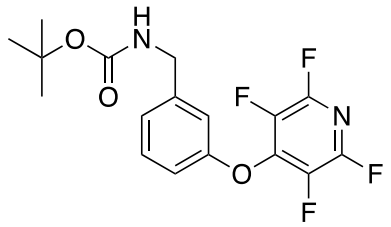

126

Using the general procedure described in **Section 7.4.6**, **123** (1.00 g, 4.47 mmol, 1.00 eq) was TFP-protected yielding **126** as an off-white solid after flash column chromatography (gradient of 100% hexane to 100% EtOAc, 1.60 g, 95%).

HRMS (TOF MS ES-): calcd for $C_{17}H_{15}F_4N_2O_3$: 371.1019; found: 371.1021.

^{1}H NMR (400 MHz, $CDCl_3$) δ 7.33 (t, 1H, ^{3}J = 7.9 Hz, Ar*H*), 7.13 (d, 1H, ^{3}J = 7.6 Hz, Ar*H*), 7.01 (t, 1H, ^{3}J = 2.0 Hz, Ar*H*), 6.94 (dd, 1H, ^{3}J = 8.2 Hz, ^{4}J = 2.7 Hz, Ar*H*), 5.10 (br, 1H, N*H*), 4.31 (d, 2H, ^{3}J = 6.2 Hz, CH_2), 1.44 (s, 9 H, ^{t}Bu-CH_3).

^{19}F NMR (400 MHz, $CDCl_3$) δ -88.68 (m, 2F), -154.21 (m, 2F).

^{13}C NMR (101 MHz, $CDCl_3$) δ 156.0, 145.6 - 145.1 (m), 143.2 - 142.7 (m), 142.0, 137.8-137.2 (m), 135.1 - 134.6 (m), 130.1, 124.0, 115.5, 115.3, 79.8, 44.1, 28.3.

7.6.11. Synthesis of *O*-TFP *m*-aminomethylphenol (111)

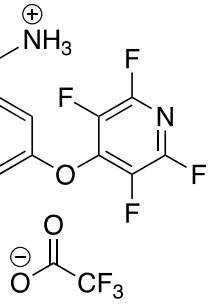

111

Using the general procedure described in **Section 7.4.4, 126** (197 mg) was Boc-deprotected to yield **111** as a light-yellow solid (265 mg, 100%).

HRMS (TOF MS ES+) calcd for $C_{12}H_9F_4N_2O$: 273.0651; found: 273.0632.

^{1}H NMR (400 MHz, DMSO) δ 8.29 (br, 3H, N*H*$_3$) 7.50 (t, 1H, ^{3}J = 7.9 Hz, Ar*H*), 7.38-7.29 (m, 3H, Ar*H*), 4.06 (q, ^{3}J = 5.8 Hz, C*H*$_2$).

^{19}F NMR (400 MHz, DMSO) δ -90.33 – -90.52 (m, 2F), -154.68 – -154.88 (m, 2F).

^{13}C NMR (101 MHz, DMSO) δ 156.1, 145.6-145.1 (m), 143.2-142.7 (m), 142.0, 137.8-137.2 (m), 137.0, 135.1 - 134.6 (m), 131.0, 125.7, 116.8, 116.6, 42.2.

7.6.12. Synthesis of *N*-Boc *p*-aminomethylphenol (124)

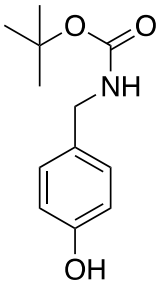

124

Using the general procedure described in **Section 7.4.3**, **121** (2.00 g, 16.2 mmol, 1.00 eq) in DCM (20 mL) was Boc-protected to yield **124** as a colourless oil (gradient of EtOAc/hexane, 2.60 g, 73%).

HRMS (TOF MS ES+): calcd for $C_{12}H_{18}NO_3$ = 224.1287; found: 224.1279.

^{1}H NMR (400 MHz, $CDCl_3$) δ 7.12 (d, 2H, ^{3}J = 8.1, Ar*H*), 6.79 (d, 2H, ^{3}J = 8.1, Ar*H*), 4.24 (d, 2H, ^{3}J = 4.2, C*H*$_2$), 1.49 (s, 9H, C*H*$_3$).

^{13}C NMR (101 MHz, $CDCl_3$) δ 156.2, 155.5, 130.3, 128.5, 115.5, 79.8, 44.2, 28.5

Physical and spectroscopic data match those previously reported.[5]

7.6.13. Synthesis of *N*-Boc, *O*-TFP p-aminomethylphenol (127)

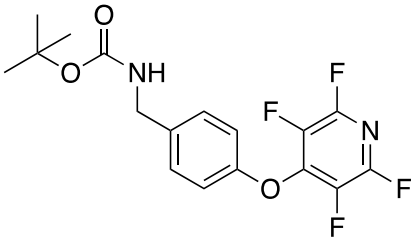

127

Using the general procedure described in **Section 7.4.6, 124** (1.00 g, 4.47 mmol, 1.00 eq) was TFP-protected using, yielding **127** as an off-white solid (1.63 g, 98%).

HRMS (TOF MS ES-): calcd for $C_{17}H_{15}F_4N_2O_3$: 371.1019; found: 371.1010.

^{1}H NMR (400 MHz, $CDCl_3$) δ 7.43-7.37 (m, 2H, Ar*H*), 7.05-7.00 (m, 2H, Ar*H*), 4.05 (s, 2H, CH_2), 1.54 (s, 9H, ^{t}Bu-CH_3).

^{19}F NMR (400 MHz, $CDCl_3$) δ -88.69 – -88.90 (m, 2F), -154.58 – -154.77 (m, 2F).

^{13}C NMR (101 MHz, $CDCl_3$) δ 161.0, 159.6, 150.3 – 149.7 (m), 147.9 – 147.2 (m), 143.1 – 142.6 (m), 142.2, 140.5 – 140.0 (m), 133.8, 121.4, 83.1, 47.9, 33.4.

7.6.14. Synthesis of *O*-TFP *p*-aminomethylphenol (112)

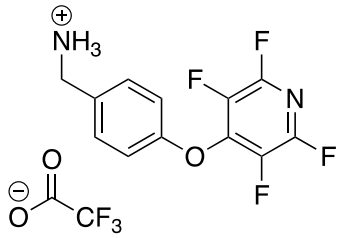

112

Using the general procedure described in **Section 7.4.4**, **127** (1.00 g, 2.7 mmol, 1.00 eq) was Boc-deprotected, yielding **112** as a yellow waxy solid (1.17 quant.).

HRMS (TOF MS ES+) calcd for $C_{12}H_9F_4N_2O$: 273.0651; found: 273.0643.

^{1}H NMR (400 MHz, DMSO) δ 8.29 (br, 3H, NH_3), 7.60-7.50 (m, 2H, Ar*H*), 7.40-7.32 (m, 2H, Ar*H*), 4.06 (s, 2H, CH_2).

^{19}F NMR (400 MHz, DMSO) δ -90.49 – -90.70 (m, 2F), -154.87 – -155.09 (m, 2F).

^{13}C NMR (101 MHz, DMSO) δ 145.5 - 144.9 (m), 143.2 - 142.5 (m), 138.6 - 137.8 (m), 135.8 -135.2 (m), 131.5, 131.1, 130.9, 116.9, 115.8, 42.0.

7.6.15. Synthesis of 2-bromo-1-piperidinyl ethanone (129)

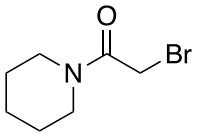

129

A solution of **128** (1.00 g, 5.46 mmol, 1.00 eq) in DCM (10 mL) was added dropwise to a solution of piperidine (0.50 g, 5.46 mmol, 1.00 eq) and DIPEA (1.41 mL, 5.46 mmol, 1.00 eq) in anhydrous DCM (10 mL), at 0°C, in N_2 atmosphere. This reaction mixture was stirred for 1 hour. It was then partitioned between H_2O and DCM, the aqueous layer was extracted with DCM twice, the organics were combined and dried over $MgSO_4$. The resulting suspension was filtered and concentrated *in vacuo*. **129** was collected as a light brown oil (0.80 g, 76%). No purification was performed.

HRMS (TOF MS ES+): calcd for $C_7H_{13}NOBr$: 206.0181; found: 206.0187.

^{1}H NMR (400 MHz, $CDCl_3$) δ 3.88 (s, 2H, C*H*$_2$), 3.58-3.51 (m, 2H, pip-C*H*$_2$), 3.47-3.40 (m, 2H, pip-C*H*$_2$), 1.69-1.51 (m, 6H, pip-C*H*$_2$).

^{13}C NMR (101 MHz, $CDCl_3$) δ 165.4, 48.0, 43.4, 26.2, 26.0, 25.4, 24.2.

Physical and spectroscopic data match those previously reported.[1]

7.6.16. Substitution of *O*-TFP *o*-aminomethylphenol (107) with piperidyl ethanone to form 138

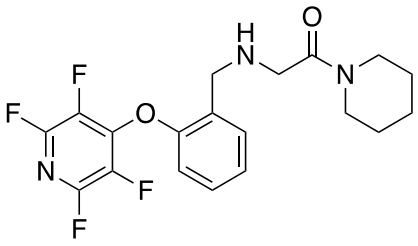

138

A suspension of **110** (180 mg, 0.47 mmol, 2.00 eq) and Cs_2CO_3 (304 mg, 0.47 mmol, 2.00 eq) in 5 mL was stirred at RT for 10 mins before **129** (48 mg, 0.24 mmol, 1.00 eq) was added. The resulting reaction mixture was brought to 80°C and stirred for 2 h. Subsequently,

the mixture was filtered and partitioned between EtOAc (10 mL), and water (10 mL) and the aqueous phase was extracted with EtOAc thrice. The organics were combined, dried with $MgSO_4$, filtered and concentrated *in vacuo*. The obtained residue was purified by flash column chromatography, and the fractions containing the desired product were combined and concentrated *in vacuo*, which yielded **137** as an off-white solid (21%, 38 mg).

HRMS (TOF MS ES+): calcd for $C_{19}H_{20}F_4N_3O_2$: 398.1492; found: 398.1472.
^{1}H NMR (400 MHz, $CDCl_3$) δ 7.35 – 7.26 (m, 2H, Ar*H*), 6.99 (td, *J* = 7.5, 1.1 Hz, 1H, Ar*H*), 6.91 (m, 1H, Ar*H*), 6.34 (br, 1H, N*H*), 4.82 (s, 2H, CH_2), 4.76 (s, 2H, CH_2), 3.62 (t, ^{3}J = 5.6 Hz, 2H, pip-CH_2), 3.42 (t, ^{3}J = 5.4 Hz, 2H, pip-CH_2), 1.74-1.56 (m, pip-CH_2, 6H).
^{19}F NMR (400 MHz, $CDCl_3$) δ -94.96 – -95.21 (m, 2F), -162.59 – -162.85 (m, 2F)
^{13}C NMR (101 MHz, $CDCl_3$) δ 171.2, 165.6, 156.5, 130.0, 129.6, 121.8, 112.1, 66.2, 45.7, 45.0, 43.2, 26.4, 25.4, 24.4. (C-F signals too weak – not detectable).

7.6.17. Synthesis of 2-benzyloxy-1-(1-piperidinyl)ethanone (143)

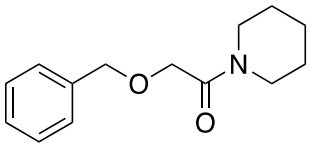

143

A solution of piperidine (0.54 mL, 0.73 mmol, 1.00 eq) in THF (10 mL) was treated with benzyloacetyl chloride (**142**) (0.85 mL, 0.73 mmol, 1.00 eq) and TEA (0.82 mL, 0.87 mmol, 1.20 eq). The resulting reaction mixture was stirred overnight and subsequently concentrated *in vacuo* before being partitioned between DCM (20 mL) and a 1 M solution of citric acid (20 mL). The aqueous layer was extracted with DCM twice. The organics were combined, dried with $MgSO_4$, filtered and concentrated *in vacuo*. The desired product **143** was recovered as a yellow oil (201 mg, 99%).

HRMS (TOF MS ES+): calcd for $C_{14}H_{20}NO_2$: 234.1494; found: 234.1490.
^{1}H NMR (400 MHz, $CDCl_3$) δ 7.37-7.27 (m, 5H, Ar*H*), 4.60 (s, 2H, CH_2), 4.17 (s, 2H, CH_2), 3.57 (t, 2H, ^{3}J = 5.6 Hz, pip-CH_2), 3.40 (t, 2H, J = 5.6 Hz, pip-CH_2), 1.66-1.49 (m, 6H, pip-CH_2)
^{13}C NMR (101 MHz, $CDCl_3$) δ 167.3, 137.5, 128.4, 128.0, 127.8, 73.0, 69.4, 46.0, 42.8, 26.4, 25.6, 24.4.

7.6.18. Synthesis of 2-hydroxy-1-(1-piperidyl)ethanone (144)

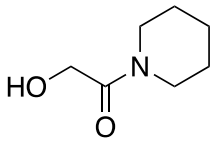

144

143 (530 mg, 2.27 mmol, 1.00 eq) was hydrogenated using the general procedure in section **7.4.5**. **144** was recovered as a yellow oil (320 mg, 98%).

HRMS (TOF MS ES+): calcd for $C_7H_{14}NO_2$: 144.1025; found: 144.1020.

^{1}H NMR (400 MHz, $CDCl_3$) δ 4.16 (s, 2H, CH_2), 3.60 (t, 2H, ^{3}J = 5.6 Hz, pip-CH_2), 3.19 (t, 2H, ^{3}J = 5.6 Hz, pip-CH_2), 1.54-1.70 (m, 6H, pip-CH_2)

^{13}C NMR (101 MHz, $CDCl_3$) δ 169.7, 59.7, 44.4, 43.5, 26.1, 25.4, 24.3.

Physical and spectroscopic data match those previously reported.[6]

7.6.19. Synthesis of *N*-Ns, *O*-TFP *p*-aminomethylphenol (146)

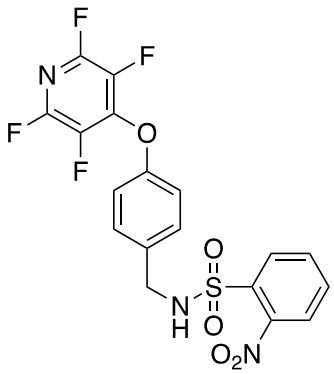

146

To a solution of **145** (66 mg, 0.428 mmol, 1 eq) and TEA (0.12 mL, 0.51 mmol, 1.20 eq) in DCM (2 mL) was added a TFA salt of **112** (150 mg, 0.39 mmol, 1.10 eq), at 0 °C. The reaction mixture was allowed to warm up to RT and stir overnight, before being diluted with DCM (5 mL) and washed with 1 M solution of citric acid (5 mL). The aqueous phase was then extracted with DCM twice. The organics were combined, dried with $MgSO_4$, filtered and concentrated *in vacuo*. **146** was collected as a pale-yellow wax (157 mg, 88%).

HRMS (TOF MS ES+): calcd for $C_{18}H_{12}N_3O_5S$: 458.0434; found: 458.0420.

^{1}H NMR (400 MHz, $CDCl_3$) δ 8.03 (m, 1H, Ar*H*), 7.86 (m, 1H, Ar*H*), 7.74-7.68 (m, 2H, Ar*H*), 7.31-7.27 (m, 2H, Ar*H*), 6.97-6.92 (m, 2H, Ar*H*), 4.36 (s, 2H, CH_2)

^{19}F NMR (400 MHz, $CDCl_3$) δ -88.08 – -88.27 (m, 2F), -153.99 – -154.18 (m 2F)

^{13}C NMR (101 MHz, $CDCl_3$) δ 155.4, 147.8, 145.7 – 145.1 (m), 143.2 – 142.7 (m), 137.7 – 137.1 (m), 135.0 – 134.5 (m), 134.0, 133.6, 132.9, 132.8, 130.9, 129.7, 125.4, 116.7, 47.0.

7.6.20. Substitution of *N*-Ns *O*-TFP *p*-aminomethylphenol (146) with piperidyl ethanone to form 147

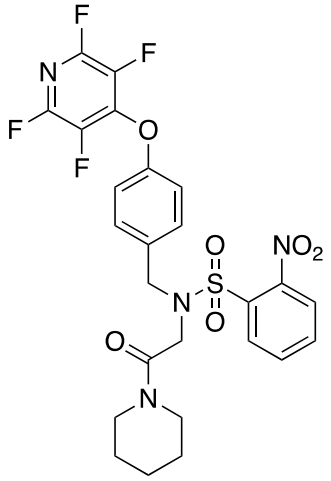

147

At 0°C, under N_2, to a solution of **146** (40 mg, 8.8 x 10^{-2} mmol, 1 eq) and DIPEA (15 µL, 8.8 x 10^{-2} mmol, 1.00 eq) in THF (2 mL) was added **129** (18 mg, 9.7 x 10^{-2} mmol, 1.10 eq). The mixture was brought to RT and stirred for 2 hours, before volatiles were evaporated *in vacuo*. The residue was purified by flash column chromatography, using a gradient of 100% hexane to 100% EtOAc, and **147** was recovered as a white solid (38 mg, 49%).

HRMS (TOF MS ES+): calcd for $C_{25}H_{22}F_4N_4O_6S$: 582.1196; found: 582.1247.

^{1}H NMR (400 MHz, $CDCl_3$) δ 8.15 (m, 1H, Ar*H*), 7.73-7.67 (m, 2H, Ar*H*), 7.65 (m, 1H, Ar*H*), 7.39-7.33 (m, 2H, Ar*H*), 7.05-7.00 (m, 2H, Ar*H*), 4.74 (s, 2H, CH_2), 4.10 (s, 2H, CH_2), 4.42 (t, 2H, ^{3}J = 5.6 Hz, pip-CH_2), 3.23 (t, 2H, ^{3}J = 5.6 Hz, pip-CH_2), 1.66-1.44 (m, 6H, pip-CH_2)

^{19}F NMR (400 MHz, $CDCl_3$) δ -88.10 – -88.43 (m, 2F), -154.03 – -154.27 (m, 2F)

^{13}C NMR (101 MHz, $CDCl_3$) δ 164.87, 155.55, 148.04, 145.83-145.04 (m), 143.36-142.98 (m), 141.95, 137.67-137.13 (m), 135.1-134.6 (m), 133.6, 133.4, 132.2, 131.7, 130.7, 130.5, 124.1, 116.9, 51.2, 47.1, 45.9, 43.1, 26.0, 25.4, 24.3.

7.6.21. Synthesis of *N*-Boc, *O*-Bnz *o*-aminomethylphenol (150)

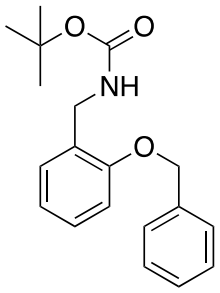

150

Using the general procedure described in **Section 7.4.8**, **122** (500 mg, 2.20 mmol, 1.00 eq), was reacted with benzyl bromide (0.27 mL, 2.64 mmol, 1.20 eq). After workup and purification, 645 mg (92%) of **150** was recovered as a white waxy solid.

HRMS (TOF MS ES-): calcd for $C_{19}H_{22}NO_3$: 312.1600; found: 312.1607.

^{1}H NMR (400 MHz, $CDCl_3$) δ 7.22-7.48 (m, 7H, Ar*H*), 6.96 (t, 2H, ^{3}J = 8.0 Hz, Ar*H*), 5.13 (s, 2H, CH_2), 4.39 (s, 2H, CH_2), 1.46 (s, 9H, ^{t}Bu-CH_3).

^{13}C NMR (126 MHz, $CDCl_3$) δ 156.57, 156.12, 136.94, 129.37, 128.66, 128.60, 128.00, 127.45, 127.25, 120.94, 111.62. 79.2, 70.0, 40.5, 28.5.

Physical and spectroscopic data match those previously reported.[7]

7.6.22. Synthesis of *N*-Boc, *O*-Bnz *m*-aminomethylphenol (151)

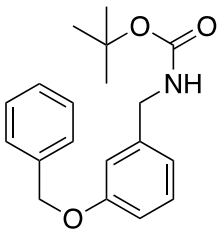

151

Using the general procedure described in **Section 7.4.8**, **123** (555 mg, 2.49 mmol, 1.00 eq) was reacted with benzyl bromide (363 μL, 3.00 mmol, 1.20 eq). After workup and purification, 650 mg (84%) of **151** was recovered as a pale-yellow oil.

HRMS (TOF MS ES+): calcd for $C_{19}H_{24}NO_3$: 314.1756; found: 314.1754.

^{1}H NMR (400 MHz, $CDCl_3$) δ 7.34-7.49 (m, 5H, Ar*H*), 7.28 (t, 1H, J = 8 Hz, Ar*H*), 6.89-7.00 (m, 3H, Ar*H*), 5.07 (s, 2H, CH_2), 4.32 (s, 2H, CH_2), 1.53 (s, 9 H, ^{t}Bu-CH_3)

^{13}C NMR (126 MHz, $CDCl_3$) δ 159.1, 156.0, 140.8, 137.0, 129.7, 128.7, 128.63 128.0, 127.6, 120.0, 113.9,113.6, 79.4, 69.9, 44.6, 28.5.

Physical and spectroscopic data match those previously reported.[8]

7.6.23. Synthesis of *N*-Boc, *O*-Bnz *p*-aminomethylphenol (152)

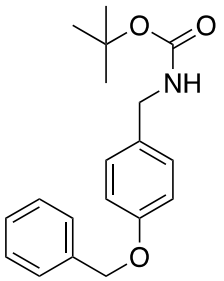

152

Using the general procedure described in **Section 7.4.8**, **124** (625 mg, 2.80 mmol, 1.00 eq) was reacted with benzyl bromide (327 μL, 3.40 mmol, 1.20 eq). After workup and purification, 607 mg (69%) of **152** was recovered as a white solid.

HRMS (TOF MS ES+): calcd for $C_{19}H_{24}NO_3$: 314.1756; found: 314.1748.

^{1}H NMR (400 MHz, $CDCl_3$) δ 7.31-7.49 (m, 5H, Ar*H*), 7.23 (d, 2H, ^{3}J = 8.1 Hz, Ar*H*), 6.96 (d, 2H, ^{3}J = 8.1 Hz, Ar*H*), 5.08 (s, 2H, CH_2), 4.27 (s, 2H, CH_2), 1.48 (s, 9H, ^{t}Bu-CH_3)

^{13}C NMR (126 MHz, $CDCl_3$) δ 158.1, 155.84 137.0, 132.0, 131.3, 128.9, 128.6, 128.0, 127.5, 115.0, 77.1, 70.1, 44.2, 28.4.

Physical and spectroscopic data match those previously reported.[9]

7.6.24. Synthesis of *O*-Bnz *o*-aminomethylphenol (153)

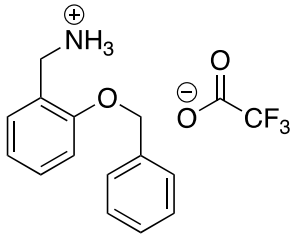

153

Using the general procedure described in **Section 7.4.4**, **150** (600 mg, 1.90 mmol, 1.00 eq) was treated with a cleavage solution. **153** was recovered as a pale-yellow oil (815 mg, quant).

HRMS (TOF MS ES-): calcd for $C_{14}H_{16}NO$: 214.1232; found: 214.1230.

^{1}H NMR (400 MHz, $CDCl_3$) δ 7.57 (br, 3H, N*H*$_3$), 7.34-7.43 (m, 6H, Ar*H*), 7.23 (dt, 1H, ^{3}J = 7.5, ^{4}J = 1.4 Ar*H*), 6.95-7.03 (m, 2H, Ar*H*), 5.16 (s, 2H, C*H*$_2$), 4.16 (s, 2H, C*H*$_2$).

^{13}C NMR (126 MHz, $CDCl_3$) δ 156.7, 135.7, 131.4, 131.0, 128.9, 128.6, 127.6, 121.6, 119.8, 112.1, 70.56 41.4.

Physical and spectroscopic data match those previously reported.[10]

7.6.25. Synthesis of *O*-Bnz *m*-aminomethylphenol (154)

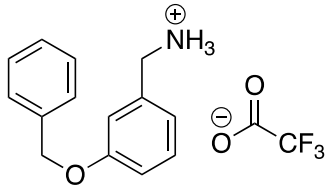

154

Using the general procedure described in **Section 7.4.4**, **151** (650 mg, 2.10 mmol, 1.00 eq) was treated with a cleavage solution. **154** was recovered as a white solid (quant).

HRMS (TOF MS ES+): calcd for $C_{14}H_{16}NO$: 214.1232; found: 214.1228.

^{1}H NMR (400 MHz, CD_3OD) δ 7.29-7.48 (m, 6H, Ar*H*), 7.02-7.14 (m, 3H, Ar*H*), 5.13 (s, 2H, C*H*$_2$), 4.10 (s, 2H, C*H*$_2$).

^{13}C NMR (126 MHz, CD_3OD) 159.4, 137.0, 134.5, 130.0, 128.2, 127.7, 127.2, 120.8, 115.2, 115.0, 69.6, 42.8.

Physical and spectroscopic data match those previously reported.[11]

7.6.26. Synthesis of *O*-Bnz *p*-aminomethylphenol (155)

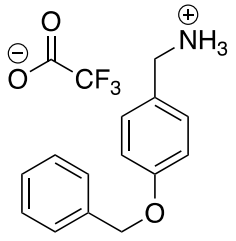

155

Using the general procedure described in **Section 7.4.4**, **152** (600 mg, 1.90 mmol, 1.00 eq) was treated with a cleavage solution. **155** was recovered as a white solid (quant).

HRMS (TOF MS ES+) calcd for $C_{14}H_{16}NO$: 214.1232; found: 214.1232.

^{1}H NMR (400 MHz, DMSO) δ 8.07 (br, 3H, N*H*$_3$), 7.28-7.50 (m, 7H, Ar*H*), 7.03-7.09 (m, 2H, Ar*H*), 5.14 (s, 2H, C*H*$_2$), 3.96 (s, 2H, C*H*$_2$).

^{13}C NMR (126 MHz, DMSO) δ 158.9, 137.4, 131.0, 129.0, 128.3, 128.1, 126.6, 115.4, 69.6, 42.3.

Physical and spectroscopic data match those previously reported.[11]

7.6.27. Synthesis of the model peptoid containing aniline (130)

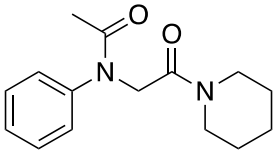

130

Using the general procedure in **Section 7.4.9**, **129** (80 mg, 0.39 mmol, 1.00 eq) in 10 mL ACN was reacted with aniline (148 μL, 1.55 mmol, 4.00 eq). The crude was then acetylated. After workup and purification, **130** was recovered as a pale-yellow oil (71 mg, 68%).

HRMS (TOF MS ES+): calcd for $C_{15}H_{20}N_2O_2$: 261.1603; found: 261.1597.

^{1}H NMR (599 MHz, $CDCl_3$) δ **major conformation (*trans*)**: 7.42-7.27 (m, 5H, Ar*H*), 4.43 (s, 2H, C*H*$_2$), 3.51 (t, 2H, ^{3}J = 3.6 Hz, pip-C*H*$_2$), 3.33 (t, 2H, ^{3}J = 3.6 Hz, pip-C*H*$_2$), 1.91 (s, 3H, ac-C*H*$_3$), 1.63-1.46 (m, 6H, pip-C*H*$_2$). **minor conformation (*cis*)**: Peaks unassignable.

^{13}C NMR (151 MHz, $CDCl_3$) δ 170.9, 165.8, 143.8, 129.5, 128.2, 127.9, 51.1, 45.8, 43.2, 26.2, 25.4, 24.4, 22.3. **minor conformation (*cis*)**: Peaks unassignable.

^{1}H NMR (599 MHz, CD_3CN) δ **major conformation (*trans*)**: 7.42-7.27 (m, 5H, Ar*H*), 4.43 (s, 2H, CH_2), 3.51 (t, 2H, ^{3}J = 3.6 Hz, pip-CH_2), 3.33 (t, 2H, 3J = 3.6 Hz, pip-CH_2), 1.83 (s, 3H, ac-CH_3), 1.63-1.46 (m, 6H, pip-CH_2). **minor conformation (*cis*)**: Peaks unassignable.
^{13}C NMR (151 MHz, CD_3CN) δ **major conformation (*trans*)**: 170.5, 166.7, 144.8, 130.0 129.0, 128.4, 118.0, 51.4, 46.1, 43.3, 26.8, 26.1, 24.8, 22.2. **minor conformation (*cis*)**: Peaks unassignable.
^{1}H NMR (599 MHz, CD_3OD) δ **major conformation (*trans*)**: 7.45-7.31 (m, 5H, Ar*H*), 4.51 (s, 2H, CH_2), 3.51 (t, 2H, 3J = 5.6 Hz, pip-CH_2), 3.41 (t, 2H, 3J = 5.6 Hz, pip-CH_2), 1.89 (s, 3H, ac-CH_3), 1.67-1.49 (m, 6H, pip-CH_2). **minor conformation (*cis*)**: Peaks unassignable.
^{13}C NMR (151 MHz, CD_3OD) δ **major conformation (*trans*)**: 171.8, 166.4, 143.5, 129.3, 128.0, 127.6, 50.9, 45.6, 43.0, 25.8, 25.2, 23.9, 20.9. **minor conformation (*cis*)**: Peaks unassignable.
Physical and spectroscopic data match those previously reported.[12]

7.6.28. Synthesis of the model peptoid containing benzylamine (40)

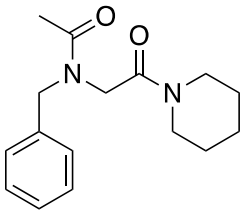

40

Using the general procedure described in **Section 7.4.9**, **129** (80 mg, 0.39 mmol, 1.00 eq) in 10 mL ACN was reacted with benzylamine (430 μL, 1.55 mmol, 4.00 eq). The crude was then acetylated. After workup and purification, **40** was recovered as a pale-yellow oil (118 mg, 99%).

HRMS (TOF MS ES+): calcd for $C_{16}H_{23}N_2O_2$: 275.1760; found: 275.1765.
^{1}H NMR (599 MHz, $CDCl_3$) δ **major conformation (*trans*)**: 7.37-7.16 (m, 5H, Ar*H*), 4.56 (s, 2H, CH_2), 4.12 (s, 2H, CH_2), 3.52 (t, 2H, ^{3}J = 5.5 Hz, pip-CH_2), 3.29 (t, 2H, ^{3}J = 5.5 Hz, pip-CH_2), 2.19 (s, 3H, ac-CH_3), 1.65-1.43 (m, 6H, pip-CH_2). **minor conformation (*cis*)**: 7.37-7.16 (m, 5H, Ar*H*), 4.63 (s, 2H, CH_2), 3.90 (s, 2H, CH_2), 3.54 (t, 2H, ^{3}J = 3.6 Hz, pip-CH_2), 3.20 (t, 2H, ^{3}J = 3.6 Hz, pip-CH_2), 2.07 (s, 3H, ac-CH_3), 1.65-1.43 (m, 6H, pip-CH_2).

^{13}C NMR (151 MHz, $CDCl_3$) δ **major conformation (*trans*)**: 171.7, 166.3, 136.7, 129.0, 127.8, 126.8, 52.8, 46.0, 46.0, 43.2, 26.3, 25.5, 24.5, 21.5. **minor conformation (*cis*)**: 171.7, 165.6, 137.5, 128.7, 128.5, 127.5, 49.6, 48.4, 45.8, 43.5, 26.5, 25.7, 24.4, 21.6.

^{1}H NMR (599 MHz, CD_3CN) δ **minor conformation (*trans*)**: 7.41-7.22 (m, 5H, Ar*H*), 4.48 (s, 2H, CH_2), 4.05 (s, 2H, CH_2), 3.49 (t, 2H, ^{3}J = 3.7 Hz, pip-CH_2), 3.26 (t, 2H, ^{3}J = 3.7 Hz, pip-CH_2), 2.97 (s, 3H, ac- CH_3), 1.66-1.45 (m, 6H, pip-CH_2). **major conformation (*cis*)**: 7.41-7.22 (m, 5H, Ar*H*), 4.57 (s, 2H, CH_2), 4.07 (s, 2H, CH_2), 3.46 (t, 2H, ^{3}J = 4.0 Hz, pip-CH_2), 3.30 (t, 2H, ^{3}J = 4.0 Hz, pip-CH_2), 2.09 (s, 3H, ac-CH_3), 1.66-1.45 (m, 6H, pip-CH_2).

^{13}C NMR (151 MHz, CD_3CN) δ **minor conformation (*trans*)**: 170.9, 166.0, 137.6, 128.7, 127.3, 127.0, 52.5, 46.4, 45.3, 42.5, 25.9, 25.4, 24.2. **major conformation (*cis*)**: 171.5, 165.8, 138.2, 128.4, 127.8, 126.9, 49.4, 49.2, 45.3, 42.8, 26.0, 25.4, 24.1.

^{1}H NMR (599 MHz, CD_3OD) δ **major conformation (*trans*)**: 7.41-7.22 (m, 5H, Ar*H*), 4.65 (s, 2H, CH_2), 4.19 (s, 2H, CH_2), 3.52 (m, 2H, pip-CH_2), 3.37 (t, 2H, ^{3}J = 5.6 Hz, pip-CH_2), 2.19 (s, 3H, ac-CH_3), 1.69-1.47 (m, 6H, pip-CH_2). **minor conformation (*cis*)**: 7.41-7.22 (m, 5H, Ar*H*), 4.57 (s, 2H, CH_2), 4.19 (s, 2H, CH_2), 3.52 (m, 2H, pip-CH_2), 3.34-3.29 (m, 2H, pip-CH_2), 2.07 (s, 3H, ac-CH_3), 1.69-1.47 (m, 6H, pip-CH_2).

^{13}C NMR (151 MHz, CD_3OD) δ **major conformation (*trans*)**: 172.9, 166.6, 136.4, 128.6, 127.4, 126.6, 52.8, 46.6, 45.5, 42.9, 25.8, 25.2 23.9, 20.0. **minor conformation (*cis*)**: 173.3, 166.3, 136.8, 128.2, 127.9, 127.1, 49.6, 48.6, 45.4, 43.1, 25.9, 25.3, 23.9, 20.0.

Physical and spectroscopic data match those previously reported.[13]

7.6.29. Synthesis of the model peptoid containing *O*-TFP *o*-aminophenol (135)

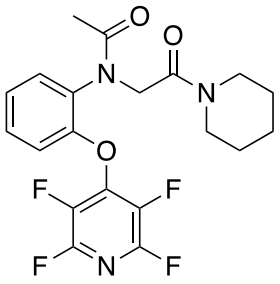

135

Using the general procedure described in **Section 7.4.9**, **129** (300 mg, 1.46 mmol, 1.00 eq) in 10 mL ACN was reacted with **107** (452 mg, 1.75 mmol, 1.20 eq). The crude was then acetylated. After workup and purification, **135** was recovered as a pale-yellow oil (29 mg, 5%).

HRMS (TOF MS ES+): calcd for $C_{20}H_{20}F_4N_3O_3$: 426.1446; found: 426.1441.

^{19}F NMR (376 MHz, $CDCl_3$) δ -87.43 – -87.67 (m, 2F), -154.43 – -154.66 (m, 2F).

^{1}H NMR (599 MHz, $CDCl_3$) δ **major conformation (*trans*)**: 7.84 (dd, 1H, ^{3}J = 7.9 Hz, ^{4}J = 1.7 Hz, Ar*H*), 7.32 (td, 1H, ^{3}J = 7.8 Hz, ^{4}J = 1.7 Hz, Ar*H*), 7.24 (td, 2H, ^{3}J = 7.5 Hz, ^{4}J = 1.3 Hz, Ar*H*), 7.15 (dq, 1H, ^{3}J = 8.4 Hz, ^{4}J = 1.3 Hz, Ar*H*), 5.11 (d, 1H, ^{3}J = 16.0 Hz, CH_2), 3.70 (d, 1H, ^{3}J = 16.0 Hz, CH_2), 3.59-3.25 (m, 4H, pip-CH_2), 1.95 (s, 3H, ac-CH_3), 1.68-1.45 (m, 6H, pip-CH_2). **minor conformation (*cis*)**: Peaks unassignable.

^{13}C NMR (151 MHz, $CDCl_3$) δ **major conformation (*trans*)**: 170.9, 165.6, 151.1, 145.2-144.7 (m), 143.5-143.1 (m), 137.0-136.7 (m), 135.2-134.8 (m), 133.0, 132.3, 129.7, 126.1, 115.9, 49.6, 45.9, 43.2, 26.1, 25.4, 24.4, 21.5. **minor conformation (*cis*)**: Peaks unassignable.

^{19}F NMR (376 MHz, CD_3CN) δ **major conformation (*trans*)**: -91.18 – -91.56 (m, 2F), -154.43 – -154.66 (m, 2F). **minor conformation (*cis*)**: -91.96 – -92.29 (m, 2F), -156.48 – -156.81 (m, 2F).

^{1}H NMR (599 MHz, CD_3CN) δ **major conformation (*trans*)**: 7.75 (dd, 1H, ^{3}J = 7.9 Hz, ^{4}J = 1.9 Hz, Ar*H*), 7.40 (td, 1H, ^{3}J = 8.1 Hz, ^{4}J = 1.9 Hz, Ar*H*), 7.31 (td, 1H, ^{3}J = 7.8 Hz, ^{4}J = 1.6 Hz, Ar*H*), 7.13 (1H, m, Ar*H*), 4.6 (d, 1H, ^{3}J = 16.2 Hz, CH_2), 3.85 (d, 1H, ^{3}J = 16.2 Hz, CH_2), 3.53-3.26 (m, 4H, pip-CH_2), 1.88 (d, 3H, ^{3}J = 1.9 Hz), 1.66-1.41 (m, 6H, pip- CH_2). **minor conformation (*cis*)**: 7.47 (dt, 1H, ^{3}J = 7.9 Hz, ^{4}J = 1.9 Hz, Ar*H*), 7.31 (m, 2H, Ar*H*), 7.19 (d, ^{3}J = 8.2 Hz, Ar*H*), 3.53-3.26 (m, 4H, pip-CH_2), 1.99 (d, 3H, ^{3}J = 1.9 Hz, ac-CH_3), 1.66-1.41 (m, 6H, pip-CH_2), other peaks overlap with major conformer.

^{13}C NMR (151 MHz, CD_3CN) δ **major conformation (*trans*)**: 170.1, 165.7, 151.3, 145.1-144.7 (m), 143.4 - 143.2 (m), 137.5 - 137.1 (m), 135.7-135.3 (m), 133.0, 131.7, 129.8, 125.9, 116.7, 49.6, 45.4, 42.6, 25.9, 25.3, 24.1, 20.9. **minor conformation (*cis*)**: 171.5, 165.8, 151.1, 134.0, 130.4, 128.6, 126.0, 118.0, 52.4, 49.6, 45.4, 45.3, 42.9, 42.6, 25.4, 24.0, other peaks overlap with major conformer.

^{19}F NMR (376 MHz, CD_3OD) δ **major conformation (*trans*)**: -91.40 – -91.72 (m, 2F), -156.90 – -157.26 (m, 2F). **minor conformation (*cis*)**: -91.78 – -92.05 (m, 2F), -157.11 – -157.56 (m, 2F).

^{1}H NMR (599 MHz, CD_3OD) δ **major conformation (*trans*)**: 7.71 (dd, 1H, ^{3}J = 7.9 Hz, ^{4}J = 1.7 Hz, Ar*H*), 7.42 (td, 1H, ^{3}J = 8.3 Hz, ^{3}J = 7.5 Hz, ^{4}J = 1.7 Hz, Ar*H*), 7.31 (td, 1H, ^{3}J = 7.7 Hz, ^{4}J = 1.3 Hz, Ar*H*), 7.17 (m, 1H, Ar*H*), 5.00 (d, 1H, ^{3}J = 16.3 Hz, CH_2), 3.98 (d, 1H, ^{3}J = 16.3 Hz, CH_2), 3.59-3.34 (m, 4H, pip-CH_2), 1.95 (s, 3H, ac-CH_3), 1.68-1.50 (m, 6H, pip-CH_2). **minor conformation (*cis*)**: 7.48 (dd, 1H, ^{3}J = 7.9 Hz, ^{4}J = 1.7 Hz, Ar*H*), 7.36 – 7.33 (m, 1H, Ar*H*), 7.25 (m, 1H, Ar*H*), 2.11 (s, 3H, ac-CH_3), other peaks overlap with major conformer.

^{13}C NMR (151 MHz, CD_3OD) δ **major conformation (*trans*)**: 172.3, 166.1, 145.0-144.7 (m), 143.5-143.1 (m), 137.3-137.0 (m), 135.1-135.2 (m), 132.4, 130.8, 130.1, 125.7, 116.3, 49.9, 45.7, 43.0, 25.8, 25.3, 23.9, 20.2. **minor conformation (*cis*)**: 173.3, 166.2, 132.9, 129.9, 128.9, 125.6, 117.4, 52.5, 45.5, 43.2, 25.9, 25.5, 23.8, 20.1, other peaks overlap with major conformer.

7.6.30. Synthesis of the model peptoid containing *O*-TFP *m*-aminophenol (136)

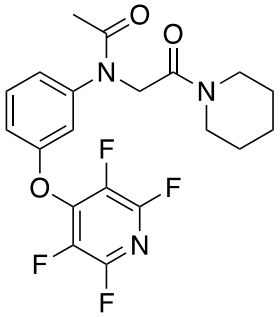

136

Using the general procedure described in **Section 7.4.9**, **129** (300 mg, 1.46 mmol, 1.00 eq) in 10 mL ACN was reacted with **107** (452 mg, 1.75 mmol, 1.20 eq). The crude was then acetylated. After workup and purification, **136** was recovered as a pale-yellow wax (35 mg, 7%).

HRMS (TOF MS ES+): calcd for $C_{20}H_{20}F_4N_3O_3$: 426.1441; found: 426.1442.

^{19}F NMR (376 MHz, $CDCl_3$) δ -87.99 – -88.30 (m, 2F), -153.92 – -154.24 (m, 2F).

^{1}H NMR (599 MHz, $CDCl_3$) δ **major conformation (*trans*)**: 7.41 (t, *J* = 8.1 Hz, 1H, Ar*H*), 7.31 – 7.26 (m, 2H, Ar*H*), 7.04 (dd, *J* = 8.3, 3.0 Hz, 1H, Ar*H*), 4.43 (s, 2H, CH_2), 3.53 (t, *J* = 5.7 Hz, 2H, pip-CH_2), 3.35 (t, *J* = 5.6 Hz, 2H, pip-C*H*2), 1.77 (s, 3H, ac-CH_3), 1.67 – 1.51 (m, 6H, pip-CH_2). **minor conformation (*cis*):** peaks not assignable.

^{13}C NMR (151 MHz, $CDCl_3$) δ **major conformation (*trans*)**: 170.5, 165.5, 156.0, 145.5, 145.2 – 144.8 (m), 143.7 – 143.1 (m), 137.1 – 136.6 (m), 135.3 – 134.8 (m), 130.8, 125.1, 117.1, 116.2, 50.9, 45.9, 43.3, 26.2, 25.4, 24.4, 22.2. **minor conformation (*cis*):** peaks not assignable.

^{19}F NMR (376 MHz, CD_3CN) δ -91.40 – -91.77 (m, 2F), -155.99 – -156.29 (m, 2F).

^{1}H NMR (700 MHz, CD_3CN) δ **major conformation (*trans*)**: 7.38 (t, *J* = 8.1 Hz, 1H. Ar*H*), 7.26 – 7.18 (m, 2H, Ar*H*), 7.09 – 7.07 (m, 2H, Ar*H*), 4.34 (s, 2H, CH_2), 3.36 (t, *J* = 5.7 Hz, 2H, pip-CH_2), 3.26 (t, *J* = 5.6 Hz, 2H, pip-CH_2), 1.77 (s, 3H, ac-CH_3), 1.55 – 1.34 (m, 6H, pip-CH_2). **minor conformation (*cis*)**: peaks not assignable.

^{13}C NMR (176 MHz, CD_3CN) δ **major conformation (*trans*)**: 170.2, 166.3, 156.5, 146.2, 144.2 – 143.8 (m), 138.1 – 137.7 (m), 136.5 – 136.2 (m), 131.3, 125.6, 117.4, 116.4, 51.1, 45.9, 43.1, 26.5, 25.9, 24.6, 22.1. **minor conformation (*cis*):** peaks not assignable.

^{19}F NMR (376 MHz, CD_3OD) δ -90.92 – -93.02 (m, 2F), -156.24 – -157.55 (m, 2F).

^{1}H NMR (599 MHz, CD_3OD) δ **major conformation (*trans*)**: 7.51 (t, *J* = 8.2 Hz, 1H, Ar*H*), 7.35 – 7.29 (m, 2H, Ar*H*), 7.26 – 7.21 (m, 1H, Ar*H*), 4.52 (s, 2H, *CH*$_2$), 3.53 (m, 2H, pip-*CH*$_2$), 3.44 (m, 2H, pip-*CH*$_2$), 1.93 (s, 3H, ac-*CH*$_3$), 1.70 – 1.50 (m, 6H, pip-*CH*$_2$). **minor conformation (*cis*)**: peaks not assignable.

^{13}C NMR (151 MHz, CD_3OD) δ **major conformation (*trans*)**: 171.6, 166.3, 156.3, 145.0, 143.8 – 142.9 (m), 137.4 – 136.9 (m), 135.7 – 135.2 (m), 130.9, 124.4, 116.2, 50.8, 45.6, 43.0, 25.8, 25.2, 23.9, 20.8. **minor conformation (*cis*):** peaks not assignable.

7.6.31. Synthesis of the model peptoid containing *O*-TFP *p*-aminophenol (137)

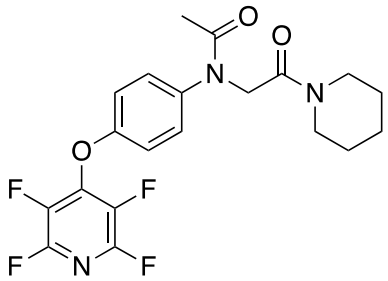

137

Using the general procedure described in **Section 7.4.9**, **129** (300 mg, 1.46 mmol, 1.00 eq) was reacted with **108** (452 mg, 1.75 mmol, 1.20 eq). The crude was then acetylated. After workup and purification, **137** was recovered as a pale-yellow wax (39 mg, 6%).

HRMS (TOF MS ES+): calcd for $C_{15}H_{20}F_4N_3O_3$: 426.1441; found: 426.1420.

^{19}F NMR (400 MHz, $CDCl_3$) δ **major conformation (*trans*)**: -87.87 – -88.11 (m, 2F), -153.82 – -154.03 (m, 2F). **minor conformation (*cis*)**: -87.61 – -88.21 (m, 2F), -154.33 – 154.58 (m, 2F).

^{1}H NMR (599 MHz, $CDCl_3$) δ **major conformation (*trans*)**: 7.47 (d, 2H, ^{3}J = 8.4 Hz, Ar*H*), 7.05 (d, 2H, ^{3}J = 8.4 Hz, Ar*H*), 4.42 (s, 2H, CH_2), 3.52 (t, 2H, ^{3}J = 5.6 Hz, pip-CH_2), 3.34 (t, 2H, ^{3}J = 5.6 Hz, pip-CH_2), 1.91 (s, 3H, ac-CH_3), 1.67-1.49 (m, 6H, pip-CH_2). **minor conformation (*cis*)**: 7.55 (d, 2H, ^{3}J = 8.5 Hz, Ar*H*), 7.00 (d, 2H, ^{3}J = 8.6 Hz, Ar*H*), 2.15 (s, 3H, ac-CH_3), other peaks overlap with major conformer.

^{13}C NMR (151 MHz, $CDCl_3$) δ **major conformation (*trans*)**: 170.8, 165.6, 154.9, 145.1-144.8 (m), 143.5-143.2 (m), 137.2-136.9 (m), 135.4-135.1 (m), 140.8, 130.2, 117.5, 51.0, 45.9, 43.2, 26.2, 25.4, 24.4, 22.3. **minor conformation (*cis*)**: 121.2, 117.3, rest of peaks unassignable due to weak signals.

^{19}F NMR (400 MHz, CD_3CN) δ **major conformation (*trans*)**: -91.23 - -91.86 (m, 2F), -155.87 – -156.36 (m, 2F). **minor conformation (*cis*)**: -91.86 – -92.19 (m, 2F), -155.87 – -156.36 (m, 2F).

^{1}H NMR (599 MHz, CD_3CN) δ **major conformation (*trans*)**: 7.48 (d, 2H, ^{3}J = 8.8 Hz, Ar*H*), 7.20 (d, 2H, ^{3}J = 8.8 Hz, Ar*H*), 4.43 (s, 2H, CH_2), 3.46 (t, 2H, ^{3}J = 5.6 Hz, pip-CH_2), 3.35 (t, 2H, ^{3}J = 5.8 Hz, pip-CH_2), 1.83 (s, 3H, ac-CH_3), 1.65-1.44 (m, 6H, pip-CH_2). **minor conformation (*cis*)**: 7.60 (d, 2H, ^{3}J = 8.4 Hz, Ar*H*), 7.14-7.11 (m, 2H, Ar*H*), 4.48 (s, 2H, CH_2), 3.54-3.50 (m, 2H, pip-CH_2), 2.06 (s, 3H, ac-CH_3), other peaks overlap with major conformer.

^{13}C NMR (151 MHz, CD_3CN) δ **major conformation (*trans*)**: 169.9, 165.9, 154.9, 145.2 - 144.7 (m), 143.5 - 143.2 (m), 141.0, 137.7 - 137.3 (m), 130.3, 117.3, 117.2, 50.7, 45.4, 42.6, 26.0, 25.4, 24.1, 21.5. **minor conformation (*cis*)**: peaks not assignable.

^{19}F NMR (400 MHz, CD_3OD) δ **major conformation (*trans*)**: -91.65 – -92.04 (m, 2F), -156.77 – -157.15 (m. 2F). **minor conformation (*cis*)**: -92.26 – -92.54 (m, 2F), -157.31 (m, 2F).

^{1}H NMR (599 MHz, CD_3OD) δ **major conformation (*trans*)**: 7.51-7.47 (m, 2H, Ar*H*), 7.25-7.22 (m, 2H, Ar*H*), 4.51 (s, 2H, CH_2), 3.52 (t, 2H, ^{3}J = 3.8 Hz, pip-CH_2), 3.42 (t, 2H, ^{3}J = 3.8 Hz, pip-CH_2), 1.91 (s, 3H, ac-CH_3), 1.68-1.50 (m, 6H, pip-CH_2). **minor conformation (*cis*)**: 7.59-7.56 (m, 2H, Ar*H*), 7.13-7.10 (m, 2H, Ar*H*), 2.11 (s, 3H, ac-CH_3), other peaks overlap with major conformer.

^{13}C NMR (151 MHz, CD_3OD) δ **major conformation (*trans*)**: 171.9, 166.3, 155.4, 145.1-144.7 (m), 143.5 - 143.3 (m), 140.3, 137.4-137.1 (m), 140.3, 135.7 - 135.3 (m), 129.7, 117.2, 50.9, 45.6, 43.0, 25.8, 25.2, 23.9, 20.8. **minor conformation (*cis*)**: 128.8, 121.2, other peaks are unassignable due to weak signals.

7.6.32. Synthesis of the model peptoid containing *o*-aminophenol (60)

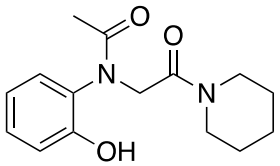

60

Using the general procedure described in **Section 7.4.7**, **135** (25.0 mg, 0.09 mmol, 1.00 eq) was TFP-deprotected. **60** was recovered as an off-white solid (23.0 mg, 74%).

HRMS (TOF MS ES+): calcd for $C_{15}H_{21}N_2O_3$: 277.1552; found: 277.1554.

^{1}H NMR (599 MHz, $CDCl_3$) δ **major conformation (*trans*)**: 10.81 (s, 1H, ArO*H*), 7.22 (m, 1H, Ar*H*), 7.05 – 6.98 (m, 2H, Ar*H*), 6.85 (m, 1H, Ar*H*), 5.23 (d, 1H, J = 16.1 Hz, CH_2), 3.64 – 3.55 (m, 2H, pip-CH_2), 3.53 (d, 1H, J = 16.0 Hz, CH_2), 3.46 – 3.31 (m, 2H, pip-CH_2), 1.88 (s, 3H, ac-CH_3), 1.75 – 1.47 (m, 6H, pip-CH_2). **minor conformation (*cis*)**: peaks not assignable.

^{13}C NMR (151 MHz, $CDCl_3$) δ **major conformation (*trans*)**: 172.1, 168.4, 154.8, 130.4, 128.4, 120.2, 118.8, 50.9, 46.1, 43.9, 26.0, 25.3, 24.2, 21.3. **minor conformation (*cis*)**: peaks not assignable.

^{1}H NMR (599 MHz, CD_3CN) δ **major conformation (*trans*)**: 10.87 (s, 1H, ArO*H*), 7.26 (m, 1H, Ar*H*), 7.18 (dd, *J* = 7.8, 1.7 Hz, 1H, Ar*H*), 6.95 – 6.88 (m, 2H, Ar*H*), 5.12 (d, *J* = 16.5 Hz, 1H, CH_2), 3.79 (d, *J* = 16.5 Hz, 1H, CH_2), 3.68 (d, *J* = 16.5 Hz, 1H, pip-CH_2), 3.61 – 3.47 (m, 1H, pip-CH_2), 3.35 – 3.47 (m, 2H, pip-CH_2), 1.74 (s, 3H, ac-CH_3), 1.68 – 1.47 (m, 6H, pip-CH_2). **minor conformation (*cis*)**: peaks not assignable.

^{13}C NMR (151 MHz, CD_3CN) δ **major conformation (*trans*)**: 171.7, 169.2, 155.7, 131.0, 130.2, 129.1, 119.8, 117.9, 50.8, 45.7, 43.4, 25.7, 25.3, 23.9, 20.5. **minor conformation (*cis*)**: peaks not assignable.

^{1}H NMR (599 MHz, CD_3OD) δ **major conformation (*trans*)**: 7.25 (m, 1H, Ar*H*), 7.20 (dd, *J* = 7.8, 1.6 Hz, 1H, Ar*H*), 6.94 (dd, *J* = 8.2, 1.4 Hz, 1H, Ar*H*), 6.90 (m, 1H, Ar*H*), 4.96 (d, *J* = 16.5 Hz, 1H, CH_2), 3.95 (d, *J* = 16.5 Hz, 1H, CH_2), 3.63 – 3.38 (m, 4H, pip-CH_2), 1.82 (s, 3H, ac-CH_3), 1.72 – 1.50 (m, 6H, pip-CH_2). **minor conformation (*cis*)**: peaks not assignable.

^{13}C NMR (151 MHz, CD_3OD) δ **major conformation (*trans*)**: 172.8, 168.4, 154.0, 130.4, 130.1, 128.6, 120.2, 117.7, 50.7, 45.7, 43.4, 25.7, 25.1, 23.9, 19.9. **minor conformation (*cis*)**: peaks not assignable.

Physical and spectroscopic data match those previously reported.[12]

7.6.33. Synthesis of the model peptoid containing *m*-aminophenol (103)

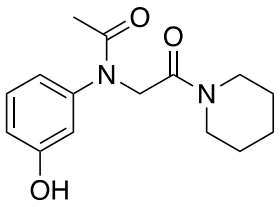

103

Using the general procedure described in **Section 7.4.7**, **136** (47.0 mg, 0.11 mmol, 1.00 eq) was TFP-deprotected. **103** was recovered as an off-white solid (23.0 mg, 74%).

HRMS (TOF MS ES+): calcd for $C_{15}H_{21}N_2O_3$: 277.1552; found: 277.1548.

^{1}H NMR (599 MHz, $CDCl_3$) δ **major conformation (*trans*)**: 7.80 (br, 1H, ArO*H*), 7.19 (t, 1H, ^{3}J = 8.0 Hz, Ar*H*), 7.03 (t, 1H, ^{3}J = 2.2 Hz, Ar*H*), 6.78 – 6.82 (m, 2H, Ar*H*), 4.46 (s, 2H, CH_2), 3.51 (t, 2H, ^{3}J = 5.6 Hz, pip-CH_2), 3.35 (t, 2H, ^{3}J = 5.4 Hz, pip-CH_2), 1.93 (s, 3H, ac-CH_3), 1.68-1.45 (m, 6H, pip-CH_2). **minor conformation (*cis*)**: peaks not assignable.

^{13}C NMR (151 MHz, $CDCl_3$) δ **major conformation (*trans*)**: 171.43, 166.31, 157.77, 144.37, 130.29, 118.92, 115.62, 115.24, 51.09, 46.00, 43.42, 26.10, 25.35, 24.31, 22.14. **minor conformation (*cis*)**: peaks not assignable.

^{1}H NMR (599 MHz, CD_3CN) δ **major conformation (*trans*)**: 7.30 (br, 1H, ArO*H*), 7.23 (t, 1H, ^{3}J = 8.0 Hz, Ar*H*), 6.92-6.87 (m, 2H, Ar*H*), 6.80 (m, 1H, Ar*H*), 4.40 (s, 2H, CH_2), 3.47 (t, 2H, ^{3}J = 5.5 Hz, pip-CH_2), 3.35 (t, 2H, ^{3}J = 5.5 Hz, pip-CH_2), 1.85 (s, 3H, ac-CH_3), 1.64-1.44 (m, 6H, pip-CH_2). **minor conformation (*cis*)**: peaks not assignable.

^{13}C NMR (151 MHz, CD_3CN) δ **major conformation (*trans*)**: 169.8, 165.7, 157.6, 145.2, 130.1, 119.5, 115.1, 114.7, 50.7, 45.4, 42.6, 26.0, 25.4, 24.1, 21.4. **minor conformation (*cis*)**: peaks not assignable.

^{1}H NMR (599 MHz, CD_3OD) δ **major conformation (*trans*)**: 7.25 (t, 1H, ^{3}J = 7.9 Hz, Ar*H*), 6.93-6.88 (m, 2H, Ar*H*), 6.80 (m, 1H, Ar*H*), 4.48 (s, 2H, CH_2), 3.52 (t, 2H, ^{3}J = 5.5 Hz, pip-CH_2), 3.39 (t, 2H, ^{3}J = 5.5 Hz, pip-CH_2), 1.93 (s, 3H. ac-CH_3), 1.70 – 1.52 (m, 6H, pip-CH_2). **minor conformation (*cis*)**: Peak unassignable.

^{13}C NMR (151 MHz, CD_3OD) δ **major conformation (*trans*)**: 168.9, 165.4, 158.5, 144.1, 130.2, 118.1, 115.2, 114.2, 61.6, 50.7, 45.3, 42.8, 25.8, 25.1, 23.9, 20.6. **minor conformation (*cis*)**: Peak unassignable.

7.6.34. Synthesis of the model peptoid containing *p*-aminophenol (59)

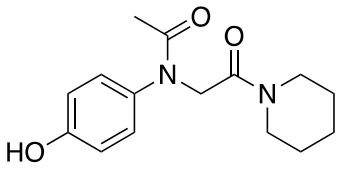

59

Using the general procedure described in **Section 7.4.7**, **137** (39.0 mg, 9.15 x 10^{-2} mmol, 1 eq) was TFP-deprotected. **59** was recovered as an off-white solid (22.0 mg, 88%).

HRMS (TOF MS ES+): calcd for $C_{15}H_{21}N_2O_3$: 277.1552; found: 277.1549.

^{1}H NMR (400 MHz, $CDCl_3$) δ **major conformation (*trans*)**: 8.01 (br, 1H, ArO*H*), 7.16-7.11 (m, 2H, Ar*H*), 6.78-6.70 (m, 2H, Ar*H*), 4.47 (s, 2H, CH_2), 3.52 (t, 2H, ^{3}J = 5.4 Hz, pip-CH_2), 3.39 (t, 2H, ^{3}J = 5.4 Hz, pip-CH_2), 1.89 (s, 3H, ac-CH_3), 1.66-1.50 (m, 6H, pip-CH_2). **minor conformation (*cis*)**: peaks not assignable.

^{13}C NMR (151 MHz, $CDCl_3$) δ **major conformation (*trans*)**: 171.7, 166.5, 156.6, 135.0, 129.0, 116.4, 51.2, 46.1, 43.4, 26.2, 25.4, 24.3, 22.1. **minor conformation (*cis*)**: peaks not assignable.

^{1}H NMR (599 MHz, CD_3CN) δ **major conformation (*trans*)**: 7.27 – 7.22 (m, 2H, Ar*H*), 6.84 – 6.80 (m, 2H, Ar*H*), 4.38 (s, 2H, Ar*H*), 3.46 (t, 2H, ^{3}J = 5.7 Hz, pip-CH_2), 3.34 (t, 2H, ^{3}J = 5.6 Hz, pip-CH_2), 1.80 (s, 3H, ac-CH_2), 1.63 – 1.44 (m, 6H, pip- CH_2). **minor conformation (*cis*)**: peaks not assignable.

^{13}C NMR (151 MHz, CD_3CN) δ **major conformation (*trans*)**: 171.2, 167.0, 157.3, 137.1, 130.5, 122.3, 116.6, 116.0, 51.8, 46.3, 43.5, 26.9, 26.3, 25.1, 22.4. **minor conformation (*cis*)**: peaks not assignable.

^{1}H NMR (599 MHz, CD_3OD) δ **major conformation (*trans*)**: 7.23 – 7.19 (m, 2H, Ar*H*), 6.81 – 6.77 (m, 2H, Ar*H*), 4.45 (s, 2H, CH_2), 3.51(m, 2H, pip-CH_2), 3.40 (m, 2H, pip-CH_2), 1.87 (s, 3H, ac-CH_3), 1.67 – 1.49 (m, 6H, pip-CH_2). **minor conformation (*cis*)**: peaks not assignable.

^{13}C NMR (151 MHz, CD_3OD) δ **major conformation (*trans*)**: 173.9, 168.0, 158.7, 136.5, 130.1, 117.0, 52.5, 49.0, 47.0, 44.4, 27.2, 26.6, 25.4, 22.2. **minor conformation (*cis*)**: peaks not assignable.

Physical and spectroscopic data match those previously reported.[12]

7.6.35. Synthesis of the model peptoid containing *O*-TFP *o*-aminomethylphenol (141)

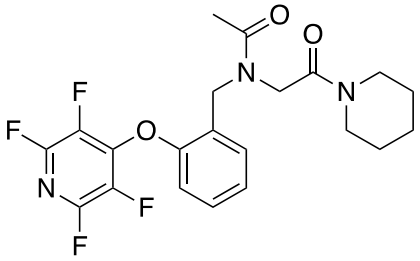

141

A solution of **138** (35 mg, 8.8 x 10^{-2} mmol, 1.0 eq) in DCM (2 mL) was treated with DIPEA (31 μL, 0.18 mmol, 2.00 eq) and then, acetyl chloride (6.3 μL, 0.18 mmol, 2.00 eq) was added dropwise and left to stir for 20 minutes. The mixture was washed with a solution of 1.0 M citric acid (5 mL), and the aqueous layer was extracted with DCM (5 mL) thrice. The organics were combined, dried with $MgSO_4$, filtered and concentrated. The crude material was

purified by flash column chromatography, using a gradient of 100% hexane to 100% EtOAc. **141** was recovered as a pale-yellow oil (39.0 mg, 85%).

HRMS (TOF MS ES+): calcd for $C_{21}H_{21}N_3O_3F_4$: 440.1597; found: 440.1596.

^{19}F NMR (376 MHz, $CDCl_3$) δ **major conformation (*trans*)**: -87.68 – -88.07 (m, 2F), -154.92 – -155.18 (m, 2F). **minor conformation (*cis*)**: -88.17 – -88.55 (m, 2F), -155.20 – 155.43 (m, 2F).

^{1}H NMR (700 MHz, $CDCl_3$) δ **major conformation (*trans*)**: 7.28 – 7.11 (m, 3H, Ar*H*), 6.75 (d, *J* = 8.1 Hz, 1H, Ar*H*), 4.78 (s, 2H, CH_2), 4.11 (s, 2H, CH_2), 3.48 (m, 2H, pip-CH_2), 3.27 (t, *J* = 5.6 Hz, 2H, pip-CH_2), 2.15 (s, 3H, ac-CH_3), 1.61 – 1.42 (m, 6H, pip-CH_2). **minor conformation (*cis*)**: 7.36 (m, 1H, Ar*H*), 7.28 – 7.11 (m, 2H, Ar*H*), 6.73 (d, *J* = 8.2 Hz, 1H, Ar*H*), 4.75 (s, 1H, CH_2), 3.95 (s, 1H, CH_2), 3.48 (m, 2H, pip-CH_2), 3.20 (t, *J* = 5.6 Hz, 2H, pip-CH_2), 2.00 (s, 3H, ac-CH_3), 1.61 – 1.42 (m, 6H, pip-CH_2).

^{13}C NMR (176 MHz, $CDCl_3$) δ **major conformation (*trans*)**: 171.7, 165.9, 153.9, 145.0 – 114.7 (m), 143.6 – 143.3 (m), 137.0 – 136.6 (m), 135.5 – 135.1 (m), 129.3, 128.6, 126.6, 125.6, 115.5, 48.0, 46.0, 45.9, 44.0, 43.1, 26.2, 25.4, 24.4, 21.2. **minor conformation (*cis*)**: δ 171.7, 165.3, 154.2, 145.0, 145.0 – 114.7 (m), 143.6 – 143.3 (m), 137.0 – 136.6 (m), 135.5 – 135.1 (m), 131.2, 129.0, 127.3, 115.4, 48.0, 46.0, 45.9, 44.0, 43.1, 26.3, 25.5, 24.3, 21.4.

^{19}F NMR (376 MHz, CD_3CN) δ **major conformation (*trans*)**: -91.57 – -91.84 (m, 2F), -157.10 – 157.37 (m, 2F). **minor conformation (*trans*)**: -91.57 – -91.84 (m, 2F), -156.87 – -157.09 (m, 2F).

^{1}H NMR (599 MHz, CD_3CN) δ **major conformation (*cis*)**: 7.41 – 7.22 (m, 3H, Ar*H*), 7.00 (m, 1H, Ar*H*), 4.65 (s, 2H, CH_2), 4.14 (s, 2H, CH_2), 3.50 (m, 2H, pip-CH_2), 3.27 (m, 2H, pip-CH_2), 1.96 (s, 3H, ac-CH_3), 1.65 – 1.46 (m, 6H, pip-CH_2). **minor conformation (*trans*)**: 7.41 – 7.22 (m, 3H, Ar*H*), 7.00 (m, 1H, Ar*H*), 4.75 (s, 1H, CH_2), 4.14 (s, 1H CH_2), 3.46 (t, *J* = 5.6 Hz, 2H, pip-CH_2), 3.32 (t, *J* = 5.5 Hz, 2H, pip-CH_2), 2.10 (s, 3H, ac-CH_3), 1.65 – 1.46 (m, 6H, pip-CH_2).

^{13}C NMR (151 MHz, CD_3CN) δ **major conformation (*cis*)**: 171.7, 165.8, 154.0, -145.0 – -144.6 (m), 143.6 – 143.0 (m), 137.5 – 136.8 (m), 135.9 – 135.1 (m), 130.2, 128.8, 127.7, 125.4, 116.0, 49.6, 45.2, 44.5, 42.8, 25.9, 24.1, 20.7. **minor conformation (*trans*)**: 171.0, 165.9, 154.0, -145.0 – -144.6 (m), -143.6 – -143.0 (m), 137.5 – -136.8 (m), -135.9 – 135.1 (m), 129.2, 129.1, 126.9, 125.5, 116.0, 49.6, 45.2, 44.5, 42.8, 25.4, 24.1, 20.5.

^{19}F NMR (376 MHz, CD_3OD) δ **major conformation (*trans*)**: -91.70 – -91.98 (m, 2F), -157.61 – -157.86 (m, 2F). **minor conformation (*cis*)**: -92.03 – -92.30 (m, 2F), -157.86 – -158.06 (m, 2F).

^{1}H NMR (599 MHz, CD_3OD) δ **major conformation (*trans*)**: 7.40 – 7.18 (m, 3H, Ar*H*), 7.05 (dd, *J* = 8.2, 1.1 Hz, 1H, Ar*H*), 4.82 (s, 2H, CH_2), 4.21 (s, 2H, CH_2), 3.50 (m, 2H, pip-CH_2), 3.35 (m, 2H, pip-CH_2), 2.20 (s, 3H, ac-CH_3), 1.69 – 1.49 (m, 6H, pip-CH_2). **minor conformation (*cis*)**: 7.40 – 7.18 (m, 3H, Ar*H*), 7.02 (dd, *J* = 8.2, 1.1 Hz, 1H, Ar*H*), 4.74 (s, 2H, CH_2), 4.26 (s, 2H, CH_2), 3.54 – 3.47 (m, 2H, pip-CH_2), 3.39 – 3.32 (m, 2H, 2.04 (s, 2H), 1.69 – 1.49 (m, 6H).

^{13}C NMR (151 MHz, CD_3OD) δ **major conformation (*trans*)**: 173.0, 166.5, 154.1, 145.3 – 144.6 (m), 143.8 – 142.8 (m), 137.4 – 136.8 (m), 135.7 – 134.7 (m), 129.4, 128.9, 125.8, 125.3, 115.6, 48.0, 46.3, 45.5, 42.9, 25.7, 25.2, 23.9, 19.8. **minor conformation (*cis*)**: 173.4, 166.2, 154.3, 145.3 – 144.57 (m), 143.8 – 142.8 (m), 137.4 – 136.83 (m), 135.7 – 134.7 (m), 130.3, 129.1, 126.4, 125.2, 115.6, 48.9, 45.5, 45.5, 45.4, 44.4, 43.1, 25.9, 25.2, 23.9, 20.0.

7.6.36. Synthesis of the model peptoid containing *O*-Bnz *o*-aminomethylphenol (159)

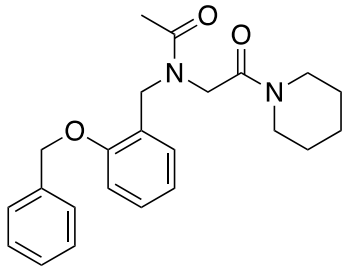

159

Using the general procedure described in **Section 7.4.9**, **129** (100 mg, 0.49 mmol, 1.00 eq) in THF (5 mL) was reacted with a solution of **153** (634 mg, 1.96 mmol, 4.00 eq) and DIPEA (338 μL, 1.96 mmol, 4.00 eq) in THF (7.5 mL). The crude was then acetylated. After workup and purification by FC chromatography using a gradient of 100% hexane to 100% EtOAc, **159** was recovered as a pale-yellow oil (52.0 mg, 28%).

HRMS (TOF MS ES+): calcd for $C_{23}H_{29}N_2O_3$: 381.2178; found: 381.2176.

^{1}H NMR (599 MHz, $CDCl_3$) δ **major conformation (*trans*)**: 7.42-7.30 (m, 6H, Ar*H*), 7.27 (1H, td, ^{3}J = 6.5 Hz, ^{4}J = 1.7 Hz, Ar*H*), 7.12 (m, 1H, Ar*H*), 6.96 (m, 1H, Ar*H*), 5.05 (s, 2H,

CH_2), 4.63 (s, 2H, CH_2), 4.10 (s, 2H, CH_2), 3.50 (t, 2H, ^{3}J = 5.6 Hz, pip-CH_2), 3.21 (t, 2H, ^{3}J = 5.6 Hz, pip-CH_2), 2.08 (s, 3H, ac-CH_3), 1.62-1.41 (m, 6H, pip-CH_2). **minor conformation (*cis*)**: 7.36 (m, 6H, Ar*H*), 7.22 (1H, td, ^{3}J = 7.8 Hz, ^{4}J = 1.8 Hz, Ar*H*), 6.94 – 6.92 (m, 2H, Ar*H*), 5.04 (s, 2H, CH_2), 4.63 (s, 2H, CH_2), 3.97 (s, 2H, CH_2), 3.44 (t, 2H, ^{3}J = 5.6 Hz, pip-CH_2), 2.94 (t, 2H, ^{3}J = 5.6 Hz, pip-CH_2), 1.99 (s, 3H, ac-CH_3), 1.62-1.41 (m, 6H, pip-CH_2).

^{13}C NMR (151 MHz, $CDCl_3$) δ **major conformation (*trans*)**: 171.9 166.3, 156.7, 136.4, 128.9, 128.7, 128.3, 128.2, 127.2, 125.1, 120.8, 111.7, 70.1, 49.0, 46.3, 45.7, 43.0, 26.2, 25.4, 24.4, 21.3. **minor conformation (*cis*)**: 171.7, 165.8, 156.8, 136.9, 131.0, 128.6, 128.5, 128.3, 128.0, 126.2, 121.1, 111.6, 70.2, 49.8, 45.4, 45.3, 43.2, 26.2, 25.4, 24.3, 21.5.

^{1}H NMR (599 MHz, CD_3CN) δ **minor conformation (*trans*)**: 7.48-7.43 (m, 7H, Ar*H*), 7.04 (m, 1H, Ar*H*), 6.94 (td, 1H, ^{3}J = 7.5, 1.1 Hz, Ar*H*), 5.11 (s, 2H, CH_2), 4.48 (s, 2H, CH_2), 4.06 (s, 2H, CH_2), 3.43 (m, 2H, pip-CH_2), 3.09 (t, 2H, ^{3}J = 5.6 Hz, 2H, pip-CH_2), 2.01 (s, 3H, ac-CH_3), 1.61-1.37 (m, 6H, pip-CH_2). **major conformation (*cis*)**: 7.48-7.43 (m, 7H, Ar*H*), 7.19 (m, 1H, Ar*H*), 6.98 (td, 1H, 3J = 7.5, 1.1 Hz), 5.13 (s, 2H, CH_2), 4.56 (s, 2H, CH_2), 4.04 (s, 2H, CH_2), 3.43 (m, 2H, pip-CH_2), 3.20 (m, 2H, pip-CH_2), 1.92 (s, 3H, ac-CH_3), 1.61-1.37 (m, 6H, pip-CH_2).

^{13}C NMR (151 MHz, CD_3CN) δ **minor conformation (*trans*)**: 171.5, 166.1, 156.7, 137.2, 128.8, 128.5, 128.5, 127.9, 127.7, 125.5, 120.6, 111.9, 69.8, 48.3, 46.2, 45.1, 42.7, 25.9, 25.4, 24.1, 20.8. **major conformation (*cis*)**: 170.9, 166.0, 156.6, 137.4, 129.6, 128.5, 128.3, 128.0, 126.4, 127.9, 120.8, 111.9, 69.9, 50.0, 45.3, 45.2, 42.5, 25.9, 25.3, 24.1, 20.6.

^{1}H NMR (599 MHz, CD_3OD) δ **major conformation (*trans*)**: 7.47-7.22 (m, 7H, Ar*H*), 7.10 (dd, 1H, ^{3}J = 8.2, ^{4}J = 1.0 Hz, Ar*H*), 6.96 (td, 1H, ^{3}J = 7.4, ^{4}J = 1.0 Hz, Ar*H*), 5.09 (s, 2H, CH_2), 4.57 (s, 2H, CH_2), 4.06 (s, 2H, CH_2), 3.45 (t, 2H, ^{3}J = 5.6 Hz, pip-CH_2), 3.18 (t, 2H, ^{3}J = 5.6 Hz, pip-CH_2), 2.05 (s, 3H, ac-CH_3), 1.63-1.39 (m, 6H, pip-CH_2). **minor conformation (*cis*)**: 7.47-7.22 (m, 7H, Ar*H*), 7.16 (m, 1H, Ar*H*), 6.96 (td, 1H, ^{3}J = 7.5, ^{4}J = 1.1 Hz, Ar*H*), 5.08 (s, 2H, CH_2), 4.57 (s, 2H, CH_2), 4.14 (s, 2H, CH_2), 3.40 (t, 2H, ^{3}J = 5.6 Hz, pip- CH_2), 3.05 (t, 2H, ^{3}J = 5.6 Hz, pip-CH_2), 1.97 (s, 3H), 1.63-1.39 (m, 6H, pip-CH_2).

^{13}C NMR (151 MHz, CD_3CN) δ **major conformation (*trans*)**: 172.9, 166.7, 156.9, 136.8, 129.1, 129.0, 128.3, 127.8, 127.3, 124.3, 120.5, 111.9, 70.0, 49.0, 46.2, 45.4, 42.9, 25.7, 25.1, 23.9, 20.1. **minor conformation (*cis*)**: 173.2, 166.5, 156.9, 137.1, 130.3, 128.6, 128.24 127.8, 127.7, 125.2, 120.6, 111.9, 69.9, 49.3, 45.2, 45.1, 43.0, 25.8, 25.1, 23.8, 20.1.

7.6.37. Synthesis of the model peptoid containing *O*-Bnz *m*-aminomethylphenol (160)

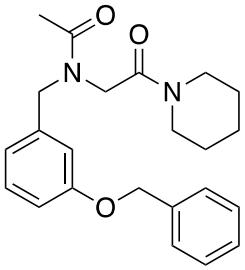

160

Using the general procedure described in **Section 7.4.9**, **129** (100 mg, 0.49 mmol, 1.00 eq) in THF (5 mL) was reacted with a solution of **154** (634 mg, 1.96 mmol, 4.00 eq) and DIPEA (338 μL, 1.96 mmol, 4.00 eq) in THF (7.5 mL). The crude was then acetylated. After workup and purification by FC chromatography using a gradient of 100% hexane to 100% EtOAc, **160** was recovered as a pale-yellow oil (49.0 mg, 26%).

HRMS (TOF MS ES+): calcd for $C_{23}H_{29}N_2O_3$: 381.2178; found: 381.2181.

^{1}H NMR (599 MHz, $CDCl_3$) δ **major conformation (*trans*)**: 7.43-7.18 (m, 5H, Ar*H*), 6.91-6.75 (m, 4H, Ar*H*), 5.05 (s, 2H, CH_2), 4.62 (s, 2H, CH_2), 4.10 (s, 2H, CH_2), 3.51 (t, 2H, ^{3}J = 5.5 Hz, pip-CH_2), 3.29 (t, 2H, ^{3}J = 5.5 Hz, pip-CH_2), 2.17 (s, 3H, ac-CH_3), 1.65-1.49 (m, 6H, pip- CH_2). **minor conformation (*cis*)**: 7.43-7.18 (m, 5H, Ar*H*), 6.91-9.75 (m, 4H, Ar*H*), 5.03 (s, 2H, CH_2), 4.61 (s, 2H, CH_2), 3.86 (s, 2H, CH_2), 3.53 (t, 2H, ^{3}J = 5.8 Hz, pip-CH_2), 3.18 (t, 2H, ^{3}J = 5.8 Hz, pip-CH_2), 2.06 (s, 3H, ac-CH_3), 1.65-1.49 (m, 6H, pip-CH_2).

^{13}C NMR (151 MHz, $CDCl_3$) δ **major conformation (*trans*)**: 171.5, 165.4, 159.0, 139.0, 137.0, 129.6, 128.5, 127.9, 127.5, 120.9, 114.6, 113.8, 69.9, 49.3, 48.3, 45.7, 43.3, 26.4, 25.5, 24.3, 21.5. **minor conformation (*cis*)**: 171.5, 166.1, 159.3, 138.4, 136.7, 130.0, 128.6, 128.0, 127.4, 119.1, 113.8, 113.2, 70.0, 52.6, 46.0, 45.8, 43.0, 26.2, 25.4, 24.4, 21.3.

^{1}H NMR (599 MHz, CD_3CN) δ **minor conformation (*trans*)**: 7.47-7.22 (m, 5H, Ar*H*), 6.94-9.82 (m, 4H, Ar*H*), 5.11 (d, 2H, ^{3}J = 1.6 Hz, CH_2), 4.55 (s, 2H, CH_2), 4.06 (d, 2H, ^{3}J = 1.7 Hz, CH_2), 3.46 (t, 2H, ^{3}J = 5.6 Hz, pip-CH_2), 3.29 (t, 2H, ^{3}J = 5.6 Hz, pip-CH_2), 2.06 (d, 3H, ^{3}J = 1.6 Hz, ac-CH_3), 1.65-1.46 (m, 6H, pip-CH_2). **major conformation (*cis*)**: 7.47-7.22 (m, 5H, Ar*H*), 6.94-9.82 (m, 4H, Ar*H*), 5.09 (d, 2H, ^{3}J = 1.6 Hz, CH_2), 4.46 (s, 2H, CH_2), 4.02 (d, 2H, ^{3}J = 1.6 Hz, CH_2), 3.49 (t, 2H ^{3}J = 5.6 Hz, pip-CH_2), 3.24 (t, 2H, ^{3}J = 5.6 Hz, pip-CH_2), 1.97 (d, 3H, ^{3}J = 1.6 Hz, ac-CH_3), 1.65-1.46 (m, 6H, pip-CH_2).

^{13}C NMR (151 MHz, CD_3CN) δ **minor conformation (*trans*)**: 170.8, 166.0, 159.1, 139.3, 137.4, 129.9, 128.5, 127.9, 127.7, 119.3, 113.7, 113.4, 69.6, 52.4, 46.5, 45.3, 42.5, 25.9, 25.4, 24.2, 20.7. **major conformation (*cis*)**: 171.5, 165.8, 158.9, 139.9, 137.5, 129.5, 128.5, 127.9, 127.7, 120.3, 114.2, 113.3, 69.5, 49.3, 49.2, 45.3, 42.8, 26.0, 25.4, 24.1, 20.7.

^{1}H NMR (599 MHz, CD_3OD) δ **major conformation (*trans*)**: 7.41-7.19 (m, 5H, Ar*H*), 6.93-6.78 (m, 4H, Ar*H*), 5.08 (s, 2H, CH_2), 4.58 (s, 2H, CH_2), 4.11 (s, 2H, CH_2), 3.49 (m, 2H, pip-CH_2), 3.29 (m, 2H, pip-CH_2), 2.13 (s, 3H, ac-CH_3), 1.65-1.45 (m, 6H, pip-CH_2). **minor conformation (*cis*)**: 7.41-7.19 (m, 5H, Ar*H*), 6.93-6.78 (m, 4H, Ar*H*), 5.05 (s, 2H, CH_2), 4.52 (s, 2H, CH_2), 4.11 (s, 2H, CH_2), 3.31 (m, 2H, pip-CH_2), 3.27 (m, 2H, pip-CH_2), 2.04 (s, 3H, ac-CH_3), 1.65-1.45 (m, 6H, pip-CH_2).

^{13}C NMR (151 MHz, CD_3OD) δ **major conformation (*trans*)**: 172.9, 166.6, 159.3, 138.0, 137.3, 129.7, 128.1, 127.5, 127.1, 119.0, 114.0, 113.0, 69.5, 52.7, 46.5, 45.5, 42.9, 25.8, 25.2, 23.9, 20.0. **minor conformation (*cis*)**: 173.3, 166.2, 159.0, 138.4, 137.3, 129.3, 128.1, 127.4, 127.1, 120.4, 114.4, 113.7, 69.5, 49.5, 48.5, 45.4, 43.1, 23.9, 20.6.

7.6.38. Synthesis of the model peptoid containing *O*-Bnz *p*-aminomethylphenol (161)

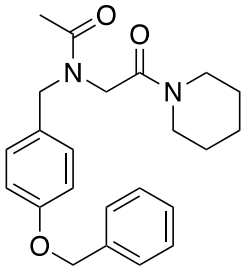

161

Using the general procedure described in **Section 7.4.9**, **129** (100 mg, 0.49 mmol, 1.00 eq) in THF (5 mL) was reacted with a solution of **155** (634 mg, 1.96 mmol, 4.00 eq) and DIPEA (338 μL, 1.96 mmol, 4.00 eq) in THF (7.5 mL). The crude was then acetylated. After workup and purification by FC chromatography using a gradient of 100% hexane to 100% EtOAc, **161** was recovered as a pale-yellow solid (43.0 mg, 23%).

HRMS (TOF MS ES+): calcd for $C_{23}H_{29}N_2O_3$: 381.2178; found: 381.2188.

^{1}H NMR (599 MHz, $CDCl_3$) δ **major conformation (*trans*)**: 7.43-7.29 (m, 5H, Ar*H*), 7.11 (d, 2H, ^{3}J = 8.6 Hz, Ar*H*), 6.95 (d, 2H, ^{3}J = 8.6 Hz, Ar*H*), 5.04 (s, 2H, CH_2), 4.59 (s, 2H, CH_2),

4.09 (s, 2H, CH_2), 3.52 (t, 2H, ^{3}J = 5.5 Hz, pip-CH_2), 3.29 (t, 2H, ^{3}J = 5.5 Hz, pip-CH_2), 2.21 (s, 3H, ac-CH_3), 1.65-1.44 (m, 6H, pip-CH_2). **minor conformation (*cis*)**: 7.43-7.29 (m, 5H, Ar*H*), 7.15 (d, 2H, ^{3}J = 8.5 Hz, Ar*H*), 6.91 (d, 2H, ^{3}J = 8.5 Hz, Ar*H*), 5.03 (s, 2H, CH_2), 4.56 (s, 2H, CH_2), 3.88 (s, 2H, CH_2), 5.53 (t, 2H, ^{3}J = 5.5 Hz, pip-CH_2), 3.20 (t, 2H, ^{3}J = 5.5 Hz, pip-CH_2), 2.06 (s, 2H), 1.65-1.44 (m, 6H, pip-CH_2).

^{13}C NMR (151 MHz, CD_3OD) δ **major conformation (*trans*)**: 171.4, 166.2, 158.4, 136.8, 129.8, 128.6, 128.1, 128.0, 127.4, 115.2, 70.1, 52.1, 45.9, 45.6, 43.1, 26.2, 25.4, 24.4, 21.4. **minor conformation (*cis*)**: 171.45, 165.45, 158.2, 136.9, 129.7, 128.7, 128.6, 128.1, 128.0, 114.9, 70.0, 48.8, 48.1, 45.7, 43.4, 26.4, 25.5, 24.3, 21.5.

^{1}H NMR (599 MHz, CD_3CN) δ **minor conformation (*trans*)**: 7.49-7.30 (m, 5H, Ar*H*), 7.18 (td, 2H, ^{3}J = 8.6 Hz, ^{4}J = 1.5 Hz, Ar*H*), 7.04-6.95 (m, 2H, Ar*H*), 5.10 (s, 2H, CH_2), 4.51 (s, 2H, CH_2), 4.05 (s, 2H, CH_2), 2.10 (s, 3H, ac-CH_3), 1.65-1.45 (m, 6H, pip-CH_2). **major conformation (*cis*)**: 7.49-7.30 (m, 5H), 7.18 (td, 2H, ^{3}J = 8.6 Hz, ^{4}J = 1.5 Hz), 6.94 (m, 2H), 5.09 (s, 2H, CH_2), 4.41 (s, 2H, pip-CH_2), 4.05 (d, 2H, ^{3}J = 1.4 Hz, pip-CH_2), 1.95 (s, 3H, ac-CH_3), 1.65-1.45 (m, 6H, pip-CH_2)**.**

^{13}C NMR (151 MHz, CD_3CN) δ **minor conformation (*trans*)**: 170.7, 166.0, 158.1, 137.4, 130.4, 129.6, 128.5, 127.9, 127.6, 114.7, 69.6, 51.9, 46.1, 45.3, 42.5, 25.9, 25.4, 24.2, 20.8. **major conformation (*cis*)**: 171.4, 165.8, 157.9, 137.5, 129.3, 128.5, 128.4, 127.9, 127.6, 114.7, 69.6, 48.9, 48.8, 45.3, 42.8, 26.0, 25.4, 24.1, 20.8.

^{1}H NMR (599 MHz, CD_3OD) δ **major conformation (*trans*)**: 7.42-7.25 (m, 5H, Ar*H*), 7.17-7.13 (m, 2H, Ar*H*), 7.00-6.97 (m, 2H, Ar*H*), 5.06 (s, 2H, CH_2), 4.55 (s, 2H, CH_2), 4.12 (s, 2H CH_2), 3.48 (m, 2H, pip-CH_2), 3.32 (m, 2H, pip- CH_2), 2.19 (s, 3H, ac-CH_3), 1.66-1.45 (m, 6H, pip-CH_2). **minor conformation (cis)**: 7.42-7.25 (m, 5H, Ar*H*), 7.17-7.13 (m, 2H, Ar*H*), 6.94-6.91 (m, 2H, Ar*H*), 5.05 (s, 2H, CH_2), 4.48 (s, 2H, CH_2), 4.12 (s, 2H, CH_2), 3.48 (m, 2H, pip-CH_2), 3.28 (m, 2H, pip-CH_2), 2.08 (s, 3H, ac CH_3), 1.66-1.45 (m, 6H, pip-CH_2).

^{13}C NMR (151 MHz, CD_3OD) δ **major conformation (*trans*)**: 172.8, 166.6, 158.5, 137.52, 129.5, 128.2, 128.1, 127.5 127.1, 115.0, 69.6, 52.3, 46.1, 45.5, 42.9, 25.8, 25.2, 23.9, 20.0. **minor conformation (*cis*)**: ^{13}C NMR (176 MHz, CD_3OD) δ 173.2, 166.3, 158.4, 137.2, 128.9, 128.40, 128.1, 127.4, 127.1, 114.7, 69.5, 49.0, 48.2, 45.4, 43.1, 25.9, 25.3, 23.9, 20.1.

7.6.39. Synthesis of the model peptoid containing *o*-aminomethylphenol (104)

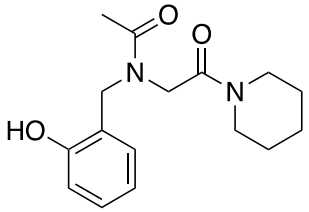

126

Using the general procedure described in **Section 7.4.5**, **159** (50.0 mg, 0.13 mmol, 1.00 eq) was hydrogenated, yielding **104** as an off-white solid (37.0 mg, 97%).

HRMS (TOF MS ES+): calcd for $C_{16}H_{23}N_2O_3$: 291.1709; found: 291.1696.

^{1}H NMR (599 MHz, $CDCl_3$) δ **minor conformation (*trans*)**: 7.18 (m, 1H, Ar*H*), 7.05 (m, 1H, Ar*H*), 6.92 (m, 1H, Ar*H*), 6.86 (m, 1H, Ar*H*), 4.56 (s, 2H, CH_2), 4.05 (s, 2H, CH_2), 3.53 – 3.50 (m, 2H, pip-CH_2), 3.39 – 3.35 (m, 2H, pip-CH_2), 2.21 (s, 3H, ac-CH_3), 1.71-1.54 (m, 6H, pip-CH_2). **major conformation (*cis*)**: 9.41 (s, 1H, ArO*H*), 7.21 (td, 1H, ^{3}J = 7.7 Hz, ^{4}J = 1.7 Hz, Ar*H*), 6.99 (dd, 1H, , ^{3}J = 7.4 Hz, ^{4}J = 1.8 Hz, Ar*H*), 6.91 (dd, 1H, ^{3}J = 8.1 Hz, ^{4}J = 1.2 Hz, Ar*H*), 6.77 (td, 1H, ^{3}J = 7.3 Hz, ^{4}J = 1.2 Hz, Ar*H*), 4.45 (s, 2H), 4.01 (s, 2H, CH_2), 3.58 (t, 2H, ^{3}J = 5.6 Hz, pip-CH_2), 3.33 (t, 2H, ^{3}J = 5.6 Hz, pip-CH_2), 2.03 (s, 3H, ac-CH_3), 1.71-1.54 (m, 6H, pip-CH_2).

^{13}C NMR (151 MHz, $CDCl_3$) δ 129.6, 122.9, 120.5, 117.6, 49.5, 46.4, 45.4, 26.2, 21.9, rest of the peaks unassignable due to weak signals. **major conformation (*cis*)**: 174.0, 164.5, 156.5, 131.0, 130.3, 121.7, 119.1, 117.6, 48.9, 48.1, 45.8, 43.5, 26.5, 25.5, 24.37, 21.0.

^{1}H NMR (599 MHz, CD_3CN) δ **minor conformation (*trans*)**: 7.17 – 7.10 (m, 2H, Ar*H*), 6.90 – 6.85 (m, 2H, Ar*H*), 4.53 (s, 2H, CH_2), 4.08 (s, 2H, CH_2), 3.47 – 3.45 (m, 2H, pip-CH_2), 3.33 – 3.29 (m, 2H, pip-CH_2), 2.11 (s, 3H, ac-CH_3), 1.69 – 1.47 (m, 6H, pip-CH_2). **major conformation (*cis*)**: 9.59 (s, 1H ArO*H*), 7.21 – 7.17 (m, 2H, Ar*H*), 6.82 – 6.77 (m, 2H, Ar*H*), 4.37 (s, 2H, CH_2), 4.19 (s, 2H, CH_2), 3.48 (m, 2H, pip-CH_2), 3.35 (m, 2H, pip-CH_2), 1.96 (s, 3H, ac-CH_3), 1.69 – 1.47 (m, 6H, pip-CH_2).

^{13}C NMR (151 MHz, CD_3CN) δ **minor conformation (*trans*)**: 129.0, 128.8, 120.0, 115.8, 48.4, 46.0, 42.7, 25.9, 20.8, rest of the peaks unassignable due to weak signals. **major conformation (*cis*)**: 174.6, 165.0, 156.3, 131.4, 129.8, 122.8, 119.1, 116.7, 49.9, 47.7, 45.4, 42.9, 26.0, 25.4, 24.1, 20.4.

^{1}H NMR (599 MHz, CD_3OD) δ **major conformation (*trans*)**: 7.17 – 7.05 (m, 2H, Ar*H*), 6.84 – 6.73 (m, 2H, Ar*H*), 4.56 (s, 2H, CH_2), 4.15 (s, 2H, CH_2), 3.51 (m, 2H, pip-CH_2), 3.26 (m,

2H, pip-CH_2), 2.24 (s, 3H, ac-CH_3), 1.68 – 1.49 (m, 6H, pip-CH_2). **minor conformation (*cis*)**: 7.17 – 7.05 (m, 2H, Ar*H*), 6.84 – 6.73 (m, 2H, Ar*H*), 4.50 (s, 2H, CH_2), 4.26 (m, 2H, CH_2), 3.51 (m, 2H, pip-CH_2), 3.26 (m, 2H, pip-CH_2), 2.02 (s, 3H, ac-CH_3), 1.68 – 1.49 (m, 6H, pip-CH_2).

^{13}C NMR (151 MHz, CD_3OD) δ **major conformation (*trans*)**: 173.0, 166.8, 155.6, 128.8, 128.8, 122.1, 119.2, 114.8, 48.5, 45.7, 45.5, 43.0, 25.8, 25.21, 24.0, 20.0. **minor conformation (*cis*)**: 173.8, 166.4, 155.6, 130.5, 128.8, 122.6, 119.2, 115.2, 48.8, 45.5, 45.1, 43.1, 25.8, 25.3, 23.9, 20.0.

7.6.40. Synthesis of the model peptoid containing *m*-aminomethylphenol (105)

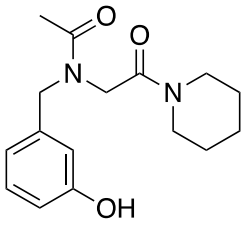

105

Using the general procedure described in **Section 7.4.5**, **160** (48.0 mg, 0.13 mmol, 1.00 eq) was hydrogenated, yielding **105** as a white solid (28.0 mg, 76%).

HRMS (TOF MS ES+): calcd for $C_{16}H_{23}N_2O_3$: 291.1709; found: 291.1692.

^{1}H NMR (599 MHz, $CDCl_3$) δ **major conformation (*trans*)**: 8.52 (br, 1H, ArO*H*), 7.16 (t, 1H, ^{3}J = 7.8 Hz, Ar*H*), 6.79 (m, 1H, Ar*H*), 6.70 (t, 1H, ^{3}J = 2.0 Hz, Ar*H*), 6.63 (m, 1H, Ar*H*), 4.75 (s, 2H, CH_2), 4.13 (s, 2H, CH_2), 3.51 (t, 2H, ^{3}J = 5.6 Hz, pip- CH_2), 3.27 (t, 2H, ^{3}J = 5.6 Hz, pip- CH_2), 2.18 (s, 3H, ac-CH_3), 1.65-1.45 (m, 6H, pip-CH_2). **minor conformation (*cis*)**: 7.12 (t, 1H, ^{3}J = 7.8 Hz, Ar*H*), 6.77-6.74 (m, 2H, Ar*H*), 6.66 (m, 1H, Ar*H*), 4.75 (s, 1H, CH_2), 3.94 (s, 2H, CH_2), 3.53 (t, 2H, ^{3}J = 5.5 Hz, pip-CH_2), 3.21 (t, 2H, ^{3}J = 5.5 Hz, pip-CH_2), 2.07 (s, 3H, ac-CH_3), 1.65-1.45 (m, 6H, pip-CH_2).

^{13}C NMR (151 MHz, $CDCl_3$) δ **major conformation (*trans*)**: 172.3, 166.2, 157.8, 137.6, 130.1, 117.8, 115.1, 113.2, 52.8, 46.3, 45.9, 43.3, 26.1 25.4, 24.3, 21.2. **minor conformation (*cis*)**: 172.5, 165.3, 157.6, 138.1, 129.6, 119.7, 115.2, 115.0, 49.6, 48.4, 45.8, 43.5, 26.3, 25.5, 24.2, 21.2.

^{1}H NMR (599 MHz, CD_3CN) δ **major conformation (*trans*)**: 7.20 (t, 1H, ^{3}J = 7.8 Hz, Ar*H*), 6.75-6.69 (m, 2H, Ar*H*) 4.52 (s, 2H, CH_2), 4.11 (s, 2H, CH_2), 3.53 (m, 2H, pip-CH_2), 3.28 (m,

2H, pip-CH_2), 2.09 (s, 3H, ac-CH_3), 1.65-1.45 (m, 6H, pip-CH_2). **minor conformation (*cis*)**: 7.16-7.13 (m, 1H, Ar*H*), 6.75-6.69 (m, 2H), 4.43 (s, 2H, CH_2), 4.06 (s, 2H, CH_2), 3.53 (m, 2H, pip-CH_2), 3.28 (m, 2H, pip-CH_2), 1.98 (s, 3H, ac-CH_3), 1.65-1.45 (m, 6H, pip-CH_2).

^{13}C NMR (151 MHz, CD_3CN) δ **major conformation (*trans*)**: 171.2, 166.1, 157.5, 139.7, 129.5, 119.2, 114.6, 113.5, 52.4, 46.6, 45.3, 42.9, 26.0, 25.4, 24.1, 20.7. **minor conformation (*cis*)**: 171.8, 165.8, 157.2, 139.1, 129.9, 118.1, 114.2, 114.0, 49.3, 49.1, 45.4, 42.6, 25.9, 25.4, 24.1, 20.7.

^{1}H NMR (599 MHz, CD_3OD) δ **major conformation (*trans*)**: 7.17 (t, 1H, ^{3}J = 7.9 Hz, Ar*H*), 6.71-6.63 (m, 3H, Ar*H*), 4.55 (s, 2H), 4.16 (s, 2H, CH_2), 3.51 (m, 2H, pip-CH_2), 3.35 (t, 2H, ^{3}J = 3.6 Hz, pip-CH_2), 2.17 (s, 3H, ac-CH_3), 1.66-1.46 (m, 6H, pip-CH_2). **minor conformation (*cis*)**: 7.11 (t, 1H, ^{3}J = 7.8 Hz, Ar*H*), 6.71-6.63 (m, 3H, Ar*H*), 4.48 (s, 2H, CH_2), 4.15 (s, 2H, CH_2), 3.50 (m, 2H, pip-CH_2), 3.30 (m, 2H, pip-CH_2), 2.05 (s, 3H, ac-CH_3), 1.66-1.46 (m, 6H, pip-CH_2).

^{13}C NMR (151 MHz, CD_3OD) δ **major conformation (*trans*)**: 172.9, 166.6, 157.8, 137.9, 129.7, 117.5, 114.3, 113.3, 52.7, 46.5, 45.6, 42.9, 25.8, 25.2, 23.9, 20.0. **minor conformation (*cis*)**: 173.2, 166.3, 157.5, 138.2, 129.3, 119.0, 114.7, 114.1, 49.4, 48.4, 45.4, 43.1, 25.9, 25.3, 23.9, 20.1.

7.6.41. Synthesis of the model peptoid containing *p*-aminomethylphenol (106)

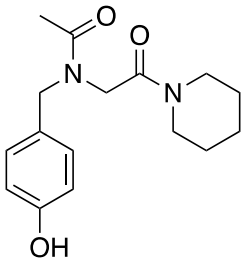

106

Using the general procedure described in **Section 7.4.5**, **161** (43.0 mg, 0.11 mmol, 1.00 eq) was hydrogenated, yielding **106** as a white solid (32.0 mg, 98%).

HRMS (TOF MS ES+): calcd for $C_{16}H_{23}N_2O_3$: 291.1709; found: 291.1702.

^{1}H NMR (599 MHz, $CDCl_3$) δ **major conformation (*trans*)**: 7.48 (br, 1H, ArO*H*), 7.01-6.97 (m, 2H, Ar*H*), 6.86-6.81 (m, 2H, Ar*H*), 4.54 (s, 2H, CH_2), 4.09 (s, 2H, CH_2), 3.51 (t, 2H, ^{3}J = 5.8 Hz, pip-CH_2), 3.28 (t, 2H, ^{3}J = 5.8 Hz, pip-CH_2), 2.21 (s, 3H, ac-CH_3), 1.66-1.45 (m, 6H, pip-CH_2). **minor conformation (*cis*)**: 7.06-7.03 (m, 2H, Ar*H*), 6.81-6.76 (m, 2H, Ar*H*), 4.53

(s, 2H, CH_2), 3.91 (s, 2H, CH_2), 3.54 (t, 2H, ^{3}J = 5.6 Hz, pip-CH_2), 3.21 (t, 2H, ^{3}J = 5.6 Hz, pip-CH_2), 2.07 (s, 3H, ac-CH_3), 1.66-1.45 (m, 6H, pip-CH_2).

^{13}C NMR (151 MHz, $CDCl_3$) δ **major conformation (*trans*)**: 172.1, 166.4, 156.6, 129.8, 128.1, 115.9, 52.4, 45.9, 45.8, 43.3, 26.1, 25.4, 24.3, 21.3. **minor conformation (*cis*)**: 172.2, 165.5, 156.4, 128.1, 127.0, 115.7, 49.1, 48.1, 45.8, 43.5, 26.3, 25.5, 24.2, 21.5.

^{1}H NMR (599 MHz, CD_3CN) δ **minor conformation (*trans*)**: 7.46 (br, 1H, ArO*H*), 7.11-7.06 (m, 2H, Ar*H*), 6.83-6.79 (m, 2H, Ar*H*), 4.48 (s, 2H, CH_2), 4.02 (s, 2H, CH_2), 3.53-3.44 (m, 2H, pip-CH_2), 3.29 (t, 2H, ^{3}J = 5.6 Hz, pip-CH_2), 2.11 (s, 3H, ac-CH_2), 1.65-1.45 (m, 6H, pip-CH_2). **major conformation (*cis*)**: 7.46 (br, 1H, ArO*H*), 7.11-7.06 (m, 2H, Ar*H*), 6.78-6.75 (m, 2H, Ar*H*), 4.40 (s, 2H, CH_2), 4.06 (s, 2H, CH_2), 3.48 (m, 2H, pip-CH_2), 3.25 (t, 2H, ^{3}J = 5.5 Hz, pip-CH_2), 1.96 (s, 3H, ac-CH_3), 1.65-1.45 (m, 6H, pip-CH_2).

^{13}C NMR (151 MHz, CD_3CN) δ **minor conformation (*trans*)**: 171.0, 166.2, 156.5, 129.5, 128.8, 115.4, 52.0, 46.1, 45.4, 42.66, 25.9, 25.4, 24.1, 20.8. **major conformation (*cis*)**: 171.7, 165.9, 156.3, 128.5, 128.1, 115.1, 48.8, 48.7, 45.3, 42.9, 26.0, 25.4, 24.1, 20.8.

^{1}H NMR (599 MHz, CD_3OD) δ **major conformation (*trans*)**: 7.08-7.03 (m, 2H, Ar*H*), 6.80-6.74 (m, 2H, Ar*H,* CH_2), 4.51 (s, 2H, CH_2), 4.12 (s, 2H, CH_2), 3.49 (m, 2H, pip-CH_2), 3.33 (m, 2H, pip-CH_2), 2.19 (s, 3H, ac-CH_3), 1.65-1.46 (m, 6H, pip-CH_2). **minor conformation (*cis*)**: 7.08-7.03 (m, 2H, Ar*H*), 6.74-6.70 (m, 2H, Ar*H*), 4.45 (s, 2H, CH_2), 4.12 (s, 2H, CH_2), 3.49 (m, 2H, pip-CH_2), 3.29 (m, 2H, pip-CH_2), 2.03 (s, 3H, ac-CH_3), 1.65-1.46 (m, 6H, pip-CH_2).

^{13}C NMR (151 MHz, CD_3OD) δ **major conformation (*trans*)**: 172.7, 166.6, 156.9, 128.3, 126.7, 115.3, 52.4, 46.0, 45.6, 42.9, 25.8, 25.2, 23.9, 20.1. **minor conformation (*cis*)**: 173.2, 166.3, 156.8, 129.6, 127.2, 115.0, 48.9, 48.0, 45.4, 43.1, 25.9, 25.3, 23.9, 20.2.

7.6.42. Synthesis *N*-Boc aminomethyl aniline (164)

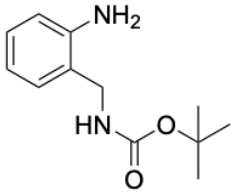

164

Using the general procedure described in **Section 7.4.3**, **163** (0.63 g, 5.2 mmol, 1.00 eq) was Boc-protected, yielding the desired product **164** as an off-white wax (1.00 g, 87%).

HRMS (TOF MS ES+): calcd for $C_{12}H_{18}N_2O_2$: 223.1447; found: 223.1452.

^{1}H NMR (400 MHz, $CDCl_3$) δ 7.10 (td, *J* = 7.7, 1.6 Hz, 1H, Ar*H*), 7.03 (m, 1H, Ar*H*), 6.70 – 6.64 (m, 2H, Ar*H*), 4.24 (d, *J* = 6.2 Hz, 2H, CH_2), 1.45 (s, 9H, ^{t}Bu-CH_3).

^{13}C NMR (101 MHz, $CDCl_3$) δ 156.5, 146.4, 130.3, 129.1, 122.5, 118.0, 115.7, 77.0, 41.47, 28.4.

Physical and spectroscopic data match those previously reported.[14]

7.6.43. Synthesis *N*-Boc, *N*-Cbz aminomethyl aniline (165)

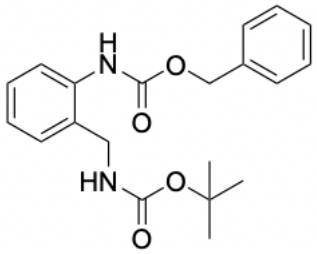

165

164 (330 g, 1.49 mmol, 1.00 eq) was dissolved in DCM (10 mL) and treated with $NaHCO_3$ (137 mg, 1.64 mmol, 1.10 eq). Then, 1.00 eq of benzoyl chloride (191 µL, 1.64 mmol, 1.10 eq) was added to this mixture and it was stirred at RT overnight. The mixture was concentrated *in vacuo*. The residue was partitioned between DCM and a 1 M solution of citric acid (10 mL). The phases were separated, and the aqueous phase was extracted twice with DCM (10 mL), dried with $MgSO_4$, filtered and concentrated under reduce pressure. The desired product **165** was recovered as an off-white solid (509 mg, 96%).

HRMS (TOF MS ES+): calcd $C_{20}H_{25}N_2O_4$: 357.1814; found: 357.1816.

^{1}H NMR (400 MHz, $CDCl_3$) δ 7.49 – 7.44 (m, 2H, Ar*H*), 7.41 – 7.29 (m, 5H, Ar*H*), 7.16 (dd, *J* = 7.6 Hz, 1.6 Hz, 1H, Ar*H*), 7.05 (td, *J* = 7.5 Hz, 1.2 Hz, 1H, Ar*H*), 5.26 (s, 2H, CH_2), 4.29 (d, *J* = 6.6 Hz, 2H, CH_2), 1.44 (s, 9H, ^{t}Bu-CH_3).

^{13}C NMR (101 MHz, $CDCl_3$) δ 154.3, 136.6, 136.5, 130.3, 129.1, 128.5, 128.0, 127.6, 127.1, 117.5, 115.4, 80.6, 43.1, 29.0, 27.0.

7.6.44. Synthesis *N*-Cbz aminomethyl aniline (166)

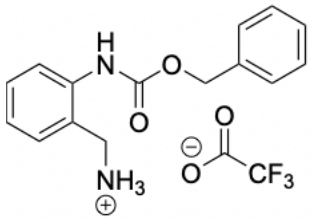

166

Using the general procedure described in **Section 7.4.4**, **165** (0.30 g, 0.56 mmol, 1.00 eq) was treated with a cleavage solution. **166** was recovered as a white solid (0.37 mg, quant).

HRMS (TOF MS ES+): calcd for $C_{15}H_{17}N_2O_2$: 257.1290; found: 257.1303.

^{1}H NMR (400 MHz, CD_3CN) δ 7.96 (br, 3H, N*H*$_3$), 7.53 (m, 1H, Ar*H*), 7.48 – 7.36 (m, 7H, Ar*H*), 7.30 (m, 1H, Ar*H*), 5.20 (s, 2H, C*H*$_2$), 4.12 (s, 2H, C*H*$_2$).

^{13}C NMR (101 MHz, CD_3CN) δ 156.3, 136.6, 136.5, 131.5, 130.1, 128.6, 128.2, 127.9, 126.7, 117.5, 80.6, 67.1, 39.7.

Physical and spectroscopic data match those previously reported.[15]

7.6.45. Synthesis of model peptoid containing *N*-Cbz *o*-amino benzylamine (167)

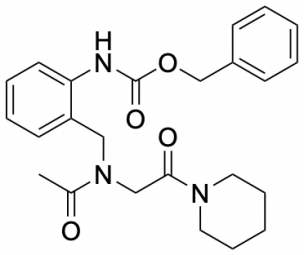

167

Using the general procedure described in **Section 7.4.9**, **129** (52.0 mg, 0.25 mmol, 1.00 eq) in THF (5 mL) was reacted with a solution of **166** (370 mg, 1.00 mmol, 4.00 eq) and DIPEA (172 µL, 1.0 mmol, 4.00 eq) in THF (10 mL). The crude was then acetylated. After workup and purification by FC chromatography using a gradient of 100% hexane to 100% EtOAc, **167** was recovered as a yellow oil (13.0 mg, 9%).

HRMS (TOF MS ES+): calcd for $C_{24}H_{30}N_3O_4$: 424.2236; found: 424.2223.

^{1}H NMR (599 MHz, $CDCl_3$) δ **major conformation (*cis*)**: 9.15 (br, 1H, N*H*), 7.46 – 7.42 (m, 2H, Ar*H*), 7.36 – 7.26 (m, 5H, Ar*H*), 7.04 (m, 1H, Ar*H*), 6.95 (m, 1H, Ar*H*), 5.22 (s, 2H, C*H*$_2$), 4.54 (s, 2H, C*H*$_2$), 3.93 (s, 2H, C*H*$_2$), 3.55 (t, *J* = 5.6 Hz, 2H, pip-C*H*$_2$), 3.27 (t, *J* = 5.6 Hz, 2H,

pip-CH_2), 2.01 (s, 3H, ac-CH_3), 1.69 – 1.52 (m, 6H, pip-CH_2). **minor conformation (*trans*)**: 7.46 – 6.92 (m, 9H, Ar*H*), 5.19 (s, 2H, CH_2), 4.62 (s, 2H, CH_2), 4.01 (s, 2H, CH_2), 3.55 (t, *J* = 5.6 Hz, 2H, pip-CH_2), 3.27 (t, *J* = 5.6 Hz, 2H, pip-CH_2), 2.20 (s, 3H, ac-CH_3), 1.69 – 1.52 (m, 6H, pip-CH_2).

^{13}C NMR (151 MHz, $CDCl_3$) δ **major conformation (*cis*)**: 172.7, 164.7, 154.3, 138.0, 136.9, 131.0, 129.3, 128.4, 127.9, 127.8, 124.8, 122.5, 121.0, 66.3, 48.1, 47.4, 45.8, 43.5, 26.4, 25.6, 24.3, 21.3. **minor conformation (*trans*)**: 128.9, 128.6, 128.4, 125.6, 67.1, 49.5, 45.9, 45.2, 43.3, 21.6. Other peaks unassignable due to weak signals.

^{1}H NMR (700 MHz, CD_3CN) δ **major conformation (*cis*)**: 9.46 (br, 1H, N*H*), 7.45 – 7.24 (m, 8H, Ar*H*), 7.02 (td, *J* = 7.4, 1.3 Hz, 1H, Ar*H*), 5.18 (s, 2H, CH_2), 4.43 (s, 2H, CH_2), 4.11 (s, 2H CH_2), 3.43 (t, *J* = 5.7 Hz, 2H, pip-CH_2), 3.30 (m, 2H, pip-CH_2), 1.92 (s, 3H, ac-CH_3), 1.65 – 1.43 (m, 6H, pip-CH_2). **minor conformation (*trans*)**: 7.50 – 6.98 (m, 9 H, Ar*H*), 5.19 (s, 2H, CH_2), 4.59 (s, 2H, CH_2), 4.01 (s, 2H, CH_2), 3.41 (m, 2H, pip-CH_2), 3.20 (t, *J* = 5.6 Hz, 2H, pip-CH_2), 2.09 (s, 3H, ac-CH_3), 1.65 – 1.43 (m, 6H, pip-CH_2).

^{13}C NMR (176 MHz, CD_3CN) δ **major conformation (*cis*)**: 173.8, 165.7, 154.7, 138.3, 137.7, 131.9, 129.3, 129.1, 128.5, 128.3, 123.5, 66.6, 49.6, 47.9, 45.9, 43.4, 26.6, 24.7, 21.2. **minor conformation (*trans*)**: 131.9, 129.0, 128.8, 128.1, 127.6, 126.1, 66.4, 49.9, 46.1, 45.6, 42.7, 26.0, 26.0, 25.5, 24.2, 21.0. Other peaks unassignable due to weak signals.

^{1}H NMR (700 MHz, CD_3OD) δ **major conformation (*cis*)**: 7.46 – 7.24 (m, 8H, Ar*H*), 7.13 (td, *J* = 7.5, 1.2 Hz, 1H, Ar*H*), 5.20 (s, 2H, CH_2), 4.59 (s, 2H, CH_2), 4.24 (s, 2H, CH_2), 3.50 (m, 2H, pip-CH_2), 3.35 (m, 2H, pip-CH_2), 2.05 (s, 3H, ac-CH_3), 1.67 – 1.49 (m, 6H, pip-CH_2). **minor conformation (*trans*)**: 7.45 – 7.11 (m, 9H, Ar*H*), 5.18 (s, 2H, CH_2), 4.66 (s, 2H, CH_2), 4.14 (m, 2H, CH_2), 3.51 (t, *J* = 5.6 Hz, 2H, pip-CH_2), 3.25 (m, 2H, pip-CH_2), 2.15 (s, 3H, ac-CH_3), 1.70 – 1.50 (m, 6H, pip-CH_2).

^{13}C NMR (176 MHz, CD_3OD) δ **major conformation (*cis*)**: 173.97, 166.00, 155.06, 136.77, 135.71, 130.20, 128.37, 128.19, 128.13, 127.80, 127.67, 127.64, 127.51, 66.3, 48.6, 46.6, 45.4, 43.1, 25.9, 25.3, 23.9, 20.0. **minor conformation (*trans*)**: 173.1, 166.6, 155.7, 136.8, 136.6, 128.2, 128.1, 128.1, 128.0, 127.5, 127.3, 126.4, 124.2, 66.6, 49.5, 46.4, 45.5, 43.0, 25.7, 25.2, 24.0, 19.9.

7.6.46. Synthesis of the model peptoid containing *o*-amino benzylamine (168)

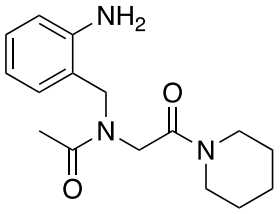

168

Using the general procedure described in **Section 7.4.5**, **167** (13.0 mg, 0.13 mmol, 1.00 eq) was hydrogenated, yielding **168** as an amber oil (37.0 mg, 97%).

HRMS (TOF MS ES+): calcd for $C_{16}H_{24}N_3O_2$: 290.1869; found 290.1870.

^{1}H NMR (599 MHz, $CDCl_3$) δ **major conformation (*cis*)**: 7.10 (td, *J* = 7.7, 1.6 Hz, 1H, Ar*H*), 6.93 (dd, *J* = 7.3, 1.6 Hz, 1H, Ar*H*), 6.65 – 6.57 (m, 2H, Ar*H*), 4.55 (d, *J* = 2.2 Hz, 2H, CH_2), 3.92 (s, 2H, CH_2), 3.57 (t, *J* = 5.7 Hz, 3H, pip-CH_2), 3.27 (t, *J* = 5.7 Hz, 3H, pip-CH_2), 2.05 (s, 3H, ac-CH_3), 1.68 – 1.47 (m, 6H, pip-CH_2). **minor conformation (*trans*)**: 7.13 (d, *J* = 7.7 Hz, 1H, Ar*H*), 7.00 (d, *J* = 7.5 Hz, 1H, Ar*H*), 6.78 (m, 1H, Ar*H*), 6.69 (d, *J* = 7.9 Hz, 1H, Ar*H*), 4.53 (m, 7H, CH_2), 4.09 (s, 2H, CH_2), 3.49 (t, *J* = 5.7 Hz, 2H, pip-CH_2), 3.32 – 3.26 (m, 2H, pip-CH_2), 2.23 (s, 3H, ac-CH_3), 1.68 – 1.44 (m, 6H, pip-CH_2).

^{13}C NMR (151 MHz, $CDCl_3$) δ **major conformation (*cis*)**: 172.1, 165.1, 146.5, 131.6, 129.4, 119.5, 116.9, 115.3, 47.4, 47.1, 45.8, 43.4, 26.4, 25.6, 24.3, 21.4. **minor conformation (*trans*)**: 172.0, 166.3, 145.0, 128.8, 128.2, 120.3, 118.9, 116.4, 49.7, 45.9, 45.3, 43.1, 26.1, 25.4, 24.4, 21.6.

^{1}H NMR (599 MHz, CD_3CN) δ **major conformation (cis)**: 7.22 – 6.55 (m, 4H, Ar*H*), 4.37 (s, 2H), 4.00 (s, 2H), 3.50 (m, 2H, pip-CH_2), 3.29 (m, 2H, pip-CH_2), 1.94 (s, 3H, ac-CH_3), 1.68 – 1.45 (m, 6H, pip-CH_2). **minor conformation (*trans*)**: 7.22 – 6.55 (m, 4H, Ar*H*), 4.44 (s, 2H, CH_2), 4.05 (s, 2H, CH_2), 3.44 (m, 2H, pip-CH_2), 3.22 (m, 2H, pip-CH_2), 2.08 (s, 3H, ac-CH_3), 1.68 – 1.45 (m, 6H, pip-CH_2).

^{13}C NMR (151 MHz, CD_3CN) δ **major conformation (*cis*)**: 172.2, 165.4, 146.9, 131.3, 129.0, 119.8, 116.3, 114.8, 47.9, 46.6, 45.3, 42.9, 26.0, 25.4, 24.1, 20.8. **minor conformation (*trans*):** 128.3, 127.6, 117.8, 115.6, 109.6, 49.3, 45.9, 42.6, 25.8. Rest of the peaks are unassignable due to weak signal.

^{1}H NMR (700 MHz, CD_3OD) δ **minor conformation (*cis*)**: 7.12 – 6.63 (m, 4H, Ar*H*), 4.52 (s, 2H, CH_2), 4.16 (s, 2H, CH_2), 3.55 – 3.34 (m, 4H, pip-CH_2), 2.07 (s, 3H, ac-CH_3), 1.72 – 1.48 (m, 6H, pip-CH_2). **major conformation (*trans*)**: 7.12 – 6.63 (m, 4H, Ar*H*), 4.54 (s, 2H, CH_2),

4.18 (s, 2H, CH_2), 3.55 – 3.34 (m, 4H, pip-CH_2), 2.21 (s, 3H, ac-CH_3), 1.72 – 1.48 (m, 6H, pip-CH_2).

^{13}C NMR (176 MHz, CD_3OD) δ **minor conformation (*cis*)**:173.6, 166.1, 146.4, 130.9, 128.9, 119.6, 117.2, 115.7, 49.4, 46.6, 45.5, 43.2, 25.9, 25.3, 23.9, 20.1. **major conformation (*trans*)**: 173.3, 166.7, 145.5, 128.3, 127.1, 120.1, 118.1, 116.2, 49.4, 46.6, 45.5, 43.2, 25.7, 25.2, 24.0, 20.0.

7.6.47. Synthesis of the intermediate containing *N*-Boc *o*-aminomethyl aniline (171)

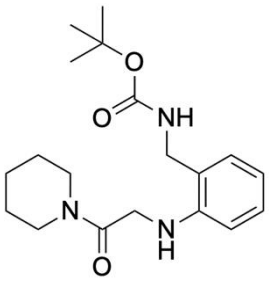

171

To a solution of **164** (370 mg, 1.0 mmol, 2 eq) in DCM (5 mL) was added Cs_2CO_3 (454 mg, 1.00 mmol, 2.00 eq), followed by dropwise addition of **129** (103 mg, 0.5 mmol, 1 eq) in DCM (5 mL) at RT. The resulting reaction mixture was stirred at RT for 1 hour. The mixture was filtered, and the filtrate was concentrated *in vacuo*. The resulting residue was purified by FC chromatography using a gradient of 100% hexane to 100% EtOAc. The desired product **171** was recovered as an amber oil (140 mg, 81%).

HRMS (TOF MS ES+): calcd for $C_{19}H_{30}N_3O_3$: 348.2291; found: 348.2287.

^{1}H NMR (400 MHz, $CDCl_3$) δ 7.24 – 7.15 (m, 2H, Ar*H*), 6.72 (td, *J* = 7.4, 1.1 Hz, 1H, Ar*H*), 6.57 (dd, *J* = 8.1, 1.2 Hz, 1H, Ar*H*), 4.33 (d, *J* = 5.7 Hz, 2H, CH_2), 3.92 (s, 2H, CH_2), 3.63 (dd, *J* = 7.6, 3.4 Hz, 2H, pip-CH_2), 3.43 (t, *J* = 5.4 Hz, 2H, pip-CH_2), 1.74 – 1.55 (m, 6H, pip-CH_2), 1.48 (s, 9H, ^{t}Bu-CH_3).

^{13}C NMR (101 MHz, $CDCl_3$) δ 165.7, 160.0, 135.5, 128.9, 127.6, 124.1, 122.8, 117.2, 63.6, 59.7, 46.8, 45.8, 43.1, 28.4, 26.3, 25.2, 24.5.

7.6.48. Synthesis of the model peptoid containing *N*-Boc *o*-aminomenyl aniline (169)

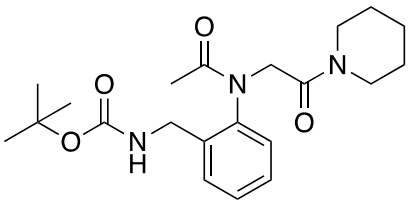

169

171 (140 mg, 0.4 mmol, 1.00 eq) was dissolved in DCM (5 mL) and treated with DIPEA (104 µL, 0.60 mmol, 1.50 eq). The reaction mixture was brought to 0ºC and treated with Ac-Cl (42.0 µL, 0.60 mmol, 1.50 eq), and stirred for 15 minutes. Then, a 1 M solution of citric acid (10 mL) was added, and the two phases were separated. The aqueous layer was extracted with DCM twice. Then, the organics were combined, dried with $MgSO_4$, filtered, and concentrated *in vacuo*. The residue was purified by FC chromatography using a gradient of 100% hexane to 100% EtOAc. The desired product **169** was recovered as white crystals (126 mg, 81%).

HRMS (TOF MS ES+): calcd for $C_{21}H_{32}N_3O_4$: 390.2393; found: 390.2396.

^{1}H NMR (599 MHz, $CDCl_3$) δ **major conformation (*trans*)**: 7.46 (d, *J* = 7.5 Hz, 2H, Ar*H*), 7.34 5 – 7.28 (m, 2H, Ar*H*), 5.57 (br, 1H, N*H*), 4.53 (d, *J* = 15.9 Hz, 1H, CH_2), 4.33 (d, *J* = 15.9 Hz, 1H, CH_2), 4.29 – 4.20 (m, 2H, CH_2), 3.53 (t, *J* = 5.4 Hz, 2H, pip-CH_2), 3.37 (t, *J* = 5.4 Hz, 2H, pip-CH_2), 1.82 (s, 3H, ac- CH_3), 1.65 – 1.49 (m, 6H, pip-CH_2), 1.41 (s, 9H, ^{t}Bu--CH_3). **minor conformation (*cis*)**: 4.43 – 4.37 (m, 2H, CH_2), 4.12 – 4.06 (m, 2H, CH_2), 2.17 (s, 3H, ac-CH_3), other signal peaks overlap with the *trans*-isomer signals.

^{13}C NMR (151 MHz, $CDCl_3$) δ **major conformation (*trans*)**: 171.2, 165.8, 156.0, 141.8, 136.9, 129.8, 129.5, 128.8, 128.7, 79.4, 50.7, 46.0, 43.2, 40.7, 28.4, 26.2, 25.4, 24.4, 21.9. **minor conformation (*cis*)**: 170.52, 165.59, 136.55, 128.21, 127.93, 45.78, 43.48, 26.35, 25.51, 24.24, 21.74, other peaks undetectable due to weak signals.

^{1}H NMR (400 MHz, CD_3CN) δ **major conformation (*trans*)**: 7.51 (m, 1H, Ar*H*), 7.45 – 7.23 (m, 3H, Ar*H*), 4.68 (d, *J* = 16.2 Hz, 1H, CH_2), 4.19 (dd, *J* = 6.3, 1.9 Hz, 2H, CH_2), 3.56 – 3.32 (m, 4H, pip-CH_2), 1.72 (s, 3H, ac-CH_3), 1.61 – 1.44 (m, 6H, pip-CH_2), 1.40 (d, *J* = 4.5 Hz, 9H, ^{t}Bu-CH_3). **minor conformation (*cis*)**: 4.61 (d, *J* = 17.9 Hz, 2H, CH_2), 2.09 (s, 3H, ac-CH_3), 1.42 (s, 9H, ^{t}Bu-CH_3), other signal peaks overlap with the *trans*-isomer signals.

^{13}C NMR (151 MHz, CD_3CN) δ **major conformation (*trans*)**: 171.13, 166.99, 156.89, 142.84, 138.47, 130.86, 130.17, 129.43, 129.14, 79.46, 51.18, 46.42, 43.58, 41.06, 28.59, 26.92, 26.32, 25.06, 22.32. **minor conformation (*cis*)**: 171.98, 166.25, 142.54, 137.43, 128.77, 128.13, 127.76, 127.60, 78.35, 53.25, 45.39, 42.98, 40.35, 26.01, 25.43, 24.03, 21.21.

^{1}H NMR (599 MHz, CD_3OD) δ **major conformation (*trans*)**: 7.55 (dd, *J* = 7.8, 1.4 Hz, 1H, Ar*H*), 7.43 (dd, *J* = 7.8, 1.6 Hz, 1H, Ar*H*), 7.38 (m, 1H, Ar*H*), 7.32 (ddd, *J* = 9.2, 6.8, 1.6 Hz, 1H, Ar*H*), 4.96 (d, *J* = 16.3 Hz, 1H, CH_2), 4.22 (qd, *J* = 15.8, 5.3 Hz, 2H, CH_2), 3.99 (d, *J* = 16.4 Hz, 1H, CH_2), 3.58 – 3.34 (m, 4H, pip-CH_2), 1.81 (s, 3H, ac-CH_2), 1.70 – 1.46 (m, 6H, pip-CH_2), 1.43 (s, 9H, ^{t}Bu-CH_3). **minor conformation (*cis*)**: peaks undetectable.

^{13}C NMR (151 MHz, CD_3OD) δ **major conformation (*trans*)**: 172.18, 166.25, 156.85, 141.23, 136.74, 129.27, 128.89, 128.73, 128.14, 78.92, 50.33, 45.62, 42.99, 39.81, 27.40, 25.84, 25.20, 23.97, 20.69. **minor conformation (*cis*)**: peaks undetectable.

7.6.49. Synthesis of the model peptoid containing o-aminomethyl aniline (170)

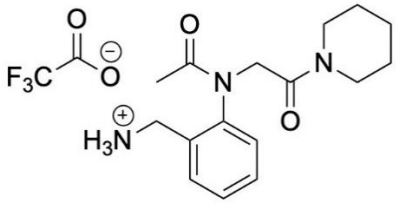

170

Using the general described procedure in **Section 7.4.4**, **169** (100 mg, 0.26 mmol, 1.00 eq) was treated with a cleavage solution. The desired **170** was recovered as a pale-yellow oil (quant).

HRMS (TOF MS ES+): calcd for $C_{16}H_{24}N_3O_2$: 290.1869; found: 290.1868.

^{1}H NMR (599 MHz, $CDCl_3$) δ **major conformation (*cis*)**: 7.27 (m, 1H, Ar*H*), 7.20 (t, *J* = 7.5 Hz, 1H, Ar*H*), 7.06 (dd, *J* = 7.6, 1.4 Hz, 1H, Ar*H*), 6.71 (d, *J* = 8.2 Hz, 1H, Ar*H*), 5.05 (s, 2H, CH_2), 4.73 (d, *J* = 21.0 Hz, 4H, pip-CH_2), 2.47 (s, 3H, CH_3), 1.74 – 1.47 (m, 6H, pip-CH_2). **minor conformation (*trans*)**: peaks undetectable.

^{13}C NMR (151 MHz, $CDCl_3$) δ **major conformation (*cis*)**: 163.5, 162.5, 134.1, 129.2, 127.2, 126.9, 118.9, 114.3, 47.9, 46.0, 43.7, 42.1, 26.5, 25.5, 24.2, 18.8. **minor conformation (*trans*)**: peaks undetectable.

^{1}H NMR (599 MHz, CD_3CN) δ **major conformation (*cis*)**: 7.35 (td, *J* = 7.8, 1.5 Hz, 1H, Ar*H*), 7.28 (t, *J* = 7.5 Hz, 1H, Ar*H*), 7.20 (d, *J* = 7.5 Hz, 1H, Ar*H*), 6.90 (d, *J* = 8.3 Hz, 1H, Ar*H*),

4.77 (s, 2H, CH_2), 4.71 (s, 2H, CH_2), 3.54 – 3.45 (m, 4H, pip-CH_2), 2.38 (s, 3H, ac-CH_3), 1.74 – 1.66 (m, 6H, CH_2). **minor conformation (*trans*)**: peaks undetectable.

^{13}C NMR (151 MHz, CD_3CN) δ **major conformation (*cis*)**: 163.9, 162.9, 134.3, 128.9, 126.9, 119.1, 115.0, 48.0, 45.7, 43.1, 41.7, 26.1, 25.3, 24.0, 18.5. **minor conformation (*trans*)**: peaks undetectable.

^{1}H NMR (700 MHz, CD_3OD) δ **major conformation (*cis*)**: 7.40 (m, 1H, Ar*H*), 7.32 (m, 1H, Ar*H*), 7.25 (m, 1H, Ar*H*), 7.00 (m, 1H, Ar*H*), 5.06 (s, 2H, CH_2), 4.78 (s, 2H, CH_2), 3.65 – 3.59 (m, 4H, pip-CH_2), 2.43 (s, 3H, ac-CH_3), 1.81 – 1.60 (m, 6H, pip-CH_2). **minor conformation (*trans*)**: peaks undetectable.

^{13}C NMR (176 MHz, CD_3OD) δ **major conformation (*cis*)**: 163.97, 163.87, 134.04, 128.89, 127.10, 126.59, 118.95, 114.87, 45.78, 43.35, 41.54, 26.11, 25.27, 23.83, 17.94. **minor conformation (*trans*)**: peaks undetectable.

7.6.50. Model peptoid $K_{cis/trans}$ and $\Delta G_{cis/trans}$ determination

Pure model peptoid was dissolved in $CDCl_3$, CD_3CN and CD_3OD for a full set of 1 D and 2 D high field NMR experiments. At least one ^{1}H NMR spectrum was recorded for each model peptoid. Protons were independently assigned by ^{1}H NMR and ^{1}H-^{1}H COSY, with individual isomers being distinguished by ^{1}H-^{1}H NOESY. Rotamer peaks arising from protons involved in isomerisation about the amide bond were distinguished by ^{1}H-^{1}H NOESY. Signals arising from the *cis*-isomer have NOEs between terminal acetal methyl protons and backbone methylene protons. ^{19}F NMR was used for further calculation of $K_{cis/trans}$ values. However, these values were reported separately to the average values of $K_{cis/trans}$. Each $K_{cis/trans}$ value was calculated as a ratio of *cis* to *trans* from a single spectrum. $\Delta G_{cis/trans}$ was calculated at 25°C using the equation $\Delta G_{cis/trans} = -RT \ln K_{cis/trans}$, R = 1.987 x 10^{-3} kcal K^{-1} mol^{-1} and T = 298 K. The $K_{cis/trans}$ values and $\Delta G_{cis/trans}$ calculated for the model peptoids are shown in **Table 7.2**.

Table 7.2. $K_{cis/trans}$ values in different solvents (CD_3OD, CD_3CN, $CDCl_3$) and their corresponding Gibbs free energy differences (ΔG in kcal mol^{-1}) of model peptoids containing different monomers. $K_{cis/trans}$ values are calculated using three sets of ^1H NMR resonances and are rounded to two decimal places.

No.	$CDCl_3$			CD_3CN			CD_3OD		
	$K_{cis/trans}$	ΔG (kcal mol^{-1})[a]	^{19}F $K_{cis/trans}$	$K_{cis/trans}$	ΔG (kcal mol^{-1})	^{19}F $K_{cis/trans}$	$K_{cis/trans}$	ΔG (kcal mol^{-1})	^{19}F $K_{cis/trans}$
60	-*	-	-	-*	-	-	-*	-	-
103	-*	-	-	-*	-	-	-*	-	-
59	0.05	1.77	-	0.05	1.77	-	0.04	1.91	-
135	-*	-	-	0.11	1.31	0.1	0.06	1.67	0.07
136	-*	-	-	-*	-		-*	-	-
137	0.04	1.91	0.02	0.18	1.02	0.03	0.04	1.91	0.3
130	-*	-	-	-*	-	-	-*	-	-
104	7.13	-1.16	-	8.70	-1.28	-	0.65	0.26	-
105	0.27	0.78	-	0.99	0.00	-	0.62	0.28	-
106	0.19	0.98	-	1.04	-0.02	-	0.75	0.17	-
141	0.35	0.62	0.33	1.40	-0.20	1.37	0.80	0.13	0.80
159	0.18	1.02	-	1.11	-0.06	-	0.49	0.42	-
160	0.26	0.80	-	1.13	-0.07	-	0.69	0.22	-
161	0.26	0.80	-	1.14	-0.08	-	0.69	0.22	-
40	0.26	0.80	-	1.15	-0.08	-	0.04	1.91	-
167	3.92	-0.81	-	7.38	-1.18	-	1.44	-0.22	-
168	2.35	-0.51	-	4.97	-0.95	-	1.93	-0.39	-
169	0.13	1.21	-	0.24	0.85	-	-	-	-
170	-**	-	-	-	-	-	-	-	-

[a] The value was calculated using the Gibbs free energy equation $\Delta G^o = -RT \ln(K_{eq})$ at 298 K, where R = 1.987 x 10^{-3} kcal K^{-1} mol^{-1}.

* Presence of only one isomer (*trans*). NMR signals corresponding to the *cis*-isomer were not detected.

** Presence of only one isomer (*cis*). NMR signals corresponding to the *trans*-isomer were not detected.

7.7. Experimental data for Chapter 4

7.7.1. Synthesis of *N*-Boc, *O*-Allyl *o*-aminomethylphenol (175)

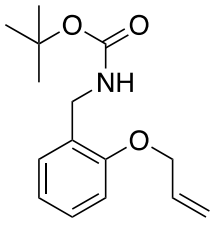

175

Using the procedure described in **Section 7.4.8**, **122** (2.00 g, 9.00 mmol, 1.00 eq) was reacted with allyl bromide (1.30 g, 10.8 mmol, 1.20 eq). After workup **175** was recovered as a pale-yellow oil (2.40 g, 94%).

HRMS (TOF MS ES-): calcd for $C_{15}H_{20}NO_3$: 262.1443; found: 262.1440.

^{1}H NMR (400 MHz, $CDCl_3$) δ 7.21-7.34 (m, 2H, Ar*H*), 6.94 (td, ^{3}J = 7.4, ^{2}J = 1.0, 1H, Ar*H*), 6.87 (d, ^{3}J = 8.0, 1H, Ar*H*), 6.08 (ddt, ^{3}J = 17.3 Hz, ^{3}J = 10.4 Hz, ^{2}J = 5.1 Hz, 1H, C*H*), 5.44 (dd, ^{3}J = 17.3 Hz, ^{2}J = 1.6 Hz, 1H, CH_2), 5.31 (dd, ^{3}J = 10.3 Hz, ^{2}J = 1.4 Hz, 1H, CH_2), 5.02 (br, 1H, N*H*), 4.59 (d, ^{3}J = 5.3 Hz, 2H, CH_2), 4.37 (d, ^{3}J = 4.37 Hz, 2H, CH_2), 1.46 (s, 9H, ^{t}Bu-CH_3)

^{13}C NMR (126 MHz, $CDCl_3$) δ 156.4, 155.9, 133.2, 129.4, 128.6, 127.4, 120.8, 117.37, 111.5, 79.2, 68.7, 40.5, 28.5.

Physical and spectroscopic data match those previously reported.[16]

7.7.2. Synthesis of *N*-Boc, *O*-Allyl *m*-aminomethylphenol (176)

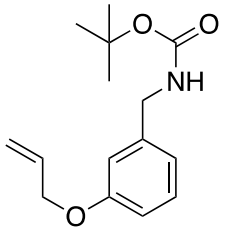

176

Using the procedure described in **Section 7.4.8**, **123** (1.70 g, 7.60 mmol, 1.00 eq) was reacted with allyl bromide (0.80 mL, 9.10 mmol, 1.20 eq). After workup and purification (1.10 g, 50%) **176** was recovered as a pale-yellow waxy solid.

HRMS (TOF MS ES+): calcd for $C_{15}H_{22}NO_3$: 264.1600; found: 264.1590.

^{1}H NMR (400 MHz, $CDCl_3$) δ 7.37 (t, J = 8.0 Hz, 1H, Ar*H*), 6.99-7.07 (m, 3H, Ar*H*), 6.07 (ddt, ^{3}J = 17.3 Hz, ^{3}J = 10.5 Hz, ^{2}J = 5.3, 1H, C*H*), 5.43 (dd, ^{3}J = 17.25 Hz, ^{2}J = 1.6 Hz, 1H, CH_2), 5.31 (dd, ^{3}J = 10.5 Hz, ^{2}J = 1.4 5 Hz, 1H, CH_2), 4.86 (br, 1H, N*H*), 4.55 (d, ^{3}J = 5.4 Hz, 2H, CH_2), 4.31 (d, ^{3}J = 6.0 Hz, 2H, CH_2) 1.48 (s, 9H, ^{t}Bu-CH_3).

^{13}C NMR (126 MHz, $CDCl_3$) δ 158.8, 155.5, 140.6, 133.2, 129.6, 119.9, 117.8, 113.8, 113.6, 68.8, 44.6, 28.4, 27.7.

Physical and spectroscopic data match those previously reported.[17]

7.7.3. Synthesis of *N*-Boc, *O*-Allyl *p*-aminomethylphenol (177)

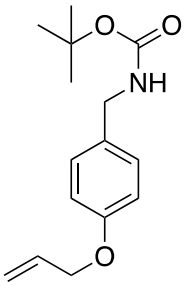

167

Using the general procedure described in **Section 7.4.8, 124** (1.10 g, 4.90 mmol, 1.00 eq) was reacted with Allyl bromide (0.52 mL, 5.90 mmol, 1.20 eq). After workup and purification (1.10 g 79%) **177** was recovered as a yellow solid.

HRMS (TOF MS ES+): calcd for $C_{15}H_{22}NO_3$: 264.1600; found: 264.1609.

^{1}H NMR (400 MHz, $CDCl_3$) δ 7.22 (d, ^{3}J = 8.2 Hz, 2H, Ar*H*), 6.87-6.92 (m, 2H, Ar*H*), 6.07 (ddt, ^{3}J = 17.3 Hz, ^{2}J = 10.6 Hz, ^{2}J = 5.3 Hz, 1H, C*H*), 5.43 (dd, ^{3}J = 17.3 Hz, ^{2}J = 1.6 Hz, 1H, CH_2), 5.31 (dd, ^{3}J = 10.5 Hz, ^{2}J = 1.4 Hz, 1H, CH_2), 4.55 (d, ^{3}J = 5.3 Hz, 2H, CH_2), 4.27 (d, ^{3}J = 5.83 Hz, 2H, CH_2), 1.48 (s, 9H, ^{t}Bu-CH_3)

^{13}C NMR (101 MHz, $CDCl_3$) δ 157.9, 156.1, 132.6, 131.0, 129.7, 117.8, 115.4, 79.4, 69.4, 44.2, 29.2.

Physical and spectroscopic data match those previously reported.[18]

7.7.4. Synthesis of *O*-Allyl *o*-aminomethylphenol (178)

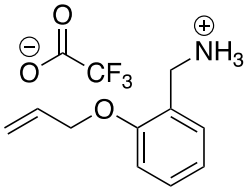

168

Using the general procedure described in **Section 7.4.4**, **175** (1.00 g, 4.70 mmol, 1.00 eq) was treated with a cleavage solution. After workup, **178** was recovered as an amber oil (1.20 g, quant.).

HRMS (TOF MS ES-): calcd for $C_{10}H_{14}NO$: 164.1075; found: 164.1073.

^{1}H NMR (400 MHz, $CDCl_3$) δ 7.40 (m, 1H, Ar*H*), 7.24 (m, 1H, Ar*H*), 6.99 (m, 1H, Ar*H*), 6.95 (d, ^{3}J = 8.4 Hz, 1H, Ar*H*), 6.07 (ddt, ^{3}J = 17.3 Hz, ^{3}J = 10.9 Hz, ^{2}J = 5.6 Hz, 1H, C*H*), 5.39 (m, 2H, CH_2), 4.65 (m, 2H, CH_2), 4.24 (d, ^{3}J = 5.4 Hz, 2H, CH_2).

^{13}C NMR (101 MHz, $CDCl_3$) δ 156.6, 132.0, 131.6, 130.9, 121.5, 119.3, 119.1, 111.9, 69.3, 41.8

Physical and spectroscopic data match those previously reported.[19]

7.7.5. Synthesis of *O*-Allyl *m*-aminomethylphenol (179)

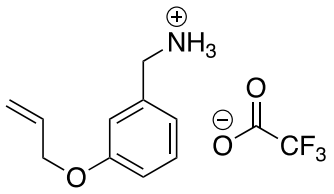

179

Using the general described procedure in **Section 7.4.4**, **176** (1.00 g, 4.70 mmol, 1.00 eq) was treated with a cleavage solution. **179** was recovered as a pale-yellow waxy solid (1.10 g, quant).

HRMS (TOF MS ES+): calcd for $C_{10}H_{14}NO$: 164.1075; found: 164.1065.

^{1}H NMR (400 MHz, CD_3OD) δ 7.37 (t, J = 8.0 Hz, 1H, Ar*H*), 6.99-7.07 (m, 3H, Ar*H*), 6.07 (ddt, ^{3}J = 17.3 Hz, ^{3}J = 10.5 Hz, ^{2}J = 5.3 Hz, 1H, C*H*), 5.43 (dd, ^{3}J = 17.25 Hz, ^{2}J = 1.6 Hz, 1H, CH_2), 5.28 (dd, 1H, ^{3}J = 10.6 Hz, ^{2}J = 1.5 Hz, CH_2), 4.60 (d, ^{3}J = 5.2 Hz, 2H, CH_2), 4.09 (s, 2H, CH_2).

^{13}C NMR (101 MHz, CD_3OD) δ 159.4, 134.5, 133.2, 130.0, 120.7, 116.2, 114.9, 114.9, 68.4, 42.8.

Physical and spectroscopic data match those previously reported.[20]

7.7.6. Synthesis of *O*-Allyl *p*-aminomethylphenol (180)

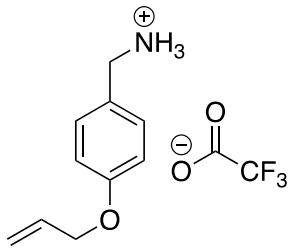

170

Using the general procedure described in **Section 7.4.4**, **177** (1.10 g, 3.80 mmol, 1.00 eq) was treated with a cleavage solution. **180** was recovered as a pale-yellow waxy solid (1.30 g, quant).

HRMS (TOF MS ES-): calcd for $C_{10}H_{14}NO$: 164.1075; found: 164.1081.

^{1}H NMR (400 MHz, CD_3OD) δ 7.35-7.41 (m, 2H, Ar*H*), 6.98-7.04 (m, 2H, Ar*H*), 6.07 (ddt, ^{3}J = 17.3, ^{3}J = 10.4, ^{2}J = 5.2, 1H, C*H*), 5.41 (dd, ^{3}J = 17.3 Hz, ^{2}J = 1.6, 1H, CH_2), 5.27 (dd, ^{3}J = 10.6 Hz, ^{2}J = 1.5 Hz, 1H, CH_2), 4.59 (d, ^{3}J = 5.2 Hz, 2H, CH_2), 4.06 (s, 2H, CH_2).

^{13}C NMR (101 MHz, CD_3OD) δ 159.4, 133.2, 130.2, 125.01 116.2, 114.9, 68.4, 42.5.

Physical and spectroscopic data match those previously reported.[21]

7.7.7. Synthesis of *N*-Alloc, *N*-Boc aminobenzylamine (183)

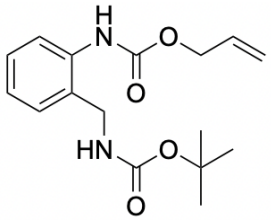

183

182 (761 mg, 3.40 mmol, 1.00 eq) was dissolved in THF (10 mL) and treated with $NaHCO_3$ (428 mg, 5.10 mmol, 1.50 eq) before the dropwise addition of allyl chloroformate (397 µL, 3.70 mmol, 1.10 eq) at 0 ºC. The reaction mixture was allowed to warm up to RT and was stirred for 1 h. Then, it was concentrated and partitioned between DCM (10 mL) and a solution of 1 M citric acid (10 mL), and the aqueous layer was extracted twice with DCM. The organic extracts were combined, dried with $MgSO_4$, filtered, and concentrated *in vacuo.* **183** was recovered as an amber oil (quant).

HRMS (TOF MS ES+): calcd for $C_{16}H_{23}N_2O_4$: 307.1658; found: 307.1673.

^{1}H NMR (400 MHz, $CDCl_3$) δ 7.39 – 7.28 (m, 2H, Ar*H*), 7.16 (dd, *J* = 7.6, 1.7 Hz, 1H, Ar*H*), 7.05 (td, *J* = 7.5 Hz, 1.3 Hz, 1H, Ar*H*), 6.01 (ddt, *J* = 17.2 Hz, 10.5 Hz, 5.5 Hz, 1H, C*H*), 5.44 – 5.23 (m, 2H, CH_2), 4.70 (dt, *J* = 5.5 Hz, 1.5 Hz, 2H, CH_2), 4.14 (s, 2H, CH_2), 1.47 (s, 9H, CH_3).

^{13}C NMR (101 MHz, $CDCl_3$) δ 170.8, 160.8, 154.3, 149.8, 131.8, 130.2, 128.6, 123.2, 121.6, 117.5, 80.3, 66.2, 60.4, 28.7.

Physical and spectroscopic data match those previously reported.[22]

7.7.8. Synthesis of *N*-Alloc aminobenzylamine (184)

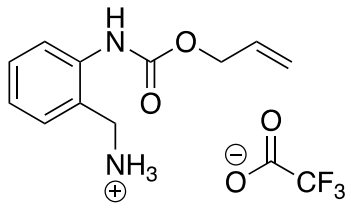

184

Using the general procedure described in **Section 7.4.4**, **183** (1.20 g, 3.40 mmol, 1.00 eq) was treated with a cleavage solution to produce **184** as an amber oil (1.40 g, quant).

HRMS (TOF MS ES+): calcd for $C_{11}H_{15}N_2O_2$: 207.1134; found: 207.1138.

^{1}H NMR (400 MHz, CD_3CN) δ 7.95 (br, 1H, N*H*), 7.56 – 7.40 (m, 2H, Ar*H*), 7.39 – 7.28 (m, 2H, Ar*H*), 7.12 (br, 3H, NH_3), 6.00 (ddt, *J* = 17.3, 10.7, 5.4 Hz, 1H, C*H*), 5.39 (dd, *J* = 17.3, 1.6 Hz, 1H, CH_2), 5.27 (dd, *J* = 10.6, 1.4 Hz, 1H, CH_2), 4.64 (d, *J* = 5.4, 2H, CH_2), 4.09 (s, 2H, CH_2).

^{13}C NMR (101 MHz, $CDCl_3$) δ 141.7, 138.0, 137.4, 135.8, 133.2, 132.4, 131.7, 105.0, 71.5, 45.5.

Physical and spectroscopic data match those previously reported.[22]

7.7.9. Synthesis of nonamer peptoids (Pep. 50 – Pep. 57)

The syntheses of a series of linear 9-mer peptoids (**Table 7.2**) were carried out using the general procedures outlined in **Section 7.4.1.c).**

Table 7.2. A tabulated summary of manually synthesised peptoid dodecamers. [a]Yield after HPLC purification.

No.	Sequence	t_R (min)	Calc. mass [M]	Obs. Mass $[M+H]^+$	Pure pdt (mg)	Isolated Yield (%)[a]
Pep. 50	*N*Lys*N*spe*N*Phe $[N\text{lys}N\text{Phe}N\text{Phe}]_2$	21.0	1298.64	1299.75	15.6	24
Pep. 51	*N*lys*N*spe*No*Tyr $[N\text{lys}N\text{Phe}No\text{Tyr}]_2$	19.7	1346.64	1347.73	2.4	4
Pep. 54	*N*lys*N*spe*No*Tyr $[N\text{lys}No\text{Tyr}No\text{Tyr}]_2$	17.8	1378.64	1379.72	0.5	1
Pep. 52	*N*lys*N*spe*Nm*Tyr $[N\text{lys}N\text{Phe}Nm\text{Tyr}]_2$	17.9	1346.64	1347.73	2.0	2
Pep. 55	*N*lys*N*spe*Nm*Tyr $[N\text{lys}Nm\text{Tyr}Nm\text{Tyr}]_2$	16.2	1378.64	1379.72	1.0	2
Pep. 53	*N*lys*N*spe*N*Tyr $[N\text{lys}N\text{Phe}N\text{Tyr}]_2$	16.9	1346.64	1347.73	8.6	14
Pep. 56	*N*lys*N*spe*N*Tyr $[N\text{lys}N\text{Tyr}N\text{Tyr}]_2$	14.2	1378.64	1379.72	2.8	3
Pep. 57	*N*2aPhe*N*spe*N*Phe $[N2\text{aPhe}N\text{Phe}N\text{Phe}]_2$	29.41	1442.78	1443.79	3.2	5

7.8. Experimental data for Chapter 5

7.8.1. Synthesis of *N*-Boc, *N*-Alloc 1,4-diaminobutane (192)

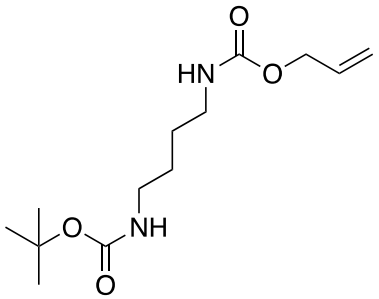

192

191 (1.00 g, 5.32 mmol, 1.00 eq) was dissolved in DCM (10 mL) and TEA (0.81 mL, 5.80 mmol, 1.10 eq) was added. The mixture was subsequently placed in an ice bath and, at 0°C, allyl chloroformate (0.56 mL, 5.80 mmol, 1.10 eq) was added dropwise. The mixture was then brought to RT and stirred for 1 h. The reaction mixture was washed with a solution of 1 M citric acid (10 mL), the layers were separated, and the aqueous phase was extracted with

DCM (10 mL) twice. The organics were combined, washed with a saturated solution of $NaHCO_3$ (10 mL), dried over $MgSO_4$, filtered, and concentrated *in vacuo* to afford the desired product **192** as a white solid (1.45 g, 100%).

HRMS (TOF MS ES+): calcd for $C_{13}H_{25}N_2O_4$: 273.1824; found: 273.1814.

^{1}H NMR (126 MHz, $CDCl_3$) δ 5.92 (m, 1H, C*H*), 5.31 (m, 2H, CH_2), 5.22 (m, 2H, CH_2), 4.57 (d, J = 5.7 Hz, 1H, CH_2), 3.18 (m, 4H, CH_2), 1.56 – 1.51 (m, 4H, CH_2), 1.46 (s, 9H, ^{t}Bu-CH_3)

^{13}C NMR (101 MHz, $CDCl_3$) δ 156.3, 156.0, 133.0, 117.6, 79.2, 65.4, 40.7, 40.2, 28.4, 27.4, 27.3.

Physical and spectroscopic data match those previously reported.[23]

7.8.2. Synthesis of *N*-Alloc 1,4-diaminobutane (193)

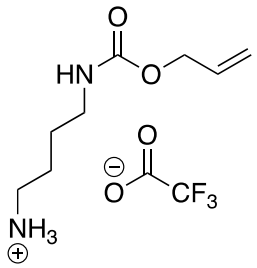

193

Using the general procedure described in **Section 7.4.4**, **192** (1.45 g, 5.32 mmol, 1.00 eq) was treated with a cleavage solution. After workup, **193** (1.45 g, 5.32 mmol, 1.00 eq) was recovered as a yellow oil (1.77 g, quant.).

HRMS (TOF MS ES+): calcd for $C_8H_{17}N_2O_2$: 173.1280; found: 173.1290.

^{1}H NMR (400 MHz, $CDCl_3$) δ 5.96 (m, 1H, C*H*), 5.31 (m, 1H, CH_2), 5.20 (dd, J = 10.5, 1.5 Hz, 1H, CH_2), 4.54 (dd, J = 5.5, 1.6 Hz, 2H, CH_2), 3.17 (t, J = 6.7 Hz, 2H, CH_2), 2.96 (t, J = 7.5 Hz, 2H, CH_2), 1.76 – 1.52 (m, 4H, CH_2).

^{13}C NMR (101 MHz, $CDCl_3$) δ 157.5, 133.1, 116.0, 64.9, 39.5, 39.0, 26.5, 24.4.

Physical and spectroscopic data match those previously reported.[23]

7.8.3. Synthesis of *N*-Alloc, *N*-Fmoc 1,4-diaminobutane (194)

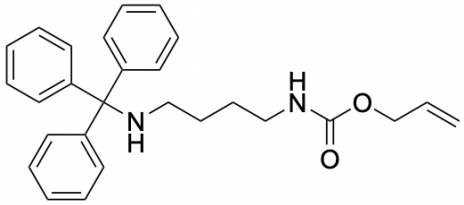

194

193 (0.73 g, 1.76 mmol, 1.00 eq) was dissolved in 5 mL of DCM. Then, TEA (0.26 mL, 3.52 mmol, 2.00 eq) was added. The flask was cooled down to 0 °C and inertised with N_2. Subsequent dropwise addition of Trt-Cl (0.53 mL. 3.52 mmol, 1.20 eq) in DCM (5 mL) followed. The reaction mixture was allowed to reach RT and was stirred overnight. It was then partitioned between EtOAc (10 mL) and water (10 mL), and the aqueous layer was extracted with ethyl acetate (10 mL) twice. The organics were combined, dried with $MgSO_4$, filtered and concentrated *in vacuo*. The desired product **194** was recovered as a white solid (0.94 mg, quant).

HRMS (TOF MS ES+): calcd for $C_{27}H_{30}N_2O_2$: 415.2374; found: 415.2386.

^{1}H NMR (400 MHz, $CDCl_3$) δ 7.52 – 7.45 (m, 5H, Ar*H*), 7.34 – 7.25 (m, 7H, Ar*H*), 7.23 – 7.17 (m, 3H, Ar*H*), 5.95 (m, 1H, C*H*), 5.32 (dd, J = 17.2, 1.6 Hz, 1H, CH_2), 5.23 (dd, J = 10.4, 1.3 Hz, 1H, CH_2), 4.57 (d, J = 5.7 Hz, 2H, CH_2), 3.18 (m, 2H, CH_2), 1.66 – 1.49 (m, 6H, CH_2).

^{13}C NMR (101 MHz, $CDCl_3$) δ 156.3, 146.2, 133.1, 128.7, 127.8, 126.3, 117.6, 70.9, 65.5, 43.3, 41.1, 26.1, 28.0.

7.8.4. Synthesis of *N*-Fmoc 1,4-diaminobutane (195)

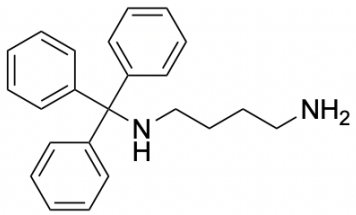

195

Phenylsilane (1.50 mL, 15.1 mmol, 10.0 eq) was added to a solution of **194** (498 mg, 1.51 mmol, 1.00 eq) in DCM (15 mL). The flask was placed under N_2 atmosphere and $Pd(PPh_3)_4$ (139 mg, 0.15 mmol, 0.10 eq) was added to the mixture at RT. The resulting reaction mixture was stirred under inert atmosphere, at ambient temperature for 1 hour. Following concentration *in vacuo*, the crude material was purified by FC chromatography, using a

gradient of 100% hexane to 100% EtOAc. The desired product **195** was recovered as a white solid (quant).

HRMS (TOF MS ES+): calcd for $C_{23}H_{27}N_2$: 331.2174; found: 331.2184.

^{1}H NMR (126 MHz, $CDCl_3$) δ 7.53 – 7.44 (m, 5H, Ar*H*), 7.32 – 7.25 (m, 7H, Ar*H*), 7.23 – 7.17 (m, 3H, Ar*H*), 2.71 (t, J = 6.5 Jz, 2H, CH_2), 2.15 (t, J = 6.1 Hz, 2H, CH_2), 1.59 – 1.45 (m, 4H, CH_2).

^{13}C NMR (101 MHz, $CDCl_3$) δ 146.2, 128.6, 127.8, 126.2, 70.9, 43.0, 41.8, 30.4, 28.1.

Physical and spectroscopic data match those previously reported.[24]

7.8.5. Synthesis of *N*-Alloc, *N*-Mmt 1,4-diaminobnutane (197)

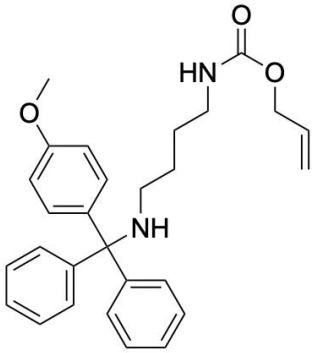

197

193 (100 mg, 0.35 mmol, 1.00 eq) was dissolved in DCM (5 mL) and treated with TEA (51.0 μL, 0.70 mmol, 2.00 eq), Mmt-Cl (130 mg, 0.42 mmol, 1.20 eq) was then added and the mixture was stirred o/n at RT. The volatiles were evaporated in vacuo. The residue was purified by flash column chromatography, using a gradient of 100% hexane to 100% EtOAc. The desired product (impure) was recovered as a white wax (178, quant.). LC/HRMS was not obtained because the Mmt group is cleaved by acidic conditions present in the system.

^{1}H NMR (400 MHz, CD_3CN) δ 7.53 – 7.14 (m, 12H, Ar*H*), 6.89 – 6.84 (m, 2H, Ar*H*), 6.12 – 5.99 (m, 1H, C*H*), 5.30 – 5.25 (m, 2 H, CH_2), 4.60 (d, J = 5.7 Hz, 2H, CH_2), 3.78 (s, 3H, CH_3), 2.17 – 2.10 (m, 2H, CH_2), 1.56 – 1.48 (s, 4H, CH_2), other signals overlap with triethylamine signals.

^{13}C NMR (101 MHz, CD_3CN) δ 162.2, 159.2, 140.9, 135.1, 132.1, 129.5, 128.7, 128.6, 127.1, 117.3, 113.9, 78.3, 65.3, 55.8, 44.3, 37.8, 28.4, 25.5.

7.8.6. Synthesis of *N*-Boc, *N*-Fmoc 1,4-diaminobutane (199)

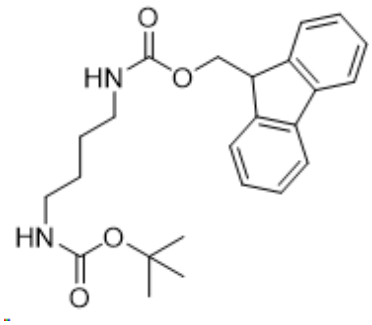

199

190 (0.50 g, 2.66 mmol, 1.00 eq) was dissolved in 10 mL of dioxane and 8 mL of acetone. Then, $NaHCO_3$ (3.50 eq, 9.31 mmol, 782 mg) in H_2O (12 mL) was added. Fmoc-OSu (1.08 g, 3.19 mmol, 1.20 eq) was added to this mixture portion wise over 10 mins. After 1 h of stirring at RT the mixture was partitioned between DCM (20 mL) and 1 M solution of citric acid (15 mL). The aqueous was extracted twice with DCM, the organics were combined, dried over $MgSO_4$, filtered and concentrated *in vacuo*. The resulting precipitate was suspended in hexane and collected upon filtration to yield the desired product **199** as a white solid (1.00 g, 95%).

HRMS (TOF MS ES+): calcd for $C_{25}H_{30}N_2O_4$: 411.2284; found: 411.2289.

^{1}H NMR (400 MHz, DMSO) δ 7.90 (d, J = 7.5 Hz, 2H, Ar*H*), 7.69 (d, J = 7.4, 2H, Ar*H*), 7.45 – 7.39 (m, 2H, Ar*H*), 7.37 – 7.31 (m, 2H, Ar*H*), 4.29 (d, *J* = 7.0 Hz, 2H, CH_2), 4.21 (t, *J* = 6.9 Hz, 1H, C*H*), 2.97 (t, *J* = 5.7 Hz, 2H, CH_2), 2.90 (t, *J* = 5.9 Hz, 2H), 1.42 – 1.31 (m, 13H, CH_2, ^{t}Bu-CH_3).

^{13}C NMR (101 MHz, DMSO) δ 156.55, 156.05, 144.42, 141.21, 128.06, 127.52, 125.61, 120.58, 77.80, 65.64, 47.25, 28.75, 27.34, 27.27.

7.8.7. Synthesis of *N*-Fmoc 1,4-diaminobutane (200)

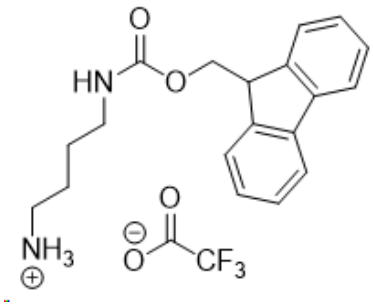

200

199 (1.00 g, 2.53 mmol, 1.00 eq), was dissolved in a solution of 25% TFA in DCM (10 mL). The mixture was stirred for 2 h at RT before it was concentrated. The desired product **200** was recovered as a waxy off-white solid (1.26 g, quant).

HRMS (TOF MS ES+): calcd for $C_{20}H_{23}N_2O_2$: 311.1676; found: 311.1675.

^{1}H NMR (400 MHz, DMSO) δ 7.82 (d, J = 7.4 Hz, 2H, Ar*H*), 7.59 (d, 7.4 Hz, 2H, Ar*H*), 7.45 – 7.40 (m, 2H, Ar*H*), 7.33 – 7.29 (m, 2H, Ar*H*), 4.33 (d, *J* = 6.9 Hz, 2H, CH_2), 4.20 (t, *J* = 6.9 Hz, 1H, C*H*), 2.94 (t, *J* = 5.7 Hz, 2H, CH_2), 2.97 (t, *J* = 5.9 Hz, 2H, CH_2), 1.65 – 1.60 (m, 2H, CH_2), 1.58 – 1.53 (m, 2H, CH_2).

^{13}C NMR (101 MHz, DMSO) δ 159.1, 144.4, 142.6, 128.8, 128.2, 126.1 121.0, 66.6, 47.1, 41.0, 36.0, 27.9, 27.2.

7.8.8. Synthesis of *N*-Fmoc, N-Mmt 1,4-diaminobutane (201)

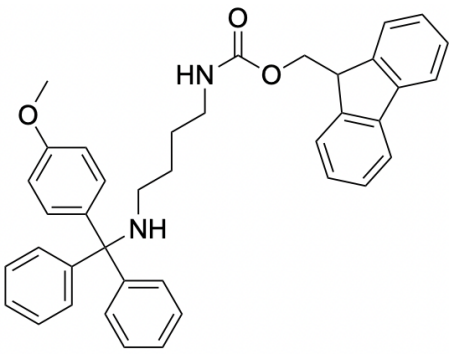

201

200 (0.5 g, 1.18 mmol, 1.0 eq) in DCM (10 mL) was treated with TEA (0.30 mL, 2.36 mmol, 2.00 eq) and Mmt-Cl (0.40 g, 2.36 mmol, 1.20 eq). The mixture was stirred for 2 hours at RT before it was concentrated. The remaining traces of TEA were co-evaporated with Et_2O (50 mL). The desired product **201** was recovered as an amber oil (0.88 g, quant). LC/HRMS was not obtained because Mmt is cleaved by acidic conditions present in the system.

^{1}H NMR (400 MHz, $CDCl_3$) δ 7.79 (d, *J* = 7.5 Hz, 2H, Ar*H*), 7.62 (d, *J* = 7.5 Hz, 2H, Ar*H*), 7.54 – 7.46 (m, 4H, Ar*H*), 7.46 – 7.37 (m, 4H, Ar*H*), 7.37 – 7.26 (m, 6H, Ar*H*), 7.25 – 7.17 (m, 2H, Ar*H*), 6.90 – 6.80 (m, 2H Ar*H*), 4.88 (s, 1H, C*H*), 4.44 (d, *J* = 6.8 Hz, 2H, CH_2), 3.83 – 3.77 (m, 2H, CH_2), (3.81 (s, 3H, CH_3), 3.23 – 3.14 (m, 2H, CH_2), 1.59 – 1.49 (m, 4H, CH_2).
^{13}C NMR (101 MHz, $CDCl_3$) δ 171.21, 157.84, 156.45, 146.48, 144.05, 142.10, 138.39, 129.79, 128.56, 127.82, 127.69, 127.06, 126.20, 125.06, 119.99, 113.11, 70.41, 66.44, 60.44, 47.36, 43.32, 41.12, 28.10, 27.95.

7.8.9. Synthesis of Boc-Tyr(TFP)-OMe (205)

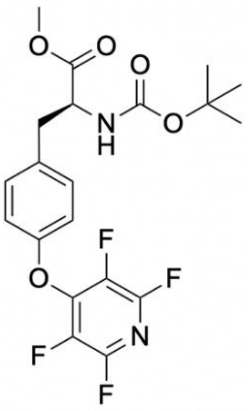

205

Using the general procedure described in **Section 7.4.6, 204** (1.00 g, 3.39 mmol, 1.00 eq) was TFP-protected, yielding the desired product **205** as a white solid (1.49 g, 100%).

HRMS (TOF MS ES+): calcd for $C_{20}H_{19}N_2O_5F_4$: 443.1230; found: 443.1236.
^{19}F NMR (376 MHz, $CDCl_3$) δ -88.30 – -88.79 (m, 2 F), -154.03 – -154.40 (m, 2 F).
^{1}H NMR (400 MHz, $CDCl_3$) δ 7.22 – 7.13 (m, 2H, Ar*H*), 7.05 – 6.97 (m, 2H, Ar*H*), 4.61 (m, 1H, C*H*), 3.73 (s, 3H, CH_3), 3.19 – 2.96 (m, 2H, CH_2), 1.44 (s, 9H, ^{t}Bu- CH_3).
^{13}C NMR (101 MHz, $CDCl_3$) δ 172.1, 159.0, 154.9, 142.6, 133.2, 130.9, 116.8, 77.2, 54.4, 52.3, 37.8, 28.3. C-F signals are too weak, so are not reportable.
Physical and spectroscopic data match those previously reported.[27]

7.8.10. Synthesis of Boc-Tyr(TFP)-OMe (206)

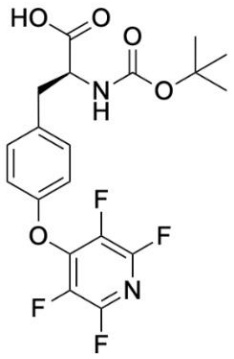

206

205 (0.50 g, 1.13 mmol, 1.00 eq) was dissolved in a mixture of THF (5 mL) and H_2O (5 mL), and treated with $LiOH.H_2O$ (71 mg, 1.70 mmol, 1.05 eq). The resulting reaction mixture was stirred for 45 minutes before it was partitioned between a solution of 1 M of citric acid (10 mL) and EtOAc (10 mL). The aqueous layer was extracted with EtOAc twice. The organics were combined, dried over $MgSO_4$, filtered and concentrated *in vacuo*. No purification was performed, and the desired product **206** (containing traces of **207**) was recovered as a white solid (0.43 g, 98%*).

* The recovered product comprised of mainly the desired product **206**.

HRMS (TOF MS ES-): calcd for $C_{19}H_{17}F_4N_2O_5$: 430.3556; found: 429.0833.

^{19}F NMR (376 MHz, CD_3OD) δ -92.17 - -92.53 (m, 2 F), -156.92 - -157.33 (m, 2F).

^{1}H NMR (400 MHz, CD_3OD) δ 7.34 – 7.27 (m, 2H, Ar*H*), 7.15 – 7.06 (m, 2H, Ar*H*), 4.37 (t, *J* = 8.5, 1H, C*H*), 3.20 (m, 1H, CH_2), 2.91 (ddd, *J* = 14.4, 9.4, 5.0 Hz, 1H, CH_2), 1.39 (s, 9H, ^{t}Bu-CH_3).

^{13}C NMR (101 MHz, CD_3OD) δ 173.8, 156.4, 155.0, 134.4, 130.7, 116.1, 79.1, 54.8, 36.6, 27.3. C-F signals are too weak, so are not detectable.

7.8.11. Synthesis of Fmoc-Tyr(tBu)-O(Allyl) (211)

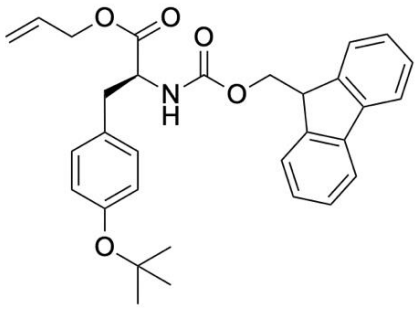

211

210 (1.00 g, 2.17 mmol, 1.00 eq) was dissolved in 10 mL of DMF and treated with $KHCO_3$ (0.34 g, 3.26 mmol, 1.50 eq) and allyl bromide (2.30 mL, 3.26 mmol, 1.50 eq). The reaction mixture was allowed to stir at RT overnight. Subsequently, the mixture was partitioned between EtOAc (20 mL) and a solution of 1 M citric acid (20 mL). The aqueous phase was extracted with EtOAc thrice. The organics were combined, washed with water, and dried with magnesium sulphate. The volatiles were evaporated *in vacuo* and the desired product **211** was recovered as a colourless oil (1.01 g, 97%).

HRMS (TOF MS ES+): calcd for $C_{31}H_{34}NO_5$: 500.2435, found: 500.2437.

^{1}H NMR (126 MHz, $CDCl_3$) δ 8.04 (br, 1H, N*H*), 7.79 (d, J = 7.5 Hz, 2H, Ar*H*), 7.60 (dd, J = 7.7, 3.7 Hz, 2H, Ar*H*), 7.47 – 7.38 (m, 2H, Ar*H*), 7.34 (tt, J = 7.4, 1.4 Hz, 2H, Ar*H*), 7.02 (d, J = 8.4 Hz, 2H, Ar*H*), 6.96 – 6.89 (m, 2H, Ar*H*), 5.91 (m, 1H, C*H*), 5.28 (m, 2H, CH_2), 4.66 (m, 2H, CH_2), 4.41 (m, 2H, CH_2), 4.24 (t, J = 7.0 Hz, 1H, C*H*), 3.10 (m, 2H, CH_2), 1.34 (s, 9H, ^{t}Bu-CH_3).

^{13}C NMR (101 MHz, $CDCl_3$) δ 171.3, 155.6, 154.5, 143.8, 141.3, 131.4, 130.4, 129.9, 127.7, 127.1, 125.1, 124.2, 120.0, 119.1, 78.5, 67.0, 66.1, 54.9, 47.2, 37.7, 28.8.

Physical and spectroscopic data match those previously reported.[25]

7.8.12. Synthesis of Fmoc-Tyr-O(Allyl) (212)

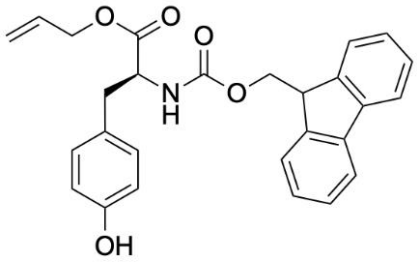

212

211 (1.00 g, 2.00 mmol, 1.00 eq) was treated with 10 mL of a solution of 25% TFA in DCM. The resulting reaction mixture was stirred at RT for 1 h before being concentrated *in vacuo*. The residual TFA was then co-evaporated with Et_2O (5 mL). **212** was collected as a white solid (0.95 g, 98%).

HRMS (TOF MS ES+): calcd for $C_{27}H_{26}NO_5$: 444.1811; found: 444.1798.

^{1}H NMR (400 MHz, CD_3CN) δ 7.85 (d, J = 7.7 Hz, 2H, Ar*H*), 7.63 (d, J = 7.5 Hz, 2H, Ar*H*), 7.44 (t, J = 7.5 Hz, 2H, Ar*H*), 7.38 – 7.31 (m, 2H, Ar*H*), 7.07 (d, J = 8.0 Hz, 2H, Ar*H*), 6.82 – 6.71 (m, 2H, Ar*H*), 6.00 – 5.85 (m, 1H, C*H*), 5.33 – 5.24 (m, 2H, CH_2), 4.61 (d, J = 5.5 Hz, 2H, CH_2), 4.35 – 4.26 (m, 2H, CH_2), 4.24 – 4.17 (m, 1H, C*H*), 3.13 – 3.03 (m, 2H, CH_2).

^{13}C NMR (101 MHz, CD_3CN) δ 171.5, 155.8, 144.1, 144.0, 141.2, 139.4, 132.2, 128.0, 127.2, 125.2, 125.2, 120.0, 117.7, 115.2, 66.4, 65.4, 55.8, 47.0, 36.4.

7.8.14. Synthesis of Fmoc-Tyr(TFP)-O(Allyl) (213)

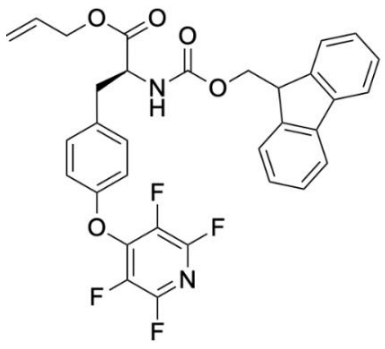

213

Using the general procedure described in **Section 7.4.6, 212** (0.95 g, 2.00 mmol, 1.00 eq) was TFP-protected, yielding the desired product **213** as a white solid (1.20 g, 95%).

HRMS (TOF MS ES+): calcd for $C_{32}H_{25}N_2O_5F_4$: 593.1700; found: 593.1721.

^{19}F NMR (376 MHz, CD_3OD) δ -88.36 – -89.03 (m, 2F), -153.95 – -154.41 (m, 2F).

^{1}H NMR (126 MHz, $CDCl_3$) δ 7.78 (d, J = 7.6 Hz, 2H, Ar*H*), 7.60 (t, J = 7.4 Hz, 2H, Ar*H*), 7.41 (t, J = 7.5 Hz, 2H, Ar*H*), 7.35 – 7.28 (m, 2H, Ar*H*), 7.16 (d, J = 8.2 Hz, 2H, Ar*H*), 6.97 (d, J = 8.2 Hz, 2H, Ar*H*), 5.96 – 5.82 (m, 1H, C*H*), 5.36 – 5.23 (m, 2H, CH_2),.64 (d, J = 5.9 Hz, 2H, CH_2), 4.51 – 4.33 (m, 2H, CH_2), 4.22 (t, J = 6.8 Hz, 1H, C*H*), 3.25 – 3.06 (m, 2H, CH_2).

^{13}C NMR (101 MHz, $CDCl_3$) δ 171.1, 155.7, 149.5, 145.9 – 145.1 (m), 143.8, 143.7, 142.6, 143.2 - 141.3 (m), 138.8, 137.8 – 137.1 (m), 135.1 – 134.6 (m), 133.1, 131.4, 131.0, 127.8, 125,1, 120.0, 119.2, 116.8, 67.0, 66.2, 55.0, 47.4, 37.5.

7.8.15. Synthesis of Fmoc-Tyr(TFP)-OH (214)

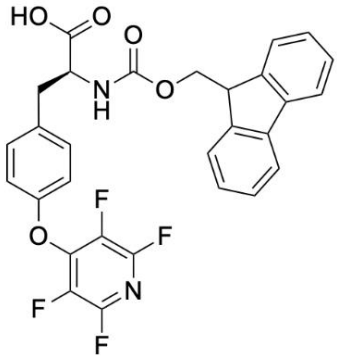

214

Under an N_2 atmosphere, at RT, **213** (1.20 g, 1.90 mmol, 1.00 eq) was dissolved in 10 mL of DCM and treated with $Pd(PPh_3)_4$ (231 mg, 0.19 mmol, 0.10 eq). The mixture was left to stir o/n. The volatiles were evaporated, and the crude material was purified by FC chromatography using a gradient of 100% hexane to 100% EtOAc. The desired product **214** was recovered as an off-white solid (1.10 g, 99%)

HRMS (TOF MS ES+): calcd for $C_{29}H_{21}F_4N_2O_5$: 553.1375; found: 553.1387.

^{19}F NMR (376 MHz, CD_3OD) δ -91.50 – -92.90 (m, 2 F), -156.69 – -157.50 (m, 2 F).

^{1}H NMR (126 MHz, CD_3OD) δ 7.83 – 7.76 (m, 2H, Ar*H*), 7.66 – 7.55 (m, 2H, Ar*H*), 7.49 – 7.36 (m, 2H, Ar*H*), 7.35 – 7.31 (m, 4H, Ar*H*), 7.10 – 7.03 (m, 2H, Ar*H*), 4.43 (dd, J = 9.7, 4.7 Hz, 1H, C*H*), 4.27 (m, 2H, CH_2), 4.17 (m, 1H, C*H*), 3.26 (dd, J = 13.9, 4.6 Hz, 1H, CH_2), 2.96 (dd, J = 13.9, 9.8 Hz, 1H, CH_2).

^{13}C NMR (101 MHz, CD_3OD) δ 172.9, 154.9, 148.9, 143.9, 143.8, 141.1, 134.4, 130.7, 127.4, 126.7, 124.9, 119.5, 116.1, 66.6, 55.4, 47.1, 36.5. C-F signals are too weak, so are not reportable.

7.8.19. Synthesis of cyclic biopolymers (Pep. 90 –95, Pep. 101)

The syntheses of a cyclic peptoids (**Pep. 90 – 95**) and peptide (**Pep.101**), shown in **Table 7.3**, were carried out using the general procedures outlined in **Sections 7.4.11.** and **7.4.12.**

Table 7.3. A tabulated summary of manually synthesised peptoid and peptide cycles. [a]after HPLC purification.

No.	Sequence	t_R (min)	Calc. mass [M]	Obs. Mass $[M+H]^+$	Pure pdt (mg)	Isolated Yield (%)[a]
Pep. 90	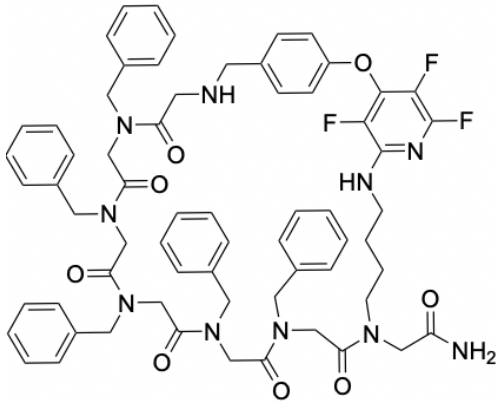	30.8	1173.31	1173.44	2.8	3

Pep. 91	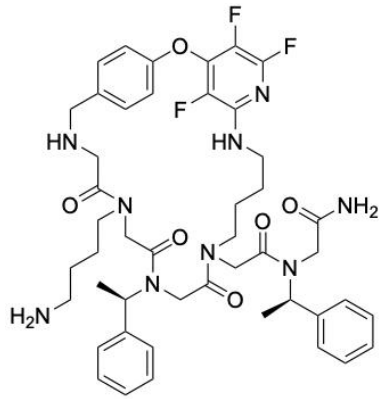	23.7	888.01	888.38	6.0	9
Pep. 92	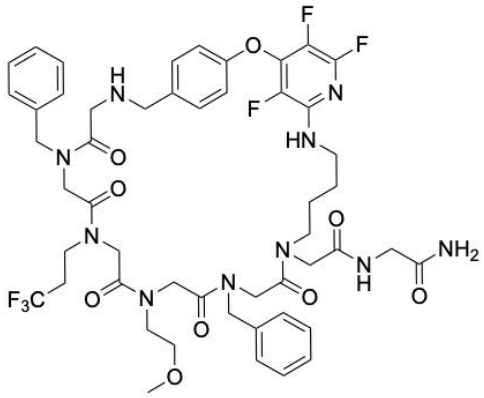	24.0	1057.07	1057.36	3.6	4

Pep. 93	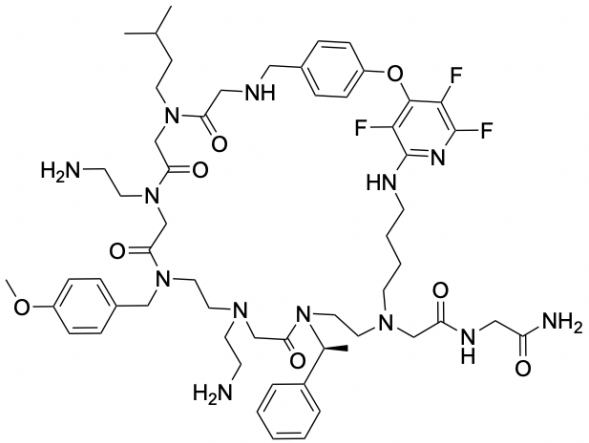	21.9	1160.34	1161.59	6.7	7
Pep. 94	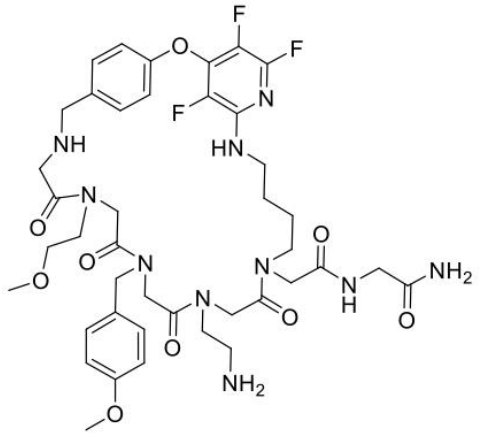	24.8	886.93	887.40	5.2	7

Pep. 95	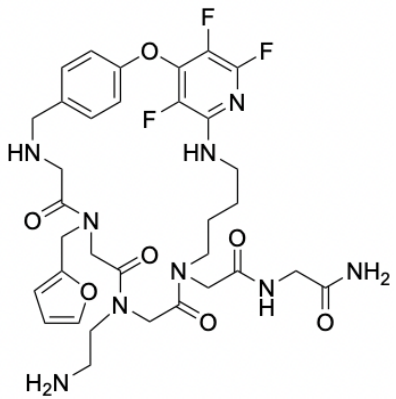	19.5	731.73	732.31	6.0	11
Pep. 101	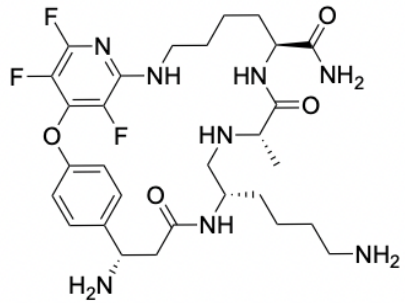	17.8	636.68	637.31	3.0	4

7.9. References for Chapter 7

[1] Wijaya, A. W., Nguyen, A. I., Roe, L. T., Butterfoss, G. L., Spencer, R. K., Li, N. K., Zuckermann, R. N., 2019, J. *Am. Chem. Soc*., **141**, 19436-19447.
[2] Jahani, F., Tajbakhsh, M., Golchoubian, H. Khaksar, S., 2011, *Tetrahedron Lett*., **52**, 1260-1264.
[3] Lee, C., Lee, D.H., Hong, J.I., 2001, 49, 8665-8668.
[4] Nhu, D., Duffy, S., Avery, V.M., Hughes, A., Baell, J.B., 2010, *Bioorg. Med. Chem. Lett*., **20**, 4496-4498.
[5] Surmiak, E., Neochoritis, C.G., Musielak, B., Twarda-Clapa, A., Kurpiewska, K., Dubin, G., Camacho, C., Holak, T.A., Dömling, A., 2017, *Eur. J. Med. Chem.,* **126**, 384-407.
[6] Morin, M.S., Toumieux, S., Compain, P., Peyrat, S., Kalinowska-Tluscik, J., 2007, *Tetrahedron Lett*., **48**, 8531-8535.
[7] Dubash, N.P., Mangu, N.K., Satyam, A., 2004, *Synth. Commun*., **34**, 1791-1799.
[8] Kankanala, J., Ribeiro, C.J., Kiselev, E., Ravji, A., Williams, J., Xie, J., Aihara, H., Pommier, Y., Wang, Z., 2019, *J. Med. Chem.,* **62**, 4669-4682.
[9] Vitaku, E., Smith, D.T., Njardarson, J.T., 2016, *Angew. Chem. Int. Ed*., **55**, 2243-2247.
[10] Dubash, N.P., Mangu, N.K., Satyam, A., 2004, *Synth. Commun*., **34**, 1791-1799.
[11] Kankanala, J., Ribeiro, C.J., Kiselev, E., Ravji, A., Williams, J., Xie, J., Aihara, H., Pommier, Y., Wang, Z., 2019, *J. Med. Chem*., **62**, 4669-4682.
[12] Stringer, J.R., Crapster, J.A., Guzei, I.A., Blackwell, H.E., 2010, *J. Org. Chem*., **75**, 6068-6078.
[13] Gorske, B.C., Stringer, J.R., Bastian, B.L., Fowler, S.A., Blackwell, H.E., 2009, *J. Am. Chem. Soc*., **131**, 16555-16567.
[14] Rodríguez-Soacha, D.A., Steinmüller, S.A., Isbilir, A., Fender, J., Deventer, M.H., Ramírez, Y.A., Tutov, A., Sotriffer, C., Stove, C.P., Lorenz, K., Lohse, M.J., 2022., *ACS Chem. Neurosci*., **13**(16), 2410-2435.
[15] Guk, D.A., Burlutskiy, R.O., Lemenovskiy, D.A., Beloglazkina, E.K., 2023, *Mendeleev Commun*., **33**(1), 14-16.
[16] Fabre, I., Perego, L.A., Bergès, J., Ciofini, I., Grimaud, L., Taillefer, M., 2016, *Eur. J. Org. Chem.,* **2016**, 5887-5896.
[17] Slavish, P.J., Cuypers, M.G., Rimmer, M.A., Abdolvahabi, A., Jeevan, T., Kumar, G., Jarusiewicz, J.A., Vaithiyalingam, S., Jones, J.C., Bowling, J.J., Price, J.E., 2023., *Eur. J. Med. Chem*., **247**, p.115035.
[18] Müller, A., Kobarg, H., Chandrasekaran, V., Gronow, J., Sçnnichsen, F.D., Lindhorst, T.K., 2015, *Synth. Azobenzene Glycoconjugates to Control Biological Function*, 101.
[19] Bennasar, M.L., Roca, T., Monerris, M., García-Díaz, D., 2006. *J. Org. Chem.,* **71**, 7028-7034.
[20] Lambruschini, C., Galante, D., Moni, L., Ferraro, F., Gancia, G., Riva, R., Traverso, A., Banfi, L., D'Arrigo, C., 2017, *Org. Biomol. Chem.,* **15**, 9331-9351.
[21] Haddenham, D., Pasumansky, L., DeSoto, J., Eagon, S., Singaram, B., 2009, *J. Org. Chem.,* **74**,1964-1970
[22] Fader, L.D., Tsantrizos, Y.S., 2002, *Org. Lett.,* **4**(1), 63-66.
[23] Henriksen, H.C., Sowers, A.J., Travis, C.R., Vulpis, T.D., Cope, T.A., Ouslander, S.K., Russell, A.F., Gagné, M.R., Pophristic, V., Liu, Z. and Waters, M.L., 2023, *J. Am. Chem. Soc*., **145**(50), 27672-27679.
[24] Thomson, A., O'Connor, S., Knuckley, B., Causey, C.P., 2014., *Bioorg. Med. Chem.,* **22**(17),4602-4608.
[25] Brittain WD, Cobb SL., 2019, *Org. Biomol. Chem.,* **17**(8):2110-5.

Appendices

A.1. Crystal structure data

For X-ray crystallography, single crystals were taken and analysed at 120 K. Samples were collected using a Brucker DB Venture, the radiation was Mo Kα (λ = 0.71073). Structures were solved by direct method and refined by full-matrix least squares on F^2 using Olex2, the refinement program was SHELXL 2017/1 (Sheldrick 2015) and the solution program was XS (Scheldrick 2008).

Sample analyses and refinement were performed by Dr Dmitry Yufit and Dr Toby Blundell, Durham University.

A1.1. Crystal determination of 59

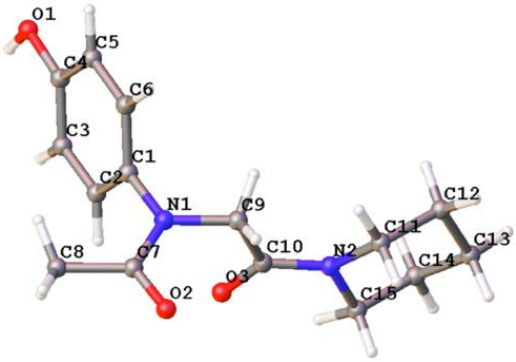

Table A.1. Crystal data and structure refinement for **59**.	
Identification code	21srv380
Empirical formula	$C_{16}H_{14}F_4N_2O_3$
Formula weight	358.29
Temperature/K	120.0
Crystal system	orthorhombic
Space group	$P2_12_12_1$
a/Å	5.2146(2)
b/Å	9.8819(4)
c/Å	30.5825(11)
α/°	90
β/°	90
γ/°	90
Volume/Å^3	1575.92(10)
Z	4
ρ_{calc}g/cm^3	1.510
μ/mm^{-1}	0.136
F(000)	736.0
Crystal size/mm^3	0.36 × 0.05 × 0.04
Radiation	Mo Kα (λ = 0.71073)

2Θ range for data collection/°	4.332 to 60
Index ranges	$-7 \leq h \leq 7$, $-13 \leq k \leq 13$, $-43 \leq l \leq 43$
Reflections collected	26508
Independent reflections	4585 [R_{int} = 0.0684, R_{sigma} = 0.0470]
Data/restraints/parameters	4585/0/249
Goodness-of-fit on F^2	1.051
Final R indexes [I>=2σ (I)]	R_1 = 0.0394, wR_2 = 0.0844
Final R indexes [all data]	R_1 = 0.0513, wR_2 = 0.0912
Largest diff. peak/hole / e $Å^{-3}$	0.25/-0.20
Flack parameter	-0.2(4)

A1.2. Crystal determination of 60

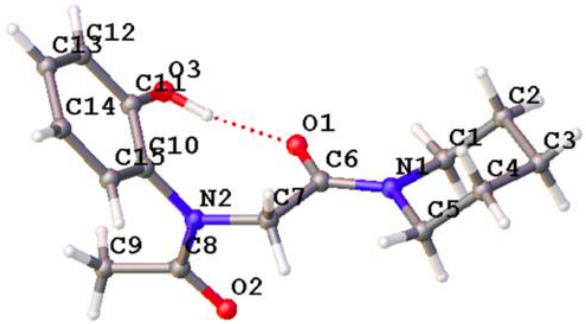

Table A.2. Crystal data and structure refinement for **60**.	
Identification code	22srv185
Empirical formula	$C_{15}H_{20}N_2O_3$
Formula weight	276.33
Temperature/K	120.00
Crystal system	monoclinic
Space group	$P2_1/c$
a/Å	8.6643(5)
b/Å	29.1323(16)
c/Å	11.5389(6)
α/°	90
β/°	91.700(2)
γ/°	90
Volume/$Å^3$	2911.3(3)
Z	8
ρ_{calc}g/cm^3	1.261
μ/mm^{-1}	0.088
F(000)	1184.0
Crystal size/mm^3	0.26 × 0.23 × 0.18
Radiation	Mo Kα (λ = 0.71073)
2Θ range for data collection/°	4.194 to 59.998
Index ranges	$-12 \leq h \leq 12$, $-40 \leq k \leq 40$, $-16 \leq l \leq 16$
Reflections collected	98647
Independent reflections	8447 [R_{int} = 0.0475, R_{sigma} = 0.0224]
Data/restraints/parameters	8447/0/522
Goodness-of-fit on F^2	1.072
Final R indexes [I>=2σ (I)]	R_1 = 0.0452, wR_2 = 0.1073

Final R indexes [all data]	R_1 = 0.0523, wR_2 = 0.1114
Largest diff. peak/hole / e Å^{-3}	0.40/-0.17

A1.3. Crystal determination of 105

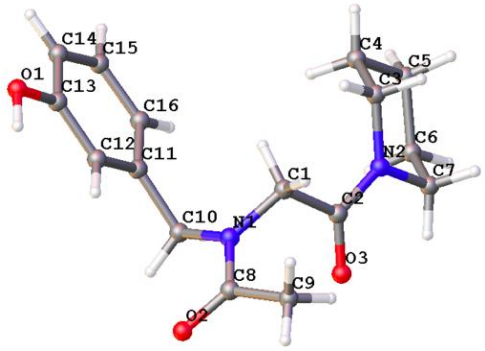

Table A.3. Crystal data and structure refinement for **105**.	
Identification code	21srv273
Empirical formula	$C_{16}H_{22}N_2O_3$
Formula weight	290.35
Temperature/K	130.0
Crystal system	monoclinic
Space group	$P2_1/c$
a/Å	8.4327(2)
b/Å	17.4960(5)
c/Å	10.5891(3)
α/°	90
β/°	99.3620(10)
γ/°	90
Volume/Å^3	1541.49(7)
Z	4
ρ_{calc}g/cm^3	1.251
μ/mm^{-1}	0.087
F(000)	624.0
Crystal size/mm^3	0.19 × 0.11 × 0.01
Radiation	MoKα (λ = 0.71073)
2Θ range for data collection/°	4.54 to 59.992
Index ranges	-11 ≤ h ≤ 11, -24 ≤ k ≤ 24, -14 ≤ l ≤ 14
Reflections collected	27798
Independent reflections	4487 [R_{int} = 0.0542, R_{sigma} = 0.0404]
Data/restraints/parameters	4487/0/278
Goodness-of-fit on F^2	1.045
Final R indexes [I>=2σ (I)]	R_1 = 0.0512, wR_2 = 0.1103
Final R indexes [all data]	R_1 = 0.0696, wR_2 = 0.1184
Largest diff. peak/hole / e Å^{-3}	0.31/-0.20

A1.4. Crystal determination of 127

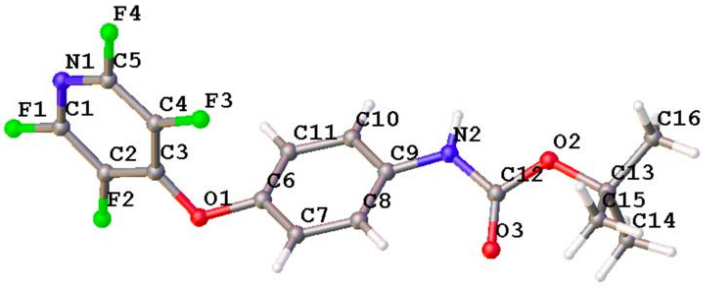

Table A.4. Crystal data and structure refinement for **127**.	
Identification code	21srv380
Empirical formula	$C_{16}H_{14}F_4N_2O_3$
Formula weight	358.29
Temperature/K	120.0
Crystal system	orthorhombic
Space group	$P2_12_12_1$
a/Å	5.2146(2)
b/Å	9.8819(4)
c/Å	30.5825(11)
α/°	90
β/°	90
γ/°	90
Volume/Å^3	1575.92(10)
Z	4
ρ_{calc}g/cm^3	1.510
μ/mm^{-1}	0.136
F(000)	736.0
Crystal size/mm^3	0.36 × 0.05 × 0.04
Radiation	Mo Kα (λ = 0.71073)
2Θ range for data collection/°	4.332 to 60
Index ranges	$-7 \leq h \leq 7$, $-13 \leq k \leq 13$, $-43 \leq l \leq 43$
Reflections collected	26508
Independent reflections	4585 [R_{int} = 0.0684, R_{sigma} = 0.0470]
Data/restraints/parameters	4585/0/249
Goodness-of-fit on F^2	1.051
Final R indexes [I>=2σ (I)]	R_1 = 0.0394, wR_2 = 0.0844
Final R indexes [all data]	R_1 = 0.0513, wR_2 = 0.0912
Largest diff. peak/hole / e Å^{-3}	0.25/-0.20
Flack parameter	-0.2(4)

A1.5. Crystal determination of 130

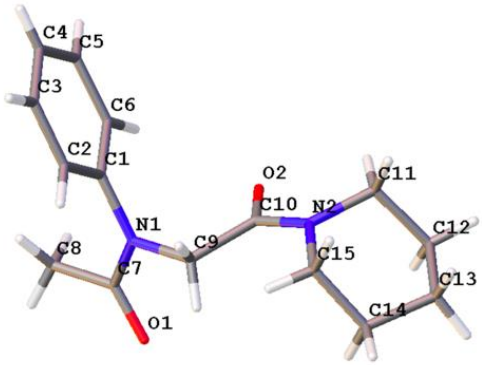

Table A.5. Crystal data and structure refinement for **130**.	
Identification code	22srv162
Empirical formula	$C_{15}H_{20}N_2O_2$
Formula weight	260.33
Temperature/K	120.00
Crystal system	monoclinic
Space group	$P2_1$
a/Å	8.0998(3)
b/Å	8.7937(3)
c/Å	10.3848(3)
α/°	90
β/°	112.0060(11)
γ/°	90
Volume/Å^3	685.79(4)
Z	2
ρ_{calc}g/cm^3	1.261
μ/mm^{-1}	0.084
F(000)	280.0
Crystal size/mm^3	0.18 × 0.13 × 0.08
Radiation	Mo Kα (λ = 0.71073)
2Θ range for data collection/°	4.23 to 59.98
Index ranges	$-11 \leq h \leq 11$, $-12 \leq k \leq 12$, $-14 \leq l \leq 14$
Reflections collected	15896
Independent reflections	3992 [R_{int} = 0.0395, R_{sigma} = 0.0402]
Data/restraints/parameters	3992/1/252
Goodness-of-fit on F^2	1.078
Final R indexes [I>=2σ (I)]	R_1 = 0.0474, wR_2 = 0.1037
Final R indexes [all data]	R_1 = 0.0521, wR_2 = 0.1058
Largest diff. peak/hole / e Å^{-3}	0.31/-0.21
Flack parameter	-0.3(5)

A1.6. Crystal determination of 131

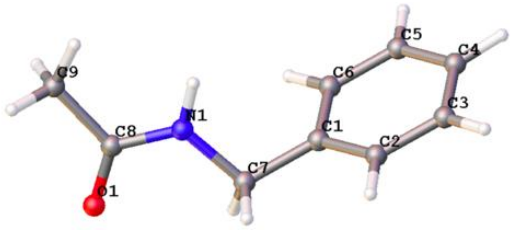

Table A.6. Crystal data and structure refinement for **131**.	
Identification code	22srv223
Empirical formula	$C_9H_{11}NO$
Formula weight	149.19
Temperature/K	120.00
Crystal system	monoclinic
Space group	$P2_1/c$
a/Å	8.6487(3)
b/Å	4.8388(2)
c/Å	19.6779(8)
α/°	90
β/°	99.248(2)
γ/°	90
Volume/Å^3	812.80(6)
Z	4
ρ_{calc}g/cm^3	1.219
μ/mm^{-1}	0.080
F(000)	320.0
Crystal size/mm^3	0.32 × 0.04 × 0.02
Radiation	Mo Kα (λ = 0.71073)
2Θ range for data collection/°	4.194 to 57.982
Index ranges	$-11 \leq h \leq 11$, $-6 \leq k \leq 6$, $-26 \leq l \leq 26$
Reflections collected	18416
Independent reflections	2166 [R_{int} = 0.0597, R_{sigma} = 0.0344]
Data/restraints/parameters	2166/0/145
Goodness-of-fit on F^2	1.179
Final R indexes [I>=2σ (I)]	R_1 = 0.0562, wR_2 = 0.1153
Final R indexes [all data]	R_1 = 0.0650, wR_2 = 0.1190
Largest diff. peak/hole / e Å^{-3}	0.22/-0.19

A1.7. Crystal determination of 136

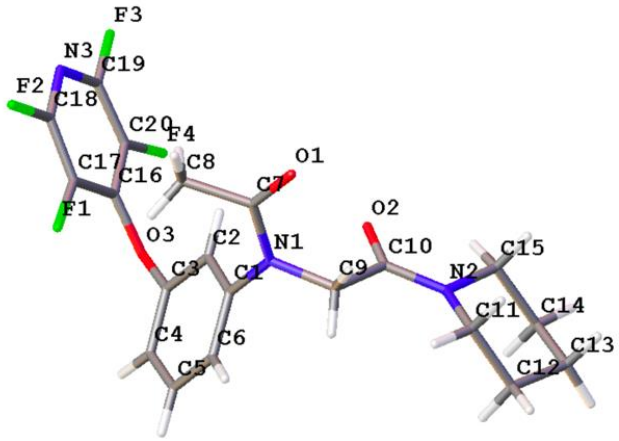

Table A.7. Crystal data and structure refinement for **136**.	
Identification code	22srv175
Empirical formula	$C_{20}H_{19}F_4N_3O_3$
Formula weight	425.38
Temperature/K	120.00
Crystal system	monoclinic
Space group	$P2_1/c$
a/Å	12.0171(4)
b/Å	13.4593(4)
c/Å	12.3689(4)
α/°	90
β/°	112.273(2)
γ/°	90
Volume/Å^3	1851.31(11)
Z	4
ρ_{calc}g/cm^3	1.526
μ/mm^{-1}	1.131
F(000)	880.0
Crystal size/mm^3	0.14 × 0.07 × 0.04
Radiation	Mo Kα (λ = 1.54178)
2Θ range for data collection/°	7.95 to 144.988
Index ranges	-14 ≤ h ≤ 14, -16 ≤ k ≤ 16, -14 ≤ l ≤ 15
Reflections collected	19647
Independent reflections	3660 [R_{int} = 0.0869, R_{sigma} = 0.0514]
Data/restraints/parameters	3660/0/347
Goodness-of-fit on F^2	1.020
Final R indexes [I>=2σ (I)]	R_1 = 0.0425, wR_2 = 0.0922
Final R indexes [all data]	R_1 = 0.0669, wR_2 = 0.1028
Largest diff. peak/hole / e Å^{-3}	0.20/-0.24

A1.8. Crystal determination of 146

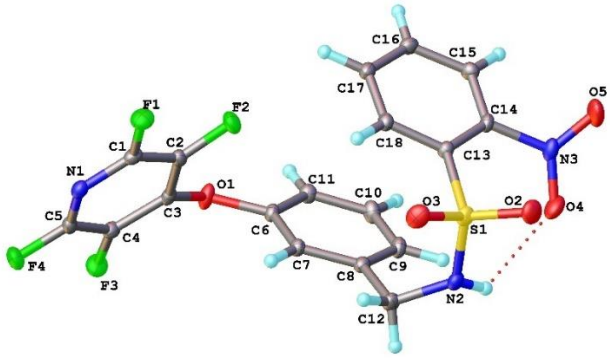

Table A.8. Crystal data and structure refinement for **146**.	
Empirical formula	$C_{18}H_{11}F_4N_3O_5S$
Formula weight	457.36
Temperature/K	120.0
Crystal system	monoclinic
Space group	C2/c
a/Å	33.9861(8)
b/Å	7.3613(2)
c/Å	14.7993(4)
α/°	90
β/°	109.2890(10)
γ/°	90
Volume/Å^3	3494.67(16)
Z	8
ρ_{calc}g/cm^3	1.739
μ/mm^{-1}	0.269
F(000)	1856.0
Crystal size/mm^3	0.32 × 0.11 × 0.08
Radiation	Mo Kα (λ = 0.71073)
2Θ range for data collection/°	5.08 to 59.996
Index ranges	-47 ≤ h ≤ 47, -10 ≤ k ≤ 10, -20 ≤ l ≤ 20
Reflections collected	40433
Independent reflections	5095 [R_{int} = 0.0353, R_{sigma} = 0.0203]
Data/restraints/parameters	5095/0/324
Goodness-of-fit on F^2	1.074
Final R indexes [I>=2σ (I)]	R_1 = 0.0362, wR_2 = 0.0868
Final R indexes [all data]	R_1 = 0.0410, wR_2 = 0.0892
Largest diff. peak/hole / e Å^{-3}	0.42/-0.35

A1.9. Crystal determination of 164

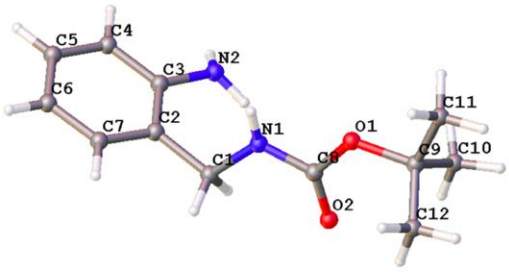

Table A.9. Crystal data and structure refinement for **164**.	
Empirical formula	$C_{12}H_{18}N_2O_2$
Formula weight	222.28
Temperature/K	120.00
Crystal system	monoclinic
Space group	$P2_1/n$
a/Å	15.1349(4)
b/Å	5.13220(10)
c/Å	15.2735(4)
α/°	90
β/°	98.7864(12)
γ/°	90
Volume/Å^3	1172.45(5)
Z	4
ρ_{calc}g/cm^3	1.259
μ/mm^{-1}	0.086
F(000)	480.0
Crystal size/mm^3	0.27 × 0.08 × 0.07
Radiation	Mo Kα (λ = 0.71073)
2Θ range for data collection/°	4.116 to 59.998
Index ranges	$-21 \leq h \leq 21$, $-7 \leq k \leq 7$, $-21 \leq l \leq 21$
Reflections collected	33625
Independent reflections	3426 [R_{int} = 0.0459, R_{sigma} = 0.0242]
Data/restraints/parameters	3426/0/217
Goodness-of-fit on F^2	1.056
Final R indexes [I>=2σ (I)]	R_1 = 0.0422, wR_2 = 0.0950
Final R indexes [all data]	R_1 = 0.0492, wR_2 = 0.0984
Largest diff. peak/hole / e Å^{-3}	0.30/-0.19

A1.10. Crystal determination of 166

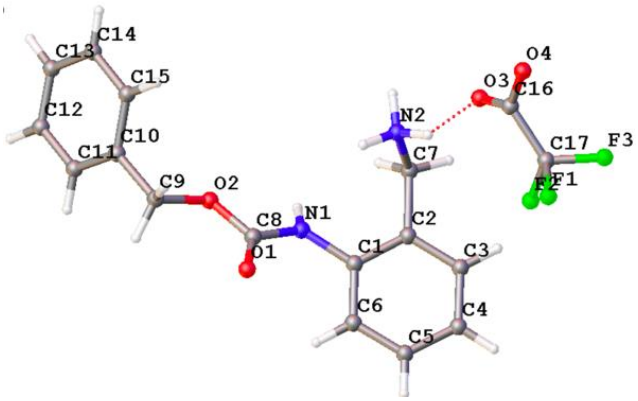

Table A.10. Crystal data and structure refinement for **166.**	
Empirical formula	$C_{11}NO_3H_{0.25}F_{0.25}$
Formula weight	199.12
Temperature/K	120.00
Crystal system	triclinic
Space group	P-1
a/Å	4.7465(16)
b/Å	13.418(5)
c/Å	14.111(5)
α/°	97.278(9)
β/°	98.164(9)
γ/°	90.535(9)
Volume/Å^3	882.1(5)
Z	4
ρ_{calc}g/cm^3	1.499
μ/mm^{-1}	0.116
F(000)	398.0
Crystal size/mm^3	0.509 × 0.28 × 0.024
Radiation	Mo Kα (λ = 0.71073)
2Θ range for data collection/°	3.962 to 59.334
Index ranges	$-6 \leq h \leq 6$, $-18 \leq k \leq 18$, $-19 \leq l \leq 19$
Reflections collected	25711
Independent reflections	4981 [R_{int} = 0.3608, R_{sigma} = 0.4036]
Data/restraints/parameters	4981/93/240
Goodness-of-fit on F^2	1.067
Final R indexes [I>=2σ (I)]	R_1 = 0.1685, wR_2 = 0.3931
Final R indexes [all data]	R_1 = 0.4162, wR_2 = 0.5229
Largest diff. peak/hole / e Å^{-3}	1.38/-0.50

A1.11. Crystal determination of 169

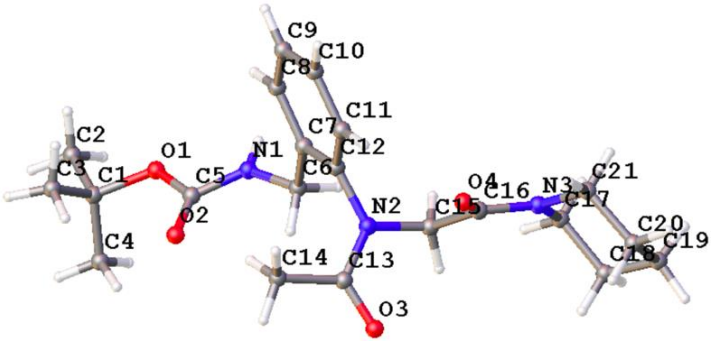

Table A.11. Crystal data and structure refinement for **169.**	
Empirical formula	$C_{21}H_{31}N_3O_4$
Formula weight	389.49
Temperature/K	120.00(10)
Crystal system	monoclinic
Space group	$P2_1/n$
a/Å	9.3809(12)
b/Å	23.453(3)
c/Å	10.4455(15)
α/°	90
β/°	107.361(15)
γ/°	90
Volume/Å^3	2193.5(5)
Z	4
ρ_{calc}g/cm^3	1.179
μ/mm^{-1}	0.082
F(000)	840.0
Crystal size/mm^3	0.109 × 0.079 × 0.051
Radiation	Mo Kα (λ = 0.71073)
2Θ range for data collection/°	4.44 to 59.146
Index ranges	$-13 \leq h \leq 13$, $-32 \leq k \leq 32$, $-14 \leq l \leq 14$
Reflections collected	14275
Independent reflections	14275 [R_{int} = ?, R_{sigma} = 0.8592]
Data/restraints/parameters	14275/207/261
Goodness-of-fit on F^2	0.562
Final R indexes [I>=2σ (I)]	R_1 = 0.0557, wR_2 = 0.0879
Final R indexes [all data]	R_1 = 0.3414, wR_2 = 0.1070
Largest diff. peak/hole / e Å^{-3}	0.25/-0.25

A1.12. Crystal determination of 171

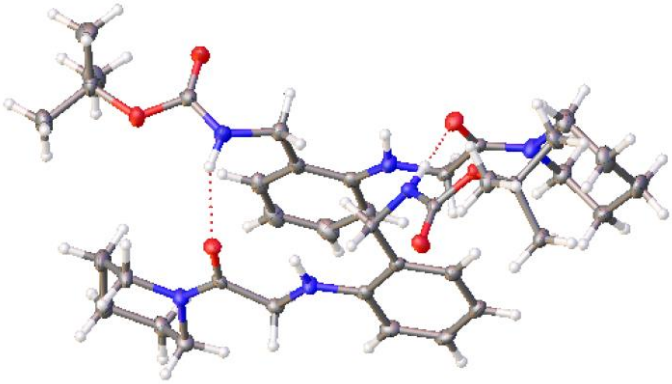

Table A.12. Crystal data and structure refinement for **171.**	
Empirical formula	$C_{19}H_{29}N_3O_3$
Formula weight	347.45
Temperature/K	120.00
Crystal system	monoclinic
Space group	$P2_1/n$
a/Å	21.2212(5)
b/Å	13.2164(3)
c/Å	28.8816(6)
α/°	90
β/°	107.9920(10)
γ/°	90
Volume/Å^3	7704.2(3)
Z	16
ρ_{calc}g/cm^3	1.198
μ/mm^{-1}	0.082
F(000)	3008.0
Crystal size/mm^3	0.243 × 0.157 × 0.077
Radiation	Mo Kα (λ = 0.71073)
2Θ range for data collection/°	3.684 to 59.216
Index ranges	-29 ≤ h ≤ 29, -18 ≤ k ≤ 18, -40 ≤ l ≤ 40
Reflections collected	180847
Independent reflections	21653 [R_{int} = 0.1101, R_{sigma} = 0.0683]
Data/restraints/parameters	21653/0/945
Goodness-of-fit on F^2	1.080
Final R indexes [I>=2σ (I)]	R_1 = 0.0756, wR_2 = 0.1364
Final R indexes [all data]	R_1 = 0.1173, wR_2 = 0.1518
Largest diff. peak/hole / e Å^{-3}	0.28/-0.25

A1.13. Crystal determination of 178

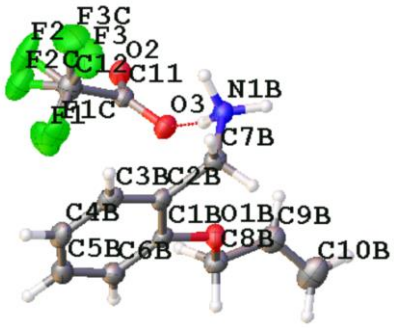

Table A.13. Crystal data and structure refinement for **178**.	
Empirical formula	$C_{12}H_{14}F_3NO_3$
Formula weight	277.24
Temperature/K	120.00
Crystal system	monoclinic
Space group	$P2_1/n$
a/Å	11.3895(4)
b/Å	11.1593(4)
c/Å	30.9413(10)
α/°	90
β/°	97.788(2)
γ/°	90
Volume/Å^3	3896.3(2)
Z	12
ρ_{calc}g/cm^3	1.418
μ/mm^{-1}	1.129
F(000)	1728.0
Crystal size/mm^3	0.36 × 0.02 × 0.01
Radiation	Mo Kα (λ = 1.54178)
2Θ range for data collection/°	5.766 to 141.994
Index ranges	-13 ≤ h ≤ 13, -13 ≤ k ≤ 13, -37 ≤ l ≤ 37
Reflections collected	46843
Independent reflections	7500 [R_{int} = 0.1611, R_{sigma} = 0.0980]
Data/restraints/parameters	7500/75/578
Goodness-of-fit on F^2	1.021
Final R indexes [I>=2σ (I)]	R_1 = 0.0579, wR_2 = 0.1278
Final R indexes [all data]	R_1 = 0.1119, wR_2 = 0.1541
Largest diff. peak/hole / e Å^{-3}	0.31/-0.26

A1.14. Crystal determination of 180

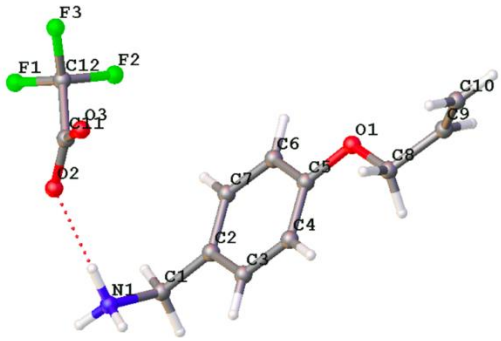

Table A.14. Crystal data and structure refinement for **180.**	
Empirical formula	$C_{12}H_{14}F_3NO_3$
Formula weight	277.24
Temperature/K	120.00(2)
Crystal system	monoclinic
Space group	$P2_1/c$
a/Å	15.3034(4)
b/Å	10.2797(3)
c/Å	8.2137(2)
α/°	90
β/°	103.2190(10)
γ/°	90
Volume/Å^3	1257.90(6)
Z	4
ρ_{calc}g/cm^3	1.464
μ/mm^{-1}	0.133
F(000)	576.0
Crystal size/mm^3	0.237 × 0.102 × 0.094
Radiation	Mo Kα (λ = 0.71073)
2Θ range for data collection/°	4.814 to 63.146
Index ranges	$-21 \leq h \leq 22$, $-15 \leq k \leq 15$, $-12 \leq l \leq 12$
Reflections collected	42076
Independent reflections	4202 [R_{int} = 0.0415, R_{sigma} = 0.0231]
Data/restraints/parameters	4202/0/184
Goodness-of-fit on F^2	1.212
Final R indexes [I>=2σ (I)]	R_1 = 0.0592, wR_2 = 0.1211
Final R indexes [all data]	R_1 = 0.0683, wR_2 = 0.1249
Largest diff. peak/hole / e Å^{-3}	0.52/-0.27

A1.15. Crystal determination of 184

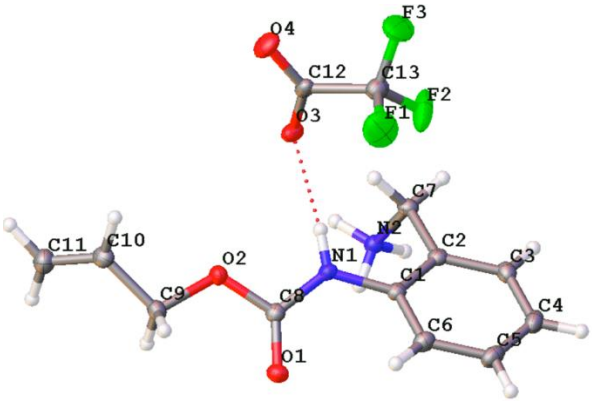

Table A.15. Crystal data and structure refinement for **184**.	
Empirical formula	$C_{13}H_{15}F_3N_2O_4$
Formula weight	320.27
Temperature/K	120.00
Crystal system	triclinic
Space group	P-1
a/Å	8.3683(3)
b/Å	8.6967(3)
c/Å	10.8153(4)
α/°	84.2627(14)
β/°	83.5254(13)
γ/°	69.2217(13)
Volume/Å^3	729.69(5)
Z	2
ρ_{calc}g/cm^3	1.458
μ/mm^{-1}	0.132
F(000)	332.0
Crystal size/mm^3	0.18 × 0.11 × 0.02
Radiation	Mo Kα (λ = 0.71073)
2Θ range for data collection/°	3.798 to 60
Index ranges	-11 ≤ h ≤ 11, -12 ≤ k ≤ 12, -15 ≤ l ≤ 15
Reflections collected	26080
Independent reflections	4254 [R_{int} = 0.0408, R_{sigma} = 0.0290]
Data/restraints/parameters	4254/0/259
Goodness-of-fit on F^2	1.061
Final R indexes [I>=2σ (I)]	R_1 = 0.0480, wR_2 = 0.1020
Final R indexes [all data]	R_1 = 0.0586, wR_2 = 0.1069
Largest diff. peak/hole / e Å^{-3}	0.40/-0.32

A1.16. Crystal determination of 195

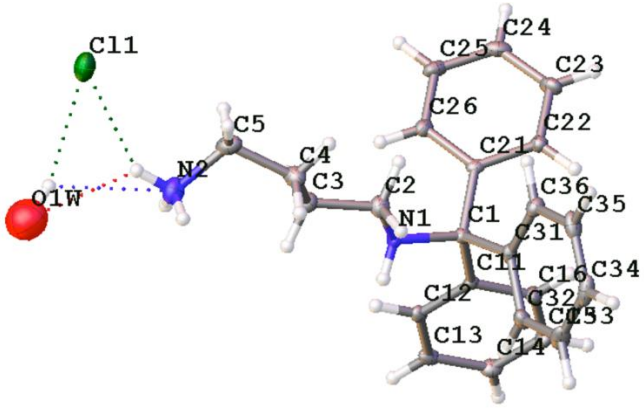

Table A.16. Crystal data and structure refinement for **195**.	
Empirical formula	$C_{23}H_{26}N_2$ x Cl x 1/3 H_2O
Formula weight	372.92
Temperature/K	120.00
Crystal system	trigonal
Space group	R3c
a/Å	34.1215(6)
b/Å	34.1215(6)
c/Å	8.9685(2)
α/°	90
β/°	90
γ/°	120
Volume/Å^3	9042.9(4)
Z	18
ρ_{calc}g/cm^3	1.233
μ/mm^{-1}	0.201
F(000)	3588.0
Crystal size/mm^3	0.19 × 0.02 × 0.01
Radiation	Mo Kα (λ = 0.71073)
2Θ range for data collection/°	4.136 to 57.994
Index ranges	-46 ≤ h ≤ 46, -46 ≤ k ≤ 46, -12 ≤ l ≤ 12
Reflections collected	84070
Independent reflections	5341 [R_{int} = 0.1055, R_{sigma} = 0.0448]
Data/restraints/parameters	5341/1/254
Goodness-of-fit on F^2	1.154
Final R indexes [I>=2σ (I)]	R_1 = 0.0640, wR_2 = 0.1360
Final R indexes [all data]	R_1 = 0.0697, wR_2 = 0.1386
Largest diff. peak/hole / e Å^{-3}	0.35/-0.60
Flack parameter	0.00(2)

A1.17. Crystal determination of 205

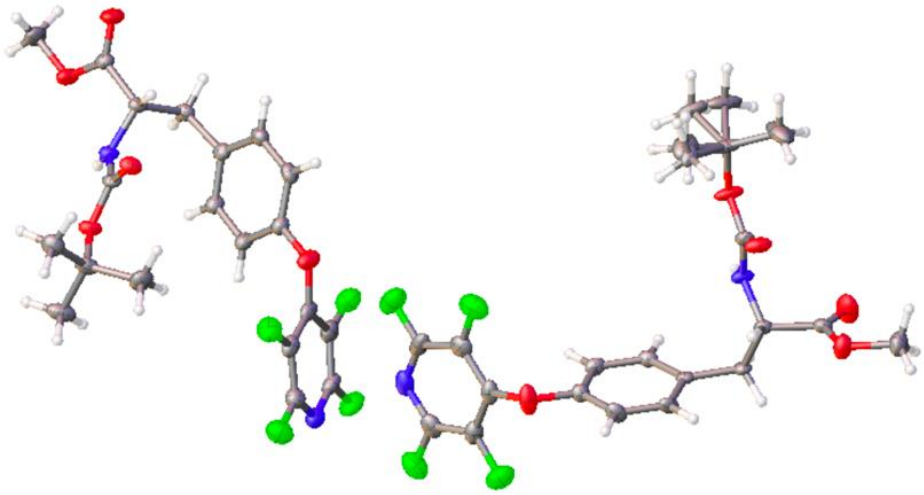

Table A.17. Crystal data and structure refinement for **205**.	
Empirical formula	$C_{20}H_{20}F_4N_2O_5$
Formula weight	444.38
Temperature/K	100.00(2)
Crystal system	monoclinic
Space group	$P2_1$
a/Å	15.7617(3)
b/Å	5.25190(10)
c/Å	25.5026(5)
α/°	90
β/°	107.8160(10)
γ/°	90
Volume/Å^3	2009.84(7)
Z	4
ρ_{calc}g/cm^3	1.469
μ/mm^{-1}	0.121
F(000)	920.0
Crystal size/mm^3	0.184 × 0.008 × 0.004
Radiation	Synchrotron (λ = 0.6889)
2Θ range for data collection/°	2.63 to 64.344
Index ranges	$-22 \leq h \leq 24$, $-8 \leq k \leq 8$, $-37 \leq l \leq 38$
Reflections collected	36881
Independent reflections	13310 [R_{int} = 0.0808, R_{sigma} = 0.1524]
Data/restraints/parameters	13310/415/596
Goodness-of-fit on F^2	0.962
Final R indexes [I>=2σ (I)]	R_1 = 0.0567, wR_2 = 0.1241
Final R indexes [all data]	R_1 = 0.1187, wR_2 = 0.1376
Largest diff. peak/hole / e Å^{-3}	0.40/-0.32
Flack parameter	-0.1(5)

A1.18. Crystal determination of 216

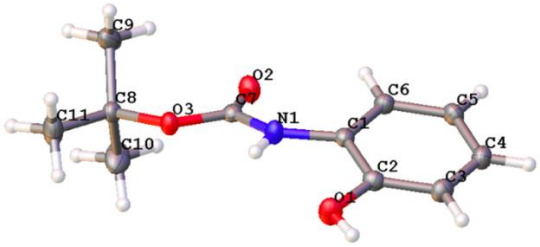

Table A.18. Crystal data and structure refinement for **216.**	
Empirical formula	$C_{11}H_{15}NO_3$
Formula weight	209.24
Temperature/K	120.00
Crystal system	monoclinic
Space group	$P2_1/n$
a/Å	8.3320(3)
b/Å	12.6977(5)
c/Å	10.7219(4)
α/°	90
β/°	100.694(2)
γ/°	90
Volume/Å^3	1114.65(7)
Z	4
ρ_{calc}g/cm^3	1.247
μ/mm^{-1}	0.091
F(000)	448.0
Crystal size/mm^3	0.467 × 0.153 × 0.107
Radiation	Mo Kα (λ = 0.71073)
2Θ range for data collection/°	5.024 to 65.406
Index ranges	$-12 \leq h \leq 12$, $-19 \leq k \leq 19$, $-16 \leq l \leq 16$
Reflections collected	22319
Independent reflections	4102 [R_{int} = 0.0865, R_{sigma} = 0.0680]
Data/restraints/parameters	4102/0/144
Goodness-of-fit on F^2	1.032
Final R indexes [I>=2σ (I)]	R_1 = 0.0548, wR_2 = 0.1272
Final R indexes [all data]	R_1 = 0.0807, wR_2 = 0.1395
Largest diff. peak/hole / e Å^{-3}	0.35/-0.24

A1.19. Crystal determination of 223

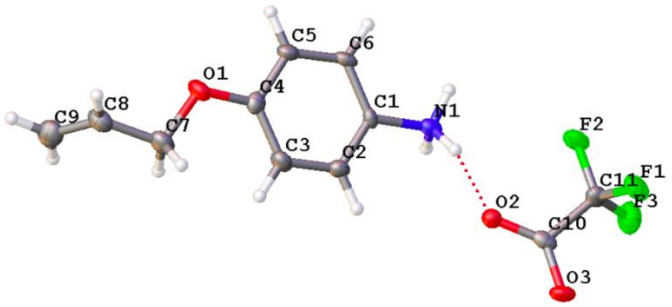

Table A.19. Crystal data and structure refinement for **223.**	
Empirical formula	$C_{11}H_{12}F_3NO_3$
Formula weight	263.22
Temperature/K	120.00(10)
Crystal system	orthorhombic
Space group	Pbcn
a/Å	10.2454(5)
b/Å	7.5316(5)
c/Å	30.2325(15)
α/°	90
β/°	90
γ/°	90
Volume/Å^3	2332.9(2)
Z	8
ρ_{calc}g/cm^3	1.499
μ/mm^{-1}	0.139
F(000)	1088.0
Crystal size/mm^3	0.094 × 0.057 × 0.032
Radiation	Mo Kα (λ = 0.71073)
2Θ range for data collection/°	4.802 to 50.054
Index ranges	-12 ≤ h ≤ 12, -8 ≤ k ≤ 8, -35 ≤ l ≤ 35
Reflections collected	6927
Independent reflections	6927 [R_{int} = ?, R_{sigma} = 0.3684]
Data/restraints/parameters	6927/0/165
Goodness-of-fit on F^2	0.635
Final R indexes [I>=2σ (I)]	R_1 = 0.0525, wR_2 = 0.0956
Final R indexes [all data]	R_1 = 0.1559, wR_2 = 0.1055
Largest diff. peak/hole / e Å^{-3}	0.16/-0.24